THE JOURNAL
OF
CHEMICAL PHYSICS

VOLUME 21, NUMBER 6 JUNE, 1953

A Statistical Theory of Order-Disorder Equilibrium at High Temperatures

PHILIP SCHWED AND GERHART GROETZINGER
Lewis Laboratory, National Advisory Committee for Aeronautics, Cleveland, Ohio
(Received October 15, 1952)

An expression for the free energy of a binary cubic alloy undergoing the order-disorder transition is derived by direct evaluation of the configurational partition function.

THE problem of accounting theoretically for the behavior of an alloy exhibiting an order-disorder transition is usually taken as being equivalent to the problem of determining its configurational partition function f. In general, an approximate expression for f is obtained by considering solely the interaction between nearest neighbors. With this simplification, the expression for f may in the case of a binary alloy $A-B$ be written as

$$f=\sum_{\lambda} n(\lambda)e^{\lambda V/kT}, \tag{1}$$

where $n(\lambda)$ is the number of configurational states with a number of bonds between unlike atoms equal to λ, and V is given by

$$V=(V_{aa}+V_{bb})/2-V_{ab}, \tag{2}$$

with V_{aa}, V_{bb}, and V_{ab} being equal to the interaction energy associated with $A-A$, $B-B$, and $A-B$ bonds, respectively.

Although the problem is completely determined by the above representation in terms of the parameter λ, in all the theories the behavior of the system is specified primarily by another parameter, the degree of long range order s. For the definition of this quantity, the lattice is considered as being made up of two interlacing lattices 1 and 2, such that all the nearest neighbors of an atom on lattice 1 are located on lattice 2. Then if N_{1A} and N_{1B} are the numbers of A and B atoms on lattice 1, respectively, and $2N$ the total number of atoms present, s is given by

$$s=(N_{1A}-N_{1B})/N. \tag{3}$$

It is easy to construct examples which demonstrate that the parameter s does not determine the energy of the configuration. However, in the theory of Bragg and Williams[1] it was assumed that E could be expressed to a good approximation as a function of s alone. Kirkwood[2] has expressed the partition function in a form in which the quantity s is introduced explicitly without the assumption that it determines the energy. Specifically, he writes the quantity f as

$$f=\sum_{s} \sigma(s); \tag{4}$$

if $n(s,\lambda)$ is the number of states of long range order s for a given value of λ, then

$$\sigma=\sum_{\lambda} n(s,\lambda)e^{\lambda V/kT}. \tag{5}$$

As far as the properties of the alloy are concerned, not f itself but the quantity $\log f$ is important, since the free energy F is given by

$$f=-kT\log f. \tag{6}$$

Thus if $\sigma(s)$ takes on a sufficiently strong maximum at some point $s=s_0$ in the range of the summation, then $\log f$ can be replaced by $\log\sigma(s_0)$ so that the behavior of the system is determined by $\sigma(s_0)$. By considering the first four terms of a power series in $1/kT$ for $\log\sigma$, Kirkwood concluded that it possesses such a maximum throughout the whole temperature range so that it was possible to replace $\log f$ by $\log\sigma(s_0)$. Furthermore, both these theories are characterized by the existence of a critical temperature T_c at which the specific heat has a discontinuity. Above this temperature s_0 is identically zero, and below it s_0 increases monotonically from zero to one as the temperature decreases. However, these

[1] W. L. Bragg and E. G. Williams, Proc. Roy. Soc. (London) **A145**, 699 (1934); **151**, 540 (1935); **152**, 231 (1935).
[2] J. G. Kirkwood, J. Chem. Phys. **6**, 70 (1938); H. A. Bethe and J. G. Kirkwood, J. Chem. Phys. **7**, 578 (1939).

two theories differ in the value of T_c and the specific heat. In the Bragg theory this latter quantity vanishes above T_c, while in the Kirkwood theory (as in an earlier theory of Bethe's[3]) it remains greater than zero.

In spite of the fact that in Kirkwood's theory the long-range order is introduced in an unobjectionable fashion, it certainly would be desirable to construct a theory without the intervention of the parameter s. The evaluation of the partition function without reference to this parameter is, of course, quite difficult. We have succeeded, however, in obtaining in this fashion an approximate expression which is valid for the case of high temperatures.

A direct evaluation of $\log f$ would require the enumeration, for each value of λ, of the number of possible arrangements of the A and B atoms over the lattice consistent with the value in question. In approximating the expression for the partition function, we shall attempt to characterize this distribution by a finite number of statistical parameters, which is equivalent to an expression in terms to these quantities. Krishna Iyer[4] has carried out an investigation of the distribution of bonds in a binary cubic lattice of the type $A-B$ and has shown that the problem of the determination of the jth cumulant is equivalent to the one of determining the parameters for the distribution of bonds in a lattice containing j A-atoms and $(2N-j)$ B-atoms. For small values of j this latter problem is much simpler than the original one so that he was able in this fashion to calculate the first four cumulants of the distribution of interest here. The most direct way of obtaining an approximation to the partition function involving these parameters is to make use of the definition of the cumulants which permits us to write

$$\log f=\sum_{j=1}^{\infty}(\kappa_j/j!)(V/kT)^j, \tag{7}$$

where κ_j is the jth cumulant. The four cumulants calculated by Iyer as $\kappa_1=\Lambda/2$, $\kappa_2=\Lambda/4$, $\kappa_3=0$, and $\kappa_4=11\Lambda/8$, where $\Lambda=6N$ is the total number of bonds may thus be used to obtain an approximation for $\log f$ good to the fourth power in $1/kT$:

$$\log f=(\Lambda/2)(V/kT)+(\Lambda/8)(V/kT)^2+(11\Lambda/192)(V/kT)^4. \tag{8}$$

This expression obviously diverges badly at low temperatures as the result of putting κ_j equal to zero for j larger than four. Unfortunately, it is impossible to deduce from the few terms given in this equation the range of validity of the series but it would appear to be reasonably good for temperatures above $T_1=V/k$.

There are, of course, a large number of distributions available which have the same first four cumulants but which behave well at low temperatures as the result of satisfying certain auxiliary conditions following from the elementary properties of the lattice. The simplest of these latter requirements is that there be no contribution from terms with $\lambda>\Lambda$. This can be assured, e.g., by approximating the distribution by a modified Gram-Charlier[5] series in terms of a set of Gaussians cut off at the point $\lambda=\Lambda$. Such a procedure leads to an expression for $\log f$ which is well behaved throughout the whole temperature range and which even displays a critical temperature. However, the cut-off procedure, and therefore the low temperature behavior deduced, are quite arbitrary, as such a procedure must necessarily be. The reason for this is that relatively improbable λ's have very little influence on the values of the early cumulants and conversely these latter fail to determine the behavior of the distribution for such values of λ. Physically this means that the early cumulants only define the behavior of the system at higher temperatures where the contribution of states with improbable λ's is unimportant. For this reason all the valid information obtainable on this approach is contained in the series given in Eq. (8).

The corresponding specific heat per atom following from Eq. (8) is equal to

$$c_v=3k[V^2/(2kT)^2+11V^4/(2kT)^4]. \tag{9}$$

The temperature T_2 at which this expression becomes invalid is of especial interest since according to the usual theories there is a critical temperature T_c at which c_v shows a discontinuity, and it would be expected that the series breaks down near this temperature. It is, of course, again not possible to give a good estimate of T_2 on the basis of Eq. (9), but roughly it appears that

$$T_2\approx 2T_1\approx 2V/k. \tag{10}$$

T_2 is thus a temperature in the vicinity of the critical temperature following from Kirkwood's theory.

The partition function and the specific heat following from our theory and those from Kirkwood's theory show perfect agreement above the critical temperature. This fact is gratifying in view of the difference in the approach and the approximations involved in the two theories.

[3] H. A. Bethe, Proc. Roy. Soc. (London) **A150**, 552 (1935).
[4] P. V. Krishna Iyer, Ann. Math. Statistics **21**, 198 (1950).
[5] See, e.g., M. J. Kendall, *The Advanced Theory of Statistics* (Chas. Griffin and Company, Ltd., London, 1947), Vol. 1, p. 147 ff.

Thermodynamic Functions from Mayer's Theory of Ionic Solutions. I. Equations for Thermodynamic Functions*

JACQUES C. POIRIER†
Department of Chemistry, University of Chicago, Chicago, Illinois
(Received November 26, 1952)

For an ionic solute, Mayer has previously derived from statistical mechanics an analytical expression for a mean activity coefficient which, however, is not usually measured. From the partial molal free energy expression defining Mayer's activity coefficient, there are derived in this paper expressions for five usually measured thermodynamic functions. These are the change in partial molal volume with concentration; the change in apparent molal volume with concentration; the relative partial molal heat content; the relative apparent molal heat content; and the stoichiometric mean ionic molar activity coefficient. Formulas for these five functions involve the coefficients of thermal expansion and isothermal compressibility of the solution and solvent; the solvent dielectric constant and its pressure and temperature derivatives; and readily computable analytic expressions arising from the theory.

A. INTRODUCTION AND DEFINITIONS

ON the basis of the statistical mechanical theory of the thermodynamics of multicomponent systems,[1] an equation has been derived[2] for f^*,[3] a mean activity coefficient of an ionic solute in solution at the absolute temperature T, under a total external pressure P and at a concentration of c moles per liter at T and P. In this paper, we will restrict ourselves to two-component systems and will denote solvent quantities by the subscript 1 and solute quantities by the subscript 2. The defining equation for f^* is

$$\bar{F}_2(c, P, T)=\bar{F}_2^{\circ}{}_c(p, T)+\nu RT \ln(f^* c_{\pm}). \quad (1)$$

Here $\bar{F}_2(c, P, T)$ is the usual partial molal free energy; $\bar{F}_2^{\circ}{}_c(p, T)$ is the standard partial molal free energy, the subscript c indicating that it is measured on the molarity scale. It should be emphasized that the standard state pressure in $\bar{F}_2^{\circ}{}_c$ is not that under which $\bar{F}_2$ is measured; this results from the fact that in the derivation of the fundamental equations the partial molal free energy of the solvent does not vary with solute concentration, and hence the external pressure at any solute concentration c must exceed the standard state pressure by the osmotic pressure of the solution. The symbol ν represents the number of ions into which one molecule of the solute dissociates, and $c_{\pm}$ is the mean molar concentration, defined by

$$c_{\pm}=c[\nu_+{}^{\nu_+}\nu_-{}^{\nu_-}]^{1/\nu}, \quad (2)$$

where ν_+ and ν_- denote the number of cations and anions, respectively, produced in dissolving one molecule of solute. Explicitly, f^* is given by the following equation,[4]

$$\ln f^*=-\frac{n_2{}^{\frac{1}{2}}(\nu c)^{\frac{1}{2}}}{(2C_0)^{\frac{1}{2}}}-\frac{A}{n_2}\sum_{\mu\geq 0}\frac{(-)^{\mu}n_{\mu}{}^2}{A^{\mu}}[f_{\mu}(\varphi)-g_{\mu}(\varphi)], \quad (3)$$

in which μ is a running index and φ is proportional to the square root of solute concentration,

$$\varphi=A(2n_2\nu c/C_0)^{\frac{1}{2}}. \quad (4)$$

The quantity A is proportional to the distance of closest approach a of oppositely charged ions and is defined by

$$A=aKkT/\epsilon^2$$
$$=a \text{ (in angstrom units)}/7.137 \ (H_2O, 25°C), \quad (5)$$

in which K is the dielectric constant of water at the standard state pressure p and temperature T, k is the Boltzmann constant, and ϵ is the electronic charge. The set of quantities n_{μ} is defined by

$$n_{\mu}=\sum_s Z_s{}^{\mu}x_s, \quad (6)$$

where Z_s is the charge in protonic units on an ion of type s, and x_s is the mole fraction of ions of type s in the solute. The quantity C_0 is defined by

$$C_0=1000[KkT/\epsilon^2]^3/2\pi N_0, \quad (7)$$

where N_0 is Avogadro's number. The sets of functions f_{μ} and g_{μ} are defined by

$$f_{\mu}(\varphi)=\frac{\varphi^2}{\mu!}\int_1^{l_{\mu}} e^{-\mu\varphi y}y^{2-\mu}dy, \quad (8)$$

$$g_{\mu}(\varphi)=\frac{\varphi^3}{4(\mu-1)!}\int_1^{l_{\mu}} e^{-\mu\varphi y}y^{3-\mu}dy, \quad (9)$$

* From a thesis submitted in partial fulfillment of the requirements for the degree of Doctor of Philosophy at the University of Chicago, Chicago, Illinois.

† Atomic Energy Commission Predoctoral Fellow. Present address: Department of Chemistry, Yale University, New Haven, Connecticut.

[1] W. G. McMillan and J. E. Mayer, J. Chem. Phys. **13**, 276 (1945).

[2] J. E. Mayer, J. Chem. Phys. **18**, 1426 (1950).

[3] The activity coefficient f^* is identical with $\gamma_{\pm}$ of reference 2. In this and the following paper, an effort has been made to conform with the recommendations of the National Research Council regarding nomenclature of activity coefficients.

[4] Equations (3) and (9) are Eqs. (72) and (71) of reference 2; the delta-function appearing in the definition of f_{μ} in reference 2 has here been taken out of the summation and not included in the present definition Eq. (8). Instead the delta-function gives rise to the first terms of Eqs. (3) and (9) of the present paper.

in which the limit $l_\mu=0$ for $\mu\leqslant 2$; $l_\mu=\infty$ for $\mu\geqslant 3$. The osmotic pressure of the solution at the concentration c, the temperature T, and the pressure P is given by

$$P_{osm}/\rho kT=1-\frac{n_2{}^{\frac{1}{2}}(\nu c)^{\frac{1}{2}}}{3(2C_0)^{\frac{1}{2}}}-\frac{A}{2n_2}\sum_{\mu\geq 0}\frac{(-)^\mu n_\mu{}^2}{A^\mu}\times[f_\mu(\varphi)-2g_\mu(\varphi)], \quad (10)$$

where the total ion density ρ is given by

$$\rho=N_0\nu c/1000. \quad (11)$$

We will hereafter symbolize the first term of the right member of (3) by $\ln f^*_D$, the last term of the right member of (3) by $\ln f^*_S$, the first two terms of the right member of (10) multiplied by ρkT by P_D, and the last term of (10) by ρkT by P_S. If the Debye-Hückel κ,

$$\kappa=(4\pi N_0\epsilon^2 n_2\nu c/1000KkT)^{\frac{1}{2}}, \quad (12)$$

is used in $\ln f^*_D$, there results the familiar form

$$\ln f^*_D=-n_2\epsilon^2\kappa/2KkT, \quad (13)$$

and hence it is evident that $\ln f^*_D$ is identical with the usually derived Debye-Hückel limiting expression for the logarithm of the activity coefficient[6] at infinite dilution, (though not identical at any finite concentration). Similarly P_D is the Debye-Hückel osmotic pressure.

The purpose of this paper is to derive, from these fundamental equations, equations for the change in partial molal volume with concentration; the apparent molal volume; the relative partial molal heat content; the relative apparent molal heat content; and the relation of f^* to f, the usual stoichiometric mean ionic molar activity coefficient, defined by the equation

$$\bar F_2(c, P, T)=\bar F_2{}^\circ{}_c(P, T)+\nu RT\ln(fc_\pm), \quad (14)$$

in which the activity coefficient of an ionic solute in solution, under a pressure P and temperature T and at a concentration of c moles per liter measured under P and T, is given with reference to a standard state at the same pressure P. In Sections B through F, thermodynamic transformations will be carried out to obtain equations for the above thermodynamic functions; Section G will then apply Eqs. (1)–(11) to the problem of evaluating these functions. The general plan is to consider the standard pressure p in Eqs. (1)–(11) as depending on the concentration in such a way that the total external pressure P remains independent of concentration, then differentiation at constant P or with respect to P can be performed. In order to relate f^* to f, one needs the difference between two standard partial molal free energies at different pressures; since this involves the partial molal volume, it is more convenient to consider first the change in partial molal volume with concentration.

[6] See, for example, MacDougall, *Physical Chemistry* (The Macmillan Company, New York, 1949), revised edition, p. 507, where the stoichiometric mean ionic *rational* activity coefficient is derived. The corresponding *molar* activity coefficient contains the additional factor $d/d_1+c(\nu M_1-M_2)/1000d_1$, which, however, reduces to unity at infinite dilutions.

B. THE CHANGE IN PARTIAL MOLAL VOLUME WITH CONCENTRATION

We take as independent variables the total pressure P, the temperature T, and the numbers of moles of the various components n_1 and n_2 [which should be readily distinguishable in context from members of the set n_μ defined in (3)]. In this and subsequent sections, partial derivatives with respect to one of the above variables keeping all others constant will be needed. These derivatives will be symbolized as in the following two examples:

$$(\partial P_{osm}/\partial P)_{n_i,T}=(P_{osm})_P,$$
$$(\partial^2\bar F_2{}^\circ{}_c/\partial P^2)_{n_i,T}=(\bar F_2{}^\circ{}_c)_{PP},$$

all quantities being evaluated at P and T. We begin by expanding $\bar F_2{}^\circ{}_c(p, T)$ in a Taylor's series expansion about the total external pressure P, two terms being retained:

$$\bar F_2{}^\circ{}_c(p, T)=\bar F_2{}^\circ{}_c(P, T)-P_{osm}(\bar F_2{}^\circ{}_c)_P. \quad (15)$$

Since the partial molal volume is the partial derivative of the partial molal free energy with respect to the total external pressure P at constant temperature and mole numbers, when the equation resulting from using Eq. (15) in Eq. (1) is so differentiated, there is obtained the following equation:

$$\bar V_2=(\bar F_2{}^\circ{}_c)_P[1-(P_{osm})_P]+\nu RT[(\ln f^*)_P+(\ln c_\pm)_P]-P_{osm}(\bar F_2{}^\circ{}_c)_{PP}. \quad (16)$$

Introducing the coefficient of isothermal compressibility β, defined by

$$\beta=-V^{-1}(V)_P=(\ln c)_P, \quad (17)$$

we see from (2) that

$$(\ln c_\pm)_P=\beta. \quad (18)$$

Now if we let the number of moles of solute n_2 approach zero in Eq. (16), while keeping the total pressure P, the temperature T, and the number of moles of solvent n_1 constant, the concentration c and therefore the osmotic pressure approach zero, $(P_{osm})_P$ approaches zero, the standard state pressure p becomes the total pressure P, $\ln f^*$ approaches zero, $(\ln f^*)_P$ approaches zero, the compressibility becomes that of the pure solvent at P and T, and the partial molal volume approaches the partial molal volume at infinite dilution $\bar V_2{}^\circ$. Consequently in the limit of infinite dilution Eq. (16) reduces to the following:

$$\bar V_2{}^\circ=(\bar F_2{}^\circ{}_c)P+\nu RT\beta_1. \quad (19)$$

Substitution of (18) and (19) in (16) yields the final equation,

$$\bar V_2-\bar V_2{}^\circ=\nu RT[(\ln f^*)_P+\beta-\beta_1]+B, \quad (20)$$

where B contains the small correction terms,

$$B=(P_{osm})_P[\nu RT\beta_1-\bar{V}_2^\circ] +P_{osm}[\nu RT(\beta_1)_P-\bar{V}_2^\circ)_P], \quad (21)$$

which may usually be neglected in a numerical calculation since it contributes only a few tenths of one percent of the total value of the change in partial molal volume. The evaluation of B necessitates the evaluation of $(\bar{V}_2^\circ)_P$, which is not generally available, but which may be converted to a more convenient expression as follows. Equating the mixed third partials of the free energy, the identity,

$$(\bar{V}_2)_P=-\bar{V}_2\beta-V(\beta)_{n_2}, \quad (22)$$

is obtained, which in the limit of infinite dilution leads to the useful form,

$$(\bar{V}_2^\circ)_P=-\bar{V}_2^\circ\beta_1-V_1(\beta_1)_{n_2}, \quad (23)$$

where V_1 is the molar volume of the solvent. With (23) in (21), B can be computed from

$$B=P_{osm}[\bar{V}_2^\circ\beta_1+V_1(\beta_1)_{n_2}+\nu RT(\beta_1)_P] +(P_{osm})_P[\nu RT\beta_1-\bar{V}_2^\circ]=\nu RT\beta O(\bar{V}_2c/1000), \quad (24)$$

the order of O following from the fact that $1000P_{osm}/\nu cRT$ is approximately unity, Eq. (10).

C. THE APPARENT MOLAL VOLUME

Since a knowledge of the partial molal volume of a solute is usually derived from measurements of the apparent molal volume, an equation for this more directly measurable thermodynamic function is here given. The usual definition of the apparent molal molal volume is

$$\phi_V=(V-n_1V_1)/n_2, \quad (25)$$

where V is the total volume of solution at c, P, and T. Since the volume is a homogeneous function of first order in the mole numbers,

$$V=n_1\bar{V}_1+n_2\bar{V}_2, \quad (26)$$

where $\bar{V}_1$ and $\bar{V}_2$ are the partial molal volumes of solvent and solute, respectively. Using Eq. (26) in (25), we obtain the equation

$$\phi_V=\bar{V}_2+(n_1V_1/n_2)(\bar{V}_1/V_1-1). \quad (27)$$

If the partial molal volume of the solute at infinite dilution is known, then $\bar{V}_2$ can be calculated from (20); we shall assume that this has been done and that $\bar{V}_2$ is calculable. In order to obtain an equation for $\bar{V}_1/V_1-1$, appearing in Eq. (27), we proceed from the definition of the osmotic pressure $P-p$,

$$\bar{F}_1(c, P, T)=F_1(p, T), \quad (28)$$

where $F_1(p, T)$ is the free energy per mole of pure solvent at p, the standard state pressure. Replacing the right member of Eq. (28) by the first two terms of its Taylor series expansion about the total external pressure P, we obtain the equation

$$\bar{F}_1(c, P, T)=F_1(P, T)-V_1P_{osm}, \quad (29)$$

where the equality of V_1 and $(F_1)_P$ has been used. Differentiation of Eq. (29) with respect to the total external pressure P, holding the temperature and mole numbers constant, yields the following equation:

$$\bar{V}_1=V_1[1-(P_{osm})_P]-P_{osm}(V_1)_P. \quad (30)$$

Using Eq. (17) for the pure solvent, (30) yields the equation

$$\bar{V}_1/V_1-1=\beta_1P_{osm}-(P_{osm})_P=G. \quad (31)$$

The remaining factor in Eq. (27), namely, n_1V_1/n_2, is the volume per mole of solute if there were no change in volume of the solution and can obviously be expressed as the difference between the actual volume per mole of solute and the change in volume of the solution per mole of solute and the change in volume of the solution per mole of solute,

$$n_1V_1/n_2=1000/c-\phi_V. \quad (32)$$

Using Eqs. (31) and (32) in Eq. (27) and solving for ϕ_V, one obtains the final equation,

$$\phi_V=(\bar{V}_2+1000G/c)(1+G)^{-1}\cong\bar{V}_2+1000G/c, \quad (33)$$

where the error resulting from the last approximation is usually less than a tenth of one percent of ϕ_V.

D. THE RELATION BETWEEN f^* AND f

The activity coefficient f^* defined in Eq. (1) is not that measured experimentally. It is therefore useful to obtain the relation between f^* and f, defined in Eqs. (14), from which the two other commonly used activity coefficients, the stoichiometric mean ionic molal activity coefficient and the stoichiometric mean ionic rational activity coefficient, are easily obtainable.[6] By comparing Eqs. (1) and (14), it is seen that the defining equations for f^* and f differ only in that the standard state pressures are different. Therefore by equating the right members of Eqs. (1) and (14), one obtains the relationship

$$\ln f=\ln f^*-[\bar{F}_2^\circ{}_c(P, T)-\bar{F}_2^\circ{}_c(p, T)]/\nu RT. \quad (34)$$

By using Eqs. (15) and (19), i.e., expanding $\bar{F}_2^\circ{}_c(p, T)$ in a Taylor's series about the total pressure P, retaining only the first two terms, we immediately obtain the desired relation,

$$\ln f=\ln f^*-P_{osm}[\bar{V}_2^\circ/\nu RT-\beta_1]. \quad (35)$$

E. THE RELATIVE PARTIAL MOLAL HEAT CONTENT

We shall now obtain an equation for the relative partial molal heat content, $\bar{L}_2$, defined by

$$\bar{L}_2=\bar{H}_2-\bar{H}_2^\circ, \quad (36)$$

[6] See, for example, H. S. Harned and B. B. Owen, *The Physical Chemistry of Electrolytic Solutions* (Reinhold Publishing Corporation, New York, 1943), first edition, p. 12.

where $\bar{H}_2$ is the partial molal heat content of the solute and may be defined by

$$\bar{H}_2=\bar{F}_2-T(\bar{F}_2)_T, \tag{37}$$

and $\bar{H}_2^\circ$ is the partial molal heat content of the solute at infinite dilution. It is more convenient to carry out transformations if, for $\bar{F}_2$, Eq. (14) rather than Eq. (1) is used. Following the transformations, Eq. (35) can then be used to introduce those quantities which can be computed from the formulas of Section A. If Eq. (2) and the coefficient of thermal expansion α, defined by

$$\alpha=V^{-1}(V)_T=-(\ln c)_T, \tag{38}$$

are introduced when (14) is used in (37), the resulting equation is

$$\bar{H}_2=\bar{F}_{2c}^\circ-T(\bar{F}_{2c}^\circ)_T-\nu RT^2[(\ln f)_T-\alpha]. \tag{39}$$

Letting n_2 approach zero in Eq. (39) at constant P, T, and n_1, the quantity $\bar{F}_{2c}^\circ$ and its temperature derivative are unaffected, being independent of concentration; the coefficient of thermal expansion approaches α_1, that of the pure solvent at P and T; the derivative of $\ln f$ approaches zero; and the partial molal heat content approaches $\bar{H}_2^\circ$, yielding the equation

$$\bar{H}_2^\circ=\bar{F}_{2c}^\circ-T(\bar{F}_{2c}^\circ)_T+\nu RT^2\alpha_1. \tag{40}$$

Using Eqs. (40) and (39) in (36), there is obtained for the relative partial molal heat content,

$$\bar{L}_2/\nu RT^2=-(\ln f)_T+\alpha-\alpha_1. \tag{41}$$

Equation (35) may then be used in Eq. (41), but the temperature derivative of the correction term in Eq. (35) contributes only about one-half of one percent to the total value of $\bar{L}_2$ and hence may usually be neglected. Thus, using $(\ln f^*)_T$ for $(\ln f)_T$ one obtains the final equation,

$$\bar{L}_2/\nu RT^2=-(\ln f^*)_T+\alpha-\alpha_1. \tag{42}$$

F. THE RELATIVE APPARENT MOLAL HEAT CONTENT

Like the case of the corresponding volume quantities, the relative partial molal heat content of a solute is usually derived from measurements of the relative apparent molal heat content. Consequently an equation for this latter thermodynamic function is now given. The usual definition of the relative apparent molal heat content ϕ_L is

$$\phi_L=-\bar{H}_2^\circ+(H-n_1H_1)/n_2, \tag{43}$$

where H is the total heat content of the solution at c, P, and T. Since the total heat content is a homogeneous function of first order in the mole numbers, we have

$$H=n_1\bar{H}_1+n_2\bar{H}_2. \tag{44}$$

Using Eq. (44) in Eq. (43) along with Eq. (36), we obtain the equation

$$\phi_L=\bar{L}_2+n_1(\bar{H}_1-H_1)/n_2. \tag{45}$$

Now $\bar{H}_1$ may be defined analogously to Eq. (37) by the following equation:

$$\bar{H}_1=\bar{F}_1-T(\bar{F}_1)_T. \tag{46}$$

A convenient form for $(\bar{F}_1)_T$ is obtained by differentiation of Eq. (29) with respect to temperature at constant total external pressure P and mole numbers n_i; thus,

$$(\bar{F}_1)_T=-S_1-V_1[(P_{osm})_T+\alpha_1P_{osm}], \tag{47}$$

where Eq. (38) for the pure solvent as well as the equality of $-S_1$ and $(F_1)_T$ have been used. Substituting Eqs. (47) and (29) into Eq. (46), there is obtained the equation

$$\bar{H}_1=F_1+TS_1+V_1[P_{osm}(\alpha_1T-1)+T(P_{osm})_T]. \tag{48}$$

Since the first two terms of the right-hand member are clearly H_1, Eq. (48) may be used in Eq. (45) to give the equation,

$$\phi_L=\bar{L}_2+(n_1V_1/n_2)[P_{osm}(\alpha_1T-1)+T(P_{osm})_T], \tag{49}$$

and replacing n_1V_1/n_2 by $1000/c$ (Eq. (32) in which ϕ_V is negligibly small) one obtains the final equation,

$$\phi_L=\bar{L}_2+(1000/c)[P_{osm}(\alpha_1T-1)+T(P_{osm})_T]. \tag{50}$$

G. EXPLICIT EQUATIONS FOR FUNCTIONS AND SUMMARY

In the preceding sections, thermodynamic equations have been used to relate five thermodynamic functions, namely, $\bar{V}_2$, ϕ_V, f, $\bar{L}_2$, and ϕ_L, to $\ln f^*$, P_{osm}, and their pressure and temperature derivatives at constant temperature or pressure, respectively, and mole numbers. In this section, equations will be given in explicit analytical form so that $\ln f^*$, P_{osm}, and their derivatives may be computed given the following quantities: a, the distance of closest approach parameter for the solute; the solvent dielectric constant K and its pressure and temperature derivatives at the total external pressure P and temperature T; the molarity c; and the compressibility and thermal expansion coefficients and their derivatives for the solution and the pure solvent. The final equations of the preceding sections will then be summarized in this explicit form for purposes of computation.

It should be noted that the explicit theoretical equations for the thermodynamic functions $\ln f^*$ and P_{osm}, Eqs. (3) and (10) respectively, are functions of the variables c, T, and a, and K. However, the dielectric constant K to be used in (3) and (10) is the dielectric constant of the pure solvent at a pressure less than P by the osmotic pressure. It therefore varies with the concentration if P, the total external pressure, is considered to be fixed (at, say, one atmosphere) and independent of the concentration. We prefer to introduce at this point the more readily computable quantity $\ln f'$, given by Eq. (3) with the modification that in (3) K is now understood to mean the dielectric constant of the pure solvent at the total external pressure P and

temperature T. While $\ln f'$ is here introduced primarily as an aid in computation, it should be noted that it has thermodynamic significance. The value of $\ln f'$ is the value of $\ln f^*$ for a solute in solution under a total external pressure $P+P_{osm}$, at a temperature T and at a concentration of c moles per liter, measured at $P+P_{osm}$ and T. The defining equation is thus

$$\bar{F}_2(c, P+P_{osm}, T)=\bar{F}_2^{\circ}{}_c(P, T)+\nu RT \ln(f'c_{\pm}). \quad (51)$$

The quantity to be used in Eq. (51) for P_{osm} is to be computed from Eq. (10) using the solvent dielectric constant at the pressure P and is not identical with the quantity P_{osm} used in the definition of $\ln f^*$. Both osmotic pressures are those of solutions of the same molarity c, but the total pressures on the solutions (under which the molarity is measured) are different. Again, the two osmotic pressures are not those of the same physical solution under different total external pressures, for the external pressure change would alter the molarity by changing the volume of the solution.

The usefulness of $\ln f'$ lies in the fact that $\ln f^*$ may be expanded in a Taylor's series about the dielectric constant at the total external pressure P, this dielectric constant being hereafter written simply as K. The expansion thus obtained involves only $\ln f'$, its derivatives, and P_{osm}. Actually, the P_{osm} used in the definition of $\ln f'$ and which we use for computation is the first term of a similar Taylor's series expansion about K of the P_{osm} defined by (1), but all further terms of this expansion may be neglected since the osmotic pressure enters into the equations of the preceding sections only in correction terms. In writing these expansions and in the rest of this section, we will need derivatives of functions with respect to the logarithm of one variable from the set of variables K, c, a, and T, hereafter collectively referred to as the natural variables, keeping the other variables of this set constant. Such derivatives will be symbolized as in the following example:

$$(\partial \ln f'/\partial \ln c)_{K, a, T}=\{\ln f'\}_c,$$

that is, *braces* indicate differentiation of the inclosed function with respect to the logarithm of the natural variable written as a subscript, keeping constant all other natural variables, while as before *parentheses* indicate differentiation of the inclosed function with respect to the thermodynamic variable written as a subscript with the other members of the set P, T, and n_i constant. Carrying out the Taylor's series expansion of $\ln f^*$ about K with the additional approximation that $K(p, T)-K \cong -KP_{osm}(\ln K)_P$, the following equation, correct to two terms, is obtained:

$$\ln f^*=\ln f'-P_{osm}\{\ln f'\}_K (\ln K)_P. \quad (52)$$

The order of magnitude of the error introduced by computing P_{osm} using K is seen from the corresponding expansion of P_{osm} to be the second (neglected) term, $-P_{osm}\{P_{osm}\}_K (\ln K)_P$. Summarizing, numerical values of $\ln f^*$ are computed from Eq. (52). The quantity $\ln f'$ is computed from Eq. (3) in which $K(p, T)$ is replaced by K; P_{osm} is computed from Eq. (10) with $K(p, T)$ replaced by K; and $\{\ln f'\}_K$ is computed from the equation resulting from differentiating Eq. (3), with $K(p, T)$ replaced by K, with respect to $\ln K$. The derivation of the analytical form of this last equation [the sum of Eqs. (63) and (81)] is deferred until later, being most conveniently considered in connection with the next topic, the development of analytical expressions for the derivatives of $\ln f^*$ and P_{osm} with respect to the thermodynamic variables. These derivatives can be found as sums of partial derivatives with respect to certain of the natural variables. A partial derivative with respect to P at constant T and n_i involves only successive differentiation with respect to c (at constant K, a, and T) and K (at constant c, a, and T). The equations

$$(P_{osm})_P=\{P_{osm}\}_K (\ln K)_P+\beta\{P_{osm}\}_c, \quad (53)$$

$$(\ln f^*)_P=\{\ln f'\}_K (\ln K)_P+\beta\{\ln f'\}_c, \quad (54)$$

result, where terms coming from the second term of the right-hand member of Eq. (52) are neglected. These neglected terms involve second derivatives or the product of two first derivatives and are smaller than the first two terms of Eq. (52) by a factor of about 10^{-3}. The partial derivatives of $\ln f^*$ and P_{osm} with respect to T at constant P and n_i involve successive differentiation with respect to all four[7] natural variables in turn, the resulting equations being

$$(P_{osm})_T=\{P_{osm}\}_K (\ln K)_T-\alpha\{P_{osm}\}_c +\{P_{osm}\}_a (\ln a)_T+T^{-1}\{P_{osm}\}_T, \quad (55)$$

$$(\ln f^*)_T=\{\ln f'\}_K (\ln K)_T-\alpha\{\ln f'\}_c +\{\ln f'\}_a (\ln a)_T+T^{-1}\{\ln f'\}_T, \quad (56)$$

where again second derivatives or the product of two first derivatives, arising from the second term of the right-hand member of Eq. (52), smaller by a factor of about 10^{-3} than the other terms of Eq. (56), are neglected.

The problem of evaluating the equations of the previous sections is now reduced to finding explicit formulas for the partial derivatives $\{\ln f'\}_x$ and $\{P_{osm}\}_x$ (where x represents any one of the natural variables) appearing in the right-hand member of Eqs. (53)–(56) from the explicit Eqs. (3)–(11) (in which K is to be used). We will split Eqs. (3) and (10) into two terms; the first (indicated by a subscript D) including the Debye term in the case of $\ln f'$ and the classical and Debye terms in P_{osm}. The second terms (indicated by a subscript S) contain the higher corrections. Thus we have the following equations:

$$\ln f'=\ln f'_D+\ln f'_S, \quad (57)$$

$$\ln f'_D=-(n_2^3\nu\pi N_0\epsilon^6/1000k^3)^{\frac{1}{2}}c^{\frac{1}{2}}(KT)^{-\frac{3}{2}}, \quad (58)$$

[7] The reason for considering $(\ln a)_P=0$ but not neglecting $(\ln a)_T$ is discussed later.

$$\ln f'_S = -\frac{A}{n_2}\sum_{\mu\geq 0}\frac{(-)^\mu n_\mu^2}{A^\mu}[f_\mu(\varphi)-g_\mu(\varphi)], \quad (59)$$

$$P_{osm} = P_D + P_S, \quad (60)$$

$$P_D = (N_0\nu ckT/1000)(1+\tfrac{1}{3}\ln f'_D), \quad (61)$$

$$P_S = -(N_0\nu ckT/2000n_2)A\sum_{\mu\geq 0}\frac{(-)^\mu n_\mu^2}{A^\mu} \times[f_\mu(\varphi)-2g_\mu(\varphi)]. \quad (62)$$

Differentiating Eqs. (57) and (60) term by term with respect to the logarithm of each of the natural variables, the terms indicated by a subscript D immediately yield from Eqs. (58) and (61) the derivatives

$$\{\ln f'_D\}_K = -\tfrac{3}{2}\ln f'_D, \quad (63)$$

$$\{\ln f'_D\}_c = \tfrac{1}{2}\ln f'_D, \quad (64)$$

$$\{\ln f'_D\}_T = -\tfrac{3}{2}\ln f'_D, \quad (65)$$

$$\{P_D\}_K = (N_0\nu ckT/1000)(-\tfrac{1}{2}\ln f'_D), \quad (66)$$

$$\{P_D\}_c = (N_0\nu ckT/1000)(1+\tfrac{1}{2}\ln f'_D), \quad (67)$$

$$\{P_D\}_T = (N_0\nu ckT/1000)(1-\tfrac{1}{6}\ln f'_D). \quad (68)$$

The correction terms, Eqs. (59) and (62), involve in addition $f_\mu(\varphi)$, $g_\mu(\varphi)$, and A, functions of the natural variables. Differentiation of Eqs. (59) and (62) with respect to $\ln A$ merely introduces a factor of $(1-\mu)$ into the summations, and $\{\ln A\}_x$ may be found by differentiating Eqs. (5) to be the following:

$$\{\ln A\}_K = \{\ln A\}_a = \{\ln A\}_T = 1. \quad (69)$$

The derivatives of f_μ and g_μ with respect to $\ln\varphi$ are found by differentiating Eqs. (8) and (9) to be the following:

$$df_\mu/d\ln\varphi = 2f_\mu - 4g_\mu, \quad (70)$$

$$dg_\mu/d\ln\varphi = 3g_\mu - \frac{\mu\varphi^4}{4(\mu-1)!}\int_1^{l_\mu} e^{-\mu\varphi y}y^{4-\mu}dy. \quad (71)$$

Integrating the last integral by parts, Eqs. (71) may be converted into the following form:

$$dg_\mu/d\ln\varphi = -g_\mu - [\varphi^3 e^{-\mu\varphi}/4(\mu-1)!-\mu g_\mu]. \quad (72)$$

For the sake of brevity we shall adopt the following symbolism: $f_\mu - g_\mu$ will hereafter be written as b_μ, and the quantity in the bracket of Eq. (72) will be written as h_μ; thus

$$h_\mu = \varphi^3 e^{-\mu\varphi}/4(\mu-1)!-\mu g_\mu. \quad (73)$$

By combining Eqs. (72) with (70) and using this new symbolism, the following equations are obtained:

$$db_\mu/d\ln\varphi = 2b_\mu - g_\mu + h_\mu, \quad (74)$$

$$d(b_\mu-g_\mu)/d\ln\varphi = 2b_\mu + 2h_\mu. \quad (75)$$

Finally by combining Eqs. (4), (5), and (7), the following form is obtained for φ:

$$\varphi = (n_2\nu\pi N_0\epsilon^2/250k)^{\frac{1}{4}}c^{\frac{1}{4}}a(KT)^{-\frac{1}{4}}, \quad (76)$$

from which $\{\ln\varphi\}_x$ are easily found to be the following:

$$\{\ln\varphi\}_K = -\tfrac{1}{2}, \quad (77)$$

$$\{\ln\varphi\}_c = \tfrac{1}{2}, \quad (78)$$

$$\{\ln\varphi\}_a = 1, \quad (79)$$

$$\{\ln\varphi\}_T = -\tfrac{1}{2}. \quad (80)$$

With the aid of Eq. (69) and Eqs. (74)–(80), the partial derivatives of Eq. (59) and (62) with respect to the logarithm of the natural variables are easily found to be the following:

$$\{\ln f'_S\}_K = \frac{A}{2n_2}\sum_{\mu\geq 0}\frac{(-)^\mu n_\mu^2}{A^\mu}[2\mu b_\mu - g_\mu + h_\mu], \quad (81)$$

$$\{\ln f'_S\}_c = -\frac{A}{2n_2}\sum_{\mu\geq 0}\frac{(-)^\mu n_\mu^2}{A^\mu}[2b_\mu - g_\mu + h_\mu], \quad (82)$$

$$\{\ln f'_S\}_a = \frac{A}{n_2}\sum_{\mu\geq 0}\frac{(-)^\mu n_\mu^2}{A^\mu}[(\mu-3)b_\mu + g_\mu - h_\mu], \quad (83)$$

$$\{\ln f'_S\}_T = \frac{A}{2n_2}\sum_{\mu\geq 0}\frac{(-)^\mu n_\mu^2}{A^\mu}[2\mu b_\mu - g_\mu + h_\mu], \quad (84)$$

$$\{P_S\}_K = \frac{\rho kTA}{2n_2}\sum_{\mu\geq 0}\frac{(-)^\mu n_\mu^2}{A^\mu}[\mu b_\mu - (\mu-1)g_\mu + h_\mu], \quad (85)$$

$$\{P_S\}_c = -\frac{\rho kTA}{2n_2}\sum_{\mu\geq 0}\frac{(-)^\mu n_\mu^2}{A^\mu}[2b_\mu - g_\mu + h_\mu], \quad (86)$$

$$\{P_S\}_a = \frac{\rho kTA}{2n_2}\sum_{\mu\geq 0}\frac{(-)^\mu n_\mu^2}{A^\mu} \times[(\mu-3)b_\mu - (\mu-1)g_\mu - 2h_\mu], \quad (87)$$

$$\{P_S\}_T = \frac{\rho kTA}{2n_2}\sum_{\mu\geq 0}\frac{(-)^\mu n_\mu^2}{A^\mu} \times[(\mu-1)b_\mu - (\mu-2)g_\mu + h_\mu]. \quad (88)$$

Equations (81)–(88) may then be added to Eqs. (63)–(68) to yield explicit equations for $\{\ln f'\}_x$ and $\{P_{osm}\}_x$, which may then be used in Eqs. (53)–(56) to yield the following explicit equations for the partial derivatives of $\ln f^*$ and P_{osm}:

$$\frac{(P_{osm})_P}{\rho kT} = \beta + \tfrac{1}{2}[\beta - (\ln K)_P]\ln f'_D - \frac{\beta A}{2n_2}\sum_{\mu\geq 0}\frac{(-)^\mu n_\mu^2}{A^\mu}[2b_\mu - g_\mu + h_\mu] + \frac{(\ln K)_P A}{2n_2}\sum_{\mu\geq 0}\frac{(-)^\mu n_\mu^2}{A^\mu} \times[\mu b_\mu - (\mu-1)g_\mu + h_\mu], \quad (89)$$

$$(\ln f^*)_P=\tfrac{1}{2}[\beta-3\,(\ln K)_P]\ln f'_D$$
$$-\frac{\beta A}{2n_2}\sum_{\mu\geq 0}\frac{(-)^\mu n_\mu^2}{A^\mu}[2b_\mu-g_\mu+h_\mu]$$
$$+\frac{(\ln K)_P A}{2n_2}\sum_{\mu\geq 0}\frac{(-)^\mu n_\mu^2}{A^\mu}[2\mu b_\mu-g_\mu+h_\mu], \quad (90)$$

$$\frac{(P_{osm})_T}{\rho kT}=-\alpha+T^{-1}-\tfrac{1}{2}[\alpha+(\ln K)_T-\tfrac{1}{6}T^{-1}]\ln f'_D$$
$$+[\alpha-T^{-1}]\frac{A}{2n_2}\sum_{\mu\geq 0}\frac{(-)^\mu n_\mu^2}{A^\mu}[2b_\mu-g_\mu+h_\mu]$$
$$+[(\ln K)_T+(\ln a)_T+T^{-1}]\frac{A}{2n_2}$$
$$\times\sum_{\mu\geq 0}\frac{(-)^\mu n_\mu^2}{A^\mu}[\mu b-(\mu-1)g_\mu+h_\mu]$$
$$-[3(\ln a)_T-T^{-1}]\frac{A}{2n_2}\sum_{\mu\geq 0}\frac{(-)^\mu n_\mu^2}{A^\mu}$$
$$\times[b_\mu+h_\mu], \quad (91)$$

$$(\ln f^*)_T=-\tfrac{1}{2}[\alpha+3(\ln K)_T+3T^{-1}]\ln f'_D$$
$$+[\alpha-3(\ln a)_T]\frac{A}{2n_2}\sum_{\mu\geq 0}\frac{(-)^\mu n_\mu^2}{A^\mu}$$
$$\times[2b_\mu-g_\mu+h_\mu]+[(\ln K)_T+(\ln a)_T+T^{-1}]$$
$$\times\frac{A}{2n_2}\sum_{\mu\geq 0}\frac{(-)^\mu n_\mu^2}{A^\mu}[2\mu b_\mu-g_\mu+h_\mu]. \quad (92)$$

Equations (89)–(92) may in turn be substituted into the final equations of the previous sections, yielding the explicit formulas below for $\Delta\bar{V}_2$, ϕ_V, $\bar{L}_2$, and ϕ_L. Each is preceded by the thermodynamic equation for that function (neglecting very small terms) repeated from the earlier section for convenience:

$$\frac{\bar{V}_2-\bar{V}_2^\circ}{\nu RT}=(\ln f^*)_P+\beta-\beta_1, \quad (20)$$

$$\frac{\bar{V}_2-\bar{V}_2^\circ}{\nu RT}=\tfrac{1}{2}[\beta-3(\ln K)_P]\ln f'_D$$
$$-\frac{\beta A}{2n_2}\sum_{\mu\geq 0}\frac{(-)^\mu n_\mu^2}{A^\mu}[2b_\mu-g_\mu+h_\mu]$$
$$+\frac{(\ln K)_P A}{2n_2}\sum_{\mu\geq 0}\frac{(-)^\mu n_\mu^2}{A^\mu}$$
$$\times[2\mu b_\mu-g_\mu+h_\mu]+\beta-\beta_1, \quad (93)$$

$$\phi_V=\bar{V}_2+1000[\beta_1 P_{osm}-(P_{osm})_P]/c, \quad (33)$$

$$\frac{\phi_V-\bar{V}_2^\circ}{\nu RT}=[\beta_1-(\ln K)_P]\ln f'_D$$
$$+\frac{(\ln K)_P A}{2n_2}\sum_{\mu\geq 0}\frac{(-)^\mu n_\mu^2}{A^\mu}[\mu b_\mu+(\mu-2)g_\mu]$$
$$-\frac{\beta_1 A}{2n_2}\sum_{\mu\geq 0}\frac{(-)^\mu n_\mu^2}{A^\mu}[b_\mu-g_\mu], \quad (94)$$

$$\bar{L}_2/\nu RT^2=-(\ln f^*)_T+\alpha-\alpha_1, \quad (42)$$

$$\frac{\bar{L}_2}{\nu RT^2}=\tfrac{1}{2}[\alpha+3(\ln K)_P+3T^{-1}]\ln f'_D$$
$$-[\alpha-3(\ln a)_T]\frac{A}{2n_2}\sum_{\mu\geq 0}\frac{(-)^\mu n_\mu^2}{A^\mu}$$
$$\times[2b_\mu-g_\mu+h_\mu]-[(\ln K)_T+(\ln a)_T+T^{-1}]$$
$$\times\frac{A}{2n_2}\sum_{\mu\geq 0}\frac{(-)^\mu n_\mu^2}{A^\mu}[2\mu b_\mu-g_\mu+h_\mu]$$
$$+\alpha-\alpha_1, \quad (95)$$

$$\phi_L=\bar{L}_2+1000[P_{osm}(\alpha_1 T-1)+T(P_{osm})_T]/c, \quad (50)$$

$$\frac{\phi_L}{\nu RT^2}=[\tfrac{1}{3}\alpha_1+(\ln K)_T+T^{-1}]\ln f'_D$$
$$-[(\ln K)_T+(\ln a)_T+T^{-1}]\frac{A}{2n_2}$$
$$\times\sum_{\mu\geq 0}\frac{(-)^\mu n_\mu^2}{A^\mu}[\mu b_\mu+(\mu-2)g_\mu]$$
$$-[\alpha_1-3(\ln a)_T]\frac{A}{2n_2}\sum_{\mu\geq 0}\frac{(-)^\mu n_\mu^2}{A^\mu}$$
$$\times[b_\mu-g_\mu]. \quad (96)$$

The formula for the fifth thermodynamic function $\ln f$, obtained by using Eq. (52) in Eq. (35),

$$\ln f=\ln f'-P_{osm}[\bar{V}_2^\circ/\nu RT+\{\ln f'\}_K\,(\ln K)_P-\beta_1], \quad (97)$$

is most conveniently left in this form with $\ln f'$ given by (57), P_{osm} by Eq. (60), and $\{\ln f'\}_K$ by the sum of Eqs. (63) and (81).

The assumptions made in this paper about the variation of the effective distance of closest approach a for any particular salt with factors such as pressure, temperature, and the nature of the solvent deserves some comment. The model of a solution used in deriving the theoretical formulas of Section A is that of hard sphere ions of distance of closest approach a in a continuum of dielectric constant K. This would lead to a zero derivative of a with respect to such variables. However, al-

though the model is oversimplified, one may expect that if a is chosen to average out deviations of the actual interionic potential from a Coulombic one, it might give reasonably good answers. Therefore, if these factors affect the actual interionic potential, one would expect the derivative of a to be different from zero. The effect of a change in external pressure on a may be expected to be small, since in solutions there already exists an "internal pressure" which is very large compared to usual changes in external pressure. Hence in this paper $(a)_P$ has been assumed to be zero. There is no similar reason why the temperature derivative of a should be negligibly small, and therefore terms arising from the variation of a with temperature have been retained in the equations of this paper, though the evaluation of $(a)_T$ is somewhat problematical. Since further numerical work will be restricted to aqueous solutions, the relation between a for any particular salt and the nature of the solvent has been ignored, but there is no reason to assume that the value of a for a salt would be independent of the nature of the solvent in which it is dissolved.

The author is greatly indebted to J. E. Mayer, with whom the author had many invaluable discussions.

THE JOURNAL OF CHEMICAL PHYSICS VOLUME 21, NUMBER 6 JUNE, 1953

Thermodynamic Functions from Mayer's Theory of Ionic Solutions. II. The Stoichiometric Mean Ionic Molar Activity Coefficient*

JACQUES C. POIRIER†
Department of Chemistry, University of Chicago, Chicago, Illinois
(Received November 26, 1952)

The formula for the stoichiometric mean ionic molar activity coefficient of strong electrolytes in aqueous solution at 25°C arising from Mayer's theory is compared with published experimental data. The agreement is good for sodium chloride to a concentration of about 0.4 molar; calcium chloride to a concentration of about 0.07 molar; zinc sulfate to a concentration of about 0.01 molar; and lanthanum chloride to a concentration of about 0.017 molar. Tables facilitating the computations and practical methods for the determination of the parameter of closest interionic approach and of the activity coefficient are given.

A. INTRODUCTION

IN the preceding paper, analytic expressions for five thermodynamic functions of ionic solutes in solution were derived from the statistical mechanical theory of multicomponent systems, developed by Mayer. The reader is referred to this for the development of these expressions and for all references to statistical mechanical theory. The purpose of this paper is to compare the results of the theory for one of the five functions, namely the stoichiometric mean ionic molar activity coefficient (hereafter referred to simply as the molar activity coefficient), with published experimental data for certain representative salts of ionic types I–I, II–I, II–II, and III–I, and to present tables greatly simplifying the computations. The comparison will be restricted to single salts in aqueous solution at 25°C and one atmosphere external pressure.

Briefly summarizing the relevant equations of part I, the molar activity coefficient f for an ionic solute in solution at a concentration of c moles per liter, at the absolute temperature T, and under a total external pressure P is given by the expression

$$\ln f=\ln f'-P_{\text{osm}}[\bar{V}_2^\circ/\nu RT+\{\ln f'\}_K(\ln K)_P-\beta_1]. \quad (1)$$

The second term of the right member will be referred to as the osmotic pressure correction. In Eq. (1), ν represents the number of ions into which one molecule of solute dissociates, R is the gas constant, β_1 is the coefficient of isothermal compressibility of the pure solvent, $\bar{V}_2^\circ$ is the partial molal volume of the solute at infinite dilution, and $(\ln K)_P$ is the partial derivative with respect to pressure at constant temperature of the logarithm of the dielectric constant K of the pure solvent, all these quantities being measured at the temperature T and pressure P. The three remaining quantities in (1) are $\ln f'$, the logarithm of an unusual activity coefficient (the thermodynamic significance of which is discussed in section G of the preceding paper); $\{\ln f'\}_K$, the partial derivative of $\ln f'$ with respect to the logarithm of the solvent dielectric constant; and P_{osm}, the osmotic pressure of the solution at c, T, and P. In the explicit equation for each of these three quantities, the first term is the sum of the classical and Debye contributions, here indicated by a subscript D. The remaining terms are expressed as sums of functions of a parameter φ (proportional to the square root of concentration) defined by Eq. (12), and the functions are later tabulated. The sums also involve the param-

* From a thesis submitted in partial fulfillment of the requirements for the degree of Doctor of Philosophy at the University of Chicago.

† Atomic Energy Commission Predoctoral Fellow. Present address: Department of Chemistry, Yale University, New Haven, Connecticut.

eter A, proportional to the distance of closest interionic approach [Eq. (11)], as well as numbers n_μ determined by the ionic type [Eq. (10)]. The explicit equation for $\ln f'$ is the following:

$$\ln f' = \ln f'_D - \frac{A}{n_2} \sum_{\mu \geq 0} \frac{(-)^\mu n_\mu{}^2}{A^\mu} b_\mu(\varphi), \tag{2}$$

with $\ln f'_D$ identically the Debye-Hückel limiting law (later used as a convenient parameter):

$$\ln f'_D = -n_2 \epsilon^2 \kappa / 2KkT. \tag{3}$$

For $\{\ln f'\}_K$ we have the equation

$$\{\ln f'\}_K = \{\ln f'_D\}_K + \frac{A}{2n_2} \sum_{\mu \geq 0} \frac{(-)^\mu n_\mu{}^2}{A^\mu} \times [2\mu b_\mu(\varphi) - g_\mu(\varphi) + h_\mu(\varphi)], \tag{4}$$

where $\{\ln f'_D\}_K$ is given explicitly by the expression

$$\{\ln f'_D\}_K = 3n_2 \epsilon^2 \kappa / 4KkT. \tag{5}$$

The osmotic pressure is given by the following equation:

$$P_{\text{osm}} = P_D - \frac{\rho A kT}{2n_2} \sum_{\mu \geq 0} \frac{(-)^\mu n_\mu{}^2}{A^\mu} [b_\mu(\varphi) - g_\mu(\varphi)], \tag{6}$$

where P_D is given by the equation,

$$P_D = \rho kT[1 + \tfrac{1}{3} \ln f'_D], \tag{7}$$

in which ρ is the total ion number density,

$$\rho = N_0 \nu c / 1000, \tag{8}$$

where N_0 is Avogadro's number. In Eqs. (2)–(6), μ is a running index, k is the Boltzmann constant, ϵ is the electronic charge, and κ is the Debye-Hückel κ given by

$$\kappa = (4\pi N_0 \epsilon^2 n_2 \nu c / 1000 KkT)^{\frac{1}{2}}. \tag{9}$$

The set of quantities n_μ is defined as follows:

$$n_\mu = \sum_s Z_s{}^\mu x_s, \tag{10}$$

where Z_s is the charge in protonic units on an ion of type s and x_s is the mole fraction of ions of type s in one molecule of solute. The quantity A (further discussed in section C) is defined by the equation

$$A = aKkT/\epsilon^2, \tag{11}$$

where a is the effective distance of closest approach between oppositely charged ions in solution. The parameter φ is given by the equation

$$\varphi = A\kappa\epsilon^2/KkT = a\kappa, \tag{12}$$

the last equality following from Eq. (11). The sets of functions $g_\mu(\varphi)$, $b_\mu(\varphi)$, and $h_\mu(\varphi)$ are defined by the equations

$$g_\mu(\varphi) = \frac{\varphi^3}{4(\mu-1)!} \int_1^{l_\mu} e^{-\mu\varphi y} y^3 - \mu dy, \tag{13}$$

$$b_\mu(\varphi) = \frac{\varphi^2}{\mu!} \int_1^{l_\mu} e^{-\mu\varphi y} y^{2-\mu} (1 - \mu\varphi y/4) dy, \tag{14}$$

$$h_\mu(\varphi) = \varphi^3 e^{-\mu\varphi}/4(\mu-1)! - \mu g_\mu(\varphi), \tag{15}$$

with the limit $l_\mu = 0$ for $\mu \leqslant 2$ and $l_\mu = \infty$ for $\mu \geqslant 3$.

For computational purposes the numerical values used for the constants appearing in Eqs. (1)–(8) are those recommended by Birge:[1] $\epsilon = 4.8025_1 \times 10^{-10}$ abs. esu, $R = 8.31436 \times 10^7$ erg degree^{-1} mole^{-1}, 0°C $= 273.16$°K, $N_0 = 6.0228_3 \times 10^{23}$ mole^{-1}, and $k = 1.380474 \times 10^{-16}$ erg deg^{-1}. In addition, the following constants for water at 25°C and one atmosphere pressure are used: $K = 78.54$,[2] $\beta_1 = 4.564_6 \times 10^{-11}$ (dynes/cm^2)$^{-1}$,[3] and $(\ln K)_P = 5.854 \times 10^{-11}$ (dynes/cm^2)$^{-1}$.[4] Using these numerical values, for aqueous solutions at 25°C and one atmosphere pressure the parameters φ and a take the following form:

$$\varphi = 1.6579_0 A (n_2 \nu c)^{\frac{1}{2}}, \tag{16}$$

$$a \text{ (in angstrom units)} = 7.1345_8 \text{A}. \tag{17}$$

Equations (3), (5), and (7) become, respectively,

$$\ln f'_D = -0.82895 n_2{}^{\frac{1}{2}} (\nu c)^{\frac{1}{2}}, \tag{18}$$

$$\{\ln f'_D\}_K = 1.2434_2 n_2{}^{\frac{1}{2}} (\nu c)^{\frac{1}{2}}, \tag{19}$$

$$P_D = 2.4790 \times 10^7 \nu c [1 - 0.27631_7 n_2{}^{\frac{1}{2}} (\nu c)^{\frac{1}{2}}]. \tag{20}$$

Since the computation of the functions $b_\mu(\varphi)$, $g_\mu(\varphi)$, and $h_\mu(\varphi)$ is quite laborious, these functions are here tabulated in Tables I–III, respectively, for convenient values of φ.[5] Since solutions are electrically neutral, n_1 is always identically zero, and it is not necessary to tabulate b_1, g_1, and h_1. It may be seen from Eqs. (13) and (15) that g_0 and h_0 are identically zero, and consequently these two functions are also not tabulated. The method of using Tables I–III in obtaining the summation terms in Eqs. (2), (4), and (6) is discussed in the next section.

B. DISCUSSION OF THE BASIC EQUATION

Equation (1) is the basic equation by which activity coefficients as predicted by this theory may be compared with experimental data on activity coefficients.

[1] R. T. Birge, Revs. Modern Phys. **13**, 233 (1941).
[2] J. Wyman, Jr., and E. N. Ingalls, J. Am. Chem. Soc. **60**, 1182 (1938).
[3] R. E. Gibson, Am. J. Sci. 5, **35A**, 49 (1938).
[4] The empirical equation from which $(\ln K)_P$ is obtained is that of B. B. Owen and S. R. Brinkley, Jr., Phys. Rev. **64**, 32 (1943). The numerical values of the two parameters appearing in the equation are those of B. B. Owen and S. R. Brinkley, Jr., Ann. N. Y. Acad. Sci. **51**, 753 (1949), and B. B. Owen, J. Chem. Ed. **21**, 59 (1944).
[5] For the method used in obtaining these tabulated values, see the appendix.

TABLE I. The function $10^{\mu}b_{\mu}(\varphi)$.

φ	$b_0(\varphi)$	$10^2b_2(\varphi)$	$10^3b_3(\varphi)$	$10^4b_4(\varphi)$	$10^5b_5(\varphi)$	$10^6b_6(\varphi)$	$10^7b_7(\varphi)$	$10^8b_8(\varphi)$
0.01	−0.000 033	−0.004 939	0.045 273	0.034 447	0.037 056	0.041 428	0.044 177	0.043 781
0.02	−0.000 133	−0.019 508	0.137 326	0.116 819	0.138 763	0.148 604	0.157 400	0.154 614
0.03	−0.000 300	−0.043 554	0.253 519	0.239 245	0.268 721	0.300 299	0.315 751	0.307 176
0.04	−0.000 533	−0.076 082	0.383 43	0.380 203	0.431 051	0.480 048	0.500 703	0.482 220
0.05	−0.000 833	−0.117 48	0.520 52	0.534 446	0.609 117	0.675 111	0.697 587	0.665 328
0.06	−0.001 200	−0.167 12	0.660 59	0.694 140	0.794 855	0.875 680	0.896 659	0.845 847
0.07	−0.001 633	−0.224 71	0.800 544	0.859 069	0.981 491	1.074 299	1.090 580	1.016 414
0.08	−0.002 133	−0.289 96	0.938 223	1.020 840	1.164 740	1.265 344	1.271 51	1.171 663
0.09	−0.002 700	−0.362 57	1.072 019	1.178 440	1.340 70	1.444 755	1.435 94	1.308 343
0.10	−0.003 333	−0.442 21	1.200 784	1.329 711	1.506 74	1.609 645	1.582 799	1.424 580
0.12	−0.004 800	−0.621 67	1.440 103	1.607 474	1.801 82	1.888 95	1.815 553	1.593 449
0.14	−0.006 533	−0.826 24	1.652 001	1.846 35	2.041 17	2.096 18	1.966 513	1.680 712
0.16	−0.008 533	−1.053 92	1.835 04	2.043 43	2.222 24	2.232 08	2.040 950	1.696 036
0.18	−0.010 800	−1.302 89	1.988 93	2.198 16	2.347 14	2.301 91	2.048 433	1.652 261
0.20	−0.013 333	−1.571 45	2.114 51	2.312 19	2.419 49	2.313 52	2.000 368	1.562 944
0.22	−0.016 133	−1.857 98	2.213 29	2.388 33	2.444 33	2.275 90	1.908 463	1.440 923
0.24	−0.019 200	−2.161 00	2.287 00	2.429 85	2.429 57	2.197 98	1.783 817	1.297 585
0.26	−0.022 533	−2.479 08	2.337 70	2.440 49	2.379 65	2.088 47	1.636 399	1.142 536
0.28	−0.026 133	−2.810 93	2.367 36	2.424 30	2.301 25	1.955 52	1.474 830	0.983 547
0.30	−0.030 000	−3.155 35	2.378 13	2.384 30	2.199 52	1.806 01	1.305 91	0.826 67
0.35	−0.040 833	−4.064 04	2.335 44	2.205 67	1.879 90	1.395 76	0.886 93	0.469 968
0.40	−0.053 333	−5.028 68	2.216 26	1.952 04	1.515 52	0.993 73	0.522 85	0.189 250
0.45	−0.067 500	−6.036 20	2.045 50	1.661 66	1.151 82	0.633 51	0.230 192	−0.008 992
0.50	−0.083 333	−7.075 73	1.843 22	1.362 90	0.817 56	0.335 81	0.015 386	−0.134 420
0.55	−0.100 833	−8.138 42	1.625 16	1.074 85	0.526 49	0.104 53	−0.129 642	−0.202 746
0.60	−0.120 000	−9.216 95	1.403 26	0.809 59	0.285 18	−0.064 620	−0.217 732	−0.230 093
0.65	−0.140 833	−10.305 33	1.186 29	0.573 97	0.093 37	−0.180 251	−0.262 550	−0.230 401
0.70	−0.163 333	−11.398 83	0.980 00	0.370 83	−0.053 349	−0.252 340	−0.276 476	−0.214 408
0.75	−0.187 500	−12.493 60	0.788.64	0.200 85	−0.159 882	−0.290 741	−0.269 892	−0.190 265
0.80	−0.213 333	−13.586 70	0.614 6	0.061 394	−0.232 780	−0.304 238	−0.250 685	−0.162 947
0.85	−0.240 833	−14.675 85	0.458 4	−0.049 186	−0.278 463	−0.300 232	−0.224 760	−0.135 871
0.90	−0.270 000	−15.759 21	0.321 7	−0.133 366	−0.302 670	−0.284 655	−0.196 198	−0.110 918
0.95	−0.300 833	−16.835 63	0.202 2	−0.197 571	−0.311 346	−0.262 092	−0.168 027	−0.088 998
1.00	−0.333 333	−17.904 14	0.101 1	−0.242 135	−0.306 387	−0.235 921	−0.140 916	−0.070 395
1.10	−0.403 333	−20.015 57	−0.056 9	−0.287 743	−0.275 744	−0.181 700	−0.095 325	−0.042 530
1.20	−0.480 000	−22.091 55	−0.161 0	−0.292 921	−0.231 341	−0.133 112	−0.062 188	−0.024 767
1.30	−0.563 333	−24.133 60	−0.223 6	−0.274 259	−0.185 003	−0.094 019	−0.039 236	−0.014 020
1.40	−0.653 333	−26.143 60	−0.254 9	−0.243 381	−0.142 868	−0.064 569	−0.024 138	−0.007 755
1.50	−0.750 000	−28.124 99	−0.263 9	−0.207 997	−0.107 455	−0.043 623	−0.014 559	−0.004 209
1.60	−0.853 333	−30.081 52	−0.257 7	−0.172 827	−0.079 124	−0.028 607	−0.008 630	−0.002 250
1.70	−0.963 333	−32.016 85	−0.242 5	−0.140 485	−0.057 270	−0.018 575	−0.005 050	−0.001 161
1.80	−1.080 000	−33.934 42	−0.221 5	−0.112 193	−0.040 839	−0.011 911	−0.002 915	−0.000 616
1.90	−1.203 333	−35.837 75	−0.197 6	−0.088 304	−0.028 796	−0.007 555	−0.001 667	
2.00	−1.333 333	−37.728 68	−0.172 5	−0.068 658	−0.020 085	−0.004 746	−0.000 946	
2.50	−2.083 333	−47.085 56	−0.075 3	−0.017 090	−0.002 227	−0.000 417		
3.00	−3.000 000	−56.389 36	−0.027 6	−0.003 682	−0.000 382			
3.50	−4.083 333	−65.704 80	−0.009 4	−0.000 200				
4.00	−5.333 333	−75.041 9	−0.002 8					
4.50	−6.750 000	−84.396 0	−0.000 9					
5.00	−8.333 333	−93.760 1						
5.50	−10.083 333	−103.129 6						
6.00	−12.000 000	−112.502 2						
6.50	−14.083 333	−121.876 1						
7.00	−16.333 333	−131.250						
7.50	−18.750 000	−140.625						

Aside from $\bar{V}_2^{\circ}$, which appears in the osmotic pressure correction and which is generally to be found in the literature, four basic quantities are required for a determination of the molar activity coefficient. These are the molarity c; the number ν of ions per solute molecule and the set of numbers n_{μ}, both determined by the ionic type of the salt; and the quantity A, which distinguishes among salts of the same ionic type, and the determination of which is discussed in the next section. The most convenient way of computing the summations in Eqs. (2), (4), and (6) is to calculate φ from Eq. (16). This value of φ will in general lie between two round values of φ for which b_{μ}, g_{μ}, and h_{μ} are tabulated in Tables I–III. Using three neighboring round values of φ and the same A, n_2, and ν, Eq. (16) gives the three corresponding values of $c^{\frac{1}{2}}$. The entire summation term is then computed for the round values of φ (and their corresponding values of $c^{\frac{1}{2}}$) after which a nonlinear (Newtonian) interpolation is carried out to give the summation term for the original φ and $c^{\frac{1}{2}}$. This procedure yields a value of the summation terms of Eqs. (2), (4), and (6) accurate to four decimal places. The value obtained by using only linear interpolation rarely differs by more than one or two digits in the fourth decimal place from the value obtained by using three points and nonlinear interpolation (the exception being

TABLE I—*Continued.*

φ	$10^{9}b_{9}(\varphi)$	$10^{10}b_{10}(\varphi)$	$10^{11}b_{11}(\varphi)$	$10^{12}b_{12}(\varphi)$	$10^{13}b_{13}(\varphi)$	$10^{14}b_{14}(\varphi)$	$10^{15}b_{15}(\varphi)$	$10^{16}b_{16}(\varphi)$
0.01	0.040 265	0.034 007	0.026 805	0.019 619	0.013 419	0.008 607	0.005 196	0.002 961
0.02	0.140 230	0.117 605	0.091 707	0.066 309	0.044 798	0.028 381	0.016 919	0.009 521
0.03	0.275 601	0.228 419	0.176 348	0.125 938	0.084 022	0.052 562	0.030 937	0.017 186
0.04	0.427 857	0.350 582	0.267 699	0.188 780	0.124 348	0.076 789	0.044 610	0.024 458
0.05	0.583 625	0.472 350	0.356 818	0.248 410	0.161 504	0.098 423	0.056 418	0.030 516
0.06	0.733 410	0.586 282	0.437 855	0.300 849	0.193 000	0.116 033	0.065 603	0.034 993
0.07	0.870 741	0.687 478	0.507 275	0.343 894	0.217 611	0.129 015	0.071 915	0.037 809
0.08	0.991 477	0.772 77	0.563 244	0.376 610	0.234 977	0.137 319	0.075 426	0.039 064
0.09	1.093 291	0.840 97	0.605 158	0.398 944	0.245 318	0.141 240	0.076 401	0.038 952
0.10	1.175 17	0.891 81	0.633 269	0.411 424	0.249 213	0.141 273	0.075 204	0.037 712
0.12	1.279 68	0.944 08	0.651 771	0.410 620	0.240 897	0.132 085	0.067 909	0.032 835
0.14	1.312 04	0.939 40	0.628 856	0.383 172	0.217 003	0.114 611	0.056 615	0.026 219
0.16	1.284 68	0.890 57	0.576 305	0.338 393	0.184 127	0.093 088	0.043 805	0.019 212
0.18	1.211 719	0.811 22	0.505 184	0.284 382	0.147 605	0.070 706	0.031 233	0.012 679
0.20	1.106 758	0.712 79	0.425 010	0.227 617	0.111 311	0.049 598	0.019 943	0.007 089
0.22	0.981 919	0.605 35	0.345 921	0.172 193	0.077 780	0.031 639	0.010 467	0.002 624
0.24	0.847 029	0.496 30	0.246 533	0.121 494	0.048 455	0.015 523	0.002 959	−0.000 724
0.26	0.710 120	0.391 221	0.175 056	0.077 052	0.023 963	0.003 238	−0.002 661	−0.003 067
0.28	0.576 991	0.293 824	0.111 993	0.039 583	0.004 363	−0.006 028	−0.006 608	−0.004 567
0.30	0.451 820	0.206 443	0.058 188	0.009 133	−0.010 646	−0.012 623	−0.009 140	−0.005 398
0.35	0.189 319	0.035 699	−0.036 549	−0.039 531	−0.031 639	−0.020 218	−0.011 207	−0.005 582
0.40	0.005 280	−0.065 893	−0.083 716	−0.058 515	−0.036 513	−0.020 023	−0.009 911	−0.004 499
0.45	−0.107 013	−0.116 126	−0.098 481	−0.059 768	−0.033 147	−0.016 559	−0.007 568	−0.003 197
0.50	−0.163 163	−0.132 753	−0.094 474	−0.052 364	−0.026 699	−0.012 391	−0.005 294	−0.002 100
0.55	−0.181 248	−0.127 843	−0.081 543	−0.042 020	−0.019 968	−0.008 686	−0.003 491	−0.001 305
0.60	−0.176 809	−0.112 467	−0.065 850	−0.031 811	−0.014 187	−0.005 811	−0.002 204	−0.000 779
0.65	−0.159 079	−0.093 216	−0.050 759	−0.023 092	−0.009 703	−0.003 754	−0.001 347	−0.000 451
0.70	−0.135 972	−0.074 288	−0.037 792	−0.016 235	−0.006 444	−0.002 358	−0.000 801	−0.000 254
0.75	−0.112 090	−0.057 313	−0.027 387	−0.011 130	−0.004 179	−0.001 449	−0.000 467	−0.000 140
0.80	−0.089 616	−0.043 146	−0.019 420	−0.007 475	−0.002 659	−0.000 874	−0.000 267	−0.000 076
0.85	−0.070 140	−0.031 841	−0.013 353	−0.004 935	−0.001 664	−0.000 519	−0.000 150	−0.000 041
0.90	−0.053 904	−0.023 116	−0.009 280	−0.003 212	−0.001 027	−0.000 304	−0.000 084	−0.000 022
0.95	−0.040 802	−0.016 539	−0.006 286	−0.002 065	−0.000 627	−0.000 176	−0.000 046	−0.000 011
1.00	−0.030 491	−0.011 709	−0.004 211	−0.001 313	−0.000 378	−0.000 101	−0.000 025	
1.10	−0.016 498	−0.005 690	−0.001 838	−0.000 517	−0.000 134	−0.000 032		
1.20	−0.008 628	−0.002 671	−0.000 778	−0.000 198	−0.000 046	−0.000 010		
1.30	−0.004 393	−0.001 128	−0.000 322	−0.000 074	−0.000 016			
1.40	−0.002 187	−0.000 553	−0.000 130	−0.000 027				
1.50	−0.001 071	−0.000 117	−0.000 052					
1.60	−0.000 516							

zinc sulfate at low concentrations, for which nonlinear interpolation is necessary for accuracy to three decimal places). In case $\ln f_{\text{expt}}$ is known to only three decimal places, therefore, a linear interpolation suffices. Since the osmotic pressure correction is small, a linear interpolation of the summation terms of Eqs. (4) and (6) is sufficient.

For all ions of moderate size and for low or moderate concentrations, the osmotic pressure correction is small, and the variation of $\ln f$ with concentration and the parameter A is approximately that of $\ln f'$. Since the variation of $\ln f'$ with c and A is not readily apparent from its analytical form, the function $\ln f'$ (and therefore in a general way $\ln f$) is shown in Figs. 1–4 where, for salts of ionic type I–I, II–I, II–II, and III–I, respectively, $\ln f'$ is plotted against the square root of concentration for several values of A. The smallest value of A for which $\ln f'$ is shown is, for each type salt, approximately the smallest A for which the summation in Eq. (2) converges satisfactorily using terms through $\mu=16$. The following features of these graphs are noteworthy. At moderate concentrations, the curvature of the lines is positive and larger the larger A becomes. The curves show a minimum occurring at lower concentrations with larger A's. As compared with the other three ionic types, the curves for II–II salts are very close together, or, in other words, $\ln f'$ for II–II salts is a relatively insensitive function of the inter-ionic distance of closest approach. It has been noted[6] that the experimental activity coefficients of II–II salts have a relatively narrow spread of values. There is an interesting relation between $\ln f'$ for I–I and for II–II salts. For such symmetrical electrolytes the numbers n_μ are zero for odd μ, while for even μ they are the μth power of the charge on an ion. Consequently it follows from the form of the summation term in Eq. (2) and Eq. (16) for φ that for a II–II salt having a parameter of closest approach A, and at the molarity c, the value of $\ln f'$ will be identical with that for a I–I salt having a parameter of closest approach $A/4$, and at the molarity 64 c.

For I–I salts the $A=0.2$ curve actually intersects the Debye-Hückel limiting law line at about $c^{\frac{1}{2}}=0.25$ and $\ln f'$ is slightly less than $\ln f'_D$ at smaller concentrations, though the difference is too small to be shown on Fig. 1. The $A=0.2$ curve reapproaches the $\ln f'_D$ line from

[6] H. S. Harned and B. B. Owen, *The Physical Chemistry of Electrolytic Solutions* (Reinhold Publishing Corporation, New York, 1950), second edition, p. 426.

TABLE II. The function $10^{\mu} g_{\mu}(\varphi)$.

φ	$10^{2}g_{2}(\varphi)$	$10^{3}g_{3}(\varphi)$	$10^{4}g_{4}(\varphi)$	$10^{5}g_{5}(\varphi)$	$10^{6}g_{6}(\varphi)$	$10^{7}g_{7}(\varphi)$	$10^{8}g_{8}(\varphi)$
0.01	−0.000 012	0.004 046	0.001 117	0.000 857	0.000 930	0.001 036	0.001 115 6
0.02	−0.000 097	0.015 694	0.006 756	0.006 001	0.006 703	0.007 545 6	0.008 034 8
0.03	−0.000 325	0.034 272	0.018 669	0.017 985	0.020 456	0.023 058 4	0.024 443 0
0.04	−0.000 758	0.059 130	0.037 578	0.038 209	0.043 989	0.049 562 4	0.052 271 4
0.05	−0.001 462	0.089 66	0.063 680	0.067 309	0.078 136	0.088 141	0.092 179 1
0.06	−0.002 494	0.125 291	0.096 861	0.105 412	0.123 049	0.138 321	0.143 057 4
0.07	−0.003 907	0.165 494	0.136 815	0.152 302	0.178 381	0.199 220	0.206 634 0
0.08	−0.005 756	0.209 768	0.183 113	0.207 456	0.243 466	0.270 92	0.279 045 4
0.09	−0.008 089	0.257 641	0.235 244	0.270 28	0.317 379	0.351 97	0.359 643 5
0.10	−0.010 951	0.308 675	0.292 659	0.339 98	0.399 064	0.440 21	0.446 796 8
0.12	−0.018 437	0.418 608	0.421 046	0.496 78	0.581 170	0.634 046 7	0.634 166 7
0.14	−0.028 522	0.536 659	0.563 687	0.671 16	0.780 505	0.841 172 5	0.828 584 3
0.16	−0.041 483	0.660 034	0.716 205	0.856 49	0.988 244	1.051 142 7	1.019 219 9
0.18	−0.057 555	0.786 710	0.874 600	1.046 847	1.196 583	1.196 582 7	1.197 502 8
0.20	−0.076 941	0.914 686	1.035 321	1.236 903	1.398 919	1.446 215 0	1.357 188 3
0.22	−0.099 809	1.042 316	1.195 300	1.422 850	1.589 960	1.619 192 0	1.494 176 4
0.24	−0.126 301	1.168 210	1.351 919	1.599 293	1.765 751	1.770 577	1.606 213 5
0.26	−0.156 534	1.291 177	1.503 031	1.765 139	1.923 430	1.898 304	1.692 551 3
0.28	−0.190 599	1.410 255	1.646 680	1.917 662	2.061 069	2.001 499	1.753 614 0
0.30	−0.228 566	1.524 63	1.782 090	2.055 960	2.177 750	2.080 630	1.790 689 5
0.35	−0.340 824	1.786 14	2.076 211	2.329 933	2.377 19	2.178 301	1.791 715 3
0.40	−0.478 019	2.007 97	2.301 560	2.502 27	2.454 05	2.151 680	1.692 135 6
0.45	−0.639 893	2.187 34	2.457 09	2.580 41	2.428 72	2.037 075 5	1.529 756 9
0.50	−0.825 753	2.324 28	2.546 89	2.577 31	2.325 68	1.864 664 9	1.336 502 5
0.55	−1.034 591	2.420 66	2.578 20	2.510 05	2.168 920	1.661 328 9	1.136 086 5
0.60	−1.265 151	2.479 52	2.559 62	2.394 02	1.979 390	1.447 756 8	0.944 273 5
0.65	−1.516 029	2.504 57	2.500 26	2.243 936	1.774 121	1.238 577 5	0.770 292 5
0.70	−1.785 731	2.500 17	2.408 90	2.072 679	1.566 050	1.043 200	0.618 498 7
0.75	−2.072 690	2.470 31	2.293 361	1.890 448	1.364 440	0.867 021 6	0.489 933 9
0.80	−2.375 35	2.419 1	2.161 711	1.705 502	1.175 436	0.712 305 1	0.383 570 1
0.85	−2.692 11	2.350 7	2.019 190	1.524 069	1.002 661	0.579 322 3	0.297 238 6
0.90	−3.021 54	2.268 0	1.871 230	1.350 544	0.847 874	0.466 999 5	0.228 271 4
0.95	−3.362 12	2.175 3	1.721 979	1.188 157	0.711 478	0.373 659	0.173 910 8
1.00	−3.712 46	2.074 4	1.574 731	1.037 881	0.592 925	0.296 619	0.131 553 3
1.10	−4.437 33	1.859 6	1.295 510	0.778 670	0.404 467	0.183 555	0.073 889 0
1.20	−5.186 69	1.639 4	1.046 161	0.572 865	0.270 358	0.111 404	0.040 637 0
1.30	−5.952 50	1.425 5	0.831 767	0.414 557	0.177 686	0.066 423	0.021 961 4
1.40	−6.728 06	1.224 7	0.652 661	0.295 841	0.115 120	0.039 024	0.011 694 4
1.50	−7.507 99	1.041 5	0.506 366	0.208 646	0.073 678	0.022 646	0.006 148 9
1.60	−8.287 99	0.877 5	0.389 031	0.145 643	0.046 662	0.012 998	0.003 197 8
1.70	−9.064 79	0.734 3	0.296 331	0.100 757	0.029 275	0.007 391	0.001 646 3
1.80	−9.836 00	0.610 2	0.221 714	0.069 144	0.018 218	0.004 168	0.000 841 6
1.90	−10.599 90	0.503 6	0.168 213	0.047 127	0.011 257	0.002 333	
2.00	−11.355 29	0.412 6	0.125 553	0.031 916	0.006 910	0.001 299	
2.50	−14.993 31	0.143 9	0.027 065	0.003 977	0.000 557		
3.00	−18.424 71	0.046 3	0.005 344	0.000 511			
3.50	−21.715 40	0.014 3	0.000 417				
4.00	−24.924 6	0.004 1					
4.50	−28.090 4	0.001 2					
5.00	−31.234 3	0.000 7					
5.50	−34.368.2						
6.00	−37.496 9						
6.50	−40.623 6						
7.00	−43.749 6						
7.50	−46.874 9						

below as the concentration approaches zero. In the case of II–II salts for small A's this negative deviation from the limiting law at rather small concentrations is quite marked, as may be seen from Fig. 3, $A=0.4$. The curve $A=0.6$ also intersects the limiting law line at about $c^{\frac{1}{2}}=0.05$, but the negative deviation for this curve is too small to be shown on Fig. 3. Salts of ionic type II–I and III–I show no negative deviation from the Debye-Hückel limiting law. Negative deviations, larger in magnitude for smaller inter-ionic distances, and larger for II–II salts than for I–I salts are completely consistent with the results of the extended Debye-Hückel theory.[7] Whereas this effect is very small for I–I salts and indeed does not seem to be present for I–I salts whose A is 0.4 or larger (which includes most, if not all, actual I–I salts), the effect is pronounced for II–II salts in the range $0.6>A>0.4$. This range probably includes many real II–II salts; zinc sulfate has an A of about 0.5. This effect has been observed experimentally for zinc sulfate.[8]

While the general behavior of $\ln f$ follows that of $\ln f'$, for a numerical comparison with experiment the osmotic

[7] Gronwall, LaMer, and Sandved, Physik. Z. **29**, 358 (1928).
[8] I. A. Cowperthwaite and V. K. LaMer, J. Am. Chem. Soc. **53**, 4333 (1931).

TABLE II—*Continued.*

φ	$10^{9}g_{9}(\varphi)$	$10^{10}g_{10}(\varphi)$	$10^{11}g_{11}(\varphi)$	$10^{12}g_{12}(\varphi)$	$10^{13}g_{13}(\varphi)$	$10^{14}g_{14}(\varphi)$	$10^{15}g_{15}(\varphi)$	$10^{16}g_{16}(\varphi)$
0.01	0.001 110	0.001 027	0.000 868 0	0.000 684 1	0.000 502 0	0.000 344 2	0.000 221 4	0.000 134 0
0.02	0.007 932	0.007 205	0.006 121 1	0.004 783 2	0.003 476 7	0.002 361 3	0.001 504 0	0.000 901 5
0.03	0.023 970	0.021 674	0.018 244 0	0.014 112 2	0.010 160 8	0.006 835 2	0.004 311 8	0.002 559 3
0.04	0.050 903	0.045 589	0.038 167 6	0.029 248 7	0.020 859 9	0.013 898 6	0.008 683 1	0.005 104 2
0.05	0.089 108	0.079 285	0.065 807 9	0.049 959 6	0.035 293 5	0.023 290 5	0.014 410 6	0.008 388 9
0.06	0.138 079	0.121 871	0.100 407 8	0.075 514 3	0.052 840 6	0.034 536 4	0.021 162 8	0.012 200 2
0.07	0.196 719	0.172 100	0.140 813 2	0.104 910 5	0.072 713 6	0.047 069 9	0.028 564 7	0.016 307 6
0.08	0.263 583	0.228 67	0.185 669 9	0.137 032 5	0.094 074 7	0.060 313 6	0.036 248 4	0.020 493 5
0.09	0.337 012	0.289 85	0.233 564 2	0.170 760 7	0.116 114 1	0.073 728 9	0.043 882 8	0.024 568 8
0.10	0.415 29	0.354 09	0.283 118 4	0.205 042 1	0.138 096 6	0.086 844 5	0.051 189 4	0.028 381 2
0.12	0.579 79	0.485 75	0.382 233 5	0.271 626 4	0.179 466 6	0.110 700 0	0.063 993 4	0.034 793 6
0.14	0.744 86	0.613 04	0.474 558 6	0.330 885 9	0.214 458 9	0.129 746 4	0.073 557 3	0.039 218 8
0.16	0.900 63	0.728 10	0.554 210 5	0.379 129 2	0.241 040 8	0.143 027 2	0.079 520 7	0.041 576 2
0.18	1.039 921	0.825 48	0.617 753 3	0.414 602 6	0.258 558 3	0.150 470 3	0.082 041 5	0.042 061 7
0.20	1.158 021	0.902 59	0.663 960 8	0.437 330 9	0.267 343 3	0.152 586 2	0.081 584 9	0.041 015 3
0.22	1.252 381	0.958 29	0.688 814 9	0.447 273 6	0.268 351 6	0.153 242 4	0.078 757 5	0.038 824 1
0.24	1.322 340	0.993 24	0.705 011 8	0.446 705 2	0.262 866 6	0.144 297 1	0.074 191 2	0.035 861 6
0.26	1.368 389	1.008 880	0.703 295 4	0.437 120 2	0.252 282 4	0.135 810 5	0.068 472 6	0.032 453 0
0.28	1.392 129	1.007 383	0.689 546 3	0.420 388 2	0.237 956 8	0.125 620 4	0.062 104 8	0.028 861 4
0.30	1.395 710	0.991 171	0.666 088 0	0.398 317 9	0.221 120 3	0.114 471 8	0.055 398 1	0.025 286 1
0.35	1.333 001	0.904 004	0.579 318 6	0.330 059 0	0.174 513 0	0.086 026 9	0.039 704 2	0.017 222 0
0.40	1.201 581	0.776 084	0.474 849 9	0.257 715 6	0.129 766 8	0.060 906 8	0.026 760 6	0.011 048 9
0.45	1.036 440	0.637 464	0.372 125 1	0.192 365 3	0.092 234 1	0.041 214 9	0.017 237 9	0.006 774 2
0.50	0.863 225	0.506 479	0.281 557 2	0.138 611 6	0.063 280 1	0.026 919 0	0.010 716 7	0.004 008 3
0.55	0.699 228	0.391 061	0.207 096 6	0.097 090 4	0.042 200 1	0.017 088 6	0.006 475 3	0.002 305 0
0.60	0.554 159	0.295 123	0.148 849 7	0.066 446 8	0.027 494 8	0.010 598 0	0.003 822 1	0.001 294 8
0.65	0.430 754	0.218 451	0.104 943 4	0.044 603 6	0.017 569 5	0.006 445 9	0.002 212 5	0.000 713.3
0.70	0.329 541	0.159 212	0.072 792 4	0.029 455 1	0.011 044 3	0.003 856 6	0.001 259 8	0.000 386 5
0.75	0.248 753	0.114 412	0.049 792 2	0.019 180 9	0.006 845 6	0.002 275 1	0.000 707 2	0.000 206 5
0.80	0.185 443	0.081 242	0.033 651 0	0.012 340 0	0.004 191 9	0.001 325 9	0.000 392 2	0.000 109 0
0.85	0.136 865	0.057 091	0.022 504 2	0.007 855 4	0.002 539 8	0.000 764 5	0.000 215 2	0.000 056 9
0.90	0.100 096	0.039 752	0.014 910 9	0.004 954 2	0.001 524 5	0.000 436 7	0.000 117 0	0.000 029 4
0.95	0.072 617	0.027 449	0.009 798 9	0.003 098 8	0.000 907 5	0.000 247 4	0.000 063 1	0.000 015 1
1.00	0.052 303	0.018 824	0.006 392 4	0.001 924 1	0.000 536 2	0.000 139 1	0.000 033 7	
1.10	0.026 629	0.008 683	0.002 669 1	0.000 727 7	0.000 183 7	0.000 043 1		
1.20	0.013 272	0.003 917	0.001 090 6	0.000 269 3	0.000 061 5	0.000 013 1		
1.30	0.006 498	0.001 639	0.000 437 7	0.000 097 9	0.000 020 3			
1.40	0.003 134	0.000 760	0.000 371 1	0.000 035 0				
1.50	0.001 492	0.000 246	0.000 067 5					
1.60	0.000 702							

pressure correction cannot be neglected. The osmotic pressure correction is strongly dependent on $\bar{V}_2°$ and hence varies from salt to salt, but its order of magnitude may be seen from Table IV, which gives examples of the computed osmotic pressure correction, $\ln f - \ln f'$, including the sign prefixed in Eq. (1). Two zinc sulfate entries are omitted because they are certainly invalid; the osmotic pressure as given by Eq. (6) is decreasing with increasing concentration at 0.3 molar and is negative at 1.0 molar.

When experimental values of $\ln f$ for ionic solutions of known molarities are available, then Eq. (1) may be directly compared with experimental data. In perhaps the majority of cases, however, the quantity determined experimentally is the stoichiometric mean ionic *molal* activity coefficient f_m (hereafter called simply the molal activity coefficient), defined by the equation

$$\bar{F}_2(m, P, T) = \bar{F}_2°_m(P, T) + \nu RT \ln(f_m m_\pm), \quad (21)$$

where $\bar{F}_2$ is the partial molal free energy of the solute, $\bar{F}_2°_m$ is the standard partial molal free energy on the molality scale, and $m_\pm$ is given by the expression

$$m_\pm = m[\nu_+{}^{\nu_+}\nu_-{}^{\nu_-}]^{1/\nu}, \quad (22)$$

where m is the molality of the solution, and ν_+ and ν_- are the numbers of cations and anions produced in dissolving one molecule of salt. In these cases, the "experimental" value of $\ln f$ at the molarity c, with which Eq. (1) may be compared, may be obtained if both m and c for that solution can be found, by using the well-known equation

$$\ln f = \ln f_m + \ln d_1 + \ln(m/c), \quad (23)$$

where d_1, the density of water, is numerically 0.99707[9] at 25°C and one atmosphere pressure. In finding both m and c for a solution, use may be made of empirical equations for m/c (or c/m) often found in the literature, or else a knowledge of the density of the solution or of the apparent molal volume of the solute suffices.

C. DETERMINATION OF THE PARAMETER *A*

The present form of the summations in Eqs. (2), (4), and (6) contains only some of the terms arising from the basic theory. It is therefore to be expected that these equations will have a concentration limit of validity, above which the neglected terms will become prepon-

[9] *International Critical Tables* (McGraw-Hill Book Company, Inc., New York, 1928), first edition, Vol. 3, p. 24.

TABLE III. The function $10^{\mu}h_{\mu}(\varphi)$.

φ	$10^{2}h_{2}(\varphi)$	$10^{3}h_{3}(\varphi)$	$10^{4}h_{4}(\varphi)$	$10^{5}h_{5}(\varphi)$	$10^{6}h_{6}(\varphi)$	$10^{7}h_{7}(\varphi)$	$10^{8}h_{8}(\varphi)$
0.01	0.000 047	−0.012 016	−0.004 297	−0.003 292	−0.003 619	−0.004 016	−0.004 346
0.02	0.000 386	−0.046 142	−0.023 946	−0.022 462	−0.025 435	−0.028 670	−0.030 463
0.03	0.001 285	−0.099 730	−0.064 700	−0.065 720	−0.075 753	−0.085 417	−0.090 192
0.04	0.002 993	−0.170 295	−0.127 688	−0.136 463	−0.159 051	−0.165 925	−0.187 648
0.05	0.005 752	−0.255 531	−0.212 078	−0.235 139	−0.275 895	−0.311 133	−0.321 808
0.06	0.009 777	−0.353 321	−0.316 647	−0.360 376	−0.424 340	−0.475 462	−0.481 477
0.07	0.015 269	−0.461 728	−0.439 246	−0.509 731	−0.600 771	−0.664 919	−0.681 223
0.08	0.022 419	−0.578 960	−0.577 540	−0.689 776	−0.800 761	−0.880 96	−0.893 208
0.09	0.031 401	−0.703 360	−0.729 057	−0.867 201	−1.019 225	−1.115 67	−1.117 013
0.10	0.042 370	−0.833 423	−0.891 335	−1.068 082	−1.251 025	−1.357 203	−1.345 560
0.12	0.070 855	−1.105 126	−1.238 659	−1.496 06	−1.734 712	−1.848 064	−1.789 113
0.14	0.108 892	−1.384 609	−1.601 664	−1.936 38	−2.212 805	−2.312 327	−2.187 645
0.16	0.157 324	−1.663 284	−1.964 909	−2.365 33	−2.662 113	−2.717 575	−2.504 747
0.18	0.216 832	−1.935 330	−2.315 592	−2.764 325	−3.053 410	−3.042 148	−2.726 042
0.20	0.287 945	−2.195 245	−2.643 520	−3.118 851	−3.373 614	−3.273 590	−2.845 739
0.22	0.371 060	−2.439 018	−2.940 944	−3.422 155	−3.613 810	−3.408 199	−2.866 440
0.24	0.466 455	−2.663 520	−3.202 214	−3.659 059	−3.770 978	−3.448 091	−2.796 660
0.26	0.574 302	−2.866 412	−3.423 656	−3.836 090	−3.846 098	−3.400 057	−2.648 677
0.28	0.694 676	−3.046 152	−3.602 346	−3.949 458	−3.842 911	−3.273 951	−2.436 764
0.30	0.827 579	−3.201 72	−3.739 925	−4.004 262	−3.768 441	−3.084 117	−2.175 791
0.35	1.213 925	−3.482 96	−3.899 492	−3.888 665	−3.324 96	−2.401 446	−1.401 026
0.40	1.674 965	−3.614 34	−3.822 335	−3.488 97	−2.628 56	−1.548 440	−0.826 962
0.45	2.206 003	−3.609 12	−3.552 15	−2.897 39	−1.813 77	−0.700 847	0.112 511
0.50	2.801 129	−3.486 41	−3.138 84	−2.198 37	−0.988 71	0.053 849	0.664 402
0.55	3.453 716	−3.267 94	−2.631 62	−1.471 08	−0.229 278	0.663 810	1.043 462
0.60	4.150 946	−2.975 49	−2.073 88	−0.768 013	0.419 338	1.112 409	1.263 398
0.65	4.903 159	−2.629 71	−1.502 14	−0.127 630	0.936 388	1.406 410	1.352 474
0.70	5.686 031	−2.250 20	−0.944 82	0.425 879	1.319 287	1.566 274	1.343 515
0.75	6.498 708	−1.852 75	−0.421 811	0.882 710	1.577 126	1.617 642	1.267 649
0.80	7.334 98	−1.451 3	0.049 093	1.240 833	1.725 783	1.587 844	1.151 266
0.85	8.188 98	−1.058 0	0.462 974	1.504 677	1.784 379	1.501 382	1.014 933
0.90	9.055 65	−0.680 0	0.814 659	1.683 174	1.772 313	1.379 149	0.873 536
0.95	9.930 15	−0.326 5	1.103 809	1.786 032	1.707 689	1.236 686	0.737 060
1.00	10.808 29	0.000 2	1.332 592	1.829 290	1.606 518	1.089 924	0.611 575
1.10	12.634 44	0.557 6	1.626 774	1.772 790	1.345 379	0.807 867	0.404 055
1.20	14.292 40	0.983 7	1.740 779	1.597 430	1.065 561	0.569 375	0.255 424
1.30	15.984 48	1.282 4	1.722 891	1.367 899	0.809 272	0.386 878	0.155 956
1.40	17.627 69	1.469 4	1.617 250	1.127 258	0.594 769	0.255 162	0.092 566
1.50	19.216 76	1.562 1	1.460 284	0.901 208	0.425 657	0.164 171	0.047 521
1.60	20.750 03	1.581 1	1.279 603	0.703 093	0.297 980	0.103 491	0.030 510
1.70	22.228 65	1.541 3	1.094 668	0.537 507	0.223 065	0.064 101	0.017 061
1.80	23.655 80	1.462 0	0.927 348	0.403 995	0.138 546	0.039 107	0.009 392
1.90	25.035 83	1.357 9	0.757 398	0.299 166	0.092 437	0.023 549	
2.00	26.373 71	1.241 0	0.615 998	0.218 753	0.060 944	0.011 118	
2.50	32.618 63	0.648 5	0.187 313	0.040 770	0.006 616		
3.00	38.522 58	0.277 6	0.047 746	0.014 652			
3.50	44.408 22	0.104 7	0.013 187				
4.00	50.421 9	0.036 9					
4.50	56.461 9	0.012 0					
5.00	62.610 5	0.002 7					
5.50	68.805 9						
6.00	75.027 0						
6.50	81.262 7						
7.00	87.506 3						
7.50	93.753 5						

derant; indeed, Eq. (6) yields a negative osmotic pressure for a one molar zinc sulfate solution. The quantity A, which is independent of concentration, must here be regarded as a parameter to be determined in some manner from experimental data, since there is no adequate theory from which a satisfactory value of A can be derived. At the same time, Eq. (1) can be made to reproduce any single activity coefficient datum, even at concentrations at which the present form of the equation is invalid, by suitably choosing the quantity A. The procedure followed has been to find, for a representative strong electrolyte of each ionic type here considered, the largest concentration $c_{\max}$ at which an A can be found which, for all $c \leqslant c_{\max}$, yields values of $\ln f$ agreeing with the experimental data within experimental error. This $c_{\max}$ is then approximately the concentration limit of validity for that ionic type, and the corresponding A is approximately the "best" A for that particular salt. This procedure is laborious, and hence the following practical method is presented. At a concentration, fixed for each ionic type, not exceeding the concentration limit of validity for that ionic type as determined above, and at which experimental data are available for as many different salts as possible, $\ln f$ has been tabulated as a function of A (see appendix for details). These are Tables V–VIII, for I–I, II–I, II–II,

TABLE III—*Continued.*

φ	$10^{9}h_{9}(\varphi)$	$10^{10}h_{10}(\varphi)$	$10^{11}h_{11}(\varphi)$	$10^{12}h_{12}(\varphi)$	$10^{13}h_{13}(\varphi)$	$10^{14}h_{14}(\varphi)$	$10^{15}h_{15}(\varphi)$	$10^{16}h_{16}(\varphi)$
0.01	−0.004 322	−0.004 036	−0.003 376 6	−0.002 654 3	−0.001 942 6	−0.001 328 6	−0.000 852 3	−0.000 514 4
0.02	−0.029 960	−0.026 924	−0.023 156 7	−0.017 984 7	−0.013 002 8	−0.008 784 1	−0.005 564 9	−0.003 317 4
0.03	−0.087 931	−0.078 941	−0.066 955 4	−0.051 368 5	−0.036 680 4	−0.024 470 1	−0.015 306 8	−0.009 008 9
0.04	−0.181 271	−0.160 334	−0.135 876 5	−0.102 955 5	−0.072 592 6	−0.047 811 2	−0.029 522 7	−0.017 150 0
0.05	−0.307 779	−0.270 526	−0.227 037 2	−0.169 862 7	−0.118 233 1	−0.076 858 8	−0.046 834 6	−0.026 844 5
0.06	−0.462 245	−0.402 026	−0.335 362 2	−0.247 687 1	−0.170 146 8	−0.109 135 0	−0.065 604 7	−0.037 088 6
0.07	−0.637 789	−0.547 549	−0.454 826 6	−0.331 517 1	−0.224 684 9	−0.142 151 0	−0.084 265 8	−0.046 965 9
0.08	−0.827 002	−0.701 77	−0.579 290 2	−0.416 578 8	−0.278 461 3	−0.173 703 1	−0.101 495 4	−0.055 742 2
0.09	−1.022 310	−0.856 58	−0.703 028 1	−0.498 621 3	−0.328 602 9	−0.202 017 2	−0.116 289 5	−0.062 896 2
0.10	−1.216 75	−1.006 46	−0.821 043 3	−0.574 117 9	−0.372 860 8	−0.225 795 8	−0.179 162 9	−0.068 114 8
0.12	−1.579 60	−1.272 2	−1.024 385 8	−0.695 363 7	−0.437 898 4	−0.256 823 0	−0.140 785 5	−0.072 370 7
0.14	−1.877 71	−1.468 6	−1.167 414 3	−0.767 655 4	−0.467 520 4	−0.264 682 6	−0.139 759 0	−0.069 025 2
0.16	−2.088 491	−1.583 7	−1.241 431 5	−0.788 588 8	−0.462 798 4	−0.251 727 9	−0.127 233 1	−0.059 869 8
0.18	−2.203 132	−1.613 2	−1.247 861 7	−0.762 868 7	−0.429 206 7	−0.222 696 0	−0.106 653 9	−0.047 109 1
0.20	−2.222 837	−1.566 9	−1.195 129 4	−0.699 729 4	−0.374 280 7	−0.183 103 5	−0.081 584 9	−0.032 812 3
0.22	−2.155 844	−1.454 5	−1.088 327 4	−0.608 292 1	−0.305 920 8	−0.140 983 0	−0.055 130 3	−0.018 635 6
0.24	−2.016 051	−1.292 7	−0.958 816 0	−0.500 309 9	−0.231 322 6	−0.092 350 1	−0.029 676 5	−0.005 737 9
0.26	−1.817 895	−1.095 25	−0.801 756 7	−0.384 665 8	−0.156 415 1	−0.048 891 8	−0.006 847 3	0.005 192 4
0.28	−1.577 715	−0.877 246	−0.634 382 6	−0.269 048 4	−0.085 664 5	−0.010 049 6	0.012 421 0	0.013 853 5
0.30	−1.310 463	−0.650 720	−0.466 261 6	−0.159 327 2	−0.022 112 0	0.022 894 4	0.027 699 1	0.020 228 9
0.35	−0.605 115	−0.120 33	−0.086 897 8	0.066 011 8	0.095 982 2	0.077 424 2	0.049 630 2	0.027 555 2
0.40	0.028 518	0.314 83	0.189 940 0	0.206 172 5	0.155 720 1	0.097 450 9	0.053 521 2	0.026 517 3
0.45	0.561 932	0.599 48	0.353 518 8	0.269 311 4	0.170 633 1	0.094 794 3	0.047 404 1	0.021 677 4
0.50	0.840 996	0.737 702	0.422 326 8	0.277 223 2	0.158 200 3	0.080 757 1	0.037 508 5	0.016 033 4
0.55	1.014 125	0.773 696	0.424 548 0	0.252 434 9	0.132 930 2	0.063 227 9	0.027 524 2	0.011 064 1
0.60	1.061 565	0.737 391	0.387 009 2	0.212 629 8	0.104 480 2	0.046 631 0	0.019 110 6	0.007 251 1
0.65	1.027 061	0.659 972	0.330 571 6	0.169 493 9	0.078 184 2	0.032 874 3	0.012 721 9	0.004 565 1
0.70	0.939 464	0.562 683	0.269 332 0	0.129 602 6	0.056 326 0	0.022 368 2	0.008 188 6	0.002 782 8
0.75	0.824 003	0.463 387	0.211 616 9	0.095 904 5	0.039 362 5	0.014 788 1	0.005 127 6	0.001 651 8
0.80	0.701 130	0.370 866	0.161 525 0	0.069 103 9	0.026 828 0	0.009 546 1	0.003 137 8	0.000 958 9
0.85	0.580 905	0.289 948	0.120 397 2	0.048 703 2	0.017 905 3	0.006 039 4	0.001 883 1	0.000 546 2
0.90	0.471 162	0.222 285	0.087 974 1	0.033 688 6	0.011 738 3	0.003 755 5	0.001 111 3	0.000 306 0
0.95	0.375 344	0.167 640	0.063 202 6	0.022 931 3	0.007 577 5	0.002 300 6	0.000 646 4	0.000 169 0
1.00	0.294 463	0.124 538	0.044 746 9	0.015 392 5	0.004 826 1	0.001 391 0	0.000 371 1	
1.10	0.174 417	0.066 320	0.021 619 4	0.006 694 6	0.001 891 7	0.000 491 8		
1.20	0.099 738	0.033 975	0.010 033 9	0.002 800 7	0.000 714 0	0.000 167 5		
1.30	0.054 499	0.017 822	0.004 508 7	0.001 135 4	0.000 261 3			
1.40	0.029 165	0.008 119	0.001 972 8	0.000 448 5				
1.50	0.015 261	0.004 653	0.000 844 2					
1.60	0.007 838							

and III–I salts at concentrations (hereafter called standard concentrations, c_s) of 0.1, 0.05, 0.01, and 0.01 moles per liter, respectively. A single experimental activity coefficient datum, at or about c_s, together with these tables suffice to determine A for any particular salt as explained below.

If the molar activity coefficient is known at the standard molarity for its ionic type the following procedure is used. An approximate osmotic pressure correction is first computed using only the first (Debye) terms of P_{osm} and $\{\ln f'_D\}_K$, i.e., Eqs. (20) and (19), which do not involve A. This approximate osmotic pressure correction together with the experimental value in $\ln f$ substituted into Eq. (1) yields a first approximation for the value of $\ln f'$, from which a first approximation for A may be found by using the appropriate table from Tables V–VIII. Using this first value of A, a more exact value of the osmotic pressure correction is then obtained. Because the osmotic pressure correction is rather small at the standard concentrations, a sufficiently exact value results from using the Debye term and the terms $\mu=0$ and $\mu=2$ in Eqs. (4) and (6). These first three terms in the equations for $\{\ln f'\}_K$ and P_{osm} are then conveniently grouped and written as follows:

$$\{\ln f'\}_K(D\to\mu=2) = -\ln f'_D[0.93750+e^{-2\varphi}(0.56250-0.8750\varphi+0.250\varphi^2)]; \quad (24)$$

$$P_{osm}(D\to\mu=2) = \rho kT\left\{1+\frac{A\varphi^2}{6n_2}+\ln f'_D[0.208333+e^{-2\varphi}(0.1250-0.250\varphi)]\right\}. \quad (25)$$

This more exact osmotic pressure correction is then combined with the experimental value of $\ln f$ to give a second approximation for $\ln f'$. Linear interpolation of the appropriate table (from Tables V–VIII) yields a second approximation for A which is entirely satisfactory. A repetition of the procedure, even using the complete expressions for P_{osm} and $\{\ln f'\}_K$ does not appreciably change the second approximation for A.

Often the experimental datum from which A is to be

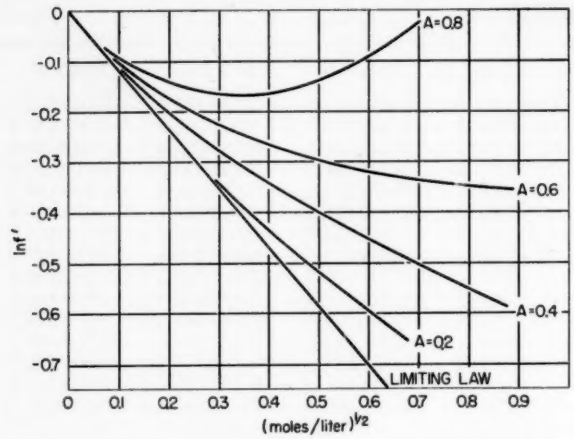

FIG. 1. The function $\ln f'$ for I–I salts in aqueous solution at 25°C.

determined is not a value of $\ln f$ for the salt in solution at the standard molarity c_s, but instead is the value of $\ln f_m$ at a molality m numerically equal to c_s. In this case Tables V–VIII may still be used if the molarity of the solution can be determined. In Eq. (23) the quantity $\ln f(c)$, where c is the molarity of the solution whose molality is numerically c_s, may be replaced by the first two terms of its Taylor's series expansion about c_s, resulting in the equation

$$\ln f(c_s)=\ln f_m+\ln d_1+\ln(c_s/c)+\{\ln f\}_c(c_s-c)/c_s. \quad (26)$$

The symbol $\{\ln f\}_c$ denotes the partial derivative of $\ln f$ with respect to the logarithm of c, and is to be evaluated here at $c=c_s$. The quantity $\{\ln f\}_c$ may be found by differentiating Eq. (1), but the terms arising from the osmotic pressure correction are small at any of the standard concentrations, and the following approximation is sufficiently accurate for the purpose for which it is to be used:

$$\{\ln f\}_c \simeq \{\ln f'\}_c. \quad (27)$$

An analytic form for $\{\ln f'\}_c$ is available as the sum of

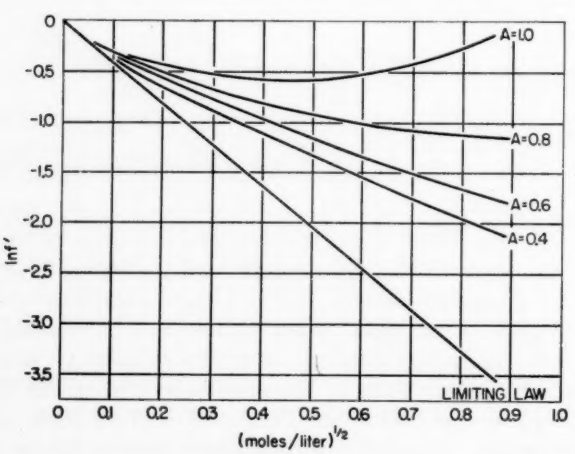

FIG. 2. The function $\ln f'$ for II–I salts in aqueous solution at 25°C.

Eqs. (64) and (82) of the preceding paper:

$$\{\ln f'\}_c=\tfrac{1}{2}\ln f'_D-\frac{A}{2n_2}\sum_{\mu\geq 0}\frac{(-)^\mu n_\mu^2}{A^\mu}\times[2b_\mu(\varphi)-g_\mu(\varphi)+h_\mu(\varphi)]. \quad (28)$$

Making the additional excellent approximation,

$$\ln(c_s/c)=-\ln(c/c_s)\simeq(c_s-c)/c_s, \quad (29)$$

Eqs. (26), (27), and (29) may be substituted into Eq. (1) at c_s to yield the equation,

$$\ln f'=\ln f_m+\ln d_1+[1+\{\ln f'\}_c](c_s-c)/c_s+P_{osm}[\bar{V}_2^\circ/\nu RT+\{\ln f'\}_K(\ln K)_P-\beta_1]. \quad (30)$$

Equation (30) may then be used in finding A as Eq. (1) was used in the preceding paragraph; the last two terms of (30) being first approximated by the Debye terms to yield a first approximation for $\ln f'$ and, through Tables V–VIII, for A. The quantity used in this step for $\{\ln f'\}_c$ is $\{\ln f'_D\}_c$, given by the equation

$$\{\ln f'_D\}_c=\tfrac{1}{2}\ln f'_D. \quad (31)$$

Using the approximate A, a more exact value of the last two terms is computed, using in addition to (24) and (25) the following form for $\{\ln f'\}_c$, which is the sum of the Debye term and the terms $\mu=0$ and $\mu=2$ in Eq. (28):

$$\{\ln f'\}_c(D\to\mu=2)=\ln f'_D[0.31250+e^{-2\varphi}(0.18750-0.6250\varphi+0.250\varphi^2)]+A\varphi^2/3n_2. \quad (32)$$

TABLE IV. The osmotic pressure correction to $\ln f'$, $\ln f-\ln f'$.

Moles/liter	NaCl	$CaCl_2$	$ZnSO_4$	$LaCl_3$
0.01	-1.4×10^{-4}	-1.5×10^{-4}	4×10^{-5}	-1.5×10^{-4}
0.30	-4.4×10^{-3}	-5.4×10^{-3}	···	-4.7×10^{-3}
1.00	-1.7×10^{-2}	-2.7×10^{-2}	···	-3.1×10^{-2}

This more exact value of the last two terms of (30) leads to a more accurate $\ln f'$ and, by interpolation in Tables V–VIII, to a value of A not further improved by a repetition of the process.

The "best" value of A may also be determined from an experimental value of $\ln f$ for a salt in solution at a known molarity c which is only approximately equal to c_s. Here $\ln f$ (c) is replaced by the first two terms of the Taylor's series expansion about c_s, and approximation (27) is made. Combining these steps with Eq. (1), the resulting final equation,

$$\ln f'=\ln f(c)+\{\ln f'\}_c(c_s-c)/c_s+P_{osm}[\bar{V}_2^\circ/\nu RT+\{\ln f'\}_K(\ln K)_P-\beta_1], \quad (33)$$

can be used as before to give A on the second approximation.

Finally if the datum used to determine A is a value of $\ln f_m$ for the salt in a solution of molality m only approximately numerically equal to c_s, the following

method is satisfactory if the molarity c of the solution can be found. Combining Eq. (23), the expansion of $\ln f(c)$ in a Taylor's series about c_s, the approximation (27), the approximation of Eq. (29) with m replacing c_s, and Eq. (1), the following equation is obtained:

$$\ln f' = \ln f_m + \ln d_1 + (m-c)/m + \{\ln f'\}_c(c_s - c)/c_s + P_{osm}[\bar{V}_2^\circ/\nu RT + \{\ln f'\}_K(\ln K)_P - \beta_1]. \quad (34)$$

Following the method of the above three paragraphs, the "best" value of A is obtained on the second approximation.

D. NUMERICAL COMPARISON

The preceding sections have outlined the computational method and the method of determining the parameter A, proportional to the distance of closest inter-ionic approach. In this section the numerical results of the theory will be compared with data, each ionic type being considered consecutively. The comparison is not intended to be exhaustive, but rather to indicate the generally good agreement for the salts here considered, and the desirability of further work with this theory.

The data used here are obtained primarily from emf measurements. T. F. Young has pointed out to the author that the "experimental" value of an activity coefficient obtained by this method, and especially from emf measurements on cells with transference, depends somewhat on the theory used in interpreting the raw data. The "experimental" values of the activity coefficients thus might differ significantly from the previously published ones used here if they were recalculated using this theory and the values of the fundamental constants used here. Perhaps this accounts for a part of the discrepancy here attributed to experimental error.

I. I-I Electrolytes

The salt chosen as representative of this type was sodium chloride. For sodium chloride $\bar{V}_2^\circ$ was taken to be 16.62 cm^3 mole^{-1}.[10] The experimental datum, $f_m = 0.778$ at 0.1 molal (reference 6, p. 562) and an empirical equation for c/m (reference 6, p. 556) in conjunction with the procedure outlined in the third paragraph of section C and Table V yielded a best value of A of 0.5464_1. Using this value of A, the concentration limit of validity of Eq. (1) for this salt was established as being about 0.4 molar, at which concentration the activity coefficient as given by Eq. (1) differed by about 1.5 percent from the experimental value. The standard concentration for I–I salts was chosen to be 0.1 molar. Table IX compares experimental values of $\ln f$ with theoretical values computed from Eq. (1). The agreement is quite good. The entry in the fourth column of Table IX, multiplied by 100, is very nearly the percent error in f. The small percent error in the very dilute solutions are probably the result of experimental error. In the most concentrated solutions considered in Table IX, the percent error in f (100 times the fourth column entry) is increasing, and probably reflects the beginning of a failure of the theoretical equation. In the case of sodium chloride, the approximations represented by Eqs. (24), (25), (27), and (32) involved in the determination of A are sufficiently accurate to determine $\ln f'$ and the theoretical $\ln f$ to five decimal places.

[10] H. E. Wirth, J. Am. Chem. Soc. **62**, 1128 (1940).

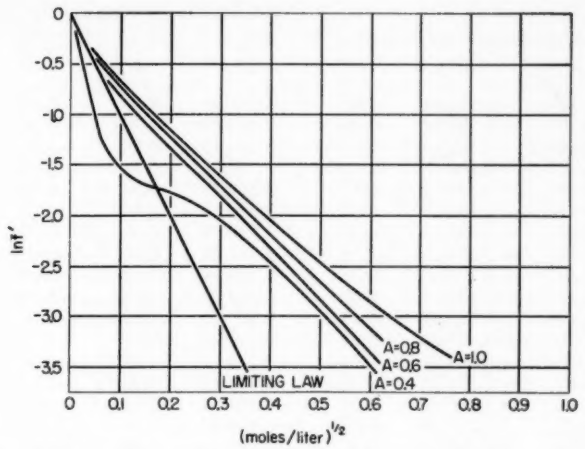

FIG. 3. The function $\ln f'$ for II–II salts in aqueous solution at 25°C.

II. II-I Electrolytes

The salt chosen as representative of this type was calcium chloride. For calcium chloride $\bar{V}_2^\circ$ was taken to be 18.25 cm^3 mole^{-1}, (reference 6, p. 253). The experimental datum, $f = 0.5834$ at 0.050000 molar[11] and Table VI were used in the procedure in the second paragraph of section C to determine the best value of A of 0.7958_2. Using this value of A, the concentration limit of validity of Eq. (1) was established as being between 0.05 and 0.1 molar; at 0.096540 molar f_{theor} differed by 3.7 percent from the experimental value. The standard concentra-

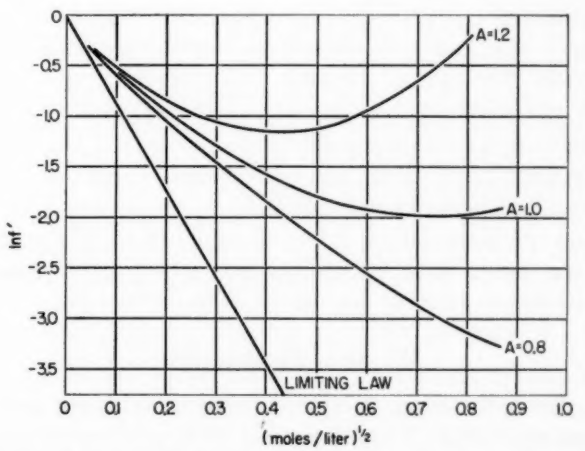

FIG. 4. The function $\ln f'$ for III–I salts in aqueous solution at 25°C.

[11] T. Shedlovsky and D. A. MacInnes, J. Am. Chem. Soc. **59**, 505 (1937).

TABLE V. The function $\ln f'$ for I–I salts at 0.1 molar as a function of A.

A	$\ln f'$	A	$\ln f'$	A	$\ln f'$	A	$\ln f'$	A	$\ln f'$	A	$\ln f'$
0.30	−0.312 51	0.47	−0.268 03	0.76	−0.179 61	1.10	−0.000 22	1.44	0.310 73	1.78	0.800 55
0.31	−0.309 51	0.48	−0.265 49	0.78	−0.171 81	1.12	0.013 95	1.46	0.334 14	1.80	0.835 90
0.32	−0.306 61	0.49	−0.262 95	0.80	−0.163 71	1.14	0.028 59	1.48	0.357 82	1.82	0.872 08
0.33	−0.303 80			0.82	−0.155 31	1.16	0.033 71	1.50	0.382 86	1.84	0.908 98
0.34	−0.301 05	0.50	−0.260 38	0.84	−0.146 60	1.18	0.059 31	1.52	0.408 19	1.86	0.946 72
0.35	−0.298 39	0.52	−0.255 17	0.86	−0.137 57	1.20	0.075 41	1.54	0.434 17	1.88	0.985 28
0.36	−0.295 74	0.54	−0.249 86	0.88	−0.128 21	1.22	0.092 01	1.56	0.460 82	1.90	1.024 65
0.37	−0.293 14	0.56	−0.244 42	0.90	−0.118 50	1.24	0.109 12	1.58	0.488 15	1.92	1.064 86
0.38	−0.290 58	0.58	−0.238 83	0.92	−0.108 44	1.26	0.126 77	1.60	0.516 16	1.94	1.105 90
0.39	−0.288 04	0.60	−0.233 08	0.94	−0.098 01	1.28	0.145 10	1.62	0.544 86	1.96	1.147 79
0.40	−0.285 52	0.62	−0.227 15	0.96	−0.087 21	1.30	0.163 68	1.64	0.574 27	1.98	1.190 54
0.41	−0.283 03	0.64	−0.221 04	0.98	−0.076 02	1.32	0.182 96	1.66	0.604 38	2.00	1.234 16
0.42	−0.280 54	0.66	−0.214 72	1.00	−0.064 44	1.34	0.202 79	1.68	0.635 22		
0.43	−0.278 15	0.68	−0.208 18	1.02	−0.052 45	1.36	0.223 18	1.70	0.666 79		
0.44	−0.275 65	0.70	−0.201 41	1.04	−0.040 04	1.38	0.244 17	1.72	0.699 10		
0.45	−0.273 05	0.72	−0.194 40	1.06	−0.027 21	1.40	0.265 75	1.74	0.732 16		
0.46	−0.270 55	0.74	−0.187 14	1.08	−0.013 94	1.42	0.287 94	1.76	0.765 97		

TABLE VI. The function $\ln f'$ for II–I salts at 0.05 molar as a function of A.

A	$\ln f'$	A	$\ln f'$	A	$\ln f'$	A	$\ln f'$	A	$\ln f'$	A	$\ln f'$
0.45	−0.671 35	0.62	−0.601 90	0.92	−0.488 12	1.22	−0.327 55	1.52	−0.086 73	1.82	0.262 14
0.46	−0.666 38	0.64	−0.594 72	0.94	−0.478 98	1.24	−0.314 33	1.54	−0.067 12	1.84	0.289 85
0.47	−0.661 59	0.66	−0.587 58	0.96	−0.469 96	1.26	−0.300 74	1.56	−0.047 08	1.86	0.318 17
0.48	−0.656 95	0.68	−0.580 45	0.98	−0.460 71	1.28	−0.286 80	1.58	−0.026 42	1.88	0.347 09
0.49	−0.652 47	0.70	−0.573 29	1.00	−0.451 20	1.30	−0.272 42	1.60	−0.005 32	1.90	0.376 62
0.50	−0.648 11	0.72	−0.566 10	1.02	−0.441 44	1.32	−0.257 67	1.62	0.016 29	1.92	0.406 78
0.51	−0.643 88	0.74	−0.558 84	1.04	−0.431 42	1.34	−0.242 52	1.64	0.038 42	1.94	0.437 55
0.52	−0.639 74	0.76	−0.551 49	1.06	−0.421 10	1.36	−0.226 95	1.66	0.061 08	1.96	0.468 96
0.53	−0.635 70	0.78	−0.554 05	1.08	−0.410 51	1.38	−0.210 97	1.68	0.084 26	1.98	0.501 02
0.54	−0.631 74	0.80	−0.536 49	1.10	−0.399 63	1.40	−0.194 57	1.70	0.107 99	2.00	0.533 72
0.55	−0.627 85	0.82	−0.528 79	1.12	−0.388 44	1.42	−0.177 73	1.72	0.132 27		
		0.84	−0.520 94	1.14	−0.376 92	1.44	−0.160 44	1.74	0.157 11		
0.56	−0.624 02	0.86	−0.512 92	1.16	−0.365 09	1.46	−0.142 71	1.76	0.182 50		
0.58	−0.616 50	0.88	−0.504 75	1.18	−0.352 92	1.48	−0.124 52	1.78	0.208 47		
0.60	−0.609 14	0.90	−0.496 36	1.20	−0.340 41	1.50	−0.105 86	1.80	0.235 01		

tion for II–I salts was chosen to be 0.05 molar. Table X compares experimental values of $\ln f$ with theoretical values computed from Eq. (1). The agreement is fairly good, though the fourth column seems to indicate that in the region of concentration studied the curve $\ln f_{\text{theor}}$ *vs* c has a smaller (positive) curvature than the corresponding experimental curve. Again the small errors at very low concentrations are probably experimental errors. For calcium chloride, in determining the best A, the use of approximations (24) and (25) in the osmotic pressure correction introduces an error only in the sixth decimal place. Since an experimental datum at the standard molarity was available, approximations (27) and (32) were not used; but had a datum at 0.05 molal been used, these approximations would have again introduced an error only in the sixth decimal place.

III. II-II Electrolytes

The salt chosen as representative of this ionic type was zinc sulfate. The value of $\bar{V}_2^\circ$ used, -7.0 cm^3 mole^{-1}, was obtained as follows. Values of the density at 25°C of solutions of known weight percent (and hence molalities) taken from reference 9, p. 65, were substituted into the equation,

$$d=(1000+Mm)/(1002.94+m\phi_V), \tag{35}$$

where M is the molecular weight of zinc sulfate and ϕ_V the apparent molal volume, yielding a series of values of ϕ_V at various molalities. These values of ϕ_V were then plotted against the square root of molality and an extrapolation to zero concentration gave $\bar{V}_2^\circ=-7.0$ cm^3 mole^{-1}. The experimental datum $f_m=0.387$ at 0.01 molal (reference 8), together with an empirically obtained value of c/m (see Table XI, note a) were used in the procedure of the third paragraph of Section C with Table IV to give a best A of 0.5245_0. Using this value of A, the concentration limit of validity of Eq.(1) was established as being about 0.01 molar; at the next largest concentration at which f_m is experimentally known the theoretical value of f differed by about 5.6 percent from the experimental value. The standard concentration for II–II salts was chosen to be 0.01 molar. Table XI compares experimental values of $\ln f$ with theoretical values computed from Eq. (1). The agreement does not appear as good as for I–I salts. The percent error in f (100 times the fourth column entry) is rather constant at about 2 percent for concentrations less than 0.01 molal. This

TABLE VII. The function $\ln f'$ for II–II salts at 0.01 molar as a function of A.

A	$\ln f'$	A	$\ln f'$	A	$\ln f'$	A	$\ln f'$	A	$\ln f'$	A	$\ln f'$
0.470	−1.090 2	0.540	−0.923 8	0.66	−0.800 6	0.80	−0.731 24	0.96	−0.682 79	1.40	−0.590 33
0.475	−1.073 5	0.545	−0.916 0	0.67	−0.794 1	0.81	−0.727 60	0.98	−0.677 76	1.45	−0.580 55
0.480	−1.057 7			0.68	−0.787 9	0.82	−0.724 07	1.00	−0.672 88	1.50	−0.570 10
0.485	−1.042 8	0.55	−0.908 6	0.69	−0.782 0	0.83	−0.720 65	1.02	−0.670 50	1.55	−0.560 73
0.490	−1.028 8	0.56	−0.894 6	0.70	−0.776 3	0.84	−0.717 33	1.04	−0.668 15	1.60	−0.550 59
0.495	−1.015 5	0.57	−0.881 6	0.71	−0.770 9	0.85	−0.714 10	1.06	−0.665 82	1.65	−0.540 24
0.500	−1.002 9	0.58	−0.869 8	0.72	−0.765 8	0.86	−0.710 92	1.08	−0.654 60	1.70	−0.529 66
0.505	−0.991 1	0.59	−0.858 9	0.73	−0.760 8	0.87	−0.707 82			1.75	−0.518 80
0.510	−0.979 9	0.60	−0.848 9	0.74	−0.756 1	0.88	−0.704 78	1.10	−0.650 26	1.80	−0.507 66
0.515	−0.969 3	0.61	−0.839 5	0.75	−0.751 54	0.89	−0.701 83	1.15	−0.639 74	1.85	−0.496 20
0.520	−0.959 2	0.62	−0.830 8	0.76	−0.747 16			1.20	−0.629 54	1.90	−0.484 38
0.525	−0.949 7	0.63	−0.822 5	0.77	−0.742 96	0.90	−0.698 94	1.25	−0.618 86	1.95	−0.472 19
0.530	−0.940 7	0.64	−0.814 5	0.78	−0.738 92	0.92	−0.693 34	1.30	−0.609 77	2.00	−0.459 61
0.535	−0.932 0	0.65	−0.807 4	0.79	−0.735 01	0.94	−0.687 97	1.35	−0.600 03		

TABLE VIII. The function $\ln f'$ for III–I salts at 0.01 molar as a function of A.

A	$\ln f'$	A	$\ln f'$	A	$\ln f'$	A	$\ln f'$	A	$\ln f'$	A	$\ln f'$
0.80	−0.599 40	1.02	−0.552 52			1.54	−0.425 27	1.72	−0.366 34	1.90	−0.296 71
0.82	−0.594 83	1.06	−0.544 15	1.38	−0.470 06	1.56	−0.419 20	1.74	−0.359 16	1.92	−0.288 24
0.84	−0.590 37	1.10	−0.535 67	1.40	−0.464 81	1.58	−0.413 02	1.76	−0.351 85	1.94	−0.279 61
0.86	−0.586 00	1.14	−0.527 03	1.42	−0.459 46	1.60	−0.406 72	1.78	−0.344 40	1.96	−0.270 83
0.88	−0.581 71	1.18	−0.518 19	1.44	−0.454 01	1.62	−0.400 30	1.80	−0.336 81	1.98	−0.261 89
		1.22	−0.509 14	1.46	−0.448 47	1.64	−0.393 76	1.82	−0.329 08	2.00	−0.252 79
0.90	−0.577 47	1.26	−0.499 82	1.48	−0.442 83	1.66	−0.387 10	1.84	−0.321 21		
0.94	−0.569 11	1.30	−0.490 22	1.50	−0.437 08	1.68	−0.380 31	1.86	−0.313 19		
0.98	−0.560 82	1.34	−0.480 31	1.52	−0.431 23	1.70	−0.373 39	1.88	−0.305 02		

is large compared to the same quantity for sodium chloride, but a 2 percent experimental error is perhaps less improbable in the case of zinc sulfate. It should be pointed out that in portions of the region where $\ln f$ deviates negatively from the limiting law, $\ln f$ is nearly as sensitive to A as it is at about 0.01 molar. Consequently a relatively small change of about 3 percent in the numerical value of $\ln f$ used in determining A would essentially eliminate the error in the deviation from the limiting law at the low concentrations. The theoretical values of the deviation from the limiting law are negative in the region within the concentration range of validity of Eq. (1). Throughout the concentration range studied, the osmotic pressure correction is negligible. The use of approximations (27) and (32) introduces an error of one digit in the fourth decimal place of $\ln f'$, which is sufficient accuracy in this case.

IV. III-I Electrolytes

The salt chosen as representative of this type was lanthanum chloride. The value of $\bar{V}_2^\circ$ for lanthanum chloride was taken to be 16.02 cm³ mole^{-1} (reference 6, p. 253). The experimental datum used for the determination of A was $f=0.5495$ at 0.010936 molar.[12] Since this concentration differs by about ten percent from 0.01 molar, chosen as the standard concentration for this ionic type, the procedure of paragraph 4, Section C, which retains only two terms of the Taylor's series expansion of $\ln f$, cannot be used. The method adopted was to calculate $\ln f'$ and the osmotic pressure correction for a molarity of 0.010936 and four different values of A, covering the expected value of A for lanthanum chloride, and so chosen that the corresponding values of φ given by Eq. (16) are successive round values listed as arguments in Tables I–III. In computing the osmotic pressure corrections, approximations (24) and (25) were adequate. From the four computed values of $\ln f$, Lagrangian interpolation yielded the value 0.8957_9 as the "best" A for lanthanum chloride. Using this value of A, the concentration limit of validity of Eq. (1) was found to be about 0.017 molar, at which concentration the theoretical value of f differed by 1.8 percent from the experimental value. The standard concentration for III–I salts, at which Table VIII is computed, was chosen to be 0.01 molar. Table XII compares experimental values of $\ln f$ with theoretical values computed from Eq. (1). The agreement is rather good. Again it is felt that the rapidly increasing percent error in f (100 times the fourth column entry) at the two largest concentrations shows the beginning of a failure of the theoretical expression (1).

E. THE DISTANCE OF CLOSEST APPROACH

The effective distance of closest inter-ionic approach, a, is readily obtained from the parameter A by using Eq. (17). Table XIII compares the values in angstrom units obtained in this manner (first column) with other values derived from activity coefficient and crystallographic data. The second column gives the value

[12] T. Shedlovsky, J. Am. Chem. Soc. **72**, 3680 (1950).

obtained for a if the particular experimental data used in this paper for the determination of A are used to determine a in the Debye-Hückel formula:

$$\log f=\frac{Gc^{\frac{1}{2}}}{1+Bac^{\frac{1}{2}}}+\log\frac{(d-0.001\ \mathrm{M}c+0.018\nu c)}{d_1}, \quad (36)$$

where G is numerically given by the expression,

$$G=0.50891(\nu/2)^{\frac{1}{2}}n_2^{\frac{3}{2}}, \quad (37)$$

while B is given by the expression,

$$B=0.32858(\nu/2)^{\frac{1}{2}}n_2^{\frac{1}{2}}. \quad (38)$$

The third column lists for three salts the value of a obtained from several equations reproducing experimental data containing, in addition to the terms of Eq. (36), terms in c or $c\log c$. For zinc sulfate column three lists the value of a obtained using the extended Debye-Hückel theory of Gronwall, LaMer, and Sandved (reference 7). The fourth column gives the crystallographic distance of closest approach. The values in the second column are, of course, unreasonable. The agreement between the a's obtained from this theory and those listed in column three is rather good, though clearly no exact agreement is expected because of the difference in form of the equations. Undoubtedly it is a result of the fact that ions are hydrated in solution that these a's are considerably larger than the sum of the crystal radii.

TABLE IX. The quantity ln$f$ for NaCl in aqueous solution at 25°C.

Molarity	ln$f_{\text{exptl.}}$	ln$f_{\text{theoret.}}$	ln$f_{\text{exptl.}}$ −ln$f_{\text{theoret.}}$
0.004984_9[a]	−0.0744[a]	−0.0754	0.0010
0.009967_0[a]	−0.1016[a]	−0.1025	0.0009
0.019934_4[a]	−0.1363[a]	−0.1372	0.0009
0.03985_8[a]	−0.1798[a]	−0.1801	0.0003
0.05976_2[a]	−0.2084[a]	−0.2089	0.0005
0.07965_8[a]	−0.2307[a]	−0.2310	0.0003
0.09952_4[b]	−0.249[c]	−0.249	0.000
0.1986_8[b]	−0.306[c]	−0.309	0.003
0.2974_7[b]	−0.337[c]	−0.347	0.010
0.3959_0[b]	−0.359[d]	−0.374	0.015

[a] A. S. Brown and D. A. MacInnes, J. Am. Chem. Soc. **57**, 1356 (1935).
[b] Calculated from round molalities and an empirical equation for c/m (reference 6, p. 556).
[c] Calculated from values of f_m (reference 6, p. 562) and an empirical equation for c/m (reference 6, p. 556).
[d] Calculated from f_m given by R. A. Robinson and R. H. Stokes, Trans. Faraday Soc. **45**, 612 (1949), and an empirical equation for c/m (reference 6, p. 556).

TABLE X. The quantity ln$f$ for $CaCl_2$ in aqueous solution at 25°C.

Molarity[a]	ln$f_{\text{exptl.}}$[a]	ln$f_{\text{theoret.}}$	ln$f_{\text{exptl.}}$ −ln$f_{\text{theoret.}}$
0.0060915	−0.2555	−0.2491	−0.0064
0.0095837	−0.3064	−0.2970	−0.0094
0.024167	−0.4286	−0.4174	−0.0112
0.037526	−0.4948	−0.4875	−0.0073
0.050000	−0.5389	−0.5389	0.0000
0.096540	−0.6396	−0.6765	0.0369

[a] Reference 11.

MATHEMATICAL APPENDIX

The tabulated values of $b_\mu(\varphi)$, $g_\mu(\varphi)$, and $h_\mu(\varphi)$, Tables I–III respectively, were obtained as follows. The function $f_\mu(\varphi)$, defined by the equation,

$$f_\mu(\varphi)=\frac{\varphi^2}{\mu!}\int_1^{l_\mu} e^{-\mu\varphi y}y^{2-\mu}dy, \quad (39)$$

and $g_\mu(\varphi)$ were the basic quantities computed. It is apparent from Eqs. (13) and (14) that $b_\mu(\varphi)$ may be obtained as the difference,

$$b_\mu(\varphi)=f_\mu(\varphi)-g_\mu(\varphi), \quad (40)$$

while $h_\mu(\varphi)$ was readily computed from Eq. (15) using computed values of $g_\mu(\varphi)$. The method of computation of $f_\mu(\varphi)$ and $g_\mu(\varphi)$ was the following. The functions $f_0(\varphi)$, $f_2(\varphi)$, and $g_3(\varphi)$ are immediately integrable, while $g_2(\varphi)$ is easily integrated by parts, the integrand

TABLE XI. The quantity ln$f$ for $ZnSO_4$ in aqueous solution at 25°C.

Molarity[a]	ln$f_{\text{exptl.}}$	ln$f_{\text{theoret.}}$	ln$f_{\text{exptl.}}$ −ln$f_{\text{theoret.}}$
0.0004985	-0.248_5[b]	-0.263_5	0.015
0.000997_1	−0.357[b]	−0.376	0.019
0.001994_2	−0.498[b]	−0.522	0.024
0.004985	−0.740[b]	−0.756	0.016
0.00997_1	−0.949[b]	−0.950	0.001
0.01994_4	−1.211[c]	−1.155	−0.056
0.04986	−1.600[c]	−1.508	−0.092

[a] Reference 9, p. 65 gives the density of zinc sulfate solutions at 25°C. for round weight percent solutions, for which the molality is readily computed. The data at the two lowest concentrations were used to determine the constants in the empirical equation: $d=0.99707+0.16_8m-0.01_{27}m^{\frac{3}{2}}$, from which the density of solutions as round molalities was found. From the molality and the density the molarity is easily obtained using the equation: $c/m=1000d/(1000+Mm)$.
[b] Calculated from values of f_m (reference 8) and values of c/m calculated as in note a above.
[c] Calculated from the values of f_m given by U. B. Bray, J. Am. Chem. Soc. **49**, 2372 (1927) (recalculated in reference 6, p. 426 to conform with the data in reference 8) and values of c/m calculated as in note a above.

being grouped as $y(e^{-2\varphi y}dy)$. The functions $f_3(\varphi)$ and $g_4(\varphi)$, apart from the factors outside the integral, are simply the exponential integral, $-Ei(-3\varphi)$ and $-Ei(-4\varphi)$, where the exponential integral function is defined as follows:

$$-Ei(-y)=\int_y^\infty e^{-t}t^{-1}dt=\int_1^\infty e^{-yt}t^{-1}dt, \quad (41)$$

and numerical values of which are available.[13] For values of the index μ exceeding three, the functions $f_\mu(\varphi)$ and $g_\mu(\varphi)$ may be converted to a form suitable for computation by repeated integration by parts until the exponent of y in the integrand has been raised to minus one, i.e., until the exponential integral function is left. This procedure leads to the following formulas

[13] Mathematical Tables Project, *Tables of Sine, Cosine, and Exponential Integrals* (Federal Works Agency, Work Projects Administration for the City of New York, 1940).

used for computation:

$$f_\mu(\varphi)=\frac{\varphi^2}{\mu!}\left\{e^{-\mu\varphi}\left[\frac{1}{\mu-3}-\frac{\mu\varphi}{(\mu-3)(\mu-4)}+\cdots\right.\right.$$
$$\left.\left.+\frac{(-\mu\varphi)^{\mu-4}}{(\mu-3)!}\right]+\frac{(-\mu\varphi)^{\mu-3}}{(\mu-3)!}[-Ei(-\mu\varphi)]\right\}, \quad (42)$$

$$g_\mu(\varphi)=\frac{\varphi^3}{4(\mu-1)!}\left\{e^{-\mu\varphi}\left[\frac{1}{\mu-4}-\frac{\mu\varphi}{(\mu-4)(\mu-5)}+\cdots\right.\right.$$
$$\left.\left.+\frac{(-\mu\varphi)^{\mu-5}}{(\mu-4)!}\right]+\frac{(-\mu\varphi)^{\mu-4}}{(\mu-4)!}[-Ei(-\mu\varphi)]\right\}. \quad (43)$$

These computations become more tedious with increasing values of the index μ. For $\mu>10$, the following approximation was used: Regrouping the exponential

TABLE XII. The quantity $\ln f$ for $LaCl_3$ in aqueous solution at 25°C.

Molarity[a]	$\ln f_{\text{exptl.}}$	$\ln f_{\text{theoret.}}$	$\ln f_{\text{exptl.}}-\ln f_{\text{theoret.}}$
0.0006070	−0.1926	−0.1835	−0.0091
0.0016628	−0.2929	−0.2836	−0.0093
0.0032179	−0.3823	−0.3719	−0.0104
0.004885	−0.4485	−0.4385	−0.0100
0.010936	−0.5987	−0.5987	0.0000
0.017188	−0.6949	−0.7129	0.0180
0.033333	−0.8465	-0.9249_5	0.0784_5

[a] Reference 12.

function in the integrand of $f_\mu(\varphi)$ and $g_\mu(\varphi)$,

$$e^{-\mu\varphi y}=e^{-\mu\varphi}(e^{-\mu\varphi})^{y-1}, \quad (44)$$

and approximating $y-1$ by $\ln y$, $f_\mu(\varphi)$ and $g_\mu(\varphi)$ take the following form:

$$f_\mu(\varphi)=\frac{\varphi^2}{\mu!}e^{-\mu\varphi}\int_1^\infty y^{-\mu(\varphi+1)+2}dy, \quad (45)$$

$$g_\mu(\varphi)=\frac{\varphi^3}{4(\mu-1)!}e^{-\mu\varphi}\int_1^\infty y^{-\mu(\varphi+1)+3}dy, \quad (46)$$

which may be immediately integrated to give the following approximate expressions for $f_\mu(\varphi)$ and $g_\mu(\varphi)$:

$$f_\mu(\varphi)=\varphi^2e^{-\mu\varphi}/\mu![\mu(\varphi+1)-3], \quad (47)$$

$$g_\mu(\varphi)=\varphi^3e^{-\mu\varphi}/4(\mu-1)![\mu(\varphi+1)-4]. \quad (48)$$

Equations (47) and (48) were used for computing $f_\mu(\varphi)$

TABLE XIII. The effective distance of closest inter-ionic approach, a, for four strong electrolytes in aqueous solution at 25°C.

Salt	This theory	Debye-Hückel	Modified Debye-Hückel	Xtal.
NaCl 0.1 molal	3.90A	6.89A	4.0A[a]	2.78A[d]
$CaCl_2$ 0.05 molal	5.68A	5.41A	5.0A[a]	2.84A[d]
$ZnSO_4$ 0.01 molal	3.74A	0.37A[e]	3.64A[b]	2.62A[e]
$LaCl_3$ 0.010936 molar	6.39A	6.01A	6.8A[a]	3.00A[b]

[a] Reference 12.
[b] Reference 8.
[c] The value, −0.31A, given in Table VI of reference 8 appears to have been obtained using the Debye-Hückel approximation for the stoichiometric mean ionic *rational* activity coefficient, given by the first term only of Eq. (36), and experimental values of the *molal* activity coefficient. The procedure used in this paper to determine the Debye-Hückel a does lead to negative values of a for zinc sulfate at concentrations less than 0.01 molal.
[d] These are averages of the values given by L. Pauling, *The Nature of the Chemical Bond* (Cornell University Press, Ithaca, New York, 1939), ch. X, and V. M. Goldschmidt, Trans. Faraday Soc. **25**, 253 (1929).
[e] Calculated assuming tetrahedral structure of the sulfate ion with O−O contact; O−O distance = 2.45A, S−O distance = 1.50A, [O. K. Rice, *Electronic Structure and Chemical Binding* (McGraw-Hill Book Company, Inc., New York, 1940), p. 308], and the average of Pauling's and Goldschmidt's radii for zinc ion (see note d above).

and $g_\mu(\varphi)$ for $11\leqslant\mu\leqslant16$. In this range of μ, it is seen by substituting (48) into (15) that $h_\mu(\varphi)$ is conveniently computed from the following form:

$$h_\mu(\varphi)=(\mu\varphi-4)g_\mu(\varphi). \quad (49)$$

Tables V–VIII were constructed in the following manner: The summation terms of Eq. (2) may be computed exactly (without interpolation) only for those values of φ listed in Table I. For each ionic type and standard concentration, Eq. (16) together with the round φ's of Table I determine the values of A for which $\ln f'$ may be exactly computed. This was done for each ionic type. The "best" A for any salt could then be found from an experimental value of $\ln f'$ by Lagrangian interpolation from these tables, but to simplify the procedure necessary to determine the best A another method was adopted. The tables of $\ln f'$ *versus* nonround A's for each ionic type were subtabulated using Newtonian interpolation to give Tables V–VIII, in which the entries are close enough together so that linear interpolation may be used. The value of A thus obtained differs negligibly from the value obtained by Lagrangian interpolation from the original exact tables of $\ln f'$ *versus* nonround A's.

The author is greatly indebted to Professor J. E. Mayer for many valuable discussions covering all phases of this work.

Electron Deficient Compounds. VII. The Structure of the Trimethylaluminum Dimer*

PAUL H. LEWIS† AND R. E. RUNDLE
Institute for Atomic Research and Department of Chemistry, Iowa State College, Ames, Iowa
(Received December 19, 1952)

The trimethylaluminum dimer has a bridge structure with a skeletal symmetry of D_{2h} within the accuracy of a structure determination by x-ray diffraction of single crystals. Bridge bonds, Al—C, equal 2.24A, *vs* Al—C bonds of 1.99A for the exterior, "normal" methyls. The bridge angle Al—C—Al=70°, the exterior angle C—Al—C=124°.

It is shown that a simple model provides the right order of magnitude for the heat of dimerization and indicates the relative importance of Al—C and Al—Al bonds. It is suggested that the sharp bridge angle required for good bridge bonding leads to metal-metal repulsions which should increase as the size of the metal increases. This probably plays a role in the instability and nature of polymers of the heavier trialkylmetal compounds.

INTRODUCTION

THE structure of the trimethylaluminum dimer, of interest because in it the number of chemical links must exceed the number of valence electron pairs, has previously been examined by electron diffraction,[1] and by use of Raman and infrared spectra.[2] The published results are inconclusive, even as to general configuration. Recent suggestions favor some sort of bridge structure. The structure of dimethylberyllium[3] and an unpublished electron diffraction study of the vapor[4] lend support to the bridge model. The number of independent parameters required to locate all heavy atoms, without recourse to assumptions concerning configuration, is so great that only an x-ray investigation of single crystals appeared likely to provide an adequate amount of data for a structure determination.

EXPERIMENTAL PROCEDURES

Preparation of Samples

Trimethylaluminum was prepared from aluminum turnings and methyl iodide as described by Pitzer and Gutowsky.[2] The water-white liquid, freezing at 15°, was distilled in an all glass system into thin-walled glass capillaries, suitable for diffraction studies, directly from the fractionating column. Purity was checked by the melting point which is depressed considerably by traces of dimethylaluminum iodide, the chief impurity.

TABLE I. Test for center of symmetry.

$N(z)$ *vs* (z), %	10	20	30	40	50	60	70	80	90
Observed	27	34	38	41	48	53	58	61	64
Centric (Theory)	25	35	42	47	52	56	59	63	66
Acentric (Theory)	9.5	18	26	33	39	45	50	55	59

Low Temperature Techniques

Methods developed in the laboratories of Fankuchen[5] and Lipscomb[6] were helpful in arriving at suitable low temperature procedures. The sample was cooled by a jet of cold air directed parallel with the x-ray beam. Air from a Pressovac pump was dried by passing it through a gallon can packed with copper turnings maintained at dry ice temperatures. Although one drying system would operate for some fifty hours without becoming clogged with ice, a tandem system was used and an interchange was made every twenty-four hours. This system, operating continuously for a month, permitted the collection of intensity data for eight reciprocal lattice levels by the Weissenberg technique from one single crystal. The dry air was cooled further by passing it through a copper coil immersed in a dry ice bath. Frosting of the sample was obviated by use of a jet tube with a wide diameter; the temperature range used, 0° to −20°C, made more elaborate techniques unnecessary. Conventional crystallization techniques were used, producing, in nearly all cases, crystals whose c axis paralleled the capillary axis.

Standard equi-inclination Weissenberg and precession cameras were used, except that the film holder and screen of the Weissenberg were slotted for their entire length, permitting work without disturbing the crystal or cooling system supported by the pin hole system.

X-Ray Data

The following x-ray data were obtained. Oscillation and rotation photographs about both the b and c axis, (hkl) data for the reciprocal levels $l=0$ to $l=7$ by the Weissenberg method, and precession photographs of the $(h0l)$ and $(h1l)$ levels. Weissenberg photographs were made by the equi-inclination technique using Ni-filtered CuK radiation, $\lambda=1.542$A, and multiple films, while precession photographs were made with Zr-

* Contribution No. 228 from the Institute for Atomic Research and Department of Chemistry, Iowa State College, Ames, Iowa. Work was performed in the Ames Laboratory of the U. S. Atomic Energy Commission.

† Present address: The Texas Company, P. O. Box 509, Beacon, New York.

[1] L. O. Brockway and N. Davidson, J. Am. Chem. Soc. **63**, 3287 (1941).

[2] K. Pitzer and H. Gutowsky, J. Am. Chem. Soc. **68**, 2204 (1946).

[3] A. I. Snow and R. E. Rundle, Acta Cryst. **4**, 348 (1951).

[4] V. Schomaker, private communication.

[5] H. S. Kaufman and I. Fankuchen, Rev. Sci. Instr. **20**, 733 (1949); Post, Schwartz, and Fankuchen, Rev. Sci. Instr. **22**, 218 (1951).

[6] Abrahams, Collins, Lipscomb, and Reed, Rev. Sci. Instr. **21**, 396 (1950).

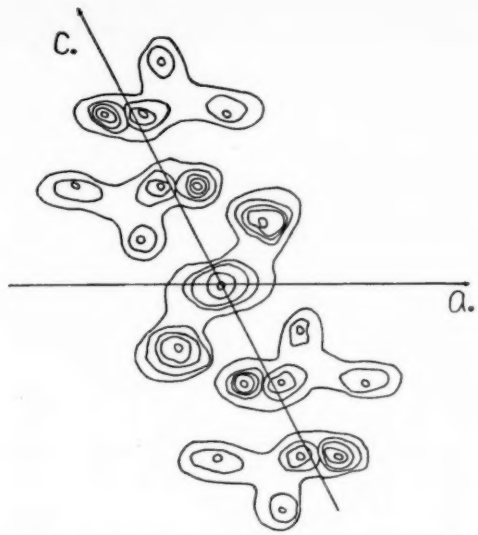

FIG. 1. "Sharpened" Patterson projection, $P(xz)$.

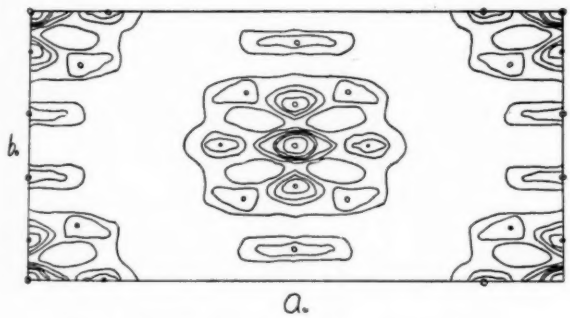

FIG. 2. "Sharpened" Patterson projection, $P(xy)$.

filtered MoK radiation, $\lambda=0.7107$A, and timed exposures.

Intensities, estimated visually, were corrected for Lorentz-polarization effects by the methods of Lu[7] and of Evans *et al.*[8] Absorption corrections were made by Albrecht's method,[9] and intensities from different levels were correlated by oscillation photographs.

STRUCTURE DETERMINATION

Unit Cell and Space Group

Trimethylaluminum is monoclinic with $a=13.0$, $b=6.96$, $c=14.7$A, $\beta=125°$. Using the density of the liquid at 20°, 0.752, the number of monomers per unit cell was calculated to be 6.8, and assumed to be 8, so that the x-ray density of the solid at $\sim-10°$ is 0.887 g/cc. Reflections (hkl) appear only when $h+k=2n$, and $(h0l)$ only when $h=2n$, $l=2n$. The space group is, then, either $C_{2h}{}^6-C2/c$ or $C_5{}^4-Cc$. The latter is made improbable by the distribution of intensities which follows closely the expected distribution for a centric crystal[10,11] (Table I). Adopting the centric space group, $C2/c$, requires a dimer molecule to have either a center of symmetry or a twofold axis.

Atomic Positions

Simple considerations show that aluminum and all carbon atoms must be placed in the general eightfold set of positions, $000, \frac{1}{2}\frac{1}{2}0\pm[x, y, z; x, \bar{y}, \frac{1}{2}+z]$. Conventional Patterson and Harker projections and Harker-Kasper inequalities were disappointing, leading to an erroneous trial structure. The "sharpened" Pattersons,[12] $P(xz)$ and $P(xy)$, however, gave clear indication of the correct structure. (See Figs. 1 and 2.) Dimer molecules with a center of symmetry seemed to be required. The structure was refined by Fourier methods, using, in the last stages, the synthetic Fourier method of Booth[13] to correct for series termination. Peaks were located by Booth's method.[14] The most useful projections, $\rho(xz)$ and $\rho(yz)$, can be seen in Figs. 3 and 4.

Structure factors were calculated using atomic scattering factors from a recent compilation[15] and were corrected by the usual empirical temperature factor with $B=3.9$A.^{2} A comparison of observed and calculated values are given in Table II. The reliability index,

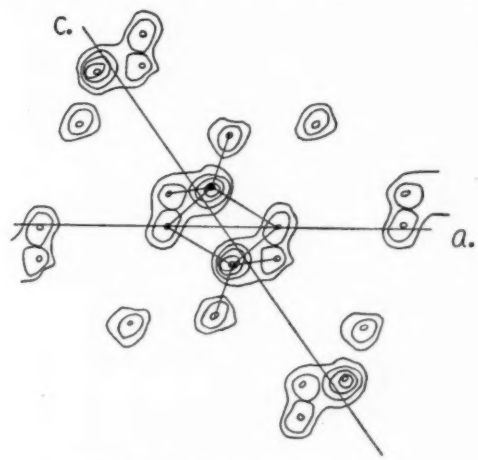

FIG. 3. Fourier projection, $\rho(xz)$.

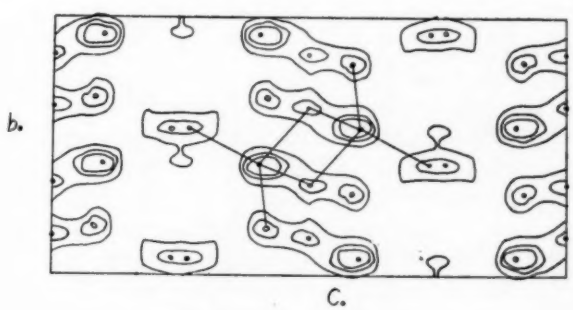

FIG. 4. Fourier projection, $\rho(yz)$.

[7] C. Lu, Rev. Sci. Instr. **14**, 331 (1943).
[8] Evans, Tilden, and Adams, Rev. Sci. Instr. **20**, 155 (1949).
[9] G. Albrecht, Rev. Sci. Instr. **10**, 221 (1933).
[10] A. J. C. Wilson, Acta Cryst. **2**, 318 (1949).
[11] Howells, Phillips, and Rogers, Acta Cryst. **3**, 210 (1950).
[12] A. L. Patterson, Z. Krist. **90**, 517 (1935).
[13] A. D. Booth, Proc. Roy. Soc. (London) **A188**, 77 (1946).
[14] A. D. Booth, *Fourier Techniques in Organic Structure Analysis* (Cambridge University Press, Cambridge, 1948), pp. 62–65.
[15] Ö. Ögrim and H. Viervoll, Acta Cryst. **2**, 277 (1949).

TABLE II. Comparison of observed and calculated structure factors for trimethylaluminum.[a] The three columns comprising each section are, from left to right, the h index, the observed, and the calculated structure factors, respectively. Unless noted otherwise the signs of the calculated factors are positive.

$h00$		
2	35	26
4	1.7	4.0
6	12	6.2
8	4.0	2.8
10	4.0	−3.4
12	2.8	−2.8

$h02$		
0	18	13
2	12	8.2
4	0.0	1.1
6	6.8	−6.2
8	5.3	−4.2
10	3.0	−3.0

$h0\bar{2}$		
2	27	22
4	6.0	6.8
6	5.8	4.6
8	9.7	9.4
10	6.2	7.0

$h04$		
0	0.0	−3.6
2	17	−10
4	22	−13
6	6.5	−4.0
8	0.0	−1.0

$h0\bar{4}$		
2	27	−17
4	28	−17
6	5.8	4.8
8	8.7	10
10	6.8	6.8
12	3.7	5.2

$h06$		
0	23	−16
2	17	−12
4	4.8	−4.6

$h0\bar{6}$		
2	14	−13
4	27	−20
6	20	−14
8	0.0	1.4
10	2.7	4.0

$h08$		
0	0.0	1.8
2	2.5	0.4
4	0.0	−1.6
6	3.2	2.0

$h0\bar{8}$		
2	5.2	−6.2
4	9.2	−9.6
6	9.5	−6.6
8	8.2	−5.8
10	6.8	−7.4
12	5.3	−4.8
14	3.2	−2.8

$h\cdot 0\cdot 10$		
0	8.2	7.4
2	3.5	2.2
4	3.5	1.8

$h\cdot 0\cdot \bar{1}0$		
2	13	9.4
4	2.5	2.0
6	2.5	−3.4
8	0.0	0.6
10	3.3	−4.6
12	7.0	−8.2
14	4.5	−4.0

$h\cdot 0\cdot 12$		
0	4.7	5.4
2	2.5	2.8

$h\cdot 0\cdot \bar{1}2$		
2	5.0	5.2
4	6.7	5.0
6	4.7	4.6
8	3.8	2.6
10	2.3	1.0

$h\cdot 0\cdot \bar{1}4$		
8	5.8	6.4
10	5.5	5.0
12	3.0	2.0

$h\cdot 0\cdot \bar{1}6$		
4	1.8	−2.2
10	2.5	3.4

$h10$		
1	19	26
3	2.3	4.4
5	5.7	4.6
7	7.1	7.2
11	1.9	−2.0

$h20$		
0	10	7.4
2	3.9	5.0
4	5.0	4.2
6	5.4	5.0
8	2.6	1.8

$h30$		
1	5.9	4.6
3	4.6	5.8
5	3.5	2.6

$h40$		
0	7.1	−7.2
2	3.9	−3.6

$h50$		
1	9.0	−9.0
3	3.7	−4.0
11	0.6	1.2

$h60$		
0	5.7	−4.4
2	4.6	−2.8
4	3.0	−2.8
6	2.8	−3.2

$h70$		
1	4.3	−3.8
3	2.9	−3.2
5	2.9	−2.4
7	1.6	−1.0

$h80$		
0	2.8	−4.0
2	2.6	−2.4
4	1.8	−1.2

$h11$		
5	1.8	−0.3
3	8.6	−11
1	7.2	−10

$h1\bar{1}$		
1	—	—
3	5.3	−6.5
5	3.0	−2.3
7	1.4	−1.9
9	2.8	4.4
11	2.2	3.8

$h21$		
6	5.1	−6.8
4	12	−11
2	13	−14
0	2.2	0.3

$h2\bar{1}$		
2	7.2	6.7
4	2.9	2.9
6	3.6	4.7
8	4.6	4.4
10	3.9	3.8
12	1.9	2.6

$h31$		
7	4.9	−5.5
5	15	−11
3	13	−16
1	7.9	−7.8

$h3\bar{1}$		
1	0.9	−1.0
3	0.0	−2.4
5	1.9	3.9
7	4.5	8.0
9	4.1	4.7
11	2.9	2.3
13	1.4	2.9

$h41$		
8	3.6	−3.2
6	4.3	−4.8
4	7.2	−9.0
2	7.2	−7.0
0	5.2	−4.8

$h4\bar{1}$		
2	4.7	−8.5
4	2.2	−4.2
6	3.1	6.0
8	3.9	5.5
10	3.0	3.0
12	1.6	3.8

$h51$		
7	3.8	−4.5
5	5.0	−7.5
3	6.0	−6.0
1	2.5	−1.5

$h5\bar{1}$		
1	1.8	−2.5
2	1.3	−2.7
5	2.6	3.9
7	3.9	6.5
9	2.3	1.1

$h61$		
8	1.6	−1.6
6	2.4	−2.9
4	2.4	−3.4
2	0.0	−1.3
0	0.0	−0.1

$h6\bar{1}$		
2	1.4	−1.2
4	1.1	−0.6
6	1.8	2.9
8	0.0	1.4

$h7\bar{1}$		
3	2.3	−1.2

$h81$		
4	1.6	1.6
2	1.6	0.3

$h12$		
3	2.6	−2.0
1	3.5	−0.3

$h1\bar{2}$		
1	11	11
3	16	20
5	12	12
7	11	11
9	11	11
11	3.1	4.8

$h22$		
4	3.5	−1.4
2	3.1	−2.5
0	3.8	−3.7

$h2\bar{2}$		
2	11	−11
4	14	15
6	7.7	9.0
8	6.7	6.5
10	5.1	5.5

$h32$		
5	2.6	3.7
3	6.7	6.3
1	2.0	0.4

$h3\bar{2}$		
1	1.4	−1.6
3	2.5	3.7
5	1.0	2.0
7	1.4	−2.5
9	0.0	−1.0

$h42$		
4	3.5	2.0
2	0.0	−0.7
0	4.6	−4.3

$h4\bar{2}$		
2	3.6	−3.0
4	0.0	−0.5
6	2.5	−1.4
8	3.1	−3.7

$h52$		
5	2.3	0.6
3	0.0	−2.7
1	4.3	−2.0

$h5\bar{2}$		
1	6.5	−3.9
3	4.3	−6.0
5	3.0	−3.7
7	4.6	−2.3
9	3.6	−3.8

$h62$		
4	2.7	−0.1
2	1.0	1.0
0	2.4	1.5

$h6\bar{2}$		
2	7.4	−6.5
4	7.4	−11
6	5.8	−7.0
8	5.3	−4.5
10	3.0	−4.4

$h72$		
3	2.5	−1.4
1	5.7	0.9

$h7\bar{2}$		
1	5.7	−1.0
3	4.5	−5.0
5	3.5	−4.1
7	2.4	−1.9
9	1.7	−2.4

$h8\bar{2}$		
2	2.5	−2.0
4	0.0	−2.5

$h13$		
7	0.0	1.3
5	1.0	0.1
3	6.1	−8.0
1	23	−18

$h1\bar{3}$		
1	13	−13
3	—	—
5	7.7	−7.5
7	4.8	−4.2
9	2.5	4.1
11	3.6	4.3

$h23$		
2	14	−13
0	13	−15

$h2\bar{3}$		
2	3.3	−1.0
4	6.5	−7.0
6	11	−15
8	4.6	−6.0
10	2.7	2.7
12	1.9	1.3

$h33$		
7	1.1	−5.5
5	2.3	−3.6
3	6.9	−8.5
1	17	−17

$h3\bar{3}$		
1	15	−14
3	8.9	−7.0
5	15	−12
7	8.9	−9.5
9	0.0	0.4
11	2.6	2.5

$h43$		
6	2.3	−3.8
4	4.2	−4.4
2	11	−11
0	18	−19

$h4\bar{3}$		
2	10	−15
4	8.1	−9.0
6	6.2	−6.5
8	0.0	0.0
10	2.6	3.2

$h53$		
7	2.7	−4.4
5	2.7	−4.0
3	2.7	−1.9
1	6.6	−5.5

$h5\bar{3}$		
1	6.2	−9.0
3	5.2	−7.0
5	5.8	−5.0
7	3.5	−3.2

$h63$		
6	1.6	−2.7
4	0.0	−0.8
2	0.0	−0.3
0	2.3	−2.5

$h6\bar{3}$		
2	3.5	−2.9
4	2.8	−2.2
6	2.3	−0.3

$h73$		
5	2.3	0.7

$h83$		
2	1.9	2.0
0	2.3	3.2

$h8\bar{3}$		
2	2.5	3.8
4	1.9	2.0
6	0.9	0.5

$h1\bar{4}$		
13	2.6	3.7
11	4.1	4.0
9	5.6	5.5
7	8.7	9.5
5	2.7	3.4
3	8.1	−8.5
1	2.2	−2.0

$h14$		
1	3.0	−4.4
3	12	−15
5	8.7	−11
7	3.2	−3.5

$h2\bar{4}$		
14	1.8	1.8
12	3.9	2.9
10	2.9	0.9
8	4.2	2.8
6	5.5	7.0
4	0.0	2.9
2	2.5	−3.1
0	0.0	−3.0

[a] Owing to modifications in the camera accommodating the cooling system, a few maxima within the sphere of reflection were either eliminated or fell in fogged regions of our films, and are not recorded in the table.

TABLE II.—*Continued.*

	*h*24			*h*6$\bar{4}$			*h*2$\bar{5}$			*h*65			*h*4$\bar{6}$			*h*27		
2	...	...	10	1.5	−0.7	2	6.7	−6.5	6	0.0	0.6	2	2.1	1.7	6	4.0	4.7
4	7.7	−6.0	8	2.7	−1.3	4	8.9	−13	4	0.0	0.9	4	5.0	4.2	4	5.9	6.5
6	4.7	−3.3	6	2.6	−4.1	6	9.9	−15	2	0.0	2.5	6	3.1	2.7	2	3.4	3.2
8	2.3	3.2	4	0.0	−1.8	8	9.9	−12	0	0.0	0.7				0	3.3	3.0
			2	1.8	2.2	10	4.9	−6.0					*h*56				
	*h*3$\bar{4}$					12	2.9	−0.8		*h*6$\bar{5}$		3	3.6	2.6		*h*2$\bar{7}$	
13	1.6	2.7		*h*64					2	3.1	−3.8	1	5.6	6.0	2	7.7	8.0
11	1.0	2.6	0	2.5	3.0		*h*35		4	3.1	−4.0				4	1.2	0.6
9	0.0	0.1	2	4.3	3.8	9	2.6	3.1	6	1.6	−1.6		*h*5$\bar{6}$		6	4.3	8.5
7	0.0	0.0	4	4.7	4.7	7	5.9	6.0	8	1.6	−2.7	1	4.5	6.0	8	3.6	−3.7
5	0.0	1.1	6	2.6	3.3	5	7.0	3.7				3	5.4	4.8			
3	5.3	−3.2				3	3.4	1.2		*h*7$\bar{5}$		5	4.4	4.8		*h*37	
1	7.2	−7.5		*h*7$\bar{4}$		1	0.0	1.5	5	2.3	1.7				7	1.9	2.0
			9	1.3	−0.7		*h*3$\bar{5}$		7	2.3	1.3		*h*66		5	4.6	5.5
	*h*34		7	1.5	−2.2	1	6.4	−4.6				2	2.7	2.7	3	5.8	6.5
1	3.5	−3.6	5	0.9	−2.5	3	11	−13		*h*16		0	3.6	5.5	1	3.9	−3.8
3	0.0	1.2	3	0.9	1.2	5	11	−12	3	6.1	−5.5						
5	0.0	1.4	1	2.3	3.0	7	11	−11	1	8.9	−11		*h*6$\bar{6}$			*h*3$\bar{7}$	
						9	7.8	−12				2	3.3	3.5	1	5.8	−6.5
	*h*4$\bar{4}$			*h*74		11	3.4	−4.8		*h*1$\bar{6}$		4	4.6	3.4	3	4.6	6.0
10	1.5	−1.6	1	...	...		*h*45		1	6.7	−8.5	6	3.6	5.5	5	1.7	−3.3
8	3.9	−2.7				8	4.4	4.6	3	8.1	−10				7	3.3	−5.5
6	0.0	−0.6		*h*8$\bar{4}$		6	3.6	2.4	5	14	−16		*h*76		9	1.8	−2.5
4	4.1	3.0	2	1.8	2.7	4	0.0	−1.1	7	6.4	−8.5	3	1.5	0.8			
2	0.9	1.3				2	0.0	0.4				1	3.0	4.7		*h*47	
				*h*15		0	2.6	−1.7		*h*26					6	1.3	1.2
	*h*44		9	2.3	1.8		*h*4$\bar{5}$		2	4.7	−4.2		*h*7$\bar{6}$		4	4.5	3.9
0	0.0	−0.9	7	3.2	3.8	2	7.7	−10	0	6.3	−7.5	1	3.3	4.9	2	4.2	4.8
2	2.6	2.2	5	1.6	−1.3	4	7.5	−6.0				3	3.0	2.3	0	4.6	5.0
4	4.1	3.7	3	2.9	−3.8	6	6.4	−3.2		*h*2$\bar{6}$		5	2.9	3.2			
			1	2.6	−4.8	8	6.8	−7.0	2	4.2	−4.5	7	2.4	3.4		*h*4$\bar{7}$	
	*h*5$\bar{4}$					10	5.8	−8.5	4	7.3	−5.5				2	5.7	6.5
11	2.0	−3.0		*h*1$\bar{5}$		12	2.6	−3.0	6	7.4	−9.0		*h*86		4	2.4	3.0
9	3.2	−2.5	1	2.0	−1.7				8	4.0	−4.7	0	2.4	4.2	6	1.8	−1.6
7	3.3	−3.0	3	1.6	−0.9		*h*55								8	1.8	−2.5
5	0.0	0.0	5	3.2	−2.9	7	3.1	2.4		*h*36			*h*8$\bar{6}$				
3	4.5	4.4	7	5.0	−5.5	5	2.3	0.9	1	5.6	−6.0	2	2.4	2.7		*h*57	
1	3.9	4.1	9	3.8	−3.7	3	0.0	2.5							5	2.4	2.2
						1	1.6	3.7		*h*3$\bar{6}$			*h*17		3	3.5	4.0
	*h*25								1	6.9	−7.0	5	2.5	2.4	1	2.5	3.1
							*h*5$\bar{5}$		3	2.1	−1.6	3	2.8	1.7			
	*h*54		8	4.4	6.0	1	4.5	−4.2	5	0.0	1.0	1	2.5	1.5		*h*5$\bar{7}$	
1	5.5	2.9	6	7.1	7.0	3	7.8	−9.5	7	0.0	−0.4				1	2.2	1.8
3	4.2	4.0	4	5.3	2.7	5	5.7	−5.0					*h*1$\bar{7}$		3	0.9	0.3
5	3.7	2.5	2	2.3	0.7	7	7.0	−3.8		*h*46		1	7.0	7.5			
			0	0.0	0.5	9	5.7	−7.0	2	2.9	2.3	3	6.0	10		*h*67	
						11	3.1	−4.3	0	0.0	1.0	5	0.9	0.1	4	1.4	1.5
												7	3.0	−4.9	2	1.7	1.6

R, ($\equiv\sum||F_{obs}|-|F_{calc}||/\sum|F_{obs}|$) is 0.23 if unobserved reflections are not included, 0.25 with them included. The relatively high value is no doubt due in part to the omission of hydrogen, which contributes 25 percent to the electron density. Crude attempts to include hydrogen positions resulted in marked decreases of R, but they were not pursued.

Parameter values for the heavy atoms are listed in Table III, while important intramolecular distances and angles are shown in Fig. 5. Errors, estimated by Cruickshank's method,[16] were about ±0.02A for bond distances and ±2° for bond angles. Intermolecular van der Waals distances between methyl groups range from 4.0 to 4.3A. An idea of the packing can be obtained from Fig. 6.

DISCUSSION

That delocalization of bonds in electron-deficient compounds results from a tendency of metals to use all low energy orbitals in bond formation, even when these exceed in number the valence electrons,[17] is no longer seriously questioned. Detailed structural information is, however, necessary for a detailed understanding of the nature of the delocalization, since otherwise there is not general agreement, even in simple cases, as to which bonds should be electron-deficient. The recent discussion by Gillespie[18] is, for example, very different from other approaches to the subject. The resemblence of the bridge bonds in dimethylberyllium[3] and trimethylaluminum are similar enough to warrant an attempt at understanding the bonding in these cases.

In the trimethylaluminum dimer C−Al distances outside the bride are 1.99A, nearly equal to the sum of the covalent radii,[19] 2.03A, while the bridge C−Al

[16] D. W. J. Cruickshank, Acta Cryst. **2**, 65 (1949).

[17] R. E. Rundle, J. Am. Chem. Soc. **69**, 1327 (1947); R. E. Rundle, J. Chem. Phys. **17**, 671 (1949).

[18] R. J. Gillespie, J. Chem. Soc. **1952**, 1002.

[19] L. Pauling, *Nature of the Chemical Bond* (Cornell University Press, Ithaca, New York, 1945), second edition, p. 179.

TABLE III. Parameters.

	x	y	z
Al	0.028	0.073	0.091
C_1	0.121	0.148	0.006
C_2	0.148	−0.072	0.230
C_3	−0.056	0.317	0.084

distances are 2.24A, approximately the length expected for half-bonds, 2.21A, using Pauling's rule.[20] Bridge Be−C bonds in dimethylberyllium are also long.[3] In both trimethylaluminum[2] and dimethylberyllium, the spectra of which we have recently examined, C−H frequencies are normal, suggesting that the electron deficiency resides entirely in the M−C bonds, contrary to the suppositions of Gillespie.[18]

Bridge angles, C−M−C, are 70° in the aluminum, 66° in the beryllium compound. The sharp bridge angle requires an Al−Al distance of 2.55A, approximately the single bond distance, 2.52A.[19] The exterior C−Al−C angle is 124°, surprisingly large, but about equal to that in B_2H_6.[21]

Two equally good ways to describe the bonding present themselves. First, a bridge electron pair can be pictured as occupying a molecular orbital formed by linear combination of one tetrahedral orbital from each of the aluminums, directed toward the bridge carbon, and a single tetrahedral orbital of the bridge carbon directed equally between them. This picture has proved useful in understanding the sharp bridge angle and its change in going to a halide bridge.[3,22] Alternately, the bridge can be thought of as a "methylated double bond" with methyls sitting in the π-bonds. In this case the short Al−Al distance seems natural due to an Al−Al σ-bond, and the exterior C−Al−C angle is expected to be large, as observed. Energetically, however, Al−C interactions must be more important than Al−Al interactions, and the tetrahedral orbitals of the bridge carbons would have to be thought of as overlapping the Al−Al σ-bond, and in the end the picture would lead to an electron distribution like that of the first view presented. Likewise, in the first view, some importance to the overlap of aluminum tetrahedral orbitals can be expected, so that the Al−Al bonding, though less prominent may not be negligible (see below).

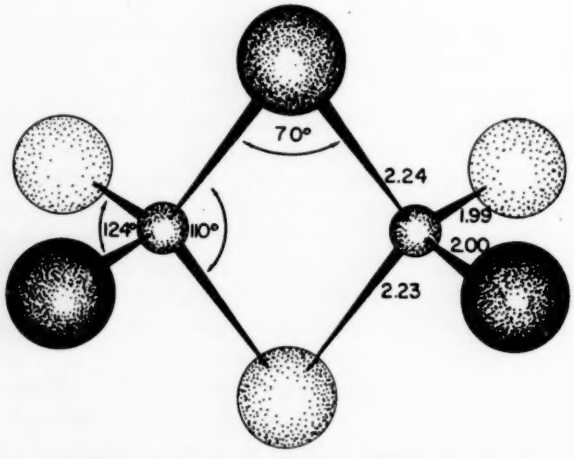

FIG. 5. Molecular structure of the trimethylaluminum dimer.

In this regard, the first picture allows an understanding of the large, exterior C−Al−C angle, since the exterior Al bonds which contain an electron pair, make more complete use of the aluminum orbitals than do the bridge orbitals. Hence if the exterior orbitals have a disproportionately large s character, the promotional energy for the bridging will be less. The C−Al−C angle at 124° suggests that the s character in the exterior aluminum orbitals exceeds one-third. In addition, for these "bent bonds," geometrical considerations (Fig. 7) would suggest that greater overlap is achieved if the aluminum orbital is not along the bond but is directed more toward the carbon orbital. This would lead to more p character in the bridge, more s character in the exterior orbitals, and a wider C−Al−C exterior angle.

A rough molecular orbital treatment of this picture of the bridge bond leads to reasonable, semiquantitative estimates of the heat of dimerization. We have made the assumptions described below.

For the reaction

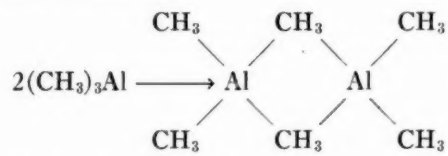

the nonbridge Al−C bonds and all C−H bonds are taken to be unaffected. Thus, though we ignore any change from trigonal to tetrahedral bonding, we must take into account some promotional energy. If, as the exterior angles of the dimer indicate, the s character in the exterior bonds exceeds one-third, say 0.4, then formally counting one electron per pair bond and one-half an electron per bridge half-bond, it is easily seen that 0.1 electron per aluminum is excited from $3s$ to $3p$. Spectroscopically the difference in levels is 82.5 kcal/mole, or for exciting 0.2 electron/dimer, the promotional energy is about 16.5 kcal/dimer. (This assumes the "valence state" for the monomer and dimer are about equally promoted from ^2P and ^4P, respectively.)

We shall calculate the heat of dimerization in terms of an Al−C bond, and set the "normal" overlap integral $\int \psi_{Al} H \psi_C d\tau$ equal to β, where both aluminum and carbon orbitals are directed along the bond. For "bent bonds" in the bridge we shall use Spitzer's approximation,[23] that the coefficient of β should be proportional to the component of the angular part of the

[20] L. Pauling, J. Am. Chem. Soc. **69**, 542 (1947).
[21] W. C. Price, J. Chem. Phys. **15**, 614 (1947).
[22] R. E. Rundle and Paul H. Lewis, J. Chem. Phys. **20**, 132 (1952).
[23] R. Spitzer, Ph.D. thesis, California Institute of Technology, 1941.

atomic wave function along the bond direction. (The carbon tetrahedral orbital makes an angle of 35° with the bond in the dimer, so that $f=\frac{1}{2}+\frac{3}{2}\cos\theta=1.727$ *vs* 2.0 for a "normal" bond, or a ratio of 0.86.) We can set up two molecular orbital treatments, ignoring Al−Al interactions (secular Eq. I; below) or considering them (Eq. II). In the latter case, considering both aluminum orbitals to make an angle of 55° with respect to the bond and estimating $\int\psi_{Al}H\psi_{Al}d\tau=\frac{1}{2}\beta$, the coefficients for these terms are obtained. The Coulomb integral for carbon is taken as $Q_{Al}+n\beta$ where, in view of the experience of others,[24] n is probably between $\frac{1}{2}$ and 2. Otherwise, the secular equations below represent the crudest sort of molecular orbital treatment of three atoms, each furnishing one atomic orbital to the final molecular orbital. The treatment applies to one-half the bridge and is thus a localized molecular orbital:

$$\begin{vmatrix} Q-W & 0.86\beta & 0 \\ 0.86\beta & Q+n\beta-W & 0.86\beta \\ 0 & 0.86\beta & Q-W \end{vmatrix}=0, \qquad \text{I}$$

$$\begin{vmatrix} Q-W & 0.86\beta & 0.23\beta \\ 0.86\beta & Q+n\beta-W & 0.86\beta \\ 0.23\beta & 0.86\beta & Q-W \end{vmatrix}=0. \qquad \text{II}$$

"Normal" Al−C bonds are found from the equation

$$\begin{vmatrix} Q-W & \beta \\ \beta & Q+n\beta-W \end{vmatrix}=0. \qquad \text{III}$$

The extra stabilization in going from one normal bond to one bridge bond is given as a function of n, both without and with aluminum contributions considered, in Table III.

The energy to break a normal Al−C bond is estimated by means of Pauling's electronegativity table and rules[25] as 67.4±5 kcal/bond, where D(C−C) =58.6, D(Al−Al) is estimated to be 30.0±10 kcal/bond, and the electronegativity difference correction is 23 kcal/bond. From this we obtain the values for the heat, ΔE, of dimerization as given in Table IV.

These calculations, though crude, are satisfactorily close to Laubengayer and Gilliam's experimental value of −20.2 kcal for ΔH of dimerization,[26] especially near the more probable values of n, near one. They strongly suggest that the contribution of highly excited structures involving 3*d* orbitals of carbon, such as suggested by Gillespie,[18] is negligible. In addition they illustrate certain interesting points.

First, the calculations indicate that though Al−C interactions predominate, Al−Al interactions are not negligible, in partial agreement with a suggestion of Schomaker[27] that metal-metal interactions and exces-

[24] C. A. Coulson, *Valence* (Oxford University Press, London 1952), p. 242.
[25] See reference 19, pp. 45–64.
[26] A. W. Laubengayer and W. F. Gilliam, J. Am. Chem. Soc. 63, 477 (1941).
[27] V. Schomaker, J. chim. phys. **46**, 262 (1949).

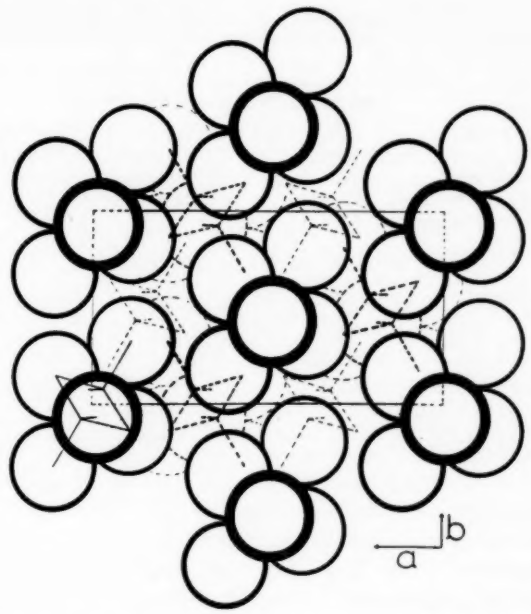

FIG. 6. Packing in trimethylaluminum crystals. Molecules are projected onto (001) along a normal to (001). Methyl groups of molecules in the first level are shown in solid heavy circles, and bond directions are indicated for the lower left-hand molecule only. Methyl groups of molecules in the second level are shown by lighter dashed circles, with all bond directions indicated by heavy dashed lines. Molecules in the third level are indicated only by light dashed bonds. Radii of circles drawn for methyl groups are approximately $\frac{3}{4}$ of the van der Waals radii of 2A. Within each level there are six molecules about any other molecule. There are also three in front and three in back in a manner approximating cubic closest packing. Molecules in alternate levels are, however, rotated 180° about *b*, so that the layer of molecules in front of the first level shown would lie approximately over the third level shown, but rotated about *b*, like in the second level shown.

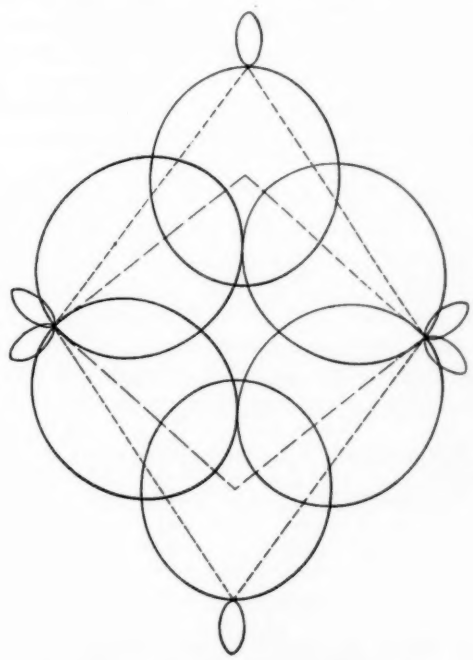

FIG. 7. Schematic representation of bonding atomic orbitals in the bridge.

TABLE IV. Calculation of dimerization energy.

n	0	1	2
	No Al—Al contribution		
Bridge bond	$2Q+2.44\beta$	$2Q+3.64\beta$	$2Q+5.15\beta$
Normal Al—C	$2Q+2\beta$	$2Q+3.24\beta$	$2Q+4.83\beta$
Coulomb term	$2Q$	$2Q+1.0\beta$	$2Q+2\beta$
Res. E/bridge bond	0.44β	0.40β	0.32β
ΔE^a (dimerization)	−13.1	−7.5	+1.1 kcal
	Al—Al contributions included		
Bridge bond	$2Q+2.64\beta$	$2Q+3.8\beta$	$2Q+5.24\beta$
Normal Al—C	$2Q+2.0\beta$	$2Q+3.24\beta$	$2Q+4.83\beta$
Coulomb term	$2Q$	$2Q+1.0\beta$	$2Q+2.0\beta$
Res. E/bond	0.64β	0.56β	0.41β
ΔE^a (dimerization)	−26.5	−17.2	−3.1 kcal

[a] Assuming D(Al—C) =67.4 kcal/bond and correcting for a promotional energy of 16.5 kcal/dimer.

sively high coordination numbers are important features of electron-deficient compounds. (That they are not general features is illustrated by the structure of tetramethylplatinum,[28] where Pt—Pt distances are too large for bonding, and the coordination number of platinum is a normal six.)

Second, both total energy of dimerization and the relative importance of metal-metal interactions become less important as the difference in electronegativity (greater n) increases. Finally, the whole effect of dimerization is proportional to the strength of metal-nonmetal bonds. All of these points having interesting application to hydrides, etc., where similar treatments may apply.

The above treatment ignores repulsions arising from dimerization. As Longuet-Higgins and Bell[29] point out, the main repulsions arise from interactions of filled shells and are probably not large in B_2H_6. We believe, however, that there is an indication that Al—Al repulsions are beginning to become important in the aluminum compound, and that metal-metal repulsions may have something to do with the odd behavior of the third group trialkyls.

The bridge angle Be—C—Be in dimethylberyllium is 66°, and even with this small angle the Be—Be distance is somewhat greater than the single bond distance.[3] With only 1s electrons below the valence shell there is probably little Be—Be repulsion at this distance. In trimethylaluminum the Al—C—Al angle is 70°, and this slightly larger bridge angle still leaves the Al—Al distance essentially equal to the single bond distance. Recent discussion of the lessened tendency for double bond formation in this and higher rows of the periodic table depend in part upon inner shell repulsions for distances shorter than single bond distances.[30] It is probably this factor that leads to a larger bridge angle in the aluminum than in the beryllium compound. For gallium and indium this effect should be increased. According to literature reports,[26,31] which contain discrepancies, it seems likely that trimethylgallium forms a weak dimer at low temperatures, but is essentially completely dissociated at higher temperatures. Trimethylindium has been reported to be a tetramer at low temperatures and a monomer at higher temperatures. It seems possible that the bridge geometry becomes rather unstable for trimethylgallium and completely unstable for trimethylindium. Since use of all low energy orbitals through delocalization of bonds should still be energetically profitable, another geometry requiring a tetramer may be found. It is noteworthy that these considerations suggest that methyl bridges of the type discussed above should always become unstable for metal atoms of large radii and large inner shell repulsions. It is noteworthy that tetramethylplatinum uses bridging methyl groups in another manner, forming a tetramer.[28]

The structure as found explains quite well the failure of Pitzer and Gutowsky[2] to find a dimer for trialkylaluminum molecules in which there was less than two hydrogens on the bridge carbon. Models show that the best possible arrangement in such cases would put carbons of the bridge alkyl groups within 1.8A of nonbridged alkyl groups. Other interactions also become very unfavorable. The effect is entirely understandable from steric considerations.

Pitzer and Gutowsky[2] pointed out that Raman data indicate a loss in symmetry in going from the aluminum trichloride dimer to the trimethylaluminum dimer. Our data indicate that within our experimental error the skeletal structure of the methyl dimer has D_{2h} symmetry, the highest possible symmetry for this molecule. To have this symmetry all methyl groups would have to be rotating or statistically arranged so as to achieve this symmetry. Nothing is known about barriers to rotation of bridge methyl groups, and it is quite possible that Pitzer and Gutowsky could be right about the lower symmetry without the skeletal structure being involved.

[28] R. E. Rundle and J. H. Sturdivant, J. Am. Chem. Soc. **69**, 1561 (1947).
[29] H. C. Longuet-Higgins and R. Bell, J. Chem. Soc. **1943**, 250.
[30] K. S. Pitzer, J. Am. Chem. Soc. **70**, 2140 (1948).
[31] L. M. Dennis and W. Patnode, J. Am. Chem. Soc. **54**, 182 (1932); Dennis, Work, Rockow, and Chamot, J. Am. Chem. Soc. **56**, 1047 (1934).

The Reactions of Methyl Radicals with the Hydrogen Isotopes

E. WHITTLE* AND E. W. R. STEACIE
Division of Pure Chemistry, National Research Council, Ottawa, Canada
(Received November 25, 1952)

The photolysis of acetone has been studied in the temperature range 130–420°C. Measurements have been made of the rates of most of the possible reactions of CH_3 and CD_3 radicals with hydrogen, deuterium, and deuterium hydride. The following activation energies for the abstraction of a hydrogen or deuterium atom have been found: CH_3+acetone, 9.7; CD_3+*d* acetone, 11.6; CH_3+D_2, 11.8; CD_3+H_2, 11.1; $CH_3+HD\rightarrow CH_4$, 10.0; $CH_3+HD\rightarrow CH_3D$, 11.3; $CD_3+HD\rightarrow CD_3H$, 10.7; $CD_3+HD\rightarrow CD_4$, 10.7 kcal. The steric factors are all of the order of 10^{-3}. The results are discussed in terms of isotope effects with particular reference to the deuterium hydride reactions.

INTRODUCTION

IT is now well established that in the photolysis of acetone between 125°C and 300°C the formation of methane and ethane occurs in the following manner:

$$CH_3COCH_3\rightarrow 2CH_3+CO \quad (1)$$

$$CH_3+CH_3\rightarrow C_2H_6 \quad (2)$$

$$CH_3+CH_3COCH_3\rightarrow CH_4+CH_2COCH_3. \quad (3)$$

If the concentration of methyl radicals does not change during the reaction, it can be shown that

$$\frac{k_3}{k_2^{\frac{1}{2}}}=\frac{(R_{CH_4})_3}{R_{C_2H_6}^{\frac{1}{2}}[Ac]},$$

where $(R_{CH_4})_3$ is the rate of production of methane by reaction (3) and [Ac] is the concentration of acetone.

If the photolysis is carried out in the presence of hydrogen, methane is also produced by the reaction

$$CH_3+H_2\rightarrow CH_4+H \quad (4)$$

so that

$$\frac{k_4}{k_2^{\frac{1}{2}}}=\frac{(R_{CH_4})_4}{R_{C_2H_6}^{\frac{1}{2}}[H_2]}.$$

$(R_{CH_4})_4$ is found from the equation

$$R_{CH_4}(\text{total})=(R_{CH_4})_4+(R_{CH_4})_3.$$

$(R_{CH_4})_3$ is calculated from data obtained for the photolysis of acetone alone. If deuterium is used we have, instead of reaction (4),

$$CH_3+D_2\rightarrow CH_3D+D. \quad (5)$$

The rate of production of CH_3D can be found by subtracting $(R_{CH_4})_3$ from the total methane or can be estimated directly by means of mass spectrometric analysis, in which case

$$\frac{k_5}{k_2^{\frac{1}{2}}}=\frac{k_3}{k_2^{\frac{1}{2}}}\cdot\frac{R_{CH_3D}}{R_{CH_4}}\cdot\frac{[Ac]}{[D_2]}.$$

The two procedures will henceforth be called Method I and Method II, respectively, and should not be confused with the two methods referred to by Trotman-Dickenson and Steacie.[1] The Method I of these authors is identical with that used here, but their Method II refers to the use of heavy acetone instead of ordinary acetone. The reactions mentioned above have been studied by Majury and Steacie,[2] and we have extended their work and also studied the reactions of deuterium hydride. In this case the methyl radical may react in two ways,

$$CH_3+HD\rightarrow CH_4+D \quad (6)$$

$$CH_3+HD\rightarrow CH_3D+H. \quad (7)$$

$(R_{CH_3D})_7$ is found directly by mass spectrometric analysis and $(R_{CH_4})_6$ is obtained by Method I.

Materials

The purification of the acetone and preparation of the deuterated acetone have been described previously.[2] The composition of the latter was determined by the mass spectrometer with the following results:

93.7 percent C_2D_6CO, 3.5 percent C_2D_5HCO,
2.8 percent $C_2D_4H_2CO$.

Commercial cylinder hydrogen and deuterium were purified by passage through a palladium thimble. The deuterium contained 5 percent HD. The deuterium hydride was prepared from lithium aluminum hydride and heavy water as described by Fookson, Pomerantz,

TABLE I. The photolysis of acetone at high temperatures.

Run	Temp °K	Time (sec)	Molecules acetone/cc $\times 10^{-18}$	Products in molecules/cc/sec $\times 10^{-13}$ CO	CH_4	C_2 fraction	% C_2H_6	% C_2H_4
100	558	1200	1.78	7.40	8.75	1.04	100	0
101	600	1230	1.64	7.68	10.4	0.556	67	33
102	628	1200	1.52	8.61	12.0	0.530	...	...
103	662	1200	1.48	9.79	14.0	0.630	...	...
104	688	905	1.42	11.0	16.5	1.00	20	80

* National Research Council of Canada Postdoctorate Fellow, 1951–1952.

[1] A. F. Trotman-Dickenson and E. W. R. Steacie, J. Chem. Phys. **19**, 163 (1951).
[2] T. G. Majury and E. W. R. Steacie, Disc. Faraday Soc. (to be published); Can. J. Chem. **30**, 800 (1952).

TABLE II. The photolysis of acetone in the presence of deuterium.

Run	Temp °K	Time (sec)	Molecules acetone/cc $\times 10^{-18}$	Molecules D_2/cc $\times 10^{-12}$	Molecules/cc/sec $\times 10^{-13}$ CO	Methane	C_2H_6	$\frac{CH_3D}{CH_4}$	$k_3/k_2^{\frac{1}{2}} \times 10^{13}$ Method I	Method II
	10 cm acetone		5 cm deuterium							
16	411	1800	2.33	1.16	5.62	1.19	4.41	0.0622		0.843
15	413	1800	2.28	1.16	5.86	1.27	4.63	0.0635		0.891
17	450	1800	2.15	1.09	5.55	2.48	3.33	0.0816		3.07
18	480	1800	2.04	1.16	5.62	3.95	2.40	0.108		7.09
19	522	1800	1.85	0.914	5.85	5.95	1.24	0.102		19.7
20	522	1800	1.95	0.972	5.96	6.49	1.16	0.104		17.8
21	563	1800	1.81	0.776	5.81	7.38	—	0.107		40.7
	10 cm acetone		20 cm deuterium							
27	410	1800	2.38	4.80	5.25	1.38	3.92	0.266	1.15	0.917
26	411	1800	2.35	4.80	7.46	1.40	4.00	0.231	1.10	0.812
25	462	1740	2.05	4.30	7.15	3.62	2.32	0.331	4.73	4.22
24	512	1800	1.89	3.65	6.92	5.92	0.985	0.411	13.7	15.6
22	564	1800	1.74	3.45	6.82	7.44	0.494	0.599	···	48.8
	5 cm acetone		10 cm deuterium							
32	408	1800	1.15	2.42	3.26	0.503	2.51	0.262	0.781	0.882
28	409	1800	1.17	2.38	3.22	0.513	2.61	0.239	0.892	0.852
29	456	1800	1.08	2.12	3.24	1.40	1.87	0.352	3.01	4.46
37	505	1800	0.984	1.96	3.38	2.81	0.978	0.383	11.2	13.3
30	508	1830	0.936	1.88	3.36	2.91	1.01	0.431	11.6	15.9
31	560	1800	0.886	1.74	3.29	4.22	0.378	0.515	33.4	46.9

and Rich.[3] Several samples were made and the average composition was found to be 94 percent HD, 4 percent H_2, and 2 percent D_2.

EXPERIMENTAL

Details of the apparatus and method of analysis have been given previously.[2] Most of the large excess of hydrogen was removed from the gaseous reaction products by compression of the mixture on to a palladium thimble at 370°C. In the experiments with acetone plus deuterium, one analysis (run 37) was made using liquid hydrogen to condense all the gases but deuterium, which was then pumped off. No change in the results was observed.

The mass spectrometer analyses were done under the direction of Dr. Lossing of these laboratories. The analyses for the $CD_4-CD_3H-CD_2H_2$ mixtures were computed assuming equal sensitivities for the isotopic molecules and using the spectra of the deuterated methanes given by Dibeler and Mohler.[4]

Nearly all the experiments were carried out to a 5 percent conversion of acetone or less. The activation energies were obtained directly by Arrhenius plots. The steric factors were then calculated by subtraction of $\frac{1}{4}RT$ from the activation energies, the mean temperature being taken as 490°K. The collision diameters used for the various molecules were acetone 5.5A, CH_3 3.5A, and H_2 2.8A.

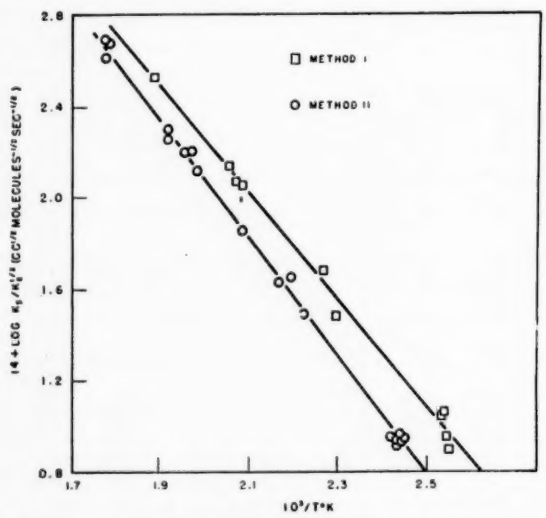

FIG. 1. Acetone plus deuterium. To avoid confusion the values of $10^3/T$ have been increased by 0.1 unit for the points marked □.

[3] Fookson, Pomerantz, and Rich, J. Research Natl. Bur. Standards **47**, 31 (1951).

The Photolysis of Acetone

The photolysis of acetone was examined in the temperature range 135–300°C and at pressures of 20 and 100 mm. The results obtained were in full agreement with those of previous workers; the value of $E_3-\frac{1}{2}E_2$ was found to be 9.7 kcal.

The photolysis was also studied in the temperature range 300–420°C, since very few experiments have been carried out in this region. The results are given in Table I. It was found that ethylene begins to form at temperatures higher than 300°C, and at 420°C it accounts for almost all the C_2 hydrocarbon produced. The ethylene could be formed by the photolysis of ketene, since the latter was found by Ferris and Haynes[5] in the high temperature photolysis of acetone. It seems clear that the photolysis becomes complicated above 300°C and that experiments which utilize acetone as a source of methyl radicals should preferably be carried out below this temperature.

[4] V. H. Dibeler and F. L. Mohler, J. Research Natl. Bur. Standards **45**, 441 (1950).

[5] R. C. Ferris and W. S. Haynes, J. Am. Chem. Soc. **72**, 893 (1950).

The Photolysis of *d* Acetone

The principal reactions occurring during the photolysis of *d*-acetone are

$$CD_3+CD_3\rightarrow C_2D_6 \quad (8)$$

$$CD_3+CD_3\cdot CO\cdot CD_3\rightarrow CD_4+CD_2\cdot CO\cdot CD_3. \quad (9)$$

The photolysis has been studied by Majury and Steacie[2] who found that $E_9-\frac{1}{2}E_8=10.6$ kcal. We have performed further experiments using a new sample of *d*-acetone and from an Arrhenius plot it is found that

$$13+\log\frac{k_9}{k_8^{\frac{1}{2}}}=6.20-\frac{2530}{T}.$$

It follows that $E_9-\frac{1}{2}E_8=11.6$ kcal and $P_9/P_8^{\frac{1}{2}}=3.3\times10^{-3}$, where P denotes the steric factor for a reaction.

The value of $E_9-\frac{1}{2}E_8=10.6$ kcal given by Majury and Steacie was based on an Arrhenius plot which tended to curve at lower temperatures. In the present work no such curvature was obtained, and so the higher value is felt to be somewhat more reliable. In the upper part of the temperature range, both sets of results agreed very well.

The Photolysis of Acetone with Deuterium

It was mentioned in the introduction that the rate of production of CH_3D by the reaction

$$CH_3+D_2\rightarrow CH_3D+D \quad (5)$$

can be determined by two methods. The results calculated by the two methods together with the experimental data obtained are given in Table II and are shown graphically in Fig. 1. A correction has been made for the presence of 5 percent HD in the deuterium. No CH_2D_2 could be detected. In the experiments in which 10 cm acetone and 5 cm D_2 were used, the calculation by Method I has not been given since the results are quite unreliable owing to the fact that the CH_4 produced by reaction (3) represents about 90 percent of the total methane.

The lines obtained from the Arrhenius plots have the following equations:

Method I	Method II
$13+\log\frac{k_5}{k_2^{\frac{1}{2}}}=5.69-\frac{2340}{T}$	$13+\log\frac{k_5}{k_2^{\frac{1}{2}}}=6.22-\frac{2570}{T}$
$E_5-\frac{1}{2}E_2=10.7$ kcal	$E_5-\frac{1}{2}E_2=11.8$ kcal
$P_5/P_2^{\frac{1}{2}}=1.0\times10^{-3}$	$P_5/P_2^{\frac{1}{2}}=3.5\times10^{-3}$

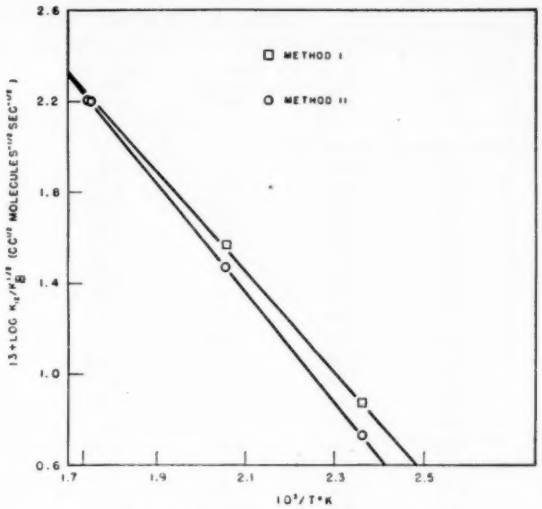

FIG. 2. *d*-acetone plus hydrogen.

The value of $E_5-\frac{1}{2}E_2$ found by Method II is identical with that found by Majury and Steacie.[2]

The Photolysis of *d*-Acetone in the Presence of Hydrogen

The methane formed in this system consists of CD_4 from reaction (9) and CD_3H from the reaction

$$CD_3+H_2\rightarrow CD_3H+H \quad (10)$$

so that the rate constant can again be calculated in two ways. The results are given in Table III, and the Arrhenius plots are shown in Fig. 2. The equations of the lines are

Method I	Method II
$13+\log\frac{k_{10}}{k_8^{\frac{1}{2}}}=6.10-\frac{2220}{T}$	$13+\log\frac{k_{10}}{k_8^{\frac{1}{2}}}=6.44-\frac{2420}{T}$
$E_{10}-\frac{1}{2}E_8=10.1$ kcal	$E_{10}-\frac{1}{2}E_8=11.1$ kcal
$P_{10}/P_8^{\frac{1}{2}}=1.84\times10^{-3}$	$P_{10}/P_8^{\frac{1}{2}}=4.10\times10^{-3}$

We have described how the rate constants for the reactions CH_3+D_2 and CD_3+H_2 may be calculated by two methods. In both cases the use of Method I leads to lower steric factors and activation energies than Method II. It seems likely that Method II is the more reliable since it depends on a direct determination of the CH_3D/CH_4 ratio, whereas the ratio is calculated

TABLE III. The photolysis of *d*-acetone in the presence of hydrogen.

Run	Temp °K	Time sec	Molecules *d* acetone/cc ×10⁻¹⁸	Molecules H_2/cc ×10⁻¹⁸	Molecules/cc/sec ×10⁻¹³ CO	methane	ethane	% CD_4	% CD_3H	% CD_2H_2	% C_2D_6 in ethane	$k_{10}/k_8^{\frac{1}{2}}\times10^{13}$ Method I	Method II
10 cm *d*-acetone, 10 cm H_2													
75	424	1800	2.27	2.37	3.48	1.18	2.59	21.1	69.9	9.1	96.3	7.22	5.34
76	487	1800	1.95	2.07	3.52	3.62	1.28	21.9	68.5	9.7	95.8	36.8	29.4
77	573	1890	1.60	1.77	3.73	...	0.294	23.4	67.4	9.2	...	...	159
78	570	1862	1.58	1.76	3.63	6.16	0.272	24.7	73.2	2.1	...	158	157

TABLE IV. The photolysis of acetone in the presence of deuterium hydride.

Run	Temp °K	Time sec	Molecules acetone/cc $\times 10^{-18}$	Molecules HD/cc $\times 10^{-18}$	Molecules/cc/sec $\times 10^{-13}$ CO	methane	C_2H_6	$\frac{CH_3D}{CH_4}$	$\frac{k_6}{k_2^{\frac{1}{2}}} \times 10^{13}$	$\frac{k_7}{k_2^{\frac{1}{2}}} \times 10^{13}$
	10 cm acetone, 10 cm HD									
43	408	1200	2.42	2.40	5.60	1.48	4.09	0.0624		0.531
86	418	1200	2.30	2.34	3.39	1.27	2.23	0.0718		0.812
47	424	1200	2.30	2.35	4.45	1.70	2.85	0.0722		0.988
45	454	1200	2.18	2.21	4.70	2.91	2.19	0.0805		2.13
51	469	1200	1.02	1.01	2.43	1.59	1.07	0.0816		3.93
50	472	1200	2.11	2.09	4.36	3.69	1.34	0.0906		4.33
52	474	1200	2.18	1.02	2.57	2.06	0.927	0.147		4.29
53	478	1200	2.03	2.03	4.11	3.66	1.17	0.0918		4.79
84	503	1214	1.94	1.92	3.51	4.07	0.626	0.0946		7.68
41	503	1200	1.95	1.83	5.77	5.49	1.20	0.0978		8.03
48	527	900	1.84	1.89	4.42	5.78	0.533	0.108		14.0
49	564	1200	1.71	1.66	4.33	6.58	0.268	0.130		30.2
42	569	1200	1.72	1.57	6.10	8.00	0.405	0.114		27.1
88	569	1200	1.73	1.70	3.64	5.56	0.178	0.113		26.2
	4 cm acetone 16 cm HD									
80	413	1800	0.942	3.67	1.81	0.572	1.24	0.183	1.51	0.714
87	414	2430	0.937	3.61	1.76	0.585	1.23	0.180	1.66	0.747
107	442	1800	0.860	3.50	3.63	1.56	2.27	0.226	3.21	1.82
90	471	1835	0.819	3.38	1.66	1.47	0.535	0.241	6.60	3.87
85	504	2400	0.756	3.06	1.78	2.17	0.315	0.254	15.2	8.54
96	506	2400	0.776	3.13	1.54	1.95	0.230	0.239	15.7	8.27
91	538	1800	0.730	2.89	1.94	2.62	0.166	0.270	23.9	16.0
89	569	2400	0.677	2.67	1.88	2.97	0.112	0.287	30.9	24.8

indirectly in Method I. The difference in the results of the two methods implies that the data obtained on the rate of reaction (3) from the photolysis of acetone alone are not strictly correct if other substances are present. It is known that the ratio $k_3/k_2^{\frac{1}{2}}$ varies slightly with pressure and this is one possible explanation of the discrepancy.

In the determination of the rate constant for the reaction

$$CH_3+HD \rightarrow CH_4+D \qquad (6)$$

we wish to know $(R_{CH_4})_3$ as accurately as possible in order to calculate the value of $(R_{CH_4})_6$. We therefore need to know the rate of reaction (3) in the presence of deuterium hydride. It is reasonable to suppose that, if the acetone photolysis is affected slightly by the presence of deuterium, it should be changed to about the same extent by the presence of deuterium hydride. From experiments on the photolysis of acetone with deuterium, we can find $(R_{CH_4})_3$ by mass spectrometric analysis and hence carry out an Arrhenius plot of $k_3/k_2^{\frac{1}{2}}$. Because of the discrepancy between Method I and Method II, the line obtained with a given pressure of acetone mixed with deuterium is not the same as the line obtained from acetone alone. Expressing the equations in the form $13+\log k_3/k_2^{\frac{1}{2}}=A-B/T$, we have

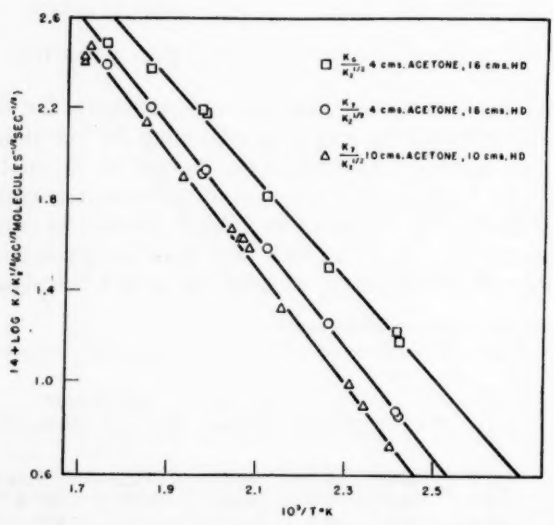

FIG. 3. Acetone plus deuterium hydride. The values of $10^3/T$ have been decreased by 0.05 unit for the points marked △.

	A	B
5 cm acetone	6.02	2120
5 cm acetone+10 cm D_2	5.92	2080
10 cm acetone	5.96	2110
10 cm acetone+20 cm D_2	5.72	1990

The same procedure has been used with *d*-acetone, but in this case the results obtained in the presence of hydrogen are used. The equations are

$$13+\log\frac{k_9}{k_8^{\frac{1}{2}}}=6.20-\frac{2530}{T} \quad \text{10 cm } d\text{-acetone},$$

$$13+\log\frac{k_9}{k_8^{\frac{1}{2}}}=5.88-\frac{2350}{T} \quad \text{10 cm } d\text{-acetone+10 cm } H_2.$$

The corrected data given here have been used in the calculation of the results of the deuterium hydride experiments.

The Photolysis of Acetone in the Presence of Deuterium Hydride

In this case, methane is produced by reaction (3) and by two other processes which are

$$CH_3+HD\rightarrow CH_4+D \quad (6)$$

$$CH_3+HD\rightarrow CH_3D+H. \quad (7)$$

The results of the experiments are given in Table IV. No CH_2D_2 was found in the methane. The rate of production of CH_3D is determined unambiguously by mass spectrometer while $(R_{CH_4})_6$ is obtained by subtracting $(R_{CH_4})_3$ from the total CH_4 which is also found by mass spectrometer. The correction $(R_{CH_4})_3$ is quite large and, as expected, the values of $k_6/k_2^{\frac{1}{2}}$ show considerable scatter. Corrections have been applied for the products of the reaction of methyl radicals with the small amounts of H_2 and D_2 present in the HD.

Two series of experiments were carried out, one using 10 cm acetone and 10 cm HD, and the other with 4 cm acetone and 16 cm HD. From the first series only the rate constants for reaction (7) have been calculated, since $(R_{CH_4})_6$ is small and cannot be reliably estimated. The Arrhenius plots are shown in Fig. 3, and the equations of the lines are given below. Using 10 cm acetone +10 cm HD

$$13+\log\frac{k_7}{k_2^{\frac{1}{2}}}=5.92-\frac{2520}{T} \qquad E_7-\tfrac{1}{2}E_2=11.5 \text{ kcal}$$

$$\frac{P_7}{P_2^{\frac{1}{2}}}=1.53\times10^{-3}. \quad (8)$$

Using 4 cm acetone and 16 cm HD,

$$13+\log\frac{k_6}{k_2^{\frac{1}{2}}}=5.48-\frac{2180}{T} \qquad E_6-\tfrac{1}{2}E_2=10.0 \text{ kcal}$$

$$P_6/P_2^{\frac{1}{2}}=0.55\times10^{-3} \quad (9)$$

$$13+\log\frac{k_7}{k_2^{\frac{1}{2}}}=5.73-\frac{2430}{T} \qquad E_7-\tfrac{1}{2}E_2=11.1 \text{ kcal}$$

$$P_7/P_2^{\frac{1}{2}}=0.98\times10^{-3}. \quad (10)$$

The Photolysis of *d*-Acetone in the Presence of Deuterium Hydride

The photolysis produces methane containing CD_4, CD_3H, and CD_2H_2. The reactions forming CD_4 and CD_3H are (9), and

$$CD_2H+CD_3\cdot CO\cdot CD_3\rightarrow CD_3H+CD_2\cdot CO\cdot CD_3 \quad (11)$$

$$CD_3+HD\rightarrow CD_3H+D \quad (12)$$

$$CD_3+HD\rightarrow CD_4+H. \quad (13)$$

$(R_{CD_4})_{13}$ is calculated in the usual way using Method I. $(R_{CD_3H})_{12}$ is found by subtracting from the total CD_3H the small amount formed by reaction (11) which can easily be estimated. The experimental results are given in Table V, and the Arrhenius plots for $k_{12}/k_8^{\frac{1}{2}}$ and $k_{13}/k_8^{\frac{1}{2}}$ are shown in Fig. 4. From the graphs it is found that

$$13+\log\frac{k_{12}}{k_8^{\frac{1}{2}}}=5.86-\frac{2340}{T} \qquad 13+\log\frac{k_{13}}{k_8^{\frac{1}{2}}}=5.63-\frac{2340}{T}$$

$$E_{12}-\tfrac{1}{2}E_8=10.7 \text{ kcal} \qquad E_{13}-\tfrac{1}{2}E_8=10.7 \text{ kcal}$$

$$P_{12}/P_8^{\frac{1}{2}}=1.26\times10^{-3} \qquad P_{13}/P_8^{\frac{1}{2}}=0.75\times10^{-3}.$$

The CD_2H_2 is produced by the reaction

$$CD_2H+HD\rightarrow CD_2H_2+D. \quad (14)$$

The relative rates of reactions (12) and (14) are given by

$$\frac{(R_{CD_3H})_{12}}{(R_{CD_2H_2})_{14}}=\frac{k_{12}[CD_3][HD]}{k_{14}[CD_2H][HD]}.$$

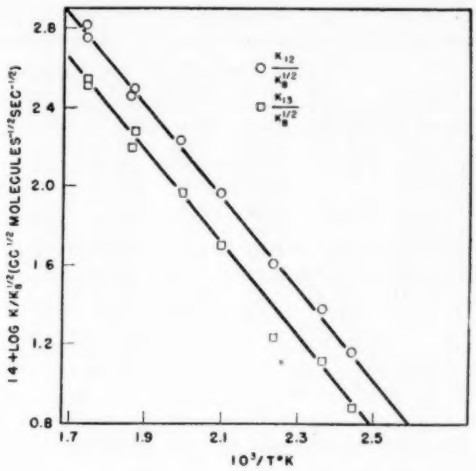

FIG. 4. *d*-acetone plus deuterium hydride.

TABLE V. The photolysis of *d*-acetone in the presence of deuterium hydride.

Run	Temp °K	Time sec	Molecules *d* acetone/cc $\times10^{-18}$	Molecules HD/cc $\times10^{-19}$	Molecules/cc/sec $\times10^{-13}$ CO	methane	ethane	% CD_4	% CD_3H	% CD_2H_2	% C_2D_6 in ethane	$\frac{k_{12}}{k_8^{\frac{1}{2}}}\times10^{13}$	$\frac{k_{13}}{k_8^{\frac{1}{2}}}\times10^{13}$
10 cm *d* acetone, 10 cm HD													
106	410	1205	2.33	2.45	6.99	0.783	6.28	50.0	43.3	6.7	—	1.44	0.757
74	423	1800	2.21	2.17	3.94	0.752	2.74	52.1	44.9	2.9	96.5	2.38	1.30
64	448	1200	2.14	2.21	3.76	1.35	2.94	50.9	42.2	6.9	96.6	4.02	1.70
65	477	1200	1.99	1.93	4.00	2.51	2.28	52.3	40.7	7.0	96.5	9.08	4.98
67	502	1229	1.88	1.90	3.89	3.53	1.52	51.5	41.7	6.8	96.2	17.1	9.20
69	534	1200	1.74	1.72	4.27	4.89	1.19	54.4	39.8	5.8	95.7	31.1	19.0
72	537	1860	1.71	1.73	3.97	4.22	0.830	54.9	40.0	5.1	95.0	28.7	15.7
71	572	1200	1.63	1.64	4.04	5.96	0.423	52.1	42.0	5.9	94.2	66.5	34.7
73	572	1800	1.65	1.61	4.00	5.43	0.416	55.4	39.2	5.5	93.0	56.7	32.7

TABLE VI.

	Reaction	$k_A/k_B^{\frac{1}{2}}\times10^{13}$ 130°C	210°C	290°C	$P_A/P_B^{\frac{1}{2}}\times10^3$	$E_A-\frac{1}{2}E_B$ kcal
(3)	$CH_3+CH_3COCH_3$	5.35	39.4	164	1.8	9.7
(9)	$CD_3+CD_3COCD_3$	0.822	9.04	50.2	3.3	11.6
(5)	$CH_3+D_2\rightarrow CH_3D$	0.689	7.85	44.9	3.5	11.8
(4)[a]	CH_3+H_2	3.3	22	87	1.6	10.0
(10)	$CD_3+H_2\rightarrow CD_3H$	2.68	26.5	137	4.1	11.1
[b]	CD_3+D_2	0.9	8.9	46	2.0	10.9
(6)	$CH_3+HD\rightarrow CH_4$	1.16	9.12	40.0	0.55	10.0
(7)	$CH_3+HD\rightarrow CH_3D$	0.497	5.09	27.0	1.2	11.3
(12)	$CD_3+HD\rightarrow CD_3H$	1.15	10.4	51.2	1.3	10.7
(13)	$CD_3+HD\rightarrow CD_4$	0.655	6.00	29.3	0.75	10.7

[a] Majury and Steacie's value corrected as indicated below.
[b] Majury and Steacie's value.

From the ethane analysis we can estimate that $CD_3/CD_2H=95/5$ so that

$$\frac{k_{14}}{k_{12}}=\frac{6}{40}\times\frac{95}{5}\approx 2.5.$$

This result implies that CD_2H radicals abstract hydrogen from HD more readily than do CD_3 radicals provided that the rates of the recombination reactions

$$CD_3+CD_3\rightarrow C_2D_6$$
$$CD_3+CD_2H\rightarrow C_2D_5H$$

are not appreciably different. This enhanced reactivity of CD_2H radicals was also observed by Majury and Steacie, when hydrogen abstraction from the molecules H_2 and $CD_3\cdot CO\cdot CD_3$ was involved.

DISCUSSION

Before discussing the results which have been obtained, it is necessary to establish the validity of the reaction mechanism which has been assumed. In particular it is necessary to consider the possibility of exchange reactions. It is found that no exchange occurs if a mixture of D_2 and CH_4 is left in contact with a palladium thimble at 370°C for two hours or if the mixture is heated to 300°C in a furnace. Deuterium hydride rapidly equilibrates in contact with a hot palladium thimble but does not exchange with CH_4.

The fate of the hydrogen atoms produced by reactions such as (6) and (7) is of great importance. It is assumed that they are removed by the reactions

$$H+CH_3COCH_3\rightarrow H_2+CH_2COCH_3 \quad (15)$$
$$D+CH_3COCH_3\rightarrow HD+CH_2COCH_3. \quad (16)$$

The accumulation of H_2 from reaction (15) is prevented by the use of small conversions. The hydrogen atoms could also bring about equilibration of the HD if their stationary concentration were sufficiently high. This may actually occur to a small extent since the average composition of the gas before a run was 94 percent HD, 4 percent H_2, 2 percent D_2 and after a run was 90 percent HD, 8 percent H_2, and 2 percent D_2.

Serious complications would occur if the hydrogen atoms reacted with the radicals present; for example,

$$CH_3+D\rightarrow CH_2D+H \quad (17)$$
$$CH_3+D\rightarrow CH_3D. \quad (18)$$

If reaction (17) occurred, some of the CH_2D radicals produced would eventually form CH_3CH_2D, but no trace of this was found in experiments with acetone and D_2 or HD. The possibility of the occurrence of reaction (18) was considered by Majury and Steacie.[2] They suggested that the reaction would probably require a third body and demonstrated that no change occurred in the photolysis of *d* acetone with hydrogen if carbon dioxide were added. It is also possible to eliminate reaction (18) from considerations of the stationary concentrations of the species observed. We wish to prove that all the hydrogen atoms react with acetone rather than methyl radicals and therefore require the relative rates of the two processes. To take the most unfavorable case, it is assumed that reaction (18) occurs at every collision and does not require a third body. It is easily seen that

$$\frac{(R_{HD})_{16}}{(R_{CH_3D})_{18}}=\frac{k_{16}[Ac]}{k_{18}[CH_3]}.$$

The value of $[CH_3]$ can be roughly estimated from the fact that $R_{C_2H_6}=k_2[CH_3]^2$, and recent work indicates that k_2 is of the order of 2×10^{-11} cc/molecule/sec. k_{16} can be estimated from the data of Harris and Steacie[6] assuming a low steric factor, since this is least favorable to our argument. It is found that at 130°C, $R_{16}/R_{18}\approx300$ and at 300°C the ratio is several thousand. Although this calculation is only approximate, it shows fairly conclusively that reaction (18) does not occur.

The results obtained for the various reactions are summarized in Table VI together with additional data obtained by Majury and Steacie. k_A, E_A, and P_A refer to the reaction between a methyl radical and the molecules concerned, while k_B, A_B, and P_B refer to the recombination of methyl radicals.

All the activation energies which have been measured are found to lie within the range 10–12 kcal, and the steric factors are of the order of 10^{-3}. There has recently been considerable discussion[7] as to whether the reaction of methyl radicals with hydrogen has an activation energy of about 14 kcal and a steric factor of 10^{-1} or an activation energy of about 10 kcal and a steric factor of about 10^{-3}. The latter value is favored by the present work. Majury and Steacie have measured the activation energy for the reaction $CH_3+H_2\rightarrow CH_4+H$ and obtained a value of 9.2 kcal. This is based on a Method I type of calculation, and consequently their results may perhaps be about 1 kcal low. A value of 10

[6] G. M. Harris and E. W. R. Steacie, J. Chem. Phys. **13**, 554 (1945).
[7] Discussions Faraday Soc. (to be published).

kcal would be more consistent with the present work, since it is unlikely that the two reactions CH_3+H_2 and CH_3+D_2 have a difference in activation energies which is greater than the difference between the zero-point energies of H_2 and D_2. If the activation energy of 10 kcal is accepted, then the value of $P_A/P_B^{\frac{1}{2}}$ becomes 1.6×10^{-3}.

Further evidence for an activation energy of 10 kcal is provided by the work of Phibbs and Darwent[8] on the photolysis of mercury dimethyl in the presence of hydrogen. From their results it is possible to plot $\log k_4/k_2^{\frac{1}{2}}$ against $1/T$ and thus correct for variations in the stationary concentration of methyl radicals. It is found that $E_4-\frac{1}{2}E_2=9.9$ kcal and $P_4/P_2^{\frac{1}{2}}=0.6\times10^{-3}$, which are in excellent agreement with the data given in Table VI.

Majury and Steacie found that the rate constants for reactions involving methyl radicals and H_2 or D_2 were changed very little if CH_3 were replaced by CD_3. For example, the following ratios of rate constants at 210°C were found:

$$\frac{CH_3+H_2}{CD_3+H_2}=0.71 \qquad \frac{CH_3+D_2}{CD_3+D_2}=0.74.$$

We have observed a similar phenomenon in the case of deuterium hydride where the corresponding ratios are

$$\frac{CH_3+HD\rightarrow CH_4}{CD_3+HD\rightarrow CD_3H}=0.88 \qquad \frac{CH_3+HD\rightarrow CH_3D}{CD_3+HD\rightarrow CD_4}=0.85.$$

A comparison of the rates of the various deuterium hydride reactions reveals the interesting fact that hydrogen abstraction is about twice as rapid as deuterium abstraction. This is shown by the following ratios of rate constants at 210°C:

$$\frac{CH_3+HD\rightarrow CH_4}{CH_3+HD\rightarrow CH_3D}=1.73 \qquad \frac{CD_3+HD\rightarrow CD_3H}{CD_3+HD\rightarrow CD_4}=1.79.$$

A similar conclusion was reached by Farkas and Farkas[9] in their work on the reactions of hydrogen and deuterium atoms with the hydrogen isotopes.

In the case of CH_3 radicals this difference in rates of hydrogen and deuterium abstraction appears as a difference in the activation energies; if CD_3 radicals are used, we find different steric factors and identical activation energies. The discrepancy is probably due to experimental error, since it is unlikely that there is really such a difference in behavior of the two radicals. For this reason we have compared rate constants rather than activation energies or steric factors.

It is interesting to compare the rates of reactions (6) and (7) in terms of the transition state theory, since the treatment is simplified by the fact that the initial reactants are the same in each case. Some of the terms in the partition functions of the transition states CH_3-H-D and CH_3-D-H such as the translational contributions are also identical. In view of the large frequencies involved, the vibrational partition functions of the two complexes should be almost equal; if a difference does exist it should be in a direction favoring CH_3D formation. The rotational contributions of the two states, however, are not the same, since the moment of inertia of the structure $CH_3\cdots H\cdots D$ is obviously larger than that of $CH_3\cdots D\cdots H$. The ratio of the two moments can be calculated approximately by means of the transition state dimensions given by Glasstone, Laidler, and Eyring.[10] It is found that

$$\frac{I(CH_3\cdots H\cdots D)}{I(CH_3\cdots D\cdots H)}=1.5.$$

The ratio is surprisingly large and almost completely accounts for the preferential formation of CH_4.

These considerations suggest that the difference in rate constants for hydrogen and deuterium atom abstraction is mainly due to a difference in steric factor rather than activation energy. If this is so, it implies that the two transition states have almost identical zero-point energies.

[8] M. K. Phibbs and B. de B. Darwent, Trans. Faraday Soc. 45, 541 (1949).

[9] A. Farkas and L. Farkas, Proc. Roy. Soc. (London) **A152**, 124 (1935).

[10] Glasstone, Laidler, and Eyring, *The Theory of Rate Processes* (McGraw-Hill Book Company, Inc., New York, 1941), p. 257.

The Photochemical Decomposition of Benzene

G. E. GIBSON, NORMAN BLAKE, AND MAX KALM
Department of Chemistry and Chemical Engineering, University of California, Berkeley, California
(Received December 17, 1952)

Under intense ultraviolet illumination with an A-H6 mercury arc, benzene solutions in rigid glass at liquid air temperatures are decomposed. If the solvent molecules contain hydrogen, hexatriene is formed (almost certainly identified by absorption spectrum and chemical behavior). In a solvent (perfluoro-2-methyl pentane) containing no hydrogen, the benzene decomposes to an entirely different product, not as yet certainly identified.

NAUMAN[1] found that when a sample of benzene in E.P.A. (5 parts ether, 5 parts isopentane, and 2 parts ethanol) was exposed to ultraviolet light at −195.8°C for a period of an hour or longer, one could notice a decrease in the phosphorescence intensity with time. He further found that when the sample was brought to room temperature, refrozen, and again exposed to the ultraviolet radiation, the phosphorescence had gone back to its original intensity. It is the purpose of this paper to present the results of work which has been done in an effort to determine the cause of this decrease in the intensity of the phosphorescence of benzene.

It was necessary at the outset to repeat and confirm Nauman's observations on the behavior of benzene upon exposure to ultraviolet radiation. For this purpose experiments were performed in which a sample of benzene in E.P.A. was exposed to ultraviolet radiation at −195.8°C, and the intensity of phosphorescence observed over a considerable time interval. The observations thus made showed that the phosphorescence intensity decreased as the time of exposure increased. Melting the sample at room temperature and then refreezing in liquid nitrogen brought the phosphorescence back nearly, but not quite, to its original intensity. Repeated exposures with intermittent returns of the sample to room temperature, showed a steady decrease in the maximum value of the phosphorescence intensity. This procedure was repeated with different concentrations of benzene in E.P.A., and it was found that the difference between the original intensity and the intensity after exposure, melting, and re-exposure was greater with more dilute solutions. The results of these experiments indicated that a definite change occurred during the exposure of benzene, and probably that some of the benzene was being converted to another compound, a compound which does not phosphoresce, and which is stable at room temperature. Furthermore, it could be deduced that the reaction which was occurring was an irreversible one.

In an effort to explain the change in the phosphorescence intensity on melting and refreezing the sample, it was reasoned that the photochemical reaction produced a region of nearly opaque material on the front surface of the sample tube, and thus prevented the ultraviolet radiation from any further excitation of the benzene molecules in the solution. On melting, the new substance formed was distributed throughout the bulk of the solution, and the intensity returned to almost its original value, the small permanent change being due mainly to the decrease in the benzene concentration.

One more experiment of this type was performed in which a sample of benzene was again exposed to the ultraviolet radiation until the phosphorescence intensity had dropped quite noticeably, and the sample was then kept at liquid nitrogen temperature for $1\frac{1}{4}$ hours without further irradiation. At the end of this time, the sample was exposed to the ultraviolet light just long enough to measure the phosphorescence intensity, and it was found that the intensity had not changed during this time.

Since a definite change seemed to have taken place in the composition of the solution during the exposure, it became desirable to compare the ultraviolet absorption spectra of this solution before and after esposure. Another sample of benzene in E.P.A. was exposed to the radiation at liquid nitrogen temperature; it was twice melted by bringing to room temperature and was refrozen. The phosphorescence intensity was observed throughout the run; at the end of three exposures the sample was brought to room temperature, and its spectrum was determined with a Cary Spectrophotometer. The comparison of this spectrum with that of the original solution showed that a definite change had occurred in the solution (see Fig. 1), since the extinction coefficient had increased enormously and the structure of the spectrum had changed completely.

The absorption spectrum of this solution was measured at liquid nitrogen temperature with the Hilger Medium Quartz Spectrograph, photographing the absorption spectrum by replacing the exciting mercury A-H6 arc with a Beckman Hydrogen Arc as a light source. It was thus possible to obtain the absorption spectrum of the original solution and then, after exposure to the ultraviolet radiation, to photograph the absorption spectrum again and determine the changes which had taken place during exposure. Two such experiments were made; one using a solution of benzene

[1] R. V. Nauman, Communication in a Seminar on Phosphorescence and the Chemical Constitution of Aromatic Compounds, University of California, 1944.

in IM_4 (4 parts methylcyclohexane and 1 part isopentane) and the other using a solution of benzene in E.P.A. Both of these solvents have been found to form a transparent glass at liquid nitrogen temperature. The same results were obtained with either solvent, the spectra showing the same difference before and after exposure to the ultraviolet radiation. In addition to an increase in the extinction coefficient, there appeared two new bands in the near-ultraviolet region of the spectrum which could not be attributed to benzene.

A solution of benzene in E.P.A. was now exposed to the radiation at room temperature; the spectrum of this solution was compared with the original spectrum, and no change was found to have taken place. It was also shown that exposure of the solvents to ultraviolet radiation *at room temperature and liquid nitrogen temperature* produced no change in their absorption spectra, and thus the observed change could not be attributed to a reaction which was taking place with the solvent alone.

In order to obtain the absorption spectrum of the new compound formed in the absence of the absorption due to benzene, another sample of benzene in IM_4 was exposed to the ultraviolet radiation for three hours with intermittent melting and refreezing, and the spectrum of this solution was measured at room temperature using the Cary Spectrophotometer. The original solution of benzene in IM_4 was used as a blank. Thus the benzene absorption was subtracted out by the instrument, and the resulting curve was the spectrum of any material which had been formed during the reaction. The only error would be the small amount of benzene which had been converted in the reaction, estimated to be less than 10 percent. The curve thus obtained showed the presence of three maxima: one at $275m\mu$, one at $264m\mu$, and one at $255m\mu$. This work was repeated using solutions of benzene in E.P.A. and benzene in ethanol; in each case the spectra were identical.

Although the spectrum thus obtained had some of the characteristics of the spectra of various substituted benzene derivatives, it was found that the extinction coefficient was much too high for any of these compounds. A calculation in which the assumption was made that all the benzene had been converted to the new substance showed that the compound would then have a maximum extinction coefficient of 371. It had previously been indicated that less than 10 percent of the benzene had been converted, hence the maximum coefficient would be much higher. This ruled out the substituted benzenes as possible products of the reaction, and another solution had to be found. It was next shown that oxygen and water were not responsible for the photochemical reaction which was taking place. A sample of benzene in IM_4 was prepared, free from both oxygen and water, and this solution was exposed to ultraviolet radiation in a similar manner to the previous samples. The results of this experiment were identical with all the previous ones.

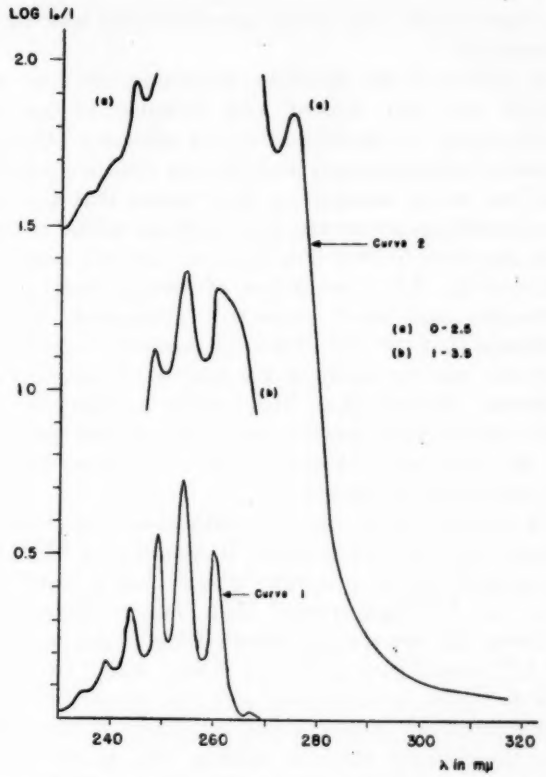

FIG. 1. Absorption spectrum of benzene in E.P.A. before irradiation (lower curve), and after irradiation (upper curve).

An attempt was next made to prepare a larger amount of the new substance in order to be able to identify it, so a number of samples of benzene in IM_4 were exposed to the ultraviolet radiation for $1\frac{1}{2}$ hours each, being melted and refrozen twice during this time. This solution was then distilled at atmospheric pressure to half its original volume, and the spectrum of the distillate showed that only benzene and solvent had been distilled from the solution. The distilland was again distilled to half its original volume, and the spectrum of this distillate showed the presence of benzene and a little of the new substance, which could be detected due to its absorption at $275m\mu$. The residue was again distilled to half its original volume; this time the distillate contained no benzene but only solvent and the new substance. The spectrum of this solution was essentially identical with the spectrum obtained previously. A small amount of the residue from the last distillation was diluted with methyl cyclohexane, and the absorption spectrum of this solution was also identical with the others. Another sample of the residue was heated on a watch glass to remove all the solvent, and a small amount of oily material remained on the watch glass. A small amount of this oily material in solution gave the same spectrum as before while, after standing in contact with the air

for three weeks, this same substance had lost all its absorption.

A portion of the distillate containing the new substance was next treated with bromine to test for unsaturation. It was found that the substance absorbed bromine instantaneously and that the resulting solution had lost all its absorption. This meant that the new compound was an unsaturated molecule whose absorption was due to this unsaturation, and no longer to aromaticity. An investigation of various unsaturated molecules and their respective absorption spectra indicated that the compound was possibly a conjugated polyene, and the study of the spectra of various such polyenes showed that they have a characteristic spectrum which is very similar to that of the spectrum of the compound resulting from the photochemical decomposition of benzene.

On comparing the spectrum with those of divinylacetylene and the hexatrienes, it was found that the compound had a spectrum which closely resembled that of 1,3,5-hexatriene.[2] The major discrepancy between the two spectra was that the entire spectrum of 1,3,5-hexatriene is shifted 7.5$m\mu$ away from the visible region as compared with the spectrum of the decomposition product. The structure of the curve and the distance between maxima was the same, and the maximum extinction coefficient was of the same order of magnitude as that estimated for our compound.

In an attempt to find a reasonable explanation for the difference between the two spectra, it was found that in conjugated polyenes geometric isomerism has an effect on the position of λ_{max} as well as on the maximum extinction coefficient.[3] It is therefore reasonable to assume that the 1,3,5-hexatriene whose spectrum was published by Woods and Schwartzman[2] might contain the *cis* isomer, whereas the product of the photochemical decomposition of benzene is the *trans* isomer which absorbs at higher wavelengths and has a higher extinction coefficient.

The possibility that the decomposition product is 1,3,5-hexatriene explains a number of observations which had heretofore been inexplicable. The molecule is highly unsaturated and would adsorb bromine readily. Hexatriene is known to polymerize on exposure to the air, and this would explain why the sample which was left exposed to the air lost all its absorption. Furthermore, one can now explain why the same product was formed regardless of which solvent was used for the reaction, while the solvent is still an essential part of the reaction.

The role of the solvent in this reaction seems to be as a contributor of hydrogen. Any solvent which has hydrogens in it and is capable of forming a glass at liquid nitrogen temperature seems to be able to cause the reaction to proceed. This was checked by using a solution of benzene in perfluoro-2-methylpentane, a solvent which formed a relatively good glass if cooled slowly. The glass was exposed to the ultraviolet radiation as before, and the spectrum of the resulting solution was obtained at room temperature on the Cary Spectrophotometer. It was shown that a change had occurred but that this new spectrum in no way resembled that of spectra obtained when IM_4 and E.P.A. had been used as solvents. The spectrum thus obtained had certain characteristics of the biphenyl spectrum, a fact which would fit in with the work which has been done on the photochemical decomposition of benzene vapor in the far ultraviolet, which is thought to go to biphenyl.[4] Thus it was shown that in the absence of hydrogen in the solvent, the decomposition goes by a different path and results in the formation of a product different from that obtained with a solvent containing hydrogen.

It was now necessary to postulate a mechanism for this reaction, in accord with the findings which have been reported. One could postulate that the first step is the breaking of one of the aromatic bonds in benzene which would result in the formation of a biradical. This biradical could then remove two hydrogens from any solvent molecule, resulting in the formation of 1,3,5-hexatriene. A competing reaction would be the removal of a hydrogen from benzene forming a phenyl radical, but such a radical could regain a hydrogen atom from any surrounding solvent molecule which would convert it back to benzene. The latter is probably the path of the formation of biphenyl, both in the vapor state and possibly in solvents which do not contain hydrogen. For biphenyl to be formed in the solid state it would be necessary to have the phenyl radical collide with a molecule of benzene. This is highly improbable *both because the concentrations used throughout the experiments never exceeded 0.0025* M *in benzene, and because the molecules are held in place in a rigid medium.* Certainly the probability of a collision between a phenyl radical and a benzene molecule would be extremely small as compared with the probability of a collision between the radical and a solvent molecule, which would convert the radical back to benzene.

It has been shown that benzene on exposure to ultraviolet radiation at liquid nitrogen temperature, undergoes a photochemical decomposition to a new compound which is stable at room temperature. It has further been shown that a solvent containing hydrogen is necessary for this reaction to occur, and that the resulting product has an absorption spectrum which is very similar to that of 1,3,5-hexatriene, and may be the *trans* isomer of this compound. A mechanism for the reaction has been postulated. Attempts have been made to determine the rate of this reaction, but these have not been successful to date. It would be desirable

[2] G. F. Woods and L. H. Schwartzman, J. Am. Chem. Soc. **70**, 3394 (1948).

[3] Pinckard, Wille, and Zechmeister, J. Am. Chem. Soc. **70**, 1938 (1948).

[4] G. I. Krassina, Acta Physicochim. U.R.S.S. **10**, 189 (1939). N. A. Prilezhaeva, Acta Physicochim. U.R.S.S. **10**, 193 (1939).

to obtain the order of the reaction with respect to light quanta. The high intensities needed to induce the reaction and the absence of decomposition at room temperature suggest that the reaction may be second order in the quanta, which would be the case if a molecule of benzene in an excited triplet state is a necessary intermediate.

It would be exceedingly useful to discover a method for producing large amounts of the decomposition product in order to characterize it definitely as to composition and structure. In order to establish definitely the geometric configuration of synthetic 1,3,5-hexatriene and of our product, one might expose a sample of our material to ultraviolet radiation in the presence of I_2 catalyst[5] and compare its spectrum before and after such exposure, or use some other method to induce the *cis-trans* equilibration.

EXPERIMENTAL

Purification of Chemicals Used

Benzene: C. P. benzene (thiophene free) was distilled and was further purified by five recrystallizations.

Diethyl Ether: Absolute ether was twice distilled from sodium metal.

Isopentane: C. P. isopentane was purified by passing through a four foot silica gel column.

Ethanol: 100 percent ethyl alcohol was twice distilled from a small amount of sodium metal.

Methyl Cyclohexane: C. P. methyl cyclohexane was first distilled from sodium metal and was then passed through a silica gel column.

Perfluoro-2-methyl pentane: This was a sample free from hydrocarbons for which we are indebted to Professor George H. Cady. While not a pure isomer it contained almost entirely molecules of the empirical formula C_6F_{14}. It was further purified immediately before using by means of a silica gel column.

Measurement of Phosphorescence Intensity

The apparatus used for measuring the phosphorescence intensity of benzene consisted of a quartz Dewar vessel which housed a quartz test tube containing the sample. Liquid nitrogen was placed in the Dewar vessel to bring the sample to −195.8°C. An A-H6 high-pressure mercury arc was used as a source of ultraviolet radiation and the phosphorescence was picked up by a photomultiplier and the intensity measured on an oscilloscope. A shutter was placed between the sample, the arc, and the photomultiplier in such a manner that it was possible to shield the photomultiplier while the sample was being irradiated and to cut off the light from the arc when the photomultiplier picked up the phosphorescence from the sample.

[5] A. Sandoval and L. Zechmeister, J. Am. Chem. Soc. **69**, 553 (1947).

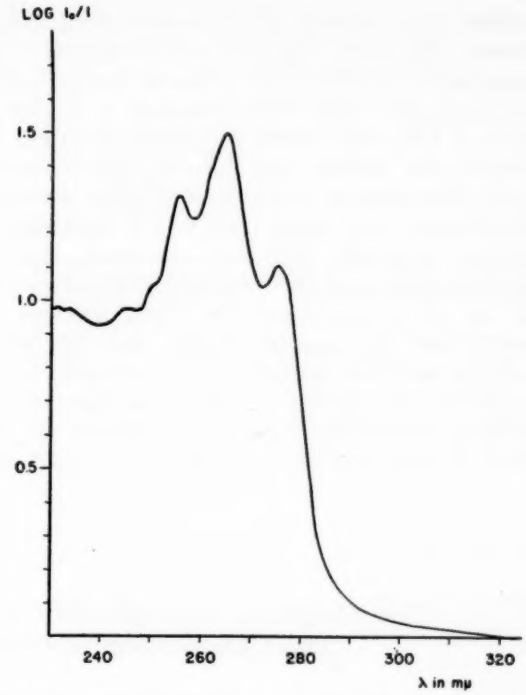

FIG. 2. Absorption spectrum of a solution in methyl cyclohexane of the purified photo-decomposition product of benzene.

Photography of the Absorption Spectra of Unexposed and Exposed Benzene Solutions

The same apparatus as that used for the phosphorescence measurements was used, except that the shutter was removed and the photomultiplier was replaced by a Hilger Medium Quartz Spectrograph. The sample was exposed to ultraviolet radiation from the A-H6 arc for a period of time. At the end of this time a Beckman Hydrogen Arc replaced the mercury arc, and served as a light source for photographing the absorption spectrum of the decomposed benzene solution.

Measurement of Absorption Spectra at Room Temperature

All spectra which were taken at room temperature were measured on a Cary Automatic Recording Spectrophotometer. Figure 1 shows the spectrum of benzene before and after exposure to the A-H6 arc. Curve 1 is the original benzene solution (concentration 0.00225 M benzene in IM_4), and curve 2 is the same solution after $1\frac{1}{2}$ hours exposure to the A-H6 arc. Figure 2 shows the spectrum of the new substance, obtained either by subtracting out the spectrum of benzene or from the distillation which removed the benzene completely.

Preparation of a Solution of Benzene Free from Oxygen and Water

The apparatus used consisted of two test tubes joined in the fashion of an inverted "U" which could be

connected to a vacuum line, separated from it by a magnetic valve and a trap. To one of the test tubes was connected a small tube containing clean potassium metal, while the other tube contained a solution of benzene in IM_4, kept frozen with liquid nitrogen. The potassium was distilled into the test tube by careful heating, thus forming a mirror of metallic potassium on its surface. The small tube which contained the potassium originally was then removed, and the system was evacuated by opening the magnetic valve. After the valve was closed, the liquid nitrogen was removed from the benzene solution and was placed around the test tube containing the potassium mirror. This allowed the solution to distill into the test tube containing the potassium metal. The sample was then allowed to melt so that any water in it could react with the potassium. This procedure was repeated three times, and at the end of this time the benzene solution was distilled back into the original test tube. The sample was frozen, and the system was evacuated to remove as much air as possible. Then with the valve closed, the sample was allowed to melt, liberating any oxygen dissolved in the solution. This was repeated until the pressure in the system was constant, indicating that no more gas was dissolved in the solution. At that point, the sample tube was sealed, still under vacuum, and was removed from the rest of the apparatus. The solution was now ready for exposure to the mercury arc, and the results obtained with this solution were identical with others containing water and oxygen, thus showing that these two materials have no influence on the path of this reaction.

THE JOURNAL OF CHEMICAL PHYSICS VOLUME 21, NUMBER 6 JUNE, 1953

The Magnetic Susceptibility of Certain Organic Compounds. Part IV. The Constitution of *Ortho*, *Meta*, and *Para* Nitroanilines

H. MIKHAIL
Faculty of Science, Fouad I University, Giza, Cairo, Egypt
(Received September 2, 1952)

Magnetic susceptibilities of *o*-, *m*-, and *p*-nitroanilines have been measured by the Gouy method. The experimental results showed that for a strong repelling group such as the amino group, the values for the *op*-derivatives are lower than the corresponding *m*-derivative. This was attributed to the fact that there is a tendency for the amino group to conjugate with the benzene nucleus in the case of *o*- and *p*-nitroanilines, accompanied by a lowering in their diamagnetic susceptibility values.

1. INTRODUCTION

SEVERAL investigators have determined the magnetic susceptibilities of different isomerides. Bhatnagar[1] and his collaborators concluded from results obtained on a series of liquid isomers that the value of χ_M is maximum for the *ortho* compounds while those of the *meta* and the *para*, like their other physical properties, are close together. They attributed this to the fact that the carbon atoms in a substituted benzene nucleus are not exactly alike as a result of the polar character of the substituent group. Cabrera and Fahlenbrach[2] have concluded that, contrary to Bhatnagar's observations, the values of χ_M for the *m*-nitrotoluene are the highest, whereas those of the *p*-nitrotoluene are the lowest. French[3] deduced from work on disubstituted benzene series that if the substituents are *op*-directing, the *m*-compounds have the highest susceptibility. She also noticed that if the nitro group is one of the constituents an apparently anomalous effect was observed. Recently, Baddar and Sugden[4] reported, from work on the contribution of the nitro group to the magnetic susceptibility of aliphatic and aromatic nitro compounds, that the difference between the magnetic susceptibilities of the $-\overset{\diagdown}{\underset{\diagup}{C}}-NO_2$ and the $-\overset{\diagdown}{\underset{\diagup}{C}}-H$ group is highest in the case of *m*-substituted nitro compounds. They attributed this to the fact that resonance as Type VIII(*b*) is impossible in the *m*-derivative.

Similar conclusions were also reported, adopting other physical constants. Tamamushi[5] found that *m*-nitroaniline is adsorbed more strongly by Al_2O_3 in benzene and more weakly by charcoal in MeOH than is the *o*-isomer. He attributed this to the fact that the *m*-derivative is a polar adsorbent and has a tendency to adsorb a more polar solute in a more nonpolar medium. Vandenbelt[6] classified the interaction of groups in band displacement from work on ultraviolet absorption spectrum of benzene derivatives into electron contributing (*op*-directing) and electron repelling (*m*-directing) types. He found that the NH_2 group, being a strongly repelling group, produces a greater displacement in the absorption of benzene bands than do single

[1] Bhatnagar, Mathur, and Mal, Phil. Mag. **10**, 101 (1930); **11**, 914 (1931).
[2] B. Cabrera, and H. Fahlenbrach, Z. Physik **89**, 697 (1934).
[3] C. M. French, Trans. Faraday Soc. **41**, 676 (1945).
[4] F. G. Baddar, and S. Sugden, J. Chem. Soc. (London) **1950**, 308.
[5] B. Tamamushi, Sci. Papers Inst. Phys. Chem. Research (Tokyo) **38**, 446 (1947).
[6] L. Doub and J. M. Vandenbelt, J. Am. Chem. Soc. **69**, 2714 (1947).

groups. Singh[7] found also a higher dipole moment for the *m*- than the *o*-nitroaniline and a similar result for the total polarization.

2. EXPERIMENTAL

The Gouy method was employed in our measurements of the magnetic susceptibilities. The apparatus consists essentially of an electromagnet of the Weiss type and a sensitive Oertling balance (sensitivity 0.05 mg). The field strength was of the order of 13 000 oersteds in a gap of 1.1 cm. The temperature was kept nearly constant during the observations.

The balance was mounted on a platform one meter above the electromagnet to avoid any direct influence resulting from the magnetic field on any part of the balance. The balance is fitted with special pans at the central bottom of which a micrometer screw adjustment is attached for the exact location of the specimen tube in the gap between the pole pieces.

The tube was made of Monax glass fitted with a glass stopper and was suspended by a fine copper wire (British S.W.G. 50) from the fine micrometer screw. Two tubes were chosen for our measurements, which we shall call (A) and (B), respectively, with approximate diameters of 0.6 cm. Sets of readings were taken for the empty tube as well as with the tube filled with the material under test up to a fixed mark.

Purified distilled water freed from air was taken as a standardizing substance whose χ_W between 20° and 25°C was taken to be -0.72×10^{-6}. The purified material was finely powdered and was uniformly packed in the specimen tube following the method adopted by Hoare.[8] Precautions were also taken with regard to the exact location of the inside flat bottom of the specimen tube centrally in the gap between the pole pieces.

The equation used for evaluating χ_S is

$$\chi_S=\frac{W-C}{S}\frac{dS}{dW}\times\chi_W+\left(1/\sigma-\frac{W}{S}\frac{dS}{dW}\times1/d\right),$$

where C is the meniscus correction which should be introduced so that both solids and liquids might have the same volume. This correction was found to be 0.0298 and 0.0301 for the tubes (A) and (B), respectively. The other symbols have their usual meanings.

Typical results for $-\chi_M\times10^6$ for the three isomerides at 25°C are shown in Table I. Typical values of dW/W for tubes A and B were taken to be 189.03 and 182.62, respectively.

Purification of materials: The solvents used for crystallization were purified as usual according to Proskauer.[9]

o-nitroaniline: Pure Kodak material was twice crystallized from ligroin to give orange-red crystals, 76.8–77°.

m-nitroaniline: Pure Kodak material was three times crystallized from alcohol in yellowish flakes, mp 115.8°.

p-nitroaniline: Pure Kodak material was twice crystallized from alcohol to give yellow prismatic needles, mp 153.0°.

Table II include the present results as well as the results of other investigators for comparison.

Referring to Table II, it will be seen that the author's value for *o*-nitroaniline differs from those of Bose and of Sugden. In the first place, this is because the value quoted by Bose was taken for the material in the molten state. He concluded from his series of measurements on crystalline and molten states of some compounds that the diamagnetic susceptibility is independent of the physical state of the compound. This statement does not seem to be invariably true as some materials show a decrease while others show an increase in their susceptibility values on melting (see reference 14). On the other hand, the values quoted by Baddar and Sugden were deduced from the additivity law of solutions assuming the law to be linear. Such an assumption does

TABLE I.

Tube	S g	$-dS$ g	$\frac{S}{dS}$	Mean of S/dS	σ g/ml	Mol wt	χ_S	χ_M
			o-Nitroaniline					
A	4.3825	0.01561	280.75		1.442	138.12	0.481	
	4.2142	0.01501	280.76	280.66				66.47
	4.1679	0.01486	280.48					
B	4.1517	0.01532	271.00		1.442			
	3.9927	0.01472	271.24	271.04		138.12	0.481	66.48
	3.8412	0.01418	270.89					
			m-Nitroaniline					
A	3.2122	0.01206	266.35		1.398			
	3.0243	0.01136	266.22	266.79		138.12	0.508	70.17
	2.7879	0.01041	267.81					
B	2.8794	0.01118	257.55		1.398			
	2.7574	0.01072	257.22	257.59		138.12	0.507	70.01
	2.6627	0.01032	258.01					
			p-Nitroaniline					
A	3.9323	0.01400	280.88		1.437			
	3.8271	0.01365	280.37	280.84		138.12	0.481	66.42
	3.6874	0.01311	281.27					
B	3.6778	0.01358	270.82		1.437			
	3.5583	0.01312	271.21	271.18		138.12	0.481	66.43
	3.4808	0.01282	271.51					

TABLE II.

Substance	Experimental values[a] (1)	(2)	(3)	(4)	Calculated values[a] (5)	(6)	(7)
o-Nitroaniline	66.47	69.3 at 73°			68.39	69.89	66.05
m-Nitroaniline	70.09		69.4		68.82	69.89	70.00
p-Nitroaniline	66.43			66.5	66.85	69.89	66.05

[a] (1) Author's values. (2) Bose's value in the molten state (see reference 10). (3) Bose's value for a single crystal, and also by Krishnan (see reference 11). (4) Garssen (see reference 12). (5) Baddar and Sugden (see reference 4). (6) Pascal's data. (7) Gray and Cruickshank (see reference 13).

[7] Sahney, Beri, Sarna, and Singh, J. Indian Chem. Soc. **26**, 329 (1949).
[8] F. E. Hoare, Proc. Roy. Soc. (London) **147**, 88 (1934).
[9] A. Weissberger and E. Proskauer, *Organic Solvents* (1935).
[10] A. Bose, Phil. Mag. **21**, 1119 (1936).
[11] K. S. Krishnan and S. Banerjee, Trans. Roy. Soc. (London) **A234**, 265 (1935).
[12] J. H. Garssen, Compt. rend. **196**, 541 (1933).
[13] F. W. Gray, and J. H. Cruickshank, Trans. Faraday Soc. **31**, 1491 (1935).
[14] S. S. Bhatnagar, and R. N. Mathur, *Physical Principles and Application of Magnetochemistry* (MacMillan and Company, Ltd., London, 1935), p. 310.

not always hold as molecular association may occur, and thus, a deviation from linearity may exist. In particular, Garssen (see reference 12) found from work on a mixture of acetone and *p*-nitroaniline a deviation amounting to 17 percent. The same solvent was used by Baddar and Sugden in their measurements.

In the Gouy method random orientation might be assumed if good powdering and even packing were followed. The results obtained from adopting such a procedure gave consistent diamagnetic susceptibility values. Nevertheless, the descending order of the author's values agrees with those of Baddar and Sugden values, namely, *meta*>*ortho* or *para* isomers.

To explain the experimental results for picric acid, it was suggested in Part II by Baddar and Mikhail[15] that the coplanar structure must contribute to the actual state of the molecule. To gain more evidence for the effect of substituents on the contribution of the coplanar structure to the normal state of the nitro compounds, the study was extended to include several other aromatic substituted and unsubstituted nitro- and polynitrobenzene derivatives of the following types:

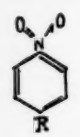

I

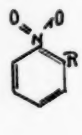

II

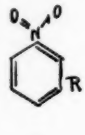

III

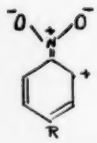

IV

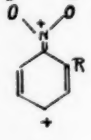

V

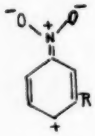

VI

where R=OH, OCH_3, CH_3, or NH_2 group.

[15] F. G. Baddar and H. Mikhail, J. Chem. Soc. 1949, 2927.

Such structures as IV, V, and VI are not so stable as I, II, and III, respectively, as they involve an unstable separation of charge. They are, therefore, expected to make a significant, though small, contribution to the normal state of the molecule. For a group such as the NH_2 group, which is a strong electron-repelling group, the resonance effect is stronger than the inductive effect, and an increase in contribution is thus expected.

The slight experimental differences between the *m*-, and the *o*-, or *p*-isomerides may, therefore, be attributed to the fact that structures VII(b) and VIII(b), which possess low calculated diamagnetic susceptibility values, contribute to the actual state of the *o*-, and *p*-nitroaniline molecules, respectively.

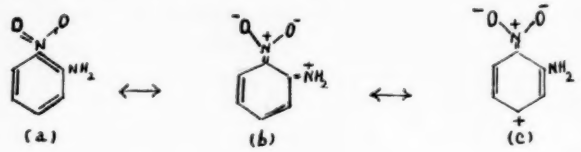

VII

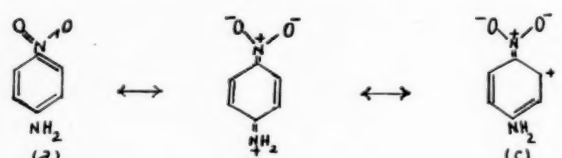

VIII

Such structures are impossible in case of metanitroaniline (see Formula IX).

IX

The Nonadditivity of the Repulsive Potential of Helium*

PHILIP ROSEN
The Johns Hopkins University, Applied Physics Laboratory, Silver Spring, Maryland
(Received December 19, 1952)

The repulsive energy of three helium atoms is calculated using the valence bond method. A great reduction of the required number of exchange integrals is found to be possible using group theoretical arguments. It is found that the effect of nonadditivity is negligible for the internuclear distances involved in most physical problems.

IN the past in developing the properties of matter using statistical mechanics or kinetic theory, it has been assumed that the potential energy of a system of molecules or atoms is simply the sum of the potential energy between all possible pairs.[1] It is, therefore, of importance to investigate the validity of this assumption. The potential is obviously nonadditive, when it is possible to form additional paired electrons as is the case in H_3. However, the problem which is of interest in statistical mechanics is the additivity of potential energy for chemically saturated structures.

There have been several investigators who have studied certain aspects of this problem. London[2] and Margenau[3] have shown that Van der Waal's dispersion forces are additive only up to the second-order perturbation. Axilrod[4] has considered the dispersion forces between three atoms using third-order perturbation theory, and he finds that nonadditivity introduces small errors. However, none of these investigators consider the first-order forces (chemical forces), although Margenau feels that these should be responsible for any important nonadditive effects. More recently Löwdin[5,6] has developed an expression for the energy of a system of atoms using the molecular orbital method in which only two-center integrals are involved. He finds that nonadditivity is important in crystals. In this work we prefer to use the valence bond method which is useful for simple systems.

The simplest problem that can be solved to test the additivity of chemical forces is the system of three helium atoms. The importance of helium in low temperature physics makes this choice an interesting one. However, because of the complexity of the problem, it is necessary to use the simplest possible atomic wave functions.

Let us consider three helium atoms, a, b, c; with electrons 1 and 2 attached to nucleus A, electrons 3 and 4 attached to nucleus B, and electrons 5 and 6 attached to nucleus C. The Hamiltonian for this system can be written symbolically as

$$H=H_a+H_b+H_c+V_{ab}+V_{ac}+V_{bc}, \tag{1}$$

where H_a is the Hamiltonian for atom a which satisfies the equation,

$$\int \psi_a^* H_a \psi_a d\tau_{12}=E_a.$$

ψ_a is the normalized atomic wave function of atom a, E_a is the energy of atom a and similarly for the other atoms. V_{ab}, V_{ac}, and V_{bc} are the interaction operators between any two atoms.

The total wave function Ψ can be written as

$$\Psi=\sum_\lambda (-1)^\lambda P_\lambda \psi_a \psi_b \psi_c, \tag{2}$$

where P_λ is any permutation operator of the symmetric group of permutations on 6 particles, which is composed of 720 elements, and λ is even or odd for even or odd permutations, respectively. Since ψ_a, ψ_b, ψ_c are antisymmetric with respect to exchanges between electons belonging to the same atom which we label the intra-atomic exchanges P_{λ_a}, P_{λ_b}, P_{λ_c}, respectively, it is convenient to consider the group P_λ as being formed from the interatomic exchanges $P_{\lambda_{abc}}$ and the intra-atomic exchanges.[7] Thus,

$$P_\lambda=P_{\lambda_{abc}}{}^{abc}P_{\lambda_a}{}^{a}P_{\lambda_b}{}^{b}P_{\lambda_c}{}^{c}. \tag{3}$$

The set of interatomic permutations $P_{\lambda_{abc}}$ represent a complex of the group P_λ which when multiplied by the intra-atomic subgroup $P_{\lambda_a}{}^{a}\cdot P_{\lambda_b}{}^{b}\cdot P_{\lambda_c}{}^{c}$ reproduces the entire group. The subgroup $P_{\lambda_a}{}^{a}\cdot P_{\lambda_b}{}^{b}\cdot P_{\lambda_c}{}^{c}$, which we denote by g_λ, for our problem is composed of 8 elements which are 1, (12), (34), (56), (12)·(34), (12)·(56), (34)·(56), and (12)·(34)·(56). Consequently, the complex $P_{\lambda_{abc}}$ contains 90 elements, one of which is unity. We shall denote the purely interatomic permutations $P_{\lambda_{abc}}{}^{abc}-1$ by Π_λ.

To obtain the elements Π_λ it is first advisable to construct a table giving the types of classes of the entire group. Using well-known rules[8] we obtain the results shown in Table I. Let us now consider the possible ways of exchanging electrons between any two atoms. There are 5 ways of permuting electrons between atoms a and b, 5 ways between a and c, and 5 ways between b and c.

* Supported by the Bureau of Ordnance, U. S. Navy, under Contract NOrd 7386.

[1] For example, see J. E. Mayer and M. G. Mayer, *Statistical Mechanics* (John Wiley and Sons, Inc., New York, 1940).
[2] F. London, Z. physik. Chem. **B11**, 222 (1930).
[3] H. Margenau, Revs. Modern Phys. **11**, 1 (1939).
[4] B. M. Axilrod, J. Chem. Phys. **19**, 719 (1951).
[5] P. O. Löwdin, J. Chem. Phys. **19**, 1396, 1570 (1951).
[6] P. O. Löwdin, thesis, University of Uppsala, Uppsala, Sweden, 1948.
[7] H. Margenau and P. Rosen, J. Chem. Phys. **21**, 394 (1953).
[8] H. Margenau and G. M. Murphy, *Mathematics of Physics and Chemistry* (D. Van Nostrand Company, Inc., New York, 1943).

TABLE I. The symmetric group of 6! permutations.

Class	Number in class	Odd or even
I	1	even
(ij)	15	odd
(ijk)	40	even
$(ij)(kl)$	45	even
$(ijkl)$	90	odd
$(ijklm)$	144	even
$(ijklmn)$	120	odd
$(ij)(klm)$	120	odd
$(ij)(kl)(mn)$	15	odd
$(ijk)(lmn)$	40	even
$(ij)(klmn)$	90	even

For example, between a and b we can have (13), (14), (23), (24), and (13)(24) or (14)(23) which is equally valid. The last two can be obtained from one another by multiplication with some member of the intra-atomic subgroup g:

$$(13)(24)\cdot(12)(34)=(14)(23),$$
$$(14)(23)\cdot(12)(34)=(13)(24).$$

We shall denote the above diatomic exchange operators by $\Pi_{\lambda ab}$, $\Pi_{\lambda ac}$, and $\Pi_{\lambda bc}$. Permutations (14), (23), and (24) are equivalent to (13), for as we shall show below, all elements which are related by the similarity transformation $g_\mu^{-1}\Pi_\lambda g_\mu$, where g_μ is an element of the intra-atomic subgroup, are equivalent in evaluating the total energy. Thus, there remain 74 purely triatomic exchange operators, which we denote by $\Pi_{\lambda abc}$ such that

$$\sum_{\lambda abc}(-1)^{\lambda abc}P_{\lambda abc}=\sum_{\lambda abc}(-1)^{\lambda abc}\Pi_{\lambda abc}+\sum_{\lambda ab}(-1)^{\lambda ab}\Pi_{\lambda ab}+\sum_{\lambda ac}(-1)^{\lambda ac}\Pi_{\lambda ac}+\sum_{\lambda bc}(-1)^{\lambda bc}\Pi_{\lambda bc}+1=\sum_{\lambda}(-1)^{\lambda}\Pi_\lambda+1. \quad (4)$$

Let us now consider the number of possible purely triatomic exchanges $\Pi_{\lambda abc}$. There are 24 ways of simultaneously exchanging two electrons on any atom with two other electrons, each belonging to different atoms. Typical elements of this set are (13)(26) with which both electrons of atom a are exchanged; (13)(46) with which both electrons of b are exchanged; (35)(26) with which both electrons of c are exchanged. All the other elements of this set can be obtained from these three by the similarity transformation $g_\mu^{-1}\Pi_\lambda g_\mu$.

There are 16 ways of cyclically permuting three electrons each of which belong to different atoms. A typical element of this set is (135); eight of the elements of this set can be obtained from (135) by using the above similarity transformation, and the remaining eight can be obtained from these by taking the inverse. We shall show below that Π_λ^{-1} and Π_λ are equivalent in evaluating the energy.

There are 8 ways of simultaneously exchanging all six electrons such that all electron pairs belonging to the same atom are transferred to different atoms. A typical element of this set is (13)(25)(46); the other elements can be obtained by using the similarity transformation.

We also have two ways of permuting all six electrons such that all electron pairs belonging to the same atom are transferred together to another atom. This is the same as permuting the nuclei cyclically. A typical element of this set is (135)(246), the other element being the inverse.

Finally, we have 24 ways of permuting any two nuclei and then exchanging any electron on these nuclei with any electron of the remaining atom. Typical elements of this set are (24)(135), (26)(135), (46)(135). One must be careful here in obtaining the other elements of this set by the similarity transformation and by taking inverses, because, if this is done, we obtain 48 elements. However, 24 of these are redundant because they can be obtained by multiplying some member of the intra-atomic subgroup by the remaining 24 elements. The most direct way of obtaining the required set of exchanges is to form the products

$$\begin{matrix}(i5)\\(i6)\end{matrix}\cdot(13)(24)\quad i=1,2,3,4$$
$$\begin{matrix}(i3)\\(i4)\end{matrix}\cdot(15)(26)\quad i=1,2,5,6$$
$$\begin{matrix}(i1)\\(i2)\end{matrix}\cdot(35)(46)\quad i=3,5,4,6.$$

There are three ways to check to see if we have the required set Π_λ. First, we notice that we have the required number of these permutations. Second, it is easily shown, using Table I, that if the products given by Eq. (3) are performed, we obtain 360 even permutations and the same number of odd permutations. Finally, none of the interatomic permutations Π_λ given above can be obtained from one another by forming the product $\Pi_\lambda g$. Table II gives all the typical interatomic permutations with the equivalent number of permutations obtained by the similarity transformation and by inversion.

TABLE II. Interatomic permutations.

Notation	Permutation	Equivalent number
$\Pi_{\lambda ab}$	(13)	4
	(13)(24)	1
$\Pi_{\lambda a}$	(15)	4
	(15)(26)	1
$\Pi_{\lambda bc}$	(35)	4
	(35)(46)	1
$\Pi_{\lambda abc}$	(13)(26)	8
	(13)(46)	8
	(35)(26)	8
	(135)	16
	(13)(25)(46)	8
	(135)(246)	2
	(24)(135)	8
	(26)(135)	8
	(46)(135)	8

CALCULATION OF THE ENERGY

The total energy of the system $\bar{H}$ can be written

$$\bar{H}=\frac{\int\psi_a^*\psi_b^*\psi_c^* H\sum_\lambda(-1)^\lambda P_\lambda\psi_a\psi_b\psi_c d\tau}{\int\psi_a^*\psi_b^*\psi_c^*\sum_\lambda(-1)^\lambda P_\lambda\psi_a\psi_b\psi_c d\tau}. \quad (5)$$

If we use the decomposition of P_λ, as given by Eq. (3), then

$$\bar{H}=\frac{\int\psi_a^*\psi_b^*\psi_c^* H\sum_{\lambda_{abc}}(-1)^{\lambda_{abc}}P_{\lambda_{abc}}\psi_a\psi_b\psi_c d\tau}{\int\psi_a^*\psi_b^*\psi_c^*\sum_{\lambda_{abc}}(-1)^{\lambda_{abc}}P_{\lambda_{abc}}\psi_a\psi_b\psi_c d\tau} \quad (6)$$

by virtue of the fact that $(-1)^{\lambda_a}P_{\lambda_a}\psi_a=\psi_a$, etc. Or since $P_{\lambda_{abc}}$ contains unity we have

$$\bar{H}=\frac{E_a+E_b+E_c+\bar{U}_{ab}+\bar{U}_{ac}+\bar{U}_{bc}+\int\psi_a^*\psi_b^*\psi_c^* H\sum_\lambda(-1)^\lambda\Pi_\lambda\psi_a\psi_b\psi_c d\tau}{1+\int\psi_a^*\psi_b^*\psi_c^*\sum_\lambda(-1)^\lambda\Pi_\lambda\psi_a\psi_b\psi_c d\tau}, \quad (7)$$

where

$$\bar{U}_{ab}=\int\psi_a^* V_{ab}\psi_a d\tau_{12}, \quad \text{etc.}$$

We will now show that Π_λ and Π_λ^{-1} yield the same contribution to Eq. (7). If we define $\Phi=\psi_a\psi_b\psi_c$ and consider cases where the integrals in Eq. (7) are real (in our case Φ will be real), then, because H is Hermitian,

$$\int\Phi^* H(-1)^\lambda\Pi_\lambda\Phi d\tau=\int\Pi_\lambda^{-1}[\Phi^* H(-1)^\lambda\Pi_\lambda\Phi]d\tau$$

$$=\int\Phi^* H(-1)^\lambda\Pi_\lambda^{-1}\Phi d\tau.$$

It was stated above that a set of Π_λ, which are related by the similarity transformation $g_\mu^{-1}\Pi_\lambda g_\mu$ are equivalent. This can be shown as follows:

$$\int\Phi^* H\Pi_\lambda\Phi d\tau=(-1)^\mu\int g_\mu^{-1}[\Phi^* H\Pi_\lambda g_\mu\Phi]d\tau$$

$$=\int\Phi^* H g_\mu^{-1}\Pi_\lambda g_\mu\Phi d\tau.$$

By use of Eqs. (1) and (4), Eq. (7) can be written

$$\bar{H}=\frac{E_a(1+\Delta_{bc})+E_b(1+\Delta_{ac})+E_c(1+\Delta_{ab})+\bar{U}_{ab}+\bar{U}_{ac}+\bar{U}_{bc}+\bar{H}_{ab}'+\bar{H}_{ac}'+\bar{H}_{bc}'+\sum_{i=1}^{4}Q_i}{1+\Delta_{ab}+\Delta_{ac}+\Delta_{bc}+\Delta_{abc}}, \quad (8)$$

where

$$\Delta_{ab}=\int\psi_a^*\psi_b^*\sum_{\lambda_{ab}}(-1)^{\lambda_{ab}}\Pi_{\lambda_{ab}}\psi_a\psi_b d\tau_{12}, \quad \text{etc.},$$

$$\Delta_{abc}=\int\psi_a^*\psi_b^*\psi_c^*\sum_{\lambda_{abc}}(-1)^{\lambda_{abc}}\Pi_{\lambda_{abc}}\psi_a\psi_b\psi_c d\tau,$$

$$\bar{H}_{ab}'=\int\psi_a^*\psi_b^*[H_a+H_b+V_{ab}]\sum_{\lambda_{ab}}(-1)^{\lambda_{ab}}\Pi_{\lambda_{ab}}\psi_a\psi_b d\tau_{12}, \quad \text{etc.},$$

$$Q_1=\int\psi_a^*\psi_b^*\psi_c^*(V_{ac}+V_{bc})\sum_{\lambda_{ab}}(-1)^{\lambda_{ab}}\Pi_{\lambda_{ab}}\psi_a\psi_b\psi_c d\tau,$$

$$Q_2=\int\psi_a^*\psi_b^*\psi_c^*(V_{ab}+V_{bc})\sum_{\lambda_{ac}}(-1)^{\lambda_{ac}}\Pi_{\lambda_{ac}}\psi_a\psi_b\psi_c d\tau,$$

$$Q_3=\int\psi_a^*\psi_b^*\psi_c^*(V_{ab}+V_{ac})\sum_{\lambda_{bc}}(-1)^{\lambda_{bc}}\Pi_{\lambda_{bc}}\psi_a\psi_b\psi_c d\tau$$

and

$$Q_4=\int\psi_a^*\psi_b^*\psi_c^* H\sum_{\lambda_{abc}}(-1)^{\lambda_{abc}}\Pi_{\lambda_{abc}}\psi_a\psi_b\psi_c d\tau.$$

It is easily seen from Eq. (8) that the total energy of a pair of atoms, for example, a and b, is

$$\bar{H}_{ab}=\frac{\bar{H}_{ab}'+E_a+E_b+\bar{U}_{ab}}{1+\Delta_{ab}}, \tag{9}$$

and the interaction energy between a and b is

$$E_{ab}=\frac{\bar{H}_{ab}'+\bar{U}_{ab}-(E_a+E_b)\Delta_{ab}}{1+\Delta_{ab}}. \tag{10}$$

The total interaction energy of the three atoms is $\bar{H}-(E_a+E_b+E_c)$, and the nonadditive part of this energy E_{abc} is

$$E_{abc}=\bar{H}-(E_a+E_b+E_c)-(E_{ab}+E_{ac}+E_{bc}),$$

which can be written by virtue of Eqs. (8) and (10)

$$\begin{aligned}E_{abc}=[&\sum_{i=1}^{4}Q_i-(E_a+E_b+E_c)\Delta_{abc}\\&-E_{ab}(\Delta_{ac}+\Delta_{bc}+\Delta_{abc})\\&-E_{ac}(\Delta_{ab}+\Delta_{bc}+\Delta_{abc})\\&-E_{bc}(\Delta_{ab}+\Delta_{ac}+\Delta_{abc})]\Delta^{-1},\end{aligned} \tag{11}$$

where

$$\Delta=1+\Delta_{ab}+\Delta_{ac}+\Delta_{bc}+\Delta_{abc}.$$

EVALUATION OF INTEGRALS

We will choose the following well-known atomic functions for our calculation:

$$\psi_a=a(1)a(2)\left(\frac{\alpha(1)\beta(2)-\beta(1)\alpha(2)}{\sqrt{2}}\right),\qquad a(1)=\left(\frac{Z^3}{\pi}\right)^{\frac{1}{2}}e^{-ZA_1}$$

$$\psi_b=b(3)b(4)\left(\frac{\alpha(3)\beta(4)-\beta(3)\alpha(4)}{\sqrt{2}}\right),\qquad b(3)=\left(\frac{Z^3}{\pi}\right)^{\frac{1}{2}}e^{-ZB_3}$$

$$\psi_c=c(5)c(6)\left(\frac{\alpha(5)\beta(6)-\beta(5)\alpha(6)}{\sqrt{2}}\right),\qquad c(5)=\left(\frac{Z^3}{\pi}\right)^{\frac{1}{2}}e^{-ZC_5},$$

where α and β are the usual spin functions, A_1 is the distance from nucleus A to electron 1, etc., and $Z=27/16$. We will write the Hamiltonian in natural units so that

$$\begin{aligned}H_a&=-(\nabla_1^2+\nabla_2^2)-4\left(\frac{1}{A_1}+\frac{1}{A_2}\right)+\frac{2}{r_{12}}\\&=\langle H_a^{(1)}\rangle+\langle H_a^{(2)}\rangle+(2Z-4)\left(\frac{1}{A_1}+\frac{1}{A_2}\right)+\frac{2}{r_{12}},\end{aligned}$$

$$V_{ab}=-4\left(\frac{1}{A_3}+\frac{1}{A_4}+\frac{1}{B_1}+\frac{1}{B_2}\right)+2\left(\frac{1}{r_{13}}+\frac{1}{r_{14}}+\frac{1}{r_{23}}+\frac{1}{r_{24}}\right)+\frac{8}{R_{ab}},$$

where r_{ij} is the distance from the ith to the jth electron and $\langle H_a^{(1)}\rangle a(1)=-Z^2a(1)$. The other parts of the Hamiltonian are similar.

If one integrates over the spin coordinates in all the expressions given in Eq. (8) and also considers the equivalence of certain exchange integrals, one finds

$$\begin{aligned}\sum_{\lambda_{abc}}(-1)^{\lambda_{abc}}\Pi\lambda_{abc}\rightarrow&2[(13)(26)+(13)(46)+(35)(26)]\\&+4[(135)]+2[(13)(25)(46)]\\&+2[(135)(246)]-4[(24)(135)\\&+(26)(135)+(46)(135)].\end{aligned}$$

Also

$$\sum_{\lambda_{ab}}(-1)^{\lambda_{ab}}\Pi\lambda_{ab}\rightarrow-2[(13)]+(13)(24),$$

with similar expressions for $\sum(-1)^{\lambda_{ac}}\Pi\lambda_{ac}$ and $\sum(-1)^{\lambda_{bc}}\Pi\lambda_{bc}$. If all the integrations are carried out, we find that‡

$$E_a=E_b=E_c=2Z^2-(27/4)Z, \tag{12}$$

$$\Delta_{ab}=-2I_{ab}^2+I_{ab}^4, \tag{13}$$

$$\begin{aligned}(1+\Delta_{ab})E_{ab}=&-4Z[4g_{ab}-2l(aa,bb)+L(ab,ab)]\\&-8ZI_{ab}[(Z-4)J_{ab}+2L(aa,ab)]\\&+ZI_{ab}^2[8Z-11-4L(aa,bb)+16g_{ab}\\&+12L(ab,ab)]+8(Z-4)ZI_{ab}^3J_{ab}\\&+I_{ab}^4[8Z/\rho-8Z^2+(27/2)Z],\end{aligned} \tag{14}$$

$$\begin{aligned}\Delta_{abc}=&4I_{ac}I_{ab}I_{bc}\\&+2[I_{ab}^2I_{ac}^2+I_{ab}^2I_{bc}^2+I_{ac}^2I_{bc}^2]\\&-4[I_{ab}^3I_{ac}I_{bc}+I_{ac}^3I_{ab}I_{bc}\\&+I_{bc}^3I_{ab}I_{ac}]+4I_{ab}^2I_{ac}^2I_{bc}^2,\end{aligned} \tag{15}$$

$$\begin{aligned}Q_1(a,b,c)=&16ZI_{ab}T(c,ab)[1-I_{ab}^2]\\&+8ZI_{ab}^2[3g_{bc}+3g_{ac}-l(aa,cc)\\&-l(bb,cc)]-8ZI_{ab}^4[g_{ac}+g_{bc}],\end{aligned}$$

$$Q_2(a,b,c)=Q_1(c,a,b),\quad Q_3(a,b,c)=Q_1(b,c,a). \tag{16}$$

For convenience we decompose Q_4 into

$$Q_4=Q_{4a}+Q_{4b}+Q_{4c}+Q_{4ab}+Q_{4ac}+Q_{4bc},$$

where

$$Q_{4a}=\int\psi_a^*\psi_b^*\psi_c^*H_a\sum_{\lambda_{abc}}(-1)^{\lambda_{abc}}\Pi\lambda_{abc}\psi_a\psi_b\psi_c d\tau$$

and

$$Q_{4ab}=\int\psi_a^*\psi_b^*\psi_c^*V_{ab}\sum_{\lambda_{abc}}(-1)^{\lambda_{abc}}\Pi\lambda_{abc}\psi_a\psi_b\psi_c d\tau;$$

‡ The symbols are defined in the Appendix.

we find

$$Q_{4a}(a,b,c)=-8Z[2I_{ab}I_{ac}I_{bc}-(Z-2)I_{ab}I_{bc}J_{ac}-I_{ab}I_{bc}L(aa,ac)]-4Z[ZI_{ab}^2I_{ac}^2+2I_{ab}^2I_{bc}^2+2I_{ac}^2I_{bc}^2$$
$$-(Z-2)(I_{bc}^2+I_{ac}^2)I_{ab}J_{ab}-(Z-2)(I_{ab}^2+I_{bc}^2)I_{ac}J_{ac}-I_{ab}I_{bc}^2L(aa,ab)-I_{ac}I_{bc}^2L(aa,ac)$$
$$-I_{ab}I_{ac}L(ab,ac)]+8Z[Z(I_{ab}^3I_{ac}I_{bc}+I_{ac}^3I_{ab}I_{bc})+2I_{bc}^3I_{ab}I_{ac}-(Z-2)I_{ab}^2I_{ac}I_{bc}J_{ab}$$
$$-(Z-2)J_{ac}(I_{ab}^3I_{bc}+2I_{ac}^2I_{ab}I_{bc}+I_{bc}^3I_{ab})-I_{ac}I_{ab}I_{bc}L(ac,ac)-I_{bc}^3I_{ab}L(aa,ac)$$
$$-I_{ab}^3I_{bc}L(ab,ac)]-4Z[2ZI_{ab}^2I_{ac}^2I_{bc}^2-3(Z-2)I_{ab}^2I_{ac}I_{bc}^2J_{ac}-(Z-2)I_{ab}I_{ac}^2I_{bc}^2J_{ab}$$
$$-I_{ab}^2I_{bc}^2L(ac,ac)-I_{ab}I_{ac}I_{bc}^2L(ab,ac)], \quad (17)$$

also

$$Q_{4b}(a,b,c)=Q_{4a}(b,c,a), \quad Q_{4c}(a,b,c)=Q_{4a}(c,a,b),$$

$$Q_{4ab}(a,b,c)=-8Z[4I_{ab}I_{ac}I_{bc}g_{ab}+2I_{ac}I_{bc}J_{ab}+2I_{ab}I_{bc}K(b,ac)-I_{ab}I_{ac}I_{bc}L(aa,bb)-I_{ac}I_{bc}L(aa,ab)$$
$$-I_{bc}L(ab,ac)-I_{bc}I_{ab}L(bb,ac)]+4Z\left[\frac{4Z}{\rho_{ab}}(I_{ab}^2I_{ac}^2+I_{ab}^2I_{bc}^2+I_{bc}^2I_{ac}^2)-2(I_{ac}^2I_{ab}^2\right.$$
$$+2I_{ac}^2I_{bc}^2+I_{ab}^2I_{bc}^2)G_{ab}-4(I_{ab}I_{ac}^2+I_{ab}I_{bc}^2)J_{ab}-2I_{ac}(I_{ab}^2+I_{bc}^2)K(b,ac)$$
$$-2I_{bc}(I_{ab}^2+I_{ac}^2)K(a,bc)+(I_{ac}^2+I_{bc}^2)L(ab,ab)+I_{ac}^2I_{bc}^2L(aa,bb)+(I_{ac}^2+I_{bc}^2)I_{ab}L(aa,ab)$$
$$+I_{bc}(I_{ac}^2+I_{ab}^2)L(aa,bc)+I_{ac}(I_{bc}^2+I_{ab}^2)L(bb,ac)+I_{ab}I_{ac}L(ab,ac)+I_{ab}I_{bc}L(ab,bc)$$
$$\left.+I_{bc}I_{ac}L(ac,bc)\right]-8Z\left[\frac{4}{\rho_{ab}}(I_{ab}^3I_{ac}I_{bc}+I_{ac}^3I_{ab}I_{bc}+I_{bc}^3I_{ab}I_{ac})-2(I_{ac}^3I_{ab}I_{bc}+I_{bc}^3I_{ab}I_{ac})G_{ab}\right.$$
$$-2(3I_{ab}^2I_{ac}I_{bc}+I_{ac}^3I_{bc}+I_{bc}^3I_{ac})J_{ab}-2(I_{ab}^3I_{bc}+2I_{ac}^2I_{ab}I_{bc}+I_{bc}^3I_{ab})K(b,ac)$$
$$-2I_{bc}^2I_{ab}I_{ac}K(a,bc)+2I_{ab}I_{bc}I_{ac}L(ab,ab)+I_{bc}^3I_{ac}L(aa,ab)+I_{bc}^2I_{ab}I_{ac}L(aa,bc)$$
$$\left.+2I_{ac}^2I_{bc}I_{ab}L(bb,ac)+(2I_{ac}^2I_{bc}+I_{bc}^3+2I_{bc}I_{ab}^2)L(ab,ac)+I_{bc}^2I_{ab}L(ac,bc)\right]$$
$$+4Z\left[\frac{8}{\rho_{ab}}I_{ab}^2I_{ac}^2I_{bc}^2-8I_{ab}I_{ac}^2I_{bc}^2J_{ab}-6I_{ab}^2I_{bc}^2I_{ac}K(b,ac)-2I_{ab}^2I_{ac}^2I_{bc}K(a,bc)\right.$$
$$\left.+I_{ac}^2I_{bc}^2L(ab,ab)+5I_{ab}I_{ac}I_{bc}^2L(ab,ac)+I_{ab}I_{ac}^2I_{bc}L(ab,bc)+I_{ab}^2I_{ac}I_{bc}L(ac,bc)\right], \quad (18)$$

also

$$Q_{4ac}(a,b,c)=Q_{4ab}(c,a,b),$$
$$Q_{4bc}(a,b,c)=Q_{4ab}(b,c,a).$$

NUMERICAL CALCULATIONS

For numerical calculations we have chosen to consider the equilateral triangular configuration and the linear symmetric configuration. One should expect that since the equilateral configuration involves the greatest overlap of wave functions that the contribution of nonadditivity will be largest in comparison to other configurations having the same triangular perimeter. The linear symmetric configuration is calculated for comparison. Another reason for this choice is the fact that the three-center integrals required for these configurations have been calculated for several values of internuclear distances.[9–11] Wherever possible we have used values given in the literature for all the necessary three-center integrals. In several cases we have used approximations which are given in the appendix. For the equilateral configuration the results for all $ZR\geqslant 3$ can be put into the form

$$\frac{E_{abc}}{E_{ab}+E_{bc}+E_{ac}}=-1.15e^{-.33(R_{ab}+R_{ac}+R_{bc})},$$

R in units of Bohr radii. For the linear symmetric case we have

$$\frac{E_{abc}}{E_{ab}+E_{bc}+E_{ac}}=9.8e^{-.66(R_{ab}+R_{ac}+R_{bc})}.$$

[9] J. O. Hirschfelder, J. Chem. Phys. **6**, 795 (1938).
[10] J. O. Hirschfelder and C. N. Weygant, J. Chem. Phys. **6**, 806 (1938).
[11] Hirschfelder, Eyring, and Rosen, J. Chem. Phys. **4**, 121 (1936).

For the equilateral configuration we find that for $ZR \geqslant 8$ the error involved in neglecting nonadditivity is 1 percent or less. The error involved for the linear symmetric case is always less than for the equilateral case and of opposite sign in the region investigated. These results show that for the distances involved in most physical situations ($ZR \geqslant 8$) the effect of nonadditivity in the repulsive forces of helium is negligible.

In the equilateral configuration at large distances we find that $E_{abc} \sim I^3$, where I is the overlap integral. Also at large distances $E_{ab} \sim I^2$. Thus $E_{abc}/3E_{ab} \sim I$. In fact, for large distances, $E_{abc}/3E_{ab} = I$ is a good approximation. Thus, if the overlap integral is small compared to unity, we expect nonadditivity to be negligible. There may be physical situations when the overlap integral is not negligible, and in these cases one should be cautious in assuming that intermolecular forces are additive.

APPENDIX

The following two-center integrals are necessary in our calculation:

$$I_{ab}(\rho_{ab}) = \int ab\, d\tau \qquad L(aa, bb) = \frac{1}{Z}\int \frac{a^2(1)b^2(2)}{r_{12}} d\tau_{12}$$

$$J_{ab}(\rho_{ab}) = \frac{1}{Z}\int \frac{ab}{A} d\tau \qquad L(ab, ab) = \frac{1}{Z}\int \frac{a(1)b(1)a(2)b(2)}{r_{12}} d\tau_{12}$$

$$G_{ab}(\rho_{ab}) = \frac{1}{Z}\int \frac{b^2}{A} d\tau \qquad L(aa, ab) = \frac{1}{Z}\int \frac{a^2(1)a(2)b(2)}{r_{12}} d\tau_{12}$$

$$g_{ab}(\rho_{ab}) = G_{ab}(\rho_{ab}) - \frac{1}{\rho_{ab}} \qquad l(aa, bb) = L(aa, bb) - \frac{1}{\rho_{ab}},$$

where $\rho = ZR$ and R is the distance between the respective nuclei.

The following three-center integrals[9–11] are required:

$$K(a, bc) = \frac{1}{Z}\int \frac{bc}{A} d\tau,$$

$$L(aa, bc) = \frac{1}{Z}\int \frac{a^2(1)b(2)c(2)}{r_{12}} d\tau_{12},$$

$$L(ab, ac) = \frac{1}{Z}\int \frac{a(1)b(1)a(2)c(2)}{r_{12}} d\tau_{12},$$

$$T(a, bc) = K(a, bc) - L(aa, bc) = \frac{\pi}{Z^3}\int a^2 bc\left(1 + \frac{1}{ZA}\right) d\tau.$$

All the two-center integrals and $K(a, bc)$ can be evaluated in closed form; however, Hirschfelder and Weygandt[10] have computed tables for these. They have also computed all the other three-center integrals for the equilateral configuration for a few values of the internuclear separation. For the linear symmetric configuration, integrals of the type $L(ab, ac)$ and $T(a, bc)$ have been computed by Hirschfelder, Eyring, and Rosen for several internuclear separations. For integrals of the type $T(a, bc)$ the latter authors give a closed expression.

Approximate expressions for integrals of the type $L(ab, ac)$ have been given by Margenau[12] which in our notation take the form

$$L(ab, ac) \cong [I_{ac} K(\langle ac\rangle, ab) + I_{ab} K(\langle ab\rangle, ac)],$$

where

$$K(\langle ac\rangle, ab) = \frac{1}{Z}\int \frac{ab}{R_{\langle ac\rangle}} d\tau,$$

where $R_{\langle ac\rangle}$ is the distance from the electron in question to the midpoint between nuclei a and c. Using Margenau's method of approximation we find for $T(a, bc)$

$$T(a, bc) \cong \tfrac{1}{4}\Big[\exp(-2ZR_{a,\langle bc\rangle})\left(1 + \frac{1}{ZR_{a,\langle bc\rangle}}\right) I_{bc} + 2\exp[-Z(R_{ab} + R_{ac})] + I_{ab}\exp[-Z(R_{a,\langle ab\rangle} + R_{c,\langle ab\rangle})]\left(1 + \frac{1}{ZR_{a,\langle ab\rangle}}\right) + I_{ac}\exp[-Z(R_{a,\langle ac\rangle} + R_{b,\langle ac\rangle})]\left(1 + \frac{1}{ZR_{a,\langle ac\rangle}}\right)\Big],$$

where $R_{a,\langle bc\rangle}$, for example, is the distance from nucleus a to the midpoint of b and c. In general, the accuracy required for integrals like $T(a, bc)$ is not great.

[12] H. Margenau, Phys. Rev. **63**, 131 (1943).

Unified Orbital Theory of the Excited States of the Fluorine Molecule

CHARLES R. MUELLER
Chemistry Department, Purdue University, West Lafayette, Indiana
(Received October 29, 1952)

The unification of the atomic orbital and molecular orbital theories of the excited states of diatomic molecules is achieved by means of semi-localized orbitals. In particular the classification of the states of the fluorine molecule arising from the interaction of two fluorine atoms in their ground state is discussed.

Quantitative calculations are made for the $^1\Sigma_g^+$ and $^3\Sigma_u^+$ states and a comparison of the singlet-triplet separation energies and binding energies from the three methods is made. Both two electron and eighteen electron calculations are made. The better molecular orbital calculations give a lower triplet than a singlet state. In the eighteen electron calculation the atomic and semi-localized orbital methods coincide, and the $^1\Sigma_g^+$ state is found to be the ground state.

PART I. CLASSIFICATION OF MOLECULAR STATES

A. Introduction

THERE are two general approaches to the classification of the electronic states of molecules. In the first method we begin with a zero nuclear separation and split up the "united atom" into the constituent atoms of a molecule. This procedure is very closely identified with the molecular orbital method.

The second method consists of an investigation of the kinds of molecular states which arise from given states of separated atoms. The procedure developed by Wigner and Witmer[1] is the basis of the atomic orbital theory of excited states.

In a series[2] of papers the author has undertaken the unification of the atomic (A.O.) and molecular orbital (M.O.) methods by use of semi-localized orbitals. The semilocalized orbitals (S.L.O.) can assume either M.O. or A.O. form depending on the value of certain variational parameter, but usually possess an intermediate character.

In carrying out such a program for the classification of molecular electronic states, the first problem is obviously to select as a beginning point either the unified or separated atom approach.

In any many-electron problem we must rely very heavily on the Slater determinantal eigenfunctions and the various techniques developed for their application. Considering the problem solely from the standpoint of the number of determinants involved, the separated atom procedure strongly recommends itself. If we pass by means of properly chosen variational parameters from A.O.'s to S.L.O.'s the number of determinants does not change, and the symmetry characteristics cannot change.

At the point where the variational parameters assume values characteristic of the M.O. eigenfunction, the number of determinants is sharply reduced, even though the symmetry properties of the eigenfunction are retained.

It is much more convenient to study this change starting from a separated atom approach. The method of Wigner and Witmer has so far been in complete accord with experiment, but there are discrepancies with experiment on the basis of the unified atom approach. This is really not surprising since molecular observations are always made at intermediate and large internuclear separations.

Having settled the question as to the type of approach to be used, we must now turn our attention to the individual one-electron eigenfunctions. According to the definition given in the first paper of this series,[1] these individual one electron orbitals will consist of a linear combination of two atomic orbitals, one on each atom of the diatomic molecule.

Suppose we consider such a linear combination, $\varphi_a+\lambda_b\varphi_b(\lambda_a\varphi_a+\varphi_b)$, at infinite internuclear separation. In the case the best orbital will be an A.O. According to our definition of atomic orbitals $\lambda_b=0(\lambda_a=0)$, and the orbital has the form $\varphi_a(\varphi_b)$. We shall call $\varphi_a(\varphi_b)$ the base atomic orbital. There are two important but equivalent restrictions on the form of the second atom orbital. First, for suitable values of the variational parameter the one-electron orbital must assume M.O. form. Second, the symmetry of the molecular eigenfunction must be independent of the value of the variational parameters.

The condition for the satisfaction of both criteria is simply that φ_a and φ_b have the same symmetry relative to the molecular axis, A. B. Coulson[3] has discussed this criterion for M.O.'s.

For the excited and ground states of fluorine, we are restricted to the combination of the P_{+1}, P_{-1}, P_0 orbitals of atom A with the P_{+1}, P_{-1}, P_0 orbitals, respectively, of atom B. In addition symmetry conditions will greatly restrict the values of the λ_i's.

[1] F. Wigner and E. Witmer, Z. Physik **51**, 859 (1928).
[2] C. Mueller and H. Eyring, J. Chem. Phys. **19**, 1945 (1951), Proc. Natl. Acad. Sci. **38**, 149 (1952). C. Mueller, J. Chem. Phys. **19**, 1497 (1951), J. Am. Chem. Soc. **74**, 3466 (1952). C. Mueller, J. Chem. Phys. **20**, 1600 (1952).
[3] C. A. Coulson, *Valence* (Oxford University Press, New York, 1952), p. 70–76.

B. Orientation of Base Atomic Orbitals

In the formation of a molecule an axial electrical field is produced which is accompanied by a quantization of angular momentum along the intermolecular axis. If the component of the angular momentum of the ith electron along such an axis is designated as M_{Li}, then the molecular state is characterized by the quantum number Λ where

$$\Lambda = |\Sigma M_{Li}|.$$

An excellent diagram for the vectoral quantization in the case of interaction between atoms in the ^2P (fluorine ground) state is given by Herzberg.[4]

We must consider states with $\Lambda = 0, 1, 2$; or Σ, Π, and Δ states. We can produce Σ states in two different ways. The base atomic orbitals for the valence electrons can be both P_Z or P_0 orbital (Z axis along the internuclear axis) or a P_{+1} orbital on one atom and a P_{-1} orbital on the other. Since the assignment of either a P_{+1} or P_{-1} orbital to an atom is arbitrary, the second kind of Σ state is degenerate.

When the base atomic orbital on one atom is P_0 and the orbital of the second atom is P_{-1} or P_{+1}, Π states arise. Again because of arbitrariness in the assignment of the orbital to individual atom, these states are degenerate.

When the base atomic orbitals for the valence electrons are both P_{+1} or P_{-1} orbitals, Δ states arise.

C. Additional Symmetry Properties

Two additional symmetry properties must be considered. If a molecular eigenfunction undergoes a sign on inversion through a center of symmetry, it is classified as a ungerade state. If no change in sign occurs as the result of such an operation, the eigenfunction is classified as gerade.

We must also characterize the eigenfunction as to its symmetry properties on reflection in a plane containing the intermolecular axis. If such an operation leaves the eigenfunction unchanged, it is called positive; if a change of sign occurs, it is negative.

The last consideration is the multiplicity. Since we have only two uncoupled electrons with spin quantum number of $\pm\frac{1}{2}$, the total spin quantum number can be 0 or 1 resulting in singlet and triplet states. The former are antisymmetric in the spin eigenfunction, the latter symmetric.

We shall consider the effects of these symmetry properties in detail for the Σ states, and when this task is completed some additional remarks about Π and Δ states will be made.

The simplest type of Σ state arises from the interaction of two P_Z orbitals, one on each atom. The base atomic orbitals are P_{Za} and P_{Zb}. The linear combinations are $P_{Za}+\lambda_b P_{Zb}$ and $\lambda_a P_{Za}+P_{Zb}$. It is sufficient to specify these linear combinations by the base atomic orbitals.

For the purposes of further simplification we will replace eighteen electron determinants such as

$$[1S_a(\alpha)\cdots P_{Za}(\alpha)1S_b(\alpha)\cdots P_{Zb}(\beta)]$$

by the two electron determinant $[P_{Za}(\alpha)P_{Zb}(\beta)]$.

Consider the case where the spins of the atomic orbitals are α and β. Two determinants specify the states equally well, namely $A=[P_{Za}(\alpha)P_{Zb}(\beta)]$ and $B=[P_{Za}(\beta)P_{Zb}(\alpha)]$. We are faced with the case of exchange degeneracy. This is removed by taking linear combination, $A+B$, and $A-B$. On expansion we find that the eigenfunction $A-B(A+B)$ is antisymmetric (symmetric) in the spins. On inversion through a center of symmetry,

$$P_{Za}+\lambda P_{Zb} \overset{i}{\rightleftarrows} +(\lambda P_{Za}+P_{Zb}). \tag{2}$$

On expansion of the eigenfunction and factorization of the spin coordinates, the first state is gerade, the second ungerade.

The eigenfunction is invariant to the operation σ_v, reflection in a plane of symmetry in both cases:

$$\Psi(^1\Sigma_g^+) = A-B, \tag{3}$$

$$\Psi(^3\Sigma_u^+) = A+B. \tag{4}$$

Note that in Eq. (2) we have tacitly assumed that $\lambda_a=\lambda_b$. This in fact must be the case if the original symmetry of the base atomic orbital is to be preserved.

The Σ state can also arise through the interaction of P_{-1} and P_{+1} orbitals. One singlet state is

$$[P_{+1a}(\alpha)P_{-1b}(\beta)]-[P_{+1a}(\beta)P_{-1b}(\alpha)]=C-D,$$

and a second singlet state is

$$[P_{+1b}(\alpha)P_{-1a}(\beta)]-[P_{+1b}(\beta)P_{-1a}(\alpha)]=E-F.$$

Similarly two triplets occur, $C+D$, and $E+F$. To remove this degeneracy we again take linear combinations,

$$\begin{aligned} \mathrm{I} &= C-D+E-F, \\ \mathrm{II} &= C-D-E+F, \\ \mathrm{III} &= C+D+E+F, \\ \mathrm{IV} &= C+D-E-F. \end{aligned} \tag{5}$$

Combinations I and II are singlet sigma-states; III and IV are triplet sigma-states. We must now classify these states as gerade or ungerade.

Now,

$$P_{+1a}+\lambda_x P_{+1b} \overset{i}{\rightleftarrows} -(P_{+1b}+\lambda_x P_{+1a}), \tag{6}$$

$$P_{-1a}+\lambda_y P_{-1b} \overset{i}{\rightleftarrows} -(P_{-1b}+\lambda_y P_{-1a}). \tag{7}$$

Note again that the symmetry reduces the number of λ_i's from 4 to 2. I is a $^1\Sigma_g$ state; II is $^1\Sigma_u$ state; III is a $^3\Sigma_g$ state; IV is $^1\Sigma_u$ state.

[4] G. Herzberg, *Spectra of Diatomic Molecules* (D. Van Nostrand Company, Inc., 1950), p. 317.

TABLE I. Σ states of fluorine molecule.

State	Valence orbitals	Determinant	Molecular orbital
$^1\Sigma_g^+$	$P_{Za}+\lambda P_{Zb}$	$A-B$	$[\sigma_g(\alpha)\sigma_g(\beta)]$
$^3\Sigma_u^+$	$\lambda P_{Za}+P_{Zb}$	$A+B$	$[\sigma_g(\alpha)\sigma_u(\beta)]+[\sigma_g(\beta)\sigma_u(\alpha)]$
$^1\Sigma_g^+$	$P_{+1a}+\lambda P_{+1b}$	$C-D+E-F$	$[\Pi_u^+(\beta)\Pi_u^-(\alpha)]-[\Pi_u^+(\alpha)\Pi_u^-(\beta)]$
$^3\Sigma_u^+$	$P_{-1a}+\lambda P_{-1b}$	$C+D-E-F$	$[\Pi_u^+(\alpha)\Pi_g^-(\beta)]+[\Pi_u^+(\beta)\Pi_g^-(\alpha)]$ $+[\Pi_u^-(\alpha)\Pi_g^+(\beta)]+[\Pi_u^-(\beta)\Pi_g^+(\alpha)]$
$^1\Sigma_u^-$	$\lambda P_{+1a}+P_{+1b}$	$C-D-E+F$	$[\Pi_u^+(\alpha)\Pi_g^-(\beta)]-[\Pi_u^+(\beta)\Pi_g^-(\alpha)]$ $-[\Pi_u^-(\alpha)\Pi_g^+(\beta)]-[\Pi_u^-(\beta)\Pi_g^+(\alpha)]$
$^3\Sigma_g^-$	$\lambda P_{-1a}+P_{-1b}$	$C+D+E+F$	$[\Pi_g^+(\alpha)\Pi_g^-(\beta)]+[\Pi_g^+(\beta)\Pi_g^-(\alpha)]$

In order for any of these states to have correct plus and minus properties the P_{+1} and P_{-1} must be functions in the polar coordinate, φ, of the form $e^{\pm i|m|\varphi}$ and $e^{\mp i|m|\varphi}$ respectively. We must use this angular part for the eigenfunction rather than $\cos m\varphi$ and $\sin m\varphi$.

On application of the operator σ_v

$$P_{-1a}+\lambda P_{-1b}\overset{\sigma_v}{\rightleftarrows}P_{-1a}+\lambda P_{+1b}, \tag{8}$$

since

$$\psi(\varphi)=e^{\pm i|m|\varphi}=\cos(|m|\varphi)\pm i\sin(|m|\varphi)\overset{\sigma_v}{\rightleftarrows}e^{\mp im\varphi}. \tag{9}$$

Notice again that the symmetry restriction reduces the variational parameters from 2 to 1. The results of this classification are given in Table I.

In the fourth column the determinants for the corresponding molecular orbitals are given. It is difficult in some cases to see the correspondence between the semi-localized and molecular orbitals. Consider first the simple $^1\Sigma_g^+$ state. When $\lambda=\pm1$ the second determinant is equal to the first, the eigenfunction becomes the single molecular orbital determinant.

In the case of the more complex $^1\Sigma_g^+$ state $C=E$, $D=F$ for $\lambda=\pm1$. For $\lambda=+1$, $P_{+1a}+\lambda P_{+1b}$ becomes Π_u^+, $P_{-1a}+\lambda P_{-1b}$, Π_u^-. For $\lambda=-1$ the eigenfunction assumes the form of a higher $^1\Sigma_g^+$ state. This is also true in the case discussed in the last paragraph.

In the case of the ungerade states, the correspondence is more complicated. All these states are pure covalent states. Regardless of the value of λ the expanded eigenfunction has atomic orbital form. All terms containing λ cancel out. This can also be shown by operation on the atomic orbital determinants for the lowest triplet $[P_{Za}(\alpha)P_{Zb}(\alpha)]$. Add the first column to the second. Subtract the second column from the first, and exchange columns. Apart from sign the atomic orbital determinant is transformed into the molecular orbital determinant. The equality for the other ungerade states can be discussed in the same way. The $^3\Sigma_u^+$, ($\dot{2}$ states) and $^1\Sigma_u^-$ states are shown to be pure covalent states.

The Π-states can be discussed in a manner similar to the degenerate Σ-states except that the positive and negative character of the eigenfunction is no longer pertinent. The symmetry restrictions are therefore less drastic. On performing an inversion through the molecular center of symmetry,

$$P_{Za}+\lambda_Z P_{Zb}\overset{i}{\rightleftarrows}P_{Zb}+\lambda_Z P_{Za}, \tag{10}$$

$$P_{+1a}+\lambda_1 P_{+1b}\overset{i}{\rightleftarrows}-(P_{+1b}+\lambda_1 P_{+1a}), \tag{11}$$

and two variational parameter λ_z and λ_1 are permissible. The σ- and π-bonds can have differing degrees of "ionic character."

The discussion of the Δ-states is analogous to that of the simple $^1\Sigma_g^+$ and $^3\Sigma_u^+$ states.

PART II. NUMERICAL CALCULATIONS

A. Two Electron Calculations for the $^1\Sigma_g^+$ and $^3\Sigma_u^+$ States

We have carried out two types of calculations of the electronic energies of the $^1\Sigma_g^+$ and $^3\Sigma_u^+$ states of the fluorine molecule. In both cases the calculations were done for molecular, atomic and semi-localized orbitals.

In the first case effective nuclear charges were used throughout. The Hamiltonian is then, in atomic units,

$$H=-\tfrac{1}{2}(\nabla_1^2+\nabla_2^2)-Z_a/r_{a1}-Z_a/r_{a2}-Z_b/r_{b1} -Z_b/r_{b2}+1/r_{12}. \tag{12}$$

Z_a and Z_b are effective nuclear charges. This charge is the result of screening of the nucleus by the electron charge cloud of the nonvalence electrons and also in an obscure way is connected with the exchange effects of these same electrons. It is obvious that these effects will vary with the distance from the nucleus, and so three separate values have been used.

If the electron is on the nucleus, the Slater effective nuclear charge is used; if in the overlap portion or on the other nucleus, a value determined by the application of Gauss'[5] theorem is used. The values are 5.20, 2.039, and 1.0108, respectively.

In the second calculation we have used the same effective nuclear charges for the overlap and opposite atom portion of the charge cloud as previously. The value of 5.20, however, has been eliminated by calculations using the eigenfunctions of Coulson and Duncanson.[6] The

[5] C. Mueller and H. Eyring, J. Chem. Phys. **19**, 934 (1951).
[6] W. C. Duncanson and C. A. Coulson, Proc. Roy. Soc. (Edinburgh) **62**, 37 (1944).

value thus obtained is, for the free atom energy, 0.57706 atomic unit. In this case the field of the electron on an atom is composed of exchange and Coulombic contribution of the remaining 8 nonvalence electrons.

At first sight it might appear that these two assumptions lead to about the same results. The energy of the free atom computed using Slater effective nuclear charges is 3.38 atomic units, and so this becomes a study in the effect of free atom energies on molecular properties. We shall use a common symbol $\mathcal{H}$ to denote the Hamiltonian in both cases.

The energy of the $^1\Sigma_g^+$ state is

$$E(^1\Sigma_g^+)=(Q+K)/(1+S^2), \tag{13}$$

and the energy of the $^3\Sigma_u^+$ state is

$$E(^3\Sigma_u^+)=(Q-K)/(1-S^2). \tag{14}$$

Here

$$Q=\int \varphi_f(1)\varphi_f'(2)\mathcal{H}\varphi_f(1)\varphi_f'(2)d\tau_1 d\tau_2, \tag{15}$$

$$K=\int \varphi_f(1)\varphi_f'(2)\mathcal{H}\varphi_f(2)\varphi_f'(1)d\tau_1 d\tau_2, \tag{16}$$

$$S=\int \varphi_f(1)\varphi_f'(1)d\tau_1, \tag{17}$$

and φ_f is a linear combination of the two P_Z valence electrons of atoms a and b:

$$\varphi_f=P_{Za}+\lambda P_{Zb};\quad \varphi_f'=\lambda P_{Za}+P_{Zb}. \tag{18}$$

When $\lambda=\pm 1$, the eigenfunction assumes molecular orbital form; when $\lambda=0$, atomic orbital form. Otherwise the eigenfunction has a semi-localized orbital form. Energy terms other than those which are involved in the free atom are calculated using Slater atomic orbitals in the linear combinations. This procedure will be followed also in the eighteen electron calculation.

The results of the two different methods are given in Tables II and III.

The calculations are in extremely poor agreement with one another in almost all quantitative respects. About the only reasonable results obtained are for the S.L.O. method with an atomic energy of 0.57706.

TABLE II. Calculation for $^1\Sigma_g^+$ and $^3\Sigma_u^+$ state of F_2 with Slater effective nuclear charge.

	Molecular orbital		Atomic orbital	Semi-localized orbital
$\lambda=$	1.00	−1.00	0.00	−0.375
$E(^1\Sigma_g^+)$	−6.47377	−7.35031	−7.01270	−7.428
Binding energy of $^1\Sigma_g^+$	0.65756	−0.21898	+0.11863	−0.297
Lowest state	$^3\Sigma_u^+$	$^1\Sigma_g^+$	$^3\Sigma_u^+$	$^1\Sigma_g^+$
Singlet triplet separation	+0.79690	−0.07964	+0.25797	−0.1573
$E(^3\Sigma_u^+)$	−7.27607	−7.27607	−7.27607	−7.27601
Binding energy of $^3\Sigma_u^+$	−0.1393	−0.1393	−0.1393	−0.1393

Kopineck[7] has done an atomic orbital calculation for the nitrogen molecule, and this calculation appears to be in good agreement with experiment. In the next section the eighteen electron calculation for fluorine indicates that the S.L.O. and A.O. calculation coincide, and that an inversion of $^1\Sigma_g^+$ and $^3\Sigma_u^+$ states occurs in the M.O. treatment.

The inversion of $^1\Sigma_g^+$ and $^3\Sigma_u^+$ states also occurs in oxygen if one uses a molecular orbital method.[8]

B. Eighteen Electron Calculation for the $^1\Sigma_g^+$ and $^3\Sigma_u^+$ States of the Fluorine Molecule

In this particular case the valence electrons are assigned to the same orbitals as in the preceding calculations. Slater atomic orbitals are used to calculate the two-center integrals, and the eigenfunctions of Coulson and Duncanson[6] are used for the calculation of one-center integrals. All Coulombic interactions are included, but any exchange interactions involving the $1s$ electrons of one atom and the electrons of the other atom are neglected. The justification for this is simply that

TABLE III. Calculation for $^1\Sigma_g^+$ and $^3\Sigma_u^+$ state of F_2 with $\epsilon_{at}=0.57706$.

	Molecular orbital		Atomic orbital	Semi-localized orbital
$\lambda=$	1.00	−1.00	0	0.25
$E(^1\Sigma_g^+)$	−1.34292	−0.58456	−1.65871	−1.770
Binding energy of $^1\Sigma_g^+$	+0.18253	+0.94089	−0.13326	−0.245
Lowest state	$^3\Sigma_u^+$	$^3\Sigma_u^+$	$^1\Sigma_g^+$	$^1\Sigma_g^+$
$E(^1\Sigma_g^+-{}^3\Sigma_u^+)$	+0.15211	+0.91047	−0.16368	−0.275
$E(^3\Sigma_u^+)$	−1.49503	−1.49503	−1.49503	−1.49503
Binding energy of $^3\Sigma_u^+$	+0.03042	+0.03042	+0.03042	+0.03042

the overlap integrals involved are about the order of 10^{-3}. This and the preceding calculations were carried out at an internuclear distance of 2.6923 atomic units, which is slightly (1 percent) less than the equilibrium internuclear distance in order to avoid time-consuming interpolations.

The energies are calculated by application of the Dirac Vector Model to the free atom and to the molecule; the energy expressions are not explicitly given because of their complexity.

The calculated total energy of the fluorine atom with reference to dissociation into nucleus and free electrons was 98.85887 atomic units. The observed total energy is 99.695 atomic units, and an error of 0.83 percent for the calculated value results.

In Table IV the results are tabulated for molecular and atomic orbital eigenfunction. The semi-localized orbitals are apparently identical with the latter. So far as the molecular orbitals are concerned, it seems that

[7] H. J. Kopineck, Z. Naturforsch., **7a**, 314 (1952).
[8] W. Moffitt, Proc. Roy. Soc. (London) **A210**, 224 (1951).

the σ_g^2 state is more stable than the σ_u^2 state. The molecular orbital method again predicts a $^3\Sigma_u^+$ ground state instead of the observed $^1\Sigma_g^+$. In general the more complicated calculations bring the atomic orbital calculation into better agreement with experiment.

In the two two-electron calculations, there is general agreement between the calculation based on an atomic energy of 0.57706 and the 18-electron calculation, especially for the case of semi-localized orbitals.

Both semi-localized orbital calculations agree as to a ground state. In the two-electron case $\lambda=+0.25$, in the 18-electron case $\lambda=0.00$. The two-electron calculation predicts a singlet triplet separation of -0.275 atomic units; the 18-electron calculation, a separation of -0.309 atomic units. The binding energy is the two-electron case is 0.245 atomic units; for the 18-electron case, 0.280 atomic units. The experimental value is much lower than this.

TABLE IV. Eighteen electron calculation of the energies of $^1\Sigma_g^+$ and $^3\Sigma_g^+$ states of the fluorine molecule.

	Molecular orbital		Semi-localized and atomic orbitals
$\lambda=$	1.00	−1.000	0.00
$E(^1\Sigma_g^+)$	−196.38680	−195.55019	197.99798
Binding energy of singlet	+1.33082	+2.16743	−0.28036
Lowest state	$^3\Sigma_u^+$	$^3\Sigma_u^+$	$^1\Sigma_g^+$
Singlet triplet separation	+1.30219	+2.13880	−0.30899
$E(^3\Sigma_u^+)$	−197.68899	−197.68899	−197.68899
Binding energy of $^3\Sigma_u^+$	+0.02863	+0.02863	+0.02863

The Photochemical Decomposition of Azomethane

M. H. JONES* AND E. W. R. STEACIE
Division of Pure Chemistry, National Research Council, Ottawa, Canada
(Received November 10, 1952)

The photolysis of azomethane has been investigated over the temperature range 24–190°C. The variation in the rates of production of nitrogen, methane, and ethane with absorbed intensity, azomethane concentration, and temperature may be accounted for quantitatively by the reactions

$$CH_3N{=}NCH_3+h\nu\rightarrow N_2+2CH_3 \quad (1)$$

$$CH_3+CH_3N{=}NCH_3\rightarrow CH_4+CH_2N{=}NCH_3 \quad (2)$$

$$CH_3+CH_3\rightarrow C_2H_6. \quad (3)$$

The quantum yield of nitrogen formation was found to be unity and independent of temperature. For the activation energy difference $E_2-\frac{1}{2}E_3$ a value of 7.6 kcal/mole was obtained. Evidence is cited for an association reaction between methyl radicals and azomethane. On the basis of an assumed mechanism, the activation energy of this process is 6.4 kcal/mole.

INTRODUCTION

THE decomposition of azomethane, both photochemical and thermal, has aroused interest because it is a potential source of radicals. Ramsperger[1] first investigated the photolysis and from the observed pressure increase formulated the reaction as

$$CH_3N{=}NCH_3+h\nu\rightarrow N_2+C_2H_6.$$

This work was carried out prior to the development of ideas concerning free radical mechanisms, and later analyses of the photolytic decomposition products[2,3] demonstrated that the reaction is not a simple molecular dissociation into nitrogen and ethane. Methane is one of the gaseous products, and the ratio of methane to ethane increases with temperature. Davis, Jahn, and Burton[4] found that nitric oxide almost completely inhibits the formation of alkanes and concluded that the initial absorption of a light quantum by azomethane results in the formation of molecular nitrogen and free methyl radicals. It has been suggested[2] that the methyls produced in the photochemical act disappear by an association reaction with the substrate, and Flowers and Taylor[5] have qualitatively accounted for the change in methane-ethane ratio by postulating secondary reactions involving the radical formed by such an association. Thus

$$CH_3+(CH_3)_2N-NCH_3\rightarrow C_2H_6+(CH_3)_2N-N$$

or

$$CH_3+(CH_3)_2N-NCH_3\rightarrow C_2H_6+CH_3N{=}NCH_3$$

$$CH_3+(CH_3)_2N-NCH_3\rightarrow CH_4+\text{liq.}$$

There is a disagreement in the reported values of the quantum yield. Those derived from pressure changes[1,6] are suspect because of the complexity of the products and their variability with concentration and temperature. Using the rate of nitrogen formation as a measure of the azomethane decomposition, Blacet and Taurog[7] and Cannon and Rice[8] obtained a value of unity for light of wavelength 3600A. They also showed that the quantum yield is independent of pressure in the range 50–600 mm. As there is, therefore, no evidence of deactivation by collision an excited molecule mechanism is unlikely. Kuchler,[9] however, reported a value of 2 for λ3130A using the same method.

The present investigation was undertaken with the object of obtaining quantitative information concerning the reactions of the methyl radicals produced in the primary process and, in particular, the activation energy of the hydrogen abstraction reaction

$$CH_3+CH_3N{=}NCH_3\rightarrow CH_4+CH_2N{=}NCH_3.$$

Such information would permit the use of azomethane as a source of methyl radicals in the investigation of reactions of the type

$$CH_3+RH\rightarrow CH_4+R.$$

EXPERIMENTAL

Azomethane was prepared by the oxidation of dimethyl hydrazine hydrochloride with cupric chloride according to the method described by Jahn.[10] The decomposition of the cuprous chloride addition complex occurred smoothly at 110–120°C, and the liberation of azomethane was accompanied by a reaction producing

* National Research Council of Canada Postdoctorate Fellow, 1950–1952.

[1] H. C. Ramsperger, J. Am. Chem. Soc. **50**, 123 (1928).
[2] Burton, Davis and Taylor, J. Am. Chem. Soc. **59**, 1038 (1937).
[3] Burton, Davis and Taylor, J. Am. Chem. Soc. **59**, 1989 (1937).
[4] Davis, Jahn, and Burton, J. Am. Chem. Soc. **60**, 10 (1938).
[5] R. G. Flowers and H. A. Taylor, J. Chem. Phys. **10**, 110 (1942).
[6] Forbes, Heidt and Sickman, J. Am. Chem. Soc. **57**, 1935 (1935).
[7] F. E. Blacet and A. Taurog, J. Am. Chem. Soc. **61**, 3024 (1939).
[8] C. V. Cannon and O. K. Rice, J. Am. Chem. Soc. **63**, 2900 (1941).
[9] L. Kuchler, Nachr. Ges. Wiss. Gottingen, Math.-physik. Kl., **1**, 215 (1937).
[10] F. P. Jahn, J. Am. Chem. Soc. **59**, 1761 (1937).

permanent gases which consisted of nitrogen and hydrocarbons. The product was dried by passing through tubes containing potassium hydroxide and phosphorous pentoxide, thoroughly degassed and purified by fractionation at −96°C; v.p. 1 mm. Several samples were prepared and no significant difference was observed in their mass spectra except in two instances where a small quantity of methyl chloride (<1 percent) was detected. The compound was stored as a liquid at −78°C; v.p. 6.6 mm.

Optical System

A Hanovia S-500 medium-pressure mercury arc run off a stabilized ac voltage supply was used as the light source. The beam was collimated by an optical system comprising two quartz lenses and two stops and was approximately parallel over the 10-cm length of the cylindrical reaction cell. It had a volume within the cell of 110 cc. Filters were used to limit the incident radiation to the longer wavelengths of the ultraviolet spectrum.

Filter A: Corning violet ultra No. 2–37 or 586, 6 mm in thickness.

Filter B: Corning H.R. clear chemical glass No. 053 or 774, 3 mm in thickness.

Most of the experiments were conducted with Filter A. As determined by a Beckman Spectrophotometer, it had a transmission of 22.5 percent at 3660A and 6.7 percent at 3340A and was opaque at wavelengths below 3150A and above 3900A. From the published data on the spectral energy distribution of the lamp and from the relative extinction coefficients of azomethane at 3660A and 3340A, we have estimated that 96 percent of the absorbed intensity consists of the longer wavelength. Filter B transmitted only wavelengths greater than 2900A and at 3660A had a transmission of 90 percent.

For quantum yield measurements using Filter A the light incident on the reaction system was determined by uranyl oxalate actinometry.[11,12] In two experiments using actinometer solutions of different concentrations values of 6.5×10^{16} and 6.05×10^{16} quanta/min were obtained. Absorption measurements were made with a Weston photronic cell coupled to a sensitive galvanometer. As individual values were liable to error, Beer's law curves were constructed for the various temperatures and the absorption for a given azomethane pressure obtained from them. (With Filter A the light was sufficiently monochromatic to make Beer's law hold to within the experimental accuracy.) The intensity of the incident radiation was varied by interposing neutral density filters of Chromel deposited on quartz in the path of the light beam.

[11] W. G. Leighton and G. S. Forbes, J. Am. Chem. Soc. **52**, 3139 (1930).

[12] G. S. Forbes and L. J. Heidt, J. Am. Chem. Soc. **56**, 2263 (1934).

Apparatus

The quartz reaction cell and manometer were isolated from the remainder of the high vacuum system by mercury cutoffs. The cell volume was 170 cc and together with connecting tubes 340 cc. In later experiments with gas mixtures mixing was facilitated by incorporating a large bulb (*ca* 300 cc. capacity) into the reaction system in which mercury could be raised and lowered. The analytical section consisted of a mercury diffusion pump, a variable temperature trap, low-temperature fractionating column,[13] McLeod gauge, Toepler pump, and gas burette. A furnace in the form of a cylindrical aluminum block with double quartz windows enclosed the cell, and a constant voltage was applied to its heating element through a Sorenson regulator. The temperature gradient along the cell did not exceed 1°C, and the absolute temperature was usually maintained to within ±1°C during a reaction.

Analysis of Products

The materials from the cell were pumped into the analysis system, condensed and the nitrogen-methane mixture removed by the Toepler pump at liquid nitrogen temperature. The column was set at −160°C, the trap being maintained at a temperature 20–30° higher to hold back the bulk of the unchanged azomethane, and the ethane fraction taken off. When carbon dioxide was added to the reaction mixture, ethane was removed at −170°C to prevent contamination. The individual fractions were analyzed by mass spectrometry and sometimes by combustion on a platinum wire. The former was found to give more consistent results, particularly for nitrogen-methane fractions containing small percentages of methane. Because of the inaccuracies involved in collecting and measuring very small volumes, no separation was attempted for reactions in which ethane constituted less than 5 percent of the total gaseous product, and the complete mixture was analyzed by the mass spectrometer. Hydrogen and ethylene were not detected, their concentrations, if present, being no greater than 0.5 percent. In some experiments at the lower temperatures small quantities of propane, invariably less than 1 percent of the total product, were found.

RESULTS

Preliminary experiments showed that for small conversions, i.e., less than 6 percent, the rates of formation of nitrogen, methane, and ethane, were independent of the amount of decomposition, and subsequent experiments were kept within this limit. No thermal reaction was observed except at the highest temperature where the rate was 1 percent of the photochemical when Filter A was used.

Table I includes the results of sets of runs conducted at temperature intervals between 24°C and 191°C

[13] D. J. LeRoy, Can. J. Research **28**, 492 (1950).

TABLE I. The variation in the rates of formation of nitrogen, methane, and ethane with azomethane concentration and temperature (Filter A used).

Run no.	Azomethane pressure (mm)	Fraction absorbed I_a	$R_{N_2}\cdot10^5$	$R_{CH_4}\cdot10^5$	$R_{C_2H_6}\cdot10^5$	$\frac{1}{2}CH_4+C_2H_6$ / N_2	$R_{CH_4}\cdot10^{-2}$ / $R_{C_2H_6}{}^{\frac{1}{2}}$[Azo]
			cc at NTP/min				
Temp. 297°K							
20	10.8	0.045	12.3	0.35	11.3	0.93	5.6
19	19.8	0.081	22.4	1.41	19.0	0.87	9.35
16	42.5	0.166	51.2	3.58	40.4	0.82	7.77
15	43.6	0.170	52.3	3.70	42.4	0.84	7.66
22	46.1	0.179	52.6	3.90	39.6	0.79	7.81
21	60.6	0.227	68.4	7.17	50.1	0.79	9.73
18	80.5	0.289	86.4	10.5	61.4	0.77	9.77
Temp. 326°K							
47	10.8		10.6	0.70	7.69	0.76	15.1
46	20.0		19.8	1.69	13.8	0.74	14.7
42	41.2		37.8	4.35	22.9	0.66	14.3
41	59.9		54.6	6.52	29.5	0.60	12.8
45	81.8		72.5	11.2	37.4	0.59	14.4
43	100.7		79.1	13.4	36.0	0.54	14.3
44	124.9		105.3	19.6	46.0	0.53	14.9
Temp. 363°K							
40	9.6		7.73	1.42	4.00	0.61	53.6
39	24.4		22.7	4.54	7.03	0.41	50.6
35	40.4		39.7	5.80	10.7	0.34	31.5
36	41.1		38.5	7.06	9.98	0.35	39.1
34	62.9		53.3	12.6	12.6	0.35	40.6
38	82.8		74.3	17.7	13.4	0.30	42.0
37	99.8		78.9	19.6	15.9	0.33	35.4
Temp. 401°K							
26	11.2	0.040	10.7	4.0	1.46	0.32	231
25	20.5	0.073	19.4	7.97	2.10	0.31	212
31	40.2	0.138	34.4	13.1	3.00	0.28	148
29	40.3	0.139	37.4	12.8	3.78	0.27	129
24	40.5	0.140	35.0	13.4	2.89	0.27	154
30	40.9	0.141	36.4	14.0	3.22	0.28	152
32	42.2	0.145	36.3	10.4	3.46	0.24	105
28	59.2	0.196	53.7	19.9	4.48	0.27	125
33	80.9	0.257	63.1	23.6	4.32	0.26	111
27	102.4	0.313	78.8	32.2	4.08	0.26	123
Temp. 437°K							
52	22.1		19.3	7.08	0.93	0.23	286
56	27.5		24.0	9.16	1.18	0.24	263
49	42.6		37.3	15.6	1.14	0.24	294
50	60.7		50.2	18.4	1.82	0.21	193
53	70.3		53.8	22.0	1.47	0.23	222
51	81.2		63.9	24.3	1.44	0.22	215
54	87.9		67.3	27.8	1.74	0.23	207
55	93.5		71.7	28.7	1.95	0.23	189
48	105.5		81.4	32.7	2.78	0.24	160
[a]75	145.5		85.0	41.2	1.66	0.26	190
Temp. 464°K							
63	41.0		36.1	16.5	0.76	0.25	421
62	57.0		48.0	21.0	0.84	0.24	368
61	99.2		77.5	34.8	0.80	0.23	359

[a] Reaction carried to 10 percent decomposition.

where, in general, the range of initial pressures of azomethane was from 10–100 mm. The results of experiments in which the incident intensity was varied, the absorption remaining sensibly constant, are given in Table II, and Table III illustrates the effect of temperature on the quantum yield of nitrogen formation. Experiments in the presence of an inert gas, carbon dioxide, are recorded in Table IV. Tables V and VI contain the values required for the calculation of the activation energies of the abstraction reactions and the reaction by which methyl radicals are considered to associate with azomethane. The latter have been derived from material balances; the method will be discussed later.

Because of small variations in light intensity and slight changes in geometry after cleaning the cell, the results of a given series of runs are somewhat more reproducible than are those for runs selected at random for all series. For this reason a separate series of runs was made to determine the effect of each of the various

TABLE II. The variation in the rates of formation of nitrogen, methane, and ethane with absorbed intensity (for Filter A).

Run no.	Azomethane pressure (mm)	$I_a \cdot 10^{-16}$ (quanta/min)	$R_{N_2} \cdot 10^5$	$R_{CH_4} \cdot 10^5$	$R_{C_2H_6} \cdot 10^5$	$\frac{R_{CH_4} \cdot 10^{-2}}{R_{C_2H_6}[Azo]}$	$\frac{R_{N_2} \cdot 10^{20}}{I_a}$ (cc/quantum)
			cc at NTP/min				
Temp. 294°K							
76	94.4	1.17	40.7	5.01	29.3	5.66	3.48
77	100.7	0.40	13.8	2.71	7.19	5.80	3.45
78	100.6	1.87	63.1	8.33	42.9	7.32	3.37
79	104.5	0.22	8.21	1.76	3.44	5.32	3.73
80	42.5	4.91	160.7	4.63	142.3	5.33	3.27
Temp. 436°K							
57	97.5	1.88	66.1				3.52
58	96.6	0.40	15.8				3.95
59	100.9	1.28	47.4				3.70
60	98.8	0.22	8.27				3.76

TABLE III. Effect of temperature on the quantum yield of nitrogen formation (Filter A used).

Run no.	Temp °K	Azomethane pressure (mm)	$I_a \cdot 10^{-16}$ (quanta/min)	$R_{N_2} \cdot 10^5$ (cc at NTP/min)	$\frac{R_{N_2} \cdot 10^{20}}{I_a}$ (cc/quantum)	ϕ_{N_2}
68	296	40.9	1.00	33.5	3.35	0.90
69	295	105.9	2.28	77.9	3.42	0.92
70	328	63.2	1.42	45.9	3.23	0.87
71	329	99.3	2.09	67.8	3.24	0.88
72	365	42.5	0.96	31.9	3.32	0.89
73	364	92.8	1.92	63.0	3.28	0.88
66	400	60.9	1.27	41.2	3.24	0.88
67	401	99.2	1.92	69.0	3.59	0.97
74	432	62.8	1.24	42.3	3.41	0.92
61	464	99.2	1.85	77.5	4.18	1.12
62	464	57.0	1.14	48.0	4.20	1.13

parameters. The results in the different tables are, therefore, not strictly comparable with one another, although the differences are slight.

A product of lower vapor pressure than azomethane was detected at the higher temperatures. This has been reported previously both for the photolysis[3] and for the thermal decomposition.[14,15] The residues from several runs at 164°C were collected after removal of the azomethane by pumping at −110°C. The mass spectrum indicated that the product was a mixture and peaks were found at mass numbers between 58 and 88, the greatest being at 72 and 88. There appeared to be no fragments between 88 and 150. In experiment 75 a larger quantity of product was obtained by using a higher pressure and by increasing the decomposition to 10 percent. The hydrocarbon rates were in agreement with those found under the normal conditions. An attempt was made to separate the mixture by low-temperature fractionation. Although there was some concentration of the 72 peak in the first fraction and the 88 peak in the second and third, the mass spectrometer cracking patterns showed that the fractions were not single components. However, a comparison of the ratio of different peak heights suggested that 72 and 88 were likely parent mass numbers. These are the molecular weights of methyl ethyl di-imide and tetramethylhydrazine. Insufficient material was obtained for an analysis.

DISCUSSION

The results for the rates of production of the permanent gases are consistent with the reaction scheme

$$CH_3N{=}NCH_3 + h\nu \rightarrow N_2 + 2CH_3 \quad (1)$$

$$CH_3 + CH_3N{=}NCH_3 \rightarrow CH_4 + CH_2N{=}NCH_3 \quad (2)$$

$$CH_3 + CH_3 \rightarrow C_2H_6 \quad (3)$$

It is interesting to note that this is an analog of the mechanism proposed for the photolysis of acetone at high temperatures.[16–18] If nitrogen, methane, and ethane are formed only by the above reactions, the rates may be expressed as follows:

$$R_{N_2} = \phi_{N_2} I_a \quad (1)$$

$$R_{CH_4} = k_2[CH_3][Azo] \quad (2)$$

$$R_{C_2H_6} = k_3[CH_3]_2. \quad (3)$$

[14] E. W. Riblett and L. C. Rubin, J. Am. Chem. Soc. **59**, 1537 (1937).
[15] H. A. Taylor and F. P. Jahn, J. Chem. Phys. **7**, 470 (1939).
[16] L. M. Dorfman and W. A. Noyes, Jr., J. Chem. Phys. **16**, 557 (1948).
[17] W. A. Noyes, Jr., and L. M. Dorfman, J. Chem. Phys. **16**, 788 (1948).
[18] A. F. Trotman-Dickenson and E. W. R. Steacie, J. Chem. Phys. **18**, 1097 (1950).

TABLE IV. Effect of carbon dioxide on the reaction at room temperature (Filter B used).

Run no.	Temp. °K	Azomethane pressure (mm)	CO_2 pressure (mm)	$R_{N_2}\cdot10^5$	$R_{CH_4}\cdot10^5$	$R_{C_2H_6}\cdot10^5$	$\frac{R_{CH_4}\cdot10^{-2}}{R_{C_2H_6}^{\frac{1}{2}}[Azo]}$	$\frac{R_{N_2}\cdot10^3}{[Azo]}$ (cc/mole)
				cc at NTP/min				
144	302	41.2	—	190.4	5.45	170.3	6.03	8.69
146	305	43.7	—	198.5	6.86	171.1	7.21	8.63
145	304	43.3	48.7	200.3	6.02	170.6	6.40	8.78
147	302	45.1	89.8	196.8	6.19	172.1	6.21	8.20
143	303	43.9	185.7	197.7	5.92	171.1	6.16	8.52

TABLE V. Effect of temperature on the values of $R_{CH_4}/R_{C_2H_6}^{\frac{1}{2}}[Azo]$.

Run no.	Temp. °K	$[Azo]\cdot10^6$ moles/cc	$R_{N_2}\cdot10^5$	$R_{CH_4}\cdot10^5$	$R_{C_2H_6}\cdot10^5$	$\frac{R_{CH_4}\cdot10^{-2}}{R_{C_2H_6}^{\frac{1}{2}}[Azo]}$
			cc at NTP/min			
Filter A						
115	297	2.57	39.0	3.69	29.9	8.29
117	315	2.64	42.3	5.41	26.5	12.6
127	330	2.67	42.9	6.78	20.8	17.6
120	339	2.60	44.2	8.06	18.5	22.8
113	362	2.42	42.2	10.3	9.84	43.0
112	386	2.41	43.6	12.9	5.72	71.0
121	424	2.47	46.6	17.6	1.49	194
123	449	2.33	46.7	20.3	0.80	308
Filter B						
116	297	2.45	193.4	8.2	171.2	8.08
118	314	2.69	231.5	14.3	186.7	12.3
126	330	2.98	246.6	22.7	182.7	17.9
119	338	2.69	236.7	23.8	156.7	22.3
114	362	2.33	213.5	31.3	104.4	41.6
111	385	2.38	232.6	52.1	67.3	84.5
122	423	2.40	232.9	71.3	25.5	186
124	451	2.45	238.3	93.1	11.9	349

TABLE VI. Effect of temperature on the values of $R_{CH_3A}/R_{C_2H_6}^{\frac{1}{2}}[Azo]$ and $R_{TMH}/R_{C_2H_6}^{\frac{1}{2}}[Azo]$ (R_{CH_3A} and R_{TMH} derived from material balances).

Run no.	Temp. °K	$R_{CH_3A}\cdot10^5$ cc at NTP/min	$\frac{R_{CH_3A}\cdot10^3}{R_{C_2H_6}^{\frac{1}{2}}}$	$\frac{R_{CH_3A}\cdot10^{-3}}{R_{C_2H_6}^{\frac{1}{2}}[Azo]}$	$R_{TMH}\cdot10^5$ cc at NTP/min	$\frac{R_{TMH}\cdot10^3}{R_{C_2H_6}^{\frac{1}{2}}}$	$\frac{R_{TMH}\cdot10^{-3}}{R_{C_2H_6}^{\frac{1}{2}}[Azo]}$
Filter A							
115	297	14.5	8.38	3.26	5.4	3.12	1.21
117	315	25.2	15.5	5.87	10.4	6.38	2.42
127	330	37.4	26.0	9.74	15.3	10.6	3.98
120	339	43.3	31.8	12.2	17.6	12.9	4.96
113	362	54.4	54.8	22.6	22.1	22.3	9.21
112	386	62.9	83.2	34.5	25.0	33.1	13.7
121	424	72.6	188	76.1	27.5	71.2	28.8
123	449	71.5	253	109	25.6	90.5	38.8
Filter B							
116	297	36.2	8.74	3.57	14.0	3.38	1.38
118	314	75.3	17.4	6.47	30.5	7.06	2.62
126	330	105.1	24.6	8.26	41.1	9.63	3.23
119	338	136.2	34.4	12.8	56.2	14.2	5.28
114	362	186.9	57.9	24.8	77.8	24.1	10.3
111	385	278.5	107.5	45.2	113.2	43.7	18.4
122	423	369	230.6	96.1	136.1	85.1	35.5
124	451	360	330	135	133.3	122	49.9

Primary Process

The data given in Table III show that the quantum yield of nitrogen formation ϕ_{N_2} is constant at temperatures between 24°C and 164°C, and it is considered to be unity within the experimental accuracy. Furthermore, the rate of nitrogen production is a linear function of the absorbed intensity I_a over a tenfold range, as is to be expected, independent of whether the incident intensity is varied (Table II) or the absorption (Fig. 1). The fact that the curves in Fig. 1 are not collinear is attributed to a slight change in the light intensity resulting from a realignment of the optical system. In these experiments Filter A was used which effectively provides that only the mercury lines at

3660A are absorbed. It appears evident that the mechanism of photolysis is independent of wavelength above 3000A. In column 9 of Table IV are given values of the ratio $R_{N_2}/[Azo]$ in the presence of various amounts of carbon dioxide. This is essentially a measure of the quantum yield when the azomethane concentration is sensibly constant. The results are in agreement with those of Cannon and Rice[8] and exclude the possibility of an excited molecule mechanism, at least within the concentration range investigated. Evidence for collisional deactivation of the electronically excited species has been observed in the higher homologs of this series, namely, azoethane[19] and azoisopropane,[20] where there are presumably sufficient internal degrees of freedom to disperse the excitation energy and thus increase the lifetime of the activated molecule to the order of the time between molecular collisions.

A quantum yield of unity which is not dependent on temperature or concentration implies that nitrogen does not arise from secondary reactions. That nitric oxide inhibits the formation of hydrocarbons but not nitrogen[4] furnishes more direct evidence of this. It would not be possible, however, to differentiate between a primary process such as Eq. (1) and one in which the initial split involved only a single carbon-nitrogen bond, provided the lifetime of the radical $CH_3N{=}N$ is short compared with its probability of collision.

The Reactions Producing Methane and Ethane

Assuming a stationary concentration of methyl it follows from Eqs. (2) and (3) that

$$R_{CH_4}/R_{C_2H_6}{}^{\frac{1}{2}} = k_2[Azo]/k_3{}^{\frac{1}{2}}. \qquad (4)$$

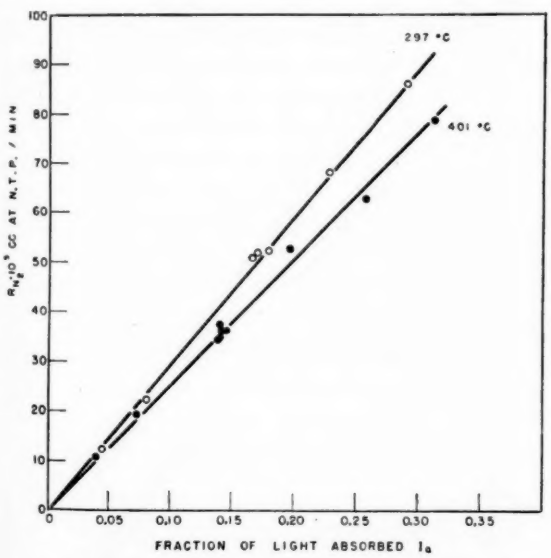

FIG. 1. Rate of nitrogen formation as a function of absorbed intensity.

[19] J. L. Weininger and O. K. Rice, "Symposium on physical and inorganic chemistry," American Chemical Society, Buffalo (March, 1952).

[20] R. Durham (private communication).

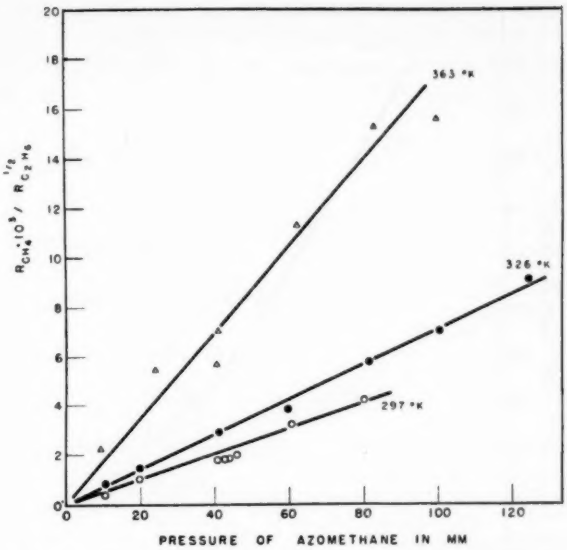

FIG. 2. $R_{CH_4}/R_{C_2H_6}{}^{\frac{1}{2}}$ as a function of azomethane pressure.

The plots of $R_{CH_4}/R_{C_2H_6}{}^{\frac{1}{2}}$ against azomethane pressure for the three lowest temperatures (Fig. 2) support the validity of reactions (2) and (3) as the sources of methane and ethane. The results at higher temperatures have not been illustrated graphically because the scatter is largely a result of the inaccuracies in estimating very small quantities of ethane, but the trend is evident. In addition, as the methyl radical concentration, which is a function of the absorbed intensity, does not enter into Eq. (4) the expression $R_{CH_4}/R_{C_2H_6}{}^{\frac{1}{2}}[Azo]$ should be independent of I_a. The results at room temperature (Table II) are in general agreement with this hypothesis. In the photolysis of acetone Linnell and Noyes[21] found that $k_2/k_3{}^{\frac{1}{2}}$ tends to increase at low pressures and have suggested that a third body may be necessary for the combination of methyls. Our results are not accurate enough to detect such an effect with certainty, and it is considered that a refinement of this nature does not affect the over-all picture.

A least squares calculation on the linear portion of the Arrhenius plot of $\log R_{CH_4}/R_{C_2H_6}{}^{\frac{1}{2}}[Azo]$ against the reciprocal of the absolute temperature (Fig. 3) yields the value of 7.6 ± 0.2 kcal/mole for the activation energy difference $E_2-\frac{1}{2}E_3$.

If it is assumed that the bimolecular combination of methyls has a zero activation energy, then the value above will be for the hydrogen abstraction reaction (2). The rates quoted are in the units cc at NTP/min, and the concentration of azomethane has been expressed in moles/cc. The expression $R_{CH_4}/R_{C_2H_6}{}^{\frac{1}{2}}[Azo]$ must, therefore, be multiplied by the constant factor $1.11\times10^{-15}/V^{\frac{1}{2}}$, where V is the reaction volume, if the ratio of the rate constant $k_2/k_3{}^{\frac{1}{2}}$ is required in the units $(\text{molecules/cc})^{-\frac{1}{2}}\ \text{sec}^{-\frac{1}{2}}$). On the assumption that there is no diffusion of radicals out of the light space, the

[21] R. H. Linnell and W. A. Noyes, Jr., J. Am. Chem. Soc. 73, 3986 (1951).

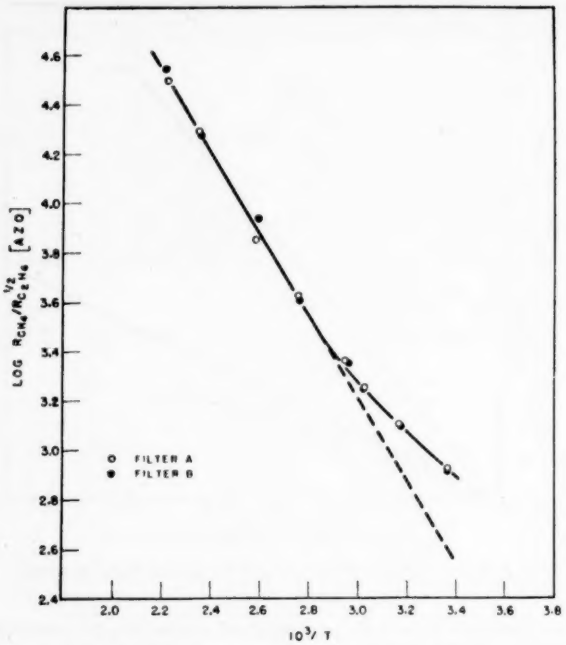

FIG. 3. Arrhenius plot for the abstraction of hydrogen from azomethane by methyl radicals.

effective reaction volume will be the light beam volume, namely, 110 cc. If values of 3.5 and 5.5A, respectively, are chosen as the collision diameters of the methyl radical and azomethane molecule, the ratio of steric factors $P_2/P_3^{\frac{1}{2}}$ is $10^{-3}-10^{-4}$ by the simple kinetic theory calculation. This is of the same order of magnitude as found by one of us[22] in previous investigations of reactions of this type.

There is a curvature in the Arrhenius plot at low temperatures which is also observed in the photolysis of acetone[23] and of mercury dimethyl.[24] For acetone it has been shown that if the light beam does not entirely fill the cell, diffusion of radicals plays some part. Above 100°C there is little diffusion out of the light beam, whereas at 25°C it is complete. This is apparent from the fact that reaction rates vary exponentially with temperature and rates of diffusion $T^{\frac{1}{2}}$. The reaction by which the methyl radical is principally removed is therefore different at high and at low temperatures. Thus, the effective reaction volume will change from that of the light beam to that of the cell. A correction of this type accounts only for part of the deviation, and Noyes[25] has considered in detail the possible causes of the anomaly. In the case of azomethane, although the results at room temperature were fairly reproducible for consecutive experiments, at different times individual values were obtained which fell below the curve in Fig. 3, but which were always equal to or higher than the extrapolated value corrected for diffusion. This suggests that the low temperature values may be sensitive to the condition of the cell, although the presence of an impurity with a low activation energy of abstraction cannot be completely ruled out since seven different samples of azomethane were used throughout the work. However, as previously mentioned, except for traces of methyl chloride in two of the samples no other impurity was detected. This alone could not cause the observed variation. Returning to the question of diffusion, carbon dioxide acting as an inert gas should reduce the effect. No change was observed in the ratio $k_2/k_3^{\frac{1}{2}}$, but the result cannot be considered conclusive as the difference between the light beam and cell volumes was small.

[22] A. F. Trotman-Dickenson and E. W. R. Steacie, J. Chem. Phys. **19**, 329 (1951).
[23] A. J. C. Nicholson, J. Am. Chem. Soc. **73**, 3981 (1951).
[24] R. E. Rebbert (private communication).
[25] W. A. Noyes, Jr., J. Phys. & Colloid Chem. **55**, 925 (1951).

The Addition of Methyl to Azomethane

If reaction (1) represents the sole primary photochemical process, for every molecule of nitrogen that appears as a product two methyls will be produced and, if reactions (2) and (3) are the only means by which these disappear, the ratio $(\frac{1}{2}CH_4+C_2H_6)/N_2$ should be unity. A value of less than unity indicates that there are simultaneous or subsequent reactions. The picture is somewhat simplified by the fact that under the conditions chosen, i.e., low conversions, there is no evidence for secondary reactions involving the hydrocarbons. An addition reaction between methyl and azomethane has been postulated.[2] In its simplest form this may be represented by

$$CH_3+A\rightarrow CH_3A, \qquad (5)$$

where A denotes a molecule of azomethane. If reaction (5) is the fate of all methyls other than those resulting in methane and ethane, or of a constant fraction of such radicals, the rate of formation of CH_3A will be

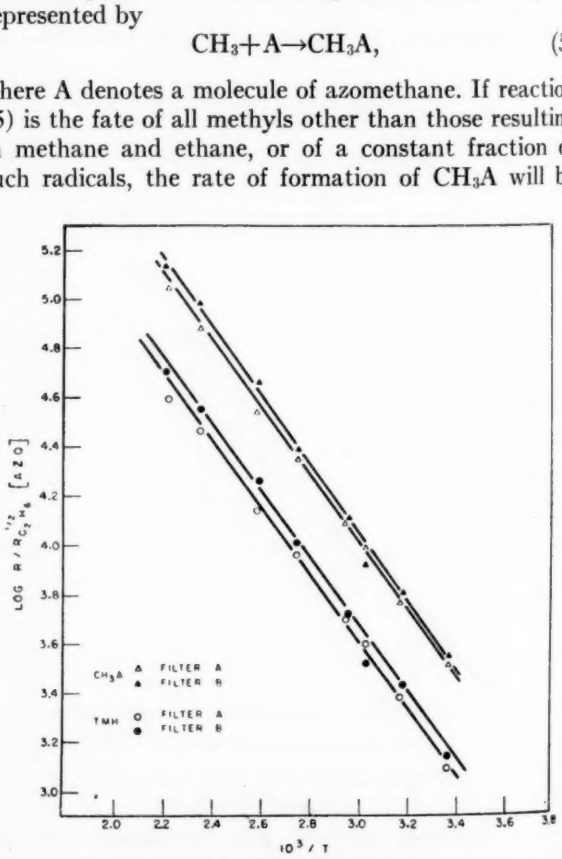

FIG. 4. Arrhenius plots for the addition of methyl radicals to azomethane.

proportional to $2R_{N_2}-(R_{CH_4}+2R_{C_2H_6})$. The values of $R_{CH_3A}/R_{C_2H_6}{}^{\frac{1}{2}}[Azo]$ calculated in this way are given in Table VI. From the Arrhenius curves (Fig. 4) $E_4-\frac{1}{2}E_3$ is 6.4 kcal/mole for both Filters A and B.

Taking into consideration the formation and fate of the radicals $CH_2N=NCH_3$ and $(CH_3)_2N-NCH_3$, the reaction scheme may be completed in the following manner:

$$CH_3+CH_3N=NCH_3\rightarrow(CH_3)_2N-NCH_3 \quad (6)$$

$$CH_3+(CH_3)_2N-NCH_3\rightarrow(CH_3)_2N-N(CH_3)_2 \quad (7)$$

$$CH_3+CH_2N=NCH_3\rightarrow C_2H_5N=NCH_3 \quad (8)$$

$$2(CH_3)_2N-NCH_3\rightarrow(CH_3)_2N-\underset{\displaystyle CH_3-N-N(CH_3)_2}{\overset{\displaystyle |}{N}}-CH_3 \quad (9)$$

$$2CH_2N=NCH_3\rightarrow(CH_2N=NCH_3)_2 \quad (10)$$

$$(CH_3)_2N-NCH_3+CH_2N=NCH_3\rightarrow(CH_3)_2N-\underset{\displaystyle CH_2N=NCH_3}{\overset{\displaystyle |}{N}}-CH_3 \quad (11)$$

Steps (6) and (7) account for the tetramethyl hydrazine and (8) for the methyl ethyl di-imide which mass spectrometer analyses of the liquid isolated from photolysis at 164°C suggest are probable products. The association of methyl and azomethane can be related to the formation of tetramethyl hydrazine if certain simplifying assumptions are made; a molecule of methyl ethyl di-imide is formed for every molecule of methane and combination of radicals by reactions (9)–(11) is small and may be neglected. Hence, from material balance considerations $R_{TMH}=\frac{1}{2}[2R_{N_2}-(2R_{CH_4}+2R_{C_2H_6})]$, where R_{TMH} is the rate of formation of tetramethyl hydrazine. Such a calculation implies that reaction (6) is the rate determining process. The plots of $\log R_{TMH}/R_{C_2H_6}{}^{\frac{1}{2}}[Azo]$ against $1/T$ for the two filters give the same value for $E_5-\frac{1}{2}E_3$, 6.3 kcal/mole. Although evidence derived from material balances must generally be accepted with reserve, the consistency between the two methods of calculation of the activation energy strengthens the argument in favor of the proposed mechanism. (This argument is, however, somewhat weakened by the fact that the temperature coefficient of R_{CH_4} is similar to that of TMH or of CH_3A, and hence, the two methods of calculation give similar results.) It should be emphasized that any uncertainty about the addition reaction does not affect the validity of the conclusions concerning the hydrogen abstraction reaction.

The Use of Azomethane as a Methyl Radical Source

It has been demonstrated that the kinetics of the formation of methane and ethane in the photolysis of azomethane are well defined. Consequently, it may be used as a convenient source of radicals for investigating the reaction

$$CH_3+RH\rightarrow CH_4+R,$$

where RH is a hydrogen donor. However, as the energy of abstraction from the substrate is low, the choice of suitable compounds is limited since in competitive experiments, considering the normal accuracy of analysis, quantitative results can only be obtained if their rates are comparable or faster. Azomethane has one advantage in that it absorbs at longer wavelengths and would, therefore, be adaptable for an investigation of the reaction of methyl with aldehydes and ketones. Such experiments are in progress.

The authors are indebted to Dr. L. C. Leitch and Mr. A. Morse for samples of dimethyl hydrazine hydrochloride, Dr. F. P. Lossing and Miss F. Gauthier for the mass spectrometer analyses, and Dr. R. N. Jones for measurements of the ultraviolet absorption spectrum of azomethane.

Absorption Coefficients of Oxygen in the Vacuum Ultraviolet

K. WATANABE, EDWARD C. Y. INN, AND MURRAY ZELIKOFF
Geophysics Research Directorate, Air Force Cambridge Research Center, Air Research and Development Command, Cambridge, Massachusetts

(Received December 22, 1952)

Absorption coefficients of oxygen were measured at several hundred wavelengths in the region 1050–1900A with a one-meter vacuum monochromator and a phosphor-coated photomultiplier as detector. The absorption intensity of the Schumann-Runge continuum was found to be somewhat less than previous results, and the intensity distribution was less symmetrical. The 19–0 and 20–0 bands of the Schumann-Runge progression were observed and the dissociation limit of the $B^3\Sigma_u^-$ state was 57140±60 cm^{-1}. Several other bands and continua were found at shorter wavelengths.

INTRODUCTION

THE study of photochemical and collision processes occurring in our upper atmosphere requires additional data on cross sections of gases involved in these processes. For example, a number of recent calculations of atmospheric layers have led to different conclusions as a result of the freedom exercised in the estimates of cross sections. For the vacuum ultraviolet, experimental data of absorption coefficients are still rather incomplete even for the most common gases.

Absorption coefficients of O_2 have been measured more extensively than those of any other gas. Ladenburg and van Voorhis[1] made the first quantitative measurement of absorption intensity in the vacuum ultraviolet and obtained data in the region 1330–1670A of the Schumann-Runge dissociation continuum. Their results were supported theoretically by Stueckelberg[2] and experimentally by Schneider,[3] who measured the absorption of dry CO_2-free air at 350 wavelengths in the region 380–1600A. Preston[4] and Williams[5] measured the absorption coefficients of O_2 at Lyman alpha but disagreed by a factor of fifty. Recently, Weissler and Po Lee,[6] and Clarke[7] reported data for both O_2 and N_2 at a number of wavelengths in the difficult region below the transmission limit of LiF. At two wavelengths where comparisons can be made, their results agreed for O_2 but not for N_2. To make the data for O_2 more complete, it would be desirable (a) to obtain values in the region 1670–1900A, (b) to fill a number of gaps in the shorter-wavelength regions, and (c) to resolve the conflicting results at Lyman alpha.

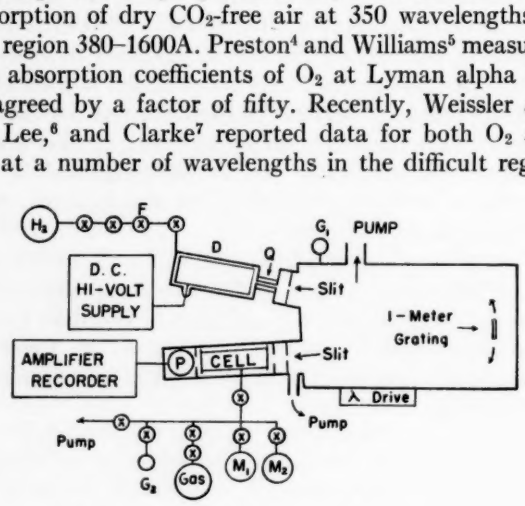

FIG. 1. Schematic diagram of apparatus.

This paper will describe some absorption measurements of O_2 made by a method somewhat different from that used by previous investigators. Measurements were made for several hundred wavelengths but were limited to the region down to 1050A, a limit set by the transmission of LiF windows of the absorption cell.

EXPERIMENTAL

The method of photographic photometry has been employed almost invariably for measurements of absorption coefficients in the vacuum ultraviolet; however, Preston's experiment[4] is an exception. He used an argon-filled Pt photocell with a LiF window for his measurement at Lyman alpha. In view of the well-known uncertainties of photographic plates, particularly for use in the region below 2000A, a 1P21 photomultiplier was selected for our detector.

In the region down to the transmission limit of LiF, it is preferable to enclose the absorbing gas in a cell rather than to use the spectrograph chamber which is usually in communication with the light source. In the former case, pressures of the absorbing gas can be more readily controlled over a wide range, and contamination of the absorbing gas as well as changes in the spectral characteristics of the light source and grating reflectivity can be minimized. By varying the pressure in the cell, it is possible to measure absorption intensity covering a range of 10^5.

The experimental arrangement is shown schematically in Fig. 1. The dispersing instrument was a Baird one-meter, vacuum monochromator. A slit width of 0.05 mm, which gave a band width of 0.85A, was used for both slits and the spectrum was scanned at 20A per minute. Wavelengths were measured to the nearest angstrom; however, occasionally the wavelength reading was in error by as much as two angstroms.

[1] R. Ladenburg and C. C. van Voorhis, Phys. Rev. **43**, 315 (1933).
[2] E. C. G. Stueckelberg, Phys. Rev. **42**, 518 (1932).
[3] E. G. Schneider, J. Opt. Soc. Am. **30**, 128 (1940).
[4] W. M. Preston, Phys. Rev. **57**, 887 (1940).
[5] S. E. Williams, Nature **145**, 68 (1940).
[6] G. L. Weissler and Po Lee, J. Opt. Soc. Am. **42**, 200 (1952); Weissler, Lee, and Mohr, J. Opt. Soc. Am. **42**, 84 (1952).
[7] K. C. Clarke, Phys. Rev. **87**, 271 (1952).

The light source (D) was a windowless hydrogen discharge tube with a quartz capillary (Q) and was operated at about 600 v×0.4 amp dc. Tank H_2 was used without purification, and its flow rate was kept constant by means of a needle valve and a simple flowmeter (F). The pressure in the main chamber of the monochromator was held at about 1×10^{-4} mm Hg when the light source was in operation. The constancy of the discharge condition was checked by the arc current, the flow rate, and the ion gauge (G_1). As a rule, the light intensity did not vary more than a few percent over a period of several hours. This was the largest source of error; however, when a more accurate result was desired, repeated measurements were made at fixed wavelengths.

The photomultiplier (P) was coated with sodium salicylate and placed in a position where it intercepted the entire beam from the exit slit. Dynode voltages from 80 to 90 volts per dynode were required for the photomultiplier. Its current was amplified and fed into a Speedomax recorder. Further details of the detector are described elsewhere.[8]

All previous investigators[1,2,4–7] placed their absorption cell between the light source and the *entrance* slit or filled their spectrograph with the absorbing gas. As observed by Ladenburg and van Voorhis,[1] photochemical change of the absorbing gas is quite possible when the cell is near the light source. Moreover, the transmission of the cell window may change due to sputtering and formation of color centers. Therefore, the absorption cell was placed at the exit slit where the number of photons passing through per hour was estimated from our thermocouple data[8] to be at least a few orders of magnitude less than the number of molecules. The Pyrex absorption cell (diameter 2.0 cm, length 4.7 cm) with LiF windows was in direct communication with a gas filling system provided with two McLeod gauges (M_1 and M_2), mercury manometer, ion gauge (G_2), and sample bottles. Cleaved LiF plates about 1 mm thick were used instead of lenses since the divergence of the beam from the exit slit was small and good transmission was desirable.

After purification of the gas to be studied, the experimental procedure was as follows. First, a sample of gas was removed directly from the gas filling system and analyzed for possible contamination, using a Consolidated Engineering Corporation mass spectrometer. In the case of O_2 the total impurity was about 0.1 percent, mostly N_2 which is, however, quite transparent in this region. Second, the absorption cell was evacuated to about 10^{-6} mm Hg and by scanning the H_2 spectrum, the spectral intensity was obtained as a recorder trace of the photomultiplier current. Third, the cell was filled with the absorbing gas at a suitable pressure, and the photomultiplier response of the transmitted light was recorded on the same trace using a different colored ink. The second and third steps of the procedure were repeated using various gas pressures to cover the absorption intensities and to determine whether Beer's Law held. In the case of O_2 pressures from 0.1- to 500-mm Hg were used.

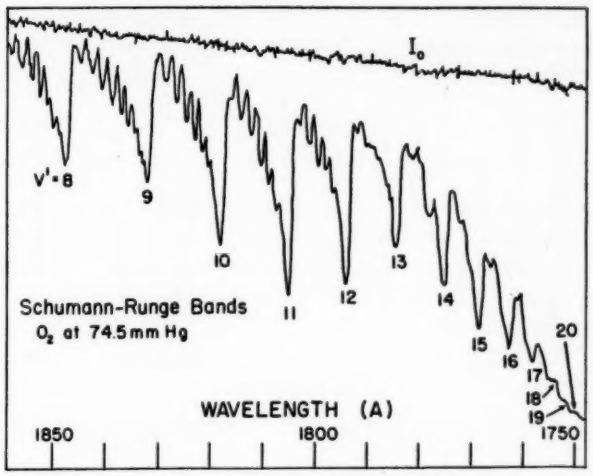

FIG. 2. Recorder trace of the Schumann-Runge bands in absorption. The upper curve represents the incident intensity of the H_2 continuum.

To obtain the absorption coefficients from the recorder traces, corrections were made whenever necessary for the scattered light and the fluorescence of the LiF window. The absorption was measured at several hundred wavelengths, one to three angstroms apart, using for each wavelength several pressures varying by a factor of at least ten. The absorption coefficient, k in cm^{-1}, is defined by $I/I_0=\exp(-kx)$ where x is the layer thickness of the absorbing gas reduced to NTP.

In order to interpret the absorption data, it is necessary to have an idea of the nature of the absorption spectrum, i.e., whether the absorption spectrum is a continuum, a diffuse band, or a sharp band. For a continuum or a very diffuse band, high resolution is not required, and as a rule Beer's Law holds at relatively low pressures. Furthermore, line sources with a sufficient number of lines may be used. On the other hand, the resolution we have used was not sufficient to give reliable k values for sharp bands, and, in general, the data showed an apparent pressure effect.[9] Figure 2 represents a recorder trace of a partially resolved spectrum of the Schumann-Runge bands (8–0 to 20–0 of ${}^3\Sigma_u^- - {}^3\Sigma_g^-$), and it can be seen that the resolution was not adequate to resolve the P and R branches of the rotational structure. For these bands the "observed coefficients" varied with pressure. Nevertheless, these "observed coefficients" give some idea of the magnitude of absorption intensity and may be useful for semiquantitative applications and for detection of intensity anomalies in a band progression.

[8] K. Watanabe and Edward C. Y. Inn, J. Opt. Soc. Am. **43**, 32 (1953).

[9] Nielson, Thornton, and Dale, Revs. Modern Phys. **16**, 307 (1944).

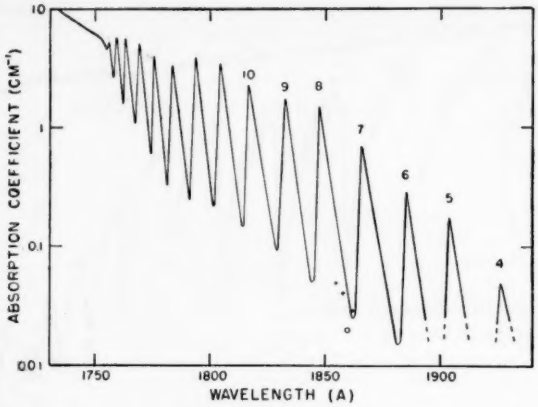

FIG. 3. Absorption coefficients of the Schumann-Runge bands.

RESULTS AND DISCUSSION

For convenience of discussion, the results given below are divided into three spectral regions: the first region extends down to the convergence limit of the Schumann-Runge bands which are vibrational bands superposed on what appears to be a continuum, the second covers the Schumann-Runge dissociation continuum, and the third includes a number of diffuse and sharp bands separated by several rather transparent windows. Papers[10–13] on the absorption spectrum of O_2 in these regions have provided helpful information as to some of the details of the spectrum which were not resolved by our equipment.

(a) Spectral Region 1900–1750A

Part of this region is accessible to quartz spectrographs; however, only a few measurements of absorption coefficients of air have been reported. Many years ago Kreusler[14] obtained the absorption coefficient of air at 1860A. Buisson, Jausseran, and Rouard[15] using line sources determined values for air at 1855, 1858, and 1863A as well as data for longer wavelengths, while the shortest wavelength reported in the extensive work of Vassy,[16] who used the H_2 continuum, was at 1898A. The rotational analyses of the Schumann-Runge bands in absorption have been made by Curry and Herzberg[17] and by Knauss and Ballard.[11]

Since only a short cell length was used here, k values below 0.02 cm^{-1} could not be measured accurately, and the lowest member of the Schumann-Runge progression measured was the 4–0 band. On the other hand, the higher members were observed readily (see Fig. 2), including what seem to be the 19–0 band and the 20–0 band which apparently have not been observed previously. Since these two bands appear rather inconspicuously in a region where the absorption intensity is changing rapidly with wavelength, they would be difficult to observe photographically.

The two bands lie beyond the accepted dissociation limit of the $B^3\sum_u^-$ state (56877 cm^{-1} by Gaydon[18] and 56859 cm^{-1} by Herzberg[19]). Since this dissociation limit was obtained by only a short extrapolation, it has been considered one of the most accurate values. Our monochromator was not designed for accurate measurements of wavelength, nevertheless, it could not be in error by more than one or two angstroms. On this basis, the 20–0 band is given as 57140 ± 60 cm^{-1}. About the time these measurements were made, Herzberg[20] had already suggested the possibility that the convergence limit of the Schumann-Runge bands may be too low by about 220 cm^{-1}. His suggestion is based on his experimentally determined dissociation limit (41219 ±40 cm^{-1} of the $^3\sum_u^+$ state obtained from his observation of the predissociation by rotation in the forbidden Herzberg bands ($^3\sum_u^+ - {}^3\sum_g^-$) under high resolution. Our result, although not precise, strongly supports his suggestion, and tentatively the dissociation energy of oxygen may be taken as 5.11 ev rather than 5.08 ev.

The absorption measurements in this region showed an apparent pressure effect (or effect of layer thickness), which we attributed to the lack of resolution, but a real pressure effect is not excluded. The "observed coefficients" varied by a factor of four or five when the pressure was changed by a factor of 70. For example, the "observed coefficients" of the head of the 14–0 band was 4.0 cm^{-1} at a pressure of 7.1-mm Hg and 0.9 cm^{-1} at 491 mm. The minima showed a smaller effect, i.e., a factor of two to three over the same pressure range. In Fig. 3, the data were smoothed out and given somewhat arbitrarily; i.e., low-pressure data were used for the maxima and high pressure data for the minima. Even so, these maxima are probably still too low and minima too high. This is supported by some data obtained with a slightly higher resolution.

For comparison, the values obtained by Kreusler[14] and by Buisson, Jausseran, and Rouard[15] are shown in Fig. 3 by O and +, respectively. Vassy[16] was able to measure the peak of the 4–0 band, but her value at 1924A converted to O_2 is less than that shown in Fig. 3 by a factor of about five. Since she used a much longer path length, but about the same resolution, the difference in the layer thickness may account for the lower "observed coefficient."

The absorption intensities of the Schumann-Runge bands have been calculated theoretically by Pillow.[21] In Table I, a comparison is made with our observed intensities. For the experimental data, the absorption intensities are relative values with that of the 12–0 band

[10] W. C. Price and G. Collins, Phys. Rev. **48**, 714 (1935).
[11] H. P. Knauss and S. S. Ballard, Phys. Rev. **48**, 796 (1935).
[12] J. J. Hopfield, Astroph. J. **104**, 208 (1946).
[13] Y. Tanaka, J. Chem. Phys. **20**, 1728 (1952).
[14] H. Kreusler, Ann. Physik. **6**, 412 (1901).
[15] Buisson, Jausseran, and Rouard, Rev. opt. **12**, 70 (1933).
[16] A. Vassy, Ann. phys. **16**, 145 (1941).
[17] J. Curry and G. Herzberg, Ann. Physik **19**, 800 (1934).
[18] A. G. Gaydon, *Dissociation Energies* (Dover Publications, Inc., New York, 1950).
[19] G. Herzberg, *Molecular Spectra and Molecular Structure I* (D. Van Nostrand Company, Inc., New York, 1950).
[20] G. Herzberg, Can. J. Phys. **30**, 185 (1952).
[21] M. E. Pillow, Proc. Phys. Soc. (London) **63A**, 940 (1950).

TABLE I. Intensities of the Schumann-Runge bands.

Band	5–0	6–0	7–0	8–0	9–0	10–0	11–0	12–0	13–0	14–0	15–0	16–0	17–0	18–0
Theoretical	1	5	20	29	51	50	78	100	90	95				
Experimental				39	42	59	90	100	87	124	146	161	166	160

arbitrarily taken as 100. The pressure of O_2 was 7.8-mm Hg, and this pressure was too low for observation of bands below 8–0. Considering the type of data being compared, the agreement is rather good; however, data obtained at higher pressures show that the decrease of intensity is less rapid from 6–0 to 4–0 than the evaluation by Pillow.

(b) Spectral Region 1750–1300A

For the Schumann-Runge dissociation continuum, ${}^3\Sigma_u^- - {}^3\Sigma_g^-$, the important absorption measurement of Ladenburg and van Voorhis[1] has been generally accepted and applied to atmospheric absorption. Their result showed a maximum absorption (k about 490 cm^{-1}) at 1450A with a nearly symmetrical intensity distribution. These results were consistent with the dispersion measurement made earlier by Ladenburg and Wolfsohn.[22] The index of refraction of O_2, obtained experimentally, was expressed by three resonance wavelengths and one of them ($\lambda_2 = 1468$A) was ascribed to the Schumann-Runge continuum. Still earlier, Koch[23] had obtained a dispersion equation with $\lambda_2 = 1421$A.

By varying the pressure over a wider range (0.1 to 50 mm), it was possible to extend the work of Ladenburg and van Voorhis to both longer and shorter wavelengths, and the result is shown in Fig. 4 by the solid curve which represents the mean of several hundred points. Within experimental error (about 5 percent) Beer's Law held over a pressure range of a factor of twenty. The result of Ladenburg and van Voorhis is shown by the dashed curve which is considerably higher over the major part of this region. The maximum in the present observation is rather flat and is 380 cm^{-1} at about 1420A (this wavelength agreeing with the value given by Koch). The intensity distribution is rather asymmetric, the short-wavelength side being rather steep, and there may be a discontinuity at about 1400A because of an interaction of potential curves ($B^3\Sigma_u^-$ and an as yet unidentified curve). Although Stueckelberg[2] obtained theoretically an intensity distribution curve agreeing fairly well with the data of Ladenburg and van Voorhis, it must be recalled that his calculation partly depended on their experimental data.

Since the discrepancy shown in Fig. 4 appears to exceed the combined experimental error, a further check was desirable and was kindly provided by the Shell Oil Research Laboratory.[24] Using a Baird monochromator, but an RCA quartz photomultiplier, they measured down to the limit of quartz transmission, and our result agrees with theirs at least in the region 1750–1570A (the lower wavelength being their limit). The following explanation might be made regarding the photometry used by Ladenburg and van Voorhis. It is reasonable to suppose that the fixed sector disks used by them for intensity calibration reduced the sizable amount of scattered light as well as the intensity of desired wavelengths. In this case, the calibration data may not be directly applicable to lines which have been greatly reduced in intensity due to the absorption of O_2, since O_2 itself would not probably have reduced the amount of scattered light, at least not as much as the sector disk. This argument is based on the "fact" that scattered light in a spectrograph consists mostly of wavelengths longer than 2000A.

Three minor maxima at 1293, 1332, and 1352A were observed on the short-wavelength slope of the continuum. These were recently found photographically by Tanaka[13] who used a Lyman continuum as source and varied the pressure of O_2. These bands or continua apparently escaped photographic detection for many years, since they are superposed on the slope of the strong continuum. Actually, by looking for them one can see them in a published photograph by Hopfield.[12] With the phosphor-coated photomultiplier they were readily observed even using the many-lined spectrum of H_2 as source. According to Tanaka, these bands appear as continua with a 3-m grazing incidence spectrograph, and the wavelengths of the maxima could

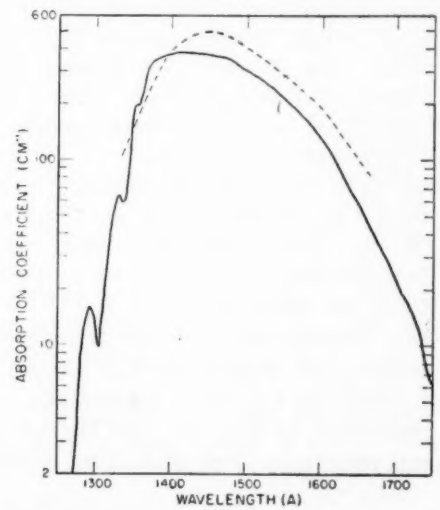

FIG. 4. Absorption coefficients of the Schumann-Runge continuum. The dashed curve was obtained Ladenburg and van Voorhis.

[22] R. Ladenburg and G. Wolfsohn, Z. Physik. 79, 42 (1932).
[23] J. Koch, Arch. Math. Astr. och Fysik 8, No. 20 (1912).
[24] Private communications with L. C. Jones, L. W. Taylor, and R. J. Greenshields.

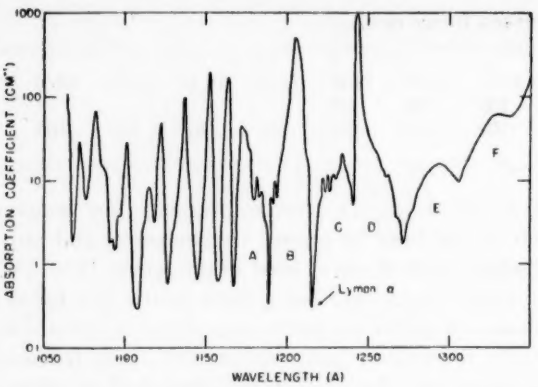

FIG. 5. Absorption coefficients of O_2 in the region 1050–1300A.

not be measured precisely. He has suggested that the first "continuum" at 1293A leads to the dissociation products $^3P+^1S$ and the other two to $^1D+^1D$ or $^3P+^1S$.

Using the formula (see reference 1),

$$f=\left(\frac{mc^2}{N\pi e^2}\right)\int_{\nu_1}^{\nu_2} k_\nu d\nu,$$

with $\nu_1=5.7\times10^4$ cm^{-1} and $\nu_2=7.8\times10^4$ cm^{-1}, the f value of 0.161 was obtained by integrating graphically the k value for the Schumann-Runge continuum. This value is somewhat smaller than the value (0.193) obtained by Ladenburg and van Voorhis.

(c) Spectral Region 1300–1050A

Molecular oxygen has a complex absorption spectrum in this region, and most of the bands still need to be classified. This region is of great importance to the study of the upper atmosphere, since solar radiation can penetrate down to the D region through the several windows of the O_2 spectrum. For example, Lyman alpha lies in one of the deepest windows, and its enhancement during chromospheric eruption may very well provide the necessary energy to account for the increased ionization and radio fadeout. Furthermore, it is important to know whether dissociation of O_2 by photons in this region of the spectrum supply an appreciable amount of metastable oxygen atoms.

At Lyman alpha the absorption coefficient was found to be 0.30 cm^{-1} at pressures of 70-mm Hg and 0.50 cm^{-1} at 490 mm. These values are in close agreement with the data obtained by Preston[4] who used pressures from 30 to 290 mm and a cell length of 21.8 cm. Since he observed a pressure effect, he extrapolated his data to zero pressure and obtained $k=0.28$ cm^{-1}. Our extrapolated value was 0.27 cm^{-1}. Incidentally, our absorption coefficients for N_2, CO_2, and H_2O at Lyman alpha agreed remarkably well with those obtained by Preston.

As a result of the complexity of the O_2 spectrum and the fact that a many-lined spectrum rather than a continuum was used as source, some of the data in this region were not reliable. In the region below 1170A the absorption bands show sharp fine structure as well as some diffuseness; therefore, the "coefficient" shown in Fig. 5 for the poorly resolved region 1060–1170A must be considered semiquantitative. As in the case of the Schumann-Runge bands, the maxima are probably too low and minima too high, although the apparent pressure effect was somewhat less. Included in the paper by Weissler and Po Lee[6] are k values at 7 wavelengths in this region. These are, in general, considerably larger, and may be explained by the fact that they used higher resolution. Although close comparison may not be justified, Schneider's values[3] for this region seem to be, in a rough way, lower than those obtained by Weissler and Po Lee.

In Fig. 5, the bands A, B, C, D, E, F are very diffuse with hardly any structure, even when observed[13] with a three-meter grazing incidence spectrograph. Price and Collins[10] who observed most of them ascribed the diffuseness to predissociation, and this was confirmed by Tanaka[13] who studied the spectrum in greater detail. The latter also reported two new progressions, one of which was suggested to be a member of the Rydberg series converging to the first ionization potential. A few members of these progressions seem to appear in our data (Fig. 5). Because of the general diffuseness of the spectrum the k values shown in Fig. 5 for the region 1170–1300A should be fairly reliable.

Price and Collins[10] observed also a weak continuum at 1105A extending toward shorter wavelengths. Our measurements support their observation; however, its intensity (order of 1 cm^{-1} in Fig. 5) is much less than the estimate (50–100 cm^{-1}) reported by Weissler and Po Lee.[6]

CONCLUSIONS

The intensity measurement using a phosphor-coated photomultiplier has given quite reproducible data of absorption coefficients of several gases, and it appears to be more reliable than the usual photographic method. As shown in the case of O_2, the method is particularly suited for measurements of diffuse bands and continua. In spite of its poor resolution, it is capable of finding new bands and continua, since it is sensitive of small differences in absorption intensities. Its present limit of resolution can be improved, and efforts are being made to extend this type of measurement to more detailed absorption studies.

We wish to thank Dr. Y. Tanaka for the use of an enlarged reproduction of the oxygen absorption spectrum in the region 1000–1300A and for his interest in this work.

Dielectric Polarization in Polar Substances

FRANK E. HARRIS* AND BERNI J. ALDER
Department of Chemistry and Chemical Engineering, University of California, Berkeley, California
(Received December 30, 1952)

A statistical mechanical theory of the static dielectric constant of polar substances is presented which differs from the previous theories of Kirkwood and Fröhlich in that a precise evaluation of the distortion polarization term is made. The theory is applied to the dielectric constant of ordinary and heavy water and yields 2 percent agreement with experiment over the entire temperature range. Furthermore, the difference between the dielectric constant of water measured at visible and microwave frequencies can be ascribed to vibrations, such as the bending of the O−H−O bond. The calculated dielectric constant of ice agrees with experimental values within a mean deviation of 3 percent over a considerable temperature range using an approximate evaluation of the Pauling model for that substance. Various other liquids are also compared with experiment.

I.

THE Clausius-Mossotti equation has long been known to be inadequate for calculating dielectric constants of polar substances, because the model used in its derivation fails to include properly the interactions caused by permanent dipoles partially oriented by an electrical field. The first successful step toward a theory recognizing the effect of interactions of permanent dipoles was taken by Onsager.[1] His model considers the interaction between a molecule in a hole of molecular dimensions and an otherwise continuous dielectric of the macroscopic dielectric constant. Since the Onsager model includes the simplifying assumption that the discrete assembly of molecules as close as the nearest neighbors may be replaced by a continuum of macroscopic properties, the results are subject to considerable error when the interactions between near neighbors are strong. Kirkwood,[2] making a further refinement of the theory, discusses the interaction of a sphere of macroscopic dimensions, in vacuum, with an applied field, and uses classical statistical mechanics to obtain a formula whereby the average polarization due to orientation of the permanent dipoles may be evaluated. However, he treats in an approximate manner the polarization induced by distortion of the molecules. The Kirkwood approximation is not adequate, and therefore his equation fails to reduce to the Clausius-Mossotti formula in the absence of permanent dipoles. The difficulty arises from his assumption that the local field to be used for the calculation of the distortion polarization is the Onsager cavity field. It will be shown below that the only part of the local field whose effect is not already included in the permanent dipole term is that part which is achieved at constant orientation of the permanent dipoles. With this modification an expression may be obtained which, in the absence of permanent electric moments, does reduce to the Clausius-Mossotti equation.

Fröhlich[3] has modified Kirkwood's treatment by assuming an alternative model in which he regards the dielectric as a continuous medium of dielectric constant n^2, in which are embedded dipolar molecules not polarizable by an external field. He then treats the interaction between the field and a sphere cut from an infinite sample of this dielectric. His results are not exact, however, because he cannot evaluate in a completely rigorous manner the interaction between his non-isolated sample and the field.

Because of the difficulty of extending Fröhlich's approach, we shall here follow Kirkwood and consider a spherical specimen of dielectric of macroscopic size, surrounded by vacuum. Contributions arising from orientation and distortion polarization will be rigorously separated and evaluated, subject to no seriously restrictive approximations. Furthermore, it will be shown that the resulting equation is consistent with the limit represented by the Clausius-Mossotti equation.

II.

Consider a macroscopic specimen of N molecules in a spherical volume V, placed in a vacuum. It can easily be demonstrated that the results are independent of the shape of the specimen. Let V_N be the potential energy of interaction of the molecules; V_N will depend upon the positions of the centers of the molecules, denoted by $\mathbf{r}=\{\mathbf{r}_1, \mathbf{r}_2, \cdots, \mathbf{r}_N\}$, the orientations of the molecules $\Omega=\{\omega_1, \omega_2, \cdots, \omega_N\}$, and the extent of polarization of the molecules (represented by such coordinates of charge $\mathbf{x}=\{\mathbf{x}_1, \mathbf{x}_2, \cdots, \mathbf{x}_N\}$ relative to the charges of the unperturbed molecule as are necessary). Call a set $(\mathbf{r}, \Omega)$ a configuration of the system, and refer to states of polarization as $\mathbf{x}$; constant configuration will therefore imply constancy of $\mathbf{r}$ and Ω, but not necessarily of $\mathbf{x}$. Also, let $\mathbf{M}$ be the total electric moment of the specimen, $\mathbf{E}_0$ the applied field in the absence of the sample (the applied field is to be thought of as produced by an external fixed charge distribution), and $\mathbf{e}$ a unit vector in the direction of $\mathbf{E}_0$. Then, the inter-

* Predoctoral Fellow, National Science Foundation.
[1] L. Onsager, J. Am. Chem. Soc. **58**, 1486 (1936).
[2] J. G. Kirkwood, J. Chem. Phys. **7**, 911 (1939).
[3] H. Fröhlich, *Theory of Dielectrics* (Oxford University Press, London, 1949).

action energy with the field for any set of the variables $(\mathbf{r}, \Omega, \mathbf{x})$ is given by $-\mathbf{M}(\mathbf{r}, \Omega, \mathbf{x}) \cdot \mathbf{E}_0$. This is exact, since all variables of the system are being held fixed. We now set down a formally exact expression for the average value of the component of $\mathbf{M}$ in the direction of $\mathbf{E}_0$, for fixed $\mathbf{E}_0$:

$$\langle \mathbf{M} \cdot \mathbf{e} \rangle_{E_0} = \frac{\int (\mathbf{M}(\mathbf{r}, \Omega, \mathbf{x}) \cdot \mathbf{e}) \exp\left[\frac{-V_N(\mathbf{r}, \Omega, \mathbf{x}) + \mathbf{M}(\mathbf{r}, \Omega, \mathbf{x}) \cdot \mathbf{E}_0}{kT}\right] (d\mathbf{r})(d\Omega)(d\mathbf{x})}{\int \exp\left(\frac{-V_N + \mathbf{M} \cdot \mathbf{E}_0}{kT}\right) (d\mathbf{r})(d\Omega)(d\mathbf{x})}. \quad (1)$$

Here, $(d\mathbf{r})$, $(d\Omega)$, and $(d\mathbf{x})$ indicate volume elements in their respective coordinate spaces, and all other previously undefined symbols have their usual significance.

We may then separate $\mathbf{M}$ into two parts, $\mathbf{M}_0(\mathbf{r}, \Omega)$ and $\mathbf{M}_d(\mathbf{r}, \Omega, \mathbf{x})$, so that

$$\mathbf{M}(\mathbf{r}, \Omega, \mathbf{x}) = \mathbf{M}_0(\mathbf{r}, \Omega) + \mathbf{M}_d(\mathbf{r}, \Omega, \mathbf{x}). \quad (2)$$

$\mathbf{M}_0(\mathbf{r}, \Omega)$ is that part of the polarization due solely to the specified configuration, including the induced moment associated therewith in the absence of an applied field. The average of $\mathbf{M}_d(\mathbf{r}, \Omega, \mathbf{x})$, with respect to $\mathbf{x}$, then represents the additional polarization, both atomic and electronic, resulting from the application of an external field to the configuration $(\mathbf{r}, \Omega)$.

Combining Eqs. (1) and (2), we arrive at the result,

$$\langle \mathbf{M} \cdot \mathbf{e} \rangle_{E_0} = \frac{\int [\mathbf{M}_0(\mathbf{r}, \Omega) \cdot \mathbf{e} + \mathbf{M}_d(\mathbf{r}, \Omega, \mathbf{x}) \cdot \mathbf{e}] \exp\left[\frac{-V_N(\mathbf{r}, \Omega, \mathbf{x}) + \mathbf{M}_0(\mathbf{r}, \Omega) \cdot \mathbf{E}_0 + \mathbf{M}_d(\mathbf{r}, \Omega, \mathbf{x}) \cdot \mathbf{E}_0}{kT}\right] (d\mathbf{r})(d\Omega)(d\mathbf{x})}{\int \exp\left[\frac{-V_N + (\mathbf{M}_0 + \mathbf{M}_d) \cdot \mathbf{E}}{kT}\right] (d\mathbf{r})(d\Omega)(d\mathbf{x})}. \quad (3)$$

To proceed further, we make the following approximations: (1) We neglect dielectric saturation. Therefore, in $\langle \mathbf{M} \cdot \mathbf{e} \rangle_{E_0}$ we discard all higher powers of $\mathbf{E}_0$ than the first. (2) All integrals with respect to $\mathbf{x}$ may be replaced by a constant multiplied by the integrand, evaluated for that value of $\mathbf{x}$ which maximizes the integrand. That is,

$$\int f(\mathbf{x}) \exp\frac{[-V_N(\mathbf{x}) + \mathbf{M}_d(\mathbf{x}) \cdot \mathbf{E}_0]}{kT} (d\mathbf{x}) = C f(\mathbf{x}_E) \exp\frac{[-V_N(\mathbf{x}_E) + \mathbf{M}_d(\mathbf{x}_E) \cdot \mathbf{E}_0]}{kT}, \quad (4)$$

where $\mathbf{x}_E$ is the value of $\mathbf{x}$ which maximizes the integrand of (4) for a given field $\mathbf{E}_0$, and C is a constant. This is equivalent to assuming that any deviation of the distribution of charges giving rise to polarization from their average value is energetically very unfavorable. This assumption, although not explicitly stated, is common to all the other dielectric theories referred to above. Its applicability demands that thermal energies be small relative to those required for charge motion. For tightly bound charged particles such as electrons and, under most conditions, nuclei, the above condition is met. In Eq. (2), then, we have included in $\mathbf{M}_d$ only the coordinates of these tightly bound charges. This makes $\mathbf{M}_d$ not explicitly dependent upon temperature, and conforms to the usual concept of electronic and atomic polarization. On the other hand, to treat loosely bound nuclei one must include their coordinates in $(\mathbf{r}, \Omega)$.

Applying the second approximation to Eq. (3), we obtain

$$\langle \mathbf{M} \cdot \mathbf{e} \rangle_{E_0} = \frac{\int [\mathbf{M}_0(\mathbf{r}, \Omega) \cdot \mathbf{e} + \mathbf{M}_d(\mathbf{r}, \Omega, \mathbf{x}_E) \cdot \mathbf{e}] \exp\left[\frac{-V_N(\mathbf{r}, \Omega, \mathbf{x}_E) + \mathbf{M}_0(\mathbf{r}, \Omega) \cdot \mathbf{E}_0 + \mathbf{M}_d(\mathbf{r}, \Omega, \mathbf{x}_E) \cdot \mathbf{E}_0}{kT}\right] (d\mathbf{r})(d\Omega)}{\int \exp\left[\frac{-V_N + (\mathbf{M}_0 + \mathbf{M}_d) \cdot \mathbf{E}_0}{kT}\right] (d\mathbf{r})(d\Omega)}. \quad (5)$$

According to the first approximation, Eq. (5) may be expanded in powers of E_0, keeping only through the linear term. To do so, we need to expand $V_N(\mathbf{r}, \Omega, \mathbf{x}_E)$ in powers of E_0 about $\mathbf{x} = 0$.

$$V_N(\mathbf{r}, \Omega, \mathbf{x}_E) = V_N(\mathbf{r}, \Omega) + \sum_j \left(\frac{\partial V_N(\mathbf{r}, \Omega, \mathbf{x})}{\partial x_j}\right)_{\mathbf{x}=0} \cdot \frac{d(x_E)_j}{dE_0} E_0 + \cdots. \quad (6)$$

$V_N(\mathbf{r}, \Omega)$ is defined as $V_N(\mathbf{r}, \Omega, 0)$.

At $\mathbf{x}=0$ the first derivatives of V_N vanish, and, through linear terms in E_0, $V_N(\mathbf{r}, \Omega, \mathbf{x}_E)=V_N(\mathbf{r}, \Omega)$. The expansion of (5) now yields

$$\langle \mathbf{M}\cdot\mathbf{e}\rangle_{E_0}=\frac{\int (d\mathbf{r})(d\Omega)\exp\left[\frac{-V_N(\mathbf{r},\Omega)}{kT}\right]\left[\mathbf{M}_0\cdot\mathbf{e}+\mathbf{M}_d(\mathbf{x}_E)\cdot\mathbf{e}\right]\left[1+\frac{E_0}{kT}\{\mathbf{M}_0\cdot\mathbf{e}+\mathbf{M}_d(\mathbf{x}_E)\cdot\mathbf{e}\}+\cdots\right]}{\int (d\mathbf{r})(d\Omega)e^{-V_N/kT}\left[1+\frac{E}{kT}\{\mathbf{M}_0\cdot\mathbf{e}+\mathbf{M}_d\cdot\mathbf{e}\}+\cdots\right]}. \tag{7}$$

The term in $(\mathbf{M}_0\cdot\mathbf{e})$ vanishes, since $\mathbf{M}_0$, which is to be averaged in the absence of the field, has equal probability in all directions. The terms of form $(\mathbf{M}_0\cdot\mathbf{e})(\mathbf{M}_d\cdot\mathbf{e})$ also vanish, since $(\mathbf{M}_d\cdot\mathbf{e})$ is symmetric upon rigid rotation of the specimen through an angle of π about an axis perpendicular to $\mathbf{e}$ (the polarizability of the molecules has this symmetry), whereas $(\mathbf{M}_0\cdot\mathbf{e})$ will change in sign. As these configurations have equal probability in the absence of a field, the average will vanish. Note that we have not introduced any assumption requiring spherical molecules. Since $\mathbf{M}_d$ is itself (through $\mathbf{x}_E$) of order E_0, terms containing $(\mathbf{M}_d\cdot\mathbf{e})^2$ and $E_0(\mathbf{M}_d\cdot\mathbf{e})$ may also be neglected. With these simplifications, Eq. (7) becomes

$$\langle \mathbf{M}\cdot\mathbf{e}\rangle_{E_0}=\frac{E_0}{kT}\langle(\mathbf{M}_0\cdot\mathbf{e})^2\rangle+\langle\mathbf{M}_d(\mathbf{x}_E)\cdot\mathbf{e}\rangle. \tag{8}$$

The averages on the right side are to be performed using the potential in the absence of the field.

The first term on the right-hand side of (8) may be simplified by the methods developed by Kirkwood.[2] Averaging over directions of $\mathbf{M}_0$, $\langle(\mathbf{M}_0\cdot\mathbf{e})^2\rangle=\langle M_0^2\rangle/3$, and since

$$\mathbf{M}_0=\sum_{j=1}^{N}(\boldsymbol{\mu}_s)_j,$$

we find $\langle M_0^2\rangle=N(\boldsymbol{\mu}_s\cdot\langle\mathbf{M}\rangle_{\mu_s})$, where $\langle\mathbf{M}\rangle_{\mu_s}$ represents the average total moment of the spherical specimen for a fixed $\boldsymbol{\mu}_s$, and $\boldsymbol{\mu}_s$ is the dipole moment of a molecule in the spherical specimen. The average of M_0^2 has been removed and the sum replaced by N, since, for a specimen of macroscopic size, the position and orientation of any given $\boldsymbol{\mu}_s$ is equivalent except for the negligible proportion of molecules near the surface. However, when $\boldsymbol{\mu}_s$ is a function of internal coordinates of a molecule which have been included in $(\mathbf{r}, \Omega)$, as for example in the case of intramolecular rotations, $\boldsymbol{\mu}_s\cdot\langle\mathbf{M}\rangle_{\mu_s}$ must be averaged over these internal coordinates. Kirkwood also shows that $\langle\mathbf{M}\rangle_{\mu_s}$ for a spherical specimen may be expressed in terms of $\langle\boldsymbol{\mu}\rangle_\mu$, the average total moment of an infinite specimen, for a fixed $\boldsymbol{\mu}$. Here $\boldsymbol{\mu}$ refers to the dipole moment of a molecule in an infinite medium, and $\langle\mathbf{M}\rangle_{\mu_s}$ and $\langle\boldsymbol{\mu}\rangle_\mu$ differ only by the effect of a spherical surface at macroscopic distances from $\boldsymbol{\mu}_s$. Use of $\langle\boldsymbol{\mu}\rangle_\mu$ is preferable, since it may readily be evaluated by the usual statistical methods, and it contains only contributions from molecules near enough to $\boldsymbol{\mu}$ to be correlated with its position, whereas $\langle\mathbf{M}\rangle_{\mu_s}$ also contains a homogeneous polarization of the entire macroscopic sample. Kirkwood's relation between $\langle\mathbf{M}\rangle_{\mu_s}$ and $\langle\boldsymbol{\mu}\rangle_\mu$ is

$$\langle\mathbf{M}\rangle_{\mu_s}=\left(\frac{3}{\epsilon+2}\right)\left(\frac{3\epsilon}{2\epsilon+1}\right)\langle\boldsymbol{\mu}\rangle_\mu. \tag{9}$$

Combining (9) with the above discussion, we find

$$\langle(\mathbf{M}_0\cdot\mathbf{e})^2\rangle=\frac{N}{3}\left(\frac{3}{\epsilon+2}\right)\left(\frac{3\epsilon}{2\epsilon+1}\right)(\boldsymbol{\mu}_s\cdot\langle\boldsymbol{\mu}\rangle_\mu). \tag{10}$$

To derive Eq. (9) the average total moment $\langle\boldsymbol{\mu}\rangle_\mu$ of a molecule and its correlated neighbors in an infinite medium must be assumed to be the same as that of the identical group of molecules in a macroscopic spherical specimen. This requires that the presence of a surface at large distances from a cluster of molecules does not have an appreciable effect. Accordingly it is confirmed in Appendix I that in order for Eq. (9) to be applicable, the macroscopic spherical specimen must be large compared to the region in which there is correlation between the dipole of a central molecule and the dipoles of its neighbors. Equation (9) may therefore be used for all materials not possessing long range polarization order, i.e., for all except ferroelectric or antiferroelectric substances. For such substances, however, $\langle\mathbf{M}\rangle_{\mu_s}$ can be evaluated by other methods.

In Eq. (10), the dipole moment of a molecule in a spherical specimen must be evaluated. The effect of the surface can again be shown to be negligible except for ferroelectric or antiferroelectric substances (see Appendix I). For all other materials $\boldsymbol{\mu}_s$ is equal to $\boldsymbol{\mu}$, the dipole moment of a molecule in an infinite medium.

The second term on the right side of Eq. (8) represents the average polarization at constant configuration during application of the field $\mathbf{E}_0$. As we restrict ourselves to isotropic media, $\langle\mathbf{M}_d\rangle$ will be in the direction of $\mathbf{E}_0$, and $\langle\mathbf{M}_d\cdot\mathbf{e}\rangle$ may simply be replaced by $|\langle\mathbf{M}_d\rangle|$. Since the molecules themselves have not been assumed to be spherically polarizable, rigorous evaluation of $\langle\mathbf{M}_d\rangle$ in terms of the molecular polarizability α will be difficult. However, it may be evaluated in terms of the high frequency dielectric constant ϵ_∞. (We use ϵ_∞ to distinguish from n^2, which, as customarily measured, does not include atomic polarization.) If a macroscopic field $\mathbf{E}'$ of frequency high enough that no molecular orientation takes place is present in the sample, the

polarization will be related to ϵ_∞ by the defining equation, $[(\epsilon_\infty-1)/(4\pi)]\mathbf{E}'=\langle\mathbf{M}_d\rangle/V$. For the spherical specimen we have been considering, the field $\mathbf{E}'$ will be related to the applied field by $\mathbf{E}'=[3/(\epsilon_\infty+2)]\mathbf{E}_0$. Therefore $|\langle\mathbf{M}_d\rangle|$ is given by

$$|\langle\mathbf{M}_d\rangle|=\frac{3V}{4\pi}\left(\frac{\epsilon_\infty-1}{\epsilon_\infty+2}\right)E_0. \tag{11}$$

We see that $|\langle\mathbf{M}_d\rangle|$ has the value one would calculate, using the Lorentz local field and a polarizability calculated assuming spherical molecules.

Substituting (10) and (11) into (8), and replacing $\boldsymbol{\mu}_z$ by $\boldsymbol{\mu}$, we find

$$\langle\mathbf{M}\cdot\mathbf{e}\rangle_{E_0}=NE_0\left(\frac{3}{\epsilon+2}\right)\left(\frac{3\epsilon}{2\epsilon+1}\right)\left(\frac{\boldsymbol{\mu}\cdot\langle\boldsymbol{\mu}\rangle_\mu}{3kT}\right)+\frac{3V}{4\pi}E_0\left(\frac{\epsilon_\infty-1}{\epsilon_\infty+2}\right). \tag{12}$$

For an applied static field $\mathbf{E}_0$, the macroscopic field in the sample $\mathbf{E}$, is given by $\mathbf{E}=[3/(\epsilon+2)]\mathbf{E}_0$. When we introduce this relation, together with the defining relation for ϵ,

$$\frac{\epsilon-1}{4\pi}E=\frac{\langle\mathbf{M}\cdot\mathbf{e}\rangle_{E_0}}{V},$$

Eq. (12) becomes

$$\epsilon-1=\frac{4\pi N}{V}\left(\frac{3\epsilon}{2\epsilon+1}\right)\left(\frac{\boldsymbol{\mu}\cdot\langle\boldsymbol{\mu}\rangle_\mu}{3kT}\right)+(\epsilon+2)\left(\frac{\epsilon_\infty-1}{\epsilon_\infty+2}\right). \tag{13}$$

Then $\boldsymbol{\mu}\cdot\langle\boldsymbol{\mu}\rangle_\mu$ may be calculated by rigorous evaluation of the formula

$$\boldsymbol{\mu}\cdot\langle\boldsymbol{\mu}\rangle_\mu=\mu^2\left\{1+\frac{N\int\cos\gamma e^{-W/kT}(d\mathbf{r}_1)(d\omega_1)}{\int e^{-W/kT}(d\mathbf{r}_1)(d\omega_1)}\right\}=g\mu^2, \tag{14}$$

in which W is the potential of average force and torque between a molecule at the origin with its dipole along the polar axis, and another molecule at the position and orientation of integration. Here γ is the angle between the two dipoles, and $(\mathbf{r}_1,\omega_1)$ is the configuration of the second molecule. Equation (14) furthermore defines g, the correlation parameter. Kirkwood has suggested the approximation

$$\boldsymbol{\mu}\cdot\langle\boldsymbol{\mu}\rangle_\mu\simeq\mu^2[1+z\langle\cos\gamma\rangle]\simeq g\mu^2, \tag{15}$$

where z is the number of nearest neighbors, and $\langle\cos\gamma\rangle$ is given by

$$\langle\cos\gamma\rangle=\frac{\int\cos\gamma e^{-W_0/kT}(d\omega_1)(d\omega_2)}{\int e^{-W_0/kT}(d\omega_1)(d\omega_2)}. \tag{16}$$

Here W_0 is the potential of average torque between nearest neighbors, and ω_1 and ω_2 indicate the relative orientations of these neighbors. Approximations involving the contributions of successive shells of neighbors have also been used (see Sec. IV of this paper).

The value of $\boldsymbol{\mu}$ may be calculated by evaluation of the average induced moment of a molecule as follows:

$$\boldsymbol{\mu}=\boldsymbol{\mu}_0+\frac{N\int\alpha_E\mathbf{E}(\mathbf{r}_1,\omega_1)e^{-W/kT}(d\mathbf{r}_1)(d\omega_1)}{\int e^{-W/kT}(d\mathbf{r}_1)(d\omega_1)}, \tag{17}$$

where $\mathbf{E}(\mathbf{r}_1,\omega_1)$ is the field at the origin resulting from a molecule at the indicated configuration, α_E is the polarizability in the direction of $\mathbf{E}(\mathbf{r}_1,\omega_1)$, and $\boldsymbol{\mu}_0$ is the vacuum dipole moment. This is the only place optical anisotropy need be specifically recognized in application of the theory. If $\mathbf{E}(\mathbf{r}_1,\omega_1)$ be approximated by the dipole field, α_E by its average value, and the integral of (17) extended only over nearest neighbors, which are assumed to be fixed at their average distances, one can obtain more readily a result for $\boldsymbol{\mu}$ valid for strong interaction of neighbors.

For small neighbor interaction, $\boldsymbol{\mu}$ may be better approximated by the Onsager formula,

$$\boldsymbol{\mu}=\boldsymbol{\mu}_0\left(\frac{\epsilon_\infty+2}{3}\right)\left(\frac{2\epsilon+1}{2\epsilon+\epsilon_\infty}\right). \tag{18}$$

III.

It is of interest to compare the result (13) with the corresponding results of Kirkwood's and Fröhlich's theories. To do so more readily, we substitute the Clausius-Mossotti equation for α,

$$\frac{\epsilon_\infty-1}{\epsilon_\infty+2}=\frac{4\pi N}{3V}\alpha, \tag{19}$$

into (13),

$$\epsilon-1=\left(\frac{4\pi N}{V}\right)\left[\left(\frac{3\epsilon}{2\epsilon+1}\right)\frac{\boldsymbol{\mu}\cdot\langle\boldsymbol{\mu}\rangle_\mu}{3kT}+\frac{\epsilon+2}{3}\alpha\right], \tag{13a}$$

and compare it with the Kirkwood expression[2]

$$\epsilon-1=\left(\frac{4\pi N}{V}\right)\left(\frac{3\epsilon}{2\epsilon+1}\right)\left[\frac{\boldsymbol{\mu}\cdot\langle\boldsymbol{\mu}\rangle_\mu}{3kT}+\alpha\right]. \tag{20}$$

The difference is to be found entirely in the distortion polarization term. This is because a different field than that employed by Kirkwood must be used for calculating the α term.

Let us compare our result, again rearranged into an appropriate form,

$$\epsilon-\epsilon_\infty=\left(\frac{4\pi N}{V}\right)\left(\frac{3\epsilon}{2\epsilon+1}\right)\left(\frac{\boldsymbol{\mu}\cdot\langle\boldsymbol{\mu}\rangle_\mu}{3kT}\right)\left(\frac{\epsilon_\infty+2}{3}\right), \tag{13b}$$

with the Fröhlich theory[3]

$$\epsilon-\epsilon_\infty=\left(\frac{4\pi N}{V}\right)\left(\frac{3\epsilon}{2\epsilon+\epsilon_\infty}\right)\left(\frac{\mathfrak{y}\cdot\langle\mathfrak{y}\rangle_\mu}{3kT}\right). \quad (21)$$

The ϵ_∞ in the denominator on the right-hand side of Fröhlich's expression would become unity upon removal of the self-energy term caused by evaluating the interaction energy between his continuous substratum and the orienting dipoles; the other difference results from further interactions which were not completely taken into account in the Fröhlich treatment.

Equation (13) reduces to the Clausius-Mossotti equation (19) for $\mathfrak{y}=0$; however it does not reduce to the Onsager equation in the limit of no short-range interaction between the dipoles. In this limit, $g=1$, as is shown in Appendix II, and $\mathfrak{y}$ is related to $\mathfrak{y}_0$ by the Onsager relation (18). Under these conditions, (13) becomes

$$\epsilon-\epsilon_\infty=\left(\frac{4\pi N}{V}\right)\left(\frac{3\epsilon}{2\epsilon+1}\right)\left(\frac{\mu^2}{3kT}\right)\left(\frac{\epsilon_\infty+2}{3}\right), \quad (13c)$$

whereas Onsager's equation[1] (his No. 26) is

$$\epsilon-\epsilon_\infty=\left(\frac{4\pi N}{V}\right)\left(\frac{3\epsilon}{2\epsilon+1}\right)\left(\frac{\mu^2}{3kT}\right)\left(\frac{2\epsilon+\epsilon_\infty}{2\epsilon+1}\right). \quad (22)$$

In Eq. (22), as in (13c), $\mathfrak{y}$ is given by (18). The discrepancy between (22) and (13c) must be due to Onsager's introduction of a cavity of molecular dimensions. This concept necessitated the *ad hoc* assumption that the volume of this cavity be exactly the molecular volume in order that the theory reduce to the Clausius-Mossotti equation (19).

IV.

To illustrate physical applications of the theory here presented, dielectric constants of various substances were recalculated, using values of g and μ obtained by earlier investigators on the basis of specific models.

1. Water

The dielectric constant of water has been calculated by Kirkwood,[2] and the calculation refined by Oster and Kirkwood.[4] The model for the water molecule assumes unbendable bonds, fixed at experimentally observed angles. Free rotation is permitted about the O—H bonds. One obtains g by calculating $\langle\cos\gamma\rangle$ for this arrangement of molecules, but instead of using $z=4$ in Eq. (15), as prescribed by the model, one uses values of z consistent with experimental values of the radial distribution function. Furthermore, μ was calculated using (18).

Pople[5] has also calculated the dielectric constant of water. Pople's model provides that each water molecule be bonded to four others, but that the bonds be bendable. The amount of bending is determined by evaluating a bending force constant such that the distribution of molecules calculated by classical statistical mechanics agrees with the experimentally determined radial distribution function at several temperatures. Free rotation is again allowed around all O—H bonds. Contributions to g are evaluated for the first three shells of neighbors, and μ is determined from a calculation of the local field of only the four nearest neighbors. Pople's calculated dielectric constant was about 20 percent lower than the experimental value, but gave approximately the correct temperature dependence.

Both Pople[5] and Kirkwood[2,4] assume the polarizability of the water molecule to be that indicated by index of refraction measurements at visible frequencies ($n^2=1.79$), although measurements at frequencies as high as 2.4×10^{10} cps indicate a value of $\epsilon_\infty=5.5$.[6] In the present calculation $\epsilon_\infty=1.79$ must be used since the difference between this value and 5.5 is caused by motions of the nuclei which are to be associated with vibration of the protons still prevailing at 2.4×10^{10} cps. In fact, the bending of the O—H—O bond as determined by Raman spectra is known to occur at still higher frequencies, probably around 500 cm^{-1}.[7] Since kT/h is approximately 210 cm^{-1} at room temperature, these vibrations in accordance with our previous discussion must be included in the orientation polarization, rather than in the distortion polarization. Pople's model is in accordance with the preceding discussion.

We have thus used Pople's model and $\epsilon_\infty=n^2$ to recalculate the dielectric constant of water, and have made an analogous calculation for D_2O, assuming the same value of the bending force constant for both the deuterium and hydrogen bonds, and the same number of neighbors in the various shells. These are probably very good assumptions, as the molar volumes of H_2O and D_2O are very nearly identical. The change in the calculated dielectric constant is then due only to the difference in the polarizability of D_2O and H_2O. Dielectric constants calculated from Pople's model, using Kirkwood's equation, Fröhlich's equation, and Eq. (13) of this paper are presented in Table I, and comparative data on D_2O are listed in Table II.

The close agreement between experimental and calculated values for both H_2O and D_2O confirms in general the model of water adopted by Pople. The constancy of difference between the calculated and experimental dielectric constants for H_2O and D_2O shown in Table II lends added support to the model proposed. The remaining small discrepancy between the experimental and calculated dielectric constant of water can be ascribed to optical anisotropy and to further possible

[4] G. Oster and J. G. Kirkwood, J. Chem. Phys. **11**, 175 (1943).
[5] J. A. Pople, Proc. Roy. Soc. (London) **A205**, 163 (1951).
[6] Collie, Hasted, and Ritson, Proc. Phys. Soc. (London) **60**, 145 (1948).
[7] W. M. Latimer, Chem. Revs. **44**, 59 (1949).

TABLE I. Comparison with experiment of the calculated dielectric constant of ordinary water.

T, °C	g	ϵ Kirkwood Eq. (20)	ϵ Fröhlich Eq. (21)	ϵ This research Eq. (13)	ϵ Expt.[a]
0.0	2.60	71.9	73.0	90.7	88.2
25.0	2.55	63.8	64.0	79.9	78.5
62.0	2.49	53.0	53.0	65.7	66.4
83.0	2.46	47.8	48.0	59.6	60.4

[a] J. Wyman, Jr. and E. N. Ingalls, J. Am. Chem. Soc. **60**, 1182 (1938).

vibrations and bendings of bonds, such as the O—O bond, which has been held fixed. These motions would tend to decrease the calculated dielectric constant. Additional shells of neighbors should probably be also taken into account in a more refined calculation of $\langle\cos\gamma\rangle$ and μ. From Pople's calculation however, it can be seen that this effect would cause an increase of less than 1 percent in the dielectric constant.

2. Ice

Powles[8] has recently calculated the dielectric constant of ice by two alternative methods. Both of these methods assume ice to be an isotropic solid. The first method is based on the Pauling model,[9] which regards ice as a rigid, tetrahedrally bonded lattice of oxygens, with hydrogens distributed randomly among the bonds, but in such a way that two hydrogens are near each oxygen, and only one hydrogen in each O—O bond. Powles fixes the configuration of one molecule, and then calculates the average net moment of the entire sample when the other hydrogens are arranged randomly, but consistently with the position of the fixed molecule. He is unable to obtain an exact solution of this problem and is forced to consider small groups of molecules, the largest of which contains 24 molecules. He presents arguments indicating that the results would not be greatly affected by a further increase in the number of molecules considered.

Powles' second calculation assumes that the possible configurations of the hydrogens are not all equally probable, because they have different energies, and must be weighted accordingly. Exact evaluation of the energy of a configuration is a formidable task, and he finds it necessary to make severe approximations. The result is a dielectric constant higher than that predicted from the Pauling model by about 30 percent.

Powles evaluates μ using the Onsager relation (18), but suggests that a calculation of the actual local field of the neighbors does not alter this result very much. He also points out that the vacuum dipole moment μ_0 may not be the same in ice as in an isolated water molecule, as the bond angles are changed. This would decrease ϵ by about 9 percent if it is assumed that the bond moments are unaltered.

The use of (18) probably does not give an unreasonable value in this case, as μ/μ_0 for water (using Pople's model) increases from 1.13 at 83° to 1.17 at 0°, while μ/μ_0 by (18) is 1.24 for ice at 0°. Since stiffening of the lattice increases μ/μ_0, 1.17 is undoubtedly too low for ice, and 1.24 is an acceptable value.

Table III gives the dielectric constant of ice, using Powles' calculation on the Pauling model, assuming $\mu/\mu_0=1.24$. The close agreement with experiment must be regarded as fortuitous, as the uncertainty in μ may affect the result considerably. The experimental data chosen for comparison are those of Auty and Cole,[10] which seem to be the best available at present. These data are also presented graphically in Fig. 1. The result indicates that a more accurate calculation would substantiate the Pauling model of ice, at least at the higher temperatures where the possible energetic differences in the various configurations of ice are of less significance.

TABLE III. Comparison with experiment of the dielectric constant of ice, calculated using Pauling's model.

T, °C	ϵ (Powles)	ϵ (This research Eq. (13))	ϵ (Exptl. Auty and Cole[a])
− 0.1	76.8	92.5	91.5
−10.8	79.8	96.2	95.0
−20.9	83.0	100.0	97.4
−32.0	86.7	104.5	100
−44.7	91.4	110.2	104
−56.8	96.4	116.4	114
−65.8	100.5	121.4	133

[a] See reference 10.

TABLE II. Comparison with experiment of the calculated dielectric constant of heavy water.

T, °C	ϵ_{D_2O} ϵ calc., Eq. (13)	ϵ_{D_2O} ϵ Expt.[a]	$[\epsilon_{H_2O}-\epsilon_{D_2O}]$ calc.	$[\epsilon_{H_2O}-\epsilon_{D_2O}]$ Expt.
5.0	87.9	85.9	—	—
25.0	79.5	78.25	0.4	0.3
62.0	65.5	66.1	0.2	0.3
83.0	59.4	60.1	0.2	0.3

[a] J. Wyman, Jr. and E. N. Ingalls, J. Am. Chem. Soc. **60**, 1182 (1938).

3. Alcohols

Oster and Kirkwood[4] have also calculated dielectric constants of straight-chain aliphatic alcohols. They assume each alcohol molecule to be hydrogen bonded to two others, thus forming long chains, and make the further assumption that molecules only interact within the same chain. They permit free rotation about all bonds, and average the sum of the R—O and O—H bond dipoles. These bond dipole moments were obtained from those in vacuum using Onsager's formula (18).

[8] J. G. Powles, J. Chem. Phys. **20**, 1302 (1952).
[9] L. Pauling, J. Am. Chem. Soc. **57**, 2680 (1935).
[10] R. P. Auty and R. H. Cole, J. Chem. Phys. **20**, 1309 (1952).

Oster and Kirkwood's assumption that the chains do not interact with each other will be least valid when the alkyl group is small and the polar groups relatively exposed, but will improve as the alkyl group becomes larger and exerts a greater screening effect.

The above model results in the same value of g, 2.57, for all the alcohols. Upon recalculation, as shown in Table IV, the dielectric constants are increased above the experimental values, the discrepancy becoming smaller as the alkyl group increases in size, as might be expected from the discussion of the model. To improve the calculation, the bending of the O−H−O bond should be taken into account as was done in the case of water. This refinement would reduce the dielectric constant to the neighborhood of the experimental values.

4. Various Liquids

Since the theory here presented yields an expression differing from the Kirkwood equation, it is of interest to see how the values of g calculated from experimental data for various liquids are altered. The results of such calculations are shown in Table V. When co-association

TABLE IV. Comparison with experiment of the calculated dielectric constant at 20°C of several aliphatic alcohols.

Alcohol	g	ϵ Kirkwood Eq. (20)	ϵ This research Eq. (13)	ϵ Exp.
methyl	2.57	29.2	36.3	32.8
ethyl	2.57	21.3	26.5	24.6
n-propyl	2.57	17.3	21.7	19.5
n-butyl	2.57	14.6	18.6	18.0
n-amyl	2.57	12.8	16.4	15.8

of molecules occurs, i.e. when the dipoles tend to orient head to tail so as to reinforce each other, values of g are larger than unity. Indeed, in HCN and ethyl ether where such co-association is expected from other experimental observations,[11] g is found to be larger than unity. However in liquids such as pyridine or nitrobenzene, where contra-association is believed to occur, values of g less than unity are observed. For chloroform and acetone $g=1.0$, which is consistent with the heretofore accepted picture of nonassociating molecules in these liquids.

APPENDIX I

It is essential in identifying $\langle \mathbf{u} \rangle_\mu$ with the average total moment of a cluster of molecules in the spherical sample that the probability of a configuration of a cluster of molecules will be the same in a spherical specimen and an infinite medium. This requires that the local field have the same value in both media. We shall show that the local field is indeed equal for the spherical and infinite regions provided that the size of a

[11] J. Norton Wilson, Chem. Rev. **25**, 377 (1939).

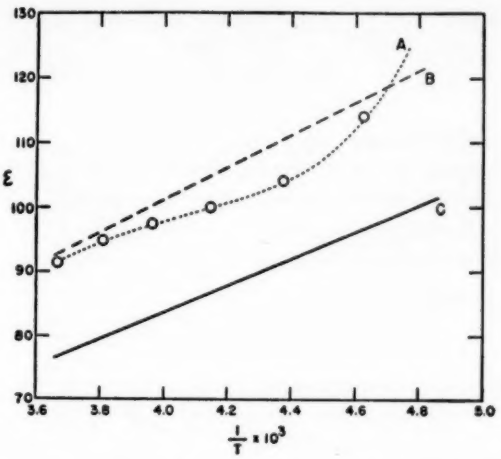

FIG. 1. Comparison of experimental and theoretical values of the static dielectric constant of ice. *A*, experimental (Auty and Cole); *B*, this research; *C*, Powles.

cluster be small compared to the dimensions of the spherical specimen. Since the field arising from a cluster itself will certainly be the same in both cases, we need only prove that the reaction fields due to the presence of the molecules outside the cluster are equal. Furthermore, equality of the local field implies equal effective dipole moments in the two media. However, the spherical and infinite specimens do differ in that the presence of the surface adds a uniform polarization to the material inside it.

To prove the above let us first consider the potential, ψ, of a system which contains a rigid dipole $\mathbf{m}$ in the direction $\theta=0$ at the center of a cavity of radius a in an otherwise continuous medium of dielectric constant ϵ.

$$\psi = -\frac{m\cos\theta}{r^2} + \frac{2m(\epsilon-1)}{a^3(2\epsilon+1)} r\cos\theta, \quad (r \leq a),$$
$$\psi = -\left(\frac{3\epsilon}{2\epsilon+1}\right)\frac{m\cos\theta}{\epsilon r^2}, \quad (r \geq a). \tag{A1}$$

Hence the reaction field inside the cavity (the difference between the field and that of the dipole in empty

TABLE V. Evaluation of the correlation factor g for various liquids.

Liquid	ϵ Expt.	n	μ_0	g Kirkwood Eq. (20)	g This research Eq. (13)
HCN	116	1.27	2.80	4.1	3.6
Ethyl ether	4.4	1.35	1.15	1.7	1.4
Acetone	21.5	1.36	2.85	1.1	1.0
Ethyl bromide	9.4	1.42	1.80	1.1	0.9
Pyridine	12.5	1.51	2.20	0.9	0.7
Chloroform	4.8	1.44	1.15	1.3	1.0
Nitrobenzene	36.1	1.55	3.90	1.1	0.8

space) is

$$\mathbf{R}=\frac{2(\epsilon-1)\mathbf{m}}{(2\epsilon+1)a^3}. \tag{A2}$$

This is the Onsager reaction field.

The potential of a system similar to that described immediately above, except that the medium of dielectric constant ϵ only be extended out to a spherical surface of radius b $(b>a)$ is

$$\psi=-\frac{m\cos\theta}{r^2}+\frac{2m(\epsilon-1)}{a^3(2\epsilon+1)} \times\left\{\frac{1-a^3/b^3}{1-\dfrac{2a^3(\epsilon-1)^2}{b^3(2\epsilon+1)(\epsilon+2)}}\right\}r\cos\theta, \quad (r\leq a),$$

$$\psi=\left[-\left(\frac{3\epsilon}{2\epsilon+1}\right)\frac{m\cos\theta}{\epsilon r^2}+\frac{2m(\epsilon-1)}{b^3(2\epsilon+1)}\left(\frac{3}{\epsilon+2}\right)r\cos\theta\right] \times\left\{\frac{1}{1-\dfrac{2a^3(\epsilon-1)^2}{b^3(2\epsilon+1)(\epsilon+2)}}\right\}, \quad (a\leq r\leq b), \tag{A3}$$

$$\psi=-\left(\frac{3\epsilon}{2\epsilon+1}\right)\left(\frac{3}{\epsilon+2}\right)\left\{\frac{1}{1-\dfrac{2a^3(\epsilon-1)^2}{b^3(2\epsilon+1)(\epsilon+2)}}\right\} \times\frac{m\cos\theta}{r^2}, \quad (r\geq b).$$

The reaction field inside this cavity is

$$\mathbf{R}=\frac{2(\epsilon-1)\mathbf{m}}{(2\epsilon+1)a^3}\left\{\frac{1-a^3/b^3}{1-\dfrac{2a^3(\epsilon-1)^2}{b^3(2\epsilon+1)(\epsilon+2)}}\right\}, \tag{A4}$$

and in the limit $b/a\rightarrow\infty$, this becomes identical with (A2).

However, the total induced moment of the spherical shell approaches a constant (nonzero) value as $b/a\rightarrow\infty$, which is responsible for the difference between $\langle\mathbf{M}\rangle_{\mu_s}$ and $\langle\boldsymbol{\mu}\rangle_\mu$. To show this, set $\langle\mathbf{M}\rangle_{\mu_s}=\langle\boldsymbol{\mu}\rangle_\mu+\mathbf{M}_s$, where $\mathbf{M}_s$ is the moment of the shell. From the basic definitions,

$$\mathbf{M}_s=\int_{a\leq r\leq b}\mathbf{P}dV=\frac{\epsilon-1}{4\pi}\int\mathbf{E}dV =\frac{\epsilon-1}{4\pi}\int(-\nabla\psi)dV, \tag{A5}$$

where ψ is given by (A3). Taking the limit, and adding $\mathbf{M}_s$ to $\langle\boldsymbol{\mu}\rangle_\mu$, Eq. (9) is obtained.

APPENDIX II

Verification that $g=1$ if no short-range interaction is present.

In this paper the term "no short-range interaction" means that the interaction between a dipolar molecule and its surroundings is just that which would exist if the surroundings were replaced by material of the macroscopic dielectric constant. Therefore, we need to show that $\langle\boldsymbol{\mu}\rangle_\mu=\boldsymbol{\mu}$ for the case of a dipole $\boldsymbol{\mu}$ in a cavity in an infinite medium of dielectric constant ϵ. To show this, set $\langle\boldsymbol{\mu}\rangle_\mu=\boldsymbol{\mu}+\mathbf{M}$, where $\mathbf{M}$ is the total moment of the surrounding medium. As above,

$$\mathbf{M}=\frac{\epsilon-1}{4\pi}\int_{r\leq a}(-\nabla\psi)dV, \tag{A6}$$

where ψ is now given by (A1). Upon integration over θ, $\mathbf{M}$ is seen to vanish.

Statistical Thermodynamics of Rubber Elasticity*

HUBERT M. JAMES, *Department of Physics, Purdue University, Lafayette, Indiana*

AND

EUGENE GUTH, *Department of Physics, University of Notre Dame, Notre Dame, Indiana*

(Received August 20, 1952)

The basic concepts and procedures underlying the theory of rubber elasticity are analyzed. The arguments advanced by Wall and Flory against the network theory of the authors are shown to be without foundation. The alternative theory which they advocate, and which is rather widely used, is criticized on two grounds: (a) it assumes a distribution of chain extensions that does not vary with network extension in the way the actual distribution functions can be shown to vary, and (b) the methods used to compute the numbers of network configurations from the distributions of chain extensions are invalid, except in the most trivial cases. The concept of "interval dilation entropy" is discussed and is shown to lack any physical basis. It is concluded that all the methods of calculation that lead to logarithmic terms in the network configuration entropy are incorrect, and that these terms, which affect the theory of swelling, should be discarded.

I. INTRODUCTION

IN a recent paper, Wall and Flory[1] have criticized our network theory of rubber elasticity[2–4] on very general grounds. Their specific objections to our theory do not appear to us to be valid; on the other hand, the theoretical basis of their own work seems to us to involve fundamental errors that are affecting a growing body of literature. In an effort to clarify the major points at issue, we wish to discuss them here in considerable detail. Our discussion of the fundamentals of the theory of rubber elasticity will not, however, be limited to the points raised by Wall and Flory; neither is it intended as an answer to all statements in their paper that we find objectionable.[5]

The theories to be discussed here are all based on the same idealization of a high-polymer molecule as a flexible chain which can take on a number of configurations, that is, a Gaussian exponential function of the distance between its ends. Such a chain will be called a Gaussian chain. In calculating the entropy of deformation of a piece of rubber-like material, we have treated it as a coherent network of Gaussian chains, neglecting the restrictions placed on the configuration of each chain by steric interferences with other chains in the network;[6] we have called this model a "Gaussian network." What we have calculated is the entropy of deformation of a given Gaussian network, or the average entropy of deformation of the different Gaussian networks that might be formed during cure of the material. Wall and Flory also treat the material as an assemblage of Gaussian chains not subject to mutual steric interferences, but they do not treat it explicitly as a network with fixed structure. Instead, they attempt to calculate the entropy of the stretched or swollen material by computing the entropy change involved in forming this material from individual high-polymer molecules in three steps:

(1) Dilution of the high-polymer molecules, if the material is swollen.

(2) Constraint of the end-to-end displacements of the individual chains to a particular distribution, intended to be the one existing in the material under the prevailing conditions of swelling and stretch.

(3) Union of the chains to form a network.

The two theories lead to concrete differences in results. For example, consider a rectangular parallelopiped of rubber-like material which in a standard, unstretched, and unswollen condition has dimensions L_{x0}, L_{y0}, L_{z0}, and has had these dimensions changed, through stretching and swelling, by factors $\alpha_x=L_x/L_{x0}$, α_y, α_z. With the idealizations mentioned above, the present authors find for the network configuration term in the entropy

$$S=\text{const}-(kK/2)(\alpha_x^2+\alpha_y^2+\alpha_z^2), \qquad (1)$$

where k is the Boltzmann constant and K is a constant that depends on the network considered. Wall's original theory,[7] based on the same idealization of the molecules, and on consideration of step (2) of the preceding para-

* Supported in part by the U. S. Office of Naval Research.

[1] F. T. Wall and P. J. Flory, J. Chem. Phys. **19**, 1435 (1951).

[2] H. M. James and E. Guth, J. Chem. Phys. **11**, 455 (1943).

[3] H. M. James and E. Guth, J. Chem. Phys. **15**, 669 (1947).

[4] H. M. James and E. Guth, J. Polymer Sci. **4**, 153 (1949).

[5] In reference 1, Wall and Flory have attributed to us ideas that we have not proposed, and have described parts of our theory in a way that appears to us to be quite misleading. We shall not here cite and answer all these points in detail, hoping that persons interested in our theory will read our own presentation of it.

[6] Neglect of these interferences is perhaps the most unsatisfactory feature of our model, since they actually reduce by a large factor the number of configurations accessible to the network. In Appendix A of reference 4 we have given our reasons for believing that in soft rubber-like materials, not too highly extended, these interferences reduce the number of configurations by a constant factor, and change the computed entropy only by an unimportant constant. On the other hand, the Gaussian network model is quite unsuited to any attempt to calculate the internal energy U, which enters our theory of ideal rubber-like materials as an unspecified function of volume and temperature, independent of the form of the material, as with a liquid.

[7] F. T. Wall, J. Chem. Phys. **10**, 485 (1942).

graph, yields

$$S=\text{const}-(k\nu/2)(\alpha_x^2+\alpha_y^2+\alpha_z^2)+k\nu\ln(\alpha_x\alpha_y\alpha_z), \quad (2)$$

where ν is the number of chains in the network. Consideration of steps (1) and (3) has now led Wall and Flory[1] to introduce another logarithmic term that cancels out half the last term in Eq. (2); they obtain

$$S=\text{const}-(k\nu/2)(\alpha_x^2+\alpha_y^2+\alpha_z^2)+(k\nu/2)\ln(\alpha_x\alpha_y\alpha_z). \quad (3)$$

The logarithmic terms in Eqs. (2) and (3) play no role in the discussion of stretch at constant volume, $\alpha_x\alpha_y\alpha_z=1$, but they affect, for example, the theory of the swelling of rubber, in a way that has not yet been subjected to experimental check.

Since there appears to be no difference in the pictures of the system used by Wall and Flory and by ourselves, nor any essential difference in the models selected for treatment, the question at issue is: which formalism is appropriate to the treatment of networks of high-polymer molecules, when the component molecules are treated as Gaussian chains, and steric interferences are neglected?

Wall and Flory have objected to our theory on two main grounds:

(1) We have considered only one particular network structure (that existing in the cured material).

(2) A distribution function occurring in our theory does not meet a symmetry condition that they propose.

These objections will be answered in Secs. II and IV of the present paper. On the other hand, we believe that the whole calculation of Wall and Flory is based on a fallacious assumption. In Sec. III of this paper we shall show that their assumed distribution of chain extensions does not change with stretch of the material in the way that actual distributions for Gaussian networks must change. In Sec. V we shall show that, in the case of a simple linear network, replacement of their assumed distribution function by the correct one eliminates the logarithmic term in S, and gives a result agreeing with our own. In Sec. VI we show what difficulties stand in the way of a similar correction of their treatment of more complicated networks. Section VII is concerned with the concept of "interval-dilation" entropy, introduced by Kuhn, Pasternak, and Kuhn.[8] Our conclusion is that there is no theoretical justification for the logarithmic terms in Eqs. (2) and (3).

II. IS IT NECESSARY TO CONSIDER MORE THAN ONE NETWORK STRUCTURE?

Equation 1 is obtained by taking

$$S=k\ln C(\alpha_x, \alpha_y, \alpha_z), \quad (4)$$

where $C(\alpha_x, \alpha_y, \alpha_z)$ is the relative number of configurations available to the network as a function of the macroscopic parameters that characterize the form of the material. We have shown[4] that one obtains Eq. (1), with appropriate values of the constants, from consideration of *any* definite Gaussian network that is effectively isotropic when $\alpha_x=\alpha_y=\alpha_z=1$. It follows, for instance, from the theory of Flory and Rehner,[9] which was based on consideration of four Gaussian chains of equal length, joined to each other at one end, with the other ends fixed at the four vertices of a regular tetrahedron; it thus underlies Flory and Rehner's theory of swelling.[10] It appears also as the limiting form, for Gaussian chains, of the results found by Isihara, Hashitsuma, and Tatibana[11] and by Wang and Guth[12] for arbitrary definite networks of non-Gaussian chains. The correctness of our calculation of the form of $C(\alpha_x, \alpha_y, \alpha_z)$ has not been challenged by Wall and Flory, except possibly through a symmetry argument that will be discussed in Sec. IV.

Wall and Flory do consider it a major error on our part that we consider one particular network structure out of the many that might be formed during cure of the material. They write, "Although the network which is formed in any given case is, to be sure, a unique structure, there are no constraints on the cross-linking process which favor this particular array of cross-linked pairs of units over the many others which are possible. . . . For the calculation of the entropy of the system, all states consistent with the macroscopic restraints must be considered." This criticism would be valid if we had concerned ourselves with calculation of the entropy change in rubber during cure. To calculate the entropy change involved in the formation of an unspecified network during cure, one would have to consider all the structures that might be formed. To compute the final entropy by consideration of a single network would imply that the process of network formation was carried out under conditions that would assure the formation of that particular network—a process which would involve a different entropy change from that occurring during ordinary cure and which might proceed to completion only after a long wait for a large entropy fluctuation to take place.

We have, however, been concerned entirely with the dependence of the entropy of the cured material on its external form. [The entropy of network formation appears only in the unspecified constant in Eq. (1).] We have assumed that the molecular network formed during cure is unchanged when the material is stretched or swelled, thus neglecting irreversible plastic flow. Once it is granted that a particular network structure exists throughout an experiment, it seems clearly possible to base the theory on consideration of that particular structure alone. There is no need to consider

[8] Kuhn, Pasternak, and Kuhn, Helv. Chim. Acta **30**, 1705 (1947).

[9] P. J. Flory and J. Rehner, Jr., J. Chem. Phys. **11**, 512 (1943).

[10] P. J. Flory and J. Rehner, Jr., J. Chem. Phys. **11**, 521 (1943).

[11] Isihara, Hashitsuma, and Tatibana, J. Chem. Phys. **19**, 1508 (1951).

[12] Ming Chen Wang and E. Guth, J. Chem. Phys. **20**, 1144 (1952).

structures that do not exist; neither is it appropriate to introduce into such a treatment a variable factor to represent the probability that the existing network would be formed under different conditions, as Wall and Flory do in a proposed emendation of our theory.

Though it is reasonable to discuss reversible processes in terms of the behavior of molecular networks of fixed structure, in practice one cannot know what particular structure is realized in a given case. One can, however, proceed by computing the shape-dependent term in the entropy for all possible structures, and then averaging the results, weighting each with the probability that the corresponding structure is the existing one.[13] If the system is a large one, there is a negligible chance that the resulting average will differ appreciably from the result obtained by considering the actually existing structure. For any specified network the entropy is a linear function of $\alpha_x^2+\alpha_y^2+\alpha_z^2$, as shown in Eq. (1); on averaging this over all networks, with weights independent of α_x, α_y, α_z, one must find exactly the same type of dependence of $\bar{S}$ on $\alpha_x^2+\alpha_y^2+\alpha_z^2$ but with an appropriately averaged multiplying constant K. Thus the multiplicity of possible networks does not lead to any logarithmic term in the shape-dependent entropy.

We do not contend that our approach to this problem is the only possible one.[14] The general approach of Wall and Flory is also a conceivable one, but we believe that all attempts to apply it thus far have involved several errors. One of these will be discussed in the next section.

III. DISTRIBUTION OF EXTENSIONS OF A CHAIN IN A NETWORK

Wall and Flory base their calculation of the entropy of network formation on an assumed form for the distribution of extensions of the chains running between junctions of a network, and on an assumption concerning the way in which this distribution is modified as α_x, α_y, and α_z are varied. It will now be shown that they have assumed a variation of the distribution with the α's which is quite different in character from the variation that can be *derived* by detailed treatment of Gaussian networks. Later, in Sec. V, it will be shown in a simple case for which the other elements of their formalism are valid, that use of their erroneous distribution function leads to a logarithmic term in the entropy, like that in Eq. (2), whereas use of the correct distribution yields an entropy function analogous to that in Eq. (1), without a logarithmic term.

We shall here limit detailed consideration to a simple one-dimensional case. In his first paper on rubber elasticity, Wall[15] considered the problem as essentially one-dimensional, and assumed that the distribution of extensions of chains in a network of relative length α would be

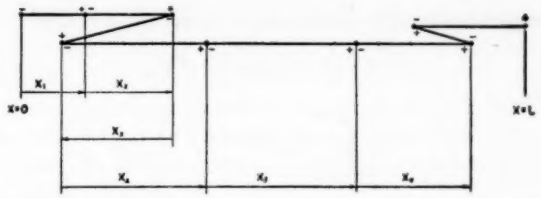

FIG. 1. Definition of extensions x_i of chains in a one-dimensional network. x_i is positive if the arrow points to the right, negative if it points to the left.

$$p'(x)=\frac{\beta}{\alpha\pi^{\frac{1}{2}}}\exp\left\{-\frac{\beta^2x^2}{\alpha^2}\right\}. \tag{5}$$

He later[16] undertook to derive this distribution function by considering the simplest possible "network," consisting of N similar chains hooked end to end, with one end of the resulting structure fixed at the point $x=0$, and the other end fixed at $x=l$. We have elsewhere[4] criticized his derivation as fallacious, and have stated the correct result. Here, for several reasons, it will be desirable to indicate our calculation in some detail, even though it is elementary. Like Wall, we shall here use the method of Lagrangian multipliers.[17]

Figure 1 represents a Gaussian network, consisting of N Gaussian chains linked end to end, with its ends fixed at $x=0$ and $x=l$. The ends of the component chains (the "junctions" of this simple network) are shown, but no attempt is made to represent the irregular configurations of the chains. Let the end of the "network" fixed at $x=0$ be taken arbitrarily as the minus end, and the end fixed at $x=l$ as the plus end. We shall also define a minus and a plus end of each chain of the network, such that as one traverses the network from its minus to its plus end one will traverse each component chain from minus to plus end, as shown in Fig. 1. Let the displacement of the plus end of the kth chain from its minus end be x_k; we shall call this the extension of the kth chain. For different configurations of the chains, different positions of the chain junctions, x_k may be positive or negative. However, for every configuration of the network consistent with the specified positions of its ends at $x=0$ and $x=l$, one must have

$$x_1+x_2+\cdots+x_N=l. \tag{6}$$

We assume that the component Gaussian chains in the network are similar, each being able to assume

$$\Delta C=K\frac{\beta}{\pi^{\frac{1}{2}}}\exp(-\beta^2x^2)\Delta x \tag{7}$$

[13] This is essentially the method used in our calculation of the increase in rigidity during cure, in reference 3.

[14] Compare, for instance, the calculations of the pressure exerted by a classical ideal gas, based on consideration of (a) the actual motions of the gas molecules in a particular case, (b) all possible motions of the gas molecules, taken with appropriate weights, and (c) the change of entropy of the gas with volume.

[15] F. T. Wall, J. Chem. Phys. **10**, 132 (1942).

[16] F. T. Wall, J. Chem. Phys. **11**, 527 (1943).

[17] Our result can be written down immediately as a special case of general results obtained by a quite different method: H. M. James, J. Chem. Phys. **15**, 651 (1947).

configurations with extension x to within Δx. Let

$$p(x)=(\beta/\pi^{\frac{1}{2}})\exp(-\beta^2x^2). \tag{8}$$

Since

$$\int_{-\infty}^{+\infty}p(x)dx=1, \tag{9}$$

it follows from Eq. (7) that K is the total number of possible configurations for the chain. The probability that a *free* chain will assume extension x to within Δx is proportional to ΔC and is exactly given by $p(x)\Delta x$; thus $p(x)$ is the probability distribution function for extensions of a free chain.

We now ask: What is the probability $p'(x)\Delta x$ of finding a chain *in the network* with extension x to within Δx? By familiar arguments it will suffice to determine the most probable distribution of chain extensions for the network—that is, the distribution of x values consistent with the largest number of network configurations. Let the entire range of x be divided into small ranges, the ith being of length Δx_i about the value x_i. A distribution of chain extensions is specified by giving the number N_i of chains with extension in the ith range, for all i. The number of configurations possible for a chain with extension in the ith range is

$$p_i=Kp(x_i)\Delta x_i. \tag{10}$$

The number of configurations of the network consistent with a specified distribution of segment extensions is then

$$C=\frac{N!}{N_0!N_1!N_2!\cdots}p_0^{N_0}p_1^{N_1}p_2^{N_2}\cdots. \tag{11}$$

The first factor on the right arises from the fact that *in this particular case* it is consistent with the structure of the network and with the conditions to which it is subject to make $N!/\prod_i N_i!$ distinct assignments of the specified extensions to the N chains of the network. We wish, then, to find the values of the N_i that maximize C, subject to the conditions that the total number of chains is N, and that the extension of the network is l,

$$\sum_i N_i=N, \tag{12}$$

$$\sum_i N_ix_i=l. \tag{13}$$

Equation (12) is, of course, a restatement of Eq. (6).

Using Stirling's approximation, one can write

$$\ln C=N\ln N-\sum_i N_i\ln(N_i/p_i). \tag{14}$$

The condition on the N_i is then that

$$\delta\ln C=0 \tag{15}$$

for all δN_i such that

$$\sum_i\delta N_i=\sum_i x_i\delta N_i=0. \tag{16}$$

It follows by the standard argument that one must have

$$N_i=p_i\exp(\lambda+\mu x_i), \tag{17}$$

where λ and μ are constant Lagrangian multipliers fixed by the conditions expressed in Eqs. (12) and (13). Equation (17) can be written, on use of Eqs. (8) and (10), as

$$N_i=\exp(\lambda-\mu^2/4\beta^2)\cdot\frac{\beta}{\pi^{\frac{1}{2}}}\cdot\exp\left(-\beta^2\left[x_i-\frac{\mu}{2\beta^2}\right]^2\right)\cdot\Delta x_i. \tag{18}$$

Converting the sums in Eqs. (12) and (13) into integrals, one obtains

$$N=\exp(\lambda-\mu^2/4\beta^2)\int_{-\infty}^{+\infty}dx\frac{\beta}{\pi^{\frac{1}{2}}}\exp\left(-\beta^2\left[x-\frac{\mu}{2\beta^2}\right]^2\right)$$

$$=\exp(\lambda-\mu^2/4\beta^2), \tag{19}$$

$$l=\exp(\lambda-\mu^2/4\beta^2)\times\int_{-\infty}^{+\infty}dx\cdot x\frac{\beta}{\pi^{\frac{1}{2}}}\exp\left(-\beta^2\left[x-\frac{\mu}{2\beta^2}\right]^2\right)$$

$$=\frac{\mu}{2\beta^2}\exp(\lambda-\mu^2/4\beta^2). \tag{20}$$

It follows that

$$\mu/2\beta^2=l/N, \tag{21}$$

and thus that

$$N_i=N(\beta/\pi^{\frac{1}{2}})\exp(-\beta^2[x-l/N]^2)\Delta x_i. \tag{22}$$

The probability distribution function that describes the extensions of chains in this "network" is consequently

$$p'(x)=\frac{\beta}{\pi^{\frac{1}{2}}}\exp\left(-\beta^2\left[x-\frac{l}{N}\right]^2\right). \tag{23}$$

Instead of Eq. (23), Wall obtains a result expressible [by use of his Eqs. (16) and (17)] as

$$N_i=N\cdot\left(\frac{CN}{2\pi l^2}\right)^{\frac{1}{2}}\exp\left(-\frac{CN}{2l^2}x^2\right)\Delta x_i, \tag{24}$$

which depends on l in a quite different way, and corresponds in form to his assumption expressed in our Eq. (5). He obtains this result because he uses, instead of our auxiliary condition, as given in Eq. (6) or (13), a quite different one,

$$C\sum_i N_ix_i^2=l^2. \tag{25}$$

To obtain this condition he starts from Eq. (6) [his Eq. (3)], squares it, and, after neglecting many terms, concludes that

$$\langle x_i^2\rangle_{\text{Av}}=l^2/N; \tag{26}$$

this he rewrites, after introducing an arbitrary constant

C, to obtain Eq. (25). The terms he neglects in deriving Eq. (26) are individually small, but they are so numerous that they cannot be neglected: exact evaluation using Eq. (23) yields

$$\langle x_i^2\rangle_{Av}=(l^2/N^2)+(1/2\beta^2). \tag{27}$$

Wall's auxiliary condition has the curious effect of requiring that $x_i=0$ for all i when $l=0$; that is, if the ends of the network are brought together the extension of every component chain must be exactly zero. His derived distribution indicates, moreover, that equal positive and negative values of x_i are equally probable, a result which is incompatible with the condition that the sum of all x_i shall be equal to l. We do not see how his treatment of this problem can be supported on either physical or mathematical grounds.

Wall and Flory have objected to our Eq. (13), not on mathematical grounds but on the basis of a symmetry principle (to be discussed in Sec. IV) and a misleading analogy. They write,[1] "Moreover, the exact profile of their distribution function for chain lengths is independent of strain, and only the center of that distribution appears to move about. This is as physically unrealistic as would be shifting the origin of the Maxwellian distribution of molecular velocities to accompany changes in temperature." The analogy between chain extensions in a network and molecular velocities in a gas can indeed be useful, but we believe the proper analog to a change in the macroscopic extension l of the network is a change in the macroscopic velocity of the gas, rather than a change in temperature. It is well known that a change in bulk velocity of a gas simply shifts the distribution of molecular velocities in velocity space, without changing its form.

Another point of view may be useful in understanding the qualitative character of our result. Consider a single chain with one end fixed at $x=0$ and the other free. The distribution of its extensions will then be given by $p(x)$ of Eq. (8). Now let this be converted into the first chain of a linear network by joining to its free end one end of a string of $N-1$ similar chains, this string having its other end fixed at $x=l$. This string of chains will jerk against the end of the first chain, exerting a net force tending to pull it toward $x=l$. This force will modify the distribution of extensions for the first chain, tending to make positive x more probable that negative x, as is indicated by our distribution function, though not by that of Wall. If the forces exerted on the end of the first chain by the second chain are replaced by a constant average force F in the direction of positive x, the probability distribution for the extensions of the first chain will have the form

$$\begin{aligned}Cp(x)\exp(Fx/kT)&=C'\exp(-\beta^2x^2+Fx/kT)\\&=C''\exp(-\beta^2[x-F/2\beta^2kT]^2).\end{aligned} \tag{28}$$

Here $\exp(Fx/kT)$ is the Boltzmann factor in the probability that corresponds to the potential energy of the applied force. Its effect is to shift the distribution for the free chain, without change of form, through a distance $F/2\beta^2kT$. Indeed, the derivation of Eq. (23) can be made complete by substituting for F the average force exerted by (or the average tension in) a string of N chains with total extension l, as given by kinetic theory (See Sec. V),

$$F=2\beta^2kTl/N. \tag{29}$$

Reference may now be made to other results concerning distributions of extensions of chains in Gaussian networks—results that can be derived from first principles, rather than assumed. One of the present authors has shown[18] that every segment of any three-dimensional Gaussian network has a probability distribution of extensions of the form

$$\begin{aligned}P_i(x,y,z)&=(\beta_i^2/\pi)^{\frac{3}{2}}\\&\quad\times\exp\{-\beta_i^2[(x-\bar{x}_i)^2+(y-\bar{y}_i)^2+(z-\bar{z}_i)^2]\}.\end{aligned} \tag{30}$$

This is a Gaussian distribution of the displacement components x, y, z, about nonzero mean values. The constant β_i, which determines the breadth of the distribution, and the mean values $\bar{x}_i$ $\bar{y}_i$, $\bar{z}_i$ are determined by the structure of the network, as well as by the number of links in the chain under consideration; the signs of $\bar{x}_i$, $\bar{y}_i$, $\bar{z}_i$ are determined only when one specifies which shall be considered to be the plus and minus ends of the chain. The quantity β_i is independent of the positions assigned to the "fixed points" of the network, but $\bar{x}_i$, $\bar{y}_i$, $\bar{z}_i$ are not. If the fixed points of the network are subjected to a homogeneous deformation, as when a cube of rubber swells or is deformed into a rectangular parallelopiped, $\bar{x}_i$, $\bar{y}_i$, $\bar{z}_i$ change proportionally to the corresponding macroscopic dimension, or the corresponding α [reference 17, Eq. (4.5)]. Thus one has

$$\bar{x}_i=\bar{x}_{i0}\alpha_x, \quad \text{etc.}, \tag{31}$$

and

$$\begin{aligned}P_i(x,y,z)=\left(\frac{\beta_i^2}{\pi}\right)^{\frac{3}{2}}\exp\Big\{&-\beta_i^2[(x-\bar{x}_{i0}\alpha_x)^2\\&+(y-\bar{y}_{i0}\alpha_y)^2+(z-\bar{z}_{i0}\alpha_z)^2]\Big\}.\end{aligned} \tag{32}$$

The distribution of extensions of all the chains in a network will be a linear combination of such distributions—a sum of Gaussian exponentials of constant form with centers at various points with coordinates that change proportionally to α_x, α_y, α_z. This is to be contrasted with the distribution assumed by Wall and Flory [compare their Eq. (7)], which is a single Gaussian exponential with fixed center and form changing with α_x, α_y, α_z,

$$\begin{aligned}P(x,y,z)=&\frac{\beta^3}{\pi^{\frac{3}{2}}\alpha_x\alpha_y\alpha_z}\\&\times\exp\left\{-\beta^2\left[\left(\frac{x}{\alpha_x}\right)^2+\left(\frac{y}{\alpha_y}\right)^2+\left(\frac{z}{\alpha_z}\right)^2\right]\right\}.\end{aligned} \tag{33}$$

[18] Reference 17, Eq. (7.5).

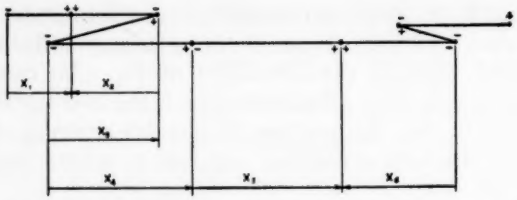

FIG. 2. Random definition of positive senses of extensions of chains in a one-dimensional network.

Finally, it may be noted that distributions of the form $(\alpha_x\alpha_y\alpha_z)^{-1}F(x/\alpha_x, y/\alpha_y, z/\alpha_z)$ can play a legitimate role in the statistical theory of rubber elasticity. The results of reference 17, as illustrated in Eq. (32), show that probability distributions for the *time-average* extensions of chains, $(\bar{x}_{i0}\alpha_x, \bar{y}_{i0}\alpha_y, \bar{z}_{i0}\alpha_z)$, simply change by scale factors when the material undergoes the homogeneous deformation described by $(\alpha_x, \alpha_y, \alpha_z)$.[19] It has also been shown in reference 17 [see Eq. (4.3)] that the computed number of configurations of a Gaussian network will be changed only by a constant factor, and the computed entropy only by an added constant, if one treats every junction as fixed at its average position, and every chain as having a fixed extension equal to its actual time-average extension.[20] Without changing the predictions of the theory one can, then, treat rubber as a system of high-polymer chains with a distribution of fixed extensions varying like $(\alpha_x\alpha_y\alpha_z)^{-1}$ $\times F(x/\alpha_x, y/\alpha_y, z/\alpha_z)$. If this is done, however, other elements of the formalism of Wall and Flory become inapplicable, as will be shown in Sec. VI.

IV. THE SYMMETRY PRINCIPLE OF WALL AND FLORY

Wall and Flory[1] have raised one further objection to our Eq. (23), an objection to which they attached great importance—that it is "incompatible with fundamental physical principles relating to symmetry." In laying the foundation for the statement of their symmetry principle, they write, "The distribution of chain lengths, and hence the probability that a chain have a certain length, can be ascertained by using as samples the vectors originating from a sufficiently large number of junction points. If all the junction points are used for determining the distribution function, then each chain will be counted twice, with opposite vector senses for each count. If less than all the junction points are used in providing samples, then some of the chains may be counted twice, others counted once, and still others may not be counted at all. It is, however, possible to pick a truly representative sample with the restriction that no chain be counted twice." They then argue that the distribution function thus obtained must be invariant to change in the signs of x, y, and z, and note that Eq. (23) does not meet this condition, whereas Eq. (5) does.

As we understand their argument, it is that one can obtain a distribution function that is symmetric in x, y, and z by counting each chain extension twice, once with either sign, or by defining the sense of the extension of each chain in an appropriately random way. With this we agree. This does not, however, reflect on the correctness of Eq. (23), which was based on a special, nonrandom definition of the sense of a positive displacement x_k. Such a definition of the signs of the x_k is necessary if Eq. 6 is to be correct with only plus signs on the left. The distribution appropriate to a random definition of the senses of the x_k, such as that illustrated in Fig. 2, can, however, be derived from the final result of our calculation by averaging the probabilities for equal positive and negative extensions. One thus obtains

$$p_s(x)=\frac{\beta}{2\pi^{\frac{1}{2}}}\left\{\exp\left(-\beta^2\left[x-\frac{l}{N}\right]^2\right)+\exp\left(-\beta^2\left[x+\frac{l}{N}\right]^2\right)\right\}. \quad (34)$$

This has the symmetry desired by Wall and Flory but it does not in the least resemble their distribution.

It will be clear from inspection of Fig. 2 how this way of defining the signs of the x_k and symmetrizing the distribution function makes Eqs. (6) and (13) invalid. It also introduces other difficulties in the application of the distributions, which will be discussed in Sec. V.

V. ENTROPY OF A SIMPLE LINEAR NETWORK

We now return to the case of the simple linear network discussed in Sec. III, to compare the procedure of Wall and Flory with our own.

We consider first a one-dimensional chain consisting of n links of fixed length a, each of which can lie parallel or antiparallel to the x direction independently of the others. It is well known that the numbers of configurations of this chain with extension x to within $\Delta x \gg a$ (extension as defined in Sec. III) is

$$\Delta C=\frac{2^n}{(2\pi na^2)^{\frac{1}{2}}}\exp\left\{-\frac{x^2}{2na^2}\right\}\Delta x \quad (35)$$

in the Gaussian approximation, valid for small x^4/n^3a^4.[21] If N such chains are joined end to end, to form a chain of Nn links, the resulting network will clearly have as the number of configurations compatible with extension l to within Δl,

$$\Delta C=\frac{2^{Nn}}{(2\pi Nna^2)^{\frac{1}{2}}}\exp\left\{-\frac{l^2}{2Nna^2}\right\}\Delta l. \quad (36)$$

[19] The difference between distributions of instantaneous extensions and of time-average extensions is well illustrated by the linear network considered in this section. The instantaneous extensions have a displaced Gaussian distribution, but the time-average extensions all have the same value, l/N.

[20] More precisely, each chain is to be treated as able to assume a number of configurations proportional to $p(\mathbf{r})_{\Delta v}$.

[21] See, for instance, reference 2, Sec. 6.

More generally, consider any Gaussian chain that can assume

$$dC=K\left(\frac{\beta}{\pi^{\frac{1}{2}}}\right)\exp\{-\beta^2x^2\}dx \tag{37}$$

configurations with the given range of extension dx. Let N such chains be joined end to end to form the "network" considered in Sec. III. It is clear from comparison with Eqs. (35) and (36), where $2^n=K$ is the total number of configurations of the chain and $1/2na^2=\beta^2$, that the network of N Gaussian chains will be able to assume

$$dC=K^N\frac{\beta}{(N\pi)^{\frac{1}{2}}}\exp\{-\beta^2l^2/N\}dl \tag{38}$$

configurations with extension l to within dl. Equations (35) and (36) are only approximations for the "folding-rule" chain, but Eq. (38) is exact if Eq. (37) is exact.

As applied to this linear network of N chains, our general method of calculating the entropy would proceed as follows. Let the negative end of the first chain be fixed at $x=\xi_0=0$, and let $\xi_1, \xi_2, \cdots \xi_N$ be the coordinates of the positive ends of the component chains. The number of configurations of the network with ξ_1 in range $d\xi_1$, ξ_2 in range $d\xi_2$ and so on is, by Eq. (38),

$$\prod_{i=1}^{N}\left[\frac{K\beta}{\pi^{\frac{1}{2}}}\exp\{-\beta^2(\xi_i-\xi_{i-1})^2\}d\xi_i\right].$$

The total number of configurations of the network with extension l to within dl is obtained by summing over all $\xi_1, \xi_2, \cdots \xi_{N-1}$ and the specified range of ξ_N,

$$dC=\left(\frac{K\beta}{\pi^{\frac{1}{2}}}\right)^N\int_l^{l+dl}d\xi_N\int_{-\infty}^{+\infty}d\xi_{N-1}\cdots\int_{-\infty}^{+\infty}d\xi_1\prod_{i=1}^{N}\exp\{-\beta^2(\xi_i-\xi_{i-1})^2\}. \tag{39}$$

This multiple integral is easily evaluated, and yields the exact result given in Eq. (38). It then follows from Boltzmann's relation that the configurational entropy of the linear network, constrained to have extension l to within dl, is

$$S(l)=k\ln(dC)=k\ln\left\{K^N\frac{\beta}{(N\pi)^{\frac{1}{2}}}dl\right\}-\frac{k\beta^2}{N}l^2. \tag{40}$$

This is the one-dimensional version of Eq. (1). If l is held fixed, the average force exerted by the thermally agitated chain in jerking against the constraints will be

$$F(l)=-T\left(\frac{\partial S}{\partial l}\right)_T=2\beta^2kTl/N, \tag{29}$$

a result already used in Sec. III.

In computing the entropy of rubber, Wall[15,16] has apparently intended to follow a familiar pattern of statistical mechanics, that of replacing the total weight of all complexions of a system by an approximation, the weight of the complexions of the most probable distribution.[22] In the present case, this amounts to calculating, not the total number of configurations of the polymer network, but the number of configurations with the most probable distribution of chain extensions. For a large network, this should be a very good approximation.

Let C_f denote the number of chain configurations consistent with any distribution of chain extensions, specified by the distribution function $f(x)$, such that

$$N_i=Nf(x_i)\Delta x_i, \tag{41}$$

with

$$\int_{-\infty}^{+\infty}f(x)dx=1. \tag{42}$$

Using Eqs. (14), (10), and (41) and converting the sum into an integral, one finds

$$\ln C_f=N\ln K+N\int_{-\infty}^{+\infty}dxf(x)\ln\{p(x)/f(x)\}. \tag{43}$$

If one takes for $f(x)$ the most probable distribution function $p'(x)$, as given in Eq. (23), this formula yields

$$\ln C_{p'}=N\ln K-\beta^2l^2/N. \tag{44}$$

This $C_{p'}$ varies with l like dC of Eq. (36). The unimportant difference in the multiplying constant arises only in part from the fact that dC is the total number of configurations of the network with extension in the range dl, $C_{p'}$ only the number of configurations consistent with a single distribution of chain extensions; in part it comes from approximations used in arriving at the integral formula of Eq. (43)

On the other hand, if one takes for $f(x)$ Wall's distribution function, as given by Eq. (5), one obtains

$$\ln C_w=N\ln K+(N/2)-N\alpha^2+N\ln\alpha, \tag{45}$$

where [see Eq. (24)]

$$\alpha^2=2\beta^2l^2/CN. \tag{46}$$

This is the form given by Wall, except for the added constant $N\ln K$; multiplying it by k, one obtains the one-dimensional analog of Eq. (2). The fact that C_w does not vary with l in the same way that dC does, and that Wall's expression for the entropy contains a logarithmic term, is due to Wall's use of a distribution function that is very different from the most probable one. Even though C_f is stationary with respect to small variations of the distribution function about its most

[22] See for instance, J. E. Mayer and M. G. Mayer, *Statistical Mechanics* (John Wiley and Sons, Inc., New York, 1940) pp. 78–86.

probable form, gross errors in the assumed distribution function will lead to important errors in C and S.

It is instructive to consider what happens when one uses the symmetrized distribution function $p_s(x)$ of Eq. (34) in the same way. The corresponding number of configurations C_s is found, after some manipulation, to be

$$\ln C_s = N\ln K - \beta^2 l^2/N - \frac{N}{\pi^{\frac{1}{2}}}\int_{-\infty}^{+\infty} dz\exp(-z^2) \times \ln\left[\frac{1+\exp\{-(4\beta l/N)[z+(\beta l/N)]\}}{2}\right]. \quad (47)$$

The last term represents the error due to use of the symmetrized distribution function. It goes to zero as l goes to zero, but approaches $+N\ln 2$ as l becomes large.

It is not difficult to see why C_s is not an approximation to dC, but an overestimate by a large and variable factor. The distribution of extensions of the chains, with random definition of positive sense, is correctly given by Eq. (34). However, the chains of the network fall into two groups, according as one traverses them in the positive sense or in the negative sense in going from $x=0$ to $x=l$. The chains of the first group have predominantly positive extensions if $l>0$, their distribution of extensions being given by the first term on the right in Eq. (34); the chains of the second group have predominantly negative extensions, with distribution given by the second term. The chains of the two groups are thus not equivalent to each other. In applying Eq. (43), however, one treats them as equivalent, since one then counts every assignment of extensions to the different chains, subject only to the specified *over-all* distribution of extensions. One counts not only the configurations of the network in which one is interested, those with extension l, but an equal number of configurations with extension $-l$ [those for which the first and second groups of chains have distributions of extensions given by the second and first terms in Eq. (27), respectively], as well as other configurations with all intermediate extensions. When $l=0$, the two parts of the symmetrized distribution coincide and no error results. When l is very large, and there is in reality very small chance that chains of the first group would have a negative extension or those of the second group a positive extension, the error in assigning signs to the extensions at random approaches a factor of 2^N.

Wall and Flory,[1] following an argument of Flory,[23] propose to add another term to the entropy as computed by Wall. Since they do not wish to limit consideration to a particular network structure, they propose, as we understand it, to add the term

$$\Delta S = k\ln A, \quad (48)$$

where A is the number of ways in which a network of the given functionality can be formed from chains with the specific distribution of extensions. In the present case of a linear network, functionality 2, it is obvious that A does not depend on l at all.[24] Given any specified assignment of extensions to the N chains, consistent with the extension l of the network, one can arrange the chains end-to-end in exactly 1 way, if a definite ordering of the chains is specified, or in $N!$ ways, if the order is not specified. In either case ΔS is a constant, and does not change the dependence of entropy on l.

VI. DIFFICULTIES IN APPLYING THE DISTRIBUTION FUNCTION METHOD TO THE GENERAL NETWORK PROBLEM

In the preceding section we have discussed a simple problem where the general procedure of Wall and Flory yields the correct result, provided one replaces their assumed chain extension distributions by the correct one. The present section will deal with the difficulties involved in applying their procedure to more complicated networks.

Let us first consider a network of definite structure, with each chain numbered according to its position in the network. For simplicity, we shall assume that each chain has the same structure. Let the most probable distribution of chain extensions be specified by the numbers $N_0, N_1, \cdots$, where N_i is the number of chains having one end displaced with respect to the other by an amount $\mathbf{r}_i$ to within $d\mathbf{r}_i$. Let

$$p_i = Kp(\mathbf{r}_i)d\mathbf{r}_i \quad (49)$$

denote the number of configurations of a chain with such an end to end displacement. The number of configurations of the set of chains consistent with this distribution is again given by

$$C = \frac{N!}{N_0!N_1!N_2!\cdots} p_0^{N_0} p_1^{N_1} p_2^{N_2}\cdots. \quad (11)$$

In the case of a linear network this is also the number of configurations of the network consistent with this distribution, since every configuration of the set of chains corresponds to one possible configuration of the network; without appreciable error, one can take C as the number of configurations possible for the network. With a more general type of network this is very far from true. The specified connectivity of the network implies the existence of a great many closed paths in the network; certain chains must form closed "triangles," others closed "quadrangles," and so on. Some assignments of vector extensions to the chains will satisfy all these conditions and correspond to configurations of the network, but the vast majority of assignments will violate one or the other of the conditions and

[23] P. J. Flory, J. Chem. Phys. 18, 108 (1950).

[24] In Sec. VI we shall apply Flory's method of calculation to obtain this result. As discussed there, we do not believe Flory's calculations are correct for functionalities greater than 2.

will not correspond to any network configuration. To take C as the number of network configurations would thus be to overestimate this quantity very greatly. In principle, the error would be the same as that made in using the symmetrized distribution function in treating the linear network, as described in Sec. V; it would consist in treating as equivalent, chains that play nonequivalent roles in the network. As in that example, one must expect that such an enumeration of configurations would be in error by a factor depending on the constraints on the network, and that the computed entropy would include a spurious form-dependent term.

It is thus clear that Wall's procedure will not yield a correct value for the entropy of a particular network structure, even if one replaces his assumed distribution function by the correct one.

For comparison with Wall's formalism, we return to the result referred to in Sec. III, that one can compute the number of configurations of a network, to within a constant factor, by treating each chain as having a fixed extension equal to its actual time-average vector extension. The number of configurations possible for such a system of chains, with extensions that are not interchangeable, is not given by Eq. (11), but is proportional to

$$C'=\prod_i [p(\mathbf{r}_i)]^{N_i}. \tag{50}$$

Calculations on this basis have been indicated in reference 4. They lead to Eq. (1), without the logarithmic term in the entropy, and with a constant K determined in terms of the assumed distribution function $(\alpha_x\alpha_y\alpha_z)^{-1}F(x/\alpha_x,\ y/\alpha_y,\ z/\alpha_z)$ for the fixed chain extensions. Wall's calculation, made with a similar distribution function, yields the logarithmic term of Eq. (2) because of the presence of the factorials in Eq. (48). If one thinks of the chains as having fixed extensions with the given distribution, inclusion of the factorials is an error in counting configurations. If, on the other hand, one takes Wall's calculation to apply to a network of fixed structure but variable chain extensions, then the logarithmic term is the resultant of two errors: assumption of an inappropriate distribution for the instantaneous extensions, and the error in Eq. (48) as a means of counting network configurations.

Next we turn to the alternative procedure of Flory,[23] as used by Wall and Flory. This involves as an essential step the solution, in some form or other, of the following problem. Let a distribution of vector chain extensions be specified. We consider a particular assignment of configurations to the N chains, one of the C complexions of the specified distribution, and ask: In how many ways can these chains be assembled to form a network—any network—of functionality f, in the volume V occupied by the system? This number is the number A of Eq. (48), if one counts as distinct the $N!$ network configurations derivable from each other by interchange of the identical chains. Then, as we understand it, Wall and Flory would take as the entropy of the network

$$S=k\ln C+k\ln A, \tag{51}$$

computed for the most probable distribution of chain extensions in the stretched and swollen material.

In essence, Flory computes A as the product of two factors:

(1) A factor proportional to the number of ways in which the N independent chains can be dispersed through volume V. This factor can be taken simply as V^N, and contributes to a term $-kN\ln v_2$ in the entropy, v_2 being the volume fraction of high polymer in the swollen material.[25]

(2) A factor giving the probability that, when the chains are arranged at random, the chain ends will all fall in sets of f within volumes $\Delta\tau$ corresponding to the network junctions.

Application of this method to the linear network with functionality 2 is very simple. The first factor is l^N. As to the second, we note that there are $N!$ ways of pairing off the $2N$ chain ends, corresponding to $N!$ possible sequences of the chains in the network. We consider one such sequence. When the ith chain in this sequence has been placed in position, and the $(i+1)$st is added at random, there is a probability $\Delta\tau/l$ that its end will fall in length $\Delta\tau$ about the appropriate end of the ith chain, as required to form the network. The probability that all N pairs of ends will fall as required is then $(\Delta\tau/l)^N$. The second factor in A is thus $N!\,(\Delta\tau/l)^N$, and A itself is independent of l, as noted in Sec. V.

In the case of networks of functionality $f>2$, Flory computes the second factor in A (which leads to his S_1 or S_3, depending on the assumed volume) as the product of a factor $(2N\Delta\tau/V)^{f-1}$, representing the probability that some $f-1$ of the $2N$ ends will fall within volume $\Delta\tau$ about an end chosen at random, a factor $((2N-f)\Delta\tau/V)^{f-1}$ representing the probability that $f-1$ other ends will fall within volume $\Delta\tau$ about another chain end chosen at random, and so on. He thus finds, in essence, that the second factor in A includes a factor $V^{-2N(f-1)/f}$, that A itself varies like $V^{-N(f-2)/f}$, and that a term

$$\Delta S=-N\frac{f-2}{f}k\ln(\alpha_x\alpha_y\alpha_z) \tag{52}$$

should be added to the network entropy computed by Wall.[26] We do not believe that this calculation is a

[25] Our N replaces ν of Flory's notation. There is another term in the entropy of swelling $(-kn\ln(1-v_2)$, where n is the number of solvent molecules) that is not included by Wall and Flory or in the present discussion.

[26] There appears to be some confusion in regard to this term in the paper of Wall and Flory. They refer to reference 23 in justifying introduction of the additional term $-\frac{1}{2}Nk\ln(\alpha_x\alpha_y\alpha_z)$ in the entropy. This would correspond to assuming $f=4$, yet they describe the term as arising from the "requirement that the selected units meet in pairs." Since there are N chains, there will be $2N$

valid one. Implicitly, it assumes that formation of each junction replaces f ends that can move through volume V independently by one junction that can move through volume V; hence the factor V^{1-f}. Actually, this cannot be so. In building up a network of functionality $f>2$ by successively forming $2N/f$ functions from the ends of N chains, one must sooner or later form junctions involving ends of chains that already have their other ends involved in other junctions of a coherent network. These ends cannot move independently through volume V before the junction is formed, and their incorporation into this junction will not introduce a factor $1/V$ into the number of possible configurations of the system. In brief, Flory's line of argument, if carried out more carefully, would indicate that a factor $1/V$ occurs in the second factor of A for each element of the system that ceases to be free to move through volume V, independently of all others, when the network is formed. Before the network is formed there are N such elements, the chains; after a fully coherent network is formed there are none. Therefore the second factor involves the factor V^{-N}, which exactly cancels out the V dependence of the first factor.

So far as this argument is concerned, one might think that A would be independent of V. Actually, a dependence on V can enter in a much more subtle way: as V changes, the appropriate distribution of chain extensions varies, and this in turn changes the number of ways of forming junctions from chain ends that *cannot* move independently in the volume V. This is an entirely different problem from that considered by Flory, and we do not see how to solve it, except by unrealistic assumptions concerning the change in the distribution of chain extensions with changing V.

It, therefore, appears to us that the procedure of Wall and Flory is impracticable, quite aside from the problem of determining an appropriate distribution of chain extensions. At any rate, we do not believe that Flory's calculations provide any justification for the logarithmic terms in Eqs. (2) or (3).

VII. PERMUTATION ENTROPY AND INTERVAL DILATION ENTROPY

Finally, we wish to comment briefly on some calculations of Kuhn and his collaborators. Kuhn and Grün[27] and Kuhn and Kuhn[28] have described calculations fundamentally similar to those of Wall and Flory. They assume that in unstretched rubber the distribution of chain extensions is the same as that for free chains, that the distribution of chain extensions changes in the way assumed by Wall and Flory, and that Eq. (48) is applicable in calculating the entropy associated with the resulting distribution. Their calculation is more elaborate than that of Wall and Flory, as they treat the distributions of orientations and elongations of the chains independently, and define corresponding separate terms in the entropy. The logarithmic term is not in evidence in their final result for the entropy, since they have restricted attention to the case of $\alpha_x\alpha_y\alpha_z=1$.

Kuhn and Kuhn have proposed the name "permutation entropy" for the term

$$S_{\text{perm}}=k\ln\left(\frac{N!}{\prod_i N_i!}\right)\cong k[N\ln N-\sum_i N_i\ln N_i], \quad (53)$$

which enters their calculation. It should be noted that the value of this quantity depends on the size of the interval used in defining the distribution of extensions, and is thus not determined uniquely.

More recently, Kuhn, Pasternak, and Kuhn[29] have reconsidered the problem, in connection with a treatment of the swelling of rubber. They recognize that presence of the permutation factor is not appropriate in a calculation of the number of configurations possible for a network of chains, though it is needed in a discussion, by their method, of a system of independent chains. However, by considering a one-dimensional problem they arrive at the striking (and false) conclusion that it makes no difference whether the permutation factor is included or not. Thereafter, for reasons of convenience, they include the permutation factor and obtain a final result having the form of Eq. (2).

Their conclusion that the permutation factor does not change the result arises in the following way. In making the calculation that includes the permutation factor, they employ Eq. (14). This gives a result independent of the size of the intervals Δx_i used in defining the distribution, since p_i and N_i both change proportionally to Δx_i, and the number of terms in the sum varies inversely with the magnitude of Δx_i. In making the calculation without the permutation factor, however, they write, in effect

$$C=\prod_i p_i^{N_i}=\prod_i [Kp(x_i)\Delta x_i]^{N_i} \quad (54)$$

or

$$\ln C=N\ln K+\sum_i N_i\ln p(x_i)+\sum_i N_i\ln(\Delta x_i). \quad (55)$$

These formulas, unlike Eq. (50), give results that do depend on the choice of the Δx_i. Furthermore, they note that when the distribution of chain extensions changes only by a scale factor proportional to α, then N_i chains, with extensions x_i to within Δx_i in the unstretched material, become N_i chains with extension αx_i to within $\alpha\Delta x_i$ in the stretched material. This observation leads them to take the ranges Δx_i in Eq. (55) to be proportional to α. Consequently, the logarithmic term

chain ends, and one would expect the requirement that these meet in pairs to introduce a term $-Nk\ln(\alpha_x\alpha_y\alpha_z)$ in the entropy; Wall and Flory's formula would then be identical with our own.

[27] W. Kuhn and F. Grün, J. Polymer Sci. **1**, 183 (1946).

[28] W. Kuhn and H. Kuhn, Helv. Chim. Acta **29**, 1615 (1946).

[29] Kuhn, Pasternak, and Kuhn, Helv. Chim. Acta **30**, 1705 (1947).

in the energy that arises from the permutation factor when Eqs. (11) or (14) are employed arises from the last term of Eq. (55) when they omit the permutation factor. Because of the origin of this term in the second calculation, they propose to call it the "interval-dilation entropy."

It must be emphasized that the calculation of Kuhn, Pasternak, and Kuhn is a purely formal one, depending on an arbitrary choice as to how Δx_i is to vary with α. There is, however, a logical basis on which to make this choice. If p_i is to denote the relative number of configurations possible to a chain in a network and is to be expressed in terms of the number of configurations per unit range in extension $Kp(x_i)$, and a range of extensions Δx_i, then Δx_i ought to be chosen to vary proportionally to the range of extensions actually available to the chain.[30] We have noted in Sec. III, in connection with Eq. (30), that the distribution of extensions of every chain in a Gaussian network has a breadth independent of the form of the material, that is, of α_x, α_y, α_z. One ought, then, to choose Δx_i the same for all α; then the logarithmic term in the entropy, as computed by Kuhn, Pasternak, and Kuhn, will disappear, and their result will agree with our own. In other words, there is no interval-dilation entropy in Gaussian networks because the physically significant intervals, the ranges of extension available to the molecular chains, do not dilate when the material is stretched.

[30] In this calculation Δx_i performs a double function, as the range used in defining the N_i and as a range proportional to the range of extensions possible for an individual chain. It is the second of these roles that fixes the variation of Δx_i with α.

THE JOURNAL OF CHEMICAL PHYSICS VOLUME 21, NUMBER 6 JUNE, 1953

The Photochlorination of Methyl Chloroformate in the Gas Phase

J. H. Brandy* and D. J. Le Roy
Department of Chemistry, University of Toronto, Toronto, Canada

(Received February 4, 1953)

Under similar conditions of concentration and light absorption the rate of the gas phase reaction is almost the same as the rate in carbon tetrachloride solution, studied previously, although the mechanism is somewhat different. The gas-phase reaction is not inhibited by products and the bimolecular chain termination step consists in the formation of chlorine, rather than monochloromethyl chloroformate. First-order removal of chlorine atoms becomes important at low light intensities.

The ratio of the rate constant for hydrogen chloride formation to that for first-order chain termination is the same in the gas phase as in carbon tetrachloride solution within the accuracy of the measurements.

IN a previous communication from this laboratory[1] it was shown that at room temperature and in carbon tetrachloride solution the photochlorination of methyl chloroformate ($CH_3OCOCl=RH_3$) to form monochloromethyl chloroformate ($CH_2ClOCOCl=RH_2Cl$) takes place by the following mechanism:

$$Cl_2+h\nu=2Cl \quad (1)$$

$$Cl+RH_3=RH_2\cdot+HCl \quad (2)$$

$$RH_2\cdot+Cl_2=RH_2Cl+Cl \quad (3)$$

$$RH_2Cl+Cl=RH_2\cdot+Cl_2 \quad (4)$$

$$RH_2\cdot+Cl=RH_2Cl \quad (5)$$

$$Cl=\tfrac{1}{2}Cl_2. \quad (6)$$

We have now shown that the reaction takes a somewhat different course in the gas phase, although the products are the same.

EXPERIMENTAL

Reagents

Commercial tank chlorine (Canadian Industries, Limited) was dried over phosphorus pentoxide, degassed by twenty or more trap-to-trap distillations, and stored over liquid air.

Hydrogen chloride (Matheson Company) was subjected to the same treatment as the chlorine.

The methyl chloroformate (RH_3), as obtained from Distillation Products Industries, contained rather large amounts of dimethyl carbonate. This impurity was removed by distillation through an eleven-plate column. The purified $RH_3(n_D^{20}=1.3870)$ was subjected to at least twenty four trap-to-trap distillations with pumping and stored over liquid air.

Monochloromethyl chloroformate (RH_2Cl) and dichloromethyl chloroformate ($RHCl_2$) were prepared by the photochlorination of methyl chloroformate in carbon tetrachloride solution followed by fractional distillation. The boiling points and refractive indices of the products were 108.0°C at 762 mm, $n_D^{20}=1.4292$, and 111.5°C at 758 mm, $n_D^{20}=1.4419$, respectively. Trichloromethyl chloroformate (RCl_3), obtained from the

* Present address, Defence Research Northern Laboratory, Fort Churchill, Manitoba.

[1] Batke, Dorfman, and Le Roy, J. Chem. Phys. 17, 566 (1949).

Defence Research Chemical Laboratories, Ottawa, was distilled under reduced pressure and the center cut taken; this had a boiling point of 49.5°C at 47.4 mm.

Infrared Analyses

In order to ascertain the experimental conditions under which the rate of formation of RH_2Cl could be studied without interference by further chlorination to $RHCl_2$ and RCl_3, a number of experiments were carried out in which the products were subjected to infrared analyses after removing chlorine and hydrogen chloride by low temperature distillation.[2]

The most suitable bands for RH_3, RH_2Cl, $RHCl_2$, and RCl_3 were found to be at 14.37, 7.43, 13.58, and 10.82 microns, respectively; the spectra were taken in the gas phase.

The analyses showed excellent agreement between the amount of RH_3 consumed and the amounts of RH_2Cl and $RHCl_2$ formed; no RCl_3 was formed in any of these experiments. It was also found that as much as half the RH_3 could be consumed before an appreciable amount of $RHCl_2$ was formed; it was therefore possible to study the formation of RH_2Cl without interference by secondary reactions.

The Reaction System

The photochemical experiments were carried out in a cylindrical Pyrex vessel 24.62 cm long and 3.42 cm in diameter (internal dimensions), with plane Pyrex windows, and provided with two small side arms, one connected directly to the cell, the other connected to the cell through a vacuum stopcock. The cell proper, consisting of the cylindrical tube and the directly connected side arm had a volume of 229 cm^3, 225 cm^3 of which could be filled with the light beam.

In filling the cell the RH_3 was added first and its pressure measured accurately on a modified Pearson gauge connected to the manifold. The RH_3 would then be condensed into the isolated side arm while the chlorine was added to the cell. After measuring its transmission, the chlorine and the RH_3 would be frozen into the directly connected side arm and then allowed to evaporate. The isolated side arm was also used in the interrupted runs to hold the cell contents during the addition of further measured quantities of reagents.

Apiezon *N* grease was used on all stopcocks.

The Optical System

Since there is no pressure change during the reaction its progress was followed by measuring the increase in light transmission as chlorine was used up; at the wavelength used chlorine was the only absorber.

The light source was a General Electric AH-4 lamp, carefully shielded from drafts and operated off a Sorensen electronic voltage regulator. The whole of the optical system, with the exception of the lamp and two diaphragms, was mounted on an optical bench inside a large black box. The light beam entered the box through a shutter. A 2.0-cm path of 2.5 percent aqueous cupric chloride solution was used to remove the longer wavelengths and together with a No. 5113 and a No. 3389 Corning filter of standard thickness, served to eliminate all wavelengths except those in the 4358A region.

The monochromatic beam was split into two beams by a Pyrex plate. The reflected beam reached a type 935 photocell after passing through a neutral density wedge. The transmitted light entered the reaction cell as a parallel beam filling its entire cross section. The light transmitted by the reaction cell could be focused either on a second type 935 photocell or on the thermopile.

In studying the effect of light intensity on the rate it was necessary to change this quantity by a large factor. This was done without changing the amount of light reaching the photocells by moving one or more filters from a position immediately behind to a position immediately in front of the reaction cell. The cell contents were shielded from light during this operation by closing shutters connected directly to the cell.

The circuit used to measure the fraction of the light transmitted by the chlorine was essentially the same as that used by Klotz and Dole.[3]

The percent transmission readings were converted to chlorine concentrations by means of the equation,

$$\log_{10} I_0/I = K(Cl_2)d, \qquad (a)$$

in which (Cl_2) is the concentration of chlorine in moles cm^{-3}, d is the length of the optical path within the cell in cm, and K is the extinction coefficient for the light used. The value of K was determined by measuring the transmission for known pressures of chlorine in the cell. $\text{Log}_{10} I_0/I$ was found to be directly proportional to chlorine concentration over the range 7 to 70-mm pressure; the value of K was found to be $(1.60 \pm 0.02) \times 10^3$, in good agreement with that found by von Halban and Seidentopf,[4] for 4358A. This suggests that the light was more nearly monochromatic than that used in our previous investigation[1] in which we found that K varied with chlorine concentration. It should be pointed out that the apparent variation of K with concentration in the previous work did not invalidate the results in as much as the values of chlorine concentration, from which the values of K were derived, were determined by chemical analysis.

The Thermopile

In order to determine quantum yields as well as numerical values of the rate constants it was necessary to know the actual value of the light intensity incident on the reactants, I_0 in Eq. (a). For this purpose a single junction compensated vacuum thermopile was con-

[2] D. J. Le Roy, Can. J. Research **B28**, 492 (1950).

[3] I. M. Klotz and M. Dole, Ind. Eng. Chem. Anal. Ed. **18**, 741 (1946).

[4] H. von Halban and K. Seidentopf, Z. physik. Chem. **103**, 84 (1922).

TABLE I.

Expt.	(Cl_2) $\times 10^7$	(RH_3) $\times 10^7$	Temp. °C	$\bar{I}_a$ $\times 10^{12}$	Variable changed	Ratio of rates	y	C[a] $\times 10^2$
1	40.9	14.4	24.9	12.70	$\bar{I}_a$ 10.28 – 1.49	3.64	0.67	2.32
2	24.7	14.2	24.5	8.44	$\bar{I}_a$ 5.48 – 0.794	4.04	0.72	2.25
3	24.4	14.1	25.1	8.15	$\bar{I}_a$ 5.72 – 0.830	4.00	0.72	2.00
4	12.2	12.6	27.2	4.59	$\bar{I}_a$ 2.84 – 0.373	4.90	0.78	2.60
5	11.3	12.6	27.2	0.56	$\bar{I}_a$ 0.465– 3.55	4.73	0.76	2.87
6	32.8	34.8	23.6	1.65	$\bar{I}_a$ 1.28 – 0.174	6.48	0.94	1.67
7	30.8	29.1	25.0	1.56	$\bar{I}_a$ 1.26 – 0.171	6.40	0.93	2.02
8	33.1	35.5	24.5	0.23	$\bar{I}_a$ 0.210– 3.20	6.80	0.96	2.00
9	24.8	14.8	25.1	8.22	b	1.00	—	2.00
10	32.2	14.4	24.5	1.63	RH_3 10.62 –25.18	2.72	1.17	2.50
11	41.1	15.1	25.0	12.75	RH_3 4.97 –17.29	3.45	0.98	2.98
12	11.9	6.2	25.2	4.53	RH_3 4.65 –19.60	5.20	1.13	1.58
13	40.2	14.4	23.8	12.41	RH_3 5.39 –22.22	4.34	1.01	2.64
14	33.7	9.4	24.6	1.69	RH_3 6.40 –35.02	5.45	1.00	2.07
15	32.5	6.2	23.5	1.64	RH_3 4.81 –32.66	6.02	0.94	1.23
16	24.5	9.2	25.0	8.15	RH_3 4.46 –36.96	7.58	0.96	2.35
								Mean 2.19

[a] Appreciable amounts of $RHCl_2$ were formed toward the end of experiments 1, 2, 3, 11, and 13; the values of C for these experiments were calculated from the first portions of the rate curves.
[b] The total pressure was increased by a factor of 7.8 by the addition of HCl.

structed. It was of the type described by Beckman and Dickenson[5] with aluminium receivers, 2.5 mm×3 mm ×0.0005 in. The circuit used to measure the thermopile voltage has been described by Burns and Dainton.[6] The output ranged from 0.2 to 10 microvolt; the corresponding precision varied from 2 percent to 0.4 percent.

The thermopile was calibrated against Bureau of Standards standard lamps. Its sensitivity was 0.228 microvolt per microwatt, corresponding to an output of 1 microvolt for a light intensity of 1.045×10^{-10} einstein cm^{-2} min^{-1} of 4358A radiation passing through the front window of the reaction cell.

RESULTS

In the order to determine the kinetics of the reaction, the influence of the following factors was taken into account: (Cl_2), (RH_3), (RH_2Cl), (HCl), in which the brackets denote concentrations in moles cm^{-3}, and $\bar{I}_a$ the average rate of light absorption in einsteins cm^{-3} min^{-1}. In none of the experiments was the light absorption greater than 35 percent, and under these conditions it can be shown that the quantity $\bar{I}_a$, defined by the relation,

$$\bar{I}_a=(I_0/d)\{1-10^{-K(Cl_2)d}\}, \qquad (b)$$

may be substituted for the *local* rate of light absorption I_a.

It was found that the rate of the reaction depended on a power of $\bar{I}_a$ between 0.5 and unity. Furthermore, the quantum yields were so large (10^4 to 10^5) that regardless of the care taken some variation in rates was found for experiments performed under supposedly identical conditions. These variations, presumably the result of variations in the amounts of residual impurities, were sufficiently large that serious errors would arise, for example, if the dependence of the rate on light intensity were determined from the results of two experiments using different light intensities but otherwise apparently identical conditions. This difficulty was largely overcome by applying the technique of the "interrupted run"[7] in which the rate of consumption of chlorine was determined immediately before and immediately after changing the light intensity by a known factor. The same procedure was used to study the effect of the other variables; after establishing a rate the experiment would be interrupted and additional chlorine, RH_3, RH_2Cl, or HCl would be added; the new rate would then be established after resuming the experiment.

In carbon tetrachloride solution the reaction is strongly inhibited by the RH_2Cl formed.[1] This was indicated by the rapid change in curvature of the (Cl_2) *vs* time curves and confirmed by experiments in which RH_2Cl was added initially. In contrast, no inhibition by RH_2Cl (or HCl) was found in the gas-phase reaction. It was also found that the concentration of chlorine had no influence on the rate except in so far as it affected the value of $\bar{I}_a$.

In Table I are given the results of the experiments designed to show the effect of $\bar{I}_a$ and (RH_3) on the rate. The initial concentrations of chlorine and RH_3 in columns 2 and 3 are given to only one decimal place; in making the calculations two decimal places were used because the changes in concentration had to be known and were known with that accuracy. The initial value of $\bar{I}_a$ is given in column 5. Under the heading "Variable changed" are given the variable changed together with its magnitude immediately before and immediately after the time of interruption. Under "Ratio of rates" is given the ratio of the larger to the smaller slope of the (Cl_2) *vs* time curve at the time of interruption. The value

[5] A. O. Beckman and R. G. Dickenson, J. Am. Chem. Soc. **52**, 124 (1930).
[6] W. G. Burns and F. S. Dainton, Trans. Faraday Soc. **48**, 39 (1952).

of y in the second to last column is defined by the expression,

$$\frac{(-d(\mathrm{Cl_2})/dt)'}{(-d(\mathrm{Cl_2})/dt)''}=(V'/V'')^{y}, \qquad (c)$$

in which V' and V'' are the values of the variable changed immediately before and immediately after the time of interruption. In the last column are given the values of the leading constant in the rate equation discussed below.

The results of the first eight experiments show that the rate depends on a power of the light intensity lying between 0.5 and unity, and that this power approaches unity at low values of $\bar{I}_a$. The results of experiment 9 show that the rate is unchanged when the total pressure is increased by a factor of 7.8 by the addition of HCl. The range of variation of (RH_3) was limited by the vapor pressure of the material. However, it seems logical to conclude from the data of experiments 10 to 16 that the rate is directly proportional to the concentration of RH_3. In one experiment, not reported in the table, it was shown that no change in chlorine concentration occurred when the reagents were left in the dark for five hours.

DISCUSSION

For the reasons discussed previously[1] the following reactions were assumed to occur:

$$\mathrm{Cl_2}+h\nu=2\mathrm{Cl} \qquad (1)$$

$$\mathrm{Cl}+\mathrm{RH_3}=\mathrm{RH_2}\cdot+\mathrm{HCl} \qquad (2)$$

$$\mathrm{RH_2}\cdot+\mathrm{Cl_2}=\mathrm{RH_2Cl}+\mathrm{Cl}. \qquad (3)$$

In addition, the following chain termination steps were considered:†

$$\mathrm{RH_2}\cdot+\mathrm{Cl}=\mathrm{RH_2Cl} \qquad (5)$$

$$2\mathrm{RH_2}\cdot=(\mathrm{RH_2})_2 \qquad (5a)$$

$$2\mathrm{Cl}=\mathrm{Cl_2} \qquad (5b)$$

$$\mathrm{Cl}=\tfrac{1}{2}\mathrm{Cl_2} \qquad (6)$$

$$\mathrm{RH_2}\cdot=\tfrac{1}{2}(\mathrm{RH_2})_2. \qquad (6a)$$

From the observed dependence of the rate on $\bar{I}_a$, it is evident that at least one first-order and one second-order process are involved in chain termination. However, a number of possible combinations are readily eliminated. For example, chain termination by (5a) and (6a) would cause the rate to be independent of (RH_3). The pairs (5a)+(6), (5)+(6a), and (5b)+(6a) can also be eliminated since they yield rate expressions in which the rate is not proportional to (RH_3) as found by experiment. It is somewhat more difficult to decide between the two remaining pairs, (5)+(6) and (5b)+(6).

† The reactions are numbered in the same way as in reference 1.

Reactions (1), (2), (3), (5), and (6) yield the rate equation

$$-d(\mathrm{Cl_2})/dt=A(\mathrm{Cl_2})\{[1+B\bar{I}_a(\mathrm{RH_3})/(\mathrm{Cl_2})]^{\frac{1}{2}}-1\}, \qquad (d)$$

while reactions (1), (2), (3), (5b), and (6) give

$$-d(\mathrm{Cl_2})/dt=\mathrm{C}(\mathrm{RH_3})\{[1+D\bar{I}_a]^{\frac{1}{2}}-1\}, \qquad (e)$$

in which $A=(k_3k_6)/(4k_5)$, $B=(16k_2k_5)/(k_3k_6^2)$, $C=(k_2k_6)/(4k_{5b})$, and $D=(16k_{5b})/(k_6^2)$. At low values of the light intensity, such that the light dependence of the rate tends toward first power, Eqs. (d) and (e) will approach the indistinguishable values

$$-d(\mathrm{Cl_2})/dt=AB(\mathrm{RH_3})\bar{I}_a/2 \qquad (f)$$

and

$$-d(\mathrm{Cl_2})/dt=CD(\mathrm{RH_3})\bar{I}_a/2. \qquad (g)$$

From the data of Table I it is seen that Eqs. (f) and (g) are in agreement with experiment under conditions of low light absorption. However, for large values of $\bar{I}_a$, such that the dependence of the rate on this quantity would be to the power 0.5, Eqs. (d) and (e) would, respectively, reduce to the expressions

$$-d(\mathrm{Cl_2})/dt=A\{B\bar{I}_a(\mathrm{RH_3})(\mathrm{Cl_2})\}^{\frac{1}{2}} \qquad (h)$$

and

$$-d(\mathrm{Cl_2})/dt=\mathrm{CD}^{\frac{1}{2}}\bar{I}_a^{\frac{1}{2}}(\mathrm{RH_3}). \qquad (i)$$

For Table I, it is seen that for the large values of $\bar{I}_a$ used in experiments 11 and 13 the rate is proportional to the first power of (RH_3), although, as shown by the results of experiments 1, 2, and 3, the $\bar{I}_a$ exponent is approaching 0.5 under these conditions. Actually, the effective value of the exponent of $\bar{I}_a$ when the average rate of light absorption is of the order of 10×10^{-12} einstein $\mathrm{cm^{-3}\ min^{-1}}$ will be closer to 0.5 than the value indicated in the "Power" column of Table I.

The first step in verifying the mechanism consisting of reactions (1), (2), (3), (5b), and (6) involved the determination of the quantity D of Eq. (e). This was done by comparing the slopes of the (Cl_2) *vs* time curves at the time of interruption of an experiment in which the variable changed was $\bar{I}_a$. For this case we have

$$\frac{(-d(\mathrm{Cl_2})/dt)'}{(-d(\mathrm{Cl_2})/dt)''}=\frac{C(\mathrm{RH_3})\{[1+D\bar{I}_a']^{\frac{1}{2}}-1\}}{C(\mathrm{RH_3})\{[1+D\bar{I}_a'']^{\frac{1}{2}}-1\}}=\frac{[1+D\bar{I}_a']^{\frac{1}{2}}-1}{[1+D\bar{I}_a'']^{\frac{1}{2}}-1}. \qquad (j)$$

The data of experiments 1 to 5 were used to obtain values of D satisfying this equation; the value so obtained was $(2.0\pm0.1)\times10^{12}$ $\mathrm{cm^3\ mole^{-1}\ min}$. The data of experiments 6, 7, and 8 were not used for this purpose, because it is readily seen that as the effective power of $\bar{I}_a$ approaches unity the ratio of the rates is not very sensitive to the value of D.

Having obtained the value of D, the experimental data for each experiment were interpreted in terms of

Eq. (e) by writing it in the form

$$\frac{-d(\mathrm{Cl_2})}{(\mathrm{RH_3})\{[1+D\bar{I}_a]^{\frac{1}{2}}-1\}}=-\varphi d(\mathrm{Cl_2})=Cdt. \qquad (k)$$

The quantity φ may be considered to be a function of (Cl_2), in view of Eq. (b) and the relation

$$(\mathrm{RH_3})_t=(\mathrm{RH_3})_0+\Delta(\mathrm{Cl_2}). \qquad (l)$$

It is clear that on the basis of this mechanism $-\int\varphi d(Cl_2)$ between the limits $t=0$ and $t=t$ should be a linear function of t for all values of (RH_3), (Cl_2), and $\bar{I}_a$ and that the slope should be equal to C. Plots of $-\int\varphi d(Cl_2)$ *vs* t gave satisfactory straight lines for all of the experiments, including those in which the interrupted run technique was used. The values of C obtained are given in the last column of Table I.

That colinearity is a sensitive criterion of mechanism was shown by treating the data of experiment 4 according to Eq. (d). A value of B was obtained by following the procedure analogous to that used in evaluating D. This value of B was then used in plotting the data of experiment 16 in the form $-\int\psi d(Cl_2)$ *vs* t in which ψ is the function analogous to φ but based on Eq. (d). The two portions of the plot were not colinear and, in fact, the slopes differed by a factor of approximately 2.4. We are confident, therefore, that the mechanism for the photochlorination of methyl chloroformate to monochloromethyl chloroformate in the gas phase is adequately explained in terms of reactions (1), (2), (3), (5a), and (6).

The rather large value of the mean deviation from the mean of the values of C given in Table I we attribute to the fact that the temperature varied somewhat from one experiment to another, as shown in the Table, and to the almost inevitable variation in residual impurities in the reagents which would have a marked effect on quantum yields as large as those found in the present work.

COMPARISON OF LIQUID- AND GAS-PHASE REACTIONS

The essential differences between the reaction in carbon tetrachloride solution[1] and the reaction in the gas phase are: (a) inhibition by RH_2Cl in the liquid phase due to reaction (4); (b) bimolecular chain termination by (5) in the liquid phase, by (5b) in the gas phase. The first-order chain termination step (6) is formally the same in both cases, although the detailed mechanisms might possibly be different.

In view of the fact that (4) is the reverse of (3), it is not unreasonable to expect that the former would be more likely to occur within the confines of a solvent cage than in the gas phase.

To facilitate comparison of the two mechanisms it is useful to consider the *initial* rate of the liquid phase reaction under the condition that the light absorption is of the order of 50 percent or less. In this case the *observed* rate is derived from the *local* rate by substituting $\bar{I}_a$ for I_a, and the term involving k_4 is eliminated from the rate equation. With these restrictions on the experimental conditions the rate equation for the liquid-phase reaction (Eq. vi, reference 1) becomes identical with Eq. (d).

In our previous investigation[1] we obtained values of the quantities $((k_2k_3/k_5)^{\frac{1}{2}})_L$ and $((k_6/2)k_3^{\frac{1}{2}}/(k_2k_5)^{\frac{1}{2}})_L$ at 25°C.‡ On the basis of these values, and for the conditions specified, the rate of the reaction in carbon tetrachloride solution may be written

$$R_L=(-d(\mathrm{Cl_2})/dt)_L$$
$$=A(\mathrm{Cl_2})\{[1+B\bar{I}_a(\mathrm{RH_3})/(\mathrm{Cl_2})]^{\frac{1}{2}}-1\},$$

in which

$$A=(k_3k_6/(4k_5))_L=6.5\times10^{-3}\ \mathrm{min^{-1}},$$
$$B=(16k_2k_5/(k_3k_6^2))_L=7.41\times10^{12}\ \mathrm{cm^3\ mole^{-1}\ min.}$$

For the gas-phase reaction,

$$R_G=(-d(\mathrm{Cl_2})/dt)_G=C(\mathrm{RH_3})\{[1+D\bar{I}_a]^{\frac{1}{2}}-1\},$$

in which

$$C=(k_2k_6/(4k_{5b}))_G=2.19\times10^{-2}\ \mathrm{min^{-1}},$$
$$D=(16k_{5b}/k_6^2)_G=2.0\times10^{12}\ \mathrm{cm^3\ mole^{-1}\ min.}$$

For large values of $\bar{I}_a$, $(RH_3)_L=(Cl_2)_L=(RH_3)_G$, and $(\bar{I}_a)_L=(\bar{I}_a)_G$, the rates will be of the same order of magnitude, *viz.*,

$$R_L=AB^{\frac{1}{2}}\bar{I}_a^{\frac{1}{2}}(\mathrm{RH_3})^{\frac{1}{2}}(\mathrm{Cl_2})^{\frac{1}{2}},$$

in which

$$AB^{\frac{1}{2}}=((k_2k_3/k_5)^{\frac{1}{2}})_L=1.77\times10^4\ (\mathrm{cm^3\ mole^{-1}\ min^{-1}})^{\frac{1}{2}};$$
$$R_G=CD^{\frac{1}{2}}\bar{I}_a^{\frac{1}{2}}(\mathrm{RH_3}),$$

in which

$$CD^{\frac{1}{2}}=(k_2/k_{5b}^{\frac{1}{2}})_G=3.10\times10^4\ (\mathrm{cm^3\ mole^{-1}\ min^{-1}})^{\frac{1}{2}}.$$

For small values of $\bar{I}_a$ the rates are the same within the accuracy of the measurements, *viz.*,

$$R_L=2(k_2/k_6)_L(\mathrm{RH_3})\bar{I}_a,$$
$$R_G=2(k_2/k_6)_G(\mathrm{RH_3})\bar{I}_a,$$

in which $(k_2/k_6)_L=1.20\times10^{10}\ \mathrm{cm^3\ mole^{-1}}$, and $(k_2/k_6)_G=1.10\times10^{10}\ \mathrm{cm^3\ mole^{-1}}$.

The authors are indebted to the Defence Research Board of Canada for supporting this research and for granting a scholarship to one of us (J.H.B.).

‡ The subscripts L and G will be used to indicate liquid- and gas-phase values, respectively.

Diffuse Double Layer Theory for Electrolytes of Unsymmetrical Valence Types

DAVID C. GRAHAME
Department of Chemistry, Amherst College, Amherst, Massachusetts
(Received January 23, 1953)

Equations are derived for the variation of potential with distance and for the components of charge and capacity in the diffuse double layer at a plane interface for electrolytes of the 1:2 and 2:1 valence types. Some additional relations are also deduced for other valence types.

THE theory of the diffuse double layer at a plane interface has not yet been worked out in detail for electrolytes of unsymmetrical valence type. It will now be shown how the theory can be extended to include electrolytes of these types, and particularly of the 1:2 and 2:1 types. As far as possible the choice of symbols will be the same as that already employed in a previous paper[1] discussing the corresponding problem for symmetrical electrolytes.

The basic equation, valid for electrolytes of any valence type, is given in reference 1, page 474, as follows:

$$\eta^d=\pm\left(\frac{DD_0kT}{2\pi}\sum n_{0i}[\exp(-z_i\epsilon\psi^0/kT)-1]\right)^{\frac{1}{2}}, \quad (1)$$

where the symbols have the following meanings. ψ^0 is the potential relative to that of the interior of the solution of a plane parallel to the interface and not closer to the interface than the electrical centers of all ionic types present at their respective distances of closest approach. This plane of closest approach has been called[1] the outer Helmholtz plane. η^d is the charge density in the solution (charge per unit area of interface) measured from the plane to which the potential ψ^0 refers. D is the dielectric constant of the solvent. D_0 is the "diabattivity" of free space, equal to $4\pi\kappa_0$, where κ_0 is the permittivity of free space. D_0 has the value 1.1128×10^{-12} coulomb-volt^{-1}-cm^{-1}. k is the Boltzmann constant. ϵ is the absolute value of the electronic charge. z_i is the valence (including sign) of the ith ionic type. n_{0i} is the number of ions of type i per cubic centimeter of solution measured at a place remote from the interface.

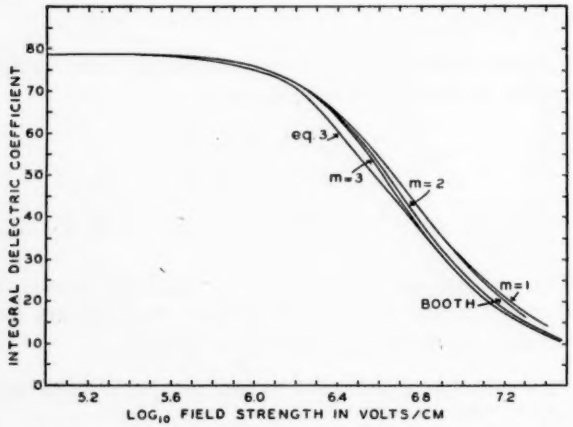

FIG. 1. Integral dielectric coefficient of water at 25°C as a function of field strength.

The summation extends over all types of ions in the solution. In the derivation of Eq. (1) it is assumed that the dielectric constant of the solvent retains its bulk value even within the diffuse double layer, up to the outer Helmholtz plane, though not necessarily beyond. Although this assumption cannot be correct, it was shown by the author in a previous work[2] that this fact does not render the theory seriously in error when the theory is used for the calculation of quantities which have a real physical meaning, such as η^d. In arriving at this conclusion the author assumed that the differential dielectric coefficient D of water could be represented as a function of the field strength E by a relation of the form

$$D=\frac{a}{[1+(b/m)E^2]^m}+3, \quad (2)$$

where b is a parameter determined by experiment ($=1.2\times10^{-13}$ cm^2/volt^2). m is a parameter of unknown magnitude and has to do with the abruptness with which the differential dielectric coefficient falls off with increasing field strength in the region where it falls off most abruptly. a is $D-3$, where D is the ordinary dielectric constant.

A decision as to the magnitude of m could not at the time be given unambiguously, although arguments were presented which showed that in all probability it did not exceed the value $m=2$. Now an independent calculation of the integral dielectric coefficient I has been given by Booth[3] [his equation (3.15)] who finds

$$I=n^2+\frac{28N_0\pi(n^2+2)\mu_v}{3\sqrt{73E}}L\left[\frac{\sqrt{73E}\mu_v(n^2+2)}{6kT}\right], \quad (3)$$

where n is the optical refractive index, μ_v the dipole moment of the water molecule, N_0 the number of molecules per cubic centimeter, and $L(x)$ the Langevin function. E is the field strength as above. It is of interest to inquire whether any value of m will reproduce Booth's equation. Figure 1 shows I as a function of E according

[1] D. C. Grahame, Chem. Revs. 41, 441 (1947).

[2] D. C. Grahame, J. Chem. Phys. 18, 903 (1950).

[3] F. Booth, J. Chem. Phys. 19, 391 (1951).

TABLE I. Calculated charge q and differential and integral capacities, C^d and K^d, of the diffuse double layer for 2:1 ($BaCl_2$ type) electrolytes in aqueous solution at 25°C. Capacities are in mfd/cm²; q's are in μ coulomb/cm².

Concentration M		Potential of outer Helmholtz plane, ψ^d 0.0 v	0.01 v	0.02 v	0.04 v	0.06 v	0.08 v	0.10 v
0.5	K^d	279.9	266.1	259.9	265.3	291.0	(336.5)	(404.8)
	C^d	279.9	256.4	254.0	297.2	396.9	(561.2)	(812.8)
	η^d	0	−2.66	−5.20	−10.61	−17.46	−(26.92)	−(40.48)
0.05	K^d	88.52	84.16	82.18	83.90	92.01	106.4	128.0
	C^d	88.52	81.07	80.32	93.98	125.5	177.5	257.0
	η^d	0	−0.842	−1.644	−3.36	−5.52	−8.51	−12.80
		0.12 v	0.14 v	0.16 v	0.18 v	0.20 v	0.22 v	0.24 v
0.005	K^d	50.22	63.77	82.50	108.3	(143.9)	(193.1)	(261.3)
	C^d	119.0	174.9	257.7	380.0	(560.6)	(827.3)	(1221)
	η^d	−6.03	−8.93	−13.20	−19.50	−(28.79)	−(42.49)	−(62.72)
0.0005	K^d	15.88	20.17	26.09	34.25	45.51	61.08	82.64
	C^d	37.62	55.30	81.48	120.2	177.3	261.6	386.1
	η^d	−1.906	−2.82	−4.17	−6.17	−9.10	−13.44	−19.83
		−0.01 v	−0.02 v	−0.04 v	−0.06 v	−0.08 v	−0.10 v	−0.12 v
0.5	K^d	303.2	338.8	463.4	(705.7)	(1165)	(2035)	(3696)
	C^d	332.1	424.5	807.3	(1691)	(3649)	(7931)	(17267)
	η^d	+3.032	+6.78	+18.54	(+42.3)	(+93.2)	(+203)	(+443)
0.05	K^d	95.89	107.1	146.8	223.2	(368.4)	(643.5)	(1169)
	C^d	105.0	134.2	255.3	534.8	(1154)	(2508)	(5460)
	η^d	+0.959	+2.143	+5.87	+13.39	(+29.47)	(+64.3)	(+140.2)

to Eq. (3) and also according to Eq. (2), using several possible values of m. The best fit is found for $m=3$, although Booth's equation (3.15) leads one to expect greater dielectric saturation at low field strengths than is predicted by any value of m. In a subsequent calculation Booth has derived an improved function for the integral dielectric coefficient, and this is presented by him only as a graph[4] (his Fig. 1). We have scaled his figure and present the result on our Fig. 1. The result shows practically complete agreement with the result obtained by setting $m=1$ in our Eq. (2). In order to obtain this agreement, the constant 3, which was chosen by us as the most likely value of the limiting value of the dielectric coefficient at high field strengths, must be changed to n^2 to agree with the choice preferred by Booth. As far as the calculations made in reference 2 are concerned, this change makes very little difference.

These considerations serve to reinforce our confidence in the conclusion reached earlier, namely, that dielectric saturation does not seriously affect the validity of calculations of observable quantities made with the assumption of a constant dielectric coefficient.

Returning to Eq. (1), let

$$A=+(DD_0kTn_0'/2\pi)^{\frac{1}{2}}, \quad (4)$$

where n_0' is the number of ions of the less abundant type per cubic centimeter of solution in the case of electrolytes of unsymmetrical valence type. Thus in a solution of $BaCl_2$, n_0' is the number of barium ions per cubic centimeter. When A is defined in this manner, the equations which involve it will be valid only for solutions containing only two ionic species in appreciable amounts.

For a 2:1 electrolyte ($BaCl_2$ type), Eq. (1) may be written

$$\eta^d=A(e^{-2y}+2e^y-3)^{\frac{1}{2}}=A(e^{-y}-1)(1+2e^y)^{\frac{1}{2}}, \quad (2:1)\ (5)$$

where

$$y=\epsilon\psi^0/kT \quad (5a)$$

and only the positive square root of $1+2e^y$ is to be taken.

The integral capacity of the diffuse double layer, K^d, is defined as $-\eta^d/\psi^0$ and is given by

$$K^d=-(A\epsilon/kTy)(e^{-y}-1)(1+2e^y)^{\frac{1}{2}}. \quad (2:1)\ (6)$$

The differential capacity of the diffuse double layer, C^d, is defined as $-d\eta^d/d\psi^0$, so that

$$C^d=-(A\epsilon/kT)[(e^y-e^{-2y})/(e^{-y}-1) \times(1+2e^y)^{\frac{1}{2}}]. \quad (2:1)\ (7)$$

As ψ^0 (and therefore y) approach zero, K^d and C^d approach the same limiting value, namely, $\sqrt{3}A\epsilon/kT$, which amounts to 395.9 $\sqrt{c_i}$ mfd/cm² in aqueous solution at 25°C where c_i is the molar concentration (moles per liter). The corresponding result[1] for a 1:1 electrolyte is 228.5 $\sqrt{c_i}$ mfd/cm² or 457.0 $\sqrt{c_i}$ for a 2:2 electrolyte. If the comparison is made, not at equimolar concentrations but at equinormal concentrations, the differences are less great, the results being for a

1:1 electrolyte, 228.5 $\sqrt{N}$ mfd/cm²,
1:2 or 2:1 electrolyte, 279.9 $\sqrt{N}$,
2:2 electrolyte, 323.2 $\sqrt{N}$.

Here N is the concentration in equivalents per liter.

[4] F. Booth, J. Chem. Phys. 19, 1327, 1615 (1951).

For convenience of reference, values of K^d and C^d and also of η^d are tabulated in Table I. It is particularly to be noted that these values of K^d and C^d are capacities of the *diffuse* double layer only and are almost invariably larger than the observed capacity of the whole double layer, even in the absence of specific adsorption, because the potential ψ^0 to which they are referred is almost inevitably smaller than the observed potential E.

In Table I numbers in parenthesis correspond to values of η^d higher than what is usually possible in practice ($\sim 25\mu$ coulomb/cm^2). The values are nevertheless listed because division by 10 gives the result for a solution 100 times more dilute.

An interesting and surprising feature of these results is that the minima in K^d and C^d do not occur at $\psi^0=0$. This is a feature which could be checked experimentally by a study of the differential capacity on mercury of very dilute solutions of 2:1 or 1:2 electrolytes.

By reversing the signs of ψ^0 and of η^d, Table I may be employed for electrolytes of valence type 1:2.

It is possible to find an explicit equation for ψ as a function of x as follows:

Gauss's law may be written for the case at hand,

$$d\psi/dx=4\pi\eta^d/DD_0, \tag{8}$$

where ψ is the potential of *any* plane parallel to the interface and no closer than the outer Helmholtz plane. η^d is now the corresponding charge density measured from *that* plane out into the solution. x is the distance of the plane from the interface.

Then from Eq. (5) (which is valid with this definition of η^d provided one writes ψ instead of ψ^0),

$$d\psi/dx=(4\pi A/DD_0)(e^{-y}-1)(1+2e^y)^{\frac{1}{2}}. \quad (2:1)\ (9)$$

From the definition of y [Eq. (5a)] now defined as $\epsilon\psi/kT$, however, because the superscript has been dropped from ψ^0,

$$dy/dx=(\epsilon/kT)(d\psi/dx)$$
$$=(4\pi A\epsilon/DD_0kT)(e^{-y}-1)(1+2e^y)^{\frac{1}{2}} \quad (2:1)\ (10)$$

and therefore

$$dx=dy/\kappa'(e^{-y}-1)(1+2e^y)^{\frac{1}{2}}, \quad (2:1)\ (11)$$

where

$$\kappa'=\left(\frac{8\pi\epsilon^2 n_0'}{DD_0kT}\right)^{\frac{1}{2}}=3.288\times10^7\sqrt{c_i}\ \text{cm}^{-1}\ \text{at}\ 25°\text{C}, \tag{12}$$

which is identical with the usual definition of κ except that it does not contain z, the valence of an ion.

Equation (11) can be integrated in terms of known functions, the result being[5]

$$\kappa'(x-x_\infty)=\kappa'x'=(1/\sqrt{3})\ln[\{(1+2e^y)^{\frac{1}{2}}+\sqrt{3}\}/\times\{(1+2e^y)^{\frac{1}{2}}-\sqrt{3}\}] \quad (2:1)\ (13)$$

for values of y greater than zero, and

$$\kappa'(x-x_\infty)=\kappa'\left(x'+\frac{2}{\sqrt{3}\kappa'}\tanh^{-1}\frac{1}{\sqrt{3}}\right)$$
$$=\frac{2}{\sqrt{3}}\tanh^{-1}\left(\frac{1+2e^y}{3}\right)^{\frac{1}{2}} \tag{13a}$$

for values of y less than zero. In both of these equations x_∞ is a constant of integration and x' is the distance of the plane in question from the plane which would have an infinite [positive Eq. (13) or negative Eq. (13a)] potential if Eq. (11) were valid at all values of x. Differences in x' are physically significant, although x' itself is not.

Equation (13) can be solved for ψ in terms of x', the result being

$$\psi=(kT/\epsilon)\ln[(p^2+4p+1)/(p-1)^2]$$
$$=(kT/\epsilon)\ln\left(1+\frac{6p}{(p-1)^2}\right), \quad (2:1)\ (14)$$

where

$$p=\exp(\sqrt{3}\kappa'x'). \tag{15}$$

When x' is large, $6p/(p-1)^2$ is small, making it possible to expand the logarithm, dropping terms after the first,

$$\psi_{\text{approx}}=(kT/\epsilon)[6p/(p-1)^2]\cong 6kT/\epsilon p$$
$$=(6kT/\epsilon)\exp(-\sqrt{3}\kappa'x'). \quad (2:1)\ (16)$$

This result shows that at sufficiently large values of x', ψ is an exponential function of x with a half-thickness of $(\ln 2)/\sqrt{3}\kappa'$ or $1.217\times10^{-8}/\sqrt{c_i}$ cm at 25°C for 1:2 or 2:1 electrolytes. The corresponding values are $2.108\times10^{-8}/\sqrt{c_i}$ for 1:1 electrolytes and $1.054\times10^{-8}/\sqrt{c_i}$ for 2:2 electrolytes. The differences are less marked if concentrations are expressed in equivalents per liter rather than moles per liter. Then

$x_{\frac{1}{2}}=2.108\times10^{-8}/\sqrt{N}$ for 1:1 electrolytes
$1.721\times10^{-8}/\sqrt{N}$ for 1:2 or 2:1 electrolytes
$1.491\times10^{-8}/\sqrt{N}$ for 2:2 electrolytes.

This is perhaps a fairer mode of comparison. It does show, as expected, that the double layer becomes thinner as the valence of either ion increases.

It might have been anticipated that these limiting values of $x_{\frac{1}{2}}$ would turn out to be inversely proportional to the values of K^d and C^d at $\psi=0$. This is so, and since it is much easier to find these values of K^d and C^d than $x_{\frac{1}{2}}$ for other valence types more complicated than these, the relationship can be used to establish $x_{\frac{1}{2}}$ for these other valence types.

In order to see how Eq. (14) differs from Eq. (16),

[5] The steps in the integration are

$$\kappa' dx=dy/e^{-y}(1-e^y)(1+2e^y)^{\frac{1}{2}}$$
$$=de^y/(1-e^y)(1+2e^y)^{\frac{1}{2}}$$
$$=-dw/w(3-2w)^{\frac{1}{2}},$$

where $w=1-e^y$. This last equation is in a form to be found in tables of integrals.

we note that

$$\psi/\psi_{\text{approx}} = (p/6)\ln[1+6p/\{p-1\}^2]. \quad (17)$$

This function lies between 0.85 and 1.15 for potentials less than 0.16 volt. It reaches a minimum at about 0.05 volt, passes through unity at about 0.135 volt and increases fairly rapidly thereafter. This calculation is independent of concentration and indicates that the simple exponential function 16 lies within 15 percent of the exact function 14 for the potentials met with in practice down to about $0.005M$ solution. (In more dilute solutions ψ can go higher than 0.16 volt.)

The above equations apply only when ψ is positive. For negative values it is necessary to return to Eq. (13a). This can be solved for ψ to give

$$\psi = \frac{kT}{\epsilon}\ln\left\{\frac{3}{2}\tanh^2\left[\frac{\sqrt{3}}{2}\kappa'(x'+c)\right]-\frac{1}{2}\right\}$$

$$= \frac{kT}{\epsilon}\ln\left\{\frac{3}{2}\tanh^2\left[\frac{\ln p}{2}+\tanh^{-1}\frac{1}{\sqrt{3}}\right]-\frac{1}{2}\right\}, \quad (2:1)\ (18)$$

where

$$c = (2/\sqrt{3}\kappa')\tanh^{-1}(1/\sqrt{3}) = 0.7602/\kappa'.$$

At large values of x', the square of the hyperbolic tangent can be approximated by

$$\tanh^2\theta \sim 1-4e^{-2\theta}.$$

Then the logarithm can be expanded, retaining only the first term, to give

$$\psi_{\text{approx}} = -(6kT/\epsilon p)\exp[-2\tanh^{-1}1/\sqrt{3}]. \quad (2:1)\ (19)$$

Then

$$\psi/\psi_{\text{approx}} = -\frac{p}{6}\left\{\frac{3}{2}\tanh^2\left[\frac{\ln p}{2}+\tanh^{-1}1/\sqrt{3}\right]-\frac{1}{2}\right\}$$

$$\times\exp[-2\tanh^{-1}1/\sqrt{3}]. \quad (2:1)\ (19a)$$

This function departs from unity rather more quickly than its counterpart for positive potentials, Eq. (17). Thus when $\psi = -0.025$ volt, the function equals 1.21, showing that Eq. (19) is already in error by 21 percent at this comparatively small potential. To generalize this result, in electrolytes of unsymmetrical valence type the variation of potential with distance is less accurately exponential when the metallic surface has the charge of the more abundant ion, the potential of the outer Helmholtz plane being held the same except for sign.

For electrolytes of valence type 1:2 the equations corresponding to 5, 6, 7, 13, and 13a are

$$\eta^d = -A(e^{2y}+2e^{-y}-3)^{\frac{1}{2}}$$

$$= -A(e^y-1)(1+2e^{-y})^{\frac{1}{2}}, \quad (1:2)\ (20)$$

$$K^d = (A\epsilon/kTy)(e^y-1)(1+2e^{-y})^{\frac{1}{2}}, \quad (1:2)\ (21)$$

$$C^d = (A\epsilon/kT)(e^{2y}-e^{-y})/(e^y-1)(1+2e^{-y})^{\frac{1}{2}}, \quad (1:2)\ (22)$$

$$\kappa'x' = (1/\sqrt{3})\ln[\{(1+2e^{-y})^{\frac{1}{2}}+\sqrt{3}\}/$$

$$\{(1+2e^{-y})^{\frac{1}{2}}-\sqrt{3}\}] \quad y<0, \quad (1:2)\ (23)$$

$$\kappa'\left(x'+\frac{2}{\sqrt{3}\kappa'}\tanh^{-1}\frac{1}{\sqrt{3}}\right)$$

$$= \frac{2}{\sqrt{3}}\tanh^{-1}\left(\frac{1+2e^{-y}}{3}\right)^{\frac{1}{2}} \quad y>0. \quad (1:2)\ (24)$$

For electrolytes of more complicated valence type the integration of the counterpart of Eq. (12) is not possible in terms of ordinary functions. Naturally a new function is defined by each such integral, and in principle all that is necessary to solve the problem is to name the function, to investigate its qualitative properties, and perhaps to tabulate it. The mathematical procedure is fully defined, so that in a real sense the problem is solved for all valence types.

It was pointed out to the author by Professor J. Th. G. Overbeek that the above type of treatment should not be employed, however, for polyelectrolytes or in general where the several loci of charge are kinetically somewhat independent. This problem has not yet been investigated.

COMPONENTS OF CHARGE AND CAPACITY OF THE DIFFUSE DOUBLE LAYER

It is worth while to inquire how much of the charge η^d is attributable to an excess or deficiency of cations and how much to anions. These ion excesses (or more properly the surface charge densities attributable to them) are called $\eta_+{}^d$ and $\eta_-{}^d$ and are formally defined by the equations

$$\eta_+{}^d = \int_x^\infty (\rho_+ - n_0{}^+z_+\epsilon)dx, \quad (25)$$

$$\eta_-{}^d = \int_x^\infty (\rho_- - n_0{}^-z_-\epsilon)dx, \quad (26)$$

where ρ_+ is the charge density per unit volume attributable to cations in the (very small) region in question. The x standing as a lower limit of the integral is the value of x at the outer Helmholtz plane. According to the Boltzmann distribution law,

$$\rho_+ = n_0{}^+z_+\epsilon e^{-z_+y}, \quad (27)$$

$$\rho_- = n_0{}^-z_-\epsilon e^{-z_-y}. \quad (28)$$

Therefore one has for any valence type

$$\eta_+{}^d = n_0{}^+z_+\epsilon\int(e^{-z_+y}-1)dx, \quad (29)$$

$$\eta_-{}^d = n_0{}^-z_-\epsilon\int(e^{-z_-y}-1)dx, \quad (30)$$

or for a 2:1 electrolyte

$$\eta_+^d = 2n_0'\epsilon \int (e^{-2y}-1)dx, \qquad (2:1)\ (31)$$

$$\eta_-^d = -2n_0'\epsilon \int (e^{y}-1)dx. \qquad (2:1)\ (32)$$

In these four equations the limits of integration are the same as in Eqs. (25) and (26).

From Eqs. (8) and (5a) (still defining y as $\epsilon\psi/kT$, however),

$$d\psi = (4\pi\eta^d/DD_0)dx = (kT/\epsilon)dy. \qquad (33)$$

Then by Eqs. (32) and (5)

$$\eta_-^d = -\frac{n_0'kTDD_0}{2\pi A}\int_y^0 \frac{e^y-1}{(e^{-2y}+2e^y-3)^{\frac{1}{2}}}dy. \quad (2:1)\ (34)$$

There is a certain mathematical impropriety in this equation in that y is used both as the variable of integration and as the lower limit of the integral. The meaning is, of course, that before integration y is taken to mean the potential (in suitable units) of a point situated anywhere within the electrical double layer, whereas after the integration it will mean the potential of the outer Helmholtz plane. This kind of double meaning for a symbol is probably less confusing, ultimately, than the alternative of defining two symbols wherever this situation arises.

Integration of Eq. (34) is effected in the manner already indicated for Eq. (11) and leads to the result

$$\eta_-^d = A[\sqrt{3}-(1+2e^y)^{\frac{1}{2}}], \qquad (2:1)\ (35)$$

where the simplification of the coefficient comes about by noting [Eq. (4)] that $kTDD_0n_0'/2\pi = A^2$. y is now defined as $\epsilon\psi^0/kT$ again.

In the same manner, or by subtracting η_-^d from η^d, one finds that

$$\eta_+^d = A[e^{-y}(1+2e^y)^{\frac{1}{2}}-\sqrt{3}]. \qquad (2:1)\ (36)$$

It is now desired to find C_+^{de} and C_-^{de}, that part of the observed capacity attributable to cations and anions in the diffuse double layer. These are defined as

$$C_+^{de} = -d\eta_+^d/dE, \qquad (37)$$

$$C_-^{de} = -d\eta_-^d/dE, \qquad (38)$$

where it is particularly to be noted that the variation is with respect to the observed potential E and not ψ^0. It is for this reason that the superscript is written de and not simply d. In the same way it is possible to define a capacity C^{de} representing the contribution of the diffuse double layer to the observed differential capacity and defined as

$$C^{de} = -d\eta^d/dE. \qquad (39)$$

Since $\eta^d = \eta_+^d + \eta_-^d$, it follows that

$$C^{de} = C_+^{de} + C_-^{de}. \qquad (40)$$

When specific adsorption of ions is absent, C^{de} may be regarded as identical with the observed differential capacity C. Thus C^{de} will be regarded as a known quantity for certain circumstances, and C_+^{de} and C_-^{de} will be expressed as functions of C^{de} and η_+^d or η_-^d not involving derivatives of these latter. The purpose of this derivation is to make it possible to evaluate C_+^{de} and C_-^{de} from observable quantities which may not be known with sufficient accuracy to make their derivatives with respect to E at all certain.

It is convenient to begin by eliminating y from Eqs. (35) and (36) to give

$$\frac{\eta_+^d}{A} = \sqrt{3}+2\left(\frac{1}{(b^2-1)^2}+\frac{1}{(b^2-1)}\right)^{\frac{1}{2}}, \quad (2:1)\ (41)$$

where $b = (\eta_-^d/A)-\sqrt{3}$.

Then by differentiation one has, after algebraic simplification,

$$-d\eta_+^d/dE = C_+^{de} = 2C_-^{de}(1+b^2)/(b^2-1)^2. \quad (2:1)\ (42)$$

Eliminating C_-^{de} or C_+^{de} with the aid of Eq. (40) gives

$$C_+^{de} = 2C^{de}(b^2+1)/(b^4+3), \qquad (2:1)\ (43)$$

$$C_-^{de} = C^{de}(b^2-1)^2/(b^4+3). \qquad (2:1)\ (44)$$

For electrolytes of the 1:2 type the corresponding equations are

$$\eta_+^d = A[(1+2e^{-y})^{\frac{1}{2}}-\sqrt{3}], \qquad (1:2)\ (45)$$

$$\eta_-^d = A[\sqrt{3}-e^y(1+2e^{-y})^{\frac{1}{2}}], \qquad (1:2)\ (46)$$

$$C_+^{de} = C^{de}(g^2-1)^2/(g^4+3), \qquad (1:2)\ (47)$$

$$C_-^{de} = 2C^{de}(g^2+1)/(g^4+3), \qquad (1:2)\ (48)$$

where $g = \sqrt{3}+(\eta_+^d/A)$.

It is necessary for the purposes of evaluating the thermodynamic properties of the electrical double layer by a method to be presented shortly to be able to evaluate dC_+^{de}/dE. This can be done with the aid of Eq. (47) to give

$$\frac{dC_+^{de}}{dE} = \frac{dC^{de}}{dE}\frac{C_+^{de}}{C^{de}} + \frac{4g(g^2+3)(g^2-1)}{(g^4+3)^2}\frac{C^{de}\cdot C_+^{de}}{A}. \qquad (1:2)\ (49)$$

In the absence of specific adsorption, dC^{de}/dE can be set equal to dC/dE and evaluated with adequate accuracy from available experimental data. C_+^{de} is given by Eq. (47), g by its defining equation together with Eq. (45), and y by Eq. (20), assuming η^d known from differential capacity measurements.[1] This is an entirely feasible sequence of calculations.

It happens that equations for C_+^{de}, C_-^{de}, and dC_+^{de}/dE have not yet been given for 1:1 electrolytes. These are found as follows: As shown in a previous

paper (reference 1, p. 482),

$$\eta_+^d = A(e^{-y/2}-1), \qquad (1:1)\ (50)$$

$$\eta_-^d = -A(e^{y/2}-1). \qquad (1:1)\ (51)$$

Eliminating y gives

$$\eta_-^d = A\eta_+^d/(A+\eta_+^d) \qquad (1:1)\ (52)$$

or after differentiation with respect to E

$$-\frac{d\eta_-^d}{dE} = \frac{C_+^{de}}{([\eta_+^d/A]+1)^2} = \frac{C_+^{de}}{(1+t)^2} = C_-^{de}, \qquad (1:1)\ (53)$$

where $t=\eta_+^d/A$. Combined with Eq. (40) this gives

$$C_+^{de} = C^{de}(1+t)^2/(t^2+2t+2), \qquad (1:1)\ (54)$$

$$C_-^{de} = C^{de}/(t^2+2t+2). \qquad (1:1)\ (55)$$

It is possible to derive somewhat more convenient equations for these quantities by making use of the fact that y can be expressed as an explicit function of η^d. For 1:1 electrolytes it has been shown (reference 1, p. 474) that

$$\eta^d = -2A\sinh(y/2) \qquad (1:1)\ (56)$$

or

$$y = -2\sinh^{-1}v, \qquad (1:1)\ (57)$$

where $v=\eta^d/2A$. Making use of the identity

$$\sinh^{-1}v = \ln[v+(1+v^2)^{\frac{1}{2}}]$$

we have

$$y = -2\ln[v+(1+v^2)^{\frac{1}{2}}], \qquad (1:1)\ (58)$$

and from Eqs. (50) and (51)

$$\eta_+^d = A[v+(1+v^2)^{\frac{1}{2}}-1], \qquad (1:1)\ (59)$$

$$\eta_-^d = A\{1-1/[v+(1+v^2)^{\frac{1}{2}}]\}. \qquad (1:1)\ (60)$$

Differentiation of Eq. (59) with respect to E gives

$$C_+^{de} = \frac{C^{de}}{2}\left(1+\frac{v}{(1+v^2)^{\frac{1}{2}}}\right), \qquad (1:1)\ (61)$$

$$C_-^{de} = C^{de}-C_+^{de} = \frac{C^{de}}{2}\left(1-\frac{v}{(1+v^2)^{\frac{1}{2}}}\right), \qquad (1:1)\ (62)$$

and finally

$$\frac{dC_+^{de}}{dE} = \frac{C^{de}}{2(1+v^2)^{\frac{1}{2}}}\left[([1+v^2]^{\frac{1}{2}}+v)\frac{dC^{de}}{C^{de}dE}+\frac{C^{de}}{2A(1+v^2)}\right]. \qquad (1:1)\ (63)$$

OTHER VALENCE TYPES

Some of the equations of the preceding section have been worked out for electrolytes of more complex valence types. In general the derivations which require integration cannot be solved explicitly in terms of common functions for electrolytes of valence types more complicated than 1:2 or 2:1. What follows is a summary, mostly without derivation because the steps are identical with those already given, of formulas for some of the above quantities for electrolytes of general valence types: (It needs to be borne in mind, however, that they are not necessarily valid if the multiple charge is distributed along a flexible chain, as in polyelectrolytes.)

$$\eta^d = (A/2)[2me^{-2y}+4e^{my}-(2m+4)]^{\frac{1}{2}} \quad (2:m),$$

$$\eta^d = (A/2)[4e^{-my}+2me^{2y}-(2m+4)]^{\frac{1}{2}} \quad (m:2),$$

$$\eta^d = (A/\sqrt{l'})[me^{-ly}+le^{my}-(m+l)]^{\frac{1}{2}} \quad (l:m),$$

where l' is the lesser of the two quantities l and m;

$$C^d = (A\epsilon m/kT)(e^{my}-e^{-2y})/[2me^{-2y}+4e^{my}-(2m+4)]^{\frac{1}{2}} \quad (2:m),$$

$$C^d = (A\epsilon m/kT)(e^{2y}-e^{my})/[4e^{-my}+2me^{2y}-(2m+4)]^{\frac{1}{2}} \quad (m:2),$$

$$C^d = (A\epsilon ml/2kT\sqrt{l'})(e^{my}-e^{-ly})/[me^{-ly}+le^{my}-(m+l)]^{\frac{1}{2}} \quad (l:m).$$

As ψ^0 approaches zero, K^d and C^d approach one and the same value, namely,

$$\lim_{\psi^0\to 0} K^d = \lim_{\psi^0\to 0} C^d = 15^{\frac{1}{2}}A\epsilon/2^{\frac{1}{2}}kT \qquad (2:3 \text{ and } 3:2)$$

$$= 6^{\frac{1}{2}}A\epsilon/kT \qquad (1:3 \text{ and } 3:1)$$

$$= [m(m+l)]^{\frac{1}{2}}A\epsilon/2^{\frac{1}{2}}kT \qquad (m:l \text{ or } l:m;\ m\geq l).$$

As indicated above, these equations can also be used to estimate the half-thickness of the diffuse double layer at distances such that the assumption of an exponential decrease is approximately valid. Then the half-thickness is given by

$$x_{\frac{1}{2}} = (2^{\frac{1}{2}}\ln 2)/\kappa'[m(m+l)]^{\frac{1}{2}} \qquad (m\geq l)$$

$$= 2.981\times 10^{-8}/[m(m+l)c_i]^{\frac{1}{2}} \text{ cm at } 25^\circ \quad (m\geq l).$$

MIXED ELECTROLYTES

For mixed electrolytes of a single valence type the diffuse double layer is the same as for a single electrolyte of the same valence type and the same total concentration. In any volume element the ratio of the ions of like charge is the same as in the bulk of the mixture. For a mixture of salts of dissimilar valence type, Eq. (1) applies, but those which follow do not. In any given case it would doubtless prove possible to carry out the

analysis numerically if not algebraically, but with such matters we are not here concerned.

CONCLUSION

The foregoing treatment shows that it is possible to carry out the analysis of the properties of the diffuse double layer for 1:2 and 2:1 electrolytes in as complete a manner as had been done previously for z:z-valent electrolytes. In addition certain other properties of the diffuse double layer have been evaluated for the first time, and equations are given for a few selected properties of the double layer in electrolytes of more complex valence type.

ACKNOWLEDGMENT

The author acknowledges with thanks the assistance of Professor Robert Breusch of the Amherst College Department of Mathematics in connection with one of the mathematical steps in the foregoing analysis. We are also grateful to the U. S. Office of Naval Research for the financial support of the project of which this work has been a part.

THE JOURNAL OF CHEMICAL PHYSICS VOLUME 21, NUMBER 6 JUNE, 1953

Infrared and Raman Spectra of Fluorinated Ethanes. VI. The Series CF_3CH_3, CF_3CH_2Cl, CF_3CHCl_2, and CF_3CCl_3*

J. Rud Nielsen and C. Y. Liang,† *Department of Physics, University of Oklahoma, Norman, Oklahoma*

AND

D. C. Smith,‡ *Naval Research Laboratory, Washington, D. C.*

(Received October 27, 1952)

The infrared spectra of gaseous CF_3CH_2Cl and CF_3CHCl_2 have been obtained in the range from 2 to 38μ, and the spectra of the liquids in the range from 2 to 22μ, with the aid of LiF, NaCl, KBr, and KRS-5 prisms. The Raman spectra of these compounds in the liquid state have been photographed with a three-prism glass spectrograph of linear dispersion 15A/mm at 4358A. Depolarization ratios were determined for most of the Raman bands.

All fundamental vibrational frequencies have been assigned; the spectra have been interpreted in detail, and thermodynamic functions have been calculated.

INTRODUCTION

METHYL fluoroform and 1,1,1-trifluoro-2,2,2-trichloroethane, the first and last compounds of this series, have been studied previously.[1–5] The fundamental vibrational frequencies of CF_3CH_3 are known with considerable certainty, and for CF_3CCl_3 all fundamentals except the torsional have been assigned although with some uncertainty about one of the a_1 fundamentals.[2,3] In the present paper spectral data are presented for the two intermediate compounds CF_3CH_2Cl and CF_3CHCl_2, their fundamental vibrational frequencies are assigned and correlated with the fundamentals of CF_3CH_3 and CF_3CCl_3, and their thermodynamic properties are calculated.

EXPERIMENTAL RESULTS

The spectra of CF_3CH_2Cl and CF_3CHCl_2 were obtained in the same manner as those reported in previous papers.[6–8] Figures 1 and 3 show the infrared absorption of these compounds in the gaseous state at 25°C. The infrared spectra of the liquids at −10°C are shown in Figs. 2 and 4. The KRS-5 regions are not included. In Tables I and II are listed the wave numbers of the observed infrared absorption maxima. The Raman frequencies observed in the liquid state at about 30°C, are listed in Tables III and IV, which include depolarization ratios and relative intensities for most of the observed Raman bands. The exciting

* A part of this work has been supported by the U. S. Atomic Energy Commission under Contract No. AT-(40-1)-1074. The Raman data are taken from a thesis presented by Ching-Yu Liang to the Faculty of the Graduate College of the University of Oklahoma in partial fullfilment of the requirements for the Degree of Doctor of Philosophy.

† Present address: Department of Physics, University of Michigan, Ann Arbor, Michigan.

‡ Present address: Phillips Petroleum Company, Bartlesville, Oklahoma.

[1] H. W. Thompson and R. B. Temple, J. Chem. Soc. 1428 (1948).

[2] Nielsen, Claassen, and Smith, J. Chem. Phys. **18**, 1471 (1950).

[3] Cowan, Herzberg, and Sinha, J. Chem. Phys. **18**, 1538 (1950); **19**, 794 (1951).

[4] G. Glockler and C. G. Sage, J. Chem. Phys. **9**, 367 (1941).

[5] Nielsen, Liang, Smith, and Smith, J. Chem. Phys. **21**, 383 (1953).

[6] Nielsen, Claassen, and Smith, J. Chem. Phys. **18**, 485 (1950).

[7] Smith, Brown, Nielsen, Smith, and Liang, J. Chem. Phys. **20**, 473 (1952).

[8] Smith, Saunders, Nielsen, and Ferguson, J. Chem. Phys. **20**, 847 (1952).

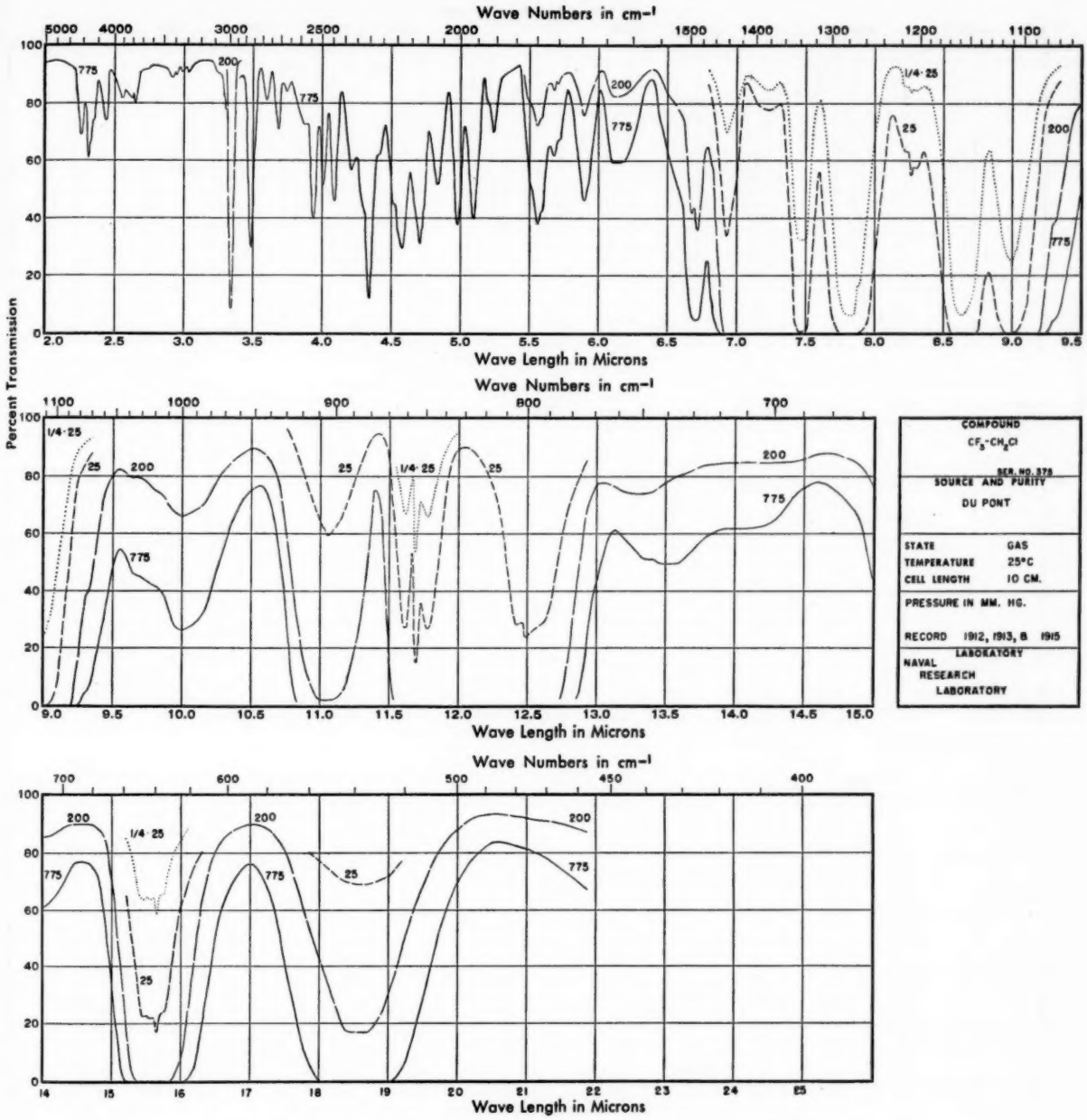

FIG. 1. Infrared spectrum of gaseous CF_3CH_2Cl. (KRS-5 region not included).

mercury lines are given by their Kohlrausch symbols.[9] The samples§ were highly purified, but no quantitative information about their purity was available. The sample of CF_3CHCl_2 apparently contained a trace of water vapor.

INTERPRETATION

1. CF_3CH_3

The fundamental vibrational frequencies of methyl fluoroform, taken from a previous paper,[2] are shown graphically at the top of Fig. 5. Solid vertical lines denote frequencies observed in infrared absorption, broken vertical lines frequencies observed in the Raman effect. Coinciding infrared and Raman frequencies are shown by slightly separated lines. Dash-dotted vertical lines represent fundamentals inferred from overtone or combination bands but not observed directly. The vibrational species are given by the usual symbols, and the approximate nature of the vibrations is indicated. The assignments are probably correct, except for a possible interchange of species for the fundamentals at 541 and 602 cm^{-1}.

[9] K. F. W. Kohlrausch, *Der Smekal-Raman-Effekt* (Julius Springer, Leipzig, 1931).

§ Kindly supplied by E. I. du Pont de Nemours and Company, Inc., Wilmington, Delaware.

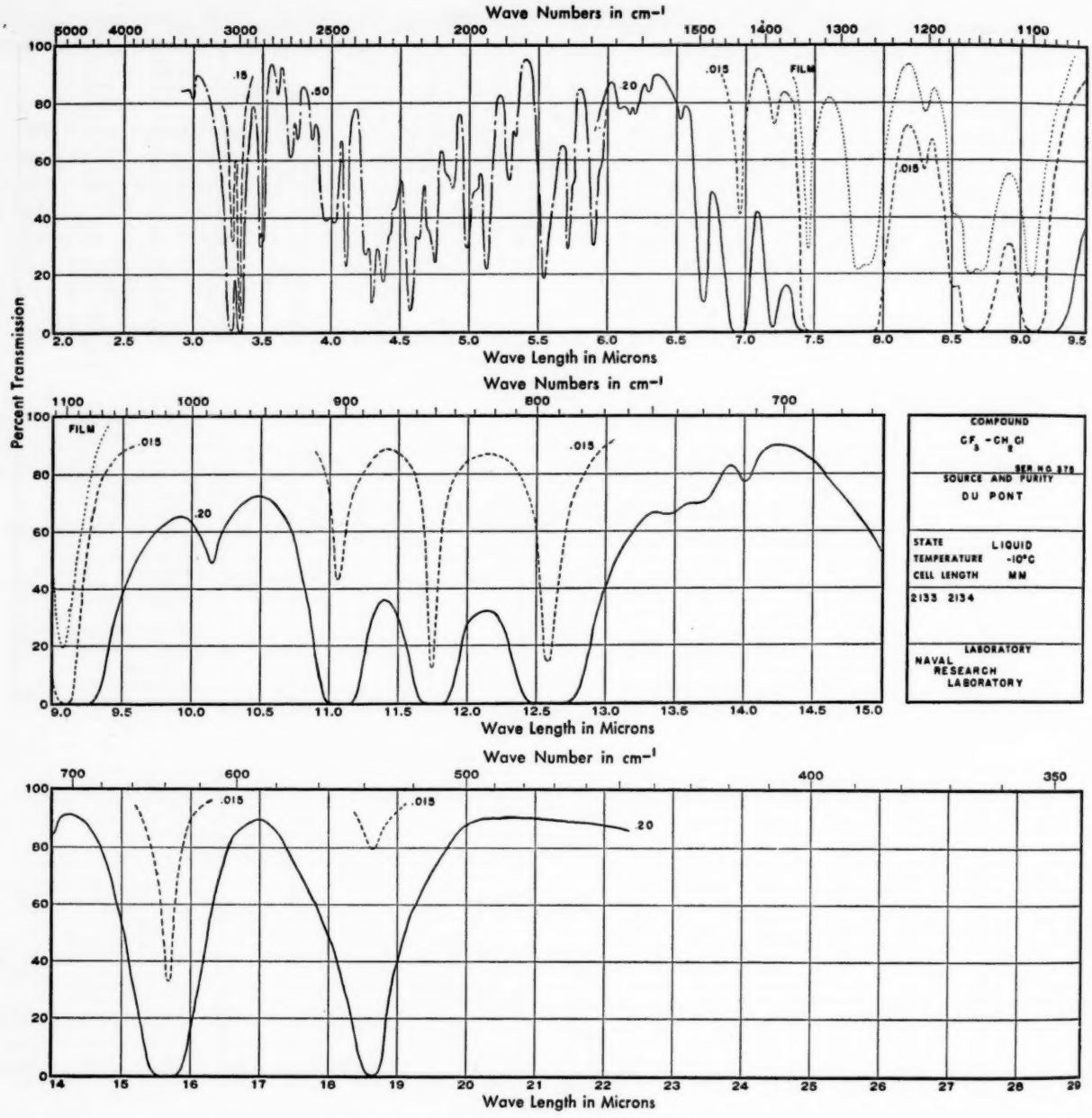

FIG. 2. Infrared spectrum of liquid CF_3CH_2Cl at $-10°C$.

2. CF_3CH_2Cl

This molecule has the symmetry C_s, and hence eleven fundamental vibrations of symmetry species a' and seven of species a''. Assuming the following interatomic distances C—H 1.093, C—C 1.54, C—F 1.36, and C—Cl 1.77A and tetrahedral angles, one obtains the principal moments of inertia 162.4, 466.3 and 467.7×10^{-40} g cm^2, the axis of smallest moment lying in the symmetry plane at an angle of 37°17′ to the C—C bond. Thus, the molecule is very nearly a symmetrical top, and fundamentals of species a'' should give rise to perpendicular bands, and fundamentals of species a' to bands that are intermediate between parallel and perpendicular bands. From the theory of Gerhard and Dennison[10] it is found that parallel infrared bands should have a PQR structure with a P—R separation of 12 cm^{-1}, while perpendicular bands should have a single maximum. Only one of the observed infrared bands has the predicted parallel-band contour, and for most of the fundamentals, infrared contours are less useful than the depolarization ratios of the Raman bands for determining the species.

The two highest fundamentals, associated with symmetric and asymmetric C—H stretching and having

[10] S. L. Gerhard and D. M. Dennison, Phys. Rev. 43, 197 (1933).

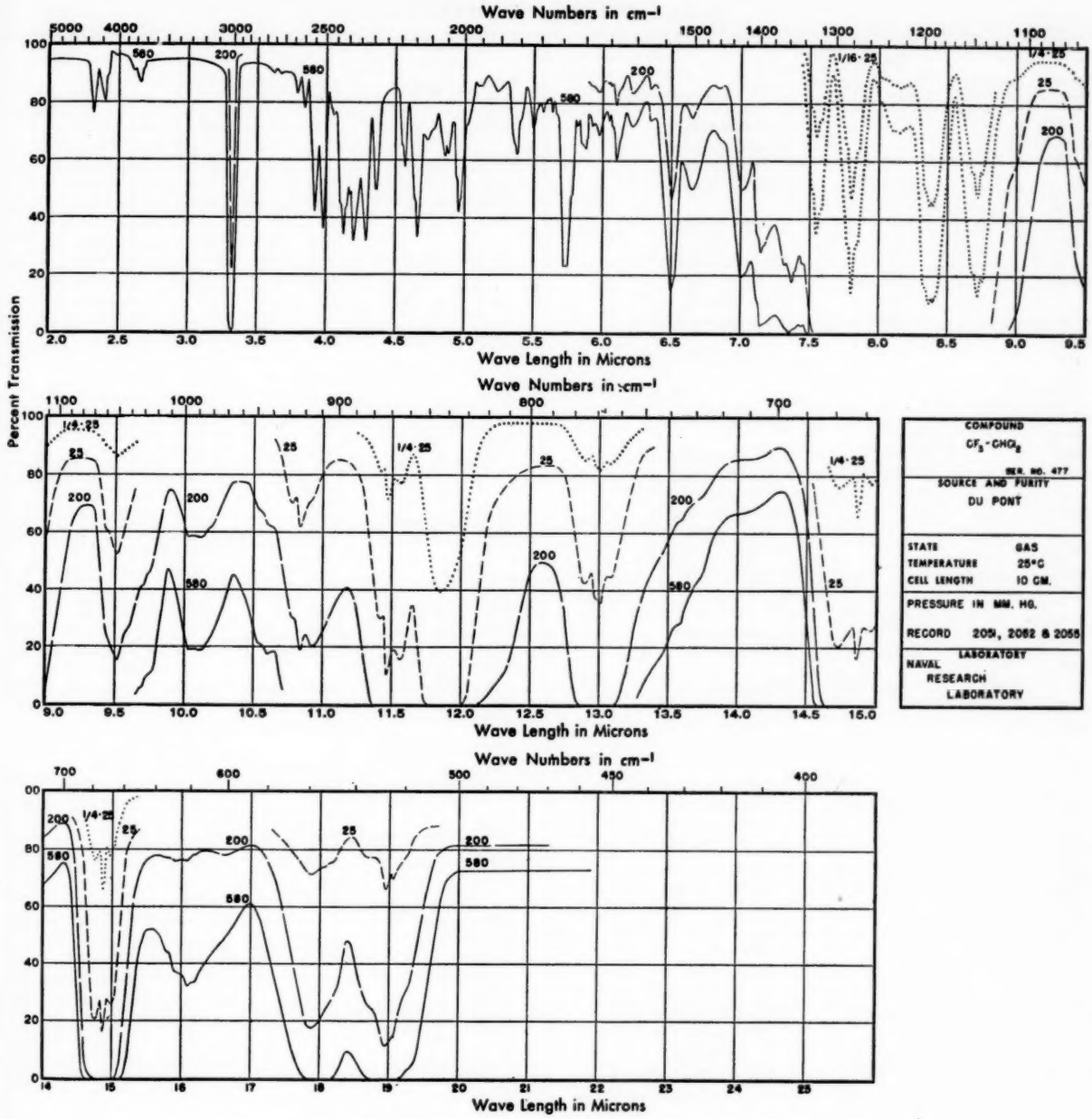

FIG. 3. Infrared spectrum of gaseous CF_3CHCl_2. (KRS-5 region not included.)

species a' and a'', respectively, are identified with the bands at 2990 and 3040 cm^{-1} (in the liquid state). The bands at 1437 cm^{-1} are taken to represent an a'' fundamental involving largely a twisting of the CH_2 group.

In both infrared and Raman spectra five strong bands appear in the region from 1100 to 1350 cm^{-1}. They are interpreted as three a' and two a'' fundamentals associated largely with C—F stretching and CH_2 deformation and rocking. The fundamental at 1103 cm^{-1} probably belongs to species a''. The other a'' fundamental is undoubtedly one of the pair at 1262 and 2181 cm^{-1}, and somewhat arbitrarily the higher frequency has been chosen. This uncertainty could be removed by making polarization measurements with 4047A excitation.

The polarized Raman bands at 903, 851, and 796 cm^{-1} and their very intense infrared counterparts are taken to represent three a' fundamentals. The infrared band at 855 cm^{-1} (in gaseous CF_3CH_2Cl) has very nearly the contour predicted for parallel bands, indicating that it is associated largely with C—C stretching. The other two a' fundamentals involve CH_2 wagging and C—Cl stretching.

The frequencies 640 and 537 cm^{-1} are both assigned as a' fundamentals and undoubtedly correspond to motions that are largely CF_3 deformation. There is some uncertainty about the value of the a'' fundamental

TABLE I. Infrared spectrum of CF_3CH_2Cl.

Gas Wave number	Gas Description	Liquid Wave number	Liquid Description	Interpretation
~330*	w			a'' fundamental
~355*	vs			a' fundamental
~455*	w			a'' fundamental
~541	s	536	s	a' fundamental
~635				
639	vs, sh	641	vs	a' fundamental
~643				
~647				109+540=649 A''
~700	w, b	713	w	2×358=716 A'
		~729	w	191+540=731 A'
~740	w, b	~740	w	109+640=749 A''
~790				
801	s	795	vs	a' fundamental
805				
849				
855	vs, sh	851	vs	a' fundamental
861				
~905	s	903	vs	a' fundamental
		984	w	191+801=992 A', 455+540=995 A''
~1000	m,b			358+640=998 A', 109+905=1014 A''
~1035				191+855=1046 A'
1072				2×540=1080 A'
1110	vs	1101	vs	a'' fundamental
		1147	vs	358+801=1159 A'
~1159	vs	1159	vs	a' fundamental
		1174	s	540+640=1180 A'
~1205				
1211	s, sh	1208	s	358+855=1213 A'
~1218				
~1267	vs	1263	vs	a' fundamental, 109+1159=1268 A''
1277	vs, b	1277	vs	a'' fundamental, 2×640=1280 A'
~1339	vs	1340	vs	a' fundamental, 540+801=1341 A'
~1389	s, b	1387	s	109+1277=1386 A'
1443	s	1435	s	a'' fundamental
1490	m, sh	1488	m	640+855=1495 A'
1497	w			358+1159=1517 A'?
~1550	w	1534	w	109+1443=1552 A', 640+905=1545 A'
		1587	w	2×801=1602 A'
		1610	w	358+1267=1625 A'
~1639	w, b	1621	w	358+1277=1635 A'', 191+1443=1634 A''
		~1645	w	540+1110=1650 A'', 801+855=1656 A'
		~1675	vw	330+1340=1670 A''
1695	w, sh	1693	w	358+1340=1698 A', 540+1159=1699 A'
1751	vw, sh	~1742	vw	640+1110=1750 A''
1761	vw, sh	1752	w	855+905=1760 A'
1799	w, sh	1803	w	640+1159=1799 A', 2×905=1810 A'
		1876	vw	540+1340=1880 A'
1908	w, sh	1890	w	801+1110=1911 A''
		1948	w	801+1159=1960 A'
1964	w, sh	1974	vw	855+1110=1965 A'', 640+1340=1980 A'
2008	w, sh	2002	w	855+1159=2014 A', 905+1110=2015 A''
		2049	w	905+1159=2064 A'?
2070	w	~2070	w	801+1277=2078 A'', 801+1267=2068 A'
2119	vw	2102	w	855+1267=2122 A'
2123	w	~2123	vw	855+1277=2132 A'', 801+1340=2141 A'
		2155	vw	905+1267=2172 A'
2183	w	2183	w	855+1340=2195 A'
~2215	vw			2×1110=2220 A'
		2242	vw	801+1443=2244 A'', 905+1340=2245 A'
2260	vw	2257	vw	1110+1159=2269 A''
2304	m, sh	2283	w	855+1443=2298 A''
~2330	w	2326	w, sh	2×1159=2318 A'
		2347	w	905+1443=2348 A''
2375	w			1110+1267=2377 A''
2445	w	2434	w, sh	1110+1340=2450 A''
2495	w	~2494	w	1159+1340=2499 A'
2538	w	~2525	w	1110+1443=2553 A'
~2590	vw			1159+1443=2602 A''
2667	vw	2670	vw	2×1340=2680 A'
2710	vw	2695	vw	1267+1443=2710 A'', 1277+1443=2720 A'
2778	vw	2770	vw	1340+1443=2783 A''
		~2858	w	(1159+2×851=2861 A')†
2865	m, sh	2866	w	2×1443=2886 A'
2994	s, sh	2992	m	a' fundamental
		3044	m	a'' fundamental
3300	vw			855+1110+1340=3305 A''
3344	vw	3339	vw	358+2994=3352 A'
3390	vw			358+3040=3398 A''
3425	vw			455+2994=3449 A''
3770	vw			801+2994=3795 A'
~3802	vw			855+2994=3849 A'
3906	vw			905+2994=3899 A'
4098	vw			1110+2994=4104 A''
4329	vw			1340+2994=4334 A'
4425	vw			1443+2994=4437 A''

* Observed with KRS-5 prism.
† Frequencies used are for liquid state.

TABLE II. Infrared spectrum of CF_3CHCl_2.

Gas Wave number	Gas Description	Liquid Wave number	Liquid Description	Interpretation
378*	s			a' fundamental
		~479	w	218+263=481 A''
~519				141+379=520 A''
525	sh			2×263=526 A'
527	s, sh	526	m	a' fundamental
~535				
~549	vw			185+357=542 A''
~553				
559	s	555	m	a'' fundamental
		575	w	218+357=575 A'
~601	w	600	vvw	218+379=597 A''
		608	vw	872−263=609 A''
~617				
622	m, sh	617	w	263+357=620 A''
~629				
~635	w	632	w	263+379=642 A'
~666				141+527=668 A''
668				
672	vs, sh	670	vs	a' fundamental
679				

* Observed with KRS-5 prism.

TABLE II.—*Continued.*

Gas Wave number	Gas Description	Liquid Wave number	Liquid Description	Interpretation
~707	vw, b	711	w	185+527=712 A', 2×357=714 A'
~727	vw	725	vw	357+2×185=727 A''
735	w	737	w	357+379=736 A''
~743				185+559=744 A'', 218+527=745 A''
~765				
769	s, sh	766	s	a' fundamental
~770				
~775				218+559=777 A'
~810	w, b	~810	m	141+672=813 A''
~844	vs, b	834	s	a'' fundamental
~865				
872	s, sh	868	s	a' fundamental
~876				
		905	m	379+527=906 A', 141+769=910 A''
~915				
923	m, sh	918	m	357+559=916 A'
~928				
943	w			379+559=938 A''
~950				185+769=954 A'
		968	w	
~980				
988	w	984	m	141+844=985 A', 218+769=987 A''
996	w	~992	w	
~1025				357+672=1029 A'', 185+844=1029 A''
~1031		1027	w	263+769=1032 A'
~1041		1034	w	
1052	s	1044	m	379+672=1051 A', 2×527=1054 A', 185+872=1057 A'
~1060				218+844=1062 A'
~1111	w			2×559=1118 A'
~1143				
1147	vs, sh	1139	vs	a' fundamental
~1152				
1192	vs, sh	1183	vs	a'' fundamental
1195	vs, sh			
1227				357+872=1229 A'', 559+672=1231 A''
~1235	s	1229	s	a'' fundamental
~1250		1245	s	379+872=1251 A'
~1274				
1284	vs, sh	1272	vs	a' fundamental
~1287				
~1318				
1325	vs, sh	1325	vs	a' fundamental
~1330				
1344	w, sh			2×672=1344 A'
~1351	vw			
1357	m, sh	1355	m	218+1147=1365 A''
~1366				527+844=1371 A'', 185+1192=1377 A''
~1395				527+872=1399 A'
1399	m, sh	1395	m	559+844=1403 A'
~1406				263+1147=1410 A', 218+1192=1410 A'
~1429	m, b	1425	m	559+872=1431 A'', 141+1282=1423 A''
1462	vw	1460	w	141+1325=1466 A'', 185+1282=1467 A'
1504	w	1490	w	357+1147=1504 A''
		1508	w	185+1325=1510 A', 672+844=1516 A''
~1534				379+1147=1526 A'
1538	m, sh	1541	m	2×769=1538 A', 672+872=1544 A', 263+1282=1545 A'
1575	vw			379+1192=1571 A''
1608	vw	1603	w	379+1235=1614 A'', 769+844=1613 A''
~1629				
1637	vw, sh	1631	w	357+1282=1639 A'', 769+872=1641 A'
1647				
1653		1658	w	379+1282=1661 A''
1672	vw			527+1147=1674 A'
1686	vw			2×844=1688 A', 357+1325=1682 A''
~1696				379+1325=1704 A'
1701	vw, sh	1699	w	559+1147=1706 A''
~1710	vw, sh			844+872=1716 A''
1718	vw, sh			527+1192=1719 A''
~1730	vvw			
~1736	vw			
1741	m, sh	1741	m	2×872=1744 A'
1744	m, sh			559+1192=1751 A'
~1764				527+1235=1762 A''
1773	vw, sh			559+1235=1794 A'
1783	vvw			
~1786	vvw			
1802	vw, sh	1805	w	527+1282=1809 A'
~1805	vvw			
~1815	vvw			
1818	vw, sh			672+1147=1819 A'
1848				527+1325=1852 A'
1859	w, sh	1848	w	672+1192=1864 A''
~1869				559+1325=1884 A''?
~1912	vw	1901	w	769+1147=1916 A', 672+1235=1907 A''
1951	vw	1940	vw	672+1282=1954 A'
1959	vw			769+1192=1961 A''
		1970	vw	844+1147=1991 A''
~1992				672+1325=1997 A'
~2012				769+1235=2004 A''
2016	w, sh	2002	w	872+1147=2019 A'
~2020				844+1192=2036 A'
2047	vw, sh	2037	w	769+1282=2051 A'
2058	vw, sh	2047	w	872+1192=2064 A''
~2092		~2088	vw	769+1325=2094 A'
2114	vw	2105	vw	872+1235=2107 A'', 844+1282=2126 A'
~2137	vvw			
2146	w, sh	2134	w	872+1282=2154 A'
~2153				844+1325=2169 A''
2188	vw, sh	2185	w	872+1325=2197 A'
~2198	vvw			
2288	w	2270	w	2×1147=2294 A'
2331	w, sh	2320	w	1147+1192=2339 A''
		2342	vw	
2381	w, sh	2364	w	1147+1235=2382 A'
2398	vw, sh			2×1192=2384 A'?
~2410				
2421	w, sh	2410	w	1192+1235=2427 A'
~2433		~2430	vw	1147+1282=2429 A'
2463	vw, sh	~2453	vw	2×1235=2470 A', 1147+1325=2472 A'
~2475				1192+1282=2474 A''
2513	w, sh	2506	w	1192+1325=2517 A''
2548	w, sh	2534	w	2×1282=2564 A', 1235+1325=2560 A''
2601	vw, sh	2591	w	1282+1325=2607 A'
2639	vw, sh	2635	w	2×1325=2650 A'
2725	vvw			
2762	vvw	2865	vw	
		2937	vw	
3012	s, sh	3008	m	a' fundamental
~3721				
3729	vw, sh			769+3012=3781 A'
3831	vw			844+3012=3856 A''
4167	vw			1147+3012=4159 A'
4310	vw			1325+3012=4337 A', 1282+3012=4294 A'

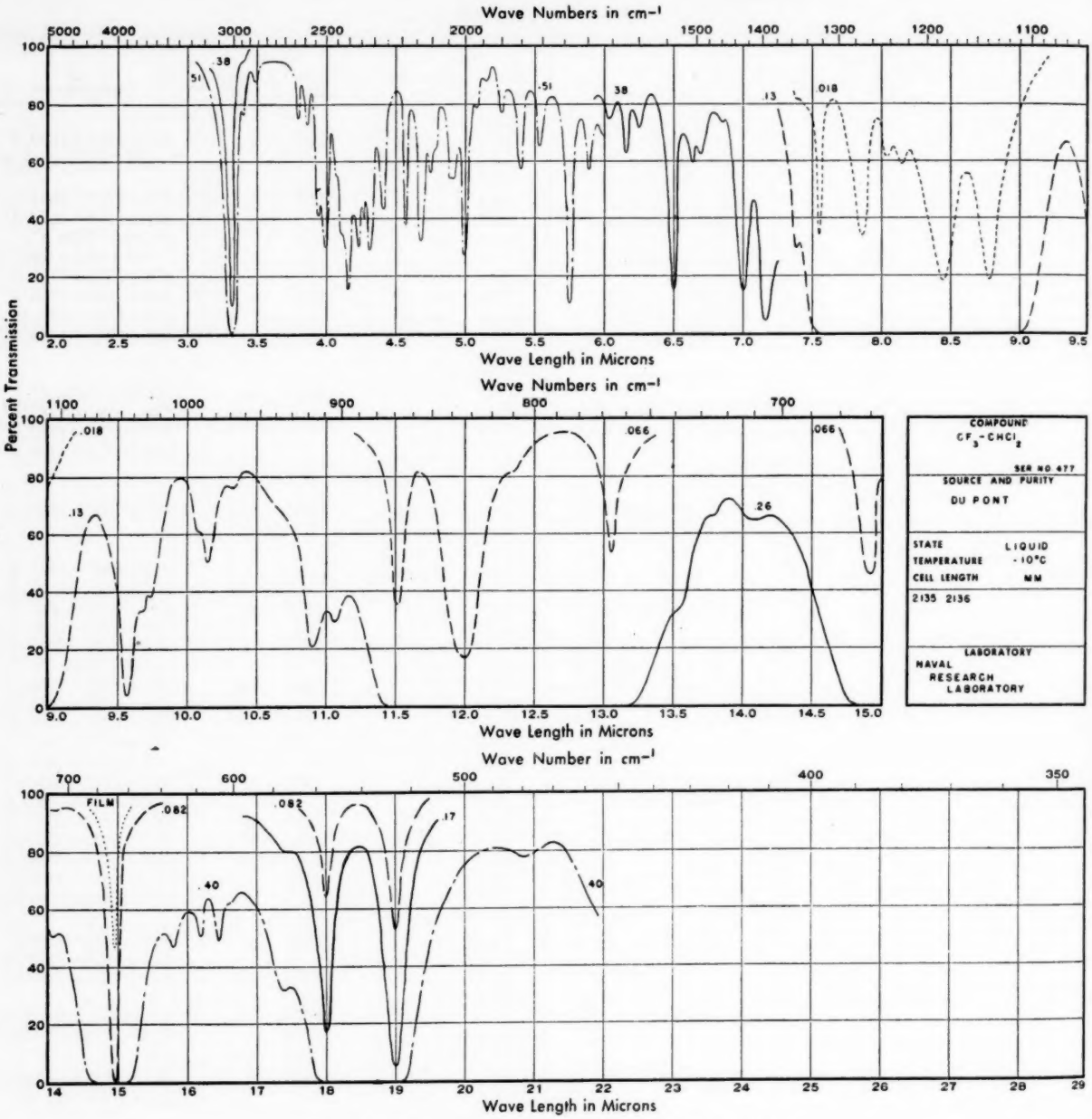

FIG. 4. Infrared spectrum of liquid CF_3CHCl_2 at $-10°C$.

involving asymmetric CF_3 deformation. It is possible that this fundamental overlaps with the a' fundamental at 640 cm^{-1}. However, since no other plausible interpretation could be found for a weak infrared band observed at 455 cm^{-1}, this band has been tentatively identified with the a'' fundamental in question.

The four remaining fundamentals, two of species a' and two of species a'', may be expected to lie below 400 cm^{-1} and to be associated with C—Cl bending, in-plane and out-of-plane rocking and torsion. Only three Raman bands have been observed in this region. The very strong polarized band at 358 cm^{-1}, which also occurs with high intensity in the infrared, is assigned as an a' fundamental. The Raman bands at 191 and 109 cm^{-1} are taken to be the two lowest fundamentals, of species a' and a'', respectively. The last a'' fundamental is tentatively identified with the weak infrared band at 330 cm^{-1} which cannot be satisfactorily interpreted otherwise.

On the basis of these assignments, listed in Table V, it has been possible to give a satisfactory interpretation of the only Raman band not assigned as a fundamental and of all of the observed infrared bands with the exception of three or four very weak bands. The interpretations are given in the last column of Tables I and III. More than one interpretation has been given for several of the bands, but not all alternatives have been listed.

TABLE III. Raman spectrum of CF_3CH_2Cl (liquid).

Wave number	Relative intensity	Depolarization ratio	Exciting Hg lines	Interpretation
109 cm^{-1}	14 d	0.85	*ek*	a'' fundamental
191	6 d	0.60	*e*	a' fundamental
358.4	34 sh	0.25	$\pm eki$	a' fundamental
537	18	0.35	$\pm ek$	a' fundamental
639	6	0.65	*ek*	a' fundamental
796	100	0.06	$\pm efkil$	a' fundamental
851.7	11 sh	0.40	*ek*	a' fundamental
903	3	0.60	*e*	a' fundamental
1104	5 d	0.85	*ek*	a'' fundamental
1152	3 d	0.60	*ek*	a' fundamental
1262 / 1285	3 d	0.75	*ek*	a' fundamental / a'' fundamental
1340	3	0.35	*ek*	a' fundamental
1439	6 vd	0.85	*ek*	a'' fundamental
2851	vvw		*e*	$2\times1439=2878$ A'
2988	84	0.08	*ekilpq*	a' fundamental
3035	w	dp	*e*	a'' fundamental

3. CF_3CHCl_2

This molecule also has the symmetry C_s. The following values were calculated for its principal moments of inertia: 410.4, 499.2, and 738.9×10^{-40} g cm^2. The axis of smallest moment makes an angle of 21°4′ with the C−C bond, and the axis of intermediate moment is perpendicular to the symmetry plane of the molecule. From the curves calculated by Badger and Zumwalt,[11] it is found that Type *B* infrared bands should be doublets with separations 3 and 14 cm^{-1} between the principal and secondary maxima, while Type *A* and Type *C* bands should have PQR structure with P−R separations of 12 and 22 cm^{-1}, respectively. The seven fundamentals belonging to species a'' should have Type *B* contours in the infrared spectrum of gaseous CF_3CHCl_2, while the eleven fundamentals of species a' should have contours intermediate between Types *A* and *C*.

The band at 3012 cm^{-1}, which is strong in both spectra and polarized in the Raman effect, is undoubtedly the highest a' fundamental and is associated with C−H stretching. The band at 1325 cm^{-1} is also assigned as an a' fundamental, since it is very intense and has pronounced PQR structure in the infrared and is polarized in the Raman spectrum. It probably involves largely C−H bending. The four bands at 1282, 1235, 1192, and 1147 cm^{-1}, while so intense in the infrared that they are assigned as fundamentals, are so weak in the Raman effect that their depolarization ratios could not be measured. However, the infrared band contours indicate clearly that the first and the last of them belong to species a' and the others to a''. The motions involve C−F stretching and C−H bending.

The band at 872 cm^{-1} is interpreted as an a' fundamental associated largely with C−C stretching. The bands at 844 and 769 cm^{-1} are taken to be a'' and a' fundamentals, respectively, involving C−Cl stretching.

The bands at 672, 559, and 527 cm^{-1} are assigned as fundamentals associated largely with CF_3 deformations. That at 559 cm^{-1} apparently belongs to a'', and the others to a'.

The very intense polarized Raman band at 379 cm^{-1}, and its infrared counterpart observed only with KRS-5 prism, is interpreted as an a' fundamental, and the depolarized Raman band at 357 cm^{-1} as an a'' funda-

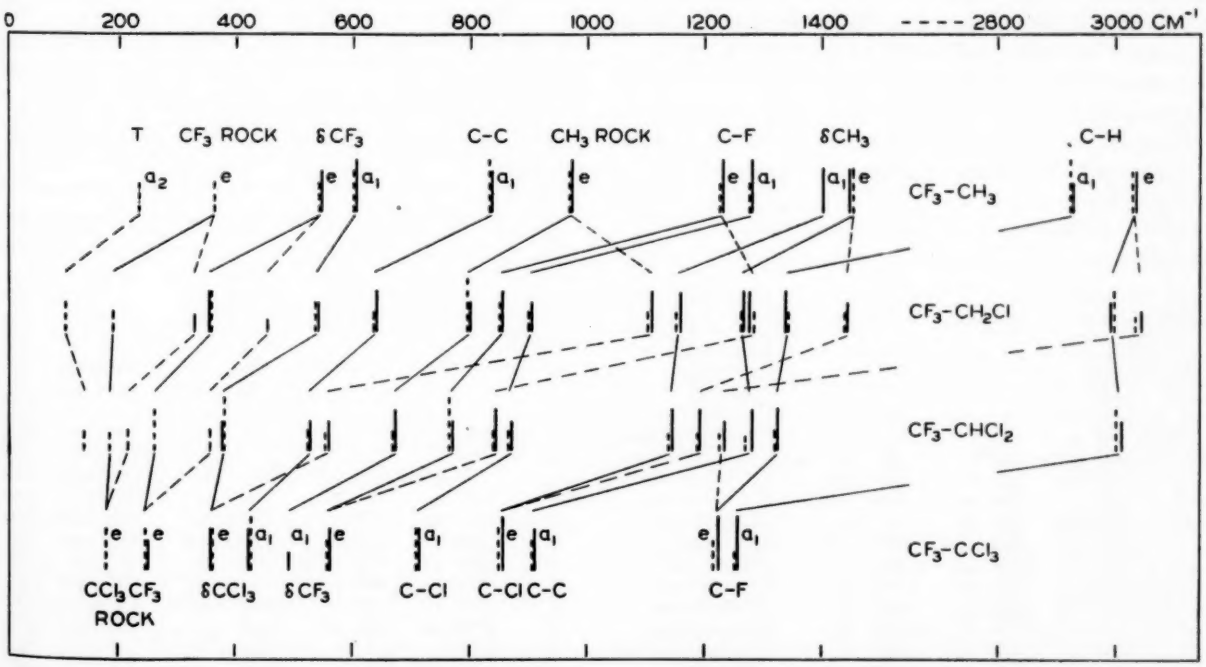

FIG. 5. Fundamental vibrational frequencies for CF_3CH_3, CF_3CH_2Cl, CF_3CHCl_2, and CF_3CCl_3.

[11] R. M. Badger and L. R. Zumwalt, J. Chem. Phys. **6**, 711 (1938).

TABLE IV. Raman spectrum of CF_3CHCl_2 (liquid).

Wave number	Relative intensity	Depolarization	Exciting Hg lines	Interpretation
105 cm^{-1}	w		*e*	Spurious?
141	m		*e*	*a''* fundamental
185	w	0.7	*e*	*a'* fundamental
218	16 d	0.8	±*e*	*a''* fundamental
263	30	0.80	±*ek*	*a'* fundamental
357	15	0.87	±*ek*	*a''* fundamental
379	74	0.25	±*ek*	*a'* fundamental
441	vvw		*e*	2×218=436 *A'*
526	14	0.37	±*ek*	*a'* fundamental
554	10 d	0.86	*e*	*a''* fundamental
671	16 sh	0.46	*ek*	*a'* fundamental
732	vvw		*e*	357+379=736 *A''*
766.5	100 sh	0.18	±*efki*	*a'* fundamental
836	10 d	0.87	*ek*	*a''* fundamental
867	7	0.8	*ek*	*a'* fundamental
1140	5 d		*e*	*a'* fundamental
1189	5 d		*e*	*a''* fundamental
1226	6 d		*e*	*a''* fundamental
1270	vw d		*e*	*a'* fundamental
1323	9	0.58	*ek*	*a'* fundamental
3003.0	70	0.23	*eki*	*a'* fundamental

mental. The motions involve CCl_2 deformation and twisting, respectively.

The Raman bands at 263, 218, and 185 cm^{-1} undoubtedly represent fundamentals. Although the depolarization ratios for these bands are not measured very accurately, it is fairly certain that the fundamental at 185 cm^{-1} belongs to *a'*, while that at 218 cm^{-1} probably belongs to *a''* and that at 263 cm^{-1} to *a'*.

There remains one low *a''* fundamental. Two Raman bands have been observed, at 105 and 141 cm^{-1}. However, because of the rather large amount of stray light in this region, their reality is not quite certain. It has been assumed that the higher frequency represents an *a''* fundamental, and that the other is spurious. The four lowest fundamentals must be associated largely with rocking and torsional motions.

The assigned fundamentals for CF_3CHCl_2 are listed in Table VI. In terms of these fundamentals, satisfactory interpretations are given in the last columns of Tables II and IV of all observed infrared absorption maxima, with the exception of about a dozen very faint maxima or shoulders, and of all observed Raman bands. All of the unassigned faint bands can be assigned as ternary combinations. However, since in each case several such interpretations are possible, these are not listed in Table II.

4. CF_3CCl_3

Infrared and Raman data for this compound, and assignments of all fundamentals except the torsional, have been presented in a previous paper.[5] The fundamental vibrational frequencies are shown graphically at the bottom of Fig. 5.

DISCUSSION

In Fig. 5 totally-symmetric fundamentals of related compounds are joined by solid slanting lines, other fundamentals by broken lines. Solid (broken) lines may not cross. The regularity of the correlation diagram supports the essential correctness of the assignments made. The advantages of this type of correlation diagram over one based on molecular group frequencies are discussed in a previous paper of this series.[7]

Although two of the *a''* fundamentals for CF_3CH_2Cl, namely, those identified with the weak infrared bands at 330 and 455 cm^{-1} and the species of the fundamentals at 1267 and 1277 cm^{-1} are uncertain, the detailed interpretation of the spectra of this compound is quite satisfactory and complete. For CF_3CHCl_2 on the other hand, there is less uncertainty about the assignment of the fundamentals, only the lowest *a''* fundamental being uncertain, but there are more faint infrared bands that cannot be interpreted as binary sums. This may be caused by a small amount of impurity, perhaps a trace of water.

TABLE V. Fundamental vibrational frequencies for CF_3CH_2Cl.

Symmetry species	Infrared cm^{-1} (gas)	Infrared cm^{-1} (liquid)	Raman cm^{-1} (liquid)	Approximate character
a''	—	—	109 s	Torsion
a'	—	—	191 m	Rocking
a''	330	—	—	Rocking
a'	355 vs	—	358.4 vs	Rocking
a''	455 w	—	—	CF_3 deformation
a'	541 s	536 s	537 s	CF_3 deformation
a'	639 vs	641 vs	639 m	CF_3 deformation
a'	801 s	795 vs	796 vvs	CCl stretching
a'	855 vs	851 vs	851.7 s	CC stretching
a'	905 s	903 vs	903 m	CH_2 wagging
a''	1110 vs	1101 vs	1104 m	CH_2 rocking
a'	1159 vs	1159 vs	1152 m	CF stretching
a'	1267 vs	1263 vs	1262 m	CF stretching
a''	1277 vs	1277 vs	~1285 m	CF stretching
a'	1339 vs	1340 vs	1340 m	CH_2 deformation
a''	1443 s	1435 s	1439 m	CH_2 twisting
a'	2994 s	2992 s	2988 vs	CH stretching
a''	—	3044 m	3035 w	CH stretching

TABLE VI. Fundamental vibrational frequencies for CF_3CHCl_2.

Symmetry species	Infrared cm^{-1} (gas)	Infrared cm^{-1} (liquid)	Raman cm^{-1} (liquid)	Approximate character
a''	—	—	~141 m	Torsion
a'	—	—	185 w	Rocking
a''	—	—	218 m	Rocking
a'	—	—	263 vs	Rocking
a''	—	—	357 m	CCl_2 twisting
a'	378 s	—	379 vvs	CCl_2 deformation
a'	527 s	526 m	526 m	CF_3 deformation
a''	559 s	555 m	554 w	CF_3 deformation
a'	672 vs	670 vs	671 m	CF_3 deformation
a'	769 s	766 s	766.5 vvs	CCl stretching
a''	844 vs	834 s	836 m	CCl stretching
a'	872 s	868 s	867 m	CC stretching
a'	1147 vs	1139 vs	1140 w	CF stretching
a''	1192 vs	1183 vs	1189 w	CH bending
a''	1235 s	1229 s	1226 w	CF stretching
a'	1282 vs	1272 vs	1270 vw	CF stretching
a'	1325 vs	1325 vs	1323 m	CH bending
a'	3012 s	3008 m	3003.0 vs	CH stretching

TABLE VII. Calculated thermodynamic functions for CF_3CH_2Cl at one atmosphere (cal/deg^{-1} mole^{-1}).

T°K		$(H^0-H_0^0)/T$	C_p^0	S^0	$-(F^0-H_0^0)/T$
167.56 (mp)	Trans+rot	7.95	7.95	62.99	55.04
	Vib	1.77	5.18	2.49	0.72
	Tors	1.24	1.92	2.26	1.02
	Total	10.96	15.05	67.74	56.78
279.26 (bp)	Trans+rot	7.95	7.95	67.05	59.10
	Vib	4.19	10.41	6.37	2.18
	Tors	1.54	2.09	3.28	1.74
	Total	13.68	20.45	76.70	63.02
298.16	Trans+rot	7.95	7.95	67.57	59.62
	Vib	4.61	11.25	7.07	2.47
	Tors	1.58	2.12	3.41	1.82
	Total	14.14	21.32	78.05	63.91
400	Trans+rot	7.95	7.95	69.90	61.96
	Vib	6.84	15.38	10.98	4.13
	Tors	1.73	2.23	4.05	2.32
	Total	16.52	25.56	84.93	68.41
500	Trans+rot	7.95	7.95	71.71	63.77
	Vib	8.89	18.62	14.97	6.08
	Tors	1.84	2.31	4.56	2.72
	Total	18.68	28.88	91.24	72.57
600	Trans+rot	7.95	7.95	73.13	65.18
	Vib	10.73	21.13	18.40	7.67
	Tors	1.92	2.33	4.99	3.06
	Total	20.60	31.41	96.52	75.91
700	Trans+rot	7.95	7.95	74.35	66.40
	Vib	12.36	23.09	21.81	9.45
	Tors	1.96	2.29	5.34	3.37
	Total	22.27	33.33	101.50	79.22

TABLE VIII. Calculated thermodynamic functions for CF_3CHCl_2 at one atmosphere (cal/deg^{-1} mole^{-1}).

T°K		$(H^0-H_0^0)/T$	C_p^0	S^0	$-(F^0-H_0^0)/T$
200	Trans+rot	7.95	7.95	66.56	58.62
	Vib	3.75	9.45	5.56	1.81
	Tors[a]	1.15	1.82	2.05	0.90
	Total	12.85	19.22	74.17	61.33
298.16	Trans+rot	7.95	7.95	69.74	61.80
	Vib	6.47	14.44	10.29	3.82
	Tors[a]	1.39	1.91	2.79	1.41
	Total	15.81	24.30	82.82	67.03
400	Trans+rot	7.95	7.95	72.08	64.13
	Vib	9.10	18.63	15.33	6.22
	Tors[a]	1.53	1.95	3.36	1.84
	Total	18.58	28.53	90.77	72.19
500	Trans+rot	7.95	7.95	73.85	65.91
	Vib	11.30	21.74	19.60	8.30
	Tors[a]	1.61	1.96	3.80	2.19
	Total	20.86	31.65	97.25	76.40
600	Trans+rot	7.95	7.95	75.30	67.35
	Vib	13.24	24.04	23.83	10.59
	Tors	1.70	2.04	4.21	2.51
	Total	22.89	34.03	103.34	80.45
700	Trans+rot	7.95	7.95	76.53	68.58
	Vib	14.91	25.75	27.57	12.66
	Tors	1.75	2.05	4.52	2.78
	Total	24.61	35.75	108.62	84.02
800	Trans+rot	7.95	7.95	77.59	69.64
	Vib	16.37	27.07	31.38	15.00
	Tors	1.79	2.08	4.80	3.01
	Total	26.11	37.10	113.77	87.65

[a] Calculated by regarding the torsional mode as an ordinary vibration.

CALCULATED THERMODYNAMIC FUNCTIONS

From the molecular dimensions given above, and, the fundamental frequencies listed in Table V and VI the heat capacity, entropy, free energy function, and heat content function, have been calculated for CF_3CH_2Cl and CF_3CHCl_2 as ideal gases at one atmosphere and at different temperatures. To obtain the contributions of the torsional motion, the potential barrier V_0 opposing the rotation of one end of the molecule relative to the other was first estimated by the formula[12]

$$\nu=(\sigma_i/2\pi)(V_0/2I_r)^{\frac{1}{2}},$$

where ν is the torsional frequency, $\sigma_i=3$ the internal symmetry number, and I_r the reduced moment of inertia. For CF_3CH_2Cl the value 5700 cal/mole was found for the barrier height, and for CF_3CHCl_2 the value 22300 cal/mole. The torsional contributions for CF_3CH_2Cl, and for CF_3CHCl_2 above 500°K, were then obtained from the tables of Pitzer and Gwinn.[13] The range covered by these tables is not wide enough to permit calculation of the torsional contributions to the thermodynamic functions for CF_3CHCl_2 at 500°K and lower temperatures. These contributions were therefore estimated by considering the torsional mode as an ordinary vibration. The calculated thermodynamic functions are given in Tables VII and VIII. No calorimetric data appear to be available with which to compare these results.

[12] See S. Glasstone, *Theoretical Chemistry* (D. Van Nostrand Company, Inc., New York, 1944), p. 421.

[13] K. S. Pitzer and W. D. Gwinn, J. Chem. Phys. **10**, 429 (1942).

Infrared and Raman Spectra of Fluorinated Ethanes. VII. CCl_3CF_2Cl and CCl_3CFCl_2*

J. Rud Nielsen and C. Y. Liang, *Department of Physics, University of Oklahoma, Norman, Oklahoma*

and

D. C. Smith† and Morris Alpert,‡ *Naval Research Laboratory, Washington, D. C.*

(Received January 12, 1953)

The infrared spectra of liquid CCl_3CF_2Cl and of CCl_3CFCl_2 as glass and in CS_2 solution, have been obtained in the region from 2 to 38μ with the aid of LiF, NaCl, KBr, and KRS-5 prisms. The Raman spectra of these compounds in the liquid state, at about 50° and 120°C, respectively, were photographed with a three-prism glass spectrograph of linear dispersion 15A/mm at 4358A. Relative intensities and depolarization ratios were measured for all but the weakest Raman bands. Complete assignments of fundamental vibration frequencies have been made, the spectra have been interpreted in detail, and thermodynamic functions have been calculated.

INTRODUCTION

THE infrared and Raman spectra of CCl_3CF_3 have been reported and interpreted in a previous paper of this series.[1] Several investigators[2] have studied C_2Cl_6. Except for the infrared spectrum of CCl_3CF_2Cl obtained with low resolution,[3] no data have been published for the two intermediate compounds. In this paper, spectral data are presented for CCl_3CF_2Cl and CCl_3CFCl_2, their fundamental vibration frequencies are assigned, and their thermodynamic properties are calculated.

EXPERIMENTAL RESULTS

The spectral measurements were made with the same instruments and in the same general manner as described in earlier papers.[4-5] The infrared spectrum of liquid CCl_3CF_2Cl (mp$\sim$35°, bp 90.5°C) at approximately 50°C is shown in Fig. 1, and the wave numbers of the observed absorption maxima are listed in Table I. The Raman spectrum of this compound in the liquid state at 40–60°C was obtained by surrounding the Raman tube with hot water in a double-walled evacuated jacket. The data obtained are listed in Table II. The exciting mercury lines are given by their Kohlrausch symbols.[6]

The infrared spectrum of CCl_3CFCl_2 (mp 100°, bp 137°C) was obtained with the compound as a solid glass, sublimed onto a cell window and then flowed under pressure and at a temperature near the melting point to form a film of uniform thickness. The regions of strong absorption were also studied with the compound in CS_2 solution. The results are given in Fig. 2 and in Table III. The Raman data for this compound in the liquid state at 120°C, listed in Table IV, were obtained by surrounding the Raman tube by a heating coil and a vacuum jacket during exposure. Both samples were highly purified, but no quantitative information about their purity was available.

INTERPRETATION

1. CCl_3CF_2Cl

This molecule undoubtedly has the symmetry C_s, and hence eleven fundamental vibrations of symmetry species A' and seven of species A''. Since no infrared data were obtained for the gaseous phase, the determination of symmetry species must be based almost entirely upon depolarization ratios, Raman bands having depolarization ratios less than 6/7 belonging to species A'.

There should be one A'' fundamental and two A' fundamentals associated largely with C–F and C–C stretching and lying in the region from about 850 to 1300 cm^{-1}. The depolarized Raman band at 1165 cm^{-1} is undoubtedly the A'' fundamental and the strong partly polarized band at 1029 cm^{-1} one of the A' fundamentals. The band at 906 cm^{-1}, which is very weak in the Raman spectrum and of only medium intensity in the infrared, can be interpreted satisfactorily as an overtone or a combination band, and its assignment as a fundamental would result in a somewhat irregular correlation diagram. The band at 1111 cm^{-1}, which is somewhat stronger than the band at 906 cm^{-1} in the infrared but has not been observed in the Raman spectrum, has therefore been assigned as an A' fundamental. Since it can also be assigned as a

* This work has been supported in part by the U. S. Atomic Energy Commission under Contract No. AT-(40-1)-1074. The Raman data are taken from a thesis presented by Ching-Yu Liang to the Faculty of the Graduate College of the University of Oklahoma in partial fullfilment of the requirements for the degree of Doctor of Philosophy.

† Present address: Phillips Petroleum Company, Bartlesville, Oklahoma.

‡ Present address: Naval Ordnance Laboratory, Silver Spring, Maryland.

[1] Nielsen, Liang, Smith, and Smith, J. Chem. Phys. **21**, 383 (1953).

[2] See, in particular, Mizushima, Morino, Simanouti, and Kurani, J. Chem. Phys. **17**, 838 (1949), and D. T. Hamilton and F. F. Cleveland, J. Chem. Phys. **12**, 249 (1944).

[3] Lacher, McKinley, Walden, Lea, and Park, J. Am. Chem. Soc. **71**, 1334 (1949).

[4] Nielsen, Crawford, and Smith, J. Opt. Soc. Am. **37**, 296 (1947).

[5] Smith, Nielsen, and Claassen, J. Chem. Phys. **18**, 326 (1950).

[6] K. F. W. Kohlrausch, *Der Smekal-Raman-Effekt* (Julius Springer, Leipzig, 1931).

combination band, its assignment must be regarded as tentative.

In the region from about 570 to 850 cm^{-1}, one A'' and three A' fundamentals are to be expected involving

TABLE I. Infrared spectrum of CCl_3CF_2Cl (liquid).

Wave number	Description	Interpretation
331[a]	w	$A'+A''$ fundamentals
~340[a]	vw	165+183=348 A''; 81+268=349 A'
375[a]	vw	456−81=375 A'
420[a]	s	A' fundamental
444	m	A' fundamental
456	s	A'' fundamental
~473	vw	81+165+231=477 A''
486	w	165+331=496
~513	vw	183+331=514
525	w	A' fundamental; 81+445=526 A'
~543	vw	81+456=537 A'; 2×268=536 A'
~586	vw	165+421=586 A'
600	vw	268+331=599
627	s	A' fundamental
662	vw	2×331=662
675	vw	231+445=676 A'
~688	vw	268+421=689 A''; 231+456=687 A'' 165+524=689 A'
~699	vw	183+524=707 A''; 81+627=708 A''
751	s	331+421=752; 231+524=755 A'
775	vs	A' fundamental; 331+445=776
847	vs, b	$A'+A''$ fundamentals
877	s	421+456=877 A''
905	m	445+456=901 A''; 2×456=912 A'
~935	m	81+856=937 A''; 165+776=941 A'
1000	w	231+776=1007 A'
1027	vs, sh	A' fundamental
1072	m, sh	445+627=1072 A'
1080	m, sh	456+627=1083 A''; 231+844=1075 A'' 231+856=1087 A'
1111	m, sh	A' fundamental; 268+844=1112 A' 81+1027=1108 A''; 331+776=1107
1139	vw	268+421+456=1145 A'?
1163	vs	A'' fundamental
1252	w, sh	2×627=1254 A'; 231+1028=1259 A'
1290	w	445+844=1289 A''; 268+1028=1296 A''
1312	w, sh	456+856=1312 A''
1335	w	231+1111=1342 A'; 165+1164=1329 A''
1351	w	183+1164=1347 A'; 331+1028=1359
~1399	vw	627+776=1403 A'; 231+1164=1395 A''
1429	vw	268+1164=1432 A'
~1443	vw	331+1111=1442; 421+1028=1449 A'
~1471	vw	445+1028=1473 A'; 627+844=1471 A''
1481	w, sh	456+1028=1484 A''
~1550	vw	2×776=1552 A'; 524+1028=1552 A'
1618	w	456+1164=1620 A'
1650	w, sh	627+1028=1655 A'
1658	vw	421+456+776=1655 A''
~1689	vw	524+1164=1688 A''; 2×844=1688 A'
1701	w	844+856=1702 A''
~1783	vw	627+1164=1791 A''
1795	w, sh	776+1028=1804 A'
1880	vw	856+1028=1884 A'; 776+1111=1887 A'
1942	vw	776+1164=1940 A''
2016	w	856+1164=2020 A''
~2045	vw	2×1028=2056 A'
2101	vw	81+856+1164=2101 A'?
2151	vw	1028+1111=2139 A'
2188	w, sh	1028+1164=2192 A''
2237	vw	2×1111=2222 A'?
~2304	vw	81+2×1111=2303 A''?
2320	w	2×1164=2328 A'
~2400	vw	183+2×1111=2405 A''?
3335	vw	3×1111=3333 A'?
3450	vw	1111+2×1164=3439 A'?

[a] Observed with KRS-5 prism.

TABLE II. Raman spectrum of CCl_3CF_2Cl (liquid).

Wave number	Relative intensity		Polarization	Exciting Hg lines	Interpretation
81	6		dp	*ek*	A'' fundamental
165	12		0.8	*e*	A' fundamental
183	25		0.9	±*e*	A'' fundamental
231	37		0.62	±*ek*	A' fundamental
268	38	d	0.88	±*ek*	A'' fundamental
298	vvw		p?	*e*	
331	40		0.75	±*eki*	$A'+A''$ fundamentals
422	100		0.07	±*efki*	A' fundamental
441	~30		p	±*ek*	A' fundamentals Cl^{37}
445.8	77	sh	0.2	±*efki*	A' fundamentals Cl^{35}
456	21		~0.8	±*eki*	A'' fundamental
523	5		0.2	*ek*	A' fundamental
579	3		p	*e*	165+422=587 A'
598	vw			*e*	268+331=599
626.8	73	sh	0.07	±*efki*	A' fundamental
637	vvw			*e*	183+456=639 A'
751	vw			*e*	331+422=753
777	5		0.6	*ek*	A' fundamental
844	21	d	0.83	*eki*	A'' fundamental
856					A' fundamental
906	vvw			*e*	446+456=902 A''
1029	16	d	0.62	*eki*	A' fundamental
1165	8	d	0.88	*ek*	A'' fundamental

TABLE III. Infrared spectrum of CCl_3CFCl_2 (solid glass, CS_2 solution).

Wave number	Description	Interpretation
~266[a]	m	A'' fundamental
~281[a]	m,d	A' fundamental
315[a]	m	$A'+A''$ fundamentals
342[a]	w	77+265=342 A'; 2×174=348 A'
~269[a]	vw	595−227=368 A''
382[a]	w	A' fundamental
~395[a]	w	A'' fundamental
407[a]	m, sh	A' fundamental
438[a]	w	174+265=439
~470	vw	77+395=472 A'
508	m, sh	A' fundamental
~532	vw	2×265=530 A'
~565	vw	2×281=562 A'; 174+395=569
602	vw	227+382=609 A'
619	vw	227+395=622 A''
629	w	2×315=630
636	vw	227+407=634 A'
667	w	281+382=663 A'; 266+407=673 A''
~675	vvw	281+395=676 A''
~691	m	281+407=688 A'; 315+382=697
725	vs, sh	A' fundamental
~741	w	227+507=734 A'?
~773	w	265+507=772 A''; 382+395=777 A''
796	vs, sh	A'' fundamental
~803	s	395+407=802 A''; 77+724=801 A''
~820	m	315+507=822; 227+595=822 A''
847	vs, sh	A' fundamental
~880	w	77+796=873 A'
883	vs	A'' fundamental
893	m	174+724=898; 382+507=889 A'
~905	w	395+507=903 A''
907	vs	407+507=914 A'
957	w	77+883=960 A'; 227+724=951 A'
~969	vw	174+796=970
~990	w	265+724=989 A''
1010	vs, sh	2×507=1014 A'; 281+724=1005 A'
1038	m	315+724=1039
1072	m	227+847=1074 A'; 281+796=1079 A''
1101	vs, sh	A' fundamental
1109	m	227+883=1110 A''; 315+796=1111; 265+847=1112 A''
~1168	w	281+883=1164 A''; 315+847=1162

TABLE III.—*Continued.*

Wave number	Description	Interpretation
1179	m	382+796=1178 A'' 77+1101=1178 A''; 174+1010=1184
1227	m	382+847=1229 A'; 507+724=1231 A'
~1253	w	407+847=1254 A'
1272	m	265+1009=1274 A''; 174+1101=1275; 395+883=1278 A'
~1304	w	507+796=1303 A''
1351	w, sh	507+847=1354 A'
1385	w, sh	281+1101=1382 A'; 507+883=1390 A''; 382+1009=1391 A'
1418	vw	315+1101=1416; 407+1009=1416 A'
~1484	vw	382+1101=1483 A'
1513	w	507+1009=1516 A'; 407+1101=1508 A'
1600	w	724+883=1607 A''; 507+1101=1608 A'; 2×796=1592 A'
1631	w	796+847=1643 A''
~1675	vw	796+883=1679 A'
1686	w	2×847=1694 A'
1805	w, sh	796+1009=1805 A''
~1855	vw	847+1009=1856 A'
~1908	vw	796+1101=1897 A''
1938	w, sh	847+1101=1948 A'
2000	w	883+1101=1984 A''; 2×1009=2018 A'
2100	m, sh	1009+1101=2110 A'
2180	m, sh	2×1101=2202 A'

[a] Observed with KRS-5 prism.

TABLE IV. Raman spectrum of CCl_3CFCl_2 (liquid).

Wave number	Relative intensity	Depolarization	Exciting Hg lines	Interpretation
77	~14	dp	*ek*	A'' fundamental
174	14	0.87	*e*	A'+A'' fundamentals
227	54	0.59	±*ek*	A' fundamental
265	20	0.8	±*ek*	A'' fundamental
281.0	8 sh	0.17	±*ek*	A' fundamental
314	21	0.65	±*ek*	A'+A'' fundamentals
381.5	71 sh	0.3	±*eki*	A' fundamental
395	~20	dp	±*eki*	A'' fundamental
407.8	75 sh	0.2	±*eki*	A' fundamental
488	vw		*e*	227+265=492 A''
505.4	100 sh	0.08	±*eki*	A' fundamental
723	vw		*e*	A' fundamental
797	4 d	0.88	*ek*	A'' fundamental
848	10 d	0.68	*ek*	A' fundamental
882	15 d	0.59	*ek*	A'' fundamental [382+507=889 A']
907	vw		*ek*	395+507=902 A''
1008	13	0.37	*ek*	A' fundamental
1100	5	0.83	*ek*	A' fundamental

largely C−Cl stretching. Although their proximity prevents measurement of separate depolarization ratios, the strong Raman band at 856 cm^{-1} appears to be polarized and that at 844 cm^{-1} to be depolarized. They are therefore interpreted as A' and A'' fundamentals, respectively. In the infrared these bands are not resolved, but only a single broad absorption maximum is observed. The two other A' fundamentals in this spectral region are readily identified with the bands at 776 and 627 cm^{-1}.

In the region from 300 to 600 cm^{-1} there should lie four A' and two A'' fundamentals involving deformations of the end groups of the molecule. Six Raman bands have been observed in this region. However, the sharp band at 441 cm^{-1} lies close to the roughly three-times stronger band at 445 cm^{-1} and probably arises from molecules having a Cl^{37} atom in the CF_2Cl group. Thus, there is one band too few. Either the missing fundamental is too weak to be observable or it overlaps another fundamental. It has been tentatively assumed that the strong band at 331 cm^{-1}, which has a rather high depolarization ratio, represents a superposition of an A' and an A'' fundamental. In the infrared spectrum the absorption maximum at 331 cm^{-1} is accompanied by a weaker maximum at about 340 cm^{-1} which may be evidence of the assumed overlapping. The bands at 421 and 445 cm^{-1} undoubtedly represent A' fundamentals, while the band at 456 cm^{-1} must be interpreted as an A'' fundamental. The last A' fundamental in this region has been identified with the band at 524 cm^{-1} which is fairly weak in both spectra but cannot be interpreted as 81+445=526 A'', since it is definitely polarized in the Raman spectrum.

TABLE V. Fundamental vibration frequencies for CCl_3CF_2Cl.

Symmetry species	Wave number Raman (liquid)		Wave number Infrared (liquid)		Approximate character
A''	81	w	—		Torsion
A'	165	w	—		CCl_3 rocking
A''	183	m	—		CCl_3 rocking
A'	231	s	—		CCl_3 deformation
A''	268	s	—		CF_2Cl rocking
A'+A''	331	s	331	w	CCl_3 deformations
A'	422	vvs	420	s	CCl_3 deformation
A'	445.8	vs	444	m	CF_2Cl deformation
A''	456	m	456	s	CF_2Cl deformation
A'	523	w	525	w	CF_2Cl deformation
A'	626.8	vs	627	s	CCl stretching
A'	777	w	775	s	CCl stretching
A''	844	w	847	vs	CCl stretching
A'	856	m			CCl stretching
A'	1029	m	1027	vs	CC stretching
A'	—		1111	m	CF stretching
A''	1165	w	1163	vs	CF stretching

TABLE VI. Fundamental vibration frequencies for CCl_3CFCl_2.

Symmetry species	Wave number Raman (liquid)		Wave number Infrared (glass)		Approximate character
A''	77	m	—		Torsion
A'+A''	174	m	—		CCl_3 rockings
A'	227	s	—		CCl_3 deformation
A''	265	m	266	w	$CFCl_2$ rocking
A'	281.0	w	281	w	$CFCl_2$ rocking
A'+A''	314	m	315	w	CCl_3 deformations
A'	381.5	vs	—		$CFCl_2$ deformation
A''	395	m	—		$CFCl_2$ deformation
A'	407.8	vs	407	m	$CFCl_2$ deformation
A'	505.4	vvs	508	m	CCl stretching
A'	723	vw	725	vs	CCl stretching
A''	797	w	796	vs	CCl stretching
A'	848	m	847	vs	CCl stretching
A''	882	m	883	vs	CCl stretching
A'	1008	m	1009	vs	CC stretching
A'	1100	w	1101	vs	CF stretching

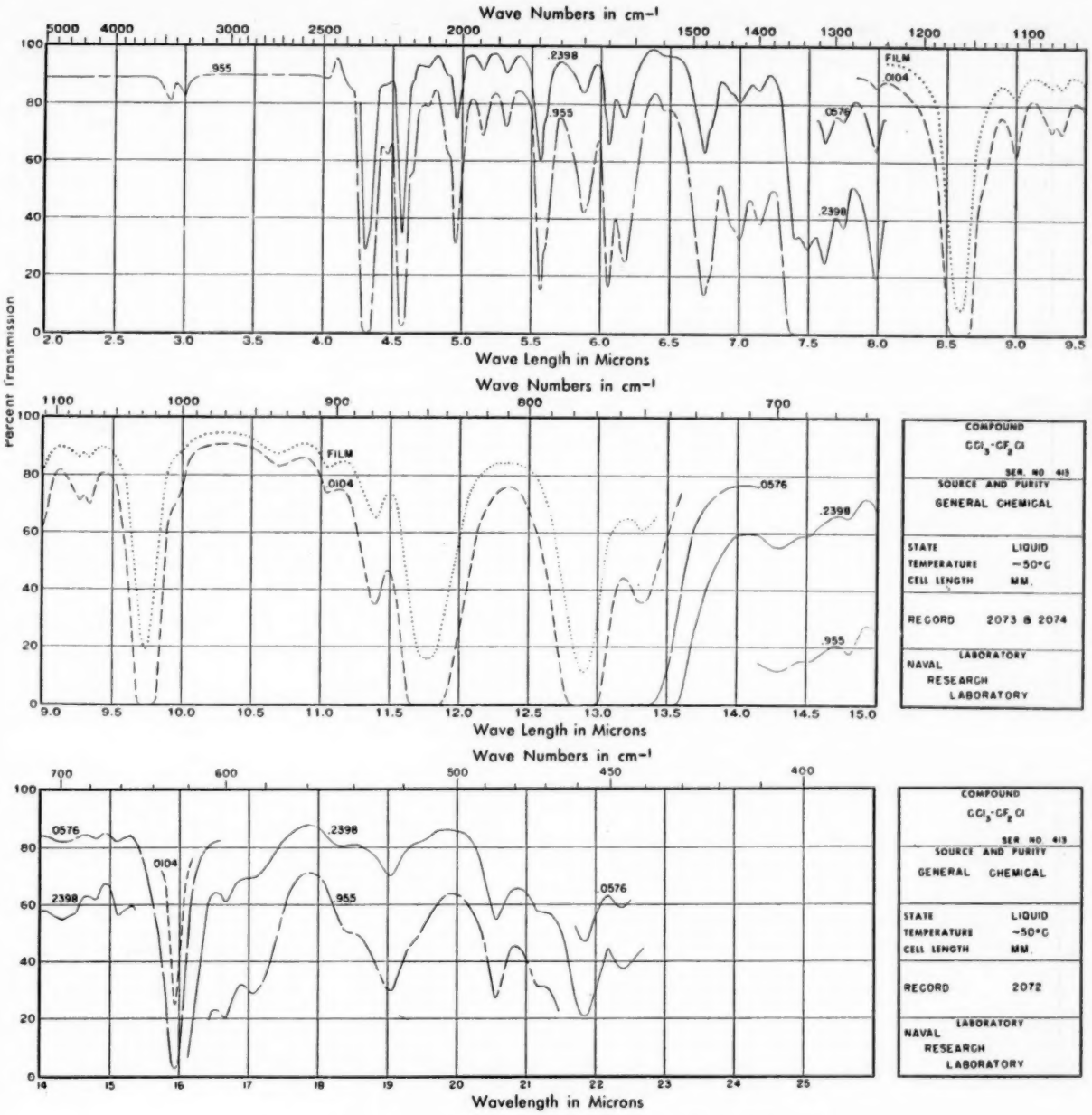

FIG. 1. Infrared spectrum of liquid CCl_3CF_2Cl at 50°C.

The remaining two A' and three A'' fundamentals, which must involve largely rocking and torsion, are identified with the observed Raman bands at 268, 231, 183, 165, and 81 cm^{-1}. That at 231 cm^{-1} definitely belongs to A' and those at 268 and 81 cm^{-1} to A''. Because of their proximity, the measured depolarization ratios for the bands at 183 and 165 cm^{-1} are not very accurate, and it is not quite certain which of them belongs to A' and which to A''.

The fundamentals assigned for CCl_3CF_2Cl are listed in Table V. On the basis of these fundamentals, it has been possible to interpret all of the observed infrared bands and all but one very faint Raman band. These interpretations are given in the last columns of Tables I and II.

2. CCl_3CFCl_2

This molecule also has the symmetry C_s and hence eleven A' and seven A'' fundamentals. The two highest Raman frequencies, 1100 and 1008 cm^{-1}, and their very strong infrared counterparts, undoubtedly represent A' fundamentals involving C—F and C—C stretching. The high depolarization ratio observed for the former probably results from overlapping with three binary combination bands of species A''. In the infrared spectrum the presence of these bands is indicated by a shoulder.

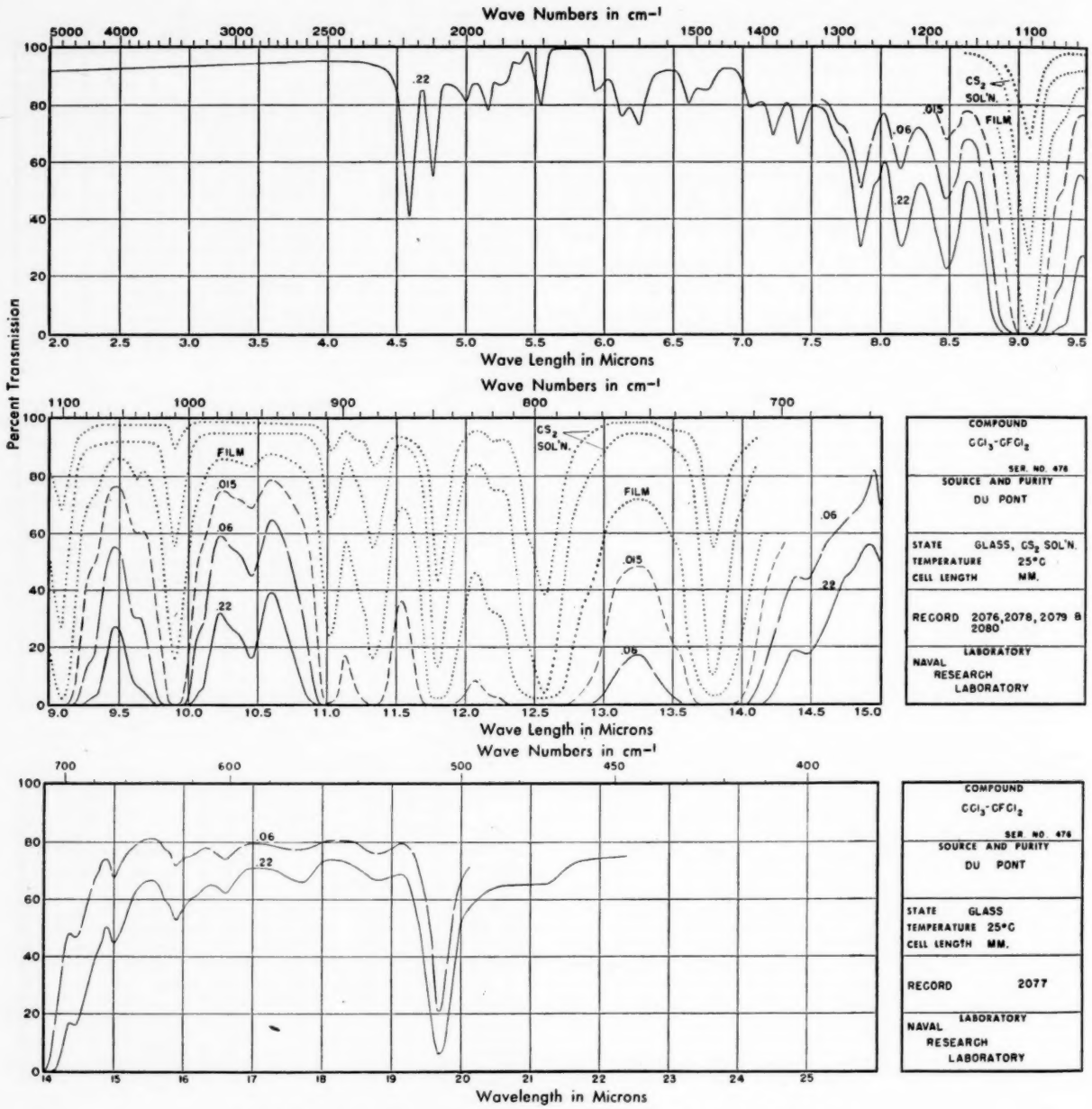

FIG. 2. Infrared spectrum of CCl_3CFCl_2 as solid (glass) and in CS_2 solution.

The bands at 883, 847, 796, 724, and 507 cm^{-1} must also be interpreted as fundamentals. They correspond to motions that are largely C—Cl stretching. The band at 796 cm^{-1} definitely belongs to A''. The other A'' fundamental in this region must then be either 883 or 847. The former has been chosen, since that makes the correlation diagram more regular, and since its low depolarization ratio can be explained by overlapping with $382+507=889$ A'.

So as to assign all of the fundamentals associated with deformation, rocking, and twisting of the molecule it has been assumed that each of the Raman bands at 174 and 314 cm^{-1} represents a superposition of A' and A'' fundamentals. The former appears actually as an unresolved doublet, and the latter has a rather high depolarization ratio. An alternative to the assumption that 314 represents two fundamentals would be the assignment of the weak infrared band at 342 cm^{-1} as an A'' fundamental. However, this band can be interpreted as $77+265=342$ A' or as $2\times174=348$ A'. The assignment of species for the remaining fundamentals in this region represents no difficulty.

The fundamental vibration frequencies assigned for the CCl_3CFCl_2 molecule are listed in Table VI. On the basis of these fundamentals all observed infrared and Raman bands have been interpreted. The interpretations are listed in the last columns of Tables III and IV.

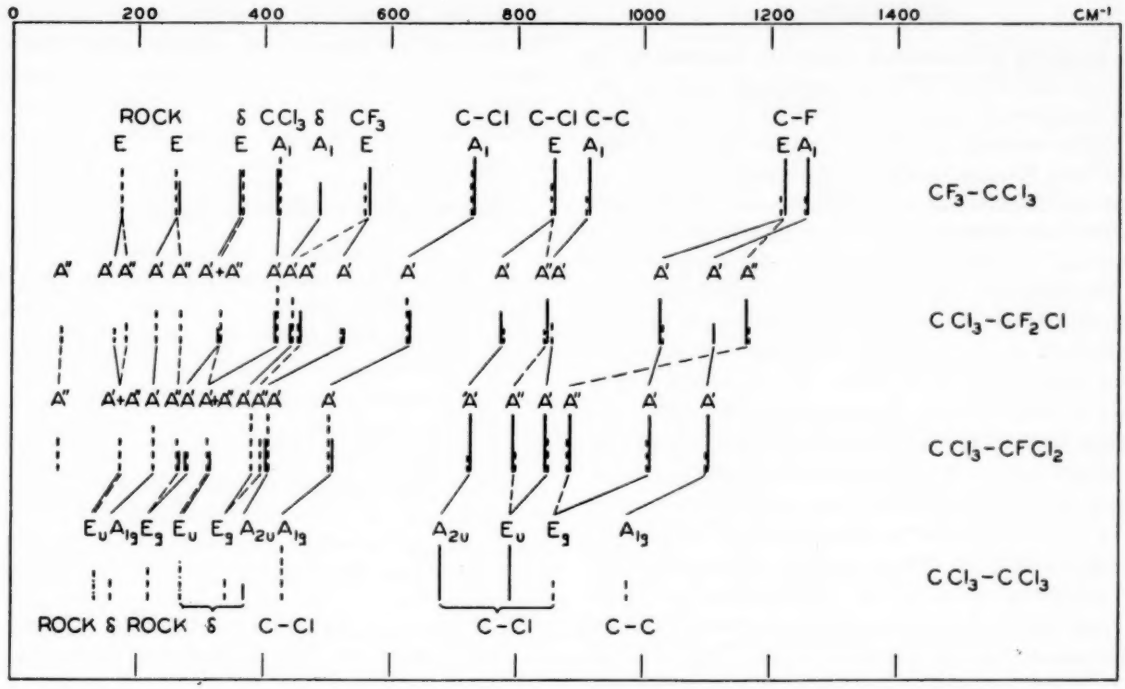

FIG. 3. Fundamental vibration frequencies of CCl_3CF_3, CCl_3CF_2Cl, CCl_3CFCl_2, and CCl_3CCl_3.

TABLE VII. Calculated thermodynamic functions for CCl_3CF_2Cl at one atmosphere (in cal/deg mole).

T°K		$(H^0-H_0^0)/T$	C_p^0	S^0	$-(F^0-H_0^0)/T$
	Tr+Rot	7.949	7.949	68.796	60.847
	Vib	5.870	13.644	8.674	2.804
200	Tor	1.464	1.932	3.088	1.624
	Total	15.28	23.52	80.56	65.28
	Tr+Rot	7.949	7.949	71.969	64.020
	Vib	9.270	19.488	15.012	5.742
298.16	Tor	1.624	1.962	3.867	2.243
	Total	18.84	29.40	90.85	72.00
	Tr+Rot	7.949	7.949	72.360	64.411
	Vib	9.782	20.214	15.996	6.214
313.16	Tor	1.642	1.964	3.965	2.323
(mp)	Total	19.37	30.13	92.32	72.95
	Tr+Rot	7.949	7.949	73.570	65.621
	Vib	11.443	22.404	19.316	7.873
364.66	Tor	1.687	1.970	4.264	2.577
(bp)	Total	21.08	32.32	97.15	76.07
	Tr+Rot	7.949	7.949	74.305	66.356
	Vib	12.439	23.626	21.369	8.930
400	Tor	1.712	1.973	4.445	2.733
	Total	22.10	33.55	100.12	78.02
	Tr+Rot	7.949	7.949	76.079	68.130
	Vib	14.965	26.332	26.952	11.987
500	Tor	1.765	1.978	4.887	3.122
	Total	24.68	36.26	107.92	83.24
	Tr+Rot	7.949	7.949	77.528	69.579
	Vib	16.970	28.107	31.873	14.903
600	Tor	1.800	1.981	5.247	3.441
	Total	26.72	38.04	114.65	87.93

TABLE VIII. Calculated thermodynamic functions for CCl_3CFCl_2 at one atmosphere (in cal/deg mole).

T°K		$(H^0-H_0^0)/T$	C_p^0	S^0	$-(F^0-H_0^0)/T$
	Tr+Rot	7.949	7.949	69.433	61.484
	Vib	6.512	15.487	9.766	3.254
200	Tor	1.487	1.937	3.186	1.699
	Total	15.95	25.37	82.38	66.44
	Tr+Rot	7.949	7.949	72.602	64.653
	Vib	10.468	21.164	16.971	6.503
298.16	Tor	1.641	1.964	3.966	2.325
	Total	20.06	31.08	93.54	73.48
	Tr+Rot	7.949	7.949	74.391	66.442
	Vib	12.933	24.139	22.177	9.244
373.16	Tor	1.707	1.973	4.409	2.702
(mp)	Total	22.59	34.06	100.98	78.39
	Tr+Rot	7.949	7.949	75.142	67.194
	Vib	13.997	25.307	24.514	10.517
410.16	Tor	1.731	1.975	4.595	2.864
(bp)	Total	23.68	35.23	104.25	80.58
	Tr+Rot	7.949	7.949	76.716	68.768
	Vib	16.229	27.417	29.739	13.510
500	Tor	1.775	1.979	4.987	3.212
	Total	25.95	37.34	111.44	85.49
	Tr+Rot	7.949	7.949	78.166	70.217
	Vib	18.037	29.022	34.690	16.653
600	Tor	1.809	1.982	5.347	3.538
	Total	27.80	38.95	118.20	90.41
	Tr+Rot	7.949	7.949	79.391	71.442
	Vib	19.860	30.096	39.452	19.592
700	Tor	1.834	1.983	5.653	3.819
	Total	29.64	40.03	124.50	94.85

DISCUSSION

The assigned fundamental vibration frequencies for CCl_3CF_2Cl and CCl_3CFCl_2 are correlated with the previously assigned fundamentals of CCl_3CF_3 and C_2Cl_6 in Fig. 3. Solid vertical lines denote infrared bands, broken vertical lines Raman bands. Dash-dotted lines indicate frequencies inferred from overtone or combination bands but not observed directly. Coincident infrared and Raman frequencies are shown by slightly separated lines. The height of each vertical line roughly indicates the band intensity. Corresponding totally-symmetric fundamentals of the different molecules are joined by slanting solid lines, and other corresponding fundamentals by broken lines. No solid lines may cross, and no broken lines may cross. For this reason such a correlation diagram is more useful than one connecting corresponding "group frequencies."

The regularity of the correlation diagram supports the assignments made. As already mentioned, the highest A' fundamental for CCl_3CF_2Cl is somewhat uncertain, as are the species of the fundamentals 165 and 183 and the assumption that 331 is double. For CCl_3CFCl_2 similar uncertainties exist for the frequencies 883, 847, 314, and 174 cm^{-1}.

One Raman band of CCl_3CF_2Cl remains uninterpreted and may be caused by an impurity. Eight of the 62 infrared absorption maxima observed for this compound are interpreted as ternary combination bands. Because of the considerable density with which such combinations are distributed over most of the frequency range and their generally low intensities, these interpretations are open to some doubt. For CCl_3CFCl_2 the interpretation of the spectra is entirely satisfactory.

CALCULATED THERMODYNAMIC FUNCTIONS

Assuming the distance C—C 1.54, C—F 1.37, and C—Cl 1.77A, and tetrahedral angles, we obtain the following principal moments of inertia: for CCl_3CF_2Cl 687.4, 906.6 and 950.6×10^{-40} $g\ cm^2$, and for CCl_3CFCl_2 823.8, 971.6 and 1118.8×10^{-40} $g\ cm^2$. From these data and the fundamental frequencies listed in Tables III and VI the heat capacity, entropy, Gibbs free-energy function, and heat-content function have been calculated for these compounds as ideal gases at one atmosphere and at different temperatures. The torsional oscillation, or lowest A'' fundamental, has been treated as an ordinary vibration, since the potential barrier opposing internal rotation is very high for these molecules. The calculated thermodynamic functions are listed in Tables VII and VIII. No calorimetric data appear to be available with which to compare these results.

The writers wish to express their indebtedness to General Chemical Division, Allied Chemical and Dye Corporation, and to E. I. duPont de Nemours and Company, Inc., for the gift of the samples.

The Infrared Spectrum of Fluoroform from 2.2 to 20μ*

H. D. Rix
The Pennsylvania State College, State College, Pennsylvania
(Received February 3, 1953)

The absorption spectrum of fluoroform has been investigated with a Perkin-Elmer double-pass spectrometer from 2.2 to 20μ. The resolution is sufficient to make possible an unequivocal assignment of all six fundamentals on the basis of the observed band envelopes. An anomaly is found in the symmetrical C-F stretching vibration; on the evidence now available this vibration should be assigned to the parallel band at 1209.3 cm^{-1} in the infrared (vapor) and to the polarized Raman line (liquid) at 1117 cm^{-1}. Overtone and combination bands measured include the A_1 and E components of the second harmonic of each of the three degenerate fundamentals. The separation of the maxima of the P and R branches of the parallel bands is discussed in relation to the theory of Gerhard and Dennison.

IN connection with some high resolution work on the overtones of fluoroform in this laboratory it was considered advisable to re-examine the fundamentals. Previous infrared work[1,2] indicated doubt as to the character of the two of lowest frequency and the value of the frequency of the symmetrical C-F stretching vibration. This study was carried out on the new double-pass Perkin-Elmer spectrometer, made available recently, which has considerably more resolving power than the Model 12-C. Measurements were made with LiF, NaCl, and KBr prisms, and the frequencies determined from calibration curves made from the spectra of CH_4, HBr, CO, H_2O, NH_3, and CH_3OH. Two different samples of the vapor were studied in a 10-cm cell, the pressures ranging from atmospheric down to low enough values to make use of the full resolving power of the spectrometer. While this instrument is not capable of resolving the rotational structure of a molecule with moments of inertia such as those of fluoroform, the envelopes of the bands for the six fundamentals, as well as those of a number of combinations and overtones, are clearly distinguished.

DISCUSSION OF THE FUNDAMENTALS

The fluoroform molecule, being a symmetric top of symmetry C_{3v}, has six fundamental modes of vibration represented by three parallel and three perpendicular type bands all of which are both infrared and Raman active.[3] A trace of the infrared spectrum for the region 2.2 to 20μ is given in Fig. 1, and the wave numbers and assignments of the bands are given in Table I. The three perpendicular fundamentals (species E) at 1375, 1152.0, and 507.6 cm^{-1} are seen to have a very simple form consisting only of a strong central absorption maximum. The various sub-bands, corresponding to different values of the quantum number K, which have been resolved in many other molecules of this symmetry class, are here so overlapped that they cannot be separated even by a spectrograph of much higher resolving power than the one employed in this work.

The other three fundamentals at 3035.0, 1209.3, and 699.2 cm^{-1} all exhibit the P, Q, R structure found in bands of species A_1 of the C_{3v} symmetric tops. The high frequency vibration representing the C-H symmetrical stretching mode is observed to have what appears to be a superfluous Q branch at 3042.0 cm^{-1}. While this 3042 cm^{-1} band should probably be ascribed to an impurity since no combination of the other fundamentals seems capable of yielding a band of this frequency, still it occurs in both samples, remains strong at low vapor pressure with only a 10-cm path, and does not appear to be found in the other freons. It may be noted that the Q branch of the 3035 cm^{-1} band has a sharp edge on the short-wavelength side as has been found in both the first and second overtones, while the 3042 cm^{-1} band is sharp on the long-wavelength side. The low frequency fundamental at 699.2 cm^{-1} shows the same separation between the maxima of the P and R branches, about 37 cm^{-1}, as the high frequency one. The P branch is somewhat distorted by atmospheric absorption. The intermediate frequency fundamental of the parallel type at 1209.3 cm^{-1} is partly covered by the very strong perpendicular band at 1152.0 cm^{-1}. However, the R and Q branches are

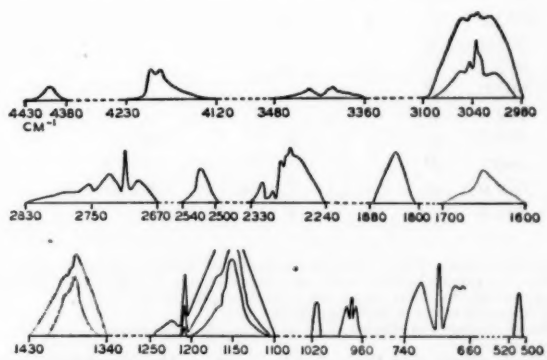

FIG. 1. Infrared absorption spectrum of CF_3H from 500 to 4430 cm^{-1} at various vapor pressures. Bands distorted by atmospheric absorption are indicated by dotted lines.

* This research was assisted by support from the U. S. Office of Naval Research.

[1] H. J. Bernstein and G. Herzberg, J. Chem. Phys. **16**, 30 (1948) (reporting the unpublished measurements of the fluoroform fundamentals of W. C. Price).

[2] E. K. Plyler and W. S. Benedict, J. Research Natl. Bur. Standards **47**, 202 (1951).

[3] G. Herzberg, *Infrared and Raman Spectra of Polyatomic Molecules* (D. Van Nostrand Company, Inc., New York, 1945).

well resolved, the separation of these two being about 16 cm^{-1}.

As mentioned above, there has been some question about the assignment of the symmetrical and the degenerate CF_3 deformation vibrations. The band here measured at 699.2 cm^{-1} has a sharp Q branch with prominent P and R branches, while the one at 507.6 cm^{-1} has only a central maximum which although not very broad is definitely not sharp on either side. Thus there can be no question that these are, respectively, parallel and perpendicular bands of species a_1 and species e. This evidence agrees with the polarization data[4] of Rank, Shull, and Pace who report a partly polarized line at 697 and a depolarized one at 508 cm^{-1}. A comparison of the infrared and Raman[5] measurements for all six fundamentals is given in Table II.

TABLE I. Infrared spectrum of fluoroform from 2.2 to 20μ.

ν_{vac}(obs) cm^{-1}	Band type and intensity[a]		Assignment	Species	ν_{vac}(calc)[b] cm^{-1}
4400	⊥	w.	$\nu_1+\nu_4$	E	4410
4189		m.	$\nu_1+\nu_5$	E	4187
4177					
3440		v.w.	$3\nu_5$	A_1+E	3456
3410		w.	$\nu_3+2\nu_4$	A_1+E	3450
3054.5	R				
3035.0	Q	v.s.	ν_1	a_1	
3017.3	P				
3042.0		m.	Impurity?		
2754.4	⊥	m.	$2\nu_4$	E	
2729.2	R				2750
2710.5	Q	m.	$2\nu_4$	A_1	
2692.9	P				
2519.8	?	m.	$\nu_4+\nu_5$	A_1+E	2527
2318	⊥	w.	$\nu_2+\nu_5$	E	2361
2305	Q?	v.w.	$\nu_1-\nu_3$	A	2336
2294.4	⊥	m.	$2\nu_5$	E	
2287.4	sh				
2283.2	Q	s.	$2\nu_5$	A_1	2304
2276.7	sh				
1849	⊥	m.	$\nu_3+\nu_5$	E	1851
1654[c]		m.	$\nu_5+\nu_6$	A_1+E	1660
1385[c]	sh		$2\nu_3$	A_1	1398
1375[c]	⊥	s.	ν_4	e	
1225.6	R				
1209.3	Q	m.	ν_2	a_1	
1185	sh		$\nu_3+\nu_6$	E	1206
1152.0	⊥	v.s.	ν_5	e	
1015.2	⊥	w.	$2\nu_6$	E	
977.8	R				1015
972.4	Q	w.	$2\nu_6$	A_1	
967.6	P				
719.5	R				
699.2	Q	s.	ν_3	a_1	
680[c]	P				
672.6	Q	w.	$2\nu_3-\nu_3$	A_1	
507.6	⊥	m.	ν_6	e	

[a] Abbreviations R, Q, P denote envelopes of R, Q, P branches of parallel bands. ⊥ = perpendicular band, sh = shoulder, v.s., s., m., w., v.w. = very strong, strong, medium, weak, very weak, respectively.
[b] Neglecting effect of anharmonicity.
[c] Band obscured or distorted by atmospheric absorption.

[4] Rank, Shull, and Pace, J. Chem. Phys. **18**, 885 (1950).
[5] Earlier Raman wave-number measurements without polarization data were made by G. Glockler and W. F. Edgell, J. Chem. Phys. **9**, 224 (1941).

Concerning the C-F stretching vibrations there is still a serious difficulty. While the infrared shows a parallel band of medium intensity at 1209.3 cm^{-1}, in which the Q branch is sharp and moderately strong, the Raman work shows a very strong, partly polarized line presumably representing the same vibration at 1117 cm^{-1}. Similarly the strongest band of the infrared system at 1152.0 cm^{-1} is clearly a perpendicular band, while there is a weak depolarized Raman line at 1160 cm^{-1}. On the basis of the band envelope, polarization, and relative intensity data it would appear that ν_3 is 92 cm^{-1} higher in the infrared (vapor) than in the Raman (liquid) spectrum, while ν_4 is 8 cm^{-1} lower; moreover, ν_3 would be of higher frequency than ν_4 in the infrared but lower in the Raman. The explanation previously advanced[2,4] to resolve this difficulty that the 1209 cm^{-1} band is a combination of $\nu_3+\nu_6$ is now seen to be untenable, as that combination would be of species E (it is apparently found in the infrared spectrum as a shoulder on ν_4 at 1185 cm^{-1}), but the present study shows the 1209 cm^{-1} band to be of species A. Also no other combination of species A should occur in this region. Further support for this infrared assignment can be found in the infrared spectrum of methyl fluoroform[6] in which the corresponding C-F stretching vibrations are assigned to the 1281(a_1) and 1234(e) cm^{-1} bands, the envelopes of which clearly mark them, respectively, as parallel and perpendicular bands.

Owing to the strongly electronegative character of the fluorine atom, frequency shifts in the liquid phase are to be anticipated. Thus the C-H stretching frequency for fluoroform is 27 cm^{-1} higher in the Raman (liquid) spectrum than in the infrared. As another example of such a shift may be mentioned the symmetrical C-F stretching frequency in difluoromethane, which is observed[7] at 1116 cm^{-1} in the infrared and 1078 cm^{-1} in the Raman.[4] If the magnitude of these shifts may be expected to increase with the number of fluorine atoms in the molecule, a shift of appreciably more than the 38 cm^{-1} observed in difluoromethane for the vibration in question should certainly be possible in fluoroform. Unless evidence to the contrary is obtained from a Raman spectrum taken in the vapor phase, it would seem that it is in this direction one should look for an explanation of the present anomalies in the infrared and Raman spectra of fluoroform.

OVERTONE AND COMBINATION BANDS

In the spectral region investigated in this study a number of overtone and combination bands could be identified using only a 10-cm absorption path. The first overtones of the perpendicular fundamentals should each be represented by two components, one perpendicular and one parallel. The perpendicular component for $2\nu_4$ appears at 2754.4 cm^{-1}, the Q branch of the parallel component at 2710.5 cm^{-1}. The separation of

[6] Cowan, Herzberg, and Sinha, J. Chem. Phys. **18**, 1538 (1950).
[7] H. B. Stewart and H. H. Nielsen, Phys. Rev. **75**, 640 (1949).

TABLE II. Fundamentals of fluoroform.

Vibration	Assignment	Price	Infrared (vapor) Plyler and Benedict	Present work	Raman (liquid) Glockler and Edgell	Rank, Shull, and Pace
Symmetric C-H stretching	$\nu_1(a_1)$	3035.6	3031	3035.0	3062.0	3062 pol.[c]
Symmetric C-F stretching	$\nu_2(a_1)$	1209	(1150?)[b]	1209.3	1116.5	1117 p.pol.
Symmetric CF_3 deformation	$\nu_3(a_1)$	703.2	700	699.2	696.7	697 p.pol.
Degenerate C-H bending	$\nu_4(e)$	1351.5	1372	1375	1376.2	1376 dep.
Degenerate C-F stretching	$\nu_5(e)$	1152.4	1152	1152.0	936.8[a]	1160 dep.
Degenerate CF_3 deformation	$\nu_6(e)$	509.4	507	507.6	508.1	508 dep.

[a] This line is apparently due to an impurity. The authors did not observe the weak line at 1160 cm^{-1}, which shows up clearly in the polarization plates of Rank, Shull, and Pace but is barely resolved from the heavy 1117 cm^{-1} line on the ordinary Raman plate.
[b] This is a hypothetical band presumed to be covered by the strong band at 1152 cm^{-1}. The authors report a band at 1206 cm^{-1} which they assign to $\nu_3+\nu_6$.
[c] pol. =polarized, p.pol. =partly polarized, dep. =depolarized.

the maxima of the P and R branches of the parallel component is about 36 cm^{-1}, close to the corresponding separations for the fundamental bands of the parallel type. The two components of $2\nu_6$ are likewise clearly resolved, and the separation of the perpendicular component from the Q branch of the parallel component, 42.8 cm^{-1}, is about the same as for $2\nu_4$. However, in this band the P and R branch maxima are only about 10 cm^{-1} apart. For $2\nu_5$ the structure is less clearly resolved. What appears to be the Q branch of the parallel component is the central peak of the strong band at 2283.2 cm^{-1} which has partially resolved shoulders with a separation of about 10 cm^{-1} that might be the P and R branch maxima. In this same region are absorption peaks of medium intensity at 2318 and 2294 cm^{-1} with a weak band between them at 2305 cm^{-1}. One of these, probably the one at 2294 cm^{-1}, must be the perpendicular component of $2\nu_5$, while the one at 2318 cm^{-1} is possibly $\nu_2+\nu_5$, and the weak band between them could be the difference band $\nu_1-\nu_3$.

In the shortest-wavelength region investigated in this study there is a weak perpendicular band at 4400 cm^{-1}, which is $\nu_1+\nu_4$. Below this is a double-headed band with peaks at 4189 and 4177 cm^{-1} representing $\nu_1+\nu_5$. The presence of two maxima here may arise from the 3042 cm^{-1} band described above. Below the region of intense atmospheric absorption are two weak bands at 3440 and 3410 cm^{-1} which may be due to $\nu_3+2\nu_4$ and to $3\nu_5$ respectively, the resolution being too low to determine the character of the bands from their envelopes. A band of medium intensity at 2519.8 cm^{-1} is the combination $\nu_4+\nu_5$. The short-wavelength side of this band is sharp, but there is no resolution of the components for the A_1 and E states. The combination $\nu_3+\nu_5$ gives rise to a clear-cut perpendicular band at 1849 cm^{-1}. In the region of strong H_2O absorption below this there is a band which should represent the A_1 and E states of $\nu_5+\nu_6$. Beneath the overlapping water vapor band there is some suggestion of the two components expected, but there is nothing definite enough for accurate measurement. Finally, at 672.6 cm^{-1} there is a weak absorption peak which is probably the difference band $2\nu_3-\nu_3$.

MOMENTS OF INERTIA

A theoretical treatment of the relation between the separation of the maxima of the P and R branches and the moments of inertia of symmetric top molecules by Gerhard and Dennison[8] showed the separation of the maxima to be given by

$$\Delta\nu=(S/c\pi)(kT/I_B)^{\frac{1}{2}},$$

where S is a function that varies from about 1.55 for a disk-shaped molecule to 1.0 for the limiting case of a linear molecule (infinitely thin spindle). This theory yields moderately good results for the prolate tops such as the methyl halides, for which the variation of S with the ratio of the two unequal moments of inertia is small, permitting the calculation of the moment I_C about the figure axis when the other moment I_B is known. For the oblate tops such as fluoroform, however, the function S varies quite rapidly with the ratio of the two moments. Substituting the measured value[1] of I_B, 81.08×10^{-40} g cm^2, in the above equation along with an average value of $\Delta\nu$ for fluoroform of 37 cm^{-1}, one obtains a value of I_C of about 372×10^{-40} g cm^2, although the presumed value of I_C from the known bond distances and angles is of the order of 150×10^{-40} g cm^2. Inasmuch as a separation of 35 cm^{-1} would give I_C as 130×10^{-40}, it is apparent that measurements of this type cannot provide reliable information about the moments of inertia of oblate tops, since the uncertainty of the measurement is at least one or two wave numbers.

Acknowledgments are due Dr. W. H. Pearlson of the Minnesota Mining and Manufacturing Company and Dr. R. C. McHarness of the Jackson Laboratory for making available the samples of fluoroform.

[8] S. L. Gerhard and D. M. Dennison, Phys. Rev. **43**, 197 (1933).

Theory of Radiation Chemistry. II. Track Effects in Radiolysis of Water*

ARYEH H. SAMUEL AND JOHN L. MAGEE
Department of Chemistry, University of Notre Dame, Notre Dame, Indiana†
(Received January 6, 1953)

A model is presented which describes the geometrical effects in the radiolysis of water as a result of the diffusion of free radicals. The motion of secondary electrons immediately following the passage of the ionizing particle is discussed in an appendix, and it is concluded that radicals are most likely formed in pairs at the approximate sites of the original ionizations. Models for the diffusion of these radicals are shown to result in a definite fraction of radicals which undergo initial recombination for gamma- and fast beta-rays, for which the spurs are considered as diffusing independently. For alpha-rays a connected-track model is used. For the intermediate case of tritium beta-rays, a two-stage model is constructed. In each case the comparative yields of the "forward" and "radical" reactions (G_F and G_R) are calculated. Subsequent chemical effects in pure water and solutions are also considered briefly.

IN the first paper of this series,[1] the importance of track effects and spatial inhomogeneity in the consideration of radiation chemical reactions was pointed out. In this paper we construct, in some detail, a model to describe the effects in the radiolysis of water which may be ascribed to geometrical inhomogeneity.

After an ionizing particle passes through water, an initial pattern of ionizations is obtained. Only an approximately quantitative description of this pattern is possible at present, and the details are conveniently summarized by Lea.[2] Along the more or less rectilinear path of the ionizing particle, primary ionization events are separated by an average distance d which is a function of the velocity of the ionizing particle. Secondary ionizations occur within a few angstrom units of the primary events. A group of ionizations corresponding to one primary ionization, which may contain one or more ion pairs, may be designated a *spur*.[3] There are also excited molecules, both in the spurs and between them, probably one or more per ion. The distance d is of the order of thousands of angstroms for fast electrons (for example, it averages about 4600A for 450-kev electrons) and the spurs corresponding to the individual primary ionizations may be considered as isolated phenomena in the first stages of their development. In the case of alpha-particles, d is much smaller (about 9A for 6-Mev particles) and the spurs will overlap from the moment of formation. Slow electrons (for example, tritium beta-rays) constitute an intermediate case.

It has been generally assumed that the ions which are formed initially in water are transformed into radicals.[4,5] For reasons which are given in the Appendix, it appears probable that the H and OH radicals are formed in close proximity, most likely from a highly excited water molecule. Thus, after a time interval of the order of 10^{-13} seconds (see Appendix) after the passage of the ionizing particle, the spur consists of an equal number of H and OH radicals. One expects that these radicals should have a finite probability of combining chemically to form H_2, H_2O_2, and H_2O while the spur is dissipated by diffusion.

THE "FORWARD" AND "RADICAL" REACTIONS

Experimentalists[6–8] have distinguished between two *initial* reactions in the radiolysis of water: the initial formation of product molecules, which is known as the "forward" reaction (F), and the initial formation of radicals, the "radical" reaction (R),

$$(F)\quad H_2O \rightarrow \tfrac{1}{2}H_2+\tfrac{1}{2}H_2O_2,$$
$$(R)\quad H_2O \rightarrow H+OH.$$

The relative yields of these reactions have also been determined. The fraction of chemically detectable radicals which undergo the forward reaction is given by $G_F/(G_F+G_R)$; and the experimental values of this quantity for gamma-rays are 0.21 (Hart) and 0.25 (Hochanadel).

DIFFUSION MODEL FOR A SPUR

Although it is not clear *a priori* that all chemical effects in the radiolysis of water are due to H and OH radicals, it would appear that reactions of these radicals have all the features necessary to explain the observed phenomena. We have, therefore, attempted to construct a detailed theory which involves only H and OH radicals.[9] We are neglecting the possibility of significant

* Condensed from a dissertation presented by Aryeh H. Samuel as partial fulfillment of requirements for the degree of Doctor of Philosophy at the University of Notre Dame.

† A contribution from the Radiation Project of the University of Notre Dame, supported in part by the U. S. Atomic Energy Commission under contract AT(11-1)-38.

[1] J. L. Magee, J. Am. Chem. Soc. **73**, 3270 (1951).

[2] D. E. Lea, *Actions of Radiations on Living Cells* (Cambridge University Press, Cambridge, 1947), pp. 1–68.

[3] Our term "spur" corresponds to the "cluster" in the terminology of E. Kara-Michailova and D. E. Lea, Proc. Cambridge Phil. Soc. **36**, 101 (1940). We have preferred to use the term "spur" in order to avoid confusion with the cluster theory of Lind, *The Chemical Effects of Alpha-Particles and Electrons* (Reinhold Publishing Company, New York, 1935). The term also corresponds to the "hot spot" of Allen, Disc. Faraday Soc. **12**, 79 (1952), but *not* to the "hot spot" term used by that author in J. Phys. & Colloid Chem. **52**, 479 (1948).

[4] J. Weiss, Nature **153**, 748 (1944).

[5] A. O. Allen, J. Phys. & Colloid Chem. **52**, 479 (1948).

[6] E. J. Hart, J. Phys. Chem. **56**, 594 (1952).

[7] C. J. Hochanadel, J. Phys. Chem. **56**, 587 (1952).

[8] Allen, Hochanadel, Ghormley, and Davis, J. Phys. Chem. **56**, 575 (1952).

[9] A qualitative description along the same lines has already been given by A. O. Allen, Disc. Faraday Soc. **12**, 79 (1952).

TABLE I. Probability of undergoing the radical reaction for different values of N_0 and x.

N_0	$x=0.01$	0.05	0.10	0.15	0.20	0.25	0.30	0.50	1.00
2	0.9922	0.9025	0.9291	0.8991	0.8720	0.8474	0.8252	0.7533	0.6461
4	0.9815	0.9149	0.8452	0.7871	0.7379	0.6958	0.6594	0.5523	0.4163
6	0.9733	0.8805	0.7888	0.7162	0.6574	0.6089	0.5679	0.4540	0.3209
8	0.9663	0.8526	0.7455	0.6629	0.6002	0.5487	0.5063	0.3924	0.2664
10	0.9600	0.8289	0.7101	0.6230	0.5562	0.5035	0.4608	0.3492	0.2303
12	0.9543	0.8079	0.6802	0.5891	0.5208	0.4677	0.4253	0.3166	0.2044
14	0.9501	0.7893	0.6543	0.5566	0.4913	0.4384	0.3966	0.2911	0.1847
16	0.9437	0.7715	0.6304	0.5346	0.4652	0.4127	0.3716	0.2695	0.1686
18	0.9392	0.7569	0.6111	0.5140	0.4446	0.3927	0.3523	0.2530	0.1564
20	0.9348	0.7425	0.5926	0.4947	0.4256	0.3744	0.3347	0.2383	0.1459
22	0.9304	0.7292	0.5760	0.4774	0.4087	0.3581	0.3193	0.2256	0.1369
24	0.9261	0.7165	0.5606	0.4618	0.3935	0.3437	0.3056	0.2146	0.1292
26	0.9223	0.7050	0.5464	0.4476	0.3799	0.3308	0.2935	0.2048	0.1225
28	0.9186	0.6941	0.5334	0.4345	0.3675	0.3191	0.2825	0.1961	0.1166
30	0.9146	0.6835	0.5212	0.4225	0.3562	0.3085	0.2726	0.1883	0.1114
32	0.9110	0.6736	0.5099	0.4115	0.3457	0.2987	0.2635	0.1812	0.1067
34	0.9077	0.6644	0.4992	0.4011	0.3362	0.2898	0.2552	0.1748	0.1024
36	0.9041	0.6552	0.4892	0.3915	0.3271	0.2815	0.2475	0.1690	0.0986
38	0.9007	0.6468	0.4797	0.3825	0.3188	0.2752	0.2405	0.1636	0.0951
40	0.8978	0.6385	0.4708	0.3740	0.3111	0.2667	0.2339	0.1586	0.0918

contribution by several other chemical species[10] and excitons, although in special cases this may not be justified.

We consider first the diffusion of a single spur. Let the distribution of radicals in the spur be random, and let the normalized probability function for finding a radical in a volume element at distance r from the center of the spur correspond to a spherically symmetrical distribution,

$$\phi(r)=\frac{\beta^3}{\pi^{\frac{1}{2}}}\exp(-\beta^2r^2), \tag{1}$$

where β is a time-dependent variable giving the extent of diffusion:

$$\beta^2=\frac{1}{Lv(t+\tau)}. \tag{2}$$

β^{-1} has the dimensions of length and is equal to the mean distance of the radicals from the center of the spur multiplied by a factor of $\pi^{\frac{1}{2}}/2=0.886$. We define $\bar{r}=\beta^{-1}$. v is the velocity of the radicals and L their mean free path. At $t=0$, $\bar{r}=(Lv\tau)^{\frac{1}{2}}$, and the fictitious time τ is equivalent to the time, it would have taken the spur to reach its initial distribution, if it had expanded from a point.

In a volume element dV the probability of finding two radicals is $N(N-1)\phi^2(dV)^2$ (where N is the total number of radicals in the spur), and the probability of their colliding is $\sigma v/dV$ times this value (σ is the collision cross section), so that

$$-dN/dt=\sigma vN(N-1)\int\phi^2dV=\sigma vN(N-1)\int_0^\infty\frac{\beta^6}{\pi^3}\cdot\exp(-2\beta^2r^2)\cdot4\pi r^2dr, \tag{3}$$

$$-dN/dt=\sigma v\beta^3N(N-1)/(8\pi^3)^{\frac{1}{2}}=\frac{\sigma vN(N-1)}{(8\pi^3)^{\frac{1}{2}}[Lv(t+\tau)]^{\frac{1}{2}}}. \tag{4}$$

It is true that a distribution function of the type used would only be strictly maintained, if there were no loss of radicals by combination. However, we believe that the results of this treatment will be essentially correct in spite of this defect.

Separating the variables and integrating from $t=0$, $N=N_0$ to $t=\infty$, $N=N_\infty$,

$$\ln\frac{1-(1/N_0)}{1-(1/N_\infty)}=\frac{\sigma}{(2\pi^3L^3v\tau)^{\frac{1}{2}}}=\frac{\sigma}{\sqrt{2}\pi^{\frac{1}{2}}L\bar{r}_0}. \tag{5}$$

If the initial volume of the spur is directly proportional to the initial number of radicals,

$$\bar{r}_0=\bar{r}_0'N_0^{\frac{1}{3}}. \tag{6}$$

The quantity $\sigma/(2\pi^3)^{\frac{1}{2}}L\bar{r}_0'$, appears as an important parameter and will be designated as x.

$$N_\infty/N_0=\frac{1}{N_0-(N_0-1)\exp(-xN_0^{-\frac{1}{3}})}. \tag{7}$$

This result means that for a group of radicals in a spherical spur diffusing into three-dimensional space, a certain fraction will escape and remain uncombined. This separation into combined radicals and escaped radicals is just what is needed for explanation of the forward and radical reactions. The yield of the radical reaction in terms of the initial number of radicals formed is given in the present model by the number N_∞/N_0 in Eq. (7). The corresponding yield of the

[10] See, for instance, M. Haïssinsky and M. Lefort, Compt. rend. **230**, 1156 (1950).

TABLE II. Probability of undergoing the forward reaction for different values of N_0 and x.

N_0	$x=0.01$	0.05	0.10	0.15	0.20	0.25	0.30	0.50	1.00
2	...	...	...	...	...	...	...	...	...
4	0.0062	0.0284	0.0516	0.0710	0.0874	0.1014	0.1135	0.1492	0.1946
6	0.0107	0.0478	0.0845	0.1135	0.1370	0.1564	0.1728	0.2184	0.2716
8	0.0144	0.0632	0.1091	0.1445	0.1713	0.1934	0.2116	0.2604	0.3144
10	0.0178	0.0760	0.1283	0.1676	0.1973	0.2207	0.2396	0.2892	0.3421
12	0.0208	0.0873	0.1454	0.1868	0.2178	0.2420	0.2612	0.3106	0.3616
14	0.0230	0.0972	0.1596	0.2046	0.2348	0.2592	0.2785	0.3272	0.3763
16	0.0263	0.1066	0.1725	0.2172	0.2498	0.2741	0.2933	0.3409	0.3880
18	0.0286	0.1144	0.1830	0.2287	0.2614	0.2854	0.3048	0.3515	0.3970
20	0.0309	0.1220	0.1930	0.2394	0.2721	0.2963	0.3151	0.3608	0.4046
22	0.0331	0.1290	0.2019	0.2489	0.2816	0.3057	0.3241	0.3688	0.4110
24	0.0353	0.1356	0.2101	0.2574	0.2901	0.3139	0.3321	0.3756	0.4165
26	0.0373	0.1416	0.2177	0.2651	0.2976	0.3212	0.3391	0.3817	0.4212
28	0.0392	0.1473	0.2247	0.2723	0.3045	0.3278	0.3455	0.3871	0.4254
30	0.0412	0.1528	0.2311	0.2788	0.3108	0.3333	0.3512	0.3919	0.4290
32	0.0431	0.1579	0.2371	0.2848	0.3166	0.3393	0.3564	0.3962	0.4322
34	0.0448	0.1627	0.2428	0.2904	0.3218	0.3443	0.3611	0.4001	0.4352
36	0.0466	0.1674	0.2481	0.2956	0.3268	0.3490	0.3655	0.4036	0.4378
38	0.0483	0.1718	0.2531	0.3004	0.3314	0.3526	0.3695	0.4070	0.4401
40	0.0498	0.1761	0.2578	0.3050	0.3356	0.3572	0.3732	0.4099	0.4425

forward reaction is then given by

$$(1-N_\infty/N_0)(\tfrac{1}{2}N_0-1)/(N_0-1), \qquad (8)$$

allowance having been made for the occurrence of the reaction

$$H+OH\rightarrow H_2O.$$

CALCULATED $G_F/(G_F+G_R)$ FOR GAMMA- AND FAST BETA-RAYS

Since the spurs, in the case of gamma- and fast beta-rays, are separated by distances which are so large that this initial combination process will be completed before they merge, it should be possible to compare the yields of the forward and radical reactions on the basis of formulas 7 and 8. In this connection it should be noted that the greatest part of the combination takes place during the earliest period of the diffusion; at $\bar{r}=100\bar{r}_0(V=10^6V_0)$ the process is practically complete.

The yields of both reactions are functions of the spur size N_0, and it is therefore necessary to have the spur size distribution. For convenience the distribution has been taken in the analytical form

$$f(N_0)=0.65\exp(-N_0/4), \qquad (9)$$

where 0.65 is a normalization factor. This curve agrees with the experimental results of Wilson[11] for ionization frequency within their limits of error. This distribution corresponds to an average spur size of 2.54 radical pairs per primary ionization.[12]

Values of the yields of the forward and radical reactions were calculated for values of N_0 ranging from 2 to 40 and for values of x ranging from 0.01 to 1.00. These results, which express the *a priori* probability of undergoing the forward or radical reaction for a particle formed in a cluster of a certain size, are given in Tables I and II. The total probability of occurrence of the two reactions is given by multiplying these values by the appropriate weighing factors $\frac{1}{2}N_0\cdot f(N_0)=0.325N_0\exp(-\frac{1}{4}N_0)$. After summing over all values of N_0, the ratio of the yield of the forward reaction to the sum of both yields can be obtained for any value of x. This ratio should correspond to the experimentally obtained ratio $G_F/(G_F+G_R)$. Table III shows this ratio as a function of x.

A comparison of the theory with the experimental results can be made, if we can determine a reasonable value of x. If the sum of the collision radii of H and OH is 2A, so that σ is $4\pi\cdot10^{-16}$ cm^2, and if L is taken as 10^{-8} cm and $\bar{r}_0'$ as $5\cdot10^{-8}$ cm,

$$x=\sigma/(2\pi^3)^{\frac{1}{3}}L\bar{r}_0'=0.284.$$

The value of $G_F/(G_F+G_R)$ corresponding to this value of x is 0.231. The experimental values are 0.21 (Hart[6]) and 0.25 (Hochanadel[7]).

DIFFUSION MODEL FOR ALPHA-RAYS

Since the value of d for alpha-particles is of the same order as $\bar{r}_0$ for the spurs, it is assumed in this model that the spurs overlap from the moment they are formed. The expansion is then treated as that of a cylindrically

[11] C. T. R. Wilson, Proc. Roy. Soc. (London) **A104**, 192 (1923). See also W. J. Beekman, Physica **15**, 327 (1949).

[12] This value is rather lower than the average number of ion pairs per primary ionization in the gas phase. If a function is chosen which gives a higher value of this average, the result will, in general, be a higher value of $G_F/(G_F+G_R)$ for a given value of x. The lower average was chosen because it seemed to accord with the larger number of small spurs which would be expected in the liquid phase, where the effective ionization potential is lowered. In this connection it should be mentioned that the value of $G_F/(G_F+G_R)$ is not very sensitive to the actual spur size distribution function as long as a constant average number of radical pairs per spur is maintained.

symmetrical track. For this track we assume that the spatial distribution of radicals is given by the normalized probability function,

$$\phi=(\beta^2/\pi Z)\exp(-\beta^2 r^2), \tag{10}$$

where the column has length Z.

$$\frac{-dN}{dt}=\sigma v\int N^2\phi^2 dV=\sigma vN^2\int_0^\infty \frac{\beta^4}{\pi^2 Z^2}\exp(-2\beta^2 r^2)\cdot 2\pi Z r dr=\frac{\sigma vN^2}{2\pi ZLv(t+\tau)},$$

$$\frac{N}{N_0}=\frac{1}{1+(\sigma N_0/2\pi ZL)\ln[(t+\tau)/\tau]}. \tag{11}$$

(Z can be taken long enough so that N is small compared with N^2.)

It is seen that for this case, in contrast with the spherical case, the number N of free radicals surviving at time t approaches zero as t goes to infinity. It is therefore necessary to consider the largest actual value of $(t+\tau)/\tau$, which will be attained at the moment when neighboring tracks begin to overlap. Since the average distance of the radicals from the axis of the cylinder is approximately given by $\bar{r}=[Lv(t+\tau)]^{\frac{1}{2}}$, this ratio will be the same as the ratio X of the track volumes at times t and 0, if the volume is that of a cylinder with radius proportional to the average radical distance. Magee[1] has given a formula which connects the maximum value of this ratio and the dose rate. In water it is[13]

$$2\cdot 10^{12}I=\frac{DN_0}{2Zv_0^2X_m(X_m-1)}, \tag{12}$$

where I is the dose rate in rep/sec, D is the diffusion constant, v_0 is the initial track volume per unit length, and $X_m=v_m/v_0$ is the ratio of the final and initial track volumes.

For $I=200$ rep/sec, $N_0/Z=8.5\cdot 10^7$ radicals/cm (equivalent to the average ion density in a 6-Mev alpha-particle track), $v_0=\pi\cdot 10^{-14}$ cm^3/cm, $D=8\cdot 10^{-5}$, X_m is obtained as $0.93\cdot 10^8$ or (within our limits of accuracy) 10^8.

Equation (11) then becomes

$$N/N_0=1/(1+1.7\ln X). \tag{13}$$

Table IV shows the variation of N/N_0 with increasing X. At $X=2$, more than one-half of the radicals have combined, and at $X=10^4$ (0.01 percent of the life of the track having passed), 97 percent of all the radicals which are going to combine during the life of the track will have done so. This makes it possible to consider the life of an alpha-particle track as a two-stage process, with the greater part of the recombination of radicals taking part in the first stage, the duration of which is small compared to the total track life.

[13] This formula is derived from the requirement that $\nu V_m t_m/Z=1$ where ν is the number of tracks falling on 1 cm^2 of the medium, V_m is the final volume, and t_m the lifetime of a track of length Z.

TABLE III. Calculated values of $G_F/(G_F+G_R)$.

x	$G_F/(G_F+G_R)$	x	$G_F/(G_F+G_R)$
0.01	0.0134	0.25	0.2126
0.05	0.0605	0.30	0.2387
0.10	0.1088	0.50	0.3190
0.15	0.1491	1.00	0.4316
0.20	0.1830		

There is no unequivocal value of $G_F/(G_F+G_R)$ for this case, but if the initial combination stage is considered as ending at $X=10^4$, a value can be obtained as follows: The ratio G_F/G_R must be proportional to $\frac{1}{2}(1-N/N_0)\cdot N_0/N$. The factor $\frac{1}{2}$ is introduced because one-half of the recombinations result in H_2O molecules, which cannot be detected as reaction products. For $X=10^4$, the ratio $G_F/(G_F+G_R)$ then becomes 0.887. This is approximately the observed value. It is not very sensitive to the value of X and therefore does not greatly depend upon the rate of irradiation.

DIFFUSION MODEL FOR TRITIUM BETA-RAYS

The beta-rays emitted by tritium have a mean energy of only 5.7 kev, and the corresponding value of d is 150A. Using the value of 2.54 for the average number of radical pairs per cluster, $\bar{r}_0=\bar{r}_0'N_0^{\frac{1}{3}}$ and $\bar{r}_0'=5$A, this value of d is found to be equal to about nine times the initial average spur diameter. It is therefore possible to treat the expansion of the track as equivalent to the independent expansion of the spurs for $\bar{r}<9\bar{r}_0$ and consider the track as expanding as a single unit for larger values of t. In the first stage we again have

$$-\frac{dN}{dt}=\frac{\sigma vN(N-1)}{(8\pi^3)^{\frac{1}{3}}[Lv(t+\tau)]^{\frac{1}{3}}}, \tag{4}$$

$$\int_{N_0}^{N_1}\frac{dN}{N(N-1)}=\frac{\sigma}{(8\pi^3L^2v)^{\frac{1}{3}}}\int_0^t\frac{dt}{(t+\tau)^{\frac{1}{3}}}. \tag{14}$$

Since

$$\frac{1}{(Lv\tau)^{\frac{1}{3}}}=\frac{1}{\bar{r}_0}\quad\text{and}\quad\frac{1}{[Lv(t+\tau)]^{\frac{1}{3}}}=\frac{1}{9\bar{r}_0},$$

TABLE IV. N/N_0 as function of X in alpha-ray track.

X	N/N_0	X	N/N_0
1	1.0000	10^3	0.0785
2	0.4591	10^4	0.0600
5	0.2677	10^5	0.0486
10	0.2035	10^6	0.0408
20	0.1641	10^7	0.0352
100	0.1133	10^8	0.0309

this integration gives

$$\frac{N_1}{N_0}=\frac{1}{N_0-(N_0-1)\exp(-8xN_0^{-\frac{1}{3}}/9)}. \quad (15)$$

Hart[6] has obtained an experimental value of $G_F/(G_F+G_R)$ for tritium beta-rays (0.30). In order to compare this model to his result, x has been taken as 0.245, a value which, when applied to Eq. (7), gives the ratio $G_F/(G_F+G_R)=0.21$ for gamma-rays, which fits Hart's experimental conditions. Taking $N_0=5700\cdot 2/30=380$, and the same distribution of cluster sizes as in the gamma-ray case, N_1 is found to be 237.56, and F_1, 57.18. N_1 here is the average number of radicals which escape recombination, and F_1 is the average number which combine to give H_2 and H_2O_2 in the first stage of the expansion of a tritium track.

In the second stage of the expansion the track is considered as a unit. Since it expands independently in all dimensions, it will approach the shape of a prolate spheroid, although the initial shape, which is nearly cylindrical, must be corrected for. A Gaussian distribution corresponding to a prolate spheroid is

$$\phi(x,y,z)=\frac{1}{ab^2\pi^{\frac{3}{2}}}\exp(-x^2/a^2+y^2/b^2+z^2/b^2), \quad (16)$$

$$-\frac{dN}{dt}=N(N-1)\sigma v\int\phi^2dV=\frac{N(N-1)\sigma v}{2\sqrt{2}ab^2\pi^{\frac{3}{2}}}. \quad (17)$$

Let

$$a=[Lv(t+\tau_a)]^{\frac{1}{2}},\quad b=[Lv(t+\tau_b)]^{\frac{1}{2}}, \quad (18)$$

then

$$\int_{N_1}^{N_\infty}\frac{dN}{N(N-1)}=\int_0^\infty\frac{\sigma dt}{[8\pi^3L^3v(t+\tau_a)]^{\frac{1}{2}}(t+\tau_b)} \quad (19)$$

and, since $\tau_a>\tau_b$,

$$\ln\frac{1-(1/N_1)}{1-(1/N_\infty)}=-\frac{\sigma\ln\dfrac{\tau_a^{\frac{1}{2}}-(\tau_a-\tau_b)^{\frac{1}{2}}}{\tau_a^{\frac{1}{2}}+(\tau_a-\tau_b)^{\frac{1}{2}}}}{[8\pi^3L^3v(\tau_a-\tau_b)]^{\frac{1}{2}}} \quad (20)$$

and

$$\frac{N_1}{N_\infty}=N_1-(N_1-1)\exp\left[-\frac{\sigma}{2\sqrt{2}\pi^{\frac{3}{2}}L^{\frac{1}{2}}v^{\frac{1}{2}}(\tau_a-\tau_b)^{\frac{1}{2}}}\times\ln\frac{\tau_a^{\frac{1}{2}}+(\tau_a-\tau_b)^{\frac{1}{2}}}{\tau_a^{\frac{1}{2}}-(\tau_a-\tau_b)^{\frac{1}{2}}}\right]. \quad (21)$$

But $(Lv\tau_a)^{\frac{1}{2}}=\bar{r}_{a0}$ and $(Lv\tau_b)^{\frac{1}{2}}=\bar{r}_{b0}$, where $\bar{r}_{a0}$ and $\bar{r}_{b0}$ are the initial root-mean-square distances from the center of the track along the directions of the axes of the spheroid. Therefore,

$$\frac{N_1}{N_\infty}=N_1-(N_1-1)\exp\left[-\frac{\sigma}{2\sqrt{2}L\pi^{\frac{3}{2}}(\bar{r}_{a0}^2-\bar{r}_{b0}^2)^{\frac{1}{2}}}\times\ln\frac{\bar{r}_{a0}+(\bar{r}_{a0}^2-\bar{r}_{b0}^2)^{\frac{1}{2}}}{\bar{r}_{a0}-(\bar{r}_{a0}^2-\bar{r}_{b0}^2)^{\frac{1}{2}}}\right]. \quad (22)$$

An initial correction is necessary here. In order to obtain a correct initial volume (and hence initial concentration), it is necessary to allow for the initial cylindrical shape of the track. This can be done by multiplying the value of $\bar{r}_{b0}$ by a factor of $(3/2)^{\frac{1}{2}}$, since the volume of a cylinder is $\frac{3}{2}$ that of the inscribed prolate spheroid. Thus,

$\bar{r}_{b0}=9.19\cdot10^{-7}$ cm (instead of $\frac{1}{2}d=7.5\cdot10^{-7}$ cm),

$\bar{r}_{a0}=4.5\cdot10^{-5}$ cm ($\frac{1}{2}$ the range of a 5.7-kv beta-ray),

$\bar{r}_{a0}+(\bar{r}_{a0}^2-\bar{r}_{b0}^2)^{\frac{1}{2}}=8.999\cdot10^{-5}$ cm,

$$\bar{r}_{a0}-(\bar{r}_{a0}^2-\bar{r}_{b0}^2)^{\frac{1}{2}}\approx\frac{\bar{r}_{b0}^2}{2\bar{r}_{a0}}=9.38\cdot10^{-9}\text{ cm}.$$

Since we are taking $x=0.245$, $\sigma/(2\pi^3)^{\frac{1}{2}}L=0.245\cdot5\cdot10^{-8}=1.225\cdot10^{-8}$. The exponent then becomes $1.248\cdot10^{-3}$, and we obtain

$$\frac{N_\infty}{N_1}=0.7717,\quad N_\infty=183.33. \quad (23)$$

The number of radicals undergoing the forward reaction during the expansion of the spheroid is

$$F_2=\frac{N_1(1-N_\infty/N_1)(\frac{1}{2}N_1-1)}{(N_1-1)}=27.00. \quad (24)$$

For the entire expansion

$$G_F/(G_F+G_R)=(F_1+F_2)/(F_1+F_2+N_\infty)=0.315. \quad (25)$$

This value compares with the experimental result of 0.30.

APPLICATION TO AQUEOUS SYSTEMS

The description of the initial stages of radical diffusion thus yields values of $G_F/(G_F+G_R)$ which are dependent only on the parameter x and the spur weighting factors for the cases of gamma- and beta-ray irradiation and on the parameters σ/L, N_0/Z and X_m for alpha-ray irradiation. In the gamma- and beta-ray cases, this treatment exhausts all effects resulting from the inhomogeneous initial distribution, and subsequent events can be treated by the ordinary kinetic equations, which have the time as the only independent variable. In the case of the cylindrically symmetrical (alpha-ray) model, it is not possible to take all geometrical effects into consideration by a simple integration to infinity. However,

since this is a "low-background" model, in the terminology of Magee,[1] it is possible to describe the effects in the life of an average track; the total effect is then obtained by a simple summation, as all tracks are independent. It can be assumed that the recombination of radicals is confined to the first stage of the life of the track and that all other reactions are essentially confined to the second stage, comprising 99.99 percent of the life of the track. Since the steady-state concentrations of products in the alpha-ray case are high, it is possible to regard them as constant over the life of a single track; and since all reactions in which the radicals take part are first order with respect to the radical concentration, the radical concentration will then decrease exponentially. It is then possible to estimate the increment of the various products (the total amount formed or consumed) over the life of a track by integration of the kinetic formulas for any set of product concentrations.

In many aqueous solutions most of the detectable reaction occurs in the solute. This indicates a radical-solute reaction which competes efficiently with the radical-product (back) reaction. It might be expected that large concentrations of solute would tend to inhibit the forward reaction by action on the radicals in the initial combination stage, but the results of Hochanadel[7] indicate no such result for concentrations of KBr up to $1M$. In the absence of such an effect it may be inferred that the radical-solute reaction can be ignored for the initial combination stage. In this case, geometrical effects can again be neglected with the exception of the distinction between forward and radical reaction.

The authors wish to thank Professor M. Burton and Dr. H. A. Dewhurst for their helpful suggestions and criticisms.

APPENDIX: THE MOTION OF THE FREE ELECTRON

The ionization process creates a positive ion and an electron which may possess a considerable amount of kinetic energy. Here we shall consider the special case in which the electron has insufficient energy to cause further ionization. The positive ion H_2O^+ will be able to move also by charge exchange with neighboring molecules, but without loss of generality we can neglect this effect.

A rigorous treatment of the motion of a free electron in liquid water is, of course, impossible and the discussion of this section is, at best, approximate. From experimental data obtained in gas-phase work[14] it is known that the scattering cross section for electrons in the energy range of interest (one to ten ev or so) is about 10^{-16} cm^2; so we feel certain that the electron cannot go very far without suffering wide deflections resulting from scattering. If scattering were predominantly elastic, the electron would still escape from the influence of the positive ion. It is also known from experimental work[15] in the gas phase, that electrons in this energy region lose energy very readily to vibrations of the H_2O molecule. We now have the quantitative problem as to whether the electron loses its excess energy while it is still in the strong field of the ion or whether it escapes. We have constructed a classical model which gives an answer to the problem.

The critical intercharge distance r_c beyond which the electron can be considered as free is such that the Coulombic attraction is equal to the thermal energy.[16] Let us take it as

$$e^2/Dr_c=kT. \tag{26}$$

For times less than the relaxation time of water (and our calculations show that the recapture is effected in a considerably shorter time), D can be taken as 3. We then get, for $kT=1/40$ ev,

$$r_c=192\text{A}.$$

For the classical model we assume that the electron moves randomly with a relatively short mean free path. Instead of considering the entire distribution function for such motion we consider an electron which has the average r^2. Thus, in a time increment such that there are Δn mean free paths traversed, the average r^2 changes as

$$\Delta(r^2)=L^2\Delta n, \tag{27}$$

where L is the mean free path.

The kinetic energy of the electron is diminished by the collisions and because of its outward motion in the Coulombic field of the positive ion. If the fractional energy loss per collision is λ,

$$dE/dn=-\lambda E-\frac{e^2}{Dr^2}\frac{dr}{dn}=-\lambda E-\frac{e^2}{2Dr^3}\frac{d(r^2)}{dn}; \tag{28}$$

dividing through by Eq. (27) in differential form,

$$\frac{d(E)}{d(r^2)}=-\frac{\lambda E}{L^2}-\frac{e^2}{2Dr^3}. \tag{29}$$

In the general case, L and λ will be functions of E. A numerical solution is possible if they are known.

Values of L were obtained from data of Brüche.[14] His values were corrected for the density difference, under the assumption that, so far as the motion of electrons in it is concerned, water behaves like a condensed gas. For $E<1$ ev, L was taken to be the same as for 1 ev, though it is probably lower.

Values of λ for water vapor are available only up to electron energies of 1.8 volts.[15] At these low energies λ is in the vicinity of 0.04 (4 percent of the energy is lost per collision). Few values of λ in triatomic gases are

[14] E. Brüche, Ann. Physik **1**, 93 (1929).

[15] V. A. Bailey and W. E. Duncansson, Phil. Mag. [7], **10**, 145 (1930).

[16] L. Onsager, Phys. Rev. **54**, 554 (1938).

TABLE V. Minimum and maximum times for return of electron from distance R to positive ion.

R in A	t_{min} in sec	t_{max} in sec
5	$1.25\cdot10^{-15}$	$6.89\cdot10^{-15}$
10	$1.00\cdot10^{-14}$	$3.90\cdot10^{-14}$
20	$8.02\cdot10^{-14}$	$2.20\cdot10^{-13}$
30	$2.71\cdot10^{-13}$	$6.08\cdot10^{-13}$
40	$6.42\cdot10^{-13}$	$1.24\cdot10^{-12}$
50	$1.25\cdot10^{-12}$	$2.18\cdot10^{-12}$
100	$1.00\cdot10^{-11}$	$1.23\cdot10^{-11}$
12.5	$1.96\cdot10^{-14}$	$6.81\cdot10^{-14}$
17.6	$5.47\cdot10^{-14}$	$1.60\cdot10^{-13}$

available.[17–19] They show, in general, values of λ in the range 0.05 to 0.10 at moderate energies and not varying much with the energy. It can therefore be assumed that λ for water vapor is between 0.025 and 0.05 over the energy range which we are considering. These high values of λ apparently are due to the large number of vibrational degrees of freedom which can be excited in triatomic molecules.

Numerical solutions of Eq. (29) were carried out for $\lambda=0.05$ and $\lambda=0.025$. The initial condition in each case was taken to be $E=15$ ev at $r=1$A. In the first case the kinetic energy of the electron drops below the Coulombic potential energy at $r=12.5$A and in the second case at $r=17.6$A.

The time necessary for the slowing process can be obtained by a numerical integration,

$$t=\int ds/v, \tag{30}$$

$$ds=Ldn=\frac{d(r^2)}{L},$$

$$t=\int\frac{d(r^2)}{Lv}=\left(\frac{m}{2}\right)^{\frac{1}{2}}\int\frac{d(r^2)}{LE^{\frac{1}{2}}}. \tag{31}$$

Using the plot of E *vs* r^2 obtained by taking $\lambda=0.025$, the value $t=2.83\cdot10^{-14}$ sec was obtained.

Once the total energy of the electron drops below zero, it may be regarded as having been recaptured by the positive ion with formation of a highly excited H_2O molecule. It is also of interest to determine the classical time it would take the electron to return to the vicinity of the positive ion. The radial velocity of an electron in a central electric field (based on a formula of Townsend[20]) is

$$-dr/dt=\tfrac{1}{2}at=\tfrac{1}{2}\cdot\frac{Ze}{m}\cdot\frac{L}{v}=\frac{e^2L}{2mvDr^2}, \tag{32}$$

where Z is the field strength, e the electronic charge, L the mean free path of the electron, m its mass, v its velocity, and r its distance from the positive ion. The value to be taken for v will be determined by the kinetic energy of the electron, which can be no less than the thermal nor more than the Coulombic potential energy. In the former case the drift velocity is a maximum and t is at a minimum,

$$v=(3kT/m)^{\frac{1}{2}}\cdot(8/3\pi)^{\frac{1}{2}}, \tag{33}$$

where the second factor converts root-mean-square velocity to mean velocity,

$$t_{min}=-\int_R^0\frac{(3mkT)^{\frac{1}{2}}Dr^2dr}{0.46e^2L}=\frac{(mkT/3)^{\frac{1}{2}}DR^3}{0.46e^2L}. \tag{34}$$

In the second case t is a maximum,

$$E=e^2/Dr,\quad v=(2e^2/mDr)^{\frac{1}{2}}, \tag{35}$$

$$dr/dt=-\frac{eL}{2(2mDr^3)^{\frac{1}{2}}}. \tag{36}$$

If L is taken to be fixed at 10^{-8} cm (a value smaller than any obtained from Brüche's data),

$$t_{max}=\frac{(8mDr^5)^{\frac{1}{2}}}{2.5\cdot10^{-8}e}. \tag{37}$$

Taking $D=3$, $T=300$°K, the values obtained for t_{min} and t_{max} are tabulated in Table V as functions of R.

Thus a time of the order of 10^{-13} seconds suffices for the dissipation of the electron's kinetic energy and for its return to the vicinity of the positive ion. It will be noted that all assumptions regarding the values of numerical constants have been taken in a sense unfavorable to the completion of this process.

The process of electron capture by a neutral water molecule might compete with the recombination of charges. Magee and Burton[21] discuss the probability of this process and come to the conclusion that it is not exothermic unless the solvation energy of the OH^- ion which is formed is available. The solvation energy is not available in the case we are considering, which is completed in a small fraction of the time necessary for the solvation process. The cross section for the electron capture process is given as 10^{-20} cm^2, which is equivalent to about 10^{-5} of the geometrical cross section. The entire process resulting in charge recombination involves only about 10^3 collisions, and the electron capture process can, therefore, probably be disregarded.

No attempt has been made to follow the details of radical pair formation. It is sufficient for the purposes of this paper to point out that after the recapture of the electron, the qualitative difference between the ionized and the excited water molecules disappears. There are,

[17] M. F. Skinker, Phil. Mag. **44**, 994 (1922).
[18] M. F. Skinker and J. V. White, Phil. Mag. **46**, 630 (1923).
[19] H. S. W. Massey and E. H. S. Burhop, *Electronic and Ionic Impact Phenomena* (Clarendon Press, Oxford, 1952), p. 279.
[20] Sir J. Townsend, *Electrons in Gases* (Hutchinson, London, 1947).
[21] J. L. Magee and M. Burton, J. Am. Chem. Soc. **73**, 523 (1951).

instead, only water molecules with different amounts of excitation energy. These may follow any of three paths:

(a) The excitation energy is lost without dissociation into radicals (by collision, or possibly radiation, as in aromatic hydrocarbons).

(b) The molecules dissociate, but the resulting radicals recombine without escaping from the liquid cage.

(c) The molecules dissociate and escape from the cage. In this case we would not expect them to move more than a few molecular diameters through the dense medium before being thermalized.

In accordance with the notation introduced by Burton, Magee, and Samuel,[22] the molecules following paths (a) and (b) can be designated H_2O^* and those following path (c) can be designated $H_2O\dagger$. It seems reasonable to assume for the purpose of these calculations that the ionized H_2O molecules will become the $H_2O\dagger$ molecules, but this is not likely to be a complete correspondence.

In conclusion we would like to emphasize that the qualitative result of this section is not critically dependent on the exact values of the physical parameters used. However, this treatment is classical, and a correct treatment must be wave mechanical; therefore the result of this section cannot be taken as an *a priori* theoretical prediction. The success of the radical diffusion model given above lends some plausibility to the occurrence of electron capture as described by this crude calculation. Further work is clearly needed.

[22] Burton, Magee, and Samuel, J. Chem. Phys. **20**, 760 (1952).

THE JOURNAL OF CHEMICAL PHYSICS VOLUME 21, NUMBER 6 JUNE, 1953

Equation of State Calculations by Fast Computing Machines

NICHOLAS METROPOLIS, ARIANNA W. ROSENBLUTH, MARSHALL N. ROSENBLUTH, AND AUGUSTA H. TELLER,
Los Alamos Scientific Laboratory, Los Alamos, New Mexico

AND

EDWARD TELLER,* *Department of Physics, University of Chicago, Chicago, Illinois*

(Received March 6, 1953)

A general method, suitable for fast computing machines, for investigating such properties as equations of state for substances consisting of interacting individual molecules is described. The method consists of a modified Monte Carlo integration over configuration space. Results for the two-dimensional rigid-sphere system have been obtained on the Los Alamos MANIAC and are presented here. These results are compared to the free volume equation of state and to a four-term virial coefficient expansion.

I. INTRODUCTION

THE purpose of this paper is to describe a general method, suitable for fast electronic computing machines, of calculating the properties of any substance which may be considered as composed of interacting individual molecules. Classical statistics is assumed, only two-body forces are considered, and the potential field of a molecule is assumed spherically symmetric. These are the usual assumptions made in theories of liquids. Subject to the above assumptions, the method is not restricted to any range of temperature or density. This paper will also present results of a preliminary two-dimensional calculation for the rigid-sphere system. Work on the two-dimensional case with a Lennard-Jones potential is in progress and will be reported in a later paper. Also, the problem in three dimensions is being investigated.

* Now at the Radiation Laboratory of the University of California, Livermore, California.

II. THE GENERAL METHOD FOR AN ARBITRARY POTENTIAL BETWEEN THE PARTICLES

In order to reduce the problem to a feasible size for numerical work, we can, of course, consider only a finite number of particles. This number N may be as high as several hundred. Our system consists of a square† containing N particles. In order to minimize the surface effects we suppose the complete substance to be periodic, consisting of many such squares, each square containing N particles in the same configuration. Thus we define d_{AB}, the minimum distance between particles A and B, as the shortest distance between A and any of the particles B, of which there is one in each of the squares which comprise the complete substance. If we have a potential which falls off rapidly with distance, there will be at most one of the distances AB which can make a substantial contribution; hence we need consider only the minimum distance d_{AB}.

† We will use the two-dimensional nomenclature here since it is easier to visualize. The extension to three dimensions is obvious.

Our method in this respect is similar to the cell method except that our cells contain several hundred particles instead of one. One would think that such a sample would be quite adequate for describing any one-phase system. We do find, however, that in two-phase systems the surface between the phases makes quite a perturbation. Also, statistical fluctuations may be sizable.

If we know the positions of the N particles in the square, we can easily calculate, for example, the potential energy of the system,

$$E=\tfrac{1}{2}\sum_{\substack{i=1\\ i\neq j}}^{N}\sum_{j=1}^{N} V(\bar{d}_{ij}). \tag{1}$$

(Here V is the potential between molecules, and $\bar{d}_{ij}$ is the minimum distance between particles i and j as defined above.)

In order to calculate the properties of our system we use the canonical ensemble. So, to calculate the equilibrium value of any quantity of interest F,

$$\bar{F}=\left[\int F\exp(-E/kT)d^{2N}pd^{2N}q\right]\Big/\left[\int \exp(-E/kT)d^{2N}pd^{2N}q\right], \tag{2}$$

where $(d^{2n}pd^{2n}q)$ is a volume element in the $4N$-dimensional phase space. Moreover, since forces between particles are velocity-independent, the momentum integrals may be separated off, and we need perform only the integration over the $2N$-dimensional configuration space. It is evidently impractical to carry out a several hundred-dimensional integral by the usual numerical methods, so we resort to the Monte Carlo method.‡ The Monte Carlo method for many-dimensional integrals consists simply of integrating over a random sampling of points instead of over a regular array of points.

Thus the most naive method of carrying out the integration would be to put each of the N particles at a random position in the square (this defines a random point in the $2N$-dimensional configuration space), then calculate the energy of the system according to Eq. (1), and give this configuration a weight $\exp(-E/kT)$. This method, however, is not practical for close-packed configurations, since with high probability we choose a configuration where $\exp(-E/kT)$ is very small; hence a configuration of very low weight. So the method we employ is actually a modified Monte Carlo scheme, where, instead of choosing configurations randomly, then weighting them with $\exp(-E/kT)$, we choose configurations with a probability $\exp(-E/kT)$ and weight them evenly.

This we do as follows: We place the N particles in any configuration, for example, in a regular lattice. Then we move each of the particles in succession according to the following prescription:

$$\begin{aligned} X&\rightarrow X+\alpha\xi_1\\ Y&\rightarrow Y+\alpha\xi_2, \end{aligned} \tag{3}$$

where α is the maximum allowed displacement, which for the sake of this argument is arbitrary, and ξ_1 and ξ_2 are random numbers§ between (-1) and 1. Then, after we move a particle, it is equally likely to be anywhere within a square of side 2α centered about its original position. (In accord with the periodicity assumption, if the indicated move would put the particle outside the square, this only means that it re-enters the square from the opposite side.)

We then calculate the change in energy of the system ΔE, which is caused by the move. If $\Delta E<0$, i.e., if the move would bring the system to a state of lower energy, we allow the move and put the particle in its new position. If $\Delta E>0$, we allow the move with probability $\exp(-\Delta E/kT)$; i.e., we take a random number ξ_3 between 0 and 1, and if $\xi_3<\exp(-\Delta E/kT)$, we move the particle to its new position. If $\xi_3>\exp(-\Delta E/kT)$, we return it to its old position. Then, whether the move has been allowed or not, i.e., whether we are in a different configuration or in the original configuration, we consider that we are in a new configuration for the purpose of taking our averages. So

$$\bar{F}=(1/M)\sum_{j=1}^{M} F_j, \tag{4}$$

where F_j is the value of the property F of the system after the jth move is carried out according to the complete prescription above. Having attempted to move a particle we proceed similarly with the next one.

We now prove that the method outlined above does choose configurations with a probability $\exp(-E/kT)$. Since a particle is allowed to move to any point within a square of side 2α with a finite probability, it is clear that a large enough number of moves will enable it to reach any point in the complete square.|| Since this is true of all particles, we may reach any point in configuration space. Hence, the method is ergodic.

Next consider a very large ensemble of systems. Suppose for simplicity that there are only a finite number of states¶ of the system, and that ν_r is the number of

‡ This method has been proposed independently by J. E. Mayer and by S. Ulam. Mayer suggested the method as a tool to deal with the problem of the liquid state, while Ulam proposed it as a procedure of general usefulness. B. Alder, J. Kirkwood, S. Frankel, and V. Lewinson discussed an application very similar to ours.

§ It might be mentioned that the random numbers that we used were generated by the middle square process. That is, if ξ^n is an m digit random number, then a new random number ξ_{n+1} is given as the middle m digits of the complete $2m$ digit square of ξ_n.

|| In practice it is, of course, not necessary to make enough moves to allow a particle to diffuse evenly throughout the system since configuration space is symmetric with respect to interchange of particles.

¶ A state here means a given point in configuration space.

systems of the ensemble in state r. What we must prove is that after many moves the ensemble tends to a distribution

$$\nu_r \propto \exp(-E_r/kT).$$

Now let us make a move in all the systems of our ensemble. Let the *a priori* probability that the move will carry a system in state r to state s be P_{rs}. [By the *a priori* probability we mean the probability before discriminating on $\exp(-\Delta E/kT)$.] First, it is clear that $P_{rs}=P_{sr}$, since according to the way our game is played a particle is equally likely to be moved anywhere within a square of side 2α centered about its original position. Thus, if states r and s differ from each other only by the position of the particle moved and if these positions are within each other's squares, the transition probabilities are equal; otherwise they are zero. Assume $E_r > E_s$. Then the number of systems moving from state r to state s will be simply $\nu_r P_{rs}$, since all moves to a state of lower energy are allowed. The number moving from s to r will be $\nu_s P_{sr} \exp(-(E_r-E_s)/kT)$, since here we must weigh by the exponential factor. Thus the net number of systems moving from s to r is

$$P_{rs}(\nu_s \exp(-(E_r-E_s)/kT)-\nu_r). \tag{5}$$

So we see that between any two states r and s, if

$$(\nu_r/\nu_s) > [\exp(-E_r/kT)/\exp(-E_s/kT)], \tag{6}$$

on the average more systems move from state r to state s. We have seen already that the method is ergodic; i.e., that any state can be reached from any other, albeit in several moves. These two facts mean that our ensemble must approach the canonical distribution. It is, incidentally, clear from the above derivation that after a forbidden move we must count again the initial configuration. Not to do this would correspond in the above case to removing from the ensemble those systems which tried to move from s to r and were forbidden. This would unjustifiably reduce the number in state s relative to r.

The above argument does not, of course, specify how rapidly the canonical distribution is approached. It may be mentioned in this connection that the maximum displacement α must be chosen with some care; if too large, most moves will be forbidden, and if too small, the configuration will not change enough. In either case it will then take longer to come to equilibrium.

For the rigid-sphere case, the game of chance on $\exp(-\Delta E/kT)$ is, of course, not necessary since ΔE is either zero or infinity. The particles are moved, one at a time, according to Eq. (3). If a sphere, after such a move, happens to overlap another sphere, we return it to its original position.

III. SPECIALIZATION TO RIGID SPHERES IN TWO DIMENSIONS

A. The Equation of State

The virial theorem of Clausius can be used to give an equation of state in terms of $\bar{n}$, the average density of other particles at the surface of a particle. Let $\mathbf{X}_i^{(\text{tot})}$ and $\mathbf{X}_i^{(\text{int})}$ represent the total and the internal force, respectively, acting on particle i, at a position $\mathbf{r}_i$. Then the virial theorem can be written

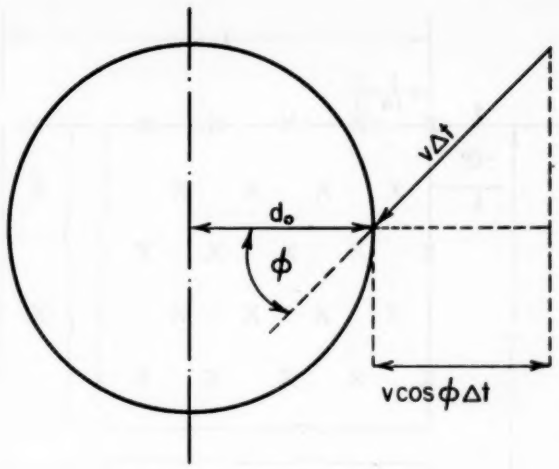

FIG. 1. Collisions of rigid spheres.

$$\langle \sum_i \mathbf{X}_i^{(\text{tot})} \cdot \mathbf{r}_i \rangle_{Av} = 2PA + \langle \sum_i \mathbf{X}_i^{(\text{int})} \cdot \mathbf{r}_i \rangle_{Av} = 2E_{\text{kin}}. \tag{7}$$

Here P is the pressure, A the area, and E_{kin} the total kinetic energy,

$$E_{\text{kin}} = N m \bar{v}^2/2$$

of the system of N particles.

Consider the collisions of the spheres for convenience as represented by those of a particle of radius d_0, twice the radius of the actual spheres, surrounded by $\bar{n}$ point particles per unit area. Those surrounding particles in an area of $2\pi d_0 v \cos\phi \Delta t$, traveling with velocity v at an angle ϕ with the radius vector, collide with the central particle provided $|\phi| < \pi/2$. (See Fig. 1.) Assuming elastic recoil, they each exert an average force during the time Δt on the central particle of

$$2mv \cos\phi/\Delta t.$$

One can see that all ϕ's are equally probable, since for any velocity-independent potential between particles the velocity distribution will just be Maxwellian, hence isotropic. The total force acting on the central particle, averaged over ϕ, over time, and over velocity, is

$$\bar{F}_i = m\bar{v}^2 \pi d_0 \bar{n}. \tag{8}$$

The sum

$$\langle \sum_i \mathbf{X}_i^{(\text{int})} \cdot \mathbf{r}_i \rangle_{Av}$$

is

$$-\tfrac{1}{2} \sum_{\substack{i \\ i \neq j}} \{ \sum_j r_{ij} F_{ij} \},$$

with F_{ij} the magnitude of the force between two particles and r_{ij} the distance between them. We see that

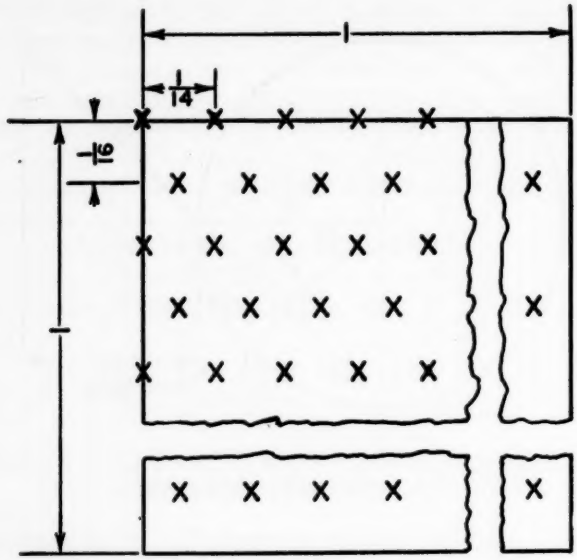

FIG. 2. Initial trigonal lattice.

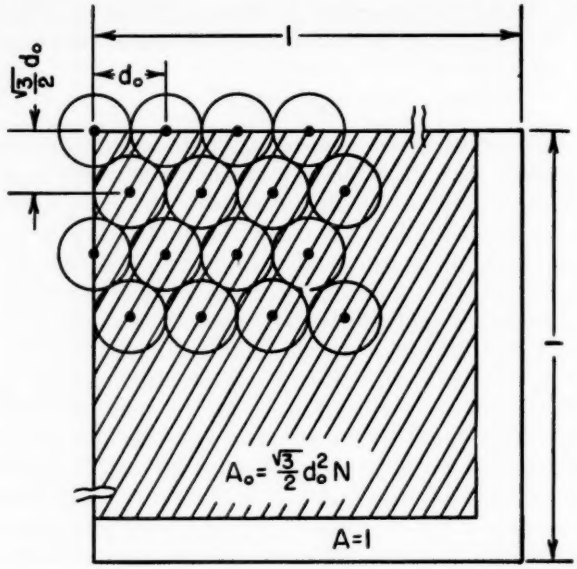

FIG. 3. The close-packed arrangement for determining A_0.

$r_{ij}=d_0$ and $\sum_j F_{ij}$ is given by Eq. (8), so we have

$$\langle \sum_i \mathbf{X}_i^{(\mathrm{int})} \cdot \mathbf{r}_i \rangle_{\mathrm{Av}} = -(Nm\bar{v}^2/2)\pi d_0^2 \bar{n}. \tag{9}$$

Substitution of (9) into (7) and replacement of $(N/2)m\bar{v}^2$ by E_{kin} gives finally

$$PA = E_{\mathrm{kin}}(1+\pi d_0^2\bar{n}/2) \equiv NkT(1+\pi d_0^2\bar{n}/2). \tag{10}$$

This equation shows that a determination of the one quantity $\bar{n}$, according to Eq. (4) as a function of A, the area, is sufficient to determine the equation of state for the rigid spheres.

B. The Actual Calculation of $\bar{n}$

We set up the calculation on a system composed of $N=224$ particles ($i=0, 1\cdots 223$) placed inside a square of unit side and unit area. The particles were arranged initially in a trigonal lattice of fourteen particles per row by sixteen particles per column, alternate rows being displaced relative to each other as shown in Fig. 2. This arrangement gives each particle six nearest neighbors at approximately equal distances of $d=1/14$ from it.

Instead of performing the calculation for various areas A and for a fixed distance d_0, we shall solve the equivalent problem of leaving $A=1$ fixed and changing d_0. We denote by A_0 the area the particles occupy in close-packed arrangement (see Fig. 3). For numerical convenience we defined an auxiliary parameter ν, which we varied from zero to seven, and in terms of which the ratio (A/A_0) and the forbidden distance d_0 are defined as follows:

$$d_0 = d(1-2^{\nu-8}), \quad d=(1/14), \tag{11a}$$

$$(A/A_0) = 1/(3^{\frac{1}{2}}d_0^2 N/2) = 1/0.98974329(1-2^{\nu-8})^2. \tag{11b}$$

The unit cell is a parallelogram with interior angle 60°, side d_0, and altitude $3^{\frac{1}{2}}d_0/2$ in the close-packed system.

Every configuration reached by proceeding according to the method of the preceding section was analyzed in terms of a radial distribution function $N(r^2)$. We chose a $K>1$ for each ν and divided the area between πd_0^2 and $K^2\pi d_0^2$ into sixty-four zones of equal area ΔA^2,

$$\Delta A^2 = (K^2-1)\pi d_0^2/64.$$

We then had the machine calculate for each configuration the number of pairs of particles N_m ($m=1, 2, \cdots 64$) separated by distances r which satisfy

$$(m-1)\Delta A^2 + \pi d_0^2 < \pi r^2 \leqslant m\Delta A^2 + \pi d_0^2. \tag{12}$$

The N_m were averaged over successive configurations according to Eq. (4), and after every sixteen cycles (a cycle consists of moving every particle once) were extrapolated back to $r^2=d_0^2$ to obtain $N_{\frac{1}{2}}$. This $N_{\frac{1}{2}}$ differs from $\bar{n}$ in Eq. (10) by a constant factor depending on N and K.

The quantity K was chosen for each ν to give reasonable statistics for the N_m. It would, of course, have been possible by choosing fairly large K's, with perhaps a larger number of zones, to obtain $N(r^2)$ at large distances. The oscillatory behavior of $N(r^2)$ at large distances is of some interest. However, the time per cycle goes up fairly rapidly with K and with the number of zones in the distance analysis. For this reason only the behavior of $N(r^2)$ in the neighborhood of d_0^2 was investigated.

The maximum displacement α of Eq. (3) was set to $(d-d_0)$. About half the moves in a cycle were forbidden by this choice, and the initial approach to equilibrium from the regular lattice was fairly rapid.

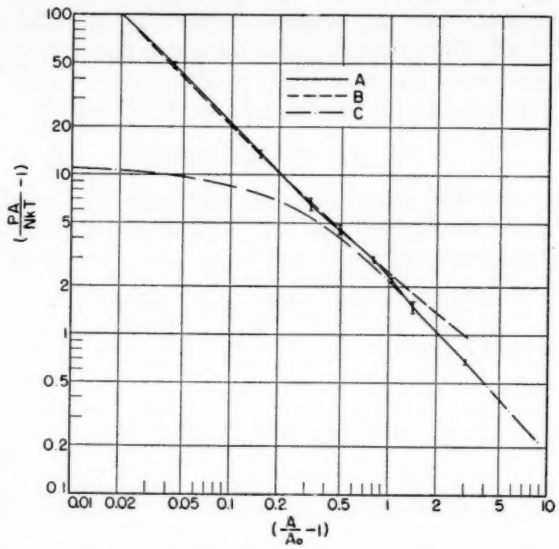

FIG. 4. A plot of $(PA/NkT)-1$ *versus* $(A/A_0)-1$. Curve A (solid line) gives the results of this paper. Curves B and C (dashed and dot-dashed lines) give the results of the free volume theory and of the first four virial coefficients, respectively.

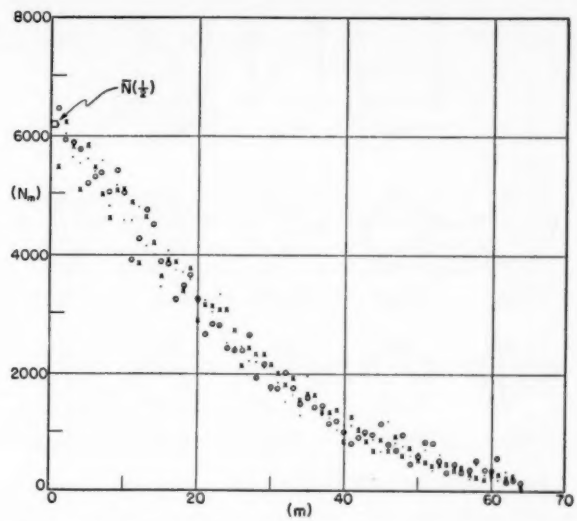

FIG. 5. The radial distribution function N_m for $\nu=5$, $(A/A_0)=1.31966$, $K=1.5$. The average of the extrapolated values of $N_{\frac{1}{2}}$ in $\bar{N}_{\frac{1}{2}}=6301$. The resultant value of $(PA/NkT)-1$ is $64\bar{N}_{\frac{1}{2}}/N^2(K^2-1)$ or 6.43. Values after 16 cycles, ●; after 32, ×; and after 48, ○.

IV. NUMERICAL RESULTS FOR RIGID SPHERES IN TWO DIMENSIONS

We first ran for something less than sixteen cycles in order to get rid of the effects of the initial regular configuration on the averages. Then about forty-eight to sixty-four cycles were run at

$$\nu=2,\ 4,\ 5,\ 5.5,\ 6,\ 6.25,\ 6.5,\ \text{and}\ 7.$$

Also, a smaller amount of data was obtained at $\nu=0$, 1, and 3. The time per cycle on the Los Alamos MANIAC is approximately three minutes, and a given point on the pressure curve was obtained in four to five hours of running. Figure 4 shows $(PA/NkT)-1$ *versus* $(A/A_0)-1$ on a log-log scale from our results (curve A), compared to the free volume equation of Wood[1] (curve B) and to the curve given by the first four virial coefficients (curve C). The last two virial coefficients were obtained by straightforward Monte Carlo integration on the MANIAC (see Sec. V). It is seen that the agreement between curves A and B at small areas and between curves A and C at large areas is good. Deviation from the free volume theory begins with a fairly sudden break at $\nu=6(A/A_0\simeq 1.8)$.

A sample plot of the radial distribution function for $\nu=5$ is given in Fig. 5. The various types of points represent values after sixteen, thirty-two, and forty-eight cycles. For $\nu=5$, least-square fits with a straight line to the first sixteen N_m values were made, giving extrapolated values of $N_{\frac{1}{2}}^{(1)}=6367$, $N_{\frac{1}{2}}^{(2)}=6160$, and $N_{\frac{1}{2}}^{(3)}=6377$. The average of these three was used in constructing PA/NkT. In general, least-square fits of the first sixteen to twenty N_m's by means of a parabola, or, where it seemed suitable, a straight line, were made.

[1] William W. Wood, J. Chem. Phys. **20**, 1334 (1952).

The errors indicated in Fig. 4 are the root-mean-square deviations for the three or four $N_{\frac{1}{2}}$ values. Our average error seemed to be about 3 percent.

Table I gives the results of our calculations in numerical form. The columns are ν, A/A_0, $(PA/NkT)-1$, and, for comparison purposes, $(PA/NkT-1)$ for the free volume theory and for the first four coefficients in the virial coefficient expansion, in that order, and finally PA_0/NkT from our results.

V. THE VIRIAL COEFFICIENT EXPANSION

One can show[2] that

$$(PA/NkT)-1=C_1(A_0/A)+C_2(A_0/A)^2+C_3(A_0/A)^3+C_4(A_0/A)^4+0(A_0/A)^5,$$

$$C_1=\pi/3^{\frac{1}{2}},\quad C_2=4\pi^2A_{3,3}/9,$$

$$C_3=\pi^3(6A_{4,5}-3A_{4,4}-A_{4,6})/3^{\frac{1}{2}},$$

$$C_4=(8\pi^3/135)\cdot[12A_{5,5}-60A_{5,6}'-10A_{5,6}''+30A_{5,7}'+60A_{5,7}''+10A_{5,7}'''-30A_{5,8}'-15A_{5,8}''+10A_{5,9}-A_{5,10}]. \quad (13)$$

TABLE I. Results of this calculation for $(PA/NkT)-1=X_1$ compared to the free volume theory (X_2) and the four-term virial expansion (X_3). Also (PA_0/NkT) from our calculations.

ν	(A/A_0)	X_1	X_2	X_3	(PA_0/NkT)
2	1.04269	49.17	47.35	9.77	48.11
4	1.14957	13.95	13.85	7.55	13.01
5	1.31966	6.43	6.72	5.35	5.63
5.5	1.4909	4.41	4.53	4.02	3.63
6	1.7962	2.929	2.939	2.680	2.187
6.25	2.04616	2.186	2.323	2.065	1.557
6.5	2.41751	1.486	1.802	1.514	1.028
7	4.04145	0.6766	0.990	0.667	0.4149

[2] J. E. Mayer and M. G. Mayer, *Statistical Mechanics* (John Wiley and Sons, Inc., New York, 1940), pp. 277–291.

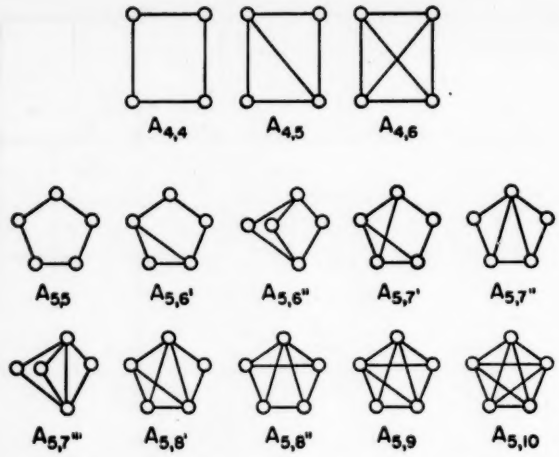

FIG. 6. Schematic diagrams for the various area integrals.

The coefficients $A_{i,k}$ are cluster integrals over configuration space of i particles, with k bonds between them. In our problem a bond is established if the two particles overlap. The cluster integral is the volume of configuration space for which the appropriate bonds are established. If k bonds can be distributed over the i particles in two or more different ways without destroying the irreducibility of the integrals, the separate cases are distinguished by primes. For example, A_{33} is given schematically by the diagram

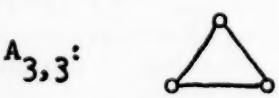

and mathematically as follows: if we define $f(r_{ij})$ by

$$f(r_{ij})=1 \quad \text{if} \quad r_{ij}<d,$$
$$f(r_{ij})=0 \quad \text{if} \quad r_{ij}>d,$$

then

$$A_{3,3}=\frac{1}{\pi^2 d^4}\int\cdots\int dx_1 dx_2 dx_3 dy_1 dy_2 dy_3 (f_{12}f_{23}f_{31}).$$

The schematics for the remaining integrals are indicated in Fig. 6.

The coefficients $A_{3,3}$, $A_{4,4}$, and $A_{4,5}$ were calculated algebraically, the remainder numerically by Monte Carlo integration. That is, for $A_{5,5}$ for example, particle 1 was placed at the origin, and particles 2, 3, 4, and 5 were put down at random, subject to $f_{12}=f_{23}=f_{34}=f_{15}=1$. The number of trials for which $f_{45}=1$, divided by the total number of trials, is just $A_{5,5}$.

The data on $A_{4,6}$ is quite reliable. We obtained

$$A_{4,6}/A_{4,4}=0.752(\pm 0.002).$$

However, because of the relatively large positive and negative terms in C_4 of Eq. (13), the coefficient C_4, being a small difference, is less accurate. We obtained

$$C_4=8\pi^3(0.585)/135 \quad (\pm\sim 5 \text{ percent}).$$

Our final formula is

$$(PA/NkT)-1=1.813799(A_0/A)+2.57269(A_0/A)^2+3.179(A_0/A)^3+3.38(A_0/A)^4+0(A_0/A)^5. \quad (14)$$

This formula is plotted in curve C of Fig. 4 and tabulated for some values of (A/A_0) in column 5 of Table I. It is seen in Fig. 4 that the curves agrees very well with our calculated equation of state for $(A/A_0)>2.5$. In this region both the possible error in our last virial coefficients and the contribution of succeeding terms in the expansion are quite small (less than our probable statistical error) so that the virial expansion should be accurate.

VI. CONCLUSION

The method of Monte Carlo integrations over configuration space seems to be a feasible approach to statistical mechanical problems which are as yet not analytically soluble. At least for a single-phase system a sample of several hundred particles seems sufficient. In the case of two-dimensional rigid spheres, runs made with 56 particles and with 224 particles agreed within statistical error. For a computing time of a few hours with presently available electronic computers, it seems possible to obtain the pressure for a given volume and temperature to an accuracy of a few percent.

In the case of two-dimensional rigid spheres our results are in agreement with the free volume approximation for $A/A_0<1.8$ and with a five-term virial expansion for $A/A_0>2.5$. There is no indication of a phase transition.

Work is now in progress for a system of particles with Lennard-Jones type interactions and for three-dimensional rigid spheres.

The Mechanism of Unimolecular Reactions

LOUIS S. KASSEL
Universal Oil Products Company, Des Plaines, Illinois
(Received January 20, 1953)

The general theory of unimolecular reactions is re-examined to determine what type of information about rate constants for specific activated states may be determined from the experimental reaction rate-pressure curves. It is found that the possibilities in this respect are very limited. Contrary to a recent statement by Johnston, data on decomposition of nitrogen pentoxide in the presence of nitric oxide are adequately fitted by the Kassel theory. Data on decomposition of nitrous oxide, however, cannot be fitted by this theory. Failure of the theory in this case is the result of too small a range of decomposition rate constants for various activated states.

THE Rice-Ramsperger-Kassel theory of unimolecular reactions was developed in the remote past.[1] This theory permits calculation, in terms of a few molecular parameters, of the variation with pressure of the first-order rate constant for a unimolecular reaction from the high pressure region in which the constant is independent of pressure down to the expected low pressure region where it is proportional to pressure. Failure of the intervening years to produce any refinement in the theory must be attributed not so much to the perfection of its original form as to the very scanty and unreliable experimental data on which it can be tested. Recently however, Mills and Johnston[2] and Johnston and Perrine[3] have presented data on the decomposition of nitrogen pentoxide in the presence of nitric oxide, and Johnston[4] has summarized the work of previous observers on the decomposition of nitrous oxide. Both of these reactions have been studied over the major part of the interesting range in which the transition from first-order to second-order kinetics takes place.

It becomes of interest to re-examine the theory in order to extract a maximum amount of information from the experimental data. The general expression for the first-order rate constant of a unimolecular reaction based on a collisional mechanism of activation is

$$k=k'M=\sum\frac{a_ic_iM}{b_iM+c_i}, \tag{1}$$

where a_i, b_i, and c_i are rate constants for collisional activation, collisional deactivation, and reaction, respectively, and M is the reactant concentration. (In the presence of added gases, M on the right side of (1) is replaced by a properly weighted sum.) At sufficiently high pressures, first-order rate constants approach a limiting value,

$$k_\infty=\sum a_ic_i/b_i, \tag{2}$$

and at sufficiently low concentrations second-order rate constants approach a limiting value,

$$k_0'=\sum a_i. \tag{3}$$

Define

$$R=k_\infty/k_0'; \tag{4}$$

R has the dimensions of a concentration, and it will be seen to represent the mid-point of the change from a first-order to a second-order reaction. Define reduced values of the observable variables

$$\left.\begin{aligned} f_1&=k/k_\infty,\\ f_2&=k'/k_0',\\ C&=M/R.\end{aligned}\right\} \tag{5}$$

It is then convenient to plot $\log f_1$ against $\log C$ for values of C greater than 1, and $\log f_2$ against $\log C$ for values of C less than 1. These two plots may be joined to give a single curve which is asymptotic to the value 0 at both $\log C=-\infty$ and $\log C=\infty$, and which reaches its lowest value at a cusp located at $\log C=0$. Making the substitutions (5) in (1) gives

$$f_1=f_2C=\sum\frac{a_ic_iC}{b_iC\sum a_ic_i/b_i+c_i\sum a_i}. \tag{6}$$

It is also convenient, moreover, to introduce reduced values of the molecular parameters:

$$\left.\begin{aligned} p_i&=a_i/\sum a_i\\ r_i&=(a_ic_i/b_i)/\sum a_ic_i/b_i.\end{aligned}\right\} \tag{7}$$

The theoretical form of the relationship between rate constant and concentration is then given by the simple expression

$$f_1=f_2C=\sum\frac{r_iC}{r_i/p_i+C}. \tag{8}$$

The maximum information about the detailed mechanism of activation, deactivation, and reaction which could be extracted from the data would be a set of

[1] For references, see L. S. Kassel, *Kinetics of Homogeneous Gas Reactions* (Chemical Catalog Company, Inc., New York, 1932), pp. 93–113.
[2] R. L. Mills and H. S. Johnston, J. Am. Chem. Soc. **73**, 938 (1951).
[3] H. S. Johnston and R. L. Perrine, J. Am. Chem. Soc. **73**, 4782 (1951).
[4] H. S. Johnston, J. Chem. Phys. **19**, 663 (1951).

values r_i and p_i. We now examine the practical problem of extracting such information.

It is convenient to have a small number of parameters which describe at least approximately the shape of the experimental curves. There are two different approaches to the determination of such parameters, depending upon whether they are based on the region near the asymptotes, or the region near the cusp. Parameters of the former type may be defined as follows:

$$\left.\begin{aligned} F&=[-df_1/d(1/C)]_{C=\infty}\\ &=[d(1/f_1)/d(1/C)]_{C=\infty}\\ &=\sum r_i^2/p_i,\\ G&=[-df_2/dC]_{C=0}\\ &=[d(1/f_2)/dC]_{C=0}\\ &=\sum p_i^2/r_i. \end{aligned}\right\} \tag{9}$$

These parameters are identical with F and G as used by Johnston.[5] The natural selections for the second type of parameter are the value and slope at the mid-point $C=1$:

$$\begin{aligned} f&=f_1(1)=f_2(1)=\sum r_ip_i/(r_i+p_i),\\ g&=(d\log f_1/d\log C)_{C=1}\\ &=1-(d\log f_2/d\log C)_{C=1}\\ &=\sum p_i\left(\frac{r_i}{r_i+p_i}\right)^2\Big/\sum p_i\left(\frac{r_i}{r_i+p_i}\right). \end{aligned} \tag{10}$$

The form of the function (8), together with the physical necessity for the r_i and p_i to be positive, places certain limitations upon the parameters. These limitations are

$$\begin{gathered} F\geqq 1,\\ G\geqq 1,\\ f\leqq \tfrac{1}{2}\\ 1-f\geqq g\geqq f. \end{gathered}$$

When there is only a single term in the sum, the shape of the curve in uniquely determined. In this case

$$\begin{gathered} F=G=1,\\ f=g=\tfrac{1}{2}. \end{gathered}$$

When the sum contains two terms, the curve is completely defined by either pair of parameters, F, G or f, g. The relation between the parameters and the r and p_i is most conveniently stated in terms of new sum and product functions:

$$\left.\begin{aligned} S&=r_1/p_1+r_2/p_2,\\ P&=r_1r_2/p_1p_2. \end{aligned}\right\} \tag{11}$$

The following relations may then be derived:

$$\left.\begin{aligned} P&=(F-1)/(G-1),\\ S&=(GF-1)/(G-1),\\ P&=(1-f-g)/(g-f),\\ S&=(1-f)(1-2f)/f(g-f). \end{aligned}\right\} \tag{12}$$

The relations between the two pairs of parameters are of particular interest. These are

$$\left.\begin{aligned} F&=(1-4f+3f^2+fg)/f(g-f),\\ G&=(1-3f+3f^2-fg)/f(1-f-g),\\ f&=(F+G-2)/(GF+F+G-3),\\ g&=(G^2F+F^2-2G-3F+3)\\ &\quad\div(GF+F+G-3)\times(F+G-2). \end{aligned}\right\} \tag{13}$$

The following three theorems, which will be helpful in the analysis of experimental data, have been proved rigorously. They are given here without the proof, which involves merely tedious algebraic manipulation.

Theorem 1: For any summation of the form (8),

$$F-(1-4f+3f^2+fg)/f(g-f)=\frac{\frac{1}{6}\sum\dfrac{p_ip_jp_k(r_i/p_i-r_j/p_j)^2(r_i/p_i-r_k/p_k)^2(r_j/p_j-r_k/p_k)^2}{(1+r_i/p_i)^2(1+r_j/p_j)^2(1+r_k/p_k)^2}}{\frac{1}{2}\sum\dfrac{p_ip_j(r_i/p_i-r_j/p_j)^2}{(1+r_i/p_i)^2(1+r_j/p_j)^2}}, \tag{14}$$

where the single summation signs indicate multiple summations over all indices. A similar relationship involving G may be obtained by making the substitutions

$$\begin{gathered} F\rightarrow G,\\ g\rightarrow 1-g,\\ p\rightarrow r,\\ r\rightarrow p. \end{gathered}$$

the right member of (14) vanishes for a summation over two terms and is clearly positive for more than two. Hence comparison with (13) shows that the minimum values of F and G consistent with a pair of values f, g are given by the uniquely determined two-term summation. Any summation over more than two terms will give larger values of F and G.

Theorem 2: Consider all summations corresponding to a given pair of values F, G. The uniquely determined two-term summation gives the smallest values of f_1 and f_2 at all values of C between 0 and ∞.

[5] H. S. Johnston, J. Chem. Phys. **20**, 1103 (1952).

Theorem 3: For any summation, f_1 and $1/f_1$ may be expanded in power series in $1/C$ as follows:

$$f_1=1-(1/C)\sum r_i^2/p_i+(1/C^2)\sum r_i^3/p_i^2-\cdots,$$
$$1/f_1=1+(1/C)\sum r_i^2/p_i$$
$$-(1/C^2)[\sum r_i^3/p_i^2-(\sum r_i^2/p_i)^2]+\cdots. \quad (15)$$

It may be shown that

$$\sum r_i^3/p_i^2-(\sum r_i^2/p_i)^2=\sum r_i r_j(r_i/p_i-r_j/p_j)^2, \quad (16)$$

which is clearly positive. This shows thst the plot of $1/f_1$ against $1/C$ has smaller curvature at the origin, and the same slope, as the plot of f_1 against $1/C$. The former plot, therefore, is more suitable for determination of the limiting slope. This means that it is better to plot $1/k$ against $1/M$, rather than k against $1/M$. In similar manner, it can be shown that for the low pressure range it is better to plot $1/k'$ against M rather than k' against M.

Johnston[5] has derived the following values from the data for the decomposition of nitrogen pentoxide in the presence of nitric oxide:

k_∞, sec^{-1}	0.277,
k_0', cc mole^{-1} sec^{-1}	1.80×10^5,
F	3.1,
G	11.4.

From his values for k_∞ and k_0', one calculates that $R=1.54\times10^{-6}$ mole/cc $=28.8$ mm. His value of F is based on a plot of k against pressure over the range of C from 76.7 to 244. His value of G is based upon a plot of k' against concentration over a range of C from 0.0025 to 0.0662. If his method of calculation is applied not to experimental data but to calculated values derived from the uniquely determined two-term distribution with values $F=3.1$, $G=11.4$, using these same ranges of C, the apparent values would be $F=2.94$, $G=5.36$. It is apparent from Theorem 1 that if the same type of calculation were made for any other distribution with the same true values of F and G, the apparent values would be even lower. Furthermore, the data used for the determination of F do not lead to as small an apparent value as is given by Johnston unless one assumes that, on the basis of unpublished work cited in his paper, the relative efficiency of activation for nitrogen has been taken as approximately one-fourth of that for the mixture of nitrogen pentoxide and nitric oxide. If this has been done, the range of C over which experimental measurements have been made is moved towards smaller values, and the maximum possible apparent value corresponding to the true value of 3.1 is again decreased. It is concluded, therefore, from study of the rate data at extreme pressures, that the correct values of F and G must be substantially greater than those given by Johnston.

This same conclusion is derived from analysis of the central portion of the curve. In this analysis we have used the values for the limiting rates given in earlier

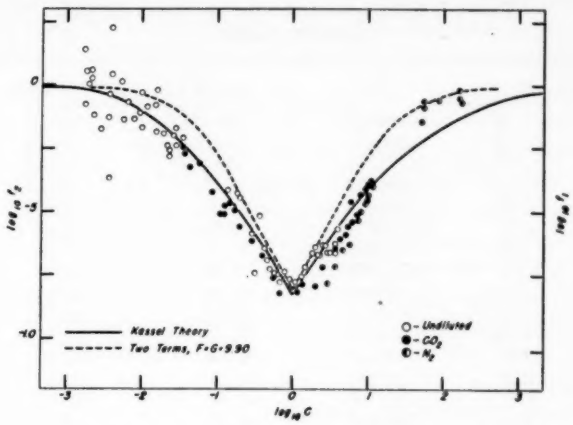

FIG. 1. Comparison of experimental rate constants for nitrogen pentoxide with theoretical curves.

references:[2,3]

k_∞ sec^{-1}	0.290,
k_0' cc mole^{-1}	1.27×10^5.

These values correspond to $R=2.28\times10^{-6}$ mole/cc $=42.7$ mm. Examination of the experimental data shows that $f=0.155$. The value of g is not determined with any accuracy, but the data are not inconsistent with $g=0.5$. It is calculated from (13) that for the unique two-term distribution with $f=0.155$, $g=0.50$, we have the values $F=G=9.90$. Any distribution with the same values of f and g which involves more than two terms will give larger values of F and G. The smallest possible value of F which is consistent with the value $f=0.155$ is given by the two-term distribution with the maximum possible value of $g=0.845$. For this combination of f and g values, the two-term distribution gives $F=5.45$, $G=\infty$. Although the experimental data do not determine g with much precision, there is no doubt that its value is substantially below 0.845. It is considered, therefore, that data in the central part of the pressure range indicate that the value of F must be very substantially greater than 5.45.

Johnston[5] has computed theoretical values of F and G on the basis of the Kassel theory for various numbers of oscillators and assumed vibration frequencies. He finds that there is no choice of these quantities which leads to theoretical values of F and G which are at all close to the "experimental" values of $F=3.1$, $G=11.4$. On the basis he states: "Thus Kassel theory fails for nitrogen pentoxide, and this failure is very large compared to experimental error." It seemed worth while, however, to subject Kassel theory to a test of a more direct character. There are two major disposable parameters in the simple form of this theory; the number of oscillators s in the molecular model, and the frequency of these oscillators, which is most conveniently replaced by the ratio m,

$$m=E/h\nu.$$

TABLE I. Calculated first-order constants for high pressure branch.

C	f_1	$-\Delta f_1/\Delta(1/C)$	$\Delta(1/f_1)/\Delta(1/C)$
1	0.149617	0.1135	3.676
2	0.206372	0.2774	4.875
4	0.275718	0.6470	6.581
8	0.356598	1.436	9.022
16	0.446354	3.021	12.52
32	0.540774	6.004	17.49
64	0.634583	11.23	24.49
128	0.722296	19.68	34.09
256	0.799164	32.26	46.82
512	0.862168	49.33	62.85
1024	0.910338	70.32	81.77
2048	0.944673	93.56	102.4
4096	0.967516	116.7	122.8
8192	0.981760	137.0	141.0
16384	0.990123	161.8	163.4
∞	1.000000		

Using fixed values $s=15$ and $E/RT=35$, f was calculated for a number of values of m with the following results:

m	f
14	0.3266
21	0.1925
25	0.1496
28	0.1269

Agreement with the experimental $f=0.155$ was considered sufficiently good at $m=25$, and the complete theoretical rate-pressure curve was calculated for this case. Comparison between the calculated curve and the experimental values is shown in Fig. 1. Agreement is clearly within the rather large experimental error except in the case of experiments where nitrogen was used as the diluent. These latter experiments fall into two distinct groups. The first group comprises experiments made at pressures less than 500 mm. In most of these experiments, the diluent:reactant ratio was about 30, and in no case was it as great as 100. All these experiments give rates which fall below the theoretical curve, as would be expected for a small molecule with few internal degrees of freedom. The second group of nitrogen points were all obtained at pressures in excess of 2000 mm, and with diluent:reactant ratios in the range 800–9000. These points were obtained in a different apparatus and with a different experimental technique than was used for any of the other measurements. In the absence of confirmatory evidence, it is not believed that these high pressure points should receive much weight.

TABLE II. Calculated second-order constants for low pressure branch.

$1/C$	f_2	$-\Delta f_2/\Delta C$	$\Delta(1/f_2)/\Delta C$
1	0.149617	0.1214	3.857
2	0.210301	0.3053	5.065
4	0.286629	0.7384	6.798
8	0.378926	1.734	9.392
16	0.487320	3.892	13.11
32	0.608941	7.791	17.51
64	0.730678	13.10	21.51
128	0.832991	18.41	24.42
256	0.904904	22.51	26.22
512	0.948875	26.18	27.59
∞	1.000000		

Table I gives calculated values of f_1 for the high pressure branch of the rate curve, extending far above the experimental range. This table shows also values for the functions $-\Delta f_1/\Delta(1/C)$ and $\Delta(1/f_1)\Delta(1/C)$ calculated between the concentrations shown and the next higher concentrations. Both of these functions approach F as a limit, and it is apparent by rough extrapolation that the value of F is about 180. It is also apparent, however, that there is no possibility of obtaining direct experimental evidence for such a value unless extremely precise rate measurements are made very near to the high pressure limit. Table II is a similar presentation of the calculated second-order rate constant f_2 for the low pressure branch of the curve. This table contains also values of the functions $-\Delta f_2/\Delta C$ and $\Delta(1/f_2)/\Delta C$. Both of these functions approach G as a limit, and it is evident that the limiting slope corresponds to approximately $G=28$.

It is evident from Tables I and II, as is expected from theorem 3, that plots of $1/k$ against p and $1/p$ are superior to plots of k for determination of G and F, respectively. Neither plot, however, is of any real value for the determination of F and G when these parameters have true values greater than about 5. Either plot is reasonably satisfactory for the limiting values k_∞ and k_0', with the plot of $1/k$ having a slight advantage.

Figure 1 contains also the calculated curve for the case $F=G=9.90$, based on the two-term distribution. It is evident that this curve fits the experimental data somewhat less well than does that based on the Kassel theory. The data can be fitted, however, by curves based on a three-term distribution. Such curves are not presented, since they are considered to have no theoretical significance. It is noteworthy, however, that distributions which fit the data involve a spread of relative rate constants for the various states of at least 1000:1. It is necessary to have a spread of at least this magnitude to fit the ends of the curves, and it is necessary to have at least one state of intermediate rate constant in order to avoid too low a value of f. Given these conditions, almost any distribution with two disposable parameters can be made to fit the experimental data. It is apparent that the shape of the reaction rate-pressure curve is a relatively feeble tool for studying the form of the distribution.

The situation is rather different in the case of nitrous oxide. The agreement between the direct measurements of Hunter[6] and the smoothed rate constants derived by Johnston[4] from the observations of all other workers is so poor that it is necessary to select one or the other of the two groups as representing the data to be fitted. The smoothed points have been chosen for this purpose,

[6] E. Hunter, Proc. Roy. Soc. (London) **A144**, 386 (1934).

largely because they extend over a wider range of concentrations. These points can be fitted very well by the empirical equation

$$10^4k=\frac{7.13}{1+3.89/10^4M}+\frac{1.211}{1+.0927/10^4M},$$

in which the constants have been evaluated by the method of least squares. The parameters calculated from this equation are as follows:

$$F=5.96, \qquad G=5.31,$$
$$f=0.232, \qquad g=0.476.$$

It will be noted that even in this case, where the values of F and G are relatively small, the method used by Johnston[5] gives unsatisfactory results. His values were $F=3.3$, $G=2.6$. In accordance with Theorem 2, the minimum value of f which is consistent with these values of F and G is 0.340, and the minimum value which could be obtained with the Kassel theory is even greater. It is not surprising, therefore, that when Johnston determines the parameters of Kassel theory from his incorrect values of F and G, he finds a poor fit with experiment in the middle part of the curve. It might be expected that by using the values of f and g as given above to determine the parameters of Kassel theory, satisfactory agreement would be obtained as in the case of nitrogen pentoxide. In fact, however, using the maximum physically possible value, $s=4$, and the maximum plausible value $m=50$, Kassel theory gives $f=0.3241$. The apparent cause of the difficulty is that for small values of s, Kassel theory predicts a relatively narrow range of reaction rate constants. Thus the successful empirical equation corresponds to a model with two activated states whose rate constants are in the approximate ratio of 42:1. For Kassel theory with $E/RT=35$, $s=4$, $m=50$, this rate constant ratio of 42:1 covers the lowest six activated states which contribute 75 percent of the limiting high pressure rate and 97.9 percent of the limiting low pressure rate. Kassel theory may be improved in this respect by a modification which involves splitting each activated state as defined by energy content alone into two states with different reaction rate constants. The more abundant states with the lower rate constant contribute largely to the low pressure limit and are relatively unimportant at high pressure. The small fraction of states with high constants make a major contribution at high pressures and only minor at low. Such a modification possesses physical plausibility, since energy stored in the different degrees of freedom might be expected to have differing effectiveness in facilitating decomposition. In a larger molecule such as nitrogen pentoxide, where the important activated states cover a relatively enormous range of rate constants, there is a better chance for the specific rates to be averaged out, and for a purely statistical theory of the Kassel type to succeed.

Study of reaction rate—pressure curves at different temperatures offers the possibility of distinguishing between total energy content and specific quantum numbers as the cause of differing specific rate constants. Further speculation along this line cannot be justified by the available data for nitrous oxide, which is not only of limited range and low accuracy, but suffers also from the possibility of a pressure shift in the ratio of the two secondary reactions:

$$O+N_2O=N_2+O_2,$$
$$O+O+M=O_2+M.$$

Such a shift would distort the rate-pressure curve.

Molecular Distribution Functions in a One-Dimensional Fluid*

ZEVI W. SALSBURG, ROBERT W. ZWANZIG, AND JOHN G. KIRKWOOD
Sterling Chemistry Laboratory, Yale University,† New Haven, Connecitut

(Received February 4, 1953)

Exact expressions are derived for the molecular distribution functions in a one-dimensional fluid whose particles interact with a nearest neighbor pair potential. The pair distribution function for rigid spheres is found to be identical with Frenkel's result. The one-dimensional form of a new set of integral equations for the molecular distribution functions is examined. The superposition principle is found to be exact in a one-dimensional fluid with nearest neighbor interactions.

WE have recently derived a new set of integral equations for the molecular distribution functions.[1] In order to understand the nature of the theoretical and mathematical problems presented by these equations, we felt that it would be profitable to study them for the case of a one-dimensional system. With certain assumptions about the intermolecular potential, an exact solution can be obtained. In this article, we derive exact expressions for the distribution functions in a one-dimensional system whose particles interact only with nearest neighbors and whose potential can be expressed as the sum of pair potentials. We then use these distribution functions to calculate the thermodynamic properties of the fluid. Finally, we discuss the integral equations for a one-dimensional system and use the known distribution function to test these equations for a system of rigid spheres having no attractive forces between them.

As an alternative to the well-known method of calculating the partition function, the thermodynamic functions of a macroscopic system can be obtained from a knowledge of the distribution functions for sets of n molecules and the forces between individual particles. When the potential of intermolecular force is approximated by a sum of pair potentials,

$$V_N=\sum_{i<j}\sum V(R_{ij}),$$

then the pair distribution function plays a central role. It has not yet been possible to calculate the pair distribution function for three-dimensional systems without using an approximation, the validity of which is hard to assess in an *a priori* way. However, in the one-dimensional system with nearest neighbor interactions, the pair and higher-order distribution functions may be evaluated exactly.

The classical statistical mechanical theory of a one-dimensional system has been developed in recent years by several authors.[2–8]

In these investigations, the partition function has been integrated exactly for several special forms of the intermolecular potential which is restricted to nearest neighbor interactions. However, a satisfactory treatment of the distribution function approach is lacking.

I. DERIVATION OF THE DISTRIBUTION FUNCTIONS

We will consider a system of N identical particles, located at the points $R_1, \cdots, R_N$ on a straight line of length L. The probability distribution function in configuration space for such a system in a canonical ensemble is

$$P^{(N)}(R_1, \cdots, R_N)=\exp[\beta(\bar{A}_N-V_N-V_W)],$$

$$\beta=1/kT,$$

$$\exp[-\beta\bar{A}_N]=\int_0^L\cdots\int_0^L \times\exp[-\beta(V_N+V_W)]\prod_{i=1}^{N}dR_i. \quad (1)$$

T is the absolute temperature and k is the Boltzmann constant. V_N is the potential of intermolecular force, and V_W is the potential of the wall forces, which act on the N particles inside the length L. $\bar{A}_N$ is the configurational contribution to the free energy of the system.

If $\varphi(R_1, \cdots, R_N)$ is a function of the coordinates of the particles, then the expectation value of φ is given by

$$\langle\varphi\rangle_N=\exp[\beta\bar{A}_N]\int_0^L\cdots\int_0^L \varphi(R_1, \cdots, R_N) \times\exp[-\beta(V_N+V_W)]\prod_{i=1}^{N}dR_i. \quad (2)$$

The most general conveniently applicable method for evaluating multiple integrals of this type is that attributable to Gürsey.[7] This is restricted to potentials that may be expressed as sums of pair potentials be-

* This work was carried out with support from the U. S. Office of Naval Research under Contract Nonr-410(00) with Yale University.
† Contribution No. 1173.

[1] J. G. Kirkwood and Z. W. Salsburg, Trans. Faraday Soc. (to be published).
[2] K. F. Herzfeld and Maria Goeppert-Mayer, J. Chem. Phys. **2**, 38 (1934).
[3] L. Tonks, Phys. Rev. **50**, 955 (1936).
[4] T. Nagamiya, Proc. Phys.-Math. Soc. Japan **22**, 705 (1940); 1034 (1940).
[5] J. Frenkel, *Kinetic Theory of Liquids* (Oxford University Press, New York, 1940), p. 126.
[6] G. Rushbrooke and H. Ursel, Proc. Cambridge Phil. Soc. **44**, 263 (1948).
[7] F. Gürsey, Proc. Cambridge Phil. Soc. **46**, 182 (1950).
[8] R. Kikuchi, J. Chem. Phys. **19**, 1230 (1951).

tween nearest neighbors. If we choose the convention

$$0<R_1<R_2<\cdots<R_N<L,$$

then the potential is

$$V_N=\sum_{i<j}\sum V(R_{ij})=\sum_{j=1}^{N-1} V(R_{j+1}-R_j). \tag{3}$$

The wall effects are easily handled if one assumes that the walls behave like particles identical with those of the system, fixed at $R=0$ and $R=L$, so that the total potential energy is

$$V_N+V_W=V(R_1)+\sum_{j=1}^{N-1} V(R_{j+1}-R_j)+V(L-R_N). \tag{4}$$

We further assume that the potential $V(R)$ has these properties:

$$\text{(a)}\quad \lim_{R\to 0} V(R)=\infty,$$

$$\text{(b)}\quad \lim_{R\to\infty} V(R)=0,$$

strongly enough that any integrals we may encounter (e.g., Eq. 29) will converge. Condition (a), which is satisfied by most of the commonly used potential functions, insures the maintenance of a given order of particles. For example, particles three and four cannot exchange places under this type of force. Therefore, we are permitted to label the particles so that $R_1<R_2<$, $\cdots$, $<R_N$ and be sure that all available configurations of the system will retain this order.

The method of Gürsey may be used only if we assume that φ is symmetric in the variables $R_1\cdots R_N$. Then

$$\begin{aligned}\langle\varphi\rangle_{Av}=N!\exp[+\beta\bar{A}_N]&\\ \times\int_0^L \exp[-\beta V(L-R_N)]dR_N&\\ \times\int_0^{R_N} \exp[-\beta V(R_N-R_{N-1})]dR_{N-1}&\\ \times\cdots\int_0^{R_2} \exp[-\beta V(R_1)]\varphi(R_1,\cdots,R_N)dR_1.&\end{aligned} \tag{5}$$

This identity can be proven by mathematical induction. In a physical sense, it is equivalent to the process of ordering the particles on the line, and prohibiting the exchange of particles. The factor $N!$ corrects for those configurations which are permutations of the order $R_1<R_2<$, $\cdots$, $<R_N$. In the case $\varphi\equiv 1$, we have

$$\begin{aligned}\exp[-\beta\bar{A}_N]=N!\int_0^L \exp[-\beta V(L-R_N)]dR_N&\\ \times\int_0^{R_N} \exp[-\beta V_{N-1,N}]dR_{N-1}&\\ \times\cdots\int_0^{R_2} \exp[-\beta V(R_1)]dR_1.&\end{aligned} \tag{6}$$

This integral is an $N+1$ fold convolution for the Laplace transform[9] of the function $\exp[-\beta V(R)]$, and one can therefore write

$$\begin{aligned}\int_0^\infty \exp[-sL-\beta\bar{A}_N]dL=N![\Omega(s)]^{N+1},&\\ \Omega(s)=\int_0^\infty \exp[-sR-\beta V(R)]dR.&\end{aligned} \tag{7}$$

The inversion formula for the Laplace transform[8] yields

$$\exp[-\beta\bar{A}_N]=\frac{N!}{2\pi i}\int_{c-i\infty}^{c+i\infty} e^{Ls}[\Omega(s)]^{N+1}ds, \tag{8}$$

where c is greater than the real parts of all the singularities of $\Omega(s)$.

We shall now express the molecular distribution functions as expectation values of certain functions over the same ensemble. The probability that the kth molecule will be between R_k and R_k+dR_k is given by

$$\begin{aligned}P^{(1)}(R_k)dR_k=\int_0^L\cdots\int_0^L&\\ \times P^{(N)}dR_1,\cdots,dR_{k-1},dR_{k+1},\cdots dR_N\cdot dR_k.&\end{aligned} \tag{9}$$

By introducing Dirac's δ-function, we can express this probability in the form

$$\begin{aligned}P^{(1)}(r)=\langle\delta(R_k-r)\rangle_{Av}&\\ =\int_0^L\cdots\int_0^L \delta(R_k-r)P^{(N)}\prod_{i=1}^{N}dR_i.&\end{aligned} \tag{10}$$

The average number density in singlet space (i.e., the probability per unit length that any molecule will be at the point r) is defined by

$$\rho^{(1)}(r)=\sum_{k=1}^{N}\langle\delta(R_k-r)\rangle_{Av}=\langle\sum_{k=1}^{N}\delta(R_k-r)\rangle_{Av}. \tag{11}$$

Similarly the average density of ordered pairs is given by

$$\rho^{(2)}(r,r')=\langle\sum_{k=1}^{N}\sum_{j=1\neq k}^{N}\delta(R_k-r)\delta(R_j-r')\rangle_{Av}, \tag{12}$$

$\rho^{(2)}$ is the probability per (unit length)^2 that one molecule will be at r and another will be at r'.

Let

$$\varphi=\sum_{k=1}^{N}\delta(R_k-r),$$

then from Eq. (11) and Eq. (5) we obtain

$$\rho^{(1)}(r)=N!\exp[\beta\bar{A}_N]\sum_{k=1}^{N} I_k^{(N)}(L,r), \tag{13}$$

[9] E.g., see G. Doetsch, *Theorie und Anwerdurg der Laplace Transformation* (Dover Publications, New York, 1943), pp. 157–167.

where

$$I_k^{(N)}(L,r)=\int_0^L \exp[-\beta V(L-R_N)]dR_N \times\cdots\int_0^{R_{k+1}} \delta(R_k-r)\exp[-\beta V_{k,k+1}]dR_k, \times\cdots\int_0^{R_2}\exp[-\beta V(R_1)]dR_1.$$

Again we recognize the convolution form for the Laplace transform and obtain

$$\int_0^\infty e^{-sL}I_k^{(N)}(L,r)dL = [\Omega(s)]^{N-k+1}\int_0^\infty \delta(L-r)h_k(L)e^{-sL}dL, = [\Omega(s)]^{N-k+1}e^{-sr}h_k(r), \quad (14)$$

where

$$h_k(r)=\int_0^r \exp[-\beta V(r-R_{k-1})]dR_{k-1} \times\cdots\int_0^{R_2}\exp[-\beta V(R_1)]dR_1=\frac{\exp[-\beta\bar{A}_{k-1}(r)]}{(k-1)!} =\frac{1}{2\pi i}\int_{c-i\infty}^{c+i\infty} e^{rt}[\Omega(t)]^k dt. \quad (15)$$

The second line follows from the first by the use of Eqs. (6) and (8). After using the inversion formula for the Laplace transform on Eq. (14) and substituting the result together with Eq. (8) into Eq. (13), we obtain

$$\rho^{(1)}(r)=\frac{\sum_{k=1}^{N}\left\{\frac{1}{2\pi i}\int_{c-i\infty}^{c+i\infty}e^{(L-r)s}[\Omega(s)]^{N-k+1}ds\right\}\left\{\frac{1}{2\pi i}\int_{c-i\infty}^{c+i\infty}e^{rt}[\Omega(t)]^k dt\right\}}{\frac{1}{2\pi i}\int_{c-i\infty}^{c+i\infty}e^{Ls}[\Omega(s)]^{N+1}ds}. \quad (16)$$

This function represents the probability per unit length of finding a particle at a distance r away from the wall. Since the wall was replaced by a fixed particle, one may state that $\rho^{(1)}(r)$ is also the probability per unit length that a particle will be found at a distance r from a given particle fixed at r' on a line of length $L+r'$. In this manner, one might anticipate the formal result for $\rho^{(2)}$ in an infinite system.

To get the analogous expression for $\rho^{(2)}$ we let

$$\varphi=\sum_{k=1}^{N}\sum_{j=1\neq k}^{N}\delta(R_k-r)\delta(R_j-r').$$

Then

$$\rho^{(2)}(r,r')=N!\exp[\beta\bar{A}_N]\sum_{k=2}^{N}\sum_{j=1}^{k-1} \times I_{jk}^{(N)}(L,r,r');\quad r>r' =N!\exp[\beta\bar{A}_N]\sum_{k=1}^{N-1}\sum_{j=k+1}^{N} \times I_{kj}^{(N)}(L,r',r);\quad r<r', \quad (17)$$

where

$$I_{jk}^{(N)}(L,r,r')=\int_0^L \exp[-\beta V(L-R_N)]dR_N \times\cdots\int_0^{R_{k+1}}\delta(R_k-r)\exp[-\beta V_{k,k+1}]dR_k, \times\cdots\int_0^{R_{j+1}}\delta(R_j-r')\exp[-\beta V_{j,j+1}]dR_j \times\cdots\int_0^{R_2}\exp[-\beta V(R_1)]dR_1.$$

The Laplace transforms of $I_{jk}^{(N)}$ and $I_{kj}^{(N)}$ can be computed since these functions have the form of a convolution, and one obtains, for example,

$$\int_0^\infty e^{-sL}I_{jk}^{(N)}(L,r,r')dL = [\Omega(s)]^{N-k+1}e^{-rs}I_j^{(k-1)}(r,r'). \quad (18)$$

By using the inversion formula and the known result for $I_j^{(k-1)}(r,r')$ we get

$$I_{jk}^{(N)}(r,r')=\left\{\frac{1}{2\pi i}\int_{c-i\infty}^{c+i\infty}e^{(L-r)s}[\Omega(s)]^{N-k+1}ds\right\} \times\left\{\frac{1}{2\pi i}\int_{c-i\infty}^{c+i\infty}e^{(r-r')t}[\Omega(t)]^{k-j}dt\right\} \times\left\{\frac{1}{2\pi i}\int_{c-i\infty}^{c+i\infty}e^{r'u}[\Omega(u)]^j du\right\}$$

and

$$I_{kj}^{(N)}(r',r)=\left\{\frac{1}{2\pi i}\int_{-i\infty}^{c+i\infty}e^{(L-r')s}[\Omega(s)]^{N-j+1}ds\right\} \times\left\{\frac{1}{2\pi i}\int_{c-i\infty}^{c+i\infty}e^{(r'-r)t}[\Omega(t)]^{j-k}dt\right\} \times\left\{\frac{1}{2\pi i}\int_{c-i\infty}^{c+i\infty}e^{ru}[\Omega(u)]^k du\right\}. \quad (19)$$

It is shown in Appendix A that asymptotic expres-

sions for $\rho^{(1)}$ and $\rho^{(2)}$ for large N take the following form:

$$\rho^{(1)}(r)=\sum_{k=1}^{N}\frac{\exp[-rc]}{[\Omega(c)]^k}\frac{1}{2\pi i}\int_{c-i\infty}^{c+i\infty}e^{rt}[\Omega(t)]^k dt, \quad (20a)$$

and

$$\rho^{(2)}(r,r')=\sum_{k=2}^{N}\sum_{i=1}^{k-1}\frac{\exp[-rc]}{[\Omega(c)]^k}$$

$$\times\left\{\frac{1}{2\pi i}\int_{c-i\infty}^{c+i\infty}e^{r's}[\Omega(s)]^i ds\right\}$$

$$\times\left\{\frac{1}{2\pi i}\int_{c-i\infty}^{c+i\infty}e^{(r-r')t}[\Omega(t)]^{k-i}dt\right\}, \quad (20b)$$

when $r>r'$.

The constant c is determined by the condition that the function

$$\sigma=\Re\left\{\frac{Ls}{N+1}+\ln\Omega(s)\right\}$$

has a stationary value at the point c on the real axis.

The integrals in Eqs. (20a) and (20b) are most conveniently evaluated by the theory of residues. In order to insure the validity of converting the complex integral into a contour integral around the origin in the complex plane, we assume that

$$\begin{aligned} V(R)&=\infty; & R<a\\ &=V(R); & a\leq R\leq\lambda \\ &=0; & R>\lambda. \end{aligned} \quad (21)$$

In the case of a hard core model with a finite range of the potential one can, for example, readily show[7] that

$$\frac{1}{2\pi i}\int_{c-i\infty}^{c+i\infty}eL^s[\Omega(s)]^{N+1}ds=\frac{1}{2\pi i}\oint eL^s[\Omega(s)]^{N+1}ds, \quad (22)$$

where $L>(N+1)a$.

Equations (20a) and (20b) include the effects of the wall, which persist for any finite values of r and r'. However, if r and r' are allowed to become infinite in such a manner that $r-r'$ remains fixed, the following expressions, calculated in appendix A, are obtained. The step function $A(R-na)$ occurs since we have explicitly introduced the hard core model, with a diameter (a).

$$\rho^{(1)}=1/la; \quad l=L/[(N+1)a] \quad (23a)$$

$$\rho^{(2)}(R)=\sum_{n-1}^{N-1}\frac{A(R-na)}{la}\frac{1}{2\pi i}$$

$$\times\int_{c-i\infty}^{c+i\infty}e^{R(s-c)}\left[\frac{\Omega(s)}{\Omega(c)}\right]^n ds, \quad (23b)$$

$$\rho^{(2)}(R)=\rho^{(2)}(-R),$$

where

$$\begin{aligned} R&=r-r'\\ A(x)&=0 \qquad x<0\\ &=1 \qquad x\geq 0. \end{aligned}$$

The average density $\rho_N^{(n)}$ of ordered sets n in a canonical ensemble of systems of N particles is given by

$$\rho_N^{(n)}(r_1,\cdots,r_n)$$

$$=\Big\langle\sum_{l_n=1}^{N}\sum_{\substack{l_{n-1}=1\\ \neq l_n}}^{N}\cdots\sum_{\substack{l_1=1\\ \neq l_j}}^{N}\prod_{\substack{i=1\\ (j=2,\cdots,n)}}^{n}\delta(R_{l_i}-r_i)\Big\rangle_{Nv}. \quad (24)$$

For a one-dimensional system in which the interactions are restricted to nearest neighbors, a fixed subset of n molecules effectively divides the system into $n+1$ independent subsystems. An extension of the analysis given in this section shows that

$$\rho^{(n)}=\sum_{l_n=n}^{N}\sum_{\substack{l_{n-1}=n-1\\ \neq l_n}}^{l_n-1}\cdots\sum_{\substack{l_1=1\\ \neq l_j}}^{l_2-1}\frac{Q_{N-l_n+1}(L-r_n)}{Q_N(L)}$$

$$\times\prod_{i=1}^{n-1}Q_{l_{i+1}-l_i}(r_{i+1}-r_i)Q_{l_1}(r_1), \quad (25)$$

where $r_n>r_{n-1}>\cdots>r_1$,

$$Q_k(r)=\frac{1}{2\pi i}\int_{-i\infty}^{c+i\infty}e^{rs}[\Omega(s)^k ds.$$

The asymptotic expression for large N takes the form

$$\rho^{(n)}=\sum_{l_n=n}^{N}\sum_{l_{n-1}=n-1}^{l_n-1}\cdots\sum_{l_1=1}^{l_2-1}\frac{\exp[-r_nc]}{[\Omega(c)]^{l_n}}$$

$$\times Q_{l_1}(r_1)\prod_{i=1}^{n-1}Q_{l_{i+1}-l_i}(r_{i+1}-r_i),$$

with $r_n>r_{n-1}>\cdots>r_1$. By substituting the expression for $Q_k(r)$ and rearranging, we obtain

$$\rho^{(n)}=\sum_{i=1}^{n-1}\left\{\sum_{k_i=1}^{N-b_i}K_i(R_{i,i+1},c)\right\}$$

$$\times\sum_{l_1=1}^{N-b_0}\frac{1}{2\pi i}\int_{c-i\infty}^{c+i\infty}e^{r_1(s-c)}\left[\frac{\Omega(s)}{\Omega(c)}\right]^{l_1}ds, \quad (25)$$

where

$$K_i(R_{i,i+1},c)=\frac{1}{2\pi i}\int_{c-i\infty}^{c+i\infty}\exp[R_{i,i+1}(s-c)]\left[\frac{\Omega(s)}{\Omega(c)}\right]^{k_i}ds,$$

$$R_{i,i+1}=r_{i+1}-r_i,$$

$$b_i=\sum_{j=i+1}^{n-1}k_j-i,$$

$$k_i=l_{i+1}-l_i$$

If we now let r_1 approach infinity in such a manner that all $R_{i,i+1}$ are held fixed, then, as the calculation in Appendix A proves, we get

$$\rho^{(n)}=\frac{1}{la}\prod_{i=1}^{n-1}\sum_{k_i=1}^{\infty}A(R_{i,i+1}-k_ia)K_i(R_{i,i+1},c)$$

$$=(la)^{n-2}\prod_{i=1}^{n-1}\rho^{(2)}(R_{i,i+1}) \quad (27)$$

$l=L/(N+1)a$.

II. THE EQUATION OF STATE

The pressure p in a thermodynamic system may be calculated from the partition function Q by the relation

$$p=kT\partial \ln Q/\partial L, \quad (28)$$

where L is the length of the system. There are several ways of deriving an expression for the pressure in terms of the distribution functions and the intermolecular potential. For example, we may use the method due to Born and Green.[10]

Since the kinetic contribution to the partition function does not depend on the length L, we can put Eqs. (1) and (28) together with the substitution $y_i=R_i/L$ to obtain

$$p=kT\exp[\beta\bar{A}_N]\frac{\partial\exp[-\beta\bar{A}_N]}{\partial L},$$

$$=kT\exp[\beta\bar{A}_N]\Big\{NL^{N-1}\int_0^1\cdots\int_0^1$$

$$\times\exp[-\beta V_N(Ly_1,\cdots,Ly_n)]\prod_{i=1}^{N}dy_i,$$

$$-\beta L^N\int_0^1\cdots\int_0^1\sum_{k=1}^{N}y_k\frac{\partial V_N}{\partial y_k}\exp[-\beta V_N]\prod_{i=1}^{N}dy_i\Big\}.$$

We have neglected the wall potential in this expression. With the assumption

$$V_N=\sum\sum_{i<j}V(R_{ij}),$$

we find that

$$\frac{pL}{NkT}=1-\frac{\beta}{2N}\int_0^L\int_0^L R\frac{\partial V(R)}{\partial R}\rho^{(2)}(r,r')drdr',$$

where $R=|r-r'|$. As N approaches infinity, at constant N/L, the equation of state takes the form

$$\frac{pL}{NkT}=1-\beta\frac{L}{N}\int_0^\infty R\frac{\partial V(R)}{\partial R}\rho^{(2)}(R)dR, \quad (29)$$

where $\rho^{(2)}(r,r')$ is a function of $R=|r-r'|$ only and is now expressed by $\rho^{(2)}(R)$.

[10] M. Born and H. S. Green, *A General Kinetic Theory of Liquids* (Cambridge University Press, New York, 1949), p. 23.

By using Eqs. (23b) and (29), we obtain

$$\frac{pL}{NkT}=1-\beta\sum_{n=1}^{\infty}\frac{1}{2\pi i}\int_{c-i\infty}^{c+i\infty}\left[\frac{\Omega(s)}{\Omega(c)}\right]^n ds$$

$$\times\int_{na}^{\infty}R\frac{\partial V}{\partial R}e^{R(s-c)}dR. \quad (30)$$

As an illustration of this equation, we consider the one-dimensional system of rigid "spheres" with diameter a, where the intermolecular potential is given by

$$V(R)=\infty; \quad R<a,$$
$$=0; \quad R\geq a.$$

Thus

$$\Omega(s)=\frac{1}{s}\exp[-as].$$

With the use of the theory of residues,[7]

$$\frac{1}{2\pi i}\int_{c-i\infty}^{c+i\infty}e^{Rs}[\Omega(s)]^n ds$$

$$=\frac{1}{2\pi i}\oint e^{Rs}[\Omega(s)]^n ds=\frac{(R-na)^{n-1}}{(n-1)!}. \quad (31)$$

Using Eqs. (23b) and (31) together with the rigid sphere value for c, $c=1/a(l-1)$, we find that for $l>1$,

$$\rho^{(2)}(x)=\frac{1}{la^2}\sum_{k=1}^{\infty}A(x-k)\left(\frac{1}{l-1}\right)^k$$

$$\times\frac{(x-k)^{k-1}}{(k-1)!}\exp\left(-\frac{x-k}{l-1}\right), \quad (32)$$

where $x=R/a$ is a reduced distance. This function can be interpreted as the probability per unit length of finding a particle at a distance $R=xa$ from an arbitrary fixed particle. This function was first derived by Frenkel[5] who used an elementary probability argument.

For this system of rigid "spheres," the equation of state is completely determined by the value of $\rho^{(2)}(x)$ at $x=1$. From Eqs. (29) and (32), we obtain the familiar Tonks'[2] equation of state,

$$pla/kT=l/(l-1). \quad (33)$$

III. INTEGRAL EQUATIONS FOR THE DISTRIBUTION FUNCTIONS

It has not yet been possible to obtain the average densities of ordered sets n for a three-dimensional system by direct integration. However, an alternative approach, which attempts to solve a set of integral equations, has been formulated and is amenable to numerical calculation. In view of the importance of these equations in the three-dimensional problem, we will consider the one-dimensional case, even though we have obtained

expressions for the distribution functions by direct integration.

In the theories of Kirkwood,[11] Born-Green,[12] Yvon,[13] and of Mayer,[14] systems of integro-differential equations for the distribution functions have been formulated in several equivalent forms. These systems have the common feature that they involve derivatives of the distribution functions with respect to suitable parameters upon which the potential of intermolecular force is assumed to depend. Integration with respect to these parameters offers difficulties, which have allowed it to be performed only after approximations, such as the superposition assumption[10] in the space of molecular triplets, has been introduced. We shall see that the superposition approximation is only true in the one-dimensional system in which we only consider nearest neighbor interactions. Recently, Kirkwood[1] has derived a new system of integral equations for the distribution functions by a method which does not depend upon the device of differentiation with respect to parameters in the potential of intermolecular force. This method leads directly to a system of integral equations rather than to a system of integro-differential equations.

The set of equations for a one-dimensional system where wall effects are neglected can be written in the form

$$g^{(n)}(1, 2, \cdots, n) = \exp[\beta(\mu^e - V_n^{(1)})]g^{(n-1)}(2, \cdots, n) + \int_0^L K^{(n)}(1, 2, \cdots, n+1) \times g^{(n)}(2, \cdots, n+1)dR_{n+1}, \tag{34}$$

$$K^{(n)}(1, 2, \cdots, n+1) = \frac{1}{la} f_{1,n+1} \exp[\beta(\mu^e - V_n^{(1)})] \times \left\{1 + \sum_{s=1}^{\nu-1} \frac{1}{(s+1)!} \int_0^L \cdots \int^L \times \rho^{(n,s)}(2, \cdots, n+1/n+2, \cdots, n+s+1) \times \prod_{\sigma=n+2}^{n+s+1} f_{1\sigma} dR_\sigma \right\},$$

$$\rho^{(n,s)}(2, \cdots, n+1/n+2, \cdots, n+s+1) = \left(\frac{1}{la}\right)^s \frac{g^{(n+s)}(2, \cdots, n+s+1)}{g^{(n)}(2, \cdots, n+1)},$$

$$\exp[-\beta\mu^e] = 1 + \sum_{s=1}^{\nu} \frac{1}{s!}\left(\frac{1}{la}\right)^s \int \cdots \int \times g^{(s)}(2, \cdots, s+1) \prod_{\sigma=2}^{s+1} f_{1\sigma} dv_\sigma,$$

$$g^{(n)} = (la)^n \rho^{(n)},$$

and

$$f_{1\sigma} = \exp[-\beta V(R_{1\sigma})] - 1,$$

$$V_n^{(1)} = \sum_{i=2}^{n} V(R_{1,i}),$$

$$l = L/Na.$$

μ^e is the excess chemical potential per molecule. $\nu+1$ is the maximum number of spheres of radius a, which can be packed into a sphere of radius λ [see Eqs. (21)]. $\rho^{(n,s)}$ is the probability per (unit length)^s that s molecules will be at the specified positions $R_{n+2}, R_{n+3}, \cdots, R_{n+s+1}$, if $2, 3, \cdots, n+1$ are fixed, and it is independent of the positions of the remaining $N-n-s-1$ molecules. $\rho^{(n)}$ is, as before, the average density of ordered sets in n tuplet space, and the correlation function $g^{(n)}$ for a subset of n molecules is defined by the last equation in (34). The derivation of these equations is given elsewhere.[1]

In principle one could solve these equations for a system in which one considers more than only nearest neighbor interactions. Since most non-ionic forces have a range of only a few molecular diameters, the number of terms in the sums of Eq. (34) could be taken to be, say, less than six. However, when we restrict our considerations to nearest neighbor interactions, a considerable simplification takes place, for as we have seen in Eq. (27) a fixed molecule effectively divides the system into two independent subsystems. If we fix molecule n of an arbitrary subset of $n+1$ molecules, then the position of molecule $n+1$ is independent of the positions of molecules $1, 2, \cdots, n-1$ and depends only on the position of molecule n. We can express this principle analytically by stating that, for nearest neighbor forces, the conditional probability

$$\frac{g^{(n+1)}(1, 2, \cdots, n, n+1)}{g^{(n)}(1, 2, \cdots, n)} = \frac{g^{(2)}(n, n+1)}{g^{(1)}(n)}. \tag{35}$$

This superposition law is exact for a one-dimensional system in which the interactions are restricted to nearest neighbors. That this result is consistent with the system of integral equations can be easily verified by substituting Eq. (35) into Eq. (34).

As an illustration of the nature of these equations, we consider the special case of a system composed of rigid "spheres." Then

$$\begin{aligned} f_{1\sigma} &= 0; \quad R_{1\sigma} > a, \\ f_{1\sigma} &= -1; \quad R_{1\sigma} < a, \end{aligned} \tag{36}$$

[11] J. G. Kirkwood, J. Chem. Phys. **3**, 300 (1935).
[12] M. Born and H. S. Green, Proc. Roy. Soc. **A188**, 10 (1946).
[13] J. Yvon, *Actualités Scientifiques et Industrielles* (Herman et Cie, Paris, 1935), p. 203.
[14] J. E. Mayer, J. Chem. Phys. **15**, 187 (1947).

where a is the diameter of a rigid sphere. Although the following discussion could be carried out in terms of an arbitrary intermolecular potential, the simplicity of the expressions for a hard sphere potential aids in the clarity of the presentation. Since we shall only attempt to illustrate the type of integral equation which one encounters, this simple model will be sufficient.

Since $\nu+1$ is the total number of particles that can possibly fit into a closed interval of length $2a$, we see that $\nu=2$. The superposition principle, Eq. (35), terminates the chain of integral equations so that we need only consider the equation for $g^{(2)}$. Equation (35), together with Eq. (34), also yields

$$\rho^{(n,s)}(2,\cdots,n+1/n+2,\cdots,n+s+1)=\left(\frac{1}{la}\right)^{s}\prod_{\sigma=n+1}^{n+s}g^{(2)}(\sigma,\sigma+1). \quad (37)$$

With these simplifications, the equation for $g^{(2)}$ takes the form

$$g^{(2)}(1,2)=0; \quad R_{12}<a,$$

$$g^{(2)}(1,2)=\exp[\beta\mu^{e}]+\int_{R_1-a}^{R_1+a}K(1,2,3)g^{(2)}(2,3)dR_3; \quad R_{12}>a,$$

$$K(1,2,3)=0; \quad R_{13}>a,$$

$$K(1,2,3)=\frac{1}{la}\exp[\beta\mu^{e}]\times\left\{-1+\frac{1}{2la}\int_{R_1-a}^{R_1+a}g^{(2)}(3,4)dR_4\right\}; \quad R_{13}>a,$$

and

$$\exp[-\beta\mu^{e}]=1-\frac{2}{l}+\frac{1}{2}\left(\frac{1}{la}\right)^{2}\int_{R_1-a}^{R_1+a}\int_{R_1-a}^{R_1+a}g^{(2)}(2,3)dR_3dR_2. \quad (39)$$

Since $g^{(2)}=g^{(2)}(R_{12})$, that is to say the radial distribution function is a function of only the relative distance between the two molecules, we let

$$R_{12}=xa, \quad R_{23}=sa, \quad R_{34}=ua. \quad (40)$$

In terms of the reduced distances x, s, u the equations take the form

$$g^{(2)}(x)=0; \quad |x|<1,$$

$$g^{(2)}(x)=\exp[\beta\mu^{e}]\times\left\{1+\frac{1}{l}\int_{x-1}^{x+1}K'(x-s)g^{(2)}(s)ds\right\}; \quad |x|>1, \quad (41)$$

where

$$K'(t)=-1+\frac{1}{l}\int_{0}^{t+1}g^{(2)}(u)du; \quad -1<t<1.$$

In addition, we obtain

$$\exp[-\beta\mu^{e}]=1+\frac{1}{l}\int_{-1}^{1}K'(t)dt. \quad (42)$$

A solution of Eq. (41) is given by Eq. (32) and has the explicit form

$$g^{(2)}(x)=l\sum_{k=1}^{\infty}A(x-k)\left(\frac{1}{l-1}\right)^{k}\frac{(x-k)^{k-1}}{(k-1)!}\times\exp\left[-\frac{x-k}{l-1}\right]. \quad (43)$$

It is shown in Appendix B that this is indeed a solution. Straightforward calculation with Eqs. (41)–(43) shows that

$$\begin{aligned}K'(t)&=-\exp[-t/(l-1)]; && 1>t>0,\\ &=-1; && 0>t>-1,\\ &=0; && |t|>1\end{aligned} \quad (44)$$

and that

$$\exp[-\beta\mu^{e}]=(l-1/l)\exp[1/(1-l)]. \quad (45)$$

This expression for the excess chemical potential μ^{e} can also be obtained by integrating the equation of state, Eq. (33).

The one-dimensional and three-dimensional formulations of the integral equations [see Eq. (34)] differ only by the replacement of the volume per molecule in the latter by the length per molecule. The major simplification that can be made in the one-dimensional problem with nearest neighbor interactions only is the superposition principle given by Eq. (35). The general form of these integral equations can be seen to be a nonhomogeneous linear form of the Fredholm type in which the kernel depends upon the distribution functions. Even under the simplifications introduced by considering a one-dimensional system of rigid spheres this general form is maintained. Therefore, the one-dimensional form of the integral equations may prove to be a useful guide in investigating the solution of the three-dimensional problem. For example, one might decide between the use of two numerical methods on the basis of the investigation of the convergence of both methods in the one-dimensional problem, where the solution is known.

APPENDIX A

In his article,[7] Gürsey investigated the partition function Q_N in the limit of large N by considering the series

$$S(Z)=\sum_{N=0}^{\infty} Q_N Z^N,$$

for then

$$\lim_{N\to\infty}(Q_N)^{1/N+1}=R,$$

where R is the radius of convergence for the series $S(Z)$. However, we will find it more convenient to obtain the asymptotic expansion for large N by a procedure which utilizes the method of steepest decent. The two approaches lead to identical results.

From Eqs. (16) and (19), we see that it is convenient to define a function M_N by

$$M_N=\frac{1}{2\pi i}\int_{c-i\infty}^{c+i\infty}\exp[(N+1)f(a)]\chi(s)ds, \qquad f(s)=(Ls/N+1)+\ln\Omega(s). \tag{A1}$$

When $\chi(s)=1$, M_N is the partition function

$$\exp[-\beta\bar{A}_N]/N\,!.$$

In the discussion of the distribution functions the function $\chi(s)$ is taken to be

$$\chi(s)=[\Omega(s)]^k\exp[-rs],$$

as stated in Part I, we first want to obtain

$$\lim_{N\to\infty} M_N.$$

As the path of integration, we take the line $s=c+iy$, which is assumed to be the line of steepest decent, which passes over the saddle point for the function $f(s)$. This saddle point is located at the point c on the positive real axis. For a system of rigid spheres one can show that $c=1/a(l-1)$. For any given potential one can readily obtain c by solving the equation,

$$(\partial f/\partial s)_{s=c}=0.$$

We now expand $f(s)$ in a power series around the point c:

$$f(s)=f(c)+\tfrac{1}{2}(s-c)^2f''(c)+\cdots, \qquad =f(c)-\tfrac{1}{2}y^2f''(c)+\cdots, \tag{A2}$$

where $iy=(s-c)$. Then

$$M_N\exp[-(N+1)f(c)]=\frac{1}{2\pi}\int_{-\infty}^{+\infty}\exp\left[-\frac{N+1}{2}f''(c)y^2\right]\chi(c+iy)dy. \tag{A3}$$

The integral is now in the form considered by G. N. Watson[15] who obtained the asymptotic expansion for such integrals. The first term of this expansion gives

$$M_N\exp[-(N+1)f(c)]\sim\frac{\chi(c)}{(2\pi(N+1)f''(c))^{\frac{1}{2}}}. \tag{A4}$$

By using Eqs. (A1) and (A4) together with Eqs. (16), (17), and (19), we obtain

$$\rho^{(1)}(r)\sim\sum_{k=1}^{N}\frac{\exp[-rc]}{[\Omega(c)]^k}\frac{1}{2\pi i}\int_{c-i\infty}^{c+i\infty}e^{rt}[\Omega(t)]^k dt \tag{A5a}$$

and

$$\rho^{(2)}(r,r')\sim\sum_{k=2}^{N}\sum_{j=1}^{k-1}\frac{\exp[-rc]}{[\Omega(c)]^k}\times\left\{\frac{1}{2\pi i}\int_{c-i\infty}^{c+i\infty}e^{r's}[\Omega(s)]^j ds\right\}\times\left\{\frac{1}{2\pi i}\int_{c-i\infty}^{c+i\infty}e^{(r-r')t}[\Omega(t)]^{k-j}dt\right\} \qquad r>r'.$$

We now wish to consider the limit as r and r' approach infinity in such a manner that $r-r'$ remains constant. From (A5a), we obtain for infinite N

$$\rho^{(1)}(r)=\frac{1}{2\pi}\int_{-\infty}^{\infty}e^{iru}\sum_{k=1}^{\infty}\left[\frac{\Omega(c+iu)}{\Omega(c)}\right]^k du. \tag{A6}$$

Within the radius of convergence of the infinite series, $\rho^{(1)}$ can be represented by

$$\rho^{(1)}(r)=\frac{1}{2\pi}\int_{-\infty}^{\infty}\frac{e^{iur}\Omega(c+iu)}{\Omega(c)-\Omega(c+iu)}du, \tag{A7}$$

and using the principle of analytic continuation, we will take this as the definition of $\rho^{(1)}(r)$ beyond the singular points of the integrand.

From the theory of residues, we obtain

$$\rho^{(1)}(r)=\sum_{\nu}\exp[iu_\nu r]\left\{-\frac{\Omega(c+iu_\nu)}{\Omega'(c+iu_\nu)}\right\}, \tag{A8}$$

where

$$\Omega'(s)=\partial\Omega/\partial s.$$

u_ν is a pole of the integrand of Eq. (A7) which has a positive imaginary part. A particular pole is $u_1=0$. for this is a solution of the equation,

$$\Omega(c)-\Omega(c+iu)=0.$$

Therefore, we obtain

$$\lim_{r\to\infty}\rho^{(1)}(r)=\frac{\Omega(c)}{-\Omega'(c)}=\frac{\int_0^\infty\exp[-cR-\beta V(R)]dR}{\int_0^\infty R\exp[-cR-\beta V(R)]dR}. \tag{A9}$$

[15] G. N. Watson, Proc. London Math. Soc. (2) **17**, 133 (1918).

The second line follows from the definition of $\Omega(c)$, Eq. (7). From the normalization condition on $\rho^{(1)}$,

$$\int_0^L \rho^{(1)}(r)dr=N,$$

we see that

$$\lim_{R\to\infty}\rho^{(1)}(r)=1/la. \tag{A10}$$

After changing the summation in Eq. (A5b), we obtain

$$\rho^{(2)}(r,r')\sim\sum_{n-1}^{N-1}\times\left\{\frac{1}{2\pi i}\int_{c-i\infty}^{c+i\infty}e^{r'(s-c)}\sum_{j=1}^{N-n}\left[\frac{\Omega(s)}{\Omega(c)}\right]^j ds\right\},$$

$$\times\left\{\frac{1}{2\pi i}\int_{c-i\infty}^{c+i\infty}e^{(r-r')(s-c)}\left[\frac{\Omega(s)}{\Omega(c)}\right]^n ds\right\}, \tag{A11}$$

where $r>r'$ and $n=k-j$. If we adopted the hard core model, Eq. (21), then $n\leq(r-r')/a$, where a is the diameter of the hard core. Then for finite $R=r-r'$ and infinite N we find that

$$\rho^{(2)}(R)=\sum_{n=1}^{\infty}\frac{A(R-na)}{la}\frac{1}{2\pi i}\times\int_{c-i\infty}^{c+i\infty}e^{R(s-c)}\left[\frac{\Omega(s)}{\Omega(c)}\right]^n ds, \tag{A12}$$

$$R=r-r'>0.$$

The step function $A(R-na)$ expresses explicitly the restriction imposed by the hard core intermolecular potential.

APPENDIX B

We wish to show here that the correlation function

$$g^{(2)}(x)=l\sum_{k=1}^{\infty}A(x-k)\left(\frac{1}{l-1}\right)^k\frac{(x-k)}{(k-1)!}\times\exp\left[-\frac{x-k}{l-1}\right] \tag{1B}$$

satisfies Eq. (41). By using Eqs. (44) and (45), the integral equation can be written in the form

$$g^{(2)}(x)=\frac{l-1}{l}\exp\left[\frac{1}{1-l}\right]\left\{1-\frac{1}{l}\int_{-1}^{0}g^{(2)}(x-u)du,\right.$$

$$\left.-\frac{1}{l}\int_0^1\exp\left[\frac{u}{1-l}\right]g^{(2)}(x-u)du\right\};$$

$$|x|>1. \tag{B2}$$

By using Eq. (B1) we find

$$\int_0^1\exp\left[\frac{u}{1-l}\right]g^{(2)}(x-u)du=l\sum_{k=1}^{\infty}\left(\frac{1}{l-1}\right)^k\frac{\exp\left[-\frac{x-k}{l-1}\right]}{(k-1)!}\times\int_0^1 A(x-k-u)(x-k-u)^{k-1}du \tag{B3}$$

$$\int_{-1}^{0}g^{(2)}(x-u)du=l\sum_{k=1}^{\infty}\left(\frac{1}{l-1}\right)^k\frac{1}{(k-1)!}\times\int_{-1}^{0}A(x-k-u)(x-k-u)^{k-1}\times\exp\left[-\frac{x-k-u}{l-1}\right]du.$$

However,

$$\int_0^1 A(x-k-u)(x-k-u)^{k-1}du=\frac{A(x-k-1)}{k}\{(x-k)^k-(x-k-1)^k\}+\frac{A(x-k)A(k+1-x)}{k}(x-k)^k, \tag{B4}$$

and

$$\int_{-1}^{0}A(x-k-u)(x-k-u)^{k-1}\exp\left[-\frac{x-k-u}{l-1}\right]du$$

$$=A(k-x)A(x-k+1)(l-1)^k(k-1)!+\sum_{\nu=0}^{k-1}A(x-k)\frac{(k-1)!(l-1)^{\nu+1}}{(k-1-\nu)!}(x-k)^{k-1-\nu}\times\exp\left[-\frac{x-k}{l-1}\right]-\sum_{\nu=0}^{k-1}\{A(x-k)+A(x-k)A(x-k+1)\}\frac{(k-1)!(l-1)^{\nu+1}}{(k-1-\nu)!}\times(x-k+1)^{k-1-\nu}\exp\left[-\frac{x-k+1}{l-1}\right].$$

By substituting Eqs. (B4) and (B3) into the right-hand side of (B2) and after interchanging summation signs

and rearranging terms, we obtain

$$\begin{aligned}\text{r.h.s.} = g^{(2)}(x) - l\sum_{k=1}^{\infty} & \times\{A(x-k)+A(x+1-k)A(k-x)\} \\ & \times\frac{(x-k+1)^{k-1}}{(l-1)^k(k-1)!}\exp\left[-\frac{x-k}{l-1}\right] \\ & +l\sum_{\nu=0}^{\infty}\sum_{k=1}^{\infty}A(x+1-k-\nu) \\ & \times\frac{(x+1-\nu-k)^{k-1}}{(k-1)!(l-1)^k}\exp\left[-\frac{x-k-\nu}{l-1}\right] \\ & -l\sum_{\nu=0}^{\infty}\sum_{k=1}^{\infty}A(x-k-\nu) \\ & \times\frac{(x-k-\nu)^{k-1}}{(k-1)!(l-1)^k}\exp\left[-\frac{x-k-\nu-1}{l-1}\right],\end{aligned} \tag{B5}$$

$$\begin{aligned}\text{r.h.s.} &= g^{(2)}(x)-\exp\left[\frac{1}{l-1}\right]g^{(2)}(x+1) \\ &\quad +\exp\left[\frac{1}{l-1}\right]\sum_{\nu=0}^{\infty}g^{(2)}(x+1-\nu) \\ &\quad -\exp\left[\frac{1}{l-1}\right]\sum_{\nu=0}^{\infty}g^{(2)}(x-\nu) \\ &= g^{(2)}(x).\end{aligned}$$

We have formally proved that the correlation function obtained by direct integration satisfies the integral equation, Eq. (42).

ADDENDUM

An alternative statistical mechanical formulation of a one-dimensional fluid in which the averages are taken for an ensemble whose systems all have a specified temperature, pressure and total number of particles has been given by Takahasi.* The probability density for this ensemble is

$$P^{(N)}(R_1, \cdots, R_N, L) = \exp[\beta(\bar{F}_N - V_N - V_W - pL)],$$

where

$$\begin{aligned}&\exp[-\beta\bar{F}_N] \\ &= \int_0^{\infty}\int_0^{L}\cdots\int_0^{L}\exp[-\beta(V_N+V_W+pL)] \\ &\qquad\qquad \times dR_1, \cdots, dR_N dL \\ &= \int_0^{\infty} e^{-\beta pL}\exp[-\beta\bar{A}_N(L)]dL.\end{aligned}$$

Since $\exp[-\beta\bar{F}_N]$ is the Laplace transform of $\exp[-\beta\bar{A}_N]$, the utilization of p and T as independent variables in place of L and T eliminates the necessity of considering the inverse of the Laplace transform (see Eqs. (7) and (8)). This method leads directly to

$$\rho^{(1)}(r) = \sum_{k=1}^{\infty}\frac{e^{-\beta pr}}{[\Omega(\beta p)]^k}\frac{1}{2\pi i}\int_{\beta p-i\infty}^{\beta p+i\infty} e^{rt}[\Omega(t)]^k dt.$$

The fact that the constant c introduced by the method of steepest descents is identically equal to βp was used by Gürsey[7] to determine the equation of state. In order to express this result for $\rho^{(1)}(r)$ in terms of the length per molecule, one would have to solve the equation of state given by $L = (\partial\bar{F}_N/\partial p)_{T,N}$ for p [see Eqs. (20)]. Since we wish to stress the integral equations for the distribution functions which are formulated in terms of the canonical ensemble, we have retained this formulation in our discussion.

* H. Takahasi, Proc. Phys.-Math. Soc., Japan **24**, 60 (1942).

Symmetry Factoring of the Kinetic and Potential Energy Matrices

BRYCE CRAWFORD, JR.
School of Chemistry, University of Minnesota, Minneapolis 14, Minnesota
(Received March 11, 1953)

In computing the kinetic-energy matrix for vibrations of large molecules of useful symmetry, a tedious double matrix multiplication is usually involved. A theorem is presented, replacing this by a shorter calculation, which may be used either to save labor or to check the result.

THE methods introduced by Wilson[1,2] have greatly facilitated normal-coordinate calculations, and the tables recently published by Decius,[3] giving explicitly the elements G_{ij} for the most usual valence-force coordinates R_i, have still further reduced the labor involved. Still, the use of symmetry involves the transformation from the G_{ij} given by Decius to the elements of the symmetry-factored G matrix, which we shall call $\bar{G}_{ij}$. The tedious multiplication of large matrices may be avoided by using the theorem we present here; it is closely related to some of the reduced expressions given by Wilson.[2]

It is possible to eliminate[4] the explicit determination of the symmetry transformation U, which we use here. However, this transformation is so easy to determine, either intuitively or by analytical methods,[5] and the perusal of it is so helpful in understanding the forms of the vibration that our current practice is to write it down explicitly. Actually, not all the transformation coefficients are needed in the equation given here.

The reader will easily see that our result also applies to the potential-energy matrix F and its transformation to the symmetry-factored $\bar{F}$.

STATEMENT OF THE THEOREM

Let the symmetry group of the molecule be **C**. Then the basic coordinates R_i will fall into equivalent sets. From the mth equivalent set of g_m coordinates we may form[6] symmetry coordinates $S_m^{(j)}$ which reduce **C**; $S_m^{(j)}$ will belong to the jth irreducible representation Γ_j of **C**, and if Γ_j is degenerate we must write $S_{ma}^{(j)}$, $S_{mb}^{(j)}$, ($S_{mc}^{(j)}$) to distinguish its 2 (or 3) components. We shall need the transformation,[7] which we take as unitary (or orthogonal if we use real coordinates),

$$S_{ma}^{(j)}=\sum_i U_{ma,i}^{(j)}R_i. \tag{1}$$

We want the element $\bar{G}_{ma,na}^{(j)}$. From the g_m coordinates of set m choose one, say R_1. Then the symmetry operations which leave R_1 unchanged form a group **H** (a subgroup of **C**). We choose R_1 so that the $S_{ma}^{(j)}$ reduce **H** as well as **C**; this may require a little foresight when choosing the $S_{ma}^{(j)}$, but it pays. Now the coordinates of set n—all equivalent under **C**—will not be all equivalent under **H**; they will fall into subsets. Let the subset A contain $g_A^{(H)}$ coordinates, equivalent under **H**, with typical member R_A; subset B contains $g_B^{(H)}$ coordinates, R_B being typical, etc.; $g_A^{(H)}+g_B^{(H)}+\cdots+g_Z^{(H)}=g_n$.

Then our useful result, which we prove below, is

$$\bar{G}_{ma,na}^{(j)}=(g_m/d_j)\sum_A g_A^{(H)} \times\sum_\alpha{}' U_{ma,1}^{(j)}U_{na,A}^{(j)*}G_{1,A}, \tag{2}$$

where α is summed over those components of Γ_j which are totally symmetric *under* **H**. The asterisk denotes the complex conjugate, meaningful only if we have chosen complex coordinates, and d_j is the degeneracy of Γ_j. It is clear that in summing over A we may look ahead and omit coordinates for which $G_{1,A}$ vanishes. The sum over components α will usually reduce to one term only.

TABLE I. Species E coordinates: $N_a=6^{-\frac{1}{2}}$, $N_b=2^{-\frac{1}{2}}$

	Δr_1	Δr_2	Δr_3	$\Delta\beta_1$	$\Delta\beta_2$	$\Delta\beta_3$	$\Delta\alpha_1$	$\Delta\alpha_2$	$\Delta\alpha_3$
S_{ra}^E	$2N_a$	$-N_a$	$-N_a$						
$S_{\beta a}^E$				$2N_a$	$-N_a$	$-N_a$			
$S_{\alpha a}^E$							$-2N_a$	N_a	N_a
S_{rb}^E		$-N_b$	N_b						
$S_{\beta b}^E$					$-N_b$	N_b			
$S_{\alpha b}^E$								N_b	$-N_b$

AN EXAMPLE

We shall illustrate with the doubly degenerate species of CH_3F, although this simple molecule scarcely calls for such methods. Number the H atoms; call the distance C—H_i r_i, the angle FCH_i β_i, and the angle H_jCH_k α_i; note that α_i is *opposite* β_i. For our coordinates we may use the Δr_i, $\Delta\alpha_i$, $\Delta\beta_i$, together with the C—F

[1] E. B. Wilson, Jr., J. Chem. Phys. **7**, 1047 (1939).
[2] E. B. Wilson, Jr., J. Chem. Phys. **9**, 76 (1941).
[3] J. C. Decius, J. Chem. Phys. **16**, 1025 (1948).
[4] See reference 2; also C. W. Lippman, thesis, Harvard University, some methods from which are quoted in J. C. Decius, J. Chem. Phys. **16**, 214 (1948).
[5] L. H. Berryman and J. R. Nielsen, J. Chem. Phys. **17**, 659 (1949).
[6] In forming coordinates in this way redundancies may be included. They may be removed from the $\bar{G}$ matrix later: Sun, Parr, and Crawford, J. Chem. Phys. **17**, 840 (1949).
[7] Our notation implies that the mth set of R_i will yield only *one* symmetry coordinate $S_{ma}^{(j)}$ for a given Γ_j and a; as is usually the case. This is not necessary for our results, however; we may have several, and write $S_{m'a}^{(j)}$, $S_{m''a}^{(j)}$, etc. But in such cases we must define U carefully, being sure that, under **C**, $S_{m'a}^{(j)}$ mixes only with $S_{m'b}^{(j)}$, and not with $S_{m''b}^{(j)}$.

distance. Then the symmetry group **C** is C_{3v}; if we consider the doubly degenerate species $\Gamma_j=E$, so that $d_j=2$, we may use the symmetry coordinates of Table I.

Let us calculate $\tilde{G}_{\beta a,\alpha a}{}^{E}$. Set m contains the three $\Delta\beta_i$, set n the $\Delta\alpha_i$. Then $g_m=3$, and we may choose $\Delta\beta_1$ as the typical coordinate R_1. The subgroup **H** becomes C_s, containing only the identity and the plane of reflection through H_1; only the a components of our E coordinates are totally symmetric under C_s, so that α in (2) refers to these components only. Under **H**, $\Delta\alpha_1$ is invariant, while $\Delta\alpha_2$ and $\Delta\alpha_3$ are equivalent: $R_A=\Delta\alpha_1$, $g_A{}^{(H)}=1$; $R_B=\Delta\alpha_2$, $g_B{}^{(H)}=2$.

We may now look up the two G elements we shall need in Decius's tables;[3] in his notation that between $\Delta\beta_1$ and $\Delta\alpha_1$ is $g_{\phi\phi}{}^{1}(\frac{1}{1})$ and that between $\Delta\beta_1$ and $\Delta\alpha_2$ is $g_{\phi\phi}{}^{2}(\frac{1}{1})$. So we have

$$\begin{aligned}\tilde{G}_{\beta a,\alpha a}{}^{E}&=(\tfrac{3}{2})[1(2N_a)(-2N_a)g_{\phi\phi}{}^{1}(\tfrac{1}{1})\\&\qquad+2(2N_a)(N_a)g_{\phi\phi}{}^{2}(\tfrac{1}{1})]\\&=-g_{\phi\phi}{}^{1}(\tfrac{1}{1})+g_{\phi\phi}{}^{2}(\tfrac{1}{1}).\end{aligned}$$

PROOF OF THE THEOREM

We begin from the basic definition

$$\tilde{G}_{ma,\,na}=\sum_{i,j}U_{ma,\,i}U_{na,\,j}{}^{*}G_{ij};\tag{3}$$

we shall omit the superscripts j when the meaning is clear. We may obtain all coordinates R_i of the set m by letting the symmetry operations C (of **C**) operate on R_1. So we obtain

$$\tilde{G}_{ma,\,na}=(g_m/h)\sum_{C}\sum_{j}U_{ma,\,C1}U_{na,\,j}{}^{*}G_{C1,\,j},\tag{4}$$

where h is the order of **C**, and the factor (g_m/h) takes care of repetitions. Now the matrix elements G_{ij} are invariant under **C**, in the sense that $G_{Ci,\,Cj}=G_{i,\,j}$; so we may write $G_{C1,\,j}=G_{1,\,C^{-1}j}=G_{1,\,k}$, if we take $CR_k\rightarrow R_j$. Then we have

$$\tilde{G}_{ma,\,na}=(g_m/h)\sum_{C}\sum_{k}U_{ma,\,C1}U_{na,\,Ck}{}^{*}G_{1,\,k}.\tag{5}$$

We now use the relation,[8] valid because the S_{ma} reduce **C**,

$$U_{ma,\,Ck}=\sum_{\beta}C_{\beta a}{}^{*}U_{m\beta,\,k},\tag{6}$$

where the $C_{\beta a}$ are the transformation matrices of the jth representation of **C**. These matrices are orthogonal,

$$\sum_{C}(C_j)_{\beta a}{}^{*}(C^k)_{\theta\epsilon}=(h/d_j)\delta_{jk}\delta_{\beta\theta}\delta_{a\epsilon}.\tag{7}$$

So (5) becomes

$$\begin{aligned}\tilde{G}_{ma,\,na}&=(g_m/h)\sum_{C}\sum_{k}\sum_{\alpha}C_{\alpha a}{}^{*}U_{ma,\,1}\sum_{\beta}C_{\beta a}U_{n\beta,\,k}{}^{*}G_{1,\,k}\\&=(g_m/d_j)\sum_{k}\sum_{\alpha}U_{ma,\,1}U_{na,\,k}{}^{*}G_{1,\,k}.\end{aligned}\tag{8}$$

For further reduction, we use the elements H of group **H**, which leave R_1 invariant; the sum over the R_k is replaced by a sum over the *nonequivalent* (under **H**) R_A, R_B, etc., each being transformed under **H** to cover its equivalent coordinates. The steps are analogous to those in the passage from Eq. (3) to Eq. (8); since the S_{ma} reduce **H**, the analog of Eq. (6) for the group **H** may be used. We write $h^{(H)}$ for the order of **H**:

$$\begin{aligned}\tilde{G}_{ma,\,na}&=(g_m/d_j)\sum_{A}\sum_{\alpha}(g_A{}^{(H)}/h^{(H)})U_{ma,\,1}\sum_{H}U_{n\alpha,\,HA}{}^{*}G_{1,\,A}\\&=(g_m/d_jh^{(H)})\sum_{A}g_A{}^{(H)}\sum_{\alpha}U_{ma,\,1}\\&\qquad\times\sum_{H}\sum_{\beta}U_{n\beta,\,A}{}^{*}H_{\beta a}G_{1,\,A}.\end{aligned}\tag{9}$$

Now using the special case of the orthogonality relation,[9]

$$\sum_{H}(H^{(j)})_{\beta a}=\sum_{H}(H^{(j)})_{\beta a}(H^{(1)})_{\gamma\gamma}{}^{*}=h^{(H)}\delta_{a\beta}\delta_{j1},\tag{10}$$

where $(H^{(1)})_{\gamma\gamma}$ refers to the totally symmetric representation Γ_1 of **H**, we immediately convert Eq. (9) into our theorem, Eq. (2).

[8] See Wilson, reference 2, Eq. (15). It is this relation which demands proper choice of $S_{m'a}$, as mentioned in footnote 7.

[9] Reference 2, Eq. (18).

Letters to the Editor

THIS section will accept reports of new work, provided these are terse and contain few figures, and especially few half-tone cuts. The Editorial Board will not hold itself responsible for opinions expressed by the correspondents. Contributions to this section should not exceed 600 words in length and must reach the office of the Editor not later than the 15th of the second month preceding that of the issue in which the Letter is to appear. No proof will be sent to the authors. A publication charge of $10.00 per Letter is made which, when honored, will entitle the Institution to 100 free reprints.

Transition Temperatures in some Dihydrogen and Dideutero Phosphates and Arsenates and their Solid Solutions

C. C. STEPHENSON, J. M. CORBELLA, AND L. A. RUSSELL
Department of Chemistry, Massachusetts Institute of Technology, Cambridge, Massachusetts
(Received April 9, 1953)

THE transitions in potassium and ammonium dihydrogen phosphates at low temperatures have been investigated extensively. These transitions, which are of the order-disorder type, are associated with the orientation of the hydrogen bonds in the tetragonal lattice. This tetragonal lattice can be maintained by replacing the potassium or ammonium ions with rubidium or cesium ions, by replacing the phosphate with the arsenate ion, or by substituting deuterium for hydrogen.

The transition temperatures of these various combinations are of interest, and Table I summarizes the results of the transition temperatures found in a cooling-curve apparatus. The temperatures reported are those found on cooling and are accurate to 0.3°; higher temperatures might be found on warming if hysteresis occurs as in the cases of the ammonium dihydrogen phosphate and arsenate.

The deutero-compounds were prepared by recrystallization three times from heavy water; although no analysis of the deuterium content was made, the increase in transition temperature between the second and third crystallizations was small enough to indicate essentially complete conversion. The marked increase in transition temperature caused by substitution of deuterium for hydrogen is qualitatively proportional to the deuterium content.

TABLE I. Transition temperatures, °K.

$NH_4H_2PO_4$[a]	147.0	$ND_4D_2PO_4$	229.7
KH_2PO_4[a]	121.97	KD_2PO_4[b]	213
RbH_2PO_4	147.1	RbD_2PO_4	...
$NH_4H_2AsO_4$[a]	215.8	$ND_4D_2AsO_4$	298.6
KH_2AsO_4	95.57	KD_2AsO_4	162.0
RbH_2AsO_4	109.9	RbD_2AsO_4	177.8
CsH_2AsO_4	143.3	CsD_2AsO_4	212.4

[a] C. C. Stephenson *et al.*, J. Am. Chem. Soc. **66**, 1397, 1402, 1405, 1409 (1944).
[b] W. Bantle, Helv. Phys. Acta **15**, 373 (1942).

The rubidium and cesium compounds were carefully purified because the transition temperature is markedly lowered by the presence of other cations. For example, K^+, Rb^+, Cs^+, and Tl^+ lower the transition temperature of $NH_4H_2PO_4$, and NH_4^+ and Rb^+ lower the temperature of the transition in KH_2PO_4. The transition was usually not found for mole fractions of a second cation exceeding ten or twenty percent. The entropy change associated with the transition was also decreased. The cooling curves permit a rough estimate of the entropy change by comparison with the known values for the potassium and ammonium salts. The entropy change for each of the pure compounds is compatible with the theoretical value[1] of $R \ln \frac{3}{2}$.

TABLE II. Transition temperatures of solid solutions of NH_4H_2PO and $NH_4H_2AsO_4$.

Mole percent $NH_4H_2AsO_4$	T, °K
8.7	152.2
41.4	172.5
55.4	183.2
62.2	187.3
79.9	201.3
92.1	210.3

It is of interest to note that a metastable form of RbH_2PO_4 has no hydrogen-bond transition between liquid air and room temperatures. The failure to observe a transition in RbD_2PO_4 and CsH_2PO_4 is no doubt due to the formation of a lattice similar to that of the metastable RbH_2PO_4, and does not preclude the existence of these compounds in the tetragonal structure.

The formation of solid solutions of phosphates and arsenates results in a regular change in transition temperature. Table II lists these temperatures for solid solution of $NH_4H_2PO_4$ and $NH_4H_2AsO_4$ as a function of composition.

The contrasting behavior of solid solutions formed by cation substitution with those formed by anion or deuterium substitution is related to the ideality of the solid solutions in a thermodynamic sense. Solid solutions of the deuterium and hydrogen compounds would approach ideal solutions. Rough measurements indicate that the phosphate-arsenate solutions are also nearly ideal, whereas those formed by cation substitution deviate considerably from ideality.

[1] J. C. Slater, J. Chem. Phys. **9**, 16 (1941).

The Statistical Interpretation of Polarization Data in Raman Spectra

MARVIN C. TOBIN
Arthur D. Little, Inc., Cambridge, Massachusetts
(Received March 31, 1953)

ALTHOUGH the use of statistical techniques[1-3] is becoming widespread in the interpretation of chemical and physical experimental data, to the writer's knowledge no application of such techniques has been made to the thorny problems connected with polarization measurements on Raman lines.

Cleveland[4] has made a quite thorough study of polarization measurements. The data in Table I of his paper will be analyzed as an illustration of what can be done in this connection. This table gives depolarization factors for the five lines of CCl_4 as measured on five different plates. Part of the variance in the measurements has been averaged out, since each entry in the table represents the mean of two independent determinations of the same line on the same plate, five microdensitometer readings being made for each determination.

One may now ask the following questions of the data:

1. Is there a systematic variation of the observed depolarization factors in going from plate to plate?

2. Is there a systematic variation of the observed depolarization factors, for the depolarized lines, in going from line to line?

TABLE I.

	Degrees of freedom	Variance	F
Lines	3	0.001039	0.906
Plates	4	0.002021	1.736
Residual	12	0.001146	
Total	19		

Critical $F = 3.26$

3. Have constant errors been eliminated so that for a large number of measurements on a depolarized line, ρ will average 0.855?

4. If a single measurement is now made using a different compound and a different plate, what criterion can be set up for deciding if a given line is polarized or depolarized?

Questions 1 and 2 may be answered by an analysis of variance[1] for the four depolarized lines on the five plates. The results are given in Table I. It is seen that the F ratios[1,2] for both lines and plates are well below the critical 5 percent probability level. The answer to these questions is, then, that the error in the measurements is purely random, and that the error in measurement is not increased by using different plates, nor does it vary significantly in going from line to line.

To answer the third question, the twenty entries in Cleveland's table are averaged to give 0.850, and the standard deviation $s=0.036$ calculated. Application of the t test[1] to test the hypothesis that this mean is not significantly different from 0.855 gives a value of $t=0.621$. Since this is well below the critical 5 percent value of $t=2.09$ (19 degrees of freedom) it may be concluded that the mean of the twenty entries is not significantly different from 0.855, and that constant errors (such as those due to nonconvergence of the illuminating beam) have been eliminated.

Question 4 is more complex. It is a good rule of thumb that only one measurement out of twenty will differ from the mean of a large series by an amount greater than twice the standard deviation of the series. For the data being analyzed here, $s=0.036$, so that there is only one chance in twenty that a depolarized Raman line measured under the conditions used by Cleveland (five readings on each of two determinations made on the same plate) will have an observed depolarization of $\rho<0.78$ or $\rho>0.93$. It may then be concluded with a 98 percent probability that a line giving a reading of $\rho<0.78$ is polarized. The analysis for lines with observed $\rho>0.78$ is rather complicated. If it is assumed that the depolarization factor for a polarized line may lie anywhere in the range 0.0–0.855 with equal probability, a polarized line chosen at random has one chance in seven of having a "true" ρ in the range 0.70–0.855. On the basis of a rule that lines with $\rho>0.78$ are to be taken as depolarized, a line with a "true" $\rho=0.70$ has one chance in forty of being taken as depolarized on the basis of a single reading, a line with a "true" $\rho=0.850$ has one chance in forty of being taken as polarized. A line with "true" $\rho=0.78$ has one chance in two of being taken as polarized on the basis of a single reading. Assuming, then, that a line chosen at random in the range $\rho=0.70$–0.855 has on the average one chance in two of incorrectly being taken as depolarized, there is one chance in fourteen of a polarized line chosen at random in the range $\rho=0.00$–0.855 giving a reading in the range $\rho=0.78$–0.86.

If half the lines in a spectrum are assumed to be polarized, there is only one chance in twenty-eight that a line with observed $\rho>0.78$ is polarized. It is therefore a reasonable working rule that a line with observed $\rho>0.78$ is depolarized.

If the question of the polarization of a Raman line is critical, it is best to make replicate measurements and apply the t test as before, the null hypothesis[2] being that the mean of the measurements is not significantly different from 0.855. An illustration of this use of the t test may be given for the polarized line of CCl_4, using Cleveland's data. The mean of the five entries is 0.072, with a standard deviation of 0.067. t turns out to be 26.8, which very greatly exceeds the 5 percent critical value of $t=2.78$ (four degrees of freedom). The null hypothesis is thus not borne out, the statistical analysis showing that the line is indeed polarized.

[1] W. J. Youden, *Statistical Methods for Chemists* (John Wiley and Sons, Inc., New York, 1951).
[2] W. L. Gore, *Statistical Methods for Chemical Experimentation* (Interscience Publishers, New York, 1952).
[3] "Statistical Methods in Chemical Production," Symposium, Ind. Eng. Chem. **43**, 2053 (1951).
[4] F. F. Cleveland, J. Chem. Phys. **13**, 101 (1945).

Macroscopic Spirals and the Dislocation Theory of Crystal Growth*

N. Cabrera
University of Virginia, Charlottesville, Virginia
(Received March 27, 1953)

THERE is now overwhelming experimental evidence in favor of the dislocation theory of crystal growth;[1] however, there are a few points which still require further clarification. One of them is the possibility for the dislocation theory to interpret the observation of macroscopic spirals centered on dislocations of very large Burgers vector. Concerning the dislocation itself, Frank[2] has shown that there must be an empty tube at the center or the dislocation, thus avoiding the high concentration of elastic energy which would otherwise be there; but we still need to understand the stabilization of the macroscopic step forming the spiral. Particularly in the case of growth from the vapor (for instance, growth of SiC crystals, Verma,[3] Amelinckx[4]) no reason has yet been proposed which would maintain the step as a multiple one, instead of being decomposed into elementary steps, forming a spiral of many branches.

The purpose of this letter is to suggest a possible explanation of this fact, applicable to those cases for which the crystal is growing in layers of thickness b, separated by stacking changes, twin boundaries, etc., having a surface energy γ' per unit surface (for instance SiC crystals, see below). It is easy to show that such a crystal will grow on a dislocation (or group of them) having a Burgers vector b (or resultant Burgers vector b), only if the supersaturation σ of the vapor satisfies the condition

$$\sigma=\ln\alpha>\sigma_c=\gamma'\Omega/kTb, \tag{1}$$

where $\alpha=p/p_0$ is the ratio of the actual vapor pressure p to the equilibrium vapor pressure p_0, and Ω is the volume per molecule. This is the necessary condition for the advance of the multiple step of height b to cause a decrease in the free energy of the crystal. It is also clear that the step will remain of height b, for any supersaturation $\sigma>\sigma_c$ because although a step of height smaller than b could then advance, it will be overtaken by the rest of the layer, which will move faster.

The critical radius of curvature ρ_c of the step of height b under a supersaturation σ will then be

$$\rho_c=\gamma\Omega/kT(\sigma-\sigma_c), \tag{2}$$

where γ is now the surface energy per unit surface of the edge of the step. The distance between successive turns of the spiral is of the order[1] $4\pi\rho_c$, and therefore may become very large if σ is sufficiently near σ_c. This explains the usual fact that whenever a macroscopic spiral is observed, the distance between successive turns is also macroscopic. To explain this fact neglecting σ_c in (2) would require an extremely small value of the supersaturation, which is not likely to occur.

The structures of SiC crystals are known[5] to consist of groups of close-packed molecular layers separated by stacking changes. The most common structure is the $Z(33)$, having macroscopic hexagonal symmetry and consisting of successive pairs of groups of three monomolecular layers each, every group being separated from the next by a stacking change. Other macroscopically hexagonal structures are possible, for instance $Z(22)$, consisting of pairs of groups of two monomolecular layers. Beside those there is a number of rombohedral structures, for instance $Z[(33)_n32]$ consisting of three successive groups of $6n+5$ monomolecular layers with stacking changes in between groups, and having $2n+1$ other stacking changes inside every group. Those rombohedral structures, which can be thought of as having a macroscopic cubic symmetry, have been shown by Frank[5] to originate from the $Z(33)$ structure by the formation of a screw dislocation of the required Burgers vector.

Although there is evidence to suggest, that the surface energies of the various possible types of stacking changes are different, let us assume for the moment that they are all equal to γ' per

unit surface. Then the hexagonal structures $Z(33)$ and $Z(32)$ should have, according to (1), a minimum supersaturation necessary for growth given, respectively, by $\sigma_{33}=(1/3)\sigma_1$ and $\sigma_{32}=(1/2)\sigma_1$, where $\sigma_1=\gamma'\Omega/kTa$, a being the height of a monomolecular layer. Also the height of the steps actually occurring on the crystal surface should not be larger than $3a$ or $2a$, because a multiple step (of height $3na$ or $2na$) will have the same minimum supersaturation for growth σ_{33} or σ_{22}, and will therefore tend to separate into its components.

However, the situation for the rhombohedral structures $Z[(33)_n32]$ is different. A multiple step of height $(6n+5)a$ will have a minimum supersaturation equal to $[2(n+1)/(6n+5)]\sigma_1$, which is somewhere between σ_{33} and σ_{22}. For higher supersaturation, the $2n+1$ layers of height $3a$ will have, when separated, a minimum supersaturation σ_{33} and the layer of height $2a$, a minimum supersaturation σ_{22}. Using velocities of advance of the form $v_{33}=C(\sigma-\sigma_{33})/3a$ and $v_{22}=C(\sigma-\sigma_{22})/2a$, where C is a constant, we see that only for a particular supersaturation $\sigma=\sigma_{33}+\sigma_{22}$, the elementary steps are able to separate from each other, because then $v_{33}=v_{22}$; at any other supersaturation $v_{33}\neq v_{22}$ and therefore the multiple step will tend to remain together. We conclude therefore that the macroscopic spirals sometime observed in SiC, should correspond according to our point of view, to a structure of the type $Z[(33)_n32]$ growing under a supersaturation very near the corresponding minimum value.

A more complete account of this work will be given later.

* Supported in part by the U. S. Office of Naval Research.

[1] F. C. Frank, Disc. Faraday Soc., No. 5, 48 (1949); Burton, Cabrera, and Frank, Trans. Roy. Soc. (London) **243**, 299 (1951), F. C. Frank, Advances in Physics, London **I**, 1 (1952).
[2] F. C. Frank, Acta Cryst. **4**, 497 (1951); F. H. Horn, Phil. Mag. **43**, 1210 (1952).
[3] A. R. Verma, Phil. Mag. **42**, 1005 (1951); **43**, 441 (1952).
[4] S. Amelinckx, J. chim. phys. **48**, 1 (1951); **49**, 411 (1952).
[5] F. C. Frank, Phil. Mag. **42**, 1014 (1951).

Pressure Virial Coefficients in Terms of Cluster Integrals

WILLIAM E. PUTNAM AND JOHN E. KILPATRICK
Department of Chemistry, The Rice Institute, Houston, Texas
(Received March 30, 1953)

EVIDENTLY it has been tacitly assumed that it is more natural to obtain density virial coefficients, rather than pressure virial coefficients, in terms of cluster integrals. This has been done for the general case by one of us.[1]

However, the pressure virial coefficients can be obtained for the general case by the procedure used by Kilpatrick[1] in a straightforward manner with slightly simpler mathematics.

The problem is to eliminate z between the two equations

$$P=kT\sum_{j=1} g_j z^j, \tag{1}$$

$$x=\frac{N}{V}=\frac{1}{v}=\sum_{j=1} j g_j z^j, \tag{2}$$

where z is the absolute activity and $g_j/g_1{}^j$ is the jth cluster integral. One can either express the pressure as a power series in the inverse volume (or molecular density) or the volume as a power series in the pressure:

$$P=kT\sum_{n=1} \alpha_n x^n, \tag{3}$$

$$v=x^{-1}=\sum_{n=1} \beta_n P^{n-2}. \tag{4}$$

Wooley[2] has given such expressions for β_1 through β_6 in a slightly different notation.

The general solution for the pressure virial coefficients can be found as follows: The equation

$$(\sum_{j=1} j g_j z^j)^{-1}=\sum_{i=1} \beta_i P^{i-2} \tag{5}$$

is multiplied by $P^{-n+1}dP$ and is integrated around the common origin of z and P. By application of Cauchy's theorem we find, after expansion by means of Taylor's theorem and the multinomial theorem,

$$\beta_n=(kT)^{-n+2}\sum_{t=0}\cdot\frac{(-)^t(n+t-2)!}{(n-2)!}\frac{1}{g_1{}^{n+t-1}}\sum_{(r_s)}\prod_{s=2}\frac{g_s{}^{r_s}}{r_s!}, \tag{6}$$
$$\sum_{s=2} r_s=t,$$
$$\sum_{s=2} s r_s=n+t-1.$$

It is not nearly so difficult to clear up this expression as it was in the case of the corresponding equation for α_n, since there is only one running summation to remove. The summation over t in Eq. (6) can be eliminated by the introduction of the net powers k_s:

$$\beta_n=(kT)^{-n+2}\sum_{(k_s)}\frac{(-)^{n-k_1-1}(2n-k_1-3)!}{(n-2)!}\frac{g_1{}^{k_1}}{g_1{}^{2n-2}}\prod_{s=2}\frac{g_s{}^{k_s}}{k_s!}, \tag{7}$$
$$\sum_{s=1} k_s=n-1,$$
$$\sum_{s=1} s k_s=2n-2.$$

The procedure for obtaining any given β_n is illustrated explicitly in reference (1). It might be noted that Eq. (7) above and Eq. (24) of reference (1) are very similar in form when β_n's are written in terms of g_j's and α_n's are written in terms of p_j's ($p_j=jg_j$).

The first six of these coefficients are

$$\beta_1=kT, \tag{8a}$$

$$\beta_2=(-g_2)/g_1{}^2, \tag{8b}$$

$$\beta_3=(-2g_3g_1+3g_2{}^2)/g_1{}^4(kT), \tag{8c}$$

$$\beta_4=(-3g_4g_1{}^2+12g_3g_2g_1-10g_2{}^3)/g_1{}^6(kT)^2, \tag{8d}$$

$$\beta_5=(-4g_5g_1{}^3+20g_4g_2g_1{}^2+10g_3{}^2g_1{}^2-60g_3g_2{}^2g_1+35g_2{}^4)/g_1{}^8(kT)^3, \tag{8e}$$

$$\beta_6=(-5g_6g_1{}^4+30g_5g_2g_1{}^3+30g_4g_3g_1{}^3-105g_4g_2{}^2g_1{}^2+280g_3g_2{}^3g_1-126g_2{}^5)/g_1{}^{10}(kT)^4. \tag{8f}$$

[1] J. E. Kilpatrick, J. Chem. Phys. **21**, 274 (1953).
[2] H. W. Wooley, J. Chem. Phys. **21**, 236 (1953).

The Charge on Combining Hydrogen Atoms

R. T. SANDERSON
Department of Chemistry, State University of Iowa, Iowa City, Iowa
(Received April 3, 1953)

IN a recent communication[1] the observation was reported that "hydrogen bridge" bonding appears to occur only when the hydrogen atoms bear partial negative charge. The relative charge on hydrogen was determined as the electronegativity difference between compound hydrogen and elementary hydrogen.

It has now been found that the charges on combined atoms may be evaluated quantitatively, if, in addition to the basic postulate that atoms adjust to equal electronegativity in a molecule, two assumptions are accepted. The first is that in an isolated molecule of NaF, the bond is 90 percent ionic. The second is that the change in electronegativity of an atom acquiring a partial charge is linear with the amount of charge. The partial charge is then simply the ratio of the actual electronegativity change undergone by an atom in going from element to compound, to the electronegativity change from zero charge to unit charge.

Partial charges calculated in this way for the individual atoms of a number of hydrogen compounds in no way alter the reported observation, but give a more realistic description of the nature of these molecules. Illustrative examples are given in Table I. Too little is known about the nature of both the hydrogen bond and the hydrogen bridge bond to justify drawing conclusions about the extent of their similarity, but it is interesting to compare

TABLE I. Partial charges on combined atoms.

$HClO_4$	H	0.39	Cl	−0.02	O −0.09	
H_3O	H	0.37	O	−0.12		
HNO_3	H	0.35	N	0.06	O −0.13	
H_2SO_4	H	0.30	S	0.12	O −0.17	
HF	H	0.30	F	−0.30		
HCl	H	0.19	Cl	−0.19		
H_2O	H	0.15	O	−0.30		
HBr	H	0.14	Br	−0.14		
$(CH_3O)_2BH$	H	0.07	B	0.30	C −0.03	O −0.38
NH_3	H	0.06	N	−0.19		
HI	H	0.04	I	−0.04		
$Ga(CH_3)_3$	H	0.01	Ga	0.12	C −0.06	
$B(CH_3)_3$	H	0.00	B	0.24	C −0.08	
$Al_2(CH_3)_6$	H	−0.03	Al	0.60	C −0.11	
Ga_2H_6	H	−0.03	Ga	0.10		
B_2H_6	H	−0.06	B	0.18		
$Al(BH_4)_3$	H	−0.08	Al	0.53	B 0.15	
$(AlH_3)_x$	H	−0.15	Al	0.45		
CaH_2	H	−0.33	Ca	0.66		
CsH	H	−0.69	Cs	0.69		

them. The hydrogen bond appears to be a bond formed between a combined hydrogen atom with partial positive charge and a atom with partial negative charge which has available an orbital with an unshared pair of electrons. The hydrogen bridge bond appears to be a bond formed between a combined hydrogen atom with partial negative charge and an atom with partial positive charge which has available an orbital with no electrons.

From data of the type given in Table I, the following tentative conclusions appear reasonable. (1) In combination with other elements, hydrogen appears to vary in partial charge between the two extremes of 0.39 and −0.69. (2) Hydrogen bridging appears to occur only when the charge on hydrogen is negative. Known compounds whose hydrogens have greater negative charge than O −0.10 are solids. (3) Stable borohydrides appear to form only when the hydrogen, with which a borine group may be considered to combine, bears a higher negative charge than that of borine hydrogen (−0.06). (4) The partial charges in the boron hydrides, although small, are sufficient to suggest that electrostatic interaction among atoms not bonded to each other may have a very significant influence on the molecular structures.

[1] R. T. Sanderson, J. Chem. Phys. 21, 571 (1953).

Evidence for One-Dimensional Rotation in NH_4I

R. C. PLUMB AND D. F. HORNIG
Metcalf Chemical Laboratories, Brown University, Providence, Rhode Island
(Received April 1, 1953)

IN a previous communication under this same title[1] it was pointed out that in the NaCl-like phase of NH_4I which exists at room temperature the only reasonable interpretation of the infrared absorption spectrum in the 7μ region led to a model in which the ammonium ion underwent one-dimensional free rotation. It was further concluded that the rotation took place about the hydrogen bond formed from one apex of the NH_4^+ tetrahedron to an adjacent I^- ion.

At the time that note was written we had, unfortunately, overlooked the beautiful investigations of the Raman spectrum of single crystals of NH_4I which had previously been published by L. C. Mathieu and J. P. Mathieu.[2] From measurements of the polarization of the Raman radiation they showed quite definitely that the threefold axis of the NH_4^+ ion coincided with the fourfold axis of the crystal. They did not reach any conclusions regarding rotation of the ion, but their prior evidence is probably less ambiguous than either the infrared spectrum or the neutron diffraction results[3] in demonstrating the one-bond model. Taken together the three investigations make this structure nearly certain.

[1] R. C. Plumb and D. F. Hornig, J. Chem. Phys. 21, 366 (1953).
[2] L. Couture-Mathieu and J. P. Mathieu, J. chim. phys. 49, 226 (1952).
[3] H. A. Levy and S. W. Peterson, J. Chem. Phys. 21, 366 (1953).

The Correlation of Solid Metal and Nonelectrolyte Solubilities*

PETER L. AUER
Research Division, Livermore Research Laboratory, California Research and Development Company, Livermore, California
(Received March 26, 1953)

TWO methods for correlating the solubilities of pure solid metals and nonelectrolytes have recently been discussed. Hildebrand has shown[1] that when the logarithm of mole fraction at saturation is plotted against the logarithm of absolute temperature, curves with constant slopes are obtained over extended temperature ranges for many systems forming regular solutions. On the other hand, Kleppa[2] has proposed that curves obtained by plotting logarithm mole fraction at saturation against reciprocal of absolute temperature can yield useful thermodynamic information and furthermore, indicate the extent of deviation from regularity.

Hildebrand's discussion for regular solutions can be extended readily to nonregular solutions in the following manner. An expression for the mole fraction of solute along the equilibrium liquidus line may be written formally as

$$\ln x = -\frac{\langle \Delta H \rangle_{sat}'}{RT} + \frac{\Delta S_f' + \langle \Delta S \rangle'^x}{R}. \tag{1}$$

Equation (1) serves to define the excess partial molar entropy of solution, $\langle \Delta S \rangle'^x$. Differentiation of Eq. (1) along the equilibrium line results in

$$\left(\frac{\partial \ln x}{\partial 1/T}\right)_{sat} = -\frac{\langle \Delta H \rangle_{sat}'/R}{1+\delta/T},$$

$$\left(\frac{\partial \ln x}{\partial \ln T}\right)_{sat} = -\frac{1}{T}\left(\frac{\partial \ln x}{\partial 1/T}\right)_{sat},$$

$$\delta = \frac{1}{R}\left\{\left(\frac{\partial \langle \Delta H \rangle_M'}{\partial \ln x}\right)_T - T\left(\frac{\partial \langle \Delta S \rangle'^x}{\partial \ln x}\right)_T\right\}. \tag{2}$$

The first relation in Eq. (2) is equivalent to Eq. (2) of reference 1.

In order to compare the merits of the reciprocal temperature and logarithm temperature plots, it will be useful to expand the heat of saturation term in Eq. (2) as follows:

$$\langle \Delta H \rangle_{sat}' = \Delta H_f' + \langle \Delta H \rangle_M',$$

$$\Delta H_f' = \Delta H_f'\{T_0\} - \Delta C_p'\{T_0\}[T_0 - T],$$

$$\langle \Delta H \rangle_M' = \langle \Delta H \rangle_M'\{T_e\} - \langle \Delta C \rangle_p^M\{T_e\}[T_e - T], \tag{3}$$

where T_0 is the fusion temperature of pure solute, T_e is the minimum temperature along the equilibrium liquidus line, and { } indicates the temperature at which the constant quantities are evaluated. If deviations from either Raoult's Law or Henry's Law are small, the quantity $(1+\delta/T)^{-1}$ may also be expanded. The expansion in Eq. (3) assumes that the series converges rapidly enough so that only the first two terms need be retained. Examination of Eqs. (2) and (3) indicate that a reciprocal temperature type of plot may be linear only if both the heat capacity terms and δ are negligibly small. However, a logarithm temperature type of plot will remain linear as long as δ is small and $\langle \Delta H \rangle_{sat}'$ is nearly linear in temperature, or if $\langle \Delta H \rangle_{sat}'$ is linear in $(T+\delta)$.

The criteria for linearity for the two different methods of plotting appear to be mutually exclusive. Obviously the ratio of slopes derived from the two plots is a function of temperature, and this ratio should vary directly as $1/T$. Experimentally, however, it is found that both methods of plotting yield straight lines in the low temperature regions. Such an apparent behavior may be observed as long as $\langle \Delta H \rangle_{sat}'$ is a slowly varying function of temperature, and δ is inappreciable at these temperatures. Experimental evidence indicates that for many systems $\langle \Delta H \rangle_{sat}'$ is nearly linear in temperature over a considerable range;[1] if the fusion and eutectoid temperatures are high for these systems, the above-mentioned slow variation condition will be fulfilled.

It is also to be expected that the δ-term will decrease as the solubility decreases. A comparison in the slopes of the two types of plots should then be made most profitably at T_e.

The application of Kleppa's method to deriving useful thermodynamic quantities characterizing nonregularity must be made with caution. In the absence of adequate heat capacity data, the assignment of simple interpretations to limiting slopes and intercepts can be made only with some uncertainty. The optimum information from a set of solubility measurements should be derivable when Kleppa's method is augmented by Hildebrand's recent proposal.

* Work performed under auspices of the U. S. Atomic Energy Commission Contract No. AT(11-1)-74.
[1] J. H. Hildebrand, J. Chem. Phys. **20**, 190 (1952).
[2] O. J. Kleppa, J. Am. Chem. Soc. **74**, 6047 (1952).

The Crystal Structure of $KVO_3 \cdot H_2O$†

C. L. Christ, Joan R. Clark, and H. T. Evans, Jr.
U. S. Geological Survey, Washington, D. C.
(Received March 23, 1953)

CRYSTALS of $KVO_3 \cdot H_2O$ were prepared by cooling a hot water solution containing roughly 2:1 mole ratio of KOH and V_2O_5, maintained at a *p*H between 7 and 8. Crystals thus obtained are colorless, transparent, prismatic elongated along [001], and of roughly equidimensional cross section. Precession and Weissenberg patterns yield the following data:

Orthorhombic: Space group—*Pnam* (D_{2h}^{16}) or *Pna* (C_{2v}^{9})
$a = 8.15_1 \pm 0.008$A Cell contents $4(KVO_3 \cdot H_2O)$
$b = 13.58_6 \pm 0.010$ Density$_{(calc)} = 2.53$ g cm^{-3}
$c = 3.69_7 \pm 0.004$ (Mo λ: $K\alpha = 0.71069$A, $K\alpha_1 = 0.70926$A)

Visual examination of the reflections obtained on patterns made by rotation of the crystal around [001] shows that corresponding reflections on all even layer lines are similar, as are those on all odd layer lines. It follows that in this structure all atoms are situated on planes parallel to (001) and $c/2$ apart. This fact suggests that all the atoms lie on the mirror planes in the space group *Pnam*, on the basis of which a satisfactory structure has been developed.

From the measured intensity data the Patterson projection on (001) was prepared. It was found possible to interpret the Patterson map in a straightforward fashion using a vector shift evaluated by the minimum function method of Buerger.[1] This procedure yielded a trial structure having a reliability index $R = 0.45$, where, as usual, $R = \Sigma||F_{obs}| - |F_{calc}||/\Sigma|F_{obs}|$. Starting with this trial structure the customary method of refinement by successive electron density computations was followed. This has given the structure shown in Fig. 1, for which $R = 0.20$, based on 153 observed reflections (calculated values for absent reflections were not included). The structure contains double, or linked, vanadium-oxygen chains in which the vanadium is fivefold coordinated by the oxygen atoms. The distorted trigonal dipyramidal polyhedra share edges, as shown, to form continuous chains parallel to the *c* axis. The departure from trigonal symmetry of the polyhedra may be due mostly to the mutual Coulombic repulsion of the vanadium atoms. The potassium ion has as nearest neighbors six oxygen atoms and two water molecules in approximately cubic coordination.

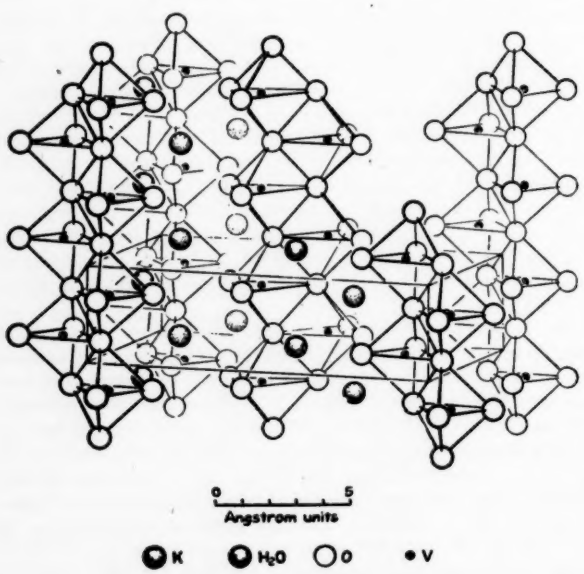

FIG. 1. Structure of $KVO_3 \cdot H_2O$.

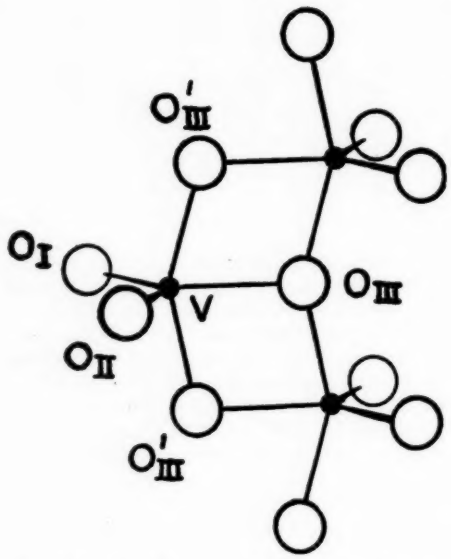

FIG. 2. Details of the oxygen-vanadium coordination.

Figure 2 shows in detail the coordination of the oxygen atoms around a vanadium atom; the corresponding vanadium-oxygen bond lengths and bond angles are listed in Table I. The same kind of distorted trigonal dipyramidal polyhedral linkage, with roughly the same V—O distances, has been found for V_2O_5 by Byström *et al.*[2] It is interesting that V_2O_5 is yellow red and $KVO_3 \cdot H_2O$ is colorless.

TABLE I. Vanadium-oxygen bond lengths and bond angles. The estimated maximum average error = 0.05A.

Bond lengths (A)		Bond angles (°)	
V—O_I	1.68	O_I—V—O_{II}	105
V—O_{II}	1.66	O_{II}—V—O_{III}	126
V—O'_{III}[a]	1.91	O'_{III}—V—O'_{III}	150
V—O_{III}	2.01	O_I—V—O_{III}	129

[a] See reference 2.

The overlapping of the O_{III} and V peaks in the electron density projection on (001) does not permit the precise fixing of the parameters of these two atoms that is desirable. Electron density sections at $(xy\frac{1}{4})$ are to be prepared to resolve this difficulty. The detailed investigation of the atomic parameters of $KVO_3 \cdot H_2O$ will be presented in a later paper.

† Publication authorized by the Director, U. S. Geological Survey.
[1] M. J. Buerger, Acta Cryst. **4**, 531 (1951).
[2] Byström, Wilhelmi, and Brotzen, Acta Chem. Scand. **4**, 1119 (1950).

Specific Influence of Solvents on the Infrared Spectra of Alcohols

ALEXANDER VERRIJN STUART*
Physics Department, University of Michigan, Ann Arbor, Michigan
(Received March 17, 1953)

THE general influence of dilution on a hydrogen bonding substance is well known to consist of a drastic decrease in intensity of the absorption band connected with the stretching vibration of the bonded group, and the simultaneous appearance and increase in intensity of a band corresponding to the same vibration in the unbonded molecule.[1] The solvents chosen are always nonpolar, and considered to be inert, but specific differences must, of course, exist between them. Few studies have been made of these specific interactions,[2] and these were made under conditions where interaction occurs only between solute and solvent molecules, but not between solute molecules mutually. In inert solvents this requires very low concentrations. At higher concentrations both associated and free molecules are present, and the intensity of the "monomer" band can be taken as a quantitative measure for the amount of monomers, using the intensity in the very dilute solution as a standard.[1] During the course of an investigation of a series of alcohols it became apparent that the solvent-solute interaction cannot be entirely neglected. In order to establish the extent of such specific effects a semi-quantitative study has been made.

As a representative alcohol propanol-1 was chosen. Spectra of the OH stretching frequency have been obtained at various concentrations in three nonpolar and three polar solvents, using a Perkin-Elmer Model 21 spectrometer equipped with a rocksalt prism, and a spectrometer designed and built in this laboratory, which was equipped with a LiF prism. The slight absorption of the polar solvents in the spectral region studied was compensated for by placing in the reference beam of the spectrometer a cell of variable thickness[3] containing the pure solvent. The temperature was not controlled, but observed to change less than 1°C during the measurements.

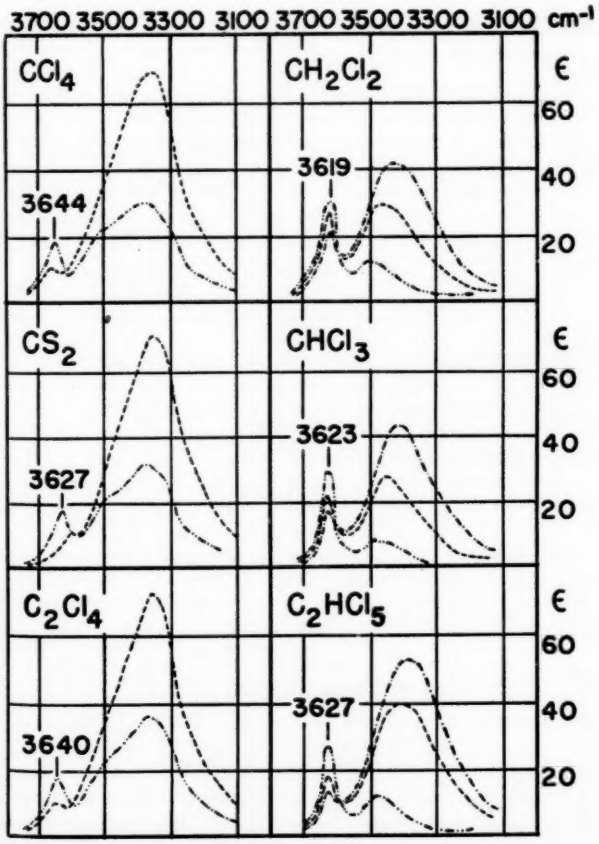

FIG. 1. Propanol-1 in six solvents. – · – 2.0 mole/liter, – – – 1.0 mole/liter, – · · – 0.25 mole/liter. Extinction coefficients ϵ are given in units 10^3 cm²/mole.

TABLE I. Solvent dependence of the OH stretching frequency. The frequencies are given in cm^{-1}; I_{mon} is given in units 10^3 cm²/mole for a concentration of 0.25 mole/liter; the intensity ratios are given for: *A* 0.25 mole/liter, *B* 1.0 mole/liter.

Nonpolar solvents	D	ν_{mon}	ν_{ass}	I_{mon}	I_{ass}/I_{mon} A	B
CCl_4	2.24	3644	doublet	17	1.77	···
C_2Cl_4	2.29	3640	doublet	17	2.06	···
CS_2	2.64	3627	doublet	17	1.88	···
Polar solvents						
C_2HCl_5	3.82	3627	3410	27	0.63	2.17
$CHCl_3$	4.82	3623	3450	28	···	1.23
CH_2Cl_2	8.3	3619	3470	31	···	1.07

(a) The frequency of the monomer band depends on the solvent used, in all cases.

(b) The association band shows two components in nonpolar solvents (at about 3300 and 3500 cm^{-1}), but in the polar solvents only a single peak appears, the position of which varies as a function of the concentration; in nonpolar solvents the 3300 cm^{-1} peak prevails at high concentrations, the other component at low concentrations.

(c) The intensity of the monomer band is higher in the polar solvents than in the nonpolar solvents, where a peak intensity of 25×10^3 cm²/mole is never exceeded at any dilution (very dilute solutions are not shown in Fig. 1).

(d) The intensity ratio of association and monomer bands, which is a measure of what might be called the "hydrogen bond breaking power" is different at identical concentrations.

The quantitative aspects of these results are listed in Table I. They indicate that differences exist, not only between the two classes of solvents, but also between the individual members of one class. A correlation with the dielectric constant suggests itself,[2b] and this quantity is listed with the results in Table I. In all cases the frequency of the monomer band is shifted to a value lower than the value 3680 cm^{-1} observed in the vapor spectrum. The assumption that such a shift would indicate hydrogen bonding between solute and solvent[2a] seems too general, but the conclusion seems warranted that the interaction is never negligible. The correlation with the dielectric constant, which is qualitatively perfect for the sequence of these shifts, holds only partially if applied to the bond breaking power. Only for the polar solvents does one find the same sequence of intensity ratios of association and monomer bands (here also the progression of the peak frequencies of the association band is indicative). For the nonpolar solvents the considerably smaller and irregular effect suggests that other factors, such as the individual bond moments of the groups closest to the solute molecule, and the size of the "hole" in the solvent "cage," may also play a part in the mechanism. Unexplained must remain the doubling of the association band in the nonpolar solvents. It seems unlikely that one deals with two different configurations (e.g., dimer and chain polymer) since a similar doubling is not observed for the OH deformation vibration. Results of an investigation of this motion will be published shortly.

The author is indebted to the Dow Chemical Company for a fellowship in support of this work.

* Now with Koninklijke/Shell Laboratorium, Amsterdam, Netherlands.
[1] Studies of these effects are reviewed by: M. M. Davies, Ann. Rep. **XLIII**, 3 (1946) and L. Kellner, Rep. Prog. Phys. **XV**, 1 (1952).
[2] W. Gordy, J. Chem. Phys. **7**, 93 (1939); R. Mecke, and W. Lüttke, Z. Elektrochem. **53**, 241 (1949).
[3] A. V. Stuart, J. Opt. Soc. Am., **43**, 212 1953.

Infrared Absorption of Solid N_2O_5†,‡

ROY TERANISHI AND J. C. DECIUS
Department of Chemistry, Oregon State College, Corvallis, Oregon
(Received April 6, 1953)

NITROGEN pentoxide in the solid state is known from x-ray diffraction data[1] to exist in the ionic form $NO_2^+NO_3^-$; the space group is $D_6{}^4{}_h$ with two molecules per unit cell. The Raman spectra[2] of the crystal, and of concentrated aqueous solutions, are different from those of solutions in nonpolar solvents, with two intense lines at 1050 and 1400 cm^{-1}, which have been assigned to the totally symmetric vibrations of the nitrate and nitronium ions, respectively.

The infrared absorption of sublimed films of N_2O_5 has been studied with a Perkin-Elmer Model 12-C spectrometer using NaCl and KBr prisms. The films were maintained at temperatures in the neighborhood of the boiling point of liquid nitrogen with a cell similar in design to that first described by Wagner and Hornig.[3] Films were condensed on AgCl and on KBr windows which were incompletely cooled with no apparent difference in the absorption, although on warming to room temperature, the KBr windows were apparently attacked, since a weak KNO_3 spectrum was observed. When the films were condensed on completely cooled windows a spectrum characteristic of gaseous N_2O_5 was observed.

The N_2O_5 was prepared by the ozonization of NO_2 obtained either by the pyrolysis of $Pb(NO_3)_2$ or from a cylinder (Matheson Company). The oxygen stream to the ozonizer was dried with concentrated H_2SO_4, KOH pellets, and $CaCl_2$. The product was trapped with a dry-ice acetone bath, and in some cases resublimed in the ozone stream before final sublimation onto the cell window.

Although the films of N_2O_5 scattered visible light strongly, the background transmission from about 3.5 to 4 microns out to 25 microns was sufficiently high, so that the strong absorption bands could be clearly identified. These were found at the positions indicated in Table I.

According to the selection rule theory for crystals as developed by Halford[4] and Hornig,[5] in the harmonic approximation the frequencies ν_2^-, ν_3^-, and ν_4^- are permitted for the NO_3^- ion, while ν_2^+ and ν_3^+ are allowed for the NO_2^+ ion, for which the site group symmetries are each D_{3h}. Hornig,[5] using a treatment of the Born-Oppenheimer type, has pointed out that molecular modes such as the degenerate frequencies ν_3^+, and ν_3^-, and ν_4^- may be split by interaction with lattice modes. It seems possible that this effect is responsible for the breadth of the very strong degenerate NO_3^- stretching mode in the vicinity of 1400 cm^{-1} and the components of the degenerate NO_3^- bending mode at 740–772 cm^{-1}. All the frequencies assigned to NO_3^- lie within about 20 cm^{-1} of the positions in which they appear in simple salts.

The frequencies of NO_2^+ are readily assigned by analogy with the isoelectronic CO_2 molecule. The bending frequency at 537 cm^{-1} seems quite low, but according to the D_{6h} unit cell symmetry it is permitted to interact with the degenerate frequencies ν_3^- and ν_4^- of the nitrate ion, both of which are found at higher values than they exhibit in simple nitrates; for this reason, and since no fundamental other than the lattice modes can be expected to occur this low, the assignment seems reasonably certain.

The unassigned frequencies may possibly be combinations involving lattice modes or may be due to HNO_3 as an impurity. Further studies are in progress, involving efforts to obtain less scattering films by control of the sublimation conditions and also involving enriched N^{15}, so as to confirm the assignments and permit a complete calculation of force constants.

TABLE I. Infrared absorption of crystalline N_2O_5.

Frequency (cm^{-1})	Relative strength	Assignment
537	strong	$\nu_3^+(E')$
740 772	medium	$\nu_4^-(E')$
819	medium	$\nu_2^-(A_2'')$
930–964	weak	
1308	weak	
1408	very strong, broad	$\nu_3^-(E')$
1680	medium	
2390	strong	$\nu_2^+(A_2'')$

† Assisted by a grant-in-aid from the Graduate School of Oregon State College.
‡ Published with the approval of the Monographs Publication Committee, Oregon State College as Research Paper No. 222, School of Science, Department of Chemistry.
[1] Grison, Eriks, and deVries, Acta Cryst. **3**, 290 (1950).
[2] J. Chedin, thèse, Paris, 1937; D. J. Millen, J. Chem. Soc. **1950**, 2606.
[3] E. L. Wagner and D. F. Hornig, J. Chem. Phys. **18**, 296 (1950).
[4] R. S. Halford, J. Chem. Phys. **14**, 8 (1946); H. Winston and R. S. Halford, J. Chem. Phys. **17**, 607 (1949).
[5] D. F. Hornig, J. Chem. Phys. **16**, 1063 (1948).

Erratum: Diffusional Processes in the Growth of Aerosol Particles

[J. Chem. Phys. **20**, 1797–1803 (1952)]

F. C. COLLINS AND H. L. FRISCH
Department of Chemistry, Polytechnic Institute of Brooklyn, Brooklyn, New York

EQUATION (37) should read

$$f=m\Phi(t)\frac{c(r,t)}{a-m\int_0^t\Phi(\tau)d\tau} \qquad (37')$$

because the probability f must be taken relative to the mean bulk concentration at the time t, which is

$$a-m\int_0^t\Phi(\tau)d\tau$$

instead of a as previously given. Equation (41) then becomes

$$\Phi(t)=\Phi_0(t)\exp\left[-\int_0^t\frac{m\Phi(\tau)d\tau}{a-m\int_0^\tau\Phi(s)ds}\right]. \qquad (41')$$

The integral in Eq. (41′) is readily evaluated in terms of

$$\Theta(t)=\int_0^t\Phi(\tau)d\tau,\quad d\Theta=\Phi(t).$$

Integration of Eq. (41′) as a whole then leads to

$$\Theta=\frac{a}{m}\left\{1-\exp\left[-\frac{m}{a}\int_0^t\Phi_0(\tau)d\tau\right]\right\}.$$

Thus we have in place of Eq. (43)

$$\frac{d\Theta}{dt}=\Phi(t)=\Phi_0\exp\left[-\frac{m}{a}\int_0^t\Phi_0(\tau)d\tau\right] \qquad (43')$$

for the flux to a given particle in the presence of a concentration m of other competing sinks.

The ν_9 Fundamental of C_2F_6*

D. E. MANN AND EARLE K. PLYLER
National Bureau of Standards, Washington, D. C.
(Received March 23, 1953)

IN connection with another investigation, it was necessary to review the assignment of the fundamentals of perfluoroethane given by Nielsen, Richards, and McMurry.[1] Apart from the torsional mode only ν_9, to which the value 216 cm^{-1} had been assigned on the basis of the plausible identification of several

binary combinations, could be regarded as uncertain. Since this vibration is infrared active, an attempt was made to observe it directly with the aid of a CsI prism. A strong band with an indistinct contour was found at 220 cm^{-1}, in very good agreement with the predicted value.

The change of ν_9 from 216 to 220 cm^{-1} would affect only very slightly the value of the barrier to internal rotation calculated by Pace and Aston.[2] Nevertheless, since recent electron diffraction and microwave studies of related molecules have made plausible structural parameters somewhat different from those used by Pace and Aston, it was considered desirable to incorporate these changes in a recalculation of the barrier. The assumption of tetrahedral bond angles, and the distances C−F:1.33A and C−C:1.48A, leads to the moments $I_A=I_B=436\times10^{-40}$, $I_C=298\times10^{-40}$ g cm^2. A barrier of 3920 cal $mole^{-1}$ gives the best fit of the calculated with experimental entropy values. The value determined by Pace and Aston is 4350 cal $mole^{-1}$.

* This work has been supported in part by the U. S. Office of Naval Research under contract NAonr 112-51.

[1] Nielsen, Richards, and McMurry, J. Chem. Phys. **16**, 67 (1948).
[2] E. L. Pace and J. G. Aston, J. Am. Chem. Soc. **70**, 566 (1948).

Flow of Oxide Layer During Oxidation of Copper

WALTER J. MOORE
Department of Chemistry, Indiana University, Bloomington, Indiana
(Received March 23, 1953)

IT has been shown[1] that the growth of cuprous oxide on copper exposed to oxygen at 800–1050° follows the rate equation $dy/dt=k/y$, where y is the thickness of oxide layer and $k=2D$, D being the diffusion coefficient of radioactive copper in cuprous oxide. Further experiments on the oxidation of copper have now been made.

Spheres of polycrystalline copper, 0.5 to 2.0 cm in diameter, were heated in air at 1000° until the oxide layer was 1 to 3 mm. After removal of the oxide, the density of the copper core was normal. This result indicates that no detectable porosity was created in the copper.[2] The oxide coat must uniformly shrink inwards as the diameter of the unoxidized copper decreases. The oxide layer is polycrystalline but free from cracks, and the plastic flow of the oxide would seem to be caused by the excess free energy produced as vacancies coalesce at the metal-to-oxide interface.

A 0.1-mm nichrome wire was tightly wound in an equatorial groove around a 2.0-cm copper sphere. After oxidation for 50 hr at 1000°, the wire was completely covered by 1.1 mm of cuprous oxide, and only 0.1 mm of oxide separated the wire girdle from the unoxidized sphere. The circumference of the wire must have decreased about 3 percent to account for its new position.

Through a copper tube 9.6 mm od with 0.58-mm wall was passed a current of pure argon, while the outside of the tube was exposed to air at 1000°. After 20 hr the inside diameter of the tube had decreased slightly from 8.4 to 8.3 mm, while 0.9 mm of oxide was formed. The copper under the oxide was hard and brittle and contained numerous cracks. In this case also, there must have been an inward flow of oxide. Evidently the vacancy current responsible for film growth cannot continue through the underlying copper, the self-diffusion coefficient of copper being much lower than the D for copper in cuprous oxide.

These results may have a bearing on the question of the sintering mechanism in oxide compacts, for a similar plastic flow of oxide may be associated with diffusion of the copper ion even in the absence of the underlying copper. Experiments on this point are in progress. This work is part of Contract AT-(11-1)-250 with the U. S. Atomic Energy Commission.

[1] W. J. Moore and B. Selikson, J. Chem. Phys. **19**, 1539 (1951); **20**, 927 (1952).
[2] Contrast this result with that of H. H. Uhlig (U. S. Office of Naval Research Forum on Corrosion Research, Washington, D. C., November 9, 1949) who oxidized a sphere of 2 percent Si−2 percent Al iron alloy for 24 hr at 1165° and found a large hole in the center.

On an Application of the Fermi-Thomas Method to Molecules

W. A. BOWERS
Physics Department, University of North Carolina, Chapel Hill, North Carolina
(Received April 7, 1953)

RECENTLY March[1] has applied the Thomas-Fermi method to molecules of tetrahedral and octahedral symmetry, using the "smoothing approximation" of Buckingham *et al.*,[2] in which the nuclear charge of the outer atoms is regarded as averaged over the surface of a sphere. This averaging makes the problem spherically symmetric and allows the application of the Thomas-Fermi method in the way familiar from the treatment of atoms. The only modification is the discontinuity in potential gradient at the sphere, proportional in magnitude to the total nuclear charge N of the outer atoms, which must be imposed on the solution. Using March's tables, one can construct appropriate solutions of the T-F equation corresponding to various values of R (radius of "smoothing" sphere) and N/Z (Z=nuclear charge of central atom); then the total energy E and also dE/dR can be calculated from March's formulas.

The purpose of this note is to give the results obtained in this way for the equilibrium sphere radius D [defined by $(dE/dR)_{R=D}=0$] and the force constant for the totally symmetric vibration k [defined by $k=(d^2E/dR^2)_{R=D}$], of tetrahedral molecules. March gave D graphically,[3] but did not calculate k. Of course one would hardly expect this treatment to give accurate results for any particular molecule; however, one might hope that some general trends, such as variation with Z or with N, would be given correctly. In any event, calculations of force constants from first principles scarcely exist for any but the simplest molecules, so that any efforts along these lines may be of some interest.

The results may be summarized as follows:

$$D=Z^{-1}g(N/Z), \tag{1a}$$

$$k=Z^3f(N/Z), \tag{1b}$$

where the functions f and g are given approximately by

$$f(x)=1980x^{3.51}\ \text{dyne/cm}, \tag{2a}$$

$$g(x)=3.12x^{-0.6}\text{A}, \tag{2b}$$

for the range of values $0.8<x<3.0$. This limitation is owing to the small number of solutions of the T-F equation available; we did not perform further numerical integrations, but simply used March's tabulated solutions. The discussion below is based on these approximate formulas; occasionally we have had to extrapolate them in an unwarranted fashion.

Comparison with the data for several tetrachlorides and tetrabromides yields the following results:

(1) The numbers predicted by Eqs. (1) and (2), using the actual values of N and Z, are in bad disagreement with the data. The internuclear distances predicted are too small by a factor which varies from 4 to 3 as one goes from CCl_4 to $PbCl_4$ and from 7 to 5 as one goes from CBr_4 to $PbBr_4$, while the force constants predicted are too high by a factor of the order 1000, which, however, decreases as one goes from CCl_4 to $PbCl_4$.

(2) Ignoring the magnitude and looking at the Z dependence of D for the series of chlorides and bromides, one finds an increase with Z predicted which is however somewhat more rapid than observed, namely $Z^{0.27}$ (predicted), and $Z^{0.12}$ (observed). The Z dependence of k predicted is a decrease as $Z^{-0.49}$; the data show likewise a decrease with Z which cannot, however, be represented over the whole range of Z by a constant exponent. For the heavier chlorides (Ge, Sn, Pb) it is about −0.45.

Although these results are not very encouraging, there is perhaps a little more to be said. March found that a more reasonable charge distribution could be obtained for CCl_4 by treating

TABLE I. Force constants of tetrachlorides.

X	C	Si	Ge	Sn	Pb
N_{eff}	6.4	6.9	9.0	9.6	10.9
k (calc) (10^5 dyne/cm)	5.4	4.5	7.4	7.5	8.9
k (exp)[a] (10^5 dyne/cm)	17.6	15.1	13.1	11.2	9.0

[a] Data from Herzberg, *Infrared and Raman Spectra*.

the outer atoms as having their inner shells compressed into the nucleus—i.e., using an effective charge in place of N. If we adopt this idea, one possible way of proceeding is to use the experimental bond lengths D together with Eq. (1a) to determine a value of N_{eff}; with this N_{eff} and the actual Z one can then calculate the force constant k and compare with experiment. The results of this sort of calculation are shown in Table I for the series of chlorides XCl_4.

The agreement is scarcely impressive; but considering that previously (i.e., using the actual N) the values of k were wrong by a factor of about 10^3, the agreement as to order of magnitude is interesting. Further, there is a clear trend toward better agreement for the heavier molecules, which is probably to be expected, as in the atomic case, when using the statistical method.

In conclusion, one may point out that since the T-F equation neglects exchange (which is certainly an important effect in molecular binding!), it would be of interest to see whether the modified equation due to Dirac,[4] which includes approximately the effect of exchange, improves these results at all. Unfortunately the Thomas-Fermi-Dirac equation is considerably harder to work with, and considering the rather violent nature of the "smoothing approximation" itself, the value of the results is not likely to be worth the effort involved.

[1] N. H. March, Proc. Cambridge Phil. Soc. **48**, 665 (1952).
[2] Buckingham, Massey, and Tibbs, Proc. Roy. Soc. (London) **A178**, 119 (1941).
[3] The scale of abscissas in Fig. 2 of March's paper should run from 2 to 10 rather than from 0 to 8.
[4] P. A. M. Dirac, Proc. Cambridge Phil. Soc. **26**, 376 (1930).

Hydrogen-Fluorine Flame Temperatures*

DAVID ALTMAN AND MILTON FARBER
Jet Propulsion Laboratory, California Institute of Technology, Pasadena, California
(Received March 23, 1953)

RECENT measurements on the heat of dissociation of fluorine[1,2] have yielded a value of about 37 kcal/mole, which is considerably lower than the previously accepted value of about 63 kcal/mole.[3] A short while ago Wilson *et al.*[4] reported a flame-temperature measurement of the stoichiometric $H_2(g)-F_2(g)$ system employing the lithium line-reversal technique with the sun as the comparison radiator. A value of 4300°K±150°K was measured which was considered in fortuitous agreement with their calculated value of 4300°K employing a heat of dissociation of 63 kcal/mole.

In view of the more recent lower value for $D_0(F_2)$, we wondered whether this temperature measurement was compatible with the new $D_0(F_2)$ and have therefore calculated flame temperatures at atmospheric pressure over a range of mole ratios for the two assumed heats of dissociation of 63.5 and 37 kcal/mole. The enthalpy and entropy tables employed were taken from the recent paper of Cole, Farber, and Elverum.[5] The results of these calculations are shown in Table I and are plotted in Fig. 1 to show the relative trends with mole ratio.

TABLE I. Calculated flame temperature for hydrogen-fluorine.

Mole ratio r (F_2/H_2)	Calculated flame temperature (1 atmos) in °K $\Delta H_{298}=63.5$ kcal/mole	$\Delta H_{298}=37$ kcal/mole
0.5	3545	3508
1.0	4252	3956
1.5	4070	3907
2.0	2871	3596
2.5	2281	2684
3.0	2130	1867
4.0	1973	1369
5.0	1871	1268

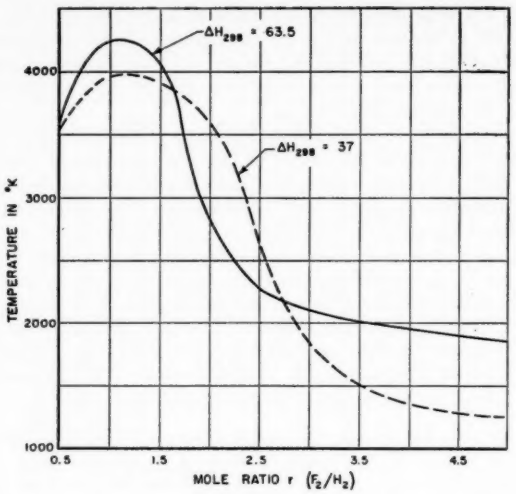

FIG. 1. Flame temperatures of the H_2-F_2 system at 1 atmosphere.

At the stoichiometric ratio, the flame temperatures for ΔH_{298} of 63.5 and 37 kcal/mole are 4252°K and 3956°K, respectively. It is clear, therefore, that the value measured by Wilson *et al.*[4] of 4300±150°K is incompatible within their admitted limit of error with the recently measured low value of $D_0(F_2)$.

We should like to point out that, if flame temperature measurements were to be made in order to decide between the two reported values for $D_0(F_2)$, a more reliable conclusion can be drawn from experiments at the higher mole ratios. Not only are the temperatures lower, permitting the use of more conventional line-reversal equipment, but also the temperature differences are larger; thus at $r=1$, ΔT is only 296°K; whereas at $r=2$, it is 725°K; and at $r=4$, it is 604°K. Furthermore, it would be desirable to make temperature measurements at two r values, perhaps $r=2.5$ and 4, since the calculated temperature ratio for $\Delta H_{298}(F_2)$ of 63.5 is 1.15, whereas that for $\Delta H_{298}(F_2)$ of 37 is 1.97. Measurements of this type which accentuate the difference also have the advantage of partially cancelling instrumental errors inherent in obtaining absolute temperature values.

* This paper presents the results of one phase of research carried out at the Jet Propulsion Laboratory under Contract No. DA-04-495-Ord 18, sponsored by the Department of the Army, Ordnance Corps.
[1] R. N. Doescher, J. Chem. Phys. **19**, 1070 (1951).
[2] H. Wise, J. Chem. Phys. **20**, 927 (1952).
[3] Wartenberg, Springer, and Taylor, Z. physik. Chem., 61 (1931).
[4] Wilson, Conway, Engelbrecht, and Grosse, J. Am. Chem. Soc. **73**, 5514 (1951).
[5] Cole, Farber, and Elverum, J. Chem. Phys. **20**, 586 (1952).

Erratum: On the Stability of Metallo-Organic Compounds

[J. Chem. Phys. **21**, 196 (1953)]

H. H. JAFFÉ AND G. O. DOAK
Venereal Disease Experimental Laboratory, U. S. Public Health Service, School of Public Health, University of North Carolina, Chapel Hill, North Carolina

TABLE I of the above paper contains an error. The entry under X_{ij}/A for *Al* should read 3.62. The last reference under *note added in proof* should read J. Chem. Phys. **21**, 156 (1953). Reference 18 should read H. H. Jaffé, J. Chem. Phys. **21**, 258 (1953).

Van der Waals' a and Ionization Potential of Inert Gases

YATENDRA PAL VARSHNI
Department of Physics, Allahabad University, Allahabad, India
(Received April 3, 1953)

VAN der Waals' a depends on the polarizability of the molecules. In case of atoms, the polarizability is dependent on the ionization potential. Thus, it is expected that a relation may hold between a and ionization potential (to be denoted by V) for similar atomic gases. For inert gases, a graph of a against $1/V^4$ is found to give a straight line. The relationship may be expressed by

$$a=-0.0004478+\frac{188.33}{V^4}, \quad (1)$$

where a is in atmos$\times$cm^4 and V is in volts.

The observed and calculated values of a are recorded in Table I.

TABLE I. a of inert gases.[a]

Inert gas	V	a calc	a obs	Percentage error
Helium	24.581	0.000068	0.000068	0
Neon	21.559	0.000424	0.00042	−1
Argon	15.756	0.00261	0.00268	+2.5
Krypton	13.996	0.00446	0.00462	+3.5
Xenon	12.127	0.00826	0.00816	−1.2
Radon	10.746	0.01367	...	

[a] Data from G. Herzberg, *Atomic Spectra and Atomic Structure*, and Hodgman, *Handbook of Chemistry and Physics*.

Considering the fact that a has no absolute value and depends on the temperature, the agreement between the observed and calculated values is fairly good.

No experimental determination of a for Radon seems to have been made. The estimated value from Eq. (1) is 0.01367.

The author is grateful to Dr. K. Majumdar for his interest in the work.

The ν_3 Raman Band of Ammonia

C. CUMMING* AND H. L. WELSH
McLennan Laboratory, University of Toronto, Toronto, Canada
(Received March 31, 1953)

AN outstanding problem associated with the ammonia molecule has been the determination of the fundamental frequency ν_3 corresponding to the doubly degenerate N−H bond-stretching vibration. The infrared band is strongly overlaid by the ν_1 band and has so far defied analysis. Barker[1] assigned the infrared band at 4μ to the $\nu_3-\nu_2$ transition and deduced the value 3414 cm^{-1} for ν_3. In a discussion of the overtone and combination bands Sutherland[2] suggested the value 3450 cm^{-1} for ν_3, which fits the isotopic relations with ND_3 much better. The Raman band at 3382 cm^{-1} in liquid ammonia[3] is probably ν_3, but the frequency is presumably shifted by the strong dipole interaction in the condensed phase. The band has apparently not been observed in the gas.[4]

In the present investigation the Raman spectrum of the gas was excited by Hg 2537 in a Raman tube with a four-mirror system for multiple reflections.[5] The spectrum was photographed using a quartz Littrow spectrograph with a reciprocal linear dispersion of 27.0 cm^{-1}/mm at 2537A. Exposures of 12 to 48 hours were made with Eastman 103a-O plates and gas pressures in the range 3 to 5 atmospheres. A microphotometer tracing of the spectrum in the region $\Delta\nu=3200$–3750 cm^{-1} is shown in Fig. 1. The frequencies of 37 maxima attributable to the ν_3 band were measured, and a partial analysis of the band was achieved.

The fundamental Raman band of a doubly degenerate vibration of a C_{3v} molecule has a very complex rotational structure, since for each initial rotational level (J, K), there are in general 20 permitted transitions according to the selection rules $\Delta J=0, \pm1, \pm2$, and $\Delta K=\pm1, \pm2$.[6] If the rotational constants, A_1 and B_1, of the upper vibrational state were very nearly equal to the ground-state values, A_0 and B_0, respectively, the most prominent features of the band would be the two series of Q_K sub-branches, corresponding to $\Delta J=0$, $\Delta K=\pm1, \pm2$, since each Q_K sub-branch represents the superposition of many single transitions. However, it was immediately apparent that the strong maxima in the ν_3 band of ammonia could not be assigned to Q_K sub-branches. It was therefore concluded that at least one of the convergence factors, B_0-B_1 and A_0-A_1, has an appreciable value.

The analysis of the band was carried out in the following way. The relative intensities of the most probable Raman transitions originating in the most highly populated rotational levels were found using the transition probabilities calculated by Placzek and Teller.[6] When the frequencies of these transitions, relative to the band origin ν_0, were calculated from the rotational constants as at present known, assignments of the strongest lines in the observed band could be made immediately. Eight lines of the series ${}^8S(J, K=J)$, for which $\Delta J=\Delta K=+2$, were identified (Fig. 1). The frequencies of these lines, corrected for centrifugal stretching according to the data of Slawsky and Dennison,[7] gave a straight line when plotted against $J+1$. Since the frequencies follow the formula

$${}^8S(J, K=J)=\nu_0+B_1+B_0+2A_1\zeta + (J+1)(B_1+4A_1+2A_1\zeta-B_0)+J^2(A_1-A_0),$$

it is evident that A_1-A_0 is small and that two relations between the constants ν_0, B_0, B_1, A_0, A_1, and $A_1\zeta$ can be obtained from the graph. The value of B_0 was taken as 9.94 cm^{-1}, as determined by us from an analysis of the rotational Raman spectrum at high dispersion. Other rotational transitions in the band were identified to give three further relationships to determine the remaining constants. The calculated values of the rotational constants vary somewhat when different lines are used in the analysis; this lack of consistency undoubtedly comes about because some of the measured lines are blended with weaker lines. When the fre-

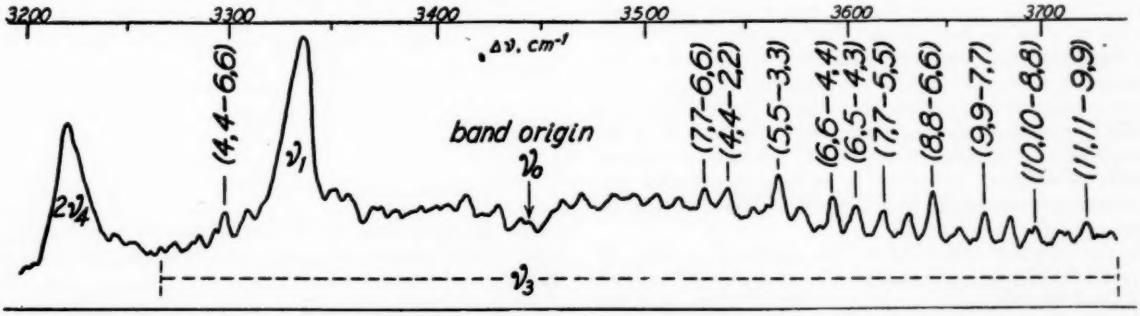

FIG. 1. Microphotometer tracing of the Raman spectrum of gaseous ammonia in the region $\Delta\nu=3200$–3750 cm^{-1}. The assignments $(J', K'-J'', K'')$ of the lines used in the analysis are indicated.

quencies of the transitions (7,7−6,6), (6,5−4,3), and (4,4−6,6), along with the series ${}^{S}S(J, K=J)$ are used, the values of the constants are: $\nu_0=3444$, $B_1=9.78$, $A_0=A_1=6.24$, and $A_1\zeta=0.28$ cm^{-1}. The value of ν_0, the frequency of the ν_3 fundamental, is probably accurate to within one cm^{-1}.

* Holder of the Nadine Phillips Fellowship, School of Graduate Studies, University of Toronto, 1951–1952.

[1] E. F. Barker, Phys. Rev. **55**, 657 (1939).
[2] G. B. B. M. Sutherland, Phys. Rev. **56**, 836 (1939).
[3] K. W. F. Kohlrausch, *Ramanspektren* (Akademische Verlagsgesellschaft Becker und Erler, Leipzig, 1943).
[4] Dickinson, Dillon, and Rasetti, Phys. Rev. **34**, 582 (1929); E. Amaldi and G. Placzek, Z. Physik **81**, 259 (1933); C. M. Lewis and W. V. Houston, Phys. Rev. **44**, 903 (1933).
[5] Welsh, Cumming, and Stansbury, J. Opt. Soc. Am. **41**, 712 (1951).
[6] G. Placzek and E. Teller, Z. Physik **81**, 209 (1933).
[7] Z. I. Slawsky and D. M. Dennison, J. Chem. Phys. **7**, 509 (1939).

Table of Bessel Functions

C. W. JONES
The University of Liverpool, Mathematical Institute, Department of Applied Mathematics, Liverpool, England
(Received February 24, 1953)

IT may be of interest to those working in theoretical chemistry and physics, in particular in calculating molecular integrals, to know of the recent publication of *A Short Table for the Bessel Functions* $I_{n+\frac{1}{2}}(x)$, $(2/\pi)K_{n+\frac{1}{2}}(x)$ (Cambridge University Press, Cambridge, 1952).

This is a pamphlet of 20 pages giving the functions to 7 or 8 figures in the ranges $x=0(.1)10$, $n=0(1)10$, with full provision for interpolation and extension of the range of x. It is published for the Royal Society Committee on Mathematical Tables, under my name.

Acoustic Wave Velocities, Elastic Constants, and Debye Characteristic Temperature for Polycrystalline MgCd†

CHARLES S. SMITH, *Physics Department, Case Institute of Technology, Cleveland, Ohio*
AND
W. E. WALLACE, *Chemistry Department, University of Pittsburgh, Pittsburgh, Pennsylvania*
(Received April 6, 1953)

THE longitudinal and transverse acoustic wave velocities in a polycrystalline magnesium-cadmium alloy containing 50.6 atomic percent cadmium were measured using the pulsed ultrasonic method. The alloy was prepared by fusing together spectroscopically pure magnesium and cadmium under a blanket of helium purified by evaporation. Experimental details concerning preparation and analysis of the alloy and the method employed in measuring the sound velocities are given elsewhere.[1,2]

Transit times were measured for a rod about 1 cm in diameter and 0.6224 cm long. The observed times were 3.60 ± 0.02 and 7.00 ± 0.02 μsec for the longitudinal and transverse waves, respectively. From the observed transit times 0.02 ± 0.05 μsec was subtracted to allow for end effects.[2] The magnitude of this correction was established mostly from experience, although it could be ascertained reasonably well for the longitudinal waves. More elaborate evaluation and control of uncertainties resulting from end effects, temperature, etc., were not warranted, since the measurements were intended merely to lead to a value of the compressibility of sufficient reliability to be used to calculate constant volume heat capacities from those determined at constant pressure.

From the corrected transit times one obtains $V_L=3.66\times10^5$ and $V_t=1.83\times10^5$ cm/sec. Employing a density[2] of 5.36 g/cm^3, $C_{11}=\rho V_L^2=7.18\times10^{11}$, and $C_{44}=\rho V_t^2=1.80\times10^{11}$ dynes/cm^2. For an isotropic medium $\beta_s^{-1}=C_{11}-4/3C_{44}=4.78\times10^{11}$ dynes/cm^2 or 4.72×10^5 atmos, where β_s is the adiabatic compressibility. β_T, the isothermal compressibility, is related to β_s by the thermodynamic expression $\beta_T-\beta_s=\alpha^2TV/C_p$. β_T is evaluated from published densities[3] and thermal expansivities[4] of magnesium-cadmium alloys, together with unpublished measurements of C_p for this alloy.[5] The result is $\beta_T=2.18\times10^{-6}$ atmos^{-1}. This value may be compared with corresponding quantities determined by Bridgeman for the pure metals[6]—β_T for Mg$=2.96\times10^{-6}$, β_T for Cd$=2.07\times10^{-6}$ atmos^{-1}. Thus, the alloy has, as expected, an intermediate compressibility, although it is somewhat less compressible than would have been anticipated from a linear interpolation between the compressibilities of the components. Such a deviation is not surprising in view of the exothermal formation of the alloy.[2,7]

The Debye characteristic temperature θ_D computed from the sound velocities is 220°K. This value compares favorably with 245°K, the value of θ_D from specific heats between 100 and 200°K.[8]

† This work was assisted by the U. S. Office of Naval Research at Case Institute of Technology and the U. S. Atomic Energy Commission at the University of Pittsburgh.

[1] Trumbore, Wallace, and Craig, J. Am. Chem. Soc. **74**, 132 (1952).
[2] Neighbors, Bratten, and Smith, J. Appl. Phys. **23**, 389 (1952).
[3] J. M. Singer and W. E. Wallace, J. Phys. Colloid Chem. **52**, 999 (1948).
[4] Hirabayashi, Nagasaki, and Nagasu, J. Jap. Inst. Metals (Sendai) **13**, No. 6 (1949).
[5] Satterthwaite, Craig, and Wallace (to be published in J. Am. Chem. Soc.).
[6] P. W. Bridgeman, Proc. Am. Acad. Art Sci. **58**, 209 (1922); **76**, 9 1945).
[7] Buck, Wallace, and Rulon, J. Am. Chem. Soc. **74**, 136 (1952).
[8] C_v values above 200°K are not appropriate in evaluating θ_D, since they contain a small configurational contribution due to the beginnings of the order-disorder transition which culminates at 528°K. The configurational contribution at 300°K is sufficiently large to make θ_D negative at that temperature.

Investigation of Rotational Isomers with Ultrasound

JOHN KARPOVICH*
Electrical Engineering Department, Imperial College of Science and Technology, London, England
(Received March 30, 1953)

A MODIFIED resonance-reverberation technique for sound absorption measurements below 600 kilocycles per second has been developed. Over 50 organic liquids and three solids have been studied. Relaxation processes have been observed in some cyclohexane derivatives, cyclohexene, methyl formate, ethyl acetoacetate, acetic anhydride, and methyl benzoate. Additional absorption measurements have been made in the relaxation regions of formic acid, ethyl formate, methyl acetate, and ethyl acetate.

A study of the cyclohexane derivatives and other similar molecules has led to the identification of the mechanism responsible for the relaxation processes in these liquids. The relaxation phenomena are attributed to the disturbance by the sound wave of equilibria between rotational isomers. The isomers in the cyclohexane derivatives result from the polar and equatorial positions assumed by the substituent groups owing to interconversion of the two chair configurations.

In cyclohexene, the equilibrium disturbed by the sound wave is that between pseudo-boat and chair configurations.

The relaxation processes in the carboxylic acids and esters, and other molecules with the

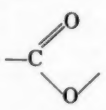

group are attributed to the disturbance of equilibria between rotational isomers which arise from rotation about the C−O bond.

Infrared absorption bands at about 1160 and 1185 cm^{-1} in the esters of carboxylic acids[1] are identified with rotational isomerism of the type postulated for the relaxation processes in these liquids.

A detailed report on these findings is now in preparation.

The author is grateful to Professor Willis Jackson for offering facilities for carrying out this program of research.

* This research was done as partial requirement for a Ph.D. degree from the University of London.

[1] H. W. Thompson and P. Torkington, J. Chem. Soc. **1945**, 640.

Green's "Correction" of Yvon's Dielectric Constant Formula

WILLIAM FULLER BROWN, JR.
Sun Physical Laboratory, Newtown Square, Pennsylvania
(Received February 3, 1953)

IN his new book on fluids,[1] H. S. Green derives a formula for the dielectric constant of a nonpolar fluid. He then comments: "This corrects the formula given by Yvon (1937), who did not discuss sufficiently the effect of the induced charge distribution."[2]

Recently, I published a calculation[3] that verified Yvon's formula. Thus, Green's result and mine are in apparent contradiction. Upon study of Green's calculation, however, I conclude that his result is only superficially different from mine, and that the two results are actually equivalent.

Green's formula [his Eq. (6.13)] is

$$(\kappa-1)(1-(4/3)\pi n\alpha)=4\pi n\alpha(1+\lambda\alpha^2), \tag{1}$$

where κ=dielectric constant, n=number density of molecules, α=polarizability, and [Eq. (6.11)]

$$n\lambda=2\int r^{-6}n_2(r)d\mathbf{r}+\int\int(rs)^{-5}\{3(\mathbf{r}\cdot\mathbf{s})^2-r^2s^2\}\times\{n_3(\mathbf{r},\mathbf{s})-nn_2(r)-nn_2(s)+n^3\}d\mathbf{r}d\mathbf{s}; \tag{2}$$

n_k is the molecular distribution function for k molecules. I have restored to the first term a lost factor 2, which was present in the step immediately preceding this equation.

In Eq. (1), terms of order α^4 have been neglected. Expansion of $1/(\kappa-1)$ to as many terms as are significant, therefore, gives

$$\frac{\kappa+2}{\kappa-1}=1+\frac{3}{\kappa-1}=\frac{3}{4\pi n\alpha}-\frac{3\lambda\alpha}{4\pi n}. \tag{3}$$

This is of the same form as my Eq. (3-10), except that C is replaced by $3\lambda\alpha/8\pi n=n\lambda\cdot(3\alpha/8\pi n^2)$.

From my Eqs. (4-8) and (4-6), C to the present approximation, and in Green's notation, is

$$C=(3\alpha/8\pi n^2)\{2\int r^{-6}n_2(r)d\mathbf{r}+2\int\int(rs)^{-3}\times[n_3-n_2(r)n_2(s)/n]P_2(\cos\theta)d\mathbf{r}d\mathbf{s}\}, \tag{4}$$

where θ is the angle between $\mathbf{r}$ and $\mathbf{s}$. Since $3(\mathbf{r}\cdot\mathbf{s})^2-r^2s^2=2r^2s^2P_2(\cos\theta)$, the only difference between C and $n\lambda\cdot(3\alpha/8\pi n^2)$ is that $n_3-n_2(r)n_2(s)/n$ in the former is replaced by $n_3-nn_2(r)-nn_2(s)+n^3$ in the latter.

In the integrals containing these quantities, let the integration over $\mathbf{r}$ be performed first. The integral that occurs in C is convergent at $r=\infty$ and at $r=0$. The integral that occurs in $n\lambda$ is convergent at $r=\infty$ but only semiconvergent at $r=0$; from Green's derivation, the reader can deduce that the order of operations must be: first, integrate over the region $r>r_0$; second, let $r_0\to0$. In the difference $C-n\lambda\cdot(3\alpha/8\pi n^2)$, we may (for given $\mathbf{s}$) safely integrate first over spherical shells r=const, then from $r=0$ to $r=\infty$. In this difference, n_3 no longer appears, and the integrand (for given $\mathbf{s}$) is of the form $f(r)P_2(\cos\theta)$; the first step of integration, therefore, gives the result zero.

Thus Green's formula is equivalent to mine and so to Yvon's.

Green's derivation is essentially the same as mine up to his Eq. (6.6), which is my Eq. (3-2). The difference from that point on lies in the method used to improve the convergence of the integrals. My expression $n_3-n_2(r)n_2(s)/n$ vanishes both at $r=\infty$ and at $r=0$. Green's expression $n_3-nn_2(r)-nn_2(s)+n^3$ remains finite at $r=0$; hence the semiconvergence.

In this discussion I have cited my own paper rather than Yvon's, because the former is more generally available to readers of this journal. With regard to Yvon's monographs, the following information may be useful. (1) In 1949 I obtained copies within less than three weeks, by ordering directly from the publishers by airmail letter. (2) The dielectric constant formula, Eq. (220) of reference 2, is quoted (with a few obvious misprints) in Science Abstracts **A39**, 300, Abstract 1318 (1936). (3) For still another derivation of Green's Eq. (2.9), p. 129, see Yvon's 1935 monograph,[4] pp. 17–19.

[1] H. S. Green, *Molecular Theory of Fluids* (Interscience Publishers, Inc., New York, 1952), pp. 207–211.

[2] J. Yvon, *Recherches sur la Théorie Cinétique des Liquides: I, Fluctuations en Densité; II, La Propagation et la Diffusion de la Lumière. Actualités Scientifiques et Industrielles, Nos. 542 and 543* (Hermann et Cie., Paris, 1937).

[3] William Fuller Brown, Jr., J. Chem. Phys. **18**, 1193–1200 (1950).

[4] J. Yvon, *La Théorie Statistique des Fluides et l'Équation d'État. Actualités Scientifiques et Industrielles, No. 203* (Hermann et Cie., Paris, 1935).

Classical Limit of Mean Thermal Vibration Amplitudes

J. C. DECIUS
Department of Chemistry, Oregon State College, Corvallis, Oregon
(Received April 6, 1953)

RECENT refinements[1] in electron diffraction studies have made possible the evaluation of the vibration amplitudes resolved along the equilibrium interatomic directions. A detailed theory[2] correlating such measurements with the analysis of the vibrational spectrum has appeared. In this theory, the vibrational frequencies and amplitudes both appear explicitly.

It is the purpose of this note to call attention to the high temperature, or classical limit of the relations developed by Morino, Kuchitsu, and Shimanouchi.

Combining their Eqs. (3) and (4), the following expression is obtained for the mean amplitude of the ith interatomic distance:

$$\langle R_i^2\rangle=\frac{h}{8\pi^2}\sum_k L_{ik}^2\left(\frac{1}{\gamma_k}\coth\frac{h\gamma_k}{2kT}\right). \tag{1}$$

If kT is large compared with $h\gamma_k$ for all γ_k, or at any rate, for all γ_k such that L_{ik} is large, this expression becomes approximately

$$\langle R_i^2\rangle=kT\sum_k\frac{L_{ik}^2}{\lambda k}, \tag{2}$$

where

$$\lambda_k=4\pi^2\gamma_k^2.$$

The summation remaining in Eq. (2) can be simplified by the following arguments. It is part of the definition of the L_{ik} that in matrix form

$$\mathbf{\Lambda}=\mathbf{L}'\mathbf{F}\mathbf{L}$$

or taking the inverse

$$\mathbf{\Lambda}^{-1}=\mathbf{L}^{-1}\mathbf{F}^{-1}(\mathbf{L}^{-1})^{-1}. \tag{4}$$

Matrix multiplying Eq. (4) on the left by $\mathbf{L}$ and on the right by $\mathbf{L}'$, one obtains

$$\mathbf{L}\mathbf{\Lambda}^{-1}\mathbf{L}'=\mathbf{F}^{-1}. \tag{5}$$

The ith diagonal element of Eq. (5) is

$$\sum_{kl}L_{ik}\Lambda_{kl}^{-1}L_{li}'=\sum_k\frac{L_{ik}^2}{\lambda k}=F_{ii}^{-1}, \tag{6}$$

since $\mathbf{\Lambda}$ and therefore $\mathbf{\Lambda}^{-1}$ are diagonal.

Thus, Eq. (2) can be written

$$\langle R_i^2\rangle=kTF_{ii}^{-1}. \tag{7}$$

The physical significance of F_{ii}^{-1} is the following: just as the potential energy can be written as a quadratic form in the internal coordinates, so it can also be written as a quadratic form in terms

of generalized forces. When it is expressed in the latter way, the proportionality constants are precisely the elements of the matrix $\mathbf{F}^{-1}$.

The usefulness of Eq. (7) as a parameter of molecular structure must certainly depend upon the possibility of finding molecules with sufficiently low fundamentals, so that the condition $h\gamma_k \ll kT$ can be satisfied under the conditions of the diffraction experiment. An interesting example might be $SnBr_4$.

[1] I. Karle and J. Karle, J. Chem. Phys. **18**, 963 (1950).
[2] Morino, Kuchitsu, and Shimanouchi, J. Chem. Phys. **20**, 726 (1952).

Note on the Vibrational Spectra of $SiHCl_3$, SiH_2Cl_2, and SiH_2Br_2*

JANET A. HAWKINS,† SANTIAGO R. POLO, AND M. KENT WILSON
Mallinckrodt Chemical Laboratory, Harvard University, Cambridge, Massachusetts
(Received March 27, 1953)

THE Raman Spectrum of liquid $SiHCl_3$ has been reported,[1] and the infrared spectrum of the gas has been examined with a NaCl prism.[2] In relation to some work being done in this laboratory, it was of interest to measure the gas frequencies of the two fundamentals, ν_2 and ν_5, and complete the study of the spectrum in the KBr region.

Measurements of the spectrum of gaseous $SiHCl_3$ were made with a Perkin-Elmer 12C Spectrograph modified for double-pass operation on a commercial sample‡ which had undergone no further purification. Gas pressures varying from 400 mm to less than 1 mm were used in a 10-cm cell. The spectrum between 450 cm^{-1} and 700 cm^{-1} is plotted in Fig. 1, and the observed frequencies and their assignments are listed in Table I.

The observed frequencies agree very well with the Raman data for the liquid.[1] The fundamental at 497 cm^{-1} is a parallel band and is identified with $\nu_2(a_1)$, while the extremely intense band at 600 cm^{-1} has no Q-branch and is assigned as the fundamental $\nu_5(e)$, in agreement with previous work.

While working with $SiHCl_3$ a resemblance was noted between the 810 cm^{-1} band of this compound and the band at the same frequency which had previously been assigned to SiH_2Cl_2.[3] Accordingly the sample of SiH_2Cl_2 was subjected to bulb-to-bulb distillation at temperatures near $-100°C$, and the spectrum of the resulting fraction was re-examined. After such treatment the 810 cm^{-1} band had decreased in intensity relative to the fundamentals of SiH_2Sl_2 and therefore, must be due to an impurity of $SiHCl_3$. Upon reinvestigation of SiH_2Cl_2 in the KBr region a shoulder at 605–620 cm^{-1} was observed on the 592 cm^{-1} band of SiH_2Cl_2. Although some of this absorption is the result of the presence of the strong 600 cm^{-1} band of the $SiHCl_3$ impurity, there is some additional absorption near 620 cm^{-1} which clearly cannot be due to the impurity.

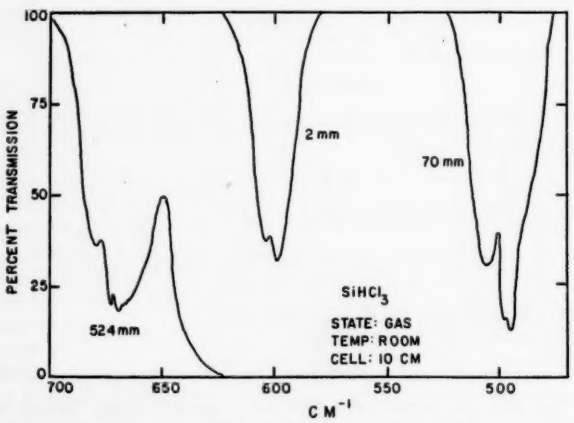

FIG. 1. The absorption spectrum of gaseous $SiHCl_3$ from 450 cm^{-1} to 700 cm^{-1}.

TABLE I. The infrared spectrum of gaseous $SiHCl_3$.

ν (cm^{-1})	Assignment
810	$\nu_4(e)$
674	$\nu_6+\nu_2(E)$
600	$\nu_5(e)$
497	$\nu_2(a_1)$

TABLE II. Thermodynamic functions for SiH_2Cl_2 (cal deg^{-1} $mole^{-1}$)

T (°K)	C_p^0	S^0	$\frac{(H^0-H_0^0)}{T}$	$\frac{-(F^0-H_0^0)}{T}$
298.15	14.83	68.06	10.79	57.27
400	17.08	72.80	12.26	60.54
800	21.53	86.21	16.11	70.10
1200	23.92	95.28	18.38	76.90

TABLE III. Fundamental frequencies of SiH_2Cl_2 and SiH_2Br_2.

SiH_2Cl_2 (cm^{-1})[a]	SiH_2Br_2 (cm^{-1})[b]	Assignment
188	122	$\nu_4(a_1)$
531	393	$\nu_3(a_1)$
592	456	$\nu_9(b_2)$
(610)[c]	(535)[c]	$\nu_7(b_1)$
710	688	$\nu_5(a_2)$
877	828	$\nu_8(b_2)$
953	925	$\nu_2(a_1)$
2200	2206	$\nu_1(a_1)$
2200	2232	$\nu_6(b_1)$

[a] See reference 3.
[b] See reference 5.
[c] See text.

Comparison with the related methane derivatives indicates that the missing rocking fundamental, $\nu_7(b_1)$, should occur at a lower frequency than the torsional mode, $\nu_5(a_2)$, which in SiH_2Cl_2 has been assigned as the 710 cm^{-1} Raman line.[3] An upper limit of the $\nu_7(b_1)$ frequency may be estimated from the corresponding carbon compounds. Since in XH_2Z_2 molecules of C_{2v} symmetry the other b_1 normal mode is essentially a X−H stretching motion, the secular equation can be reduced by splitting out the high frequency by the method of Wilson.[4] If the corresponding F-element for CH_2Cl_2 [3] is carried over to SiH_2Cl_2, a value of 615 cm^{-1} is calculated for the $\nu_7(b_1)$ mode. We, therefore, interpret the absorption near 610 cm^{-1} in SiH_2Cl_2 to be the fundamental ν_7, although the agreement between the observed and calculated values may be regarded as fortuitous. Thermodynamic functions calculated on the basis of the new assignment for SiH_2Cl_2 are given in Table II.

Francois and Buisset[5] have reported the Raman spectrum of SiH_2Br_2 and $SiHBr_3$. They assign as the torsional mode in SiH_2Br_2 the band at 761 cm^{-1} whose frequency seems to be too high when compared with the value of 710 cm^{-1} as found for this mode in SiH_2Cl_2. It appears more likely that the line at 688 cm^{-1}, assigned by François and Buisset to ν_7, corresponds to the torsional vibration, ν_5. A calculation similar to that made for SiH_2Cl_2 gives a value of 535 cm^{-1} which may be considered as an upper frequency limit for ν_7 of SiH_2Br_2. No Raman band has been reported in this region that might be assigned to ν_7. This is probably due to the fact that this band is rather weak in the Raman effect, as happens in the cases of SiH_2Cl_2 CH_2Cl_2, and CH_2Br_2. The assignments for SiH_2Cl_2 and SiH_2Br_2 are given in Table III.

* This work was supported in part by the U. S. Air Force under Contract AF 18(600)-590.
† Socony-Vacuum Predoctoral Fellow in Chemical Physics.
‡ Anderson Laboratories, Inc., Adrian, Michigan.
[1] C. A. Bradley, Phys. Rev. **40**, 908 (1932).
[2] T. G. Gibian and D. S. McKinney, J. Am. Chem. Soc. **73**, 1431 (1951).
[3] J. A. Hawkins and M. K. Wilson, J. Chem. Phys. **21**, 360 (1953).
[4] E. B. Wilson, Jr., J. Chem. Phys. **9**, 76 (1941).
[5] F. François and M. Buisset, Compt. rend. **230**, 1946 (1950).

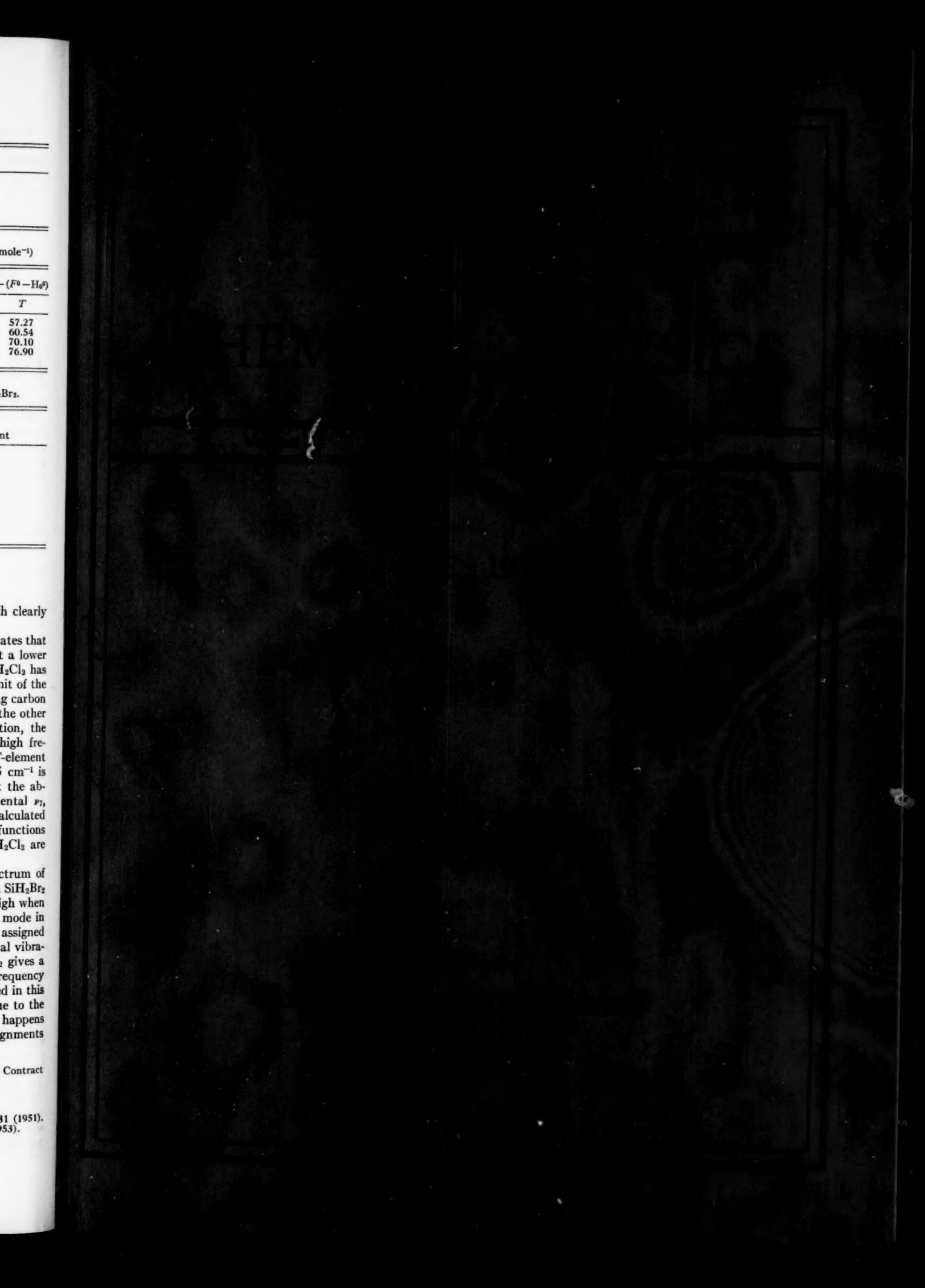

...ORS

...Jr., *Editor*

...

...

...